

Characterizing and Modeling of Silicate Modified Smart Cements, Smart Cement Grouts and Drilling Muds

A Dissertation

Presented to

the Faculty of the Department of Civil and Environmental Engineering

University of Houston

In Partial Fulfillment

of the Requirement for the Degree

Doctor of Philosophy

in Civil Engineering

by

Md Kausar Ali

December 2015

Characterizing and Modeling of Silicate Modified Smart Cements, Smart Cement Grouts and Drilling Muds

Md Kausar Ali

Approved:

Chair of the Committee
Cumaraswamy Vipulanandan, Professor,
Civil and Environmental Engineering

Committee Members:

Ramanan Krishnamoorti, Professor,
Chemical and Biomolecular Engineering

Yi-Lung Mo, Professor,
Civil and Environmental Engineering

William G. Rixey, Associate Professor,
Civil and Environmental Engineering

Yuhua Chen, Associate Professor,
Electrical and Computer Engineering

Kalyana Babu Nakshatralla, Assistant Professor,
Civil and Environmental Engineering

Suresh K. Khator, Associate Dean,
Cullen College of Engineering

Roberto Ballarini, Professor and Chair,
Civil and Environmental Engineering

ACKNOWLEDGEMENTS

First of all I acknowledge Almighty God who gave me the courage and mindset to start and continue to finish my Ph.D.

I would like to express my deepest and sincere gratitude to my research and academic advisor Dr. C. Vipulanandan for his valuable guidance, support and advice throughout my study and research. I would also like to extend my special thanks to Dr. Yi-Lung Mo, Dr. William G. Rixey, Dr. Kalyana Babu Nakshatrala, Dr. R. Krishnamoorti, and Dr. Yuhua Chen for serving in my committee with their valuable comments and advice. I want to gratefully acknowledge my fellow graduate students of the CIGMAT (Center for Innovative Grouting Materials and Technology) research group for their friendship and support throughout my study. My special thanks to the best machinist and lab technician of our department, Jeffrey Miller and Gerald McTigret.

I am eternally indebted to my loving wife, Mst. Sharmila Aktar, who agreed to leave our comfortable home and job in Bangladesh and come to the USA so that I can continue my Ph.D. study. Her support and encouragement have been unwavering, and my success as a graduate student has been largely due to her. I also want to give my special thanks to my daughter Tasfia Susmi and my son Rizwan Taseen for their sacrifices during my study. And my unexplainable gratitude to my mother and father without whom I was no one.

To my wife

Mst. Sharmila Aktar

Characterizing and Modeling of Silicate Modified Smart Cements, Smart Cement Grouts and Drilling Muds

An Abstract

Of a

Dissertation

Presented to

the Faculty of the Department of Civil and Environmental Engineering

Cullen College of Engineering

University of Houston

In Partial Fulfillment

of the Requirements for the Degree of

Doctor of Philosophy

in Civil Engineering

by

Md Kausar Ali

December 2015

Abstract

In this study, the effects of silicate based additives on the smart cements, smart cements grouts and drilling muds were investigated. Also the effects of clay soil contamination on the modified smart cement were investigated. Smart cement (Class A, Portland cement type I, Class H) was made using 0.1% conductive filler and was electrically characterized as a resistive material. In this study, a series of experiments were performed to evaluate the smart cement behavior with and without up to 0.3% of sodium meta-silicate (SMS) to determine the sensitivity in terms of electrical resistivity of the cement from curing to hardened state up to 12 months under different curing conditions. In the physical study small, large and field models were used and electrical resistance was monitored at various stages of construction and during the curing of cement in-situ.

The test results showed that the SMS reduced the electrical resistivity of the smart cement slurries and hardened cement based on the amount of SMS. For long term curing under room temperature, under moisture control curing, under water curing or at high temperature curing under dry and saturated condition, the resistivity of the hardened cement was reduced with the addition of SMS. The moisture loss from the smart cement was also reduced with addition of SMS. The resistivity with curing time was modeled with curing model develop to characterize the curing of the cement. The smart cement showed piezoresistive behavior under compressive stress. Without any SMS piezoresistivity at peak stress varied from 315% to 545% which reduced up to 145% to 230% with the addition of 0.3% SMS. The nonlinear piezoresistive model predicated the compressive stress – change in resistivity relationship of the smart cement very well. The

strength and piezoresistivity of the cement was correlated with the SMS content and curing time. The rheological properties of cement slurry with different SMS content and contamination, and the rheological properties of drilling mud with different silicates contents was modeled using Herschel–Bulkley model and Hyperbolic model. The smart cement grout showed piezoresistive behavior under compressive stress. Without any SMS, piezoresistivity at peak stress varied from 155-179% which is reduced up to 116-125% with 1% SMS. The repaired samples showed piezoresistivity varying from 48% to 62%. The strength regain of repaired damaged cement varied from 51% to 84% and the piezoresistivity regain varied from 21% to 42%.The fluid loss of the water based mud with different silicate content was modeled with API fluid loss model and the new Kinetic (Hyperbolic) Model. In the physical model study the rise of drilling mud and cement slurry in the simulated bore holes of various scales were effectively monitored using the changes in electrical resistance. The determination of resistance of the hardened cement and comparing with the predicted values were also found effective. The measured electrical resistance with curing time agreed very well with predicted resistance using the analytical models developed in this study.

TABLE OF CONTENT

Acknowledgements.....	iv
Abstracts.....	vii
TABLE OF CONTENTS.....	ix
LIST OF FIGURES.....	xv
LIST OF TABLES.....	xxix
CHAPTER 1 INTRODUCTION.....	1
1.1 General.....	1
1.2 Objective.....	4
1.3 Organization.....	4
CHAPTER 2 BACKGROUND AND LITERATURE REVIEW.....	6
2.1 Oil well cements.....	6
2.2 Smart cement for oil well.....	7
2.3 Cementing high temperature wells.....	8
2.4 Cement grouts and sodium meta-silicate.....	9
2.5 Water based drilling mud.....	10
2.6 Sodium Silicates.....	11
2.6.1 Sodium silicates in oil well cements.....	11
2.6.1.1 Hydration of oil well cement.....	14
2.6.2 Cementing high temperature wells.....	15
2.6.3 Cement grouts.....	16
2.6.4 Silicates in drilling mud.....	18
2.7 Summary.....	20
CHAPTER 3 MATERIALS AND METHODS OF TESTING.....	21

3.1 Materials.....	21
3.2 Methods of Testing.....	22
3.3 Mathematical models to characterize the materials.....	36
3.3.1 Mathematical models for rheological properties	36
3.3.2 Mathematical model to characterize fluid loss of drilling mud and cement slurry.....	37
3.3.3 Mathematical model to characterize electrical resistivity with curing time.....	39
3.3.4 Mathematical model to characterize piezoresistivity of hardened cement.....	40
CHAPTER 4 EFFECT OF SODIUM META-SILICATE ON THE SMART CEMENT BEHAVIOR.....	41
4.1 Characterizing sodium meta-silicate solution.....	41
4.1.1 pH of sodium meta-silicate solution.....	41
4.1.2 Electrical resistivity of sodium meta-silicate solution.....	41
4.2 Characterizing smart cement with SMS.....	43
4.2.1 Rheological properties.....	43
4.2.2 Fluid loss of smart cement slurry with SMS.....	47
4.2.3 Electrical Resistivity.....	47
4.2.3.1 Initial Resistivity.....	47
4.2.3.2 Resistivity during Curing Process.....	48
4.2.3.3 Curing of smart cement.....	51
4.2.3.3.1 Long time curing of the specimen at room temperature.....	51
4.2.3.3.1.1 Resistivity with curing time.....	51
4.2.3.3.1.2 Moisture loss and its effect on the resistivity.....	53
4.2.3.3.1.3 Proposed relationship between resistivity and moisture loss.....	57
4.2.3.3.2 Long time curing of the specimen without moisture loss at room temperature.....	58

4.2.3.3.3 Relationship between moisture loss and SMS content.....	60
4.2.3.3.4 Long time curing of the specimen cured under water.....	62
4.2.3.3.4.1 Resistivity with curing time.....	62
4.2.3.3.4.2 Moisture gain and its effect on the resistivity.....	65
4.2.3.3.4.3 Proposed relationship between resistivity and moisture gain.....	68
4.2.3.3.5 Minimum resistivity with respect to SMS concentration.....	69
4.2.4 Piezoresistivity and strength of smart cement.....	70
4.2.4.1 1 day of curing.....	70
4.2.4.2 7 days of curing.....	73
4.2.4.3 28 days of curing.....	75
4.2.4.4 Relationship between SMS concentration and strength/piezoresistivity.....	77
4.2.4.5 Relationship between RI24 and strength/piezoresistivity.....	79
4.2.4.6 Relationship between curing time and strength/piezoresistivity at failure.....	81
4.3 Effects of Temperature and Curing Environment on the Piezoresistive Behavior of the Smart Cement with and without Sodium Meta-silicate.....	83
4.3.1 Resistivity during curing at high temperature.....	83
4.3.2 Moisture loss/gain and its effect on the resistivity of the cement specimen.....	87
4.3.3 Piezoresistivity and strength of smart cement cured at high temperature.....	92
4.3.3.1 1 day of curing.....	92
4.3.3.2 7 days of curing.....	94
4.3.3.3 28 days of curing.....	98
4.3.4 Relationship between curing time and strength/piezoresistivity at failure.....	100
4.4 Curing and Piezoresistive Behavior of Modified Portland Cement Contaminated with Clay.....	104
4.4.1 Initial Resistivity.....	104
4.4.2 Resistivity with curing of cement.....	105

4.4.2.1 Long time curing of the specimen at room temperature.....	105
4.4.2.2 Moisture loss and its effect on the resistivity of the cement specimen.....	107
4.4.2.3 Long time curing of the specimen without moisture loss at room temperature.....	110
4.4.3 Piezoresistivity and strength of modified Portland cement.....	113
4.4.3.1 1 day of curing.....	113
4.4.3.2 7 days of curing.....	116
4.4.3.3 28 days of curing.....	118
4.4.3.4 Relationship between curing time and strength/piezoresistivity at failure.....	120
4.5 Summary.....	122
CHAPTER 5 CHARACTERIZING THE SMART CEMENT GROUTS.....	130
5.1 Curing.....	130
5.1.1 Room temperature.....	130
5.1.2 Moisture loss and resistivity.....	137
5.1.3 Minimum resistivity with respect to SMS concentration.....	141
5.2 Piezoresistivity and strength of smart cement grout and repaired specimens.....	141
5.2.1 Compressive behavior.....	142
5.2.2 Repairing of Smart Cement.....	148
5.2.2.1 1 day of Curing.....	148
5.2.2.2 7 days of Curing.....	151
5.2.2.3 28 days of Curing.....	156
5.2.3 Relationship between SMS concentration and strength/piezoresistivity.....	161
5.2.4 Relationship between RI24 and strength/piezoresistivity	166
5.2.5 Relationship between curing time and strength/piezoresistivity at failure.....	168
5.3 Summary.....	172

CHAPTER 6 CHARACTERIZATION OF DRILLING MUD.....	175
6.1 Rheological Properties of Bentonite mud.....	175
6.1.1 Apparent viscosity.....	179
6.1.2 Yield Point.....	179
6.1.3 Gel strength.....	180
6.2 Electrical Resistivity of Bentonite Drilling Mud.....	181
6.3 Fluid loss analysis.....	182
6.3.1 Modeling of the filtration process.....	183
6.3.2 Filter cake characterization.....	187
6.4 Summary.....	192
CHAPTER 7 REAL TIME MONITORING OF MODEL WELLBORE.....	195
7.1 Small lab model.....	195
7.1.1 Installation	195
7.1.1.1 Stage 1: Drilling Mud	195
7.1.1.2 Stage 2: Cement Slurry.....	197
7.1.2 Prediction of resistance in curing cement.....	200
7.1.2.1 Parameter K	200
7.1.2.2 Resistivity of the cement slurry with time.....	204
7.1.2.3 Predicted Resistance Vs Measured Resistance.....	205
7.2 Big lab model 1.....	215
7.2.1 Detecting the presence of cement slurry by resistance measurements in big lab model 1 during installation.....	215
7.2.2 Prediction and compare the measured resistance value during different curing time after cement slurry is placed in the wellbore around casing.....	219
7.2.2.1 Determination of Geometric parameter K for the different wire combination...	219
7.2.2.2 Resistivity of the cement slurry with time.....	221

7.2.2.3 Predicted Resistance Vs Measured Resistance.....	222
7.2.3 Temperature variation at different levels.....	234
7.3 Big lab model 2.....	236
7.3.1 Detecting the presence of cement slurry by resistance measurements in big lab model 2 during installation.....	236
7.3.2 Prediction and compare the measured resistance value during different curing time after cement slurry is placed in the wellbore around casing.....	240
7.3.2.1 Determination of Geometric parameter K for the different wire combination...240	
7.3.2.2 Predicted resistance Vs measured resistance.....	242
7.3.3 Temperature variation at different levels.....	252
7.4 Field model study.....	256
7.4.1 Prediction and compare the measured resistance value during different curing time after cement slurry is placed in the wellbore around casing.....	256
7.4.1.1 Determination of Geometric parameter K for the different wire combination...256	
7.4.1.2 Resistivity of the cement slurry with time.....	258
7.4.1.3 Predicted Resistance Vs Measured Resistance.....	259
7.5 Summary.....	280
CHAPTER 8 CONCLUSIONS AND RECOMMENDATIONS.....	282
8.1 Conclusions.....	282
8.2 Recommendation.....	286
REFERENCES.....	287

LIST OF FIGURES

Figure 1-1: Number blowouts for different types of oil failure during the period of 1992 to 2006 (Izon et al., 2007).....	3
Figure 3-1: Cement specimen for compressive strength and piezoresistivity test.....	23
Figure 3-2: Rotational viscometer used for rheological properties test.....	23
Figure 3-3: Direct resistivity measurement device.....	24
Figure 3-4: Typical components in the resistance measurements of the cement specimen.....	24
Figure 3-5: The K value for cement slurry with time.....	25
Figure 3-6: Schematic diagram of compression test with resistance measurements.....	26
Figure 3-7: The fluid loss test apparatus with continuous pressure arrangement.....	27
Figure 3-8: Plan and elevation of the small lab model with wire combination.....	29
Figure 3-9: A Schematic diagram of the small lab model.....	30
Figure 3-10: The actual model with partially filled cement slurry (left) and drilling mud (right).....	31
Figure 3-11: Plan and elevation of the big lab model with wire combination.....	32
Figure 3-12: Actual model after placing cement.....	33
Figure 3-13: Plan and elevation of the field model with wire combination	34
Figure 3-14: Actual casing with wire combination before placing in the wellbore.....	35
Figure 4-1: Variation of pH of water with SMS concentration (% by weight of water).....	41
Figure 4-2: Change of resistivity of SMS solution with SMS concentration	42
Figure 4-3: Shear stress – shear strain rate relationship for a smart cement slurry with and without SMS modeled with Herschel-Bulkley Model.....	45
Figure 4-4: Shear stress–shear strain rate relationship for a smart cement slurry with/without SMS modeled with Hyperbolic model.....	46
Figure 4-5: Fluid loss with time for smart cement slurry with and without SMS.....	47

Figure 4-6: Initial resistivity of the cement slurry with different concentration of SMS (C = smart cement).....	48
Figure 4-7: Variation of resistivity of curing cement slurry with time up to 24 hours....	50
Figure 4-8: Variation of resistivity for cement specimens cured at room temperature with and without SMS up to 12 months modeled with curing model.....	55
Figure 4-9: Weight loss of cement specimens cured at room temperature with and without SMS up to 12 months of curing.....	55
Figure 4-10: Change of resistivity with moisture loss of the cement specimens.....	57
Figure 4-11: Variation of resistivity of curing cement specimen with time up to 12 months for specimens having no moisture loss modeled with curing model.....	61
Figure 4-12: Variation of resistivity of curing cement specimen with time up to 12 months for specimens cured under water modeled with curing model.....	65
Figure 4-13: Weight gain of the cement specimens with time up to 12 months for specimens cured under water.....	67
Figure 4-14: Change of resistivity with moisture gain of the cement specimens.....	68
Figure 4-15: Relationship between the minimum resistivity and SMS concentration....	70
Figure 4-16: Piezoresistive response of the cement with and without SMS after 1 day of curing modeled with p-q model.....	72
Figure 4-17: Rate of change of resistivity with respect to stress vs Stress for 1 day of curing.....	73
Figure 4-18: Piezoresistive response of the cement with and without SMS after 7 days of curing modeled with p-q model.....	74
Figure 4-19: Rate of change of resistivity with respect to stress vs Stress for 7 days curing.....	75
Figure 4-20: Piezoresistive response of the cement with and without SMS after 28 days of curing.....	76
Figure 4-21: Rate of change of resistivity with respect to stress vs Stress for 28 days curing.....	77
Figure 4-22: Relationship between compressive strength and SMS concentration.....	78
Figure 4-23: Relationship between piezoresistivity at failure and SMS concentration....	80

Figure 4-24: Relationship between RI24hr and compressive strength.....	80
Figure 4-25: Relationship between compressive strength and curing time.....	82
Figure 4-26: Relationship between piezoresistivity at failure and curing time.....	83
Figure 4-27: Variation of resistivity of smart cement during curing at high temperature.....	84
Figure 4-28: Variation of resistivity of smart cement during curing at high temperature.....	88
Figure 4-29: Moisture loss of cement specimens cured at high temperature in oven with and without SMS up to 28 days.....	90
Figure 4-30: Moisture gain of cement specimens cured at high temperature in saturated sand with and without SMS up to 28 days.....	90
Figure 4-31: Relationship between resistivity and moisture loss of the smart cement cured in oven at 80°C.....	91
Figure 4-32: Relationship between resistivity and moisture gain of the smart cement cured in saturated sand at 80°C.....	92
Figure 4-33: Piezoresistive response of the smart cement with and without SMS after 1 day of high temperature curing.....	96
Figure 4-34: Rate of change of resistivity with respect to stress vs Stress for 1 day of curing.....	96
Figure 4-35: Piezoresistive response of the smart cement with and without SMS after 7 days of high temperature curing modeled with p-q model.....	97
Figure 4-36: Rate of change of resistivity with respect to stress vs Stress for 7 days curing.....	98
Figure 4-37: Piezoresistive response of the smart cement with and without SMS after 28 days of high temperature curing.....	99
Figure 4-38: Rate of change of resistivity with respect to stress vs Stress for 28 days curing.....	100
Figure 4-39: Relationship between compressive strength and the curing time for the smart cement modeled with hyperbolic model.....	102

Figure 4-40: Relationship between Piezoresistivity at failure and the curing time for the smart cement specimen modeled with hyperbolic model.....	103
Figure 4-41: Initial resistivity of the Portland cement slurry with different amount of clay contamination.....	104
Figure 4-42: Variation of resistivity for cement specimens cured at room temperature with and without clay contamination up to 28 days modeled with curing model.....	108
Figure 4-43: Moisture loss of cement specimens cured at room temperature with and without clay contamination up to 28 days.....	108
Figure 4-44: Change of resistivity with moisture loss of the cement specimens.....	109
Figure 4-45: Variation of resistivity of curing cement specimen with time up to 28 days for Portland cement with and without clay contamination having no moisture loss modeled with curing model.....	112
Figure 4-46: Piezoresistive response of the cement with and without clay contamination after 1 day of curing.....	115
Figure 4-47: Rate of change of resistivity with respect to stress vs Stress for 1 day of curing.....	115
Figure 4-48: Piezoresistive response of the cement with and without clay contamination after 7 days of curing.....	117
Figure 4-49: Rate of change of resistivity with respect to stress vs Stress for 7 days curing.....	117
Figure 4-50: Piezoresistive response of the cement with and without clay contamination after 28 days of curing.....	119
Figure 4-51: Rate of change of resistivity with respect to stress vs Stress for 28 days curing.....	119
Figure 4-52: Relationship between compressive strength and the curing time for the cement specimen modeled with hyperbolic model.....	121
Figure 4-53: Relationship between Piezoresistivity at failure and the curing time for the cement specimen modeled with hyperbolic model.....	122
Figure 5-1: Variation of resistivity for cement specimens made with smart cement grout with and without SMS up to 28 days of curing modeled with curing model.....	136

Figure 5-2: Variation of resistivity for repaired cement specimens repaired with smart cement grout with and without SMS cured up to 28 days modeled with curing model..	137
Figure 5-3: Weight loss of smart cement grout specimens cured at room temperature with and without SMS up to 28 days.....	138
Figure 5-4: Weight loss of the specimens repaired with grouts cured at room temperature up to 28 days.....	138
Figure 5-5: Relationship between resistivity and the moisture loss of the grout sample	140
Figure 5-6: Relationship between resistivity and the moisture loss of the specimens repaired with grouts.....	140
Figure 5-7: Variation of minimum resistivity with SMS concentration.....	142
Figure 5-8: Piezoresistive response of the smart cement grout after 1 day, 7 days and 28 days of curing modeled with p-q model.....	145
Figure 5-9: Rate of change of resistivity with respect to stress vs Stress for smart cement grout only after 1 day, 7 days and 28 days of curing.....	146
Figure 5-10: Piezoresistive response of the smart cement with 1% SMS after 1 day, 7 days and 28 days of curing modeled with p-q model.....	146
Figure 5-11: Rate of change of resistivity with respect to stress vs Stress for smart cement grout with 1% SMS after 1 day, 7 days and 28 days of curing.....	147
Figure 5-12: Piezoresistive response of the smart cement with 3% SMS after 1 day, 7 days and 28 days of curing modeled with p-q model.....	147
Figure 5-13: Rate of change of resistivity with respect to stress vs Stress for smart cement grout with 3% SMS after 1 day, 7 days and 28 days of curing.....	148
Figure 5-14: Piezoresistive response of the initial smart cement sample and the specimen repaired with grout after 1 day of curing modeled with p-q model.....	152
Figure 5-15: Rate of change of resistivity with respect to stress vs Stress for 1 day curing of the initial smart cement sample and the specimen repaired with grout.....	152
Figure 5-16: Piezoresistive response of the initial smart cement sample and the specimen repaired with grout with 1% SMS after 1 day of curing modeled with p-q model.....	153

Figure 5-17: Rate of change of resistivity with respect to stress vs Stress for 1 day curing of the initial smart cement sample and the specimen repaired with grout with 1% SMS.....153

Figure 5-18: Piezoresistive response of the initial smart cement sample and the specimen repaired with grout with 3% SMS after 1 day of curing modeled with p-q model.....154

Figure 5-19: Rate of change of resistivity with respect to stress vs Stress for 1 day curing of the initial smart cement sample and the specimen repaired with grout with 3% SMS.....154

Figure 5-20: Piezoresistive response of the initial smart cement sample and the specimen repaired with grout after 7 days of curing modeled with p-q model.....157

Figure 5-21: Rate of change of resistivity with respect to stress vs Stress for 7 days curing of the initial smart cement sample and the specimen repaired with grout.....157

Figure 5-22: Piezoresistive response of the initial smart cement sample and the specimen repaired with grout with 1% SMS after 7 days of curing modeled with p-q model.....158

Figure 5-23: Rate of change of resistivity with respect to stress vs Stress for 7 days curing of the initial smart cement sample and the specimen repaired with grout with 1% SMS.....158

Figure 5-24: Piezoresistive response of the initial smart cement sample and the specimen repaired with grout with 3% SMS after 7 days of curing modeled with p-q model.....159

Figure 5-25: Rate of change of resistivity with respect to stress vs Stress for 7 days curing of the initial smart cement sample and the specimen repaired with grout with 3% SMS.....159

Figure 5-26: Piezoresistive response of the initial smart cement sample and the specimen repaired with grout after 28 days of curing modeled with p-q model.....162

Figure 5-27: Rate of change of resistivity with respect to stress vs Stress for 28 days curing of the initial smart cement sample and the specimen repaired with grout.....162

Figure 5-28: Piezoresistive response of the initial smart cement sample and the specimen repaired with grout with 1% SMS after 28 days of curing modeled with p-q model.....163

Figure 5-29: Rate of change of resistivity with respect to stress vs Stress for 28 days curing of the initial smart cement sample and the specimen repaired with grout with 1% SMS.....163

Figure 5-30: Piezoresistive response of the initial smart cement sample and the specimen repaired with grout with 3% SMS after 28 days of curing modeled with p-q model....	164
Figure 5-31: Rate of change of resistivity with respect to stress vs Stress for 28 days curing of the initial smart cement sample and the specimen repaired with grout with 3% SMS.....	164
Figure 5-32: Relationship between compressive strength and SMS concentration.....	165
Figure 5-33: Relationship between piezoresistivity at failure strength and SMS concentration.....	166
Figure 5-34: Relationship between compressive strength and resistivity index after 24 hours (RI24) for the cement grout.....	167
Figure 5-35: Relationship between piezoresistivity at failure and resistivity index after 24 hours.....	168
Figure 5-36: Relationship between compressive strength and the curing time for the grout modeled with hyperbolic model.....	169
Figure 5-37: Relationship between compressive strength and the curing time for the repaired cement with grout modeled with hyperbolic model.....	170
Figure 5-38: Relationship between Piezoresistivity at failure and the curing time for the grout modeled with hyperbolic model.....	171
Figure 5-39: Relationship between Piezoresistivity at failure and the curing time for the cement specimens repaired with grout modeled with hyperbolic model.....	172
Figure 6-1: Shear stress vs shear strain rate for bentonite mud with and without SAS modeled with hyperbolic model.....	177
Figure 6-2: Shear stress vs shear strain rate for bentonite mud with and without SMS modeled with hyperbolic model.....	177
Figure 6-3: Shear stress vs shear strain rate for bentonite mud with and without SAS modeled with Herschel–Bulkley model.....	178
Figure 6-4: Shear stress vs shear strain rate for bentonite mud with and without SMS modeled with Herschel–Bulkley model.....	178
Figure 6-5: Effect of SMS and SAS on the resistivity of a 6% bentonite mud.....	182
Figure 6-6: Effect of SAS on the filtration loss of a bentonite mud modeled with API Model.....	184

Figure 6-7: Effect of SMS on the filtration loss of a bentonite mud modeled with API Model.....	184
Figure 6-8: Effect of SAS on the filtration loss of a bentonite mud modeled with new Kinetic Model.....	186
Figure 6-9: Effect of SMS on the filtration loss of a bentonite mud modeled with new Kinetic Model.....	187
Figure 6-10: Filter cake collected after fluid loss test with: (a) 6% bentonite (B) only, (b) 6%B+ 0.1% SAS, (c) 6%B+ 0.1% SMS, (d) 6%B+ 0.3% SAS and (e) 6%B+ 0.3% SMS.....	188
Figure 6-11: Effect of SAS and SMS on the filter cake thickness of 6% bentonite mud.....	189
Figure 6-12: Effect of SAS and SMS on the filter cake void ratio of 6% bentonite mud.....	190
Figure 6-13: Effect of SAS and SMS on the filter cake porosity of 6% bentonite mud.....	191
Figure 6-14: Effect of SAS and SMS on the filter cake density of 6% bentonite mud.....	191
Figure 7-1: The change of vertical resistance along wire setup A with drilling mud filling.....	196
Figure 7-2: The change of vertical resistance along wire setup B with drilling mud filling.....	196
Figure 7-3: The change of vertical resistance along wire setup C with drilling mud filling.....	197
Figure 7-4: The change of vertical resistance along wire setup A with cement slurry filling.....	198
Figure 7 5: The change of vertical resistance along wire setup B with cement slurry filling.....	199
Figure 7-6: The change of vertical resistance along wire setup C with cement slurry filling.....	200
Figure 7-7: K parameter for wire setup A.....	201
Figure 7-8: K parameter for wire setup B.....	202

Figure 7-9: K parameter for wire setup C.....	203
Figure 7-10: K parameter for horizontal wire combinations at different levels.....	204
Figure 7-11: Resistivity of cement slurry with curing time.....	205
Figure 7-12: Predicted and measured resistance for wire setup A for wire combination 1-2.....	206
Figure 7-13: Predicted and measured resistance for wire setup A for wire combination 1-3.....	207
Figure 7-14: Predicted and measured resistance for wire setup A for wire combination 1-4.....	207
Figure 7-15: Predicted and measured resistance for wire setup A for wire combination 1-5.....	208
Figure 7-16: Predicted and measured resistance for wire setup B for wire combination 1-2.....	209
Figure 7-17: Predicted and measured resistance for wire setup B for wire combination 1-3.....	209
Figure 7-18: Predicted and measured resistance for wire setup B for wire combination 1-4.....	210
Figure 7-19: Predicted and measured resistance for wire setup B for wire combination 1-5.....	210
Figure 7-20: Predicted and measured resistance for wire setup C for wire combination 1-2.....	211
Figure 7-21: Predicted and measured resistance for wire setup C for wire combination 1-3.....	211
Figure 7-22: Predicted and measured resistance for wire setup C for wire combination 1-4.....	212
Figure 7-23: Predicted and measured resistance for wire setup C for wire combination 1-5.....	213
Figure 7-24: Predicted and measured resistance for horizontal wire setup A-B at level 1.....	213

Figure 7-25: Predicted and measured resistance for horizontal wire setup A-B at level 3.....	214
Figure 7-26: Predicted and measured resistance for horizontal wire setup A-B at level 5.....	214
Figure 7-27: The change of vertical resistance along wire setup A with cement slurry filling for big lab model 1.....	216
Figure 7-28: The change of vertical resistance along wire setup C with cement slurry filling for big lab model 1.....	217
Figure 7-29: The change of horizontal resistance for wire set up A-C at different level with cement slurry filling for big lab model 1.....	218
Figure 7-30: K parameter for wire setup A for big lab model 1.....	219
Figure 7-31: K parameter for wire setup C for big lab model 1.....	220
Figure 7-32: K parameter for wire setup A-C for big lab model 1.....	221
Figure 7-33: Resistivity of cement slurry with curing time.....	222
Figure 7-34: Predicted and measured resistance for wire setup A for wire combination 1-3.....	223
Figure 7-35: Predicted and measured resistance for wire setup A for wire combination 1-5.....	223
Figure 7-36: Predicted and measured resistance for wire setup A for wire combination 1-7.....	224
Figure 7-37: Predicted and measured resistance for wire setup A for wire combination 1-9.....	225
Figure 7-38: Predicted and measured resistance for wire setup A for wire combination 1-11.....	226
Figure 7-39: Predicted and measured resistance for wire setup A for wire combination 1-13.....	226
Figure 7-40: Predicted and measured resistance for wire setup C for wire combination 1-3.....	227
Figure 7-41: Predicted and measured resistance for wire setup C for wire combination 1-5.....	228

Figure 7-42: Predicted and measured resistance for wire setup C for wire combination 1-7.....	228
Figure 7-43: Predicted and measured resistance for wire setup C for wire combination 1-9.....	229
Figure 7-44: Predicted and measured resistance for wire setup C 1-11.....	229
Figure 7-45: Predicted and measured resistance for wire setup C 1-13.....	230
Figure 7-46: Predicted and measured resistance for wire setup A-C at level 1.....	231
Figure 7-47: Predicted and measured resistance for wire setup A-C at level 3.....	231
Figure 7-48: Predicted and measured resistance for wire setup A-C at level 5.....	232
Figure 7-49: Predicted and measured resistance for wire setup A-C at level 7.....	232
Figure 7-50: Predicted and measured resistance for wire setup A-C at level 9.....	233
Figure 7-51: Predicted and measured resistance for wire setup A-C at level 11.....	233
Figure 7-52: Predicted and measured resistance for wire setup A-C at level 13.....	234
Figure 7-53: The variation of temperature throughout the curing period for thermocouples placed along wire setup A.....	235
Figure 7-54: The variation of temperature throughout the curing period for thermocouples placed along wire setup C.....	235
Figure 7-55: The change of vertical resistance along wire setup B with cement slurry filling for big lab model 2.....	237
Figure 7-56: The change of vertical resistance along wire setup D with cement slurry filling for big lab model 2.....	238
Figure 7-57: The change of horizontal resistance for wire set up B-D at different level with cement slurry filling for big lab model 2.....	239
Figure 7-58: K parameter for wire setup B for big lab model 2.....	240
Figure 7-59: K parameter for wire setup D for big lab model 2.....	241
Figure 7-60: K parameter for wire setup B-D for big lab model 2.....	242
Figure 7-61: Predicted and measured resistance for wire setup B for wire combination 1-3.....	243

Figure 7-62: Predicted and measured resistance for wire setup B for wire combination 1-5.....	244
Figure 7-63: Predicted and measured resistance for wire setup B for wire combination 1-7.....	245
Figure 7-64: Predicted and measured resistance for wire setup B for wire combination 1-9.....	245
Figure 7-65: Predicted and measured resistance for wire setup B 1-11.....	246
Figure 7-66: Predicted and measured resistance for wire setup B 1-13.....	246
Figure 7-67: Predicted and measured resistance for wire setup D for wire combination 1-3.....	247
Figure 7-68: Predicted and measured resistance for wire setup D for wire combination 1-5.....	248
Figure 7-69: Predicted and measured resistance for wire setup D for wire combination 1-7.....	248
Figure 7-70: Predicted and measured resistance for wire setup D for wire combination 1-9.....	249
Figure 7-71: Predicted and measured resistance for wire setup D 1-11.....	250
Figure 7-72: Predicted and measured resistance for wire setup D 1-13.....	250
Figure 7-73: Predicted and measured resistance for wire setup B-D at level 1.....	251
Figure 7-74: Predicted and measured resistance for wire setup B-D at level 3.....	251
Figure 7-75: Predicted and measured resistance for wire setup B-D at level 5.....	253
Figure 7-76: Predicted and measured resistance for wire setup B-D at level 7.....	253
Figure 7-77: Predicted and measured resistance for wire setup B-D at level 9.....	254
Figure 7-78: Predicted and measured resistance for wire setup B-D at level 11.....	254
Figure 7-79: Predicted and measured resistance for wire setup B-D at level 13.....	255
Figure 7-80: The variation of temperature throughout the curing period for thermocouples placed along wire setup B.....	255

Figure 7-81: The variation of temperature throughout the curing period for thermocouples placed along wire setup D.....	256
Figure 7-82: K parameter for different wire combination of the field model.....	257
Figure 7-83: Resistivity of cement slurry with curing time.....	258
Figure 7-84: Predicted and measured Resistance for wire setup E 1-2.....	260
Figure 7-85: Predicted and measured Resistance for wire setup E 2-3.....	260
Figure 7-86: Predicted and measured Resistance for wire setup E 3-4.....	261
Figure 7-87: Predicted and measured Resistance for wire setup E 4-5.....	262
Figure 7-88: Predicted and measured resistance for wire setup E 5-6.....	262
Figure 7-89: Predicted and measured resistance for wire setup E 6-7.....	263
Figure 7-90: Predicted and measured resistance for wire setup E 7-8.....	264
Figure 7-91: Predicted and measured resistance for wire setup E 8-9.....	264
Figure 7-92: Predicted and measured resistance for wire setup E 9-10.....	265
Figure 7-93: Predicted and measured resistance for wire setup E 10-11.....	265
Figure 7-94: Predicted and measured resistance for wire setup E 11-12.....	266
Figure 7-95: Predicted and measured Resistance for wire setup F 1-2.....	267
Figure 7-96: Predicted and measured resistance for wire setup F 2-3.....	267
Figure 7-97: Predicted and measured Resistance for wire setup F 3-4.....	268
Figure 7-98: Predicted and measured Resistance for wire setup F 4-5.....	269
Figure 7-99: Predicted and measured resistance for wire setup F 5-6.....	269
Figure 7-100: Predicted and measured resistance for wire setup F 6-7.....	270
Figure 7-101: Predicted and measured resistance for wire setup F 7-8.....	271
Figure 7-102: Predicted and measured resistance for wire setup F 8-9.....	271
Figure 7-103: Predicted and measured resistance for wire setup F 9-10.....	272
Figure 7-104: Predicted and measured resistance for wire setup F 10-11.....	272

Figure 7-105: Predicted and measured resistance for wire setup F 11-12.....	273
Figure 7-106: Predicted and measured Resistance for horizontal wire setup E-F at level 1.....	274
Figure 7-107: Predicted and measured Resistance for horizontal wire setup E-F at level 2.....	274
Figure 7-108: Predicted and measured Resistance for horizontal wire setup E-F at level 3.....	275
Figure 7-109: Predicted and measured Resistance for horizontal wire setup E-F at level 4.....	276
Figure 7-110: Predicted and measured resistance for horizontal wire setup E-F at level 5.....	276
Figure 7-111: Predicted and measured resistance for horizontal wire setup E-F at level 6.....	277
Figure 7-112: Predicted and measured resistance for horizontal wire setup E-F at level 7.....	278
Figure 7-113: Predicted and measured resistance for horizontal wire setup E-F at level 8.....	278
Figure 7-114: Predicted and measured resistance for horizontal wire setup E-F at level 9.....	279
Figure 7-115: Predicted and measured resistance for horizontal wire setup E-F at level 10.....	279
Figure 7-116: Predicted and measured resistance for horizontal wire setup E-F at level 11.....	281
Figure 7-117: Predicted and measured resistance for horizontal wire setup E-F at level 12.....	281

LIST OF TABLES

Table 4-1: Results of the rheological test for smart cement slurry with and without SMS.....	44
Table 4-2: Resistivity change with curing time for smart Oil Well Cement with different percentage of SMS.....	51
Table 4-3: Summary of bulk resistivity parameters for smart cement cured under room temperature with and without SMS content.....	53
Table 4-4: Model parameters for the curing model of the resistivity of smart cement modified with SMS cured under room temperature up to 12 months.....	54
Table 4-5: Summary of model parameters for the relationship between the moisture loss and the change in the resistivity.....	56
Table 4-6: Summary of model parameters for the relationship between the resistivity and the moisture loss.....	58
Table 4-7: Summary of bulk resistivity parameters for smart cement cured under no moisture loss condition at room temperature with and without SMS content.....	60
Table 4-8: Model parameters for the curing model of the resistivity of smart cement modified with SMS cured under no moisture loss condition at room temperature up to 12 months.....	63
Table 4-9: Summary of bulk resistivity parameters for smart cement cured under water at room temperature with and without SMS content.....	64
Table 4-10: Model parameters for the curing model of the resistivity of smart cement modified with SMS cured under water at room temperature up to 12 months.....	66
Table 4-11: Summary of model parameters for the relationship between the moisture gain and the change in the resistivity.....	67
Table 4-12: Summary of model parameters for the relationship between the resistivity and the moisture loss.....	69
Table 4-13: Peak stress, piezoresistivity, model parameters p_2 , q_2 and R_2 & RMSE for the piezoresistivity model for the cement specimens under compressive stress after 1 day, 7 days and 28 days.....	72
Table 4-14: Model Parameters for the relationship between strength and curing time.....	81

Table 4-15: Model Parameters for the relationship between strength and curing time...	83
Table 4-16: Summary of bulk resistivity parameters for smart cement with and without SMS cured at high temperature up to 28 days.....	86
Table 4-17: Model parameters for the curing model of the resistivity of modified smart cement with and without SMS cured at high temperature up to 28 days.....	89
Table 4-18: Peak stress, piezoresistivity, model parameters p_2 , q_2 and R_2 & RMSE for the piezoresistivity model for the smart cement specimens under compressive stress after 1 day, 7 days and 28 days.....	95
Table 4-19: Summary of bulk resistivity parameters for modified Portland cement with and without clay contamination cured under room temperature up to 28 days.....	106
Table 4-20: Model parameters for the curing model of the resistivity of modified Portland cement with and without clay contamination cured under room temperature up to 28 days.....	107
Table 4-21: Summary of bulk resistivity parameters for modified Portland cement with and without clay contamination cured under no moisture loss condition at room temperature up to 28 days.....	111
Table 4-22: Model parameters for the curing model of the resistivity of modified Portland cement with and without clay contamination cured under no moisture loss condition at room temperature up to 28 days.....	112
Table 4-23: Peak stress, piezoresistivity, model parameters p_2 , q_2 and R_2 & RMSE for the piezoresistivity model for the cement specimens under compressive stress after 1 day, 7 days and 28 days.....	114
Table 5-1: Summary of bulk resistivity parameters for smart cement grout with and without SMS cured at room temperature up to 28 days.....	132
Table 5-2: Summary of bulk resistivity parameters for damaged cement repaired with smart cement grout with and without SMS cured at room temperature up to 28 days...	132
Table 5-3: Model parameters for the curing model of the resistivity of smart cement grout with and without SMS cured at room temperature up to 28 days.....	134
Table 5-4: Model parameters for the curing model of the resistivity of damaged cement repaired with smart cement grout with and without SMS cured at room temperature up to 28 days.....	136

Table 5-5: Peak stress, piezoresistivity, model parameters p_2 , q_2 and R_2 & RMSE for the piezoresistivity model for the smart cement grout specimens after 1 day, 7 days and 28 days.....	143
Table 5-6: Model parameters p_2 , q_2 , R_2 & RMSE for the piezoresistivity model for the smart cement specimens repaired with grout after 1 day, 7 days and 28 days.....	150
Table 6-1: Results of the Rheological test for bentonite mud with and without SAS and SMS modeled with Hyperbolic model.....	176
Table 6-2: Results of the Rheological test for bentonite mud with and without SAS and SMS modeled with Herschel–Bulkley model.....	176
Table 6-3: Summary of fluid loss with SAS and SMS for a bentonite mud.....	183
Table 6-4: Model parameters for the fluid loss tests modeled with new Kinetic Model.....	186
Table 6-5: Filter cake properties of 6% bentonite mud with and without silicates (SAS/SMS).....	188
Table 7-1: Variations of K parameter for wire setup A for model 2.....	201
Table 7-2: Variations of K parameter for wire setup B for model 2.....	202
Table 7-3: Variations of K parameter for wire setup C for model 2.....	203
Table 7-4: Variations of K parameter for horizontal wire combination at different level for model 2.....	204
Table 7-5: Variations of K parameter for wire setup A for big lab model 1.....	220
Table 7-6: Variations of K parameter for wire setup C for big lab model 1.....	220
Table 7-7: Variations of K parameter for wire setup A-C for big lab model 1.....	221
Table 7-8: Variations of K parameter for wire setup B for big lab model 2.....	241
Table 7-9: Variations of K parameter for wire setup D for big lab model 2.....	241
Table 7-10: Variations of K parameter for wire setup B-D for big lab model 1.....	242
Table 7-11: Variations of K parameter for different wire combination of the field model.....	257

CHAPTER 1 INTRODUCTION

1.1 General

After drilling a wellbore and placing the metal casing, cement slurry is placed in between the borehole wall and the metal casing to provide a support to the casing and to provide a seal between the casing and the formation/borehole wall to prevent the migration of formation fluid (Nelson and Guillot, 2006). From its initial use in the late 1920s, the main purpose of using oil well cement in wellbore is to provide a complete isolation of the casing from the formation in order to protect production zones from salt water flow and to prevent hydrocarbon or liquid exchange among different formation layers, to protect the collapse of the casing under pressure, to protect the casing from corrosion, to protect the groundwater reservoir from hydrocarbon and salt contamination (Joshi and Lohtia, 1997). Oil well cement (OWC) slurry is pumped through the metal casing and pressured back to fill the annulus gap from bottom up (Powers et al., 1977; Detroit et al., 1983; Calvert, 2006). The slurry should be designed based on the wellbore geometry, mud weight and type, cement column height, formation type, depth of wellbore, temperature and pressure (Calvert and Smith, 1990).

In any successful cementing job, the cement slurry properties such as thickening time, rheology, fluid loss, free water and strength development with curing time is drastically affected by downhole temperature and pressure (Calvert and Smith, 1990). American Petroleum Institute (API) has developed a relationship based on the wellbore depth and the bottomhole temperature up to 20,000 ft (Venditto and George, 1984). Based on different well conditions, API has classified different types of cements that are currently used by oil and gas industries (Calvert and Smith, 1990) according to API Specification

API RP 10A and the physical requirements of those cements are determined according to API Specification API RP 10B (API, 1988). Although API has defined nine types of cements for oil well but, in USA, only classes A, B, C, G, and H are available of which classes G and H are widely used (smith, 1987). Throughout the world, about 80% of oil well cements are either class G or H, and, in USA, 65% of oil well cements are class H and 15% are class G (smith, 1987).

With the recent days expanding explorations of oil and gas throughout the world both in onshore and offshore, construction of new well and maintaining their lifetime monitoring has become difficult task (Vipulanandan et al., 2014). Two studies done on blowouts on the U.S. outer continental shelf (OCS) during the period of 1971 to 1991 and 1992 to 2006 clearly identified cementing failures as the major cause for blowouts (Izon et al., 2007). Cementing failures increased significantly during the second period of study when 18 of the 39 blowouts, over 40% of the failures, were due to cementing problems (Izon et al., 2007). Also, due to highly unpredictable downhole conditions of the wellbore (temperature, pressure, formation types etc.), controlling the loss of fluids to the formations and finishing the cementing job properly became a critical issue in well construction (Eoff et al., 2009; Fuller et al., 2002; Gill et al., 2005; Labibzadeh et al., 2010; and Ravi et al., 2007).

The oil well cements and their different additives which are used to control several necessary properties should also be environmentally friendly (Dom et al., 2007; Durand et al., 1995; Thaemlitz et al., 1999). In an offshore cementing, use of tracer is considered the best approach to calculate the cement returns to the seafloor and the amount of cement retained in the annulus, and having the calculation in hands the lack of cement

returns may compromise the casing support, and excess cement returns can cause problems with flow and control lines (Gill et al., 2005). Hence there is a need for monitoring the cementing operation in real time. There was no technology available to monitor the cementing operation real time from the time of placement through the entire service life of the borehole. A smart cement has been developed (Vipulanandan et al., 2014; Vipulanandan and Muhammed, 2015) which can sense any changes going on inside the borehole during cementing and during curing after cementing job. It can sense the water cement ratio, different additives, and any pressure applied to the cement sheath in terms of piezoresistivity. That cement can be modified with different additives which will show the sensing ability and, at the same time, improve other slurry properties such as rheology, fluid loss, free water, shrinkage, thickening time etc.

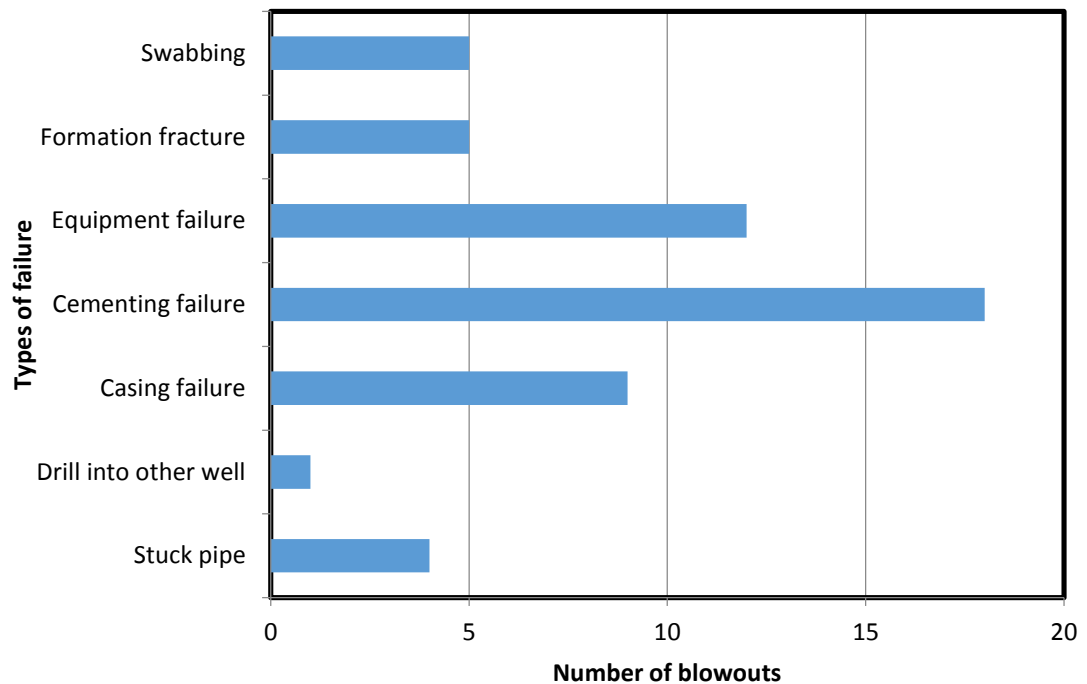


Figure 1-1: Number blowouts for different types of oil failure during the period of 1992 to 2006 (Izon et al., 2007)

1.2 Objective

The overall objective of the research study was to characterize and model silicate modified smart oil well cement, smart cement grouts and drilling mud. The specific objectives are as follows:

- (a) Investigate the effects of sodium meta-silicate on the rheological, curing and piezoresistive properties of smart oil well cement under various curing condition.
- (b) Investigate the effects of sodium meta-silicate on the curing and piezoresistive properties of grouts made of smart cement and the effectiveness of the grout to repair damaged cement.
- (c) Investigate the effects of sodium meta-silicate and sodium alumino-silicate on the rheological and fluid loss properties of water based bentonite mud
- (d) Physical model testing to verify the real time monitoring of the smart oil well cement by electrical resistivity measurements.
- (e) Develop constitutive models for silicate modified smart cement, grout and drilling mud.

1.3 Organization

Chapter 2 summarizes the background information on oil well cements and use of silicate additives with oil well cements, grouts and drilling mud. Chapter 3 involved the material identification and experimental program and mathematical models to be used to characterize the material modifications. Chapter 4 presented the experimental results on the oil well cements modified with silicate additives under different curing environments and contamination. Chapter 5 includes the characterization of smart cements grouts with silicate additives and repair of damaged cements with the grouts. Chapter 6 discussed the

characterization of water based drilling mud with addition of silicate additives. In Chapter 7 the model test results are presented for small scale lab model, medium scale lab model and full scale field model to verify the effectiveness of the resistance monitoring of the cementing job. Chapter 8 summarizes the findings and conclusions of this study.

CHAPTER 2 BACKGROUND AND LITERATURE REVIEW

2.1 Oil well cements

After drilling a wellbore and placing the metal casing, cement slurry is placed in between the borehole wall and the metal casing to provide a support to the casing and to provide a seal between the casing and the formation/borehole wall to prevent the migration of formation fluid (Nelson and Guillot, 2006). From its initial use in the late 1920s, the main purpose of using oil well cement in wellbore is to provide a complete isolation of the casing from the formation in order to protect production zones from salt water flow and to prevent hydrocarbon or liquid exchange among different formation layers, to protect the collapse of the casing under pressure, to protect the casing from corrosion, to protect the groundwater reservoir from hydrocarbon and salt contamination (Joshi and Lohtia, 1997). Oil well cement (OWC) slurry is pumped through the metal casing and pressured back to fill the annulus gap from bottom up (Powers et al., 1977; Detroit et al., 1983; Calvert, 2006). The slurry should be designed based on the wellbore geometry, mud weight and type, cement column height, formation type, depth of wellbore, temperature and pressure (Calvert and Smith, 1990).

In any successful cementing job, the cement slurry properties such as thickening time, rheology, fluid loss, free water and strength development with curing time is drastically affected by downhole temperature and pressure (Calvert and Smith, 1990). American Petroleum Institute (API) has developed a relationship based on the wellbore depth and the bottom hole temperature up to 20,000 ft (Venditto and George, 1984). Based on different well conditions, API has classified different types of cements that are currently used by oil and gas industries (Calvert and Smith, 1990) according to API Specification

API RP 10A and the physical requirements of those cements are determined according to API Specification API RP 10B (API, 1988). Although API has defined nine types of cements for oil well but, in USA, only classes A, B, C, G, and H are available of which classes G and H are widely used (smith, 1987). Throughout the world, about 80% of oil well cements are either class G or H, and, in USA, 65% of oil well cements are class H and 15% are class G (smith, 1987).

2.2 Smart cement for oil well

Vipulanandan et al., 2014 developed smart cement with class H cement and 0.075% of conductive filler which has a sensing ability in terms of electrical resistivity. If the water cement ratio of the slurry is changed and/or any kind of additives are added to the slurry, the resistivity can sense that change both in the cement slurry and hardened cement. As for example, if the water cement ratio is changed from 0.38 to 0.44, the initial resistivity is increased about 30%. Also, the resistivity after 24 hours of curing is varied from 50% to 300%. The most important characteristics is the piezoresistivity of the hardened cement (i.e., the change in resistivity due to applied stress) where the change in resistivity due to applied stress showed 1500 to 2500 times higher change than the strain of the cement. The highest change in the electrical resistivity at peak stress was found about 500% of the initial resistivity without stress. The rheological properties was not affected by the addition of 0.075% conductive filler with class H cement. This smart cement can be used to monitor the structural health of the borehole from cementing time to its entire service life by developing a wired electrical monitoring system.

This smart cement can be modified with different additive to control its different properties such as thickening time, fluid loss, rheology, shrinkage, free water etc. As the

electrical resistivity of the smart cement is sensitive to any kind of additive, the modification can be tested with its sensing property like piezoresistivity. If the modified cement shows piezoresistive behavior, then that modified cement can be used to monitor the borehole like the smart cement.

2.3 Cementing high temperature wells

American Petroleum Institute (API) has developed a relationship based on the wellbore depth and the bottomhole temperature up to 20,000 ft (Venditto and George, 1984) which showed that as the well depth is increased, the bottomhole temperature also increased. And with the increased temperature, the rate of hydration of the cement also increases; that's why sufficient retarder must be added to the cement slurry to allow adequate placement time at the maximum circulating temperature (Eoff and Buster, 1995).

Several failures in the geothermal wells has been directly attributed to degradation of cement (Radenti and Ghiringhelli, 1972). Two studies done on blowouts on the U.S. outer continental shelf (OCS) during the period of 1971 to 1991 and 1992 to 2006 clearly identified cementing failures as the major cause for blowouts (Izon et al., 2007). Cementing failures increased significantly during the second period of study when 18 of the 39 blowouts, over 40% of the failures, were due to cementing problems (Izon et al., 2007). Increasing number of projects in high-temperature environments leads the drilling service companies to adjust operations of the well construction process to the available hostile conditions, and there are fewer materials which can be applied to the conditions of the environments (Moradi and Nikolaeb, 2014).

2.4 Cement grouts and sodium meta-silicate

Cement-based grouts have been widely used in many construction areas such as grouting of soils and rocks, repairing of cracks in concrete structures and masonaries (Anagnostopoulos, 2014), coat pre-stressed cables, stabilizing ground near tunnels (Stille and Gustafson, 2010), rehabilitating historical buildings (Yeon and Han, 1997; Baltazar et al., 2012), and repair cracked oil well cement sheath (Chun et al., 2008). The cement-based grouts have been widely used since the 1800s and even earlier (Bowen, 1981). Grouting is a process of injecting the cementitious fluid that enters into fissures, cracks or voids (Nonveiller, 1989) of the damaged structure or rock and provide a sealing to the damaged part. The grouts used for repairs must be designed in a way that it can penetrate a certain distance into the fissures, cracks or voids of the damaged zone to improve integrity of the repaired material (Dragonvic and Stille, 2014; Satoh et al., 2012). The water-to-cement ratio (w/c) is the most important factor which affects both the strength development and the flow ability into the crack (Anagnostopoulos, 2014). In the oil production wells, mostly API class G or H cement is used to prepare grouts with different additives based on the property requirements (Taehee et al., 2013).

Among the different grouts used as sealer, sodium silicate-based concrete sealers have become popular to both academia and industry (Jianga et al., 2015) because sodium silicate react with portlandite (Ca(OH)_2), a weak part of the cement matrix, and forms inorganic calcium-silicate hydrates (C-S-H gels) (Franzoni et al., 2013) and hence increase the durability of the grout. Chun et al. 2008 in their study showed that sodium meta-silicate (SMS) based cement grout significantly reduces the permeability of the grouted region. In that study, sodium silicate cement grout with ordinary portland cement (OPC) showed compressive strength increase with increase in SMS concentration.

Sodium meta-silicate (SMS) is a white, water-soluble powder, which is produced through the fusing of silica (sand) with sodium carbonate at 1400°C (Nelson, 1990). From the initial use in the late 1800's sodium silicate based compounds have been used in a number of applications including cementing, grouting, emulsifying, and in cleaning agents. Heinold et al., 2002 reported that addition of 1% SMS with class G cement slurry cured at 100° F showed a reduction in compressive strength from 16.1 MPa to 13.8 MPa (72 hours) whereas with the same amount of SMS and cured at 200°F showed an increase in compressive strength from 16.1 MPa to 18.6 MPa.

2.5 Water based drilling mud

American Petroleum Institute (API) defines drilling fluid as a circulating fluid which is used in rotary drilling for any drilling operation. The main functions of drilling fluids are lubricating and cooling the drill bit, containing the cuttings of the wellbore to dispose, and providing a hydrostatic pressure to prevent formation damage by balancing the fluid pressure of the formation and the drilling fluid pressure (Brazzel, 2009; Melbouci and Sau, 2008). Drilling muds are a class of drilling fluids which are mostly used in drilling deep wells where the term mud is used due to its thick consistency of the formulations coming from bentonite (Fink, 2012). To perform the main functions of drilling a wellbore, the drilling mud must have some desirable characteristics such as rheological properties (i.e., plastic viscosity, yield point, and gel strength), less fluid loss, stability under different temperature and pressure of the well bore, and stability under possible contamination like salt, cement, calcium sulfate, and should be able to minimize fluid invasion from the drilling mud to the porous space of a reservoir (Melbouci and Sau, 2008).

Based on the continuous phase of the mud, drilling muds are generally classified as Water Based Muds (WBMs) and Oil Based Muds (OBMs). WBMs may contain oil but not as continuous phase; on the other hand, OBMs may contain water where oil is the continuous phase (Guichard et al., 2008). WBMs will contain water as its continuous phase and the amount should be at least 50% of volume percent of the entire composition, bentonite/barite, and may contain viscosifier, fluid loss control agent, lubricants, emulsifiers, corrosion inhibitors, salts and pH control agents to achieve its required properties (Fink, 2012).

2.6 Sodium Silicates

2.6.1 Sodium silicates in oil well cements

Sodium meta-silicate (SMS) is a white, water-soluble powder, which is produced through the fusing of silica (sand) with sodium carbonate at 1400°C (Nelson, 1990). From the initial use in the late 1800's sodium silicate based compounds have been used in a number of applications including cementing, grouting, emulsifying, and in cleaning agents. Of the various forms of sodium silicate based compounds, sodium meta-silicates (anhydrous) have been used in oil and gas industry related applications. Because of its emulsification and interfacial tension reduction characteristics, SMS has been used in alkaline flooding, a chemical recovery method to recover oil from various types of geological formations and sand. Larrondo et al. 1985 has used 1% sodium meta-silicate (SMS) solution as an alkaline flooding agent in chemical oil recovery method in sandstone oil reservoir and found effective in maximum oil recovery. SMS worked very well in oil recovery by steam stimulation additive as 20.8% solution where the interaction of SMS and the reservoir oil at elevated temperature produces interfacially active

material which reduces water-oil interfacial tension (Mbaba and Caballero, 1983). This causes improved recovery due to emulsification and oil displacement under lowered interfacial tension.

Sodium meta-silicate is also used as cement grout and in squeeze cementing. SMS delays the hydration reaction of cement at early stage mixture for sodium silicate cement grout (Chun et al., 2008). In that study, sodium silicate cement grout with ordinary portland cement (OPC) showed compressive strength increase with increase in SMS concentration. With OPC=17.6% and SMS=21%, 28 days compressive strength was found 570 psi whereas the strength was 360 psi with SMS=13%. Silicates have the stability to polymerize and form gel and sodium silicate provides deformability that's necessary for adhesive properties (Garba et al., 2014). In their study, squeeze practice in Zechstein halite formation showed good result with sodium meta-silicate solution (45% with water).

Nelson, 1990 mentioned that when SMS is added to portland cement, calcium silicate gel will be formed from the reaction of silicates with lime. This gel structure has enough viscosity and it allows more amount of water to the mix without excess free water and enhanced compressive strength development. It can be used at temperature up to 200°F and concentrations from 0.1 to 4% and also to make low-density slurry. Heinold et al., 2002 reported that addition of 1% SMS with class G cement slurry cured at 100°F showed a reduction in compressive strength from 2340 psi to 2000 psi (72 hours) whereas with the same amount of SMS and cured at 200°F showed an increase in compressive strength from 2340 psi to 2700 psi.

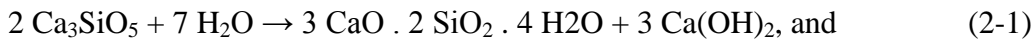
In many parts of the world, severe lost circulation and weak formations with low fracture characteristics are common. These situations require the use of low-density cement systems that reduce the hydrostatic pressure of the fluid column during the cement placement process. Hence lightweight additives (also known as extenders) are used to reduce the weight of the slurry. Malyshev et al., (2013) used SMS as the extender for a lightweight cement system of density 1500 kg/m³ (12.6 ppg) because addition of sodium silicate to cement slurry (class G) allows the use of larger quantities of mix water without excessive slurry separation. High alumina lightweight cements modified with sodium meta-silicate (density < 1.25 gm/cc) was used in a geothermal well up to temperature 300°C which retarded the thickening time of the slurry significantly thus maintained sufficient time to maintain pumpability (Sugama and Carciello, 1996). The compressive strength was decreased with increased SMS concentration. Sodium calcium silicate hydrate (Na₂Ca₂Si₂O₇.H₂O) was produced by the hydrothermal reaction occurred between CA or CA₂ in cement and SMS. At high temperature, the produced silicate hydrate becomes well-crystalized which increases the density and lowers the porosity.

Sodium silicate particles have weak agglomeration properties (Saasen et al., 1991) and sodium silicates increases the yield stress of cement slurry with class G oil well cement (0.2% - 0.54% SMS are used). Another study showed that the sodium meta-silicate was effective in controlling free water. Fasesan et al., 2005 investigated the use of 0.5% of sodium meta-silicate (by weight of cement) in 50:50 class H cement slurry to control the free water which replace the use of 2% bentonite. Hence SMS has multifunctional ability to modify the oil well cement. Ding et al., 1996 in their study used 0.25% to 1.5% of sodium silicate with high alumina cement (HAC) and concluded that

sodium silicate strongly retards the hydration of high alumina cement (HAC). Sodium silicate addition promotes formation of stratlingite in HAC paste. A small addition of sodium silicate to HAC can delay hydrogarnet formation, It is not sufficient to prevent the conversion reactions.

2.6.1.1 Hydration of oil well cement

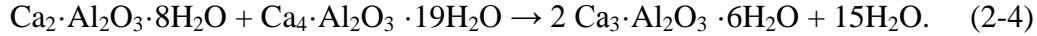
The main component of oil well cement are tri-calcium silicate- Ca_3SiO_5 (C_3S), di-calcium silicate- Ca_2SiO_4 (C_2S), tri-calcium aluminate- $\text{Ca}_3\text{Al}_2\text{O}_4$ (C_3A), tetra-calcium alumino-ferrite- $\text{Ca}_4\text{Al}_n\text{Fe}_{2-n}\text{O}_7$ (C_4AF), magnesium oxide (MgO), CaSO_4 etc. (Smith, 1987). When cement is mixed with water, chemical reactions start between water and different components of cements. Both tri-calcium silicate (Ca_3SiO_5) and di-calcium silicate (Ca_2SiO_4) creates calcium silicate hydrate reacting with water (Natarajan, 2005) as shown:



The product calcium silicate hydrate (C-S-H) gel is largely amorphous which comprises about 70% of the set cement and gives cement the mechanical properties (Malyshev et al. 2013). During initial setting, aluminate phases (C_3A) are the most reactive which plays an important role upon the rheology of the cement slurry and early strength development of the set cement though their presence are small compared to the silicates (C_3S and C_2S). Tri-calcium aluminate (C_3A) creates calcium aluminate hydrates reacting with water (Natarajan, 2005) as



The calcium aluminate hydrates (C_2AH_8 and C_4AH_{19}) are in a kind of metastable form which converts to more stable form $\text{Ca}_3 \cdot \text{Al}_2\text{O}_3 \cdot 6\text{H}_2\text{O}$ (Natarajan, 2005) as



If diluted solution of sodium silicate (Na_2SiO_3) is mixed with the cement slurry, sodium silicate reacts with the product of reaction (1) and (2) i.e. $\text{Ca}_2(\text{OH})$ and also with CaSO_4 presents in the cement which produces electrolyte and silicate cement gel (Chun et al., 2008):



2.6.2 Cementing high temperature wells

Nelson and Cassabonne, 1992 in their study showed that at high temperature up to 400°F, traditional retarders such as Lignosulfonate, Gluconate or Borax used with a class H cement and 35% silica flour provides thickening time up to 4 hour which is significantly improved up to 7 hours using a new improved retarder (composition undisclosed). The slurry must be easily mixable at ambient temperature, yet stable when heated to the maximum circulating temperature. The system must not exhibit free-water or settling tendencies, especially when cementing deviated wellbores. Excellent fluid-loss control (100 mL/30 min) is usually essential. In another study, Eilers et al., 1983 showed that the crystalline nature of hydrated Portland cement is dependent primarily on temperature. The calcium silicate hydrate (CSH) gel is produced at low temperatures and, upon curing at higher temperatures, will convert to one or more crystalline phases. The better cementing compositions contain a low lime-to-silica (CIS) ratio. Xonotlite is a phase commonly produced above 150°C (302°F) when approximately 35% fine silica is added to Portland cement. Generally, it has good strength but moderate permeability.

Truscottite, produced when an even larger quantity of silica is added to the cement, has lower permeability than xonotlite but is slightly more difficult to produce and to stabilize. Pectolite can be produced by introducing sodium into a truscottite-type formulation. Once formed, pectolite is very stable but typically has high permeability. The addition of carbonate to any of these formulations may produce scawtite. Scawtite appears to be an inferior phase by itself, but in small quantities it can be helpful in strength development.

Eoff and Buster, 1995 in their study found a copolymer named Acrylamide-Methyl propane-Sulfonic Acid (AMPS) and itaconic acid provides excellent retardation at temperatures up to 500 F for a class H, 35% silica sand cement systems without the use of an intensifier. The retarder is also unique in that compressive strength development is rapid. In another study, Johnston and Senese, 1992 found the new water dispersible weighting agent, a stable oxide of manganese which is a product of ferro-manganese manufacture, has eliminated many of the problems associated with conventional dry-blended materials (Barite, Haematite) for class G silica flour blend and for a bottom hole temperature of 132°C. Cement slurries using the new material are easily designed and exhibit excellent properties (good rheology, no sedimentation, etc.) Last minute design changes due to well conditions have been made without problem. The new weighting agent is quickly dispersed in the cement mix water; there has been no settling-out of the material.

2.6.3 Cement grouts

Anagnostopoulos (2014) presented a laboratory study of the effects of a new-generation polycarboxylate superplasticiser (PCE) on the rheological properties, mechanical strength, final setting time and bleeding of cement grouts in comparison to

that of a polynaphthalene superplasticiser (SNF). The experiments were conducted using different superplasticiser dosages with cement grouts proportioned with a water to cement ratio (w/c) of 0.33, 0.4 or 0.5. The results showed that grouts with PCE had higher viscosity, slightly increased bleeding and longer setting times compared with the SNF admixture. However, the PCE improved the final strength, especially for grouts with a w/c ratio of 0.4 and 0.5, and decreased the yield stress. Satoh et al. 2012 in a study mentioned that there were some cases in which dam foundation permeability could not be improved even by using ultrafine cement in Japan. Various measures including the design and execution of appropriate grouting were taken in such cases, but could not always solve the problem. Since cement is the basic material for dam foundation grouting it is necessary to study or develop materials of cement based grout that can be injected into small cracks or decomposed granite where improvement of permeability is generally difficult.

Jiang et al., (2015) introduced the composition and preparation process for an inorganic sodium silicate-based concrete sealer. The factors affecting water impermeability of the concrete sealer are systematically explored. In addition to the concentration of sodium silicates and the viscosity of the concrete sealer, the surface tension and gelation time of the concrete sealer also affect the waterproofing efficacy of the concrete sealer. Some super-active fluorocarbon surfactants are very effective in reducing the surface tension of the concrete sealer to an ideally low value. The gelation time of the sodium silicate-based concrete sealer surprisingly increases as the concentration of the active ingredient increases but decreases as the concentration of the catalyst increases. Additionally, the gelation time decreases as the testing temperature

increases. The good waterproofing properties of the developed sodium silicate-based concrete sealer result from its low surface tension and appropriate density, viscosity and gelation time.

2.6.4 Silicates in drilling mud

Silicate based drilling fluids such as sodium silicate was introduced in water-based drilling fluids in 1930s (Baker and Garrison, 1939; Vietti and Garrison, 1939) to use in drilling operations in shale formation (Guo et al., 2006). Because shale formations has very high clay content which tend to absorb water from drilling mud/fluid and swells resulting in wellbore collapse (Cai et al., 2012). Due to this problem with water based drilling fluid/mud, generally oil based drilling fluid was best choice to drill shale formation because oil based drilling fluid/mud provides excellent shale inhibition (Deville et al., 2011). But disposal of oil based drilling fluids provides poor environmental performance and the cost of drilling fluid is also higher compared to water based drilling mud (McDonald, 2012). That's why water based drilling fluids with silicate were found successful at drilling very reactive shale formations (Guo et al., 2006). But controlling their rheology was not easy and after several field trials undertaken in 1960s by Darley, establishing silicate based drilling fluids as an accepted system was not successful (Darley, 1970). Later, sodium silicate along with potassium ions and some polymers, a better shale stabilizing package was introduced in the 1980s (Wingrave et al., 1987). After that, having lot of research work with silicate based drilling fluids and rheology controlling additives, the industry used sodium silicate with the polymer additives that provided a shale inhibitive water-based mud system (Guo et al., 2006).

A rheologically stable field mud system has been derived by reasonable selection of additives (Ward et al., 1999) where the shale recovery test with API 13I, also known as hot rolling shale particle disintegration test, is done to determine shale inhibition with sodium silicate bases and also mixed sodium/potassium silicate mud systems. The result showed that 5% mixed sodium/potassium silicate mud system has 100% shale recovery rate, whereas, only sodium silicate was recovering upto 80% when 7.5% sodium silicate was being in use. Another particular example, 5-10% v/v silicate along with an inhibitive salt (Potassium Chloride) is used as silicate based muds in the North Sea (Stewart et al. 2000) and the hole enlargement was reduced to 1-12% compared to the 25-44% with conventional mud system, the rheological and other drilling fluid properties were easily achieved, and the rate of penetration with the silicate mud was 1.5 times faster than that of conventional bentonite mud systems. Potassium silicate based drilling fluids are also used in reactive shale formation drilling which provides better wellbore stability (Duncan and McDonald, 2004; McDonald, 2012). Potassium silicate from 5-6% along with 2% silica (SiO₂) improve 89-97% shale recovery when used with the base drilling fluid. Further research with low ratio silicates at higher concentrations of total silicate in the drilling fluid showed excellent shale stabilization (Urquhart, 1998). Environmental acceptance test was done according to ASTM standard of a potassium silicate based drilling fluid used for shale formation drilling and found the used drilling fluid as environmentally acceptable (Duncan and McDonald, 2004). Also the waste disposal cost was lower compared to oil based drilling fluid. Thus the use of silicate in drilling mud is very wide in the oil well drilling.

2.7 Summary

Based on the literature review following observations are observed:

1. Sodium meta-silicate reacts with the weak part (calcium hydroxide) of the cement hydration and produces calcium silicate hydrate which helps the durability of the hardened cement
2. Sodium meta-silicate are used as a free water controlling agent, light weight cementing agent and in cement grouting applications
3. Silicates reduces the borehole collapse in shale formation when used with water based drilling mud and it is an environmentally acceptable additive

CHAPTER 3 MATERIALS AND METHODS OF TESTING

3.1 Materials

Cement

To study the effect of sodium meta-silicate (SMS) with cement slurry, we have used API class H oil well cement.

Smart cement

Commercially available oil well cement API class H cement was modified with additives to make it a piezoresistive material. We have added 0.075% of conductive filler (CF) with the cement.

Sodium meta-silicate

Sodium meta-silicate (Na_2SiO_3), also known as disodium meta-silicate, used in this study is a white, odorless, granular anhydrous powder. Based on the data sheet provided by the chemical manufacturer, it has a molecular weight of 122 g/mol, pH of 12.5 at 10 g/l at 20 °C (68 °F), melting point of 1,090 °C (1,994 °F), density of 2.61 g/cm³ at 20 °C (68 °F), and water solubility of 350 g/L at 20 °C (68 °F).

Sodium alumino-silicate

Sodium alumino-silicate ($\text{Na}_{12}\text{AlSiO}_5$), also known as aluminum sodium salt, used in this study is a colorless, odorless, and tasteless powdered solid which is soluble in hot water. It has a specific gravity of 2.1 and pH 9-11. The chemical composition: SiO₂ - 82%, Na₂O - 8%, Al₂O₃ - 9.5%.

Bentonite

Commercially available bentonite was used to prepare water based mud.

Water based mud

The water based mud was prepared with 6% bentonite by weight of water. When any additive (sodium meta-silicate, sodium alumino-silicate) was used, the additive was first mixed with water and then the bentonite was added and mixed by a table top blender with API standard.

3.2 Methods of Testing

Sodium meta-silicate (SMS) solution

The samples were prepared by mixing selected amount of SMS powder (by weight of water) in water at room temperature. The mixture was blended using a table top blender and the pH was monitored at the end of mixing. Up to 5% SMS solution was prepared to characterize the electrical properties of SMS solution. Different percentage of SMS solution was prepared to use with the cement slurry.

Cement mix

The samples were prepared according to the API standards. Smart cement with different water-to-cement ratio varied from 0.38 to 0.45 was used in this study. For cement grout water-to-cement ratio used was varied from 0.5 to 0.8. To study the effect of SMS on the cement slurry or grout, the smart cement was mixed with SMS solution of desired concentration.

Cement specimen preparation

After mixing, specimens were prepared using cylindrical molds with a diameter of 2 inches and a height of 4 inches (Fig. 3-1). Two conductive wires were placed in all of the molds which were 2 inches apart. All specimens were capped to minimize moisture loss and were cured before testing for the piezoresistivity under compressive loading.

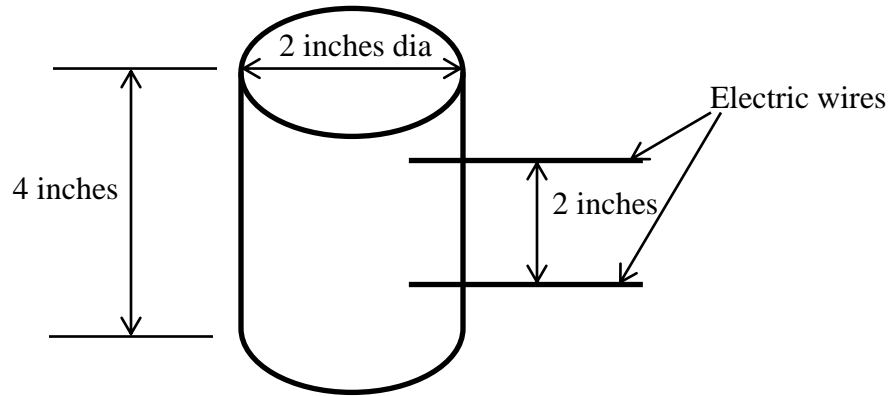


Figure 3-1: Cement specimen for compressive strength and piezoresistivity test

Rheological tests

Rheological properties determine the ability of cement to be pumped. The rheology tests were performed by utilizing a rotational viscometer (Fig. 3-2) at room pressure and temperature at rpms ranging from 3 to 600, and related shear stresses were recorded. The viscometers were calibrated using several standard solutions.



Figure 3-2: Rotational viscometer used for rheological properties test

Electrical resistivity measurement

Electrical resistivity of the slurries was measured using an API standard resistivity meter (Fig. 3-3). Further, electrical resistance was measured using an inductance–capacitance-resistance (LCR) meter during the curing time. To minimize the contact resistances, the resistance was measured at 300 kHz frequency using two-wire method (Vipulanandan et al., 2013). The procedure of measuring the resistance using LCR meter is shown in Fig. 3-4.



Figure 3-3: Direct resistivity measurement device



Figure 3-4: Typical components in the resistance measurements of the cement specimen

Mold calibration

Each specimen was calibrated to obtain the electrical resistivity (ρ) from the measured electrical resistance (R) based on the Eqn. (3-1)

$$\rho = RA/L = R/(L/A) = R/K, \quad (3-1)$$

where, L is the distance between the wires, A is the cross-sectional area through which the current is flowing, and L/A is called the geometry factor K. Where parameter $K=L/A$, the ratio of the cross-sectional area and the length of the material is defined for a particular set-up. If we know the resistivity and the resistance of the material then from the relationship in Eqn. (3-1) we can determine the parameter K. The resistivity of the cement slurry was determined using the API resistivity meter. Fig. 3-5 shows K values determine for cement slurry at different times after mixing. We found that after about 5 hours (300 min), the K value is stabilized. We used this K value for resistivity measurements of the hardened cement specimen.

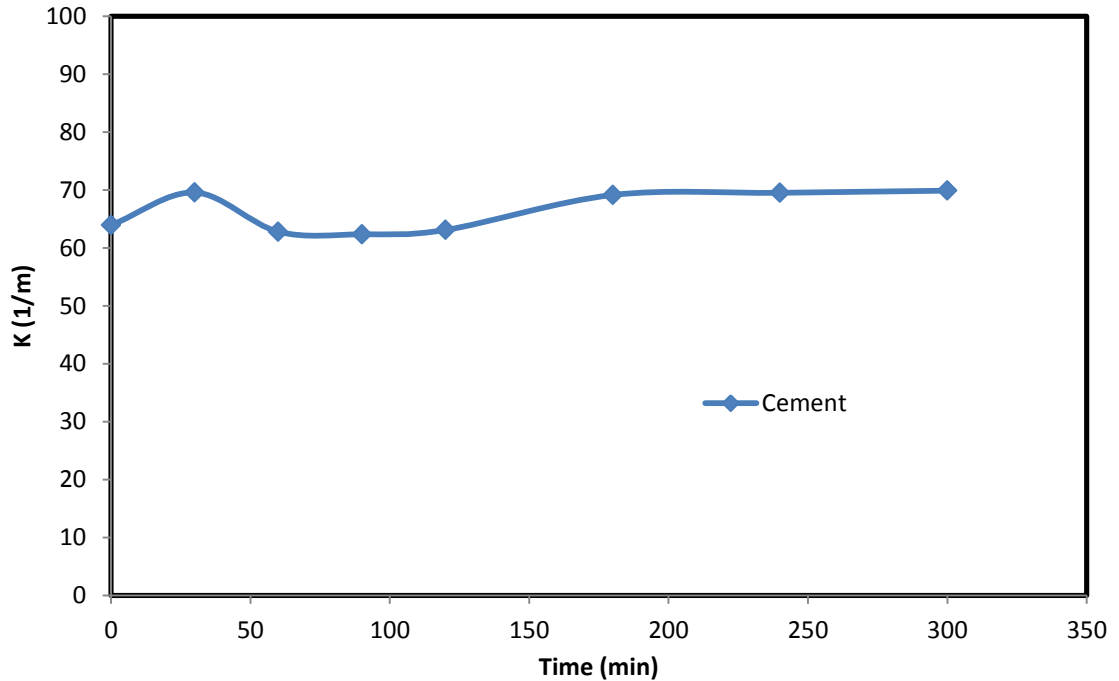


Figure 3-5: The K value for cement slurry with time

Compressive strength tests

Compressive strength of cement determines the ability of cement to stabilize casing in the wellbore. The cylindrical specimen was capped and tested at a predetermined controlled displacement rate (Fig. 3-6). Compression tests were performed on cement samples after 24 hour, 48 hours, 7 days, and 28 days of curing using a hydraulic compression machine.

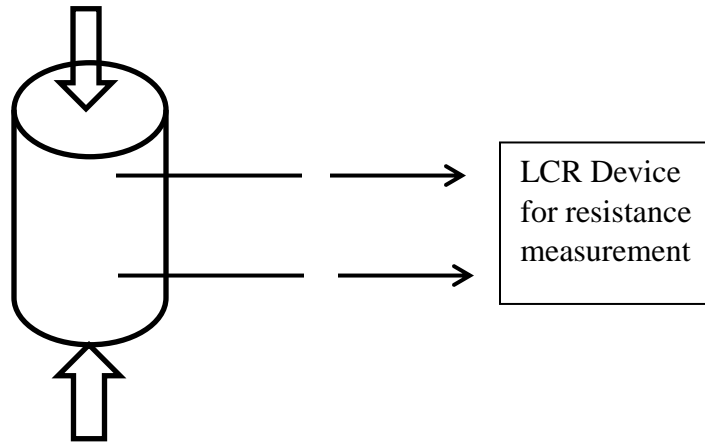


Figure 3-6: Schematic diagram of compression test with resistance measurements

Piezoresistivity tests

Piezoresistivity describes the change in electrical resistivity of a material under pressure. Since oil well cement serves as a pressure-bearing part of wells in real applications, the piezoresistivity of smart cement with and without SMS was investigated under compressive loading. During each compression test, electrical resistance was measured in the stress axis (Fig. 3-6). To eliminate the polarization effect, alternating current (AC) resistance measurements were made using a LCR meter at a frequency of 300 kHz. Furthermore, changes in resistivity were related to the applied stress.

Fluid loss test for drilling mud

Fluid loss test was done according to API Fluid loss test procedure. The pressure was maintained about 95 to 100 psi continuously until the end of the fluid loss (Fig. 3-7).

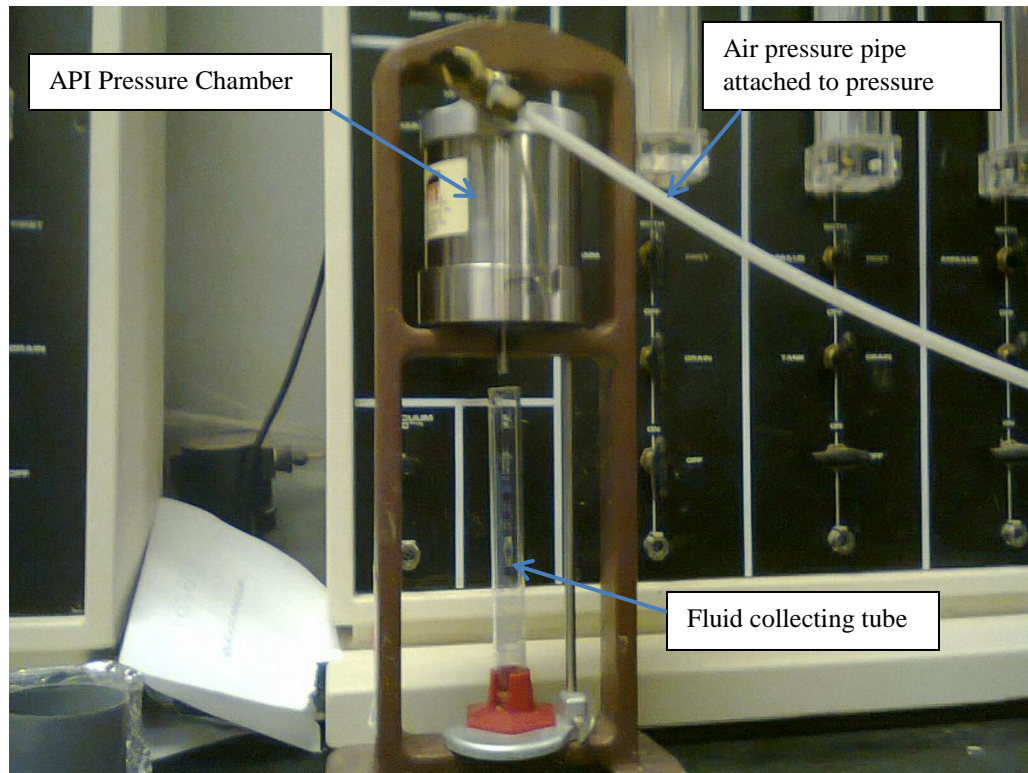


Figure 3-7: The fluid loss test apparatus with continuous pressure arrangement

Cement grout preparation and repair damaged cement with the grout

The smart cement grout samples were prepared using the API standards for mixing cement. Smart cement grout was prepared with water-to-cement ratio of 0.8 in this study. After testing the smart cement to failure the samples were submerged in the grout solution for three hours. The damaged smart cement specimens had the wires in place inside the cement at 2 inches apart. The specimens were cured under room

temperature after repairs for one day before testing. The weight and resistance of the specimens were monitored to determine moisture loss and change in the electrical resistivity before the compression and piezoresistivity test of the repaired specimens.

Physical model for wellbore and casing with wire setup

The small lab model

A small lab model of the well bore was made where the wellbore was made using a flexi-glass cylindrical mold of about 9 inches diameter and about 40 inches height. Inside of the mold we set another cylindrical pipe of 2 inches diameter and 30 inches height. The outer cylinder was acting as formation wall and the inside cylinder was working as casing. With the casing we have attached wires at 6 inches apart vertically and with 4 horizontal arrangements. The schematic diagram of the plan and elevation of the casing model with wiring are presented below. The Model consists of 4 wire combination such as A, B, C, and D (Fig. 3-8: Plan View). For each of the wire combination, there are 5 wire placed 6 inches apart from each other (Fig. 3-8: Elevation). Another schematic diagram of the whole model with wire combination is shown in Fig. 3-9. Fig. 3-10 shows actual model with partial filled cement slurry during the cementing.

Big lab model

Two big lab model of the well bore were used. The both model was 8 inches diameter and 8 ft (96 inches) height cylindrical PVC pipe. Inside of both of those molds we set another cylindrical pipe of diameter about 4 inches and 8 ft height. The outer cylinder was acting as a formation wall and the inside cylinder was working as casing. With the casing we have attached wires at 6 inches apart vertically and with 4 horizontal

arrangements. The schematic diagram of the plan and elevation of the casing model with wiring are presented below. The models consist of 4 wire combination such as A, B, C, and D (Fig. 3-11: Plan View). For each of the wire combination, there are 14 wires placed 6 inches apart (Fig. 3-11: Elevation). Fig. 3-12 shows actual model in place.

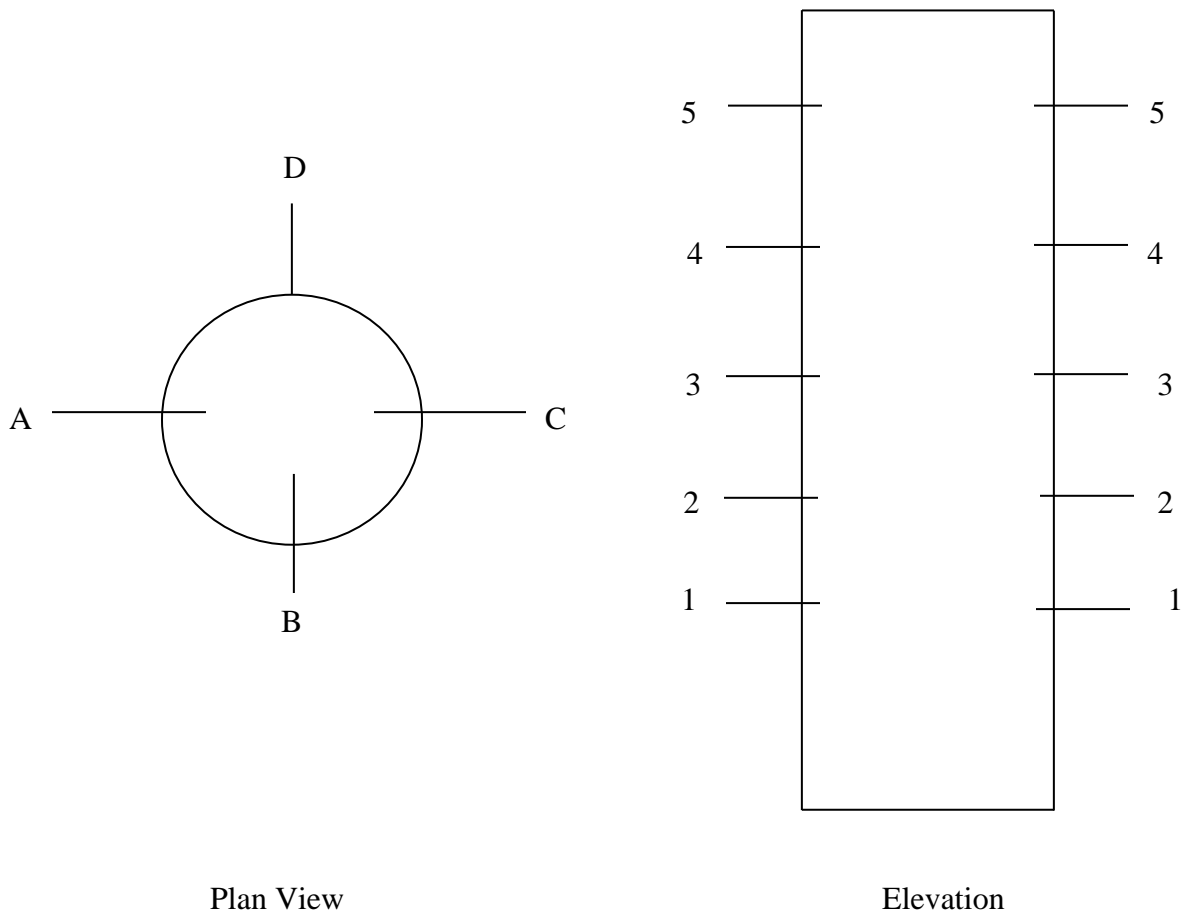


Figure 3-8: Plan and elevation of the small lab model with wire combination

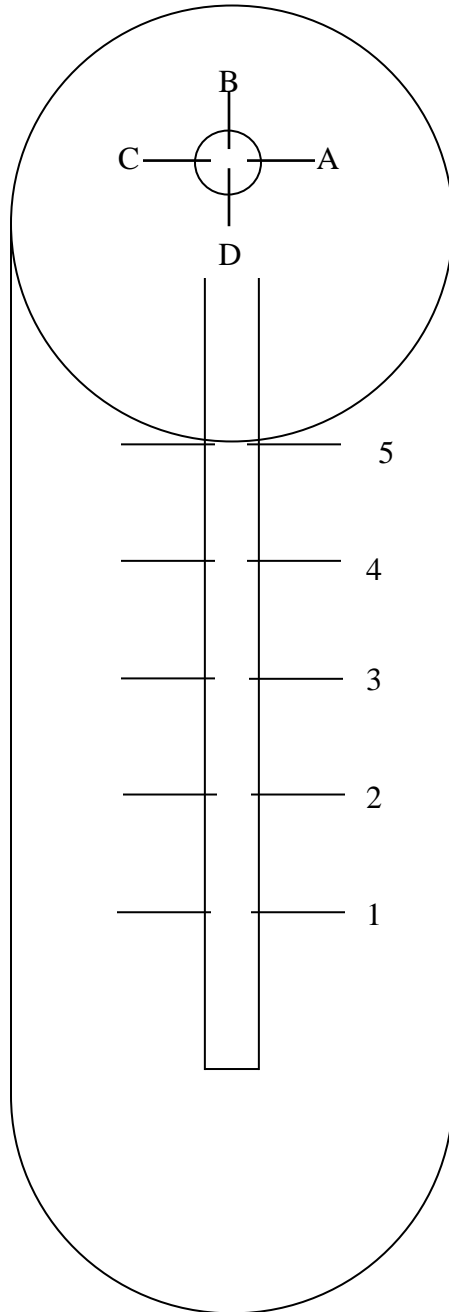


Figure 3-9: A Schematic diagram of the small lab model



Figure 3-10: The actual model with partially filled cement slurry (left) and drilling mud (right)

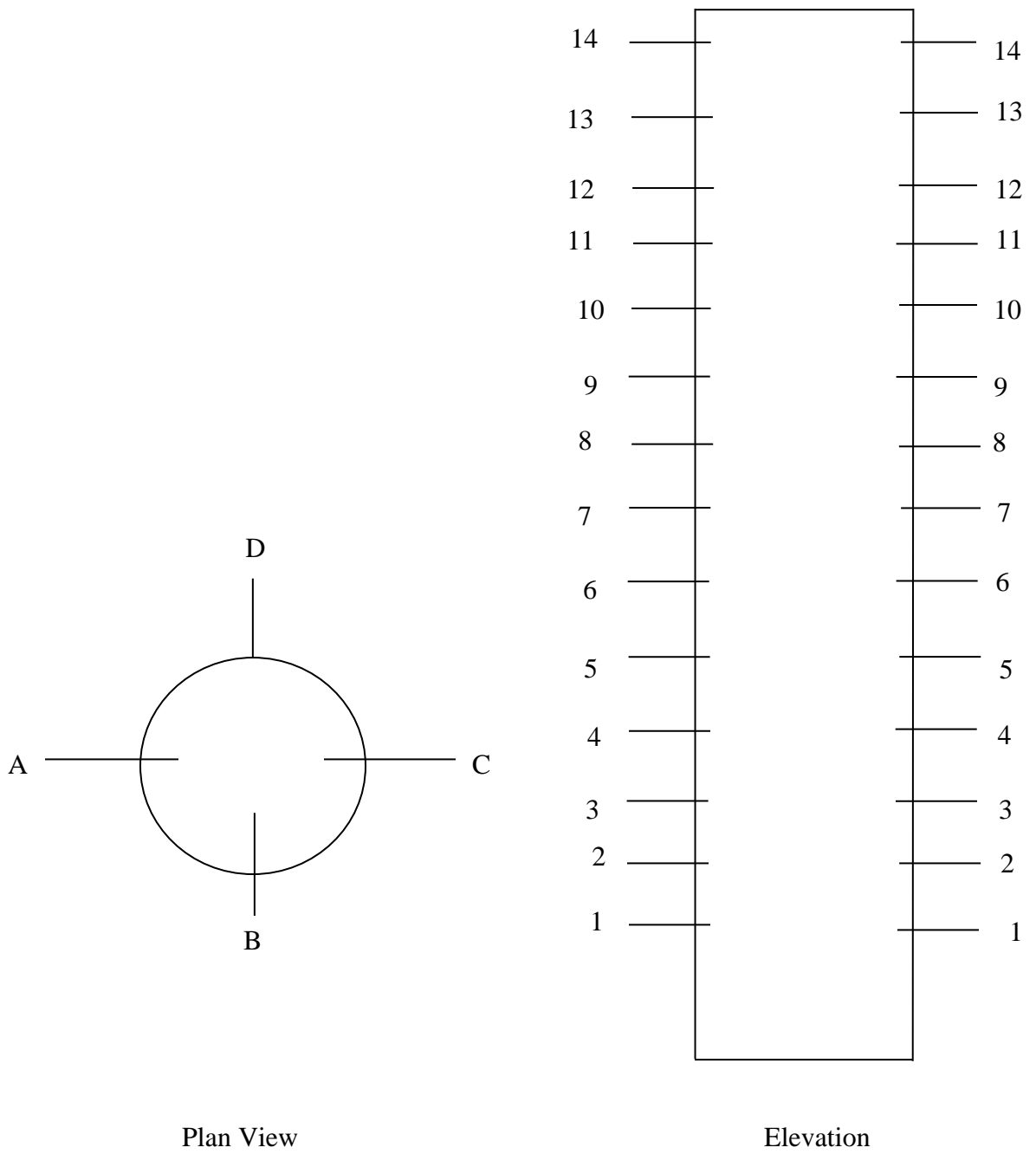


Figure 3-11: Plan and elevation of the big lab model with wire combination



Figure 3-12: Actual model after placing cement

The field model

The field model of the well bore was a 40 ft depth well made by 16 inches diameter hole underground. A 12 inches diameter steel casing was wired by 8 vertical wire set up marked as A, B, C, D, E, F, G and H (Fig. 3-13) at an angle of 45 degrees separating each other. Each vertical wire setup are divided into 15 different wire combinations whose spacing varying from 1 ft to 6 ft. The schematic diagram (Fig. 3-13) shows the wire setup and Fig. 3-14 shows actual casing with wires before placing in the wellbore.

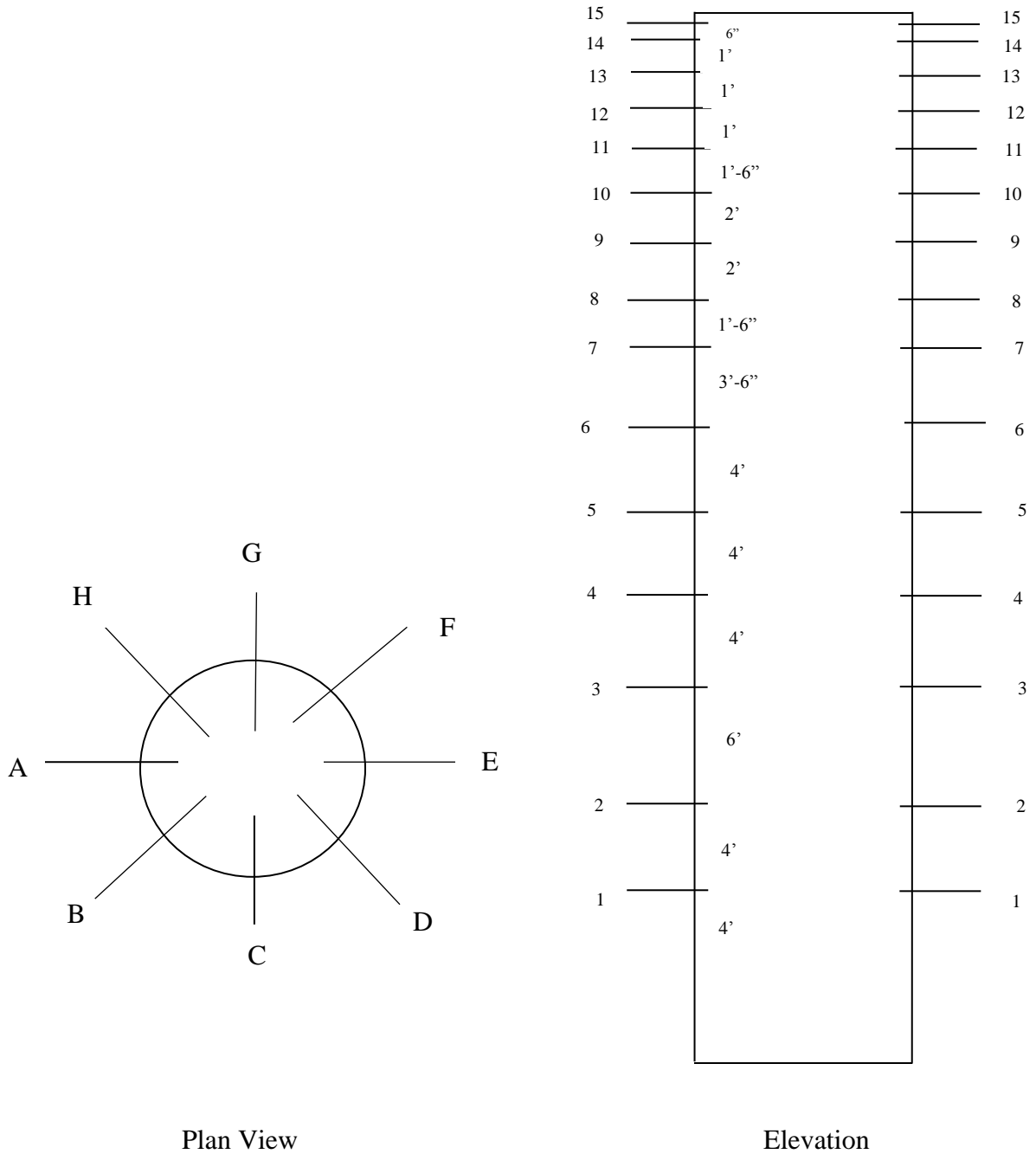


Figure 3-13: Plan and elevation of the field model with wire combination



Figure 3-14: Actual casing with wire combination before placing in the wellbore

3.3 Mathematical models to characterize the materials

3.3.1 Mathematical models for rheological properties

To characterize the rheological properties of the cement slurry and drilling mud, several mathematical models will be considered based on the behavior of the materials to best describe the material properties. The typical rheological models are:

- 1) Bingham-plastic model (two parameter model)

$$\tau = \tau_y + \eta_p \dot{\gamma} \quad (3-2)$$

where,

τ = shear stress

$\dot{\gamma}$ = shear-strain rate

τ_y = yield stress and

η_p = plastic viscosity of the fluid

- 2) Power law model (Two parameter model)

$$\tau = k \dot{\gamma}^n \quad (3-3)$$

where,

k and n are model parameters that can be fit experimentally.

- 3) Herschel-Bulkley model (Three parameter model)

$$\tau = \tau_0 + k \dot{\gamma}^n \quad (3-4)$$

where,

τ_0 = yield stress and

k and n are model parameters that can be fit experimentally.

- 4) Hyperbolic model (three parameter model) developed by Vipulanandan and Mohammed (2014)

$$\tau = \tau_0 + \frac{\dot{\gamma}}{A+B\dot{\gamma}}, \quad (3-5)$$

where,

τ_0 = yield stress and

A and B are model parameters that can be fit experimentally.

3.3.2 Mathematical model to characterize fluid loss of drilling mud and cement slurry

(1) To model the fluid loss test results, the API Fluid loss equation which is given by Eqn.

(3-6):

$$V_f - V_o = M * \sqrt{t}, \quad (3-6)$$

$$\text{where, } M = \sqrt{2k\Delta p \left(\frac{f_{sc}}{f_{sm}} - 1 \right) \frac{A_o}{\sqrt{\mu}}} \quad (3-7)$$

V_f = Volume of fluid loss at time t (cm³)

V_o = Initial volume of fluid loss (cm³)

t = Time (min)

Δp = Applied pressure (atm)

k = Drilling mud permeability (darcy)

f_{sc} = Volume fraction of solid in cake

f_{sm} = Volume fraction of solid in mud

A_o = Filter Area (cm²)

μ = Viscosity of mud (cP)

Based on the assumption that the cake forms initially, the right side of the Eqn. (3-7)

becomes constant and the model Eqn. (3-6) can be used to calculate the value of constant

M. By determining the value of M from 30 minutes fluid loss test, we can predict the

fluid loss up to any time by using Eqn. (3-7).

(2) The filtration process can also be modeled using new Kinetic (Hyperbolic) Model proposed by Vipulanandan et al. 2014 which is:

$$V_f - V_o = N * \frac{t}{C + Dt}, \quad (3-8)$$

where,

V_f = Volume of fluid loss at time t (cm³)

V_o = Initial volume of fluid loss (cm³)

t = Time (min)

C = Fluid loss parameter depends on pressure and temperature

D = Arbitrary constants (1/min)

$$\text{And } N = \sqrt{\frac{2 * k_o * \alpha_o * \Delta p * A_r}{\mu(T)}} \quad (3-9)$$

where,

k_o = initial permeability of drilling mud

α_o = arbitrary constant (1/min)

Δp = applied pressure (atm)

A_r = filter area (cm³)

$\mu(T)$ = Viscosity of the drilling mud at temperature T.

The fluid loss test results will be modeled using the model equation (3) and the model parameters will be determined. In this study, we shall have constant pressure (i.e., Δp constant), constant filter area, (i.e., A_r is constant), and for a particular drilling mud k and $\mu(T)$ will be constant thus the entire right side of equation (4) will be constant. That's why we can consider N of equation (3) as a constant.

3.3.3 Mathematical model to characterize electrical resistivity with curing time

The change of electrical resistivity with curing time for smart cement was observed for different curing condition. From the experimental results, following conditions were observed:

(i) Initial condition; when $t=0$ $\frac{1}{\rho} = \frac{1}{\rho_o}$, (3-10a)

(ii) when $0 < t < t_{min}$

$$\frac{d(\frac{1}{\rho})}{dt} > 0 \text{ and } \frac{d^2(\frac{1}{\rho})}{dt^2} < 0, \quad (3-10b)$$

(iii) when $t=t_{min}$

$$\frac{1}{\rho} = \frac{1}{\rho_{min}} \quad (3-10c)$$

$$\frac{d(\frac{1}{\rho})}{dt} = 0, \text{ and} \quad (3-10d)$$

(iv) When $t > t_{min}$ $\frac{d(\frac{1}{\rho})}{dt} < 0$ $\frac{d^2(\frac{1}{\rho})}{dt^2} > 0$. (3-10e)

Hence the model proposed by Vipulanandan and Paul (1990) was modified and used to predict the electrical resistivity of cement during hydration for different curing condition and curing time. The proposed curing model is as

$$\frac{1}{\rho} = \left(\frac{1}{\rho_{min}}\right) \left[\frac{\left(\frac{t+t_o}{t_{min}+t_o}\right)^{q_1+p_1}}{q_1+(1-p_1-q_1)*\left(\frac{t+t_o}{t_{min}+t_o}\right)+p_1*\left(\frac{t+t_o}{t_{min}+t_o}\right)^{p_1}} \right] \quad (3-11)$$

where, ρ is the electrical resistivity (Ω -m); ρ_{min} is the minimum electrical resistivity (Ω -m); t_{min} is the time corresponding to minimum electrical resistivity (ρ_{min}); $p_1(t)$, t_o , and $q_1(t)$ are model parameters and t is the curing time (min). The parameter q_1 represents the initial rate of change in the resistivity and parameter p_1+q_1 represent the ultimate resistivity.

Several characteristic resistivity parameters can be used in monitoring the curing (hardening process) of the cement. The parameters are initial resistivity (ρ_0), minimum electrical resistivity (ρ_{min}), time to reach the minimum resistivity (t_{min}) and percentage of maximum change in resistivity at the end of 24 hours (RI_{24hr}), 7 days (RI_{7days}), 28 days (RI_{28days}) were defined in Eqn. (3-12), Eqn. (3-13) and Eqn. (3-14) as follows:

$$RI_{24hr} = \frac{\rho_{24hr} - \rho_{min}}{\rho_{min}} * 100, \quad (3-12)$$

$$RI_{7days} = \frac{\rho_{7days} - \rho_{min}}{\rho_{min}} * 100, \text{ and} \quad (3-13)$$

$$RI_{28days} = \frac{\rho_{28days} - \rho_{min}}{\rho_{min}} * 100. \quad (3-14)$$

3.3.4 Mathematical model to characterize piezoresistivity of hardened cement

Piezoresistivity shall be modeled using p-q model developed by Vipulanandan and Paul (1990) which is modified as Eqn. (3-15)

$$\sigma = \frac{\sigma_{max} \times \left(\frac{(\Delta\rho/\rho)}{(\Delta\rho/\rho)_0} \right)}{q + (1-p-q) \times \left(\frac{(\Delta\rho/\rho)}{(\Delta\rho/\rho)_0} \right) + p \times \left(\frac{(\Delta\rho/\rho)}{(\Delta\rho/\rho)_0} \right)^{\frac{(p+q)}{p}}}, \quad (3-15)$$

where σ_{max} is the maximum stress at failure, $(\Delta\rho/\rho)_0$ is the piezoresistivity of the hardened cement under the maximum stress, $(\Delta\rho/\rho)$ is the piezoresistivity at any stress σ and p and q are experimentally fit parameters.

CHAPTER 4 CHARACTERIZATION OF SMART CEMENT

4.1 Characterizing sodium meta-silicate (Na_2SiO_3) solution

4.1.1 pH of sodium meta-silicate solution

Sodium meta-silicate (SMS) solution was characterized by determining its electrical property pH. Addition of SMS to the water increased the pH of SMS solution as shown in Fig. 4-1. With the addition of 0.1% SMS, the pH of water increased from 7.7 to 11.8, a 50% change in the pH. With the addition of 0.3% SMS the pH of the solution was found as 12.4, a 60% change.

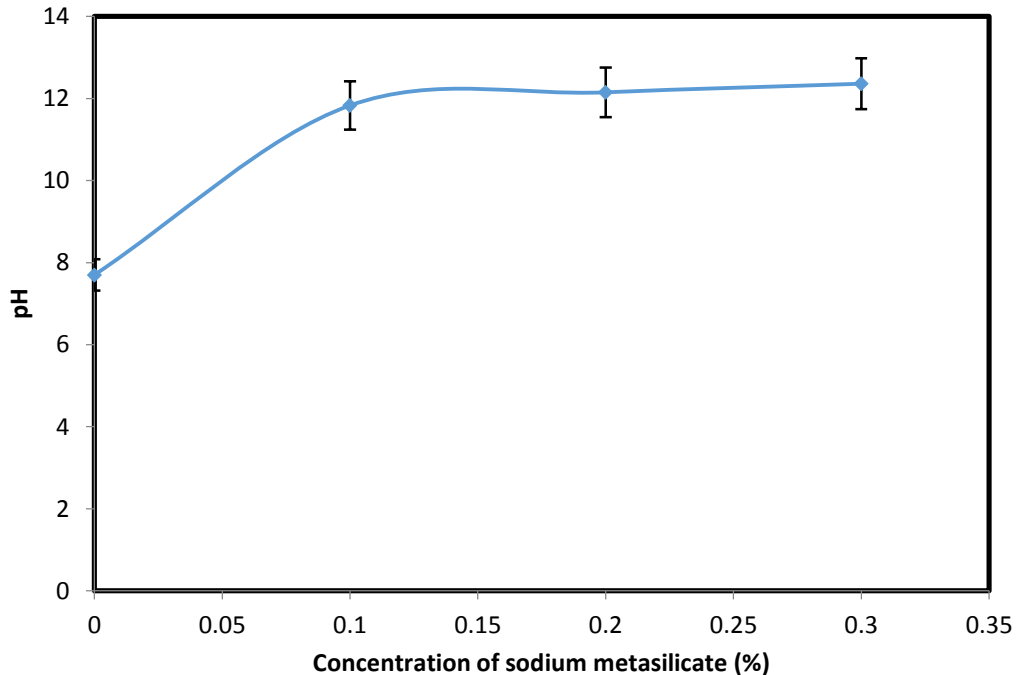


Figure 4-1: Variation of pH of water with SMS concentration (% by weight of water)

4.1.2 Electrical resistivity of sodium meta-silicate solution

The electrical resistivity of SMS solution was determined with the electrical conductivity measurement device and converting the measured conductivity to resistivity. SMS solution was very sensitive to electrical resistivity. The resistivity of water decreased from 21 Ohm-m to 4.15 Ohm-m with addition of only 0.1% SMS (Fig. 4-2),

80% reduction in resistivity. Addition of SMS further reduced the resistivity of the solution. Based on the experimental results, following relationship is proposed

$$\rho = \rho_o - S/(A + BS), \quad (4-1)$$

where,

ρ = resistivity of the SMS solution

ρ_o = resistivity of tap water without SMS (20.5 Ohm-m)

S = Concentration of SMS (% by weight).

Parameters A and B are model parameters and parameter A represent the initial rate of change and parameter B determines the ultimate resistivity. Experimental results matched very well with the proposed model with coefficient of determination (R^2) of 0.98 and parameters A and B were found as $0.0016 \text{ Ohm}^{-1}\text{-m}^{-1}$ and $0.047 \text{ Ohm}^{-1}\text{-m}^{-1}$.

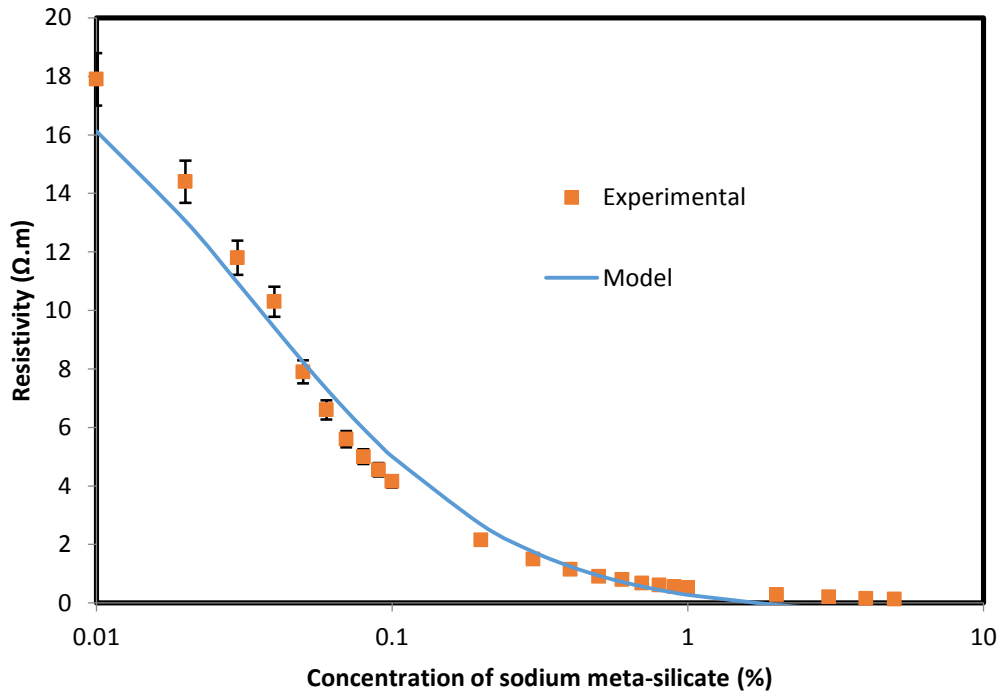


Figure 4-2: Change of resistivity of SMS solution with SMS concentration

4.2 Smart cement with SMS

4.2.1 Rheological properties

The rheological test of smart cement slurry with and without SMS was done with a rotational viscometer described in chapter 3 with RPM 3 to 600. From the experiment, the results directly found are gel strength at 10 seconds and 10 minutes, shear stress at different shear strain rate from which the apparent viscosity can be calculated. The gel strength, apparent viscosity and yield stress are summarized in Table 4-1.

Gel Strength:

For the smart cement slurry only, the 10 seconds gel strength was 12 lb/100 ft², and 10 minutes gel strength was 22 lb/100 ft² (Table 4-1). With the addition of 0.1%, 0.2%, and 0.3% SMS, the 10-second gel strength of the slurry was increased to 14 lb/100 ft², 15 lb/100 ft², and 16 lb/100 ft²; and the 10-minute gel strength was increased to 16 lb/100 ft², 17 lb/100 ft², and 19 lb/100 ft². Hence, addition of 0.3 SMS increased the 10-second gel strength by 33% and the 10-minute gel strength by 35%.

Apparent Viscosity:

From the rheological tests it was observed that the addition of SMS in smart cement slurry increased the viscosity. Addition of SMS increased the viscous behavior of the cement (Fig. 4-3, Fig 4-4, Table 4-1). For example, the viscosity of cement without SMS at a shear strain rate of 100 sec⁻¹ was 146±1.4 cP which increased to 182±1.7 cP, 225±1.6 cP, and 274±1.8 cP for slurry with 0.1%, 0.2%, and 0.3% SMS respectively. Addition of 0.3% SMS increased the viscosity about 85% at 100 sec⁻¹ shear strain rate.

Table 4-1: Results of the rheological test for smart cement slurry with and without SMS

Cement Slurry Type	Apparent Viscosity at 100 sec ⁻¹ (cP)	Gel Strength (lb/100 ft ²)		Herschel–Bulkley (H-B) model				Hyperbolic model			
		10 Sec	10 min	Yield Stress (lb/100 ft ²)	k	n	R ² Value	Yield Stress (lb/100 ft ²)	A (Pa ⁻¹)	B (Pa·sec) ⁻¹	R ² Value
Cement (C)	146±1.4	12	14	1.87	1.09	0.78	0.97	5.01	2.83	0.0015	0.97
C+0.1% SMS	182±1.7	14	16	3.4	1.75	0.72	0.97	6.5	2.55	0.0013	0.98
C+0.2% SMS	225±1.6	15	17	13.8	0.61	0.88	0.99	17.4	2.11	0.0012	0.99
C+0.3% SMS	274±1.8	16	19	14.2	0.22	0.72	0.98	19.3	1.94	0.0011	0.98

Yield stress:

The yield stress depends on the model that has been used to model the shear stress-shear strain rate behavior of the cement slurry. We have used the Herschel–Bulkley (H-B) model and Hyperbolic model (Vipulanandan and Muhammed, 2014). The Herschel–Bulkley (H-B) model is as follows:

$$\tau = \tau_o + k \gamma^n , \tag{4-2}$$

where, τ = shear stress, γ = shear-strain rate, τ_o = yield stress, k and n are constants.

And the hyperbolic model is as follows:

$$\tau = \tau_o + \gamma / (A + B\gamma) , \tag{4-3}$$

where, τ = shear stress, τ_o = yield stress, A and B are model parameters.

The experimental data for the shear stress vs shear strain rate for smart cement with/without SMS and the best fit model curves for the Herschel–Bulkley (H-B) model are shown in Fig. 4-3. The same data modeled with Hyperbolic model are shown in Fig. 4-4. Using the best fit curve the yield stress for both of the model was determined and

found that the yield stress was increased with the increase in SMS concentrations. The results are presented in Table 4-1. The yield stress was calculated by H-B model as 1.87 lb/100 ft² for smart cement slurry only which is increased to 14.2 lb/100 ft² with addition of 0.3% SMS. When modeled with Hyperbolic model, the yield stress was calculated as 5.01 lb/100 ft² for smart cement slurry only which is increased to 19.3 lb/100 ft² with addition of 0.3% SMS.

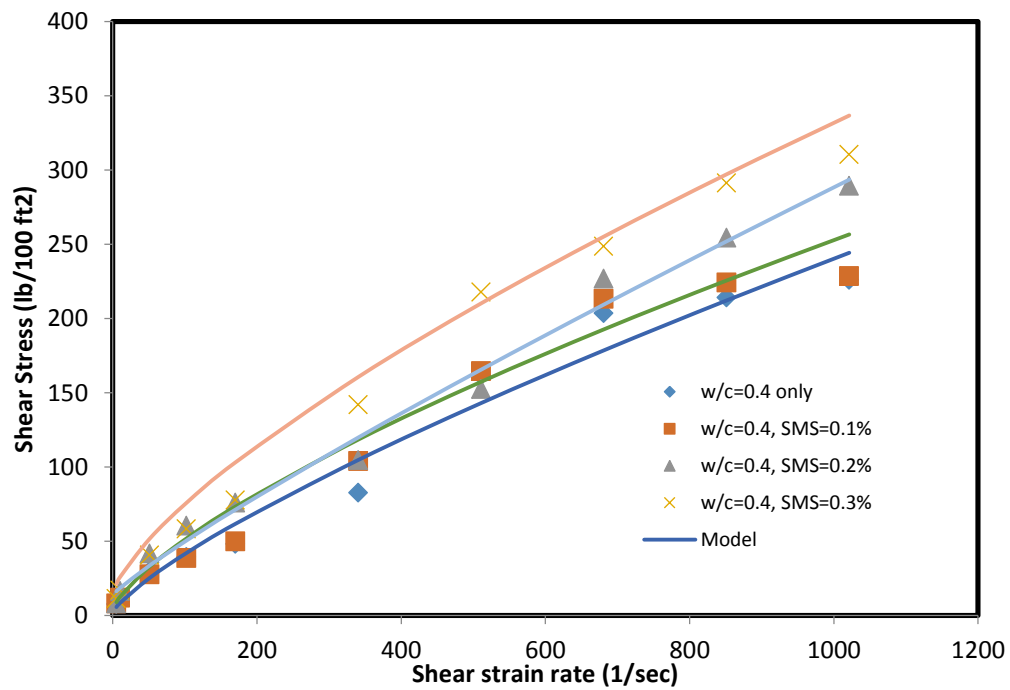


Figure 4-3: Shear stress – shear strain rate relationship for a smart cement slurry with and without SMS modeled with Herschel-Bulkley Model

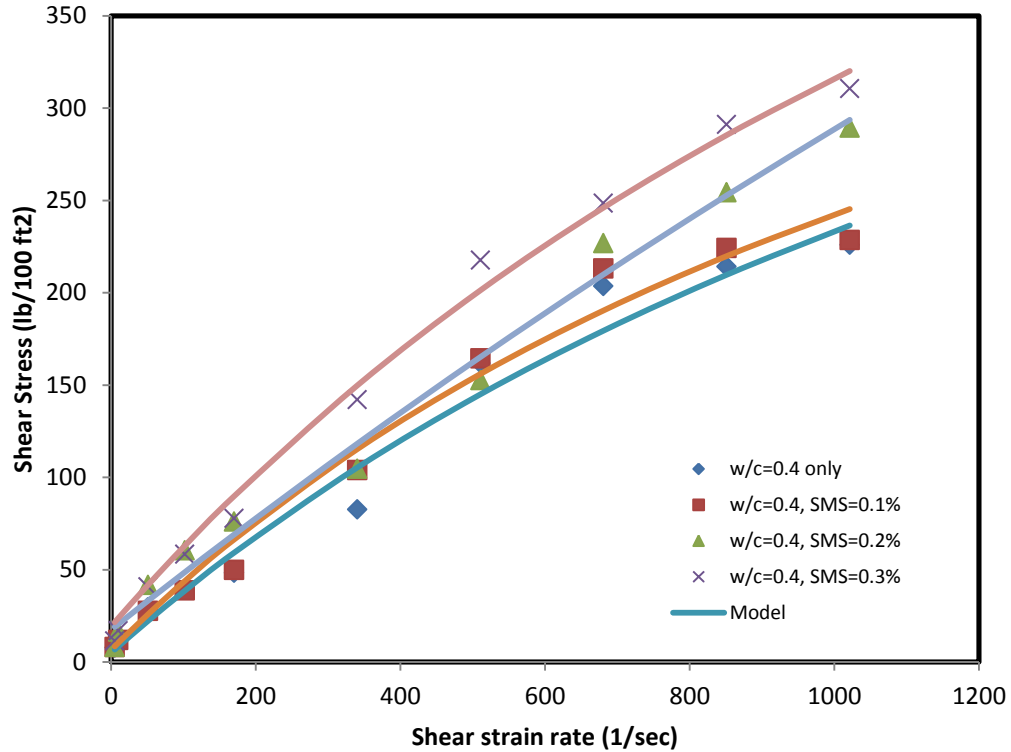


Figure 4-4: Shear stress–shear strain rate relationship for a smart cement slurry with/without SMS modeled with Hyperbolic model

Maximum shear stress:

After we have the model parameters, we can calculate the limiting value of the shear stress. As we already know that the yield stress is the shear stress at zero shear strain rate, the maximum shear stress will be the shear stress at infinite shear strain rate. If we look at the H-B model ($\tau = \tau_0 + k \gamma^n$) it is clear that the maximum shear stress at infinite shear strain rate will also be infinite which is practically impossible. If we look at the Hyperbolic model, i.e., $\tau = \tau_0 + \gamma/(A+B\gamma)$ and after rearranging we find $\tau = \tau_0 + 1/\{(A/\gamma)+B\}$. At $\gamma = \text{infinite}$, $A/\gamma = 0$ and $\tau = \tau_0 + 1/\{(A/\gamma)+B\} = \tau_0 + 1/B$. So, using yield stress and the model parameter B we can calculate maximum (limiting shear stress) with Hyperbolic model. The maximum shear stress for smart cement slurry is 672 Pa which is

increased to 763 Pa, 820 Pa and 900 Pa with addition of 0.1%, 0.2%, and 0.3% SMS. Thus the maximum shear stress is increased by 33% with addition of 0.3% SMS.

4.2.2 Fluid loss of smart cement slurry with SMS

Fluid loss test was done in an API HPHT fluid loss test cell under 100 psi pressure up to 30 min. For the smart cement slurry, the total fluid loss was 137 cc. Smart cement (w/c ratio of 0.4) with the addition of 0.2% SMS had a fluid loss of 145 cc (Fig. 4-5), hence a 6% increase in the fluid loss.

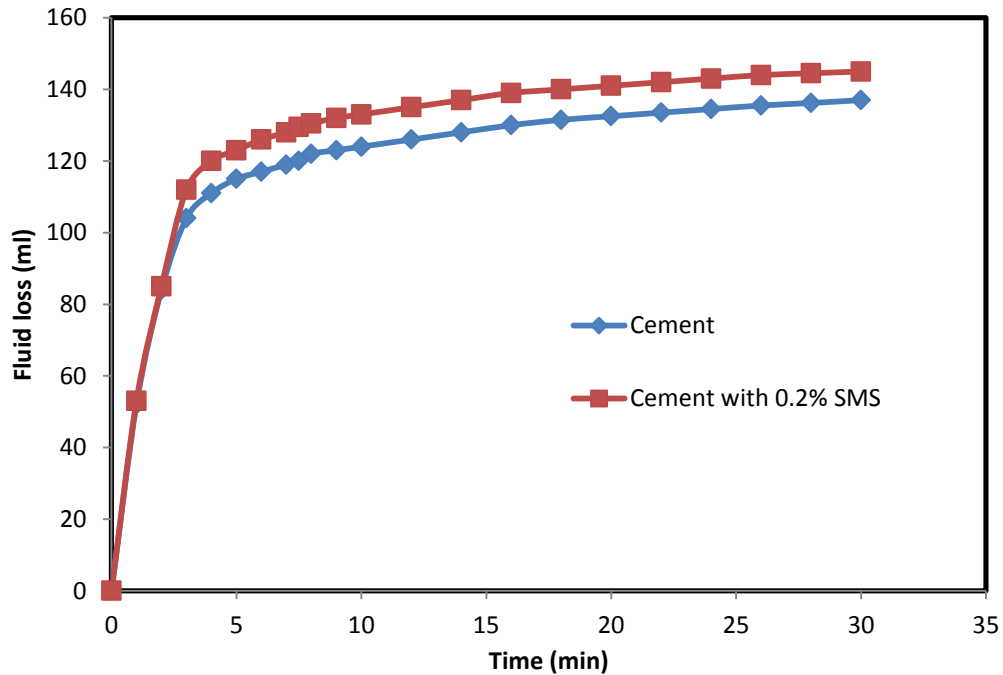


Figure 4-5: Fluid loss with time for smart cement slurry with and without SMS

4.2.3 Electrical Resistivity

4.2.3.1 Initial Resistivity

The electrical resistivity of the cement slurry with and without SMS was determined. The initial resistivity of the smart cement slurry was 0.97 Ω .m and it

decreased with the addition of sodium metasilicate as shown in Fig. 4-6. With the addition of 0.1% SMS the resistivity decreased to 0.92 $\Omega\cdot\text{m}$, a 5% reduction. With the addition of 0.2% and 0.3% SMS the resistivity were 0.9 $\Omega\cdot\text{m}$ and 0.88 $\Omega\cdot\text{m}$. Hence the resistivity was sensitive to the concentration of SMS in the cement. The resistivity was decreased to 0.8 $\Omega\cdot\text{m}$ with 1% SMS which is a 17% decrease.

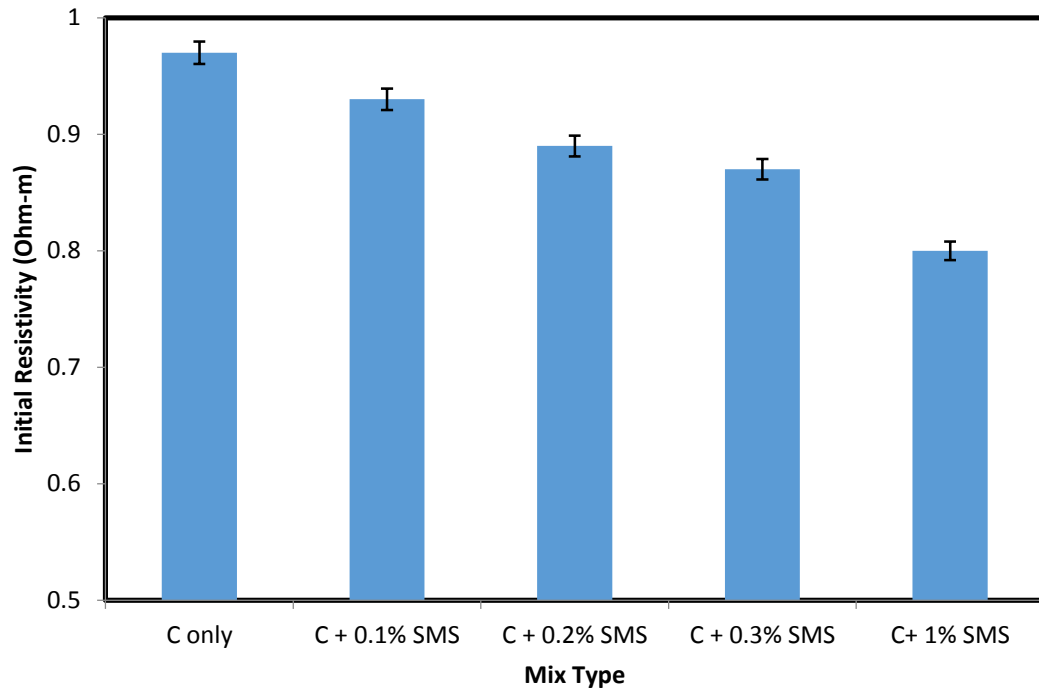


Figure 4-6: Initial resistivity of the cement slurry with different concentration of SMS (C = smart cement)

4.2.3.2 Resistivity during Curing Process

Electrical resistivity could be used as a fingerprint of the curing process. Fig. 4-7 illustrates the change in electrical resistivity (ρ) during curing time for smart cement with and without SMS. It was observed that the curves of the different samples, with and without SMS, follow a similar trend with time. The electrical resistivity dropped to a minimum value, and then gradually increased with time. After initially mixing cement with water, resistivity decreased to a minimum value (ρ_{min}), and the corresponding time

to reach the minimum resistivity was t_{min} . The decrease in resistivity immediately after mixing was due to dissolution of soluble ions from the cement particles after cement was mixed with water, and the dissolving process of the ions caused the resistivity decrease during early periods. The term t_{min} can be used as an index of speed of chemical reactions and cement set times. With the formation of resistive solid hydration products that block the conduction path, resistivity increased sharply with curing time. The following increase in electrical resistivity was caused by the formation of a large amount of hydration products in the cement matrix. Finally, a relatively stable increasing trend was reached by the ion diffusion control of hydration process. Resistivity increased steadily up to 24 hours and reached a value of ρ_{24} . Change in electrical resistivity with respect to minimum resistivity quantifies the formation of solid hydration products, which leads to the strength development in the curing cement. Therefore, by tracking the change in resistivity of oil well cement, a clear understanding of the hydration process and strength development can be obtained. Hence the Resistivity Index at 24 hours (RI₂₄) is defined as the maximum change in resistivity in 24 hours to reflect the changes in resistivity.

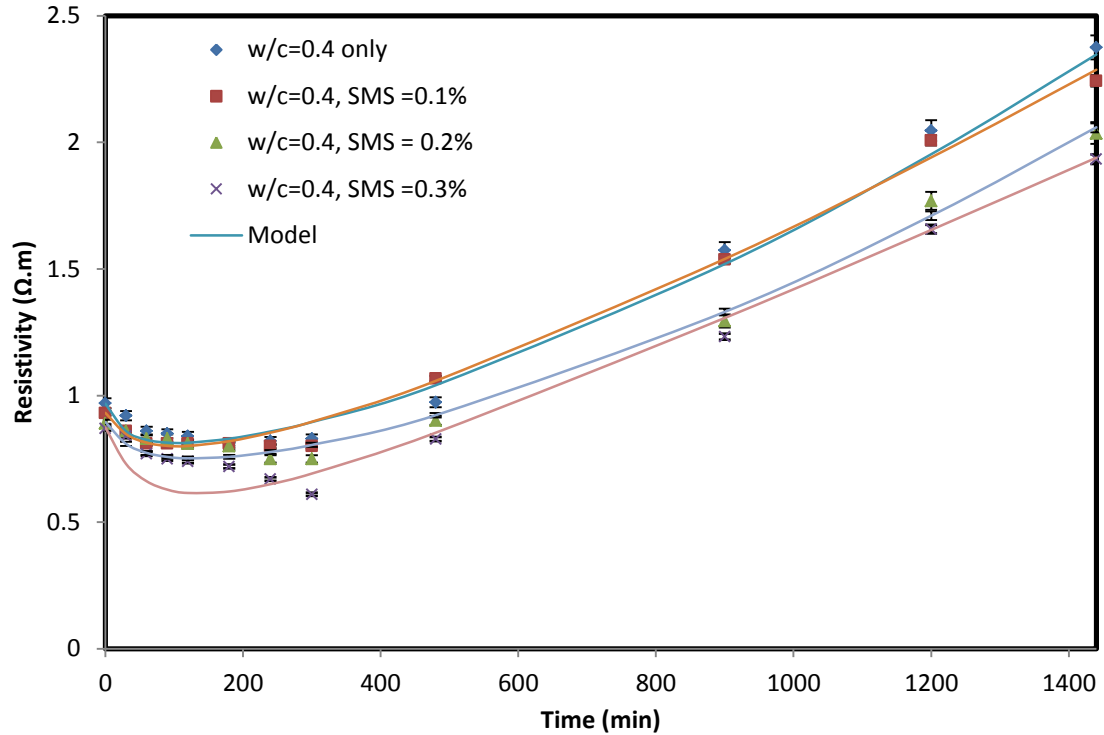


Figure 4-7: Variation of resistivity of curing cement slurry with time up to 24 hours

Variations in electrical resistivity with time for samples with different amounts of SMS are summarized in Table 4-2. Increasing SMS content decreased the minimum resistivity of cement (ρ_{\min}). This is another indicator of the increased chemical reaction between the cement and SMS. The RI_{24} value increases from 175% to 180%, 196% and 178% with addition of 0.1%, 0.2% and 0.3% SMS respectively. Time to reach the minimum resistivity was 180 min for the smart cement slurry without any SMS which increased to 240 min for 0.1% and 0.2% SMS and to 300 min for 0.3% SMS. The 24 hour resistivity was 2.23 Ohm-m for smart cement slurry without SMS. For slurry with SMS, the 24 hour resistivity were 2.24 Ohm-m, 2.22 Ohm-m and 1.7 Ohm-m for 0.1%, 0.2% and 0.3% SMS respectively (Table 4-2). In general, higher change in electrical

resistivity ($\rho_{24} - \rho_{\min}$) indicates that increased hydration products are developed in the hydrating cement system.

Table 4-2: Resistivity change with curing time for smart Oil Well Cement with different percentage of SMS

Mix Proportions		ρ_o (Ω -m)	ρ_{\min} (Ω -m)	t_{\min} (min)	ρ_1 (Ω -m)	ρ_{24} (Ω -m)	$RI_{(24)}$ (%)
w/c= 0.4	Cement (C)	0.97±0.02	0.81±0.01	180	0.86	2.23	175
	C+0.1%SMS	0.93±0.01	0.80±0.01	240	0.81	2.24	180
	C+0.2% SMS	0.89±0.01	0.75±0.02	240	0.83	2.22	196
	C+0.3% SMS	0.87±0.01	0.61±0.02	300	0.77	1.7	178
	C+ 1 % SMS	0.80±0.02	0.58±0.01	300	0.72	1.85	157

ρ_o = Initial resistivity

ρ_{\min} = Minimum resistivity

t_{\min} = Time to reach minimum resistivity

ρ_1 = Resistivity at 1 hour

ρ_{24} = Resistivity at 24 hour

$RI_{(24)}$ = Resistivity Index = $[(\rho_{24}-\rho_{\min})/\rho_{\min}]$ (%)

4.2.3.3 Curing of smart cement

The change of electrical resistivity with curing time for smart cement with different SMS content such as 0%, 0.1%, 0.2% and 0.3% was observed for different curing condition.

4.2.3.3.1 Long time curing of the specimen at room temperature

4.2.3.3.1.1 Resistivity with curing time

The resistivity of the cement specimen with different percentage (0%, 0.1%, 0.2%, 0.3% and 1%) of SMS was determined up to twelve month at room temperature. The specimens were subject to normal evaporation. Unit weight of the smart cement with w/c of 0.4 was 16.2±0.12 ppg (19.04 kN/m³) which was increased very little with SMS content. With 1% SMS, the unit weight increased to only 16.4±0.10 ppg (19.27 kN/m³). The initial electrical resistivity (ρ_o) of the smart cement with w/c ratio of 0.4 modified

with 0.075% CF was $0.99 \pm 0.02 \text{ } \Omega\text{-m}$ and the electrical resistivity reduced to reach the ρ_{\min} of $0.83 \pm 0.01 \text{ } \Omega\text{-m}$ after 180 minutes (t_{\min}) as summarized in Table 4-3. Addition of SMS decreased the initial electrical resistivity and the minimum electrical resistivity but increased the time to reach the minimum resistivity (t_{\min}). Addition of 0.3% SMS reduced the ρ_o by 15% and ρ_{\min} by 22 %. The 24 hours electrical resistivity ($\rho_{24\text{hr}}$) of the smart cement was $2.35 \text{ } \Omega\text{-m}$. Hence the maximum change in electrical resistivity after 24 hours ($RI_{24\text{hr}}$) was 183% as summarized in Table 3. The 7 days and 28 days electrical resistivity ($\rho_{7\text{days}}$ and $\rho_{28\text{days}}$) of the hardened smart cement were $11.1 \text{ } \Omega\text{-m}$ and $24.15 \text{ } \Omega\text{-m}$, hence the maximum change in electrical resistivity after 7 days and 28 days ($RI_{7\text{days}}$ and $RI_{28 \text{ days}}$) were 1239% and 2810% respectively. The addition of SMS reduced the electrical resistivity compared to that of smart cement. Addition of 0.3% SMS reduced the 24 hours, 7 days and 28 days resistivity by about 15%, 25% and 30% respectively, hence, the maximum change in electrical resistivity i.e. $RI_{24\text{hr}}$, $RI_{7\text{days}}$ and $RI_{28 \text{ days}}$ were also reduced accordingly. For long term curing after 1 year, the resistivity of the smart cement was found about $95 \text{ } \Omega\text{-m}$, whereas the cement specimen with 0.3% SMS had a resistivity of $58 \text{ } \Omega\text{-m}$ which was 38% less than that of the smart cement.

The curing model parameter q_1 for smart cement only was 0.105 at 1 day of curing and increased to 0.889 with time up to 6 months and then decreased to about 0.601 at 12 months. Addition of SMS did not affect the q_1 value that much but follow the similar trend with curing time increases. The curing model parameter p_1 for smart cement only was 0.076 at 1 day of curing and increased to 0.962 with time up to 28 days and then increased to about 1.892 for time up to 6 months but then decreased to 1.096 after time up to 12 months (Table 4-4). Addition of SMS decreases the parameter p_1 for 0.1%-0.2%

SMS content but increases for 0.3%-1% SMS content and follows the similar trend with increased curing time. The curing model (Eqn. (3-11)) predicted the measured resistivity very well (Fig. 4-8). The coefficient of determination (R^2) varied from 0.97 to 0.99 and the root mean square of error (RMSE) varied from 0.031 $\Omega.m$ to 2.107 $\Omega.m$ for 1 day and 12 months of curing respectively.

Table 4-3: Summary of bulk resistivity parameters for smart cement cured under room temperature with and without SMS content

Mix Type	Density (ppg)	Initial resistivity, ρ_o ($\Omega.m$)	ρ_{min} ($\Omega.m$)	t_{min} (min)	ρ_{24hr} ($\Omega.m$)	$\rho_{7\text{ days}}$ ($\Omega.m$)	$\rho_{28\text{ days}}$ ($\Omega.m$)	$RI_{24\text{ hr}}$ (%)	$RI_{7\text{ days}}$ (%)	$RI_{28\text{ days}}$ (%)
w/c=0.4	16.2±0.12	0.99±0.02	0.83±0.01	180	2.35	11.11	24.2	183	1239	2810
w/c=0.4 SMS=0.1%	16.2±0.11	0.91±0.01	0.82±0.01	240	2.20	9.50	17.8	168	1059	2071
w/c=0.4 SMS=0.2%	16.2±0.13	0.86±0.01	0.76±0.02	240	2.12	8.38	16.6	179	1003	2084
w/c=0.4 SMS=0.3%	16.3±0.12	0.84±0.01	0.64±0.02	300	2.01	8.18	16.1	214	1178	2416
w/c=0.4 SMS= 1%	16.4±0.10	0.80±0.02	0.58±0.01	300	1.85	6.76	14.8	219	1066	2447

4.2.3.3.1.2 Moisture loss and its effect on the resistivity

During the curing period, the weight loss of the specimens was monitored to observe any change. The percent weight loss which can be considered as moisture loss was calculated from the initial weight of the specimen. We can see from Fig. 4-9 that the rapid weight loss was happened within initial 7 days of curing. After 7 days, the weight loss were 3.4%, 3%, 2.8%, 2.7%, and 2.5% for specimens having 0%, 0.1%, 0.2%, 0.3%, and 1% SMS respectively. After 12 months of curing, the weight loss were 6.2±0.05%, 5.8±0.03%, 5.39±0.03%, 5.35±0.02%, and 4.98±0.02% for specimens having 0%, 0.1%, 0.2%, 0.3%, and 1% SMS respectively. Here we found that the specimens having more amount of SMS losing less amount of moisture inside the specimens. The specimen having 0.3% SMS losing 14% less weight compared to the specimen which had no SMS.

Table 4-4: Model parameters for the curing model of the resistivity of smart cement modified with SMS cured under room temperature up to 12 months

Mix Type	Curing Time (day)	ρ_{\min} ($\Omega.m$)	t_{\min} (min)	q_1	t_0 (min)	p_1	RMSE ($\Omega.m$)	R^2
w/c=0.4	1 day	0.83	180	0.105	40	0.076	0.031	0.99
w/c=0.4 SMS=0.1%		0.82	240	0.052	48	0.025	0.030	0.99
w/c=0.4 SMS=0.2%		0.76	240	0.066	51	0.034	0.025	0.99
w/c=0.4 SMS=0.3%		0.64	300	0.157	66	0.088	0.067	0.97
w/c=0.4 SMS= 1%		0.58	300	0.116	52	0.055	0.059	0.97
w/c=0.4	7 days	0.83	180	0.234	50	0.263	0.217	0.99
w/c=0.4 SMS=0.1%		0.82	240	0.359	80	0.461	0.166	0.99
w/c=0.4 SMS=0.2%		0.76	240	0.290	85	0.355	0.125	0.99
w/c=0.4 SMS=0.3%		0.64	300	0.464	91	0.581	0.110	0.99
w/c=0.4 SMS= 1%		0.58	300	0.483	87	0.634	0.159	0.99
w/c=0.4	28 days	0.83	180	0.563	63	0.962	0.520	0.99
w/c=0.4 SMS=0.1%		0.82	240	0.784	95	1.645	0.425	0.99
w/c=0.4 SMS=0.2%		0.76	240	0.649	92	1.254	0.309	0.99
w/c=0.4 SMS=0.3%		0.64	300	1.001	105	2.045	0.432	0.99
w/c=0.4 SMS= 1%		0.58	300	0.726	95	1.250	0.251	0.99
w/c=0.4	90 days	0.83	180	0.706	65	1.339	0.608	0.99
w/c=0.4 SMS=0.1%		0.82	240	0.745	95	1.515	0.413	0.99
w/c=0.4 SMS=0.2%		0.76	240	0.735	93	1.516	0.377	0.99
w/c=0.4 SMS=0.3%		0.64	300	0.987	105	2.046	0.323	0.99
w/c=0.4 SMS= 1%		0.58	300	0.861	99	1.636	0.355	0.99
w/c=0.4	180 days	0.83	180	0.889	68	1.892	0.967	0.99
w/c=0.4 SMS=0.1%		0.82	240	0.839	95	1.812	0.489	0.99
w/c=0.4 SMS=0.2%		0.76	240	0.778	94	1.655	0.428	0.99
w/c=0.4 SMS=0.3%		0.64	300	1.210	109	2.808	0.569	0.99
w/c=0.4 SMS= 1%		0.58	300	1.188	105	2.690	0.808	0.99
w/c=0.4	360 days	0.83	180	0.601	63	1.096	2.107	0.99
w/c=0.4 SMS=0.1%		0.82	240	0.626	92	1.194	1.308	0.99
w/c=0.4 SMS=0.2%		0.76	240	0.730	93	1.510	0.668	0.99
w/c=0.4 SMS=0.3%		0.64	300	0.933	104	1.931	1.075	0.99
w/c=0.4 SMS= 1%		0.58	300	1.248	105	2.937	1.016	0.99

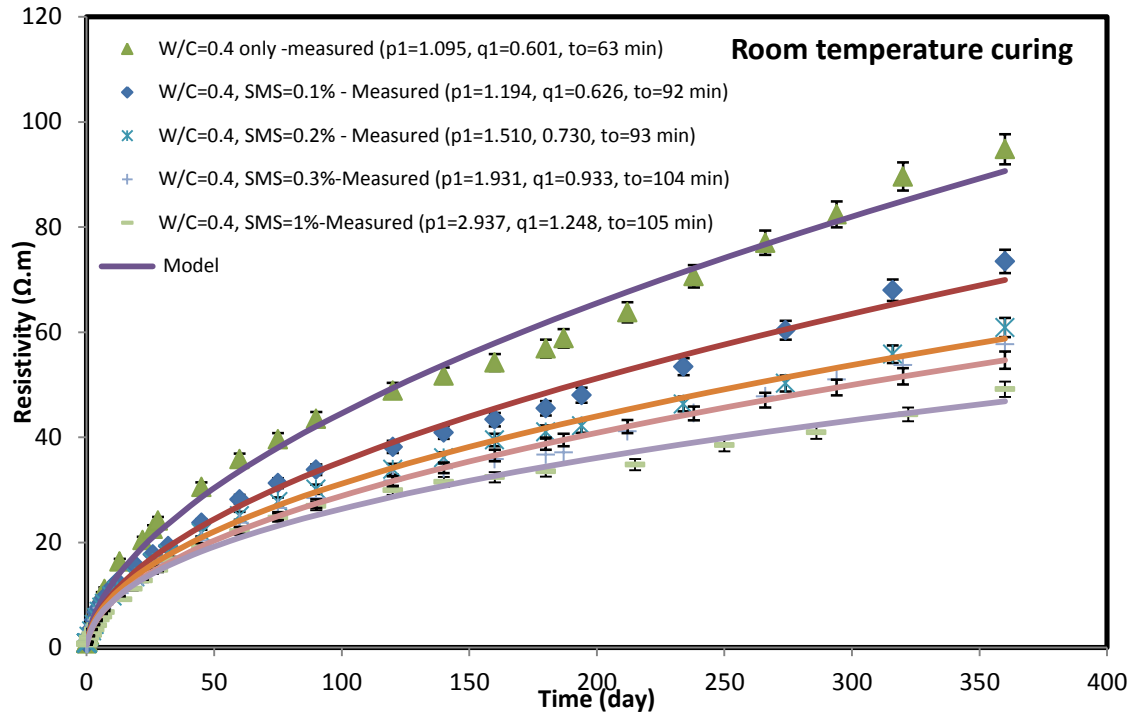


Figure 4-8: Variation of resistivity for cement specimens cured at room temperature with and without SMS up to 12 months modeled with curing model.

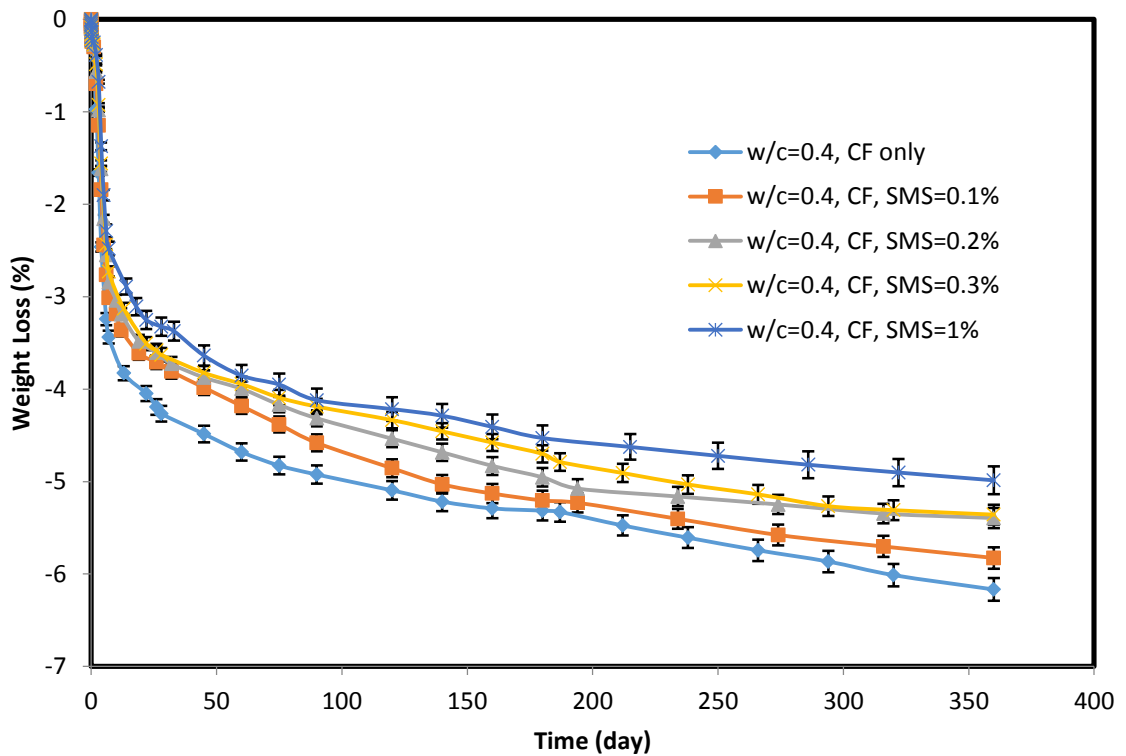


Figure 4-9: Weight loss of cement specimens cured at room temperature with and without SMS up to 12 months of curing.

The relationship between the moisture loss ($\Delta w/w_0$) and the change in the resistivity

($\Delta\rho/\rho_o$) for the smart cement sample with and without SMS was observed and a polynomial relationship was found. The relation was

$$\Delta\rho/\rho_o = C*(\Delta w/w_o)^n. \quad (4-4)$$

The experimental results matched very well (Fig. 4-10) with the model equation (4-4) and the model parameters C and n are presented in Table 4-5. The constant C varies from 0.11 to 0.54 and the constant n varies from 2.89 to 3.73. We can see from Table that the R^2 values are almost 0.99 with very good RMSE.

Table 4-5: Summary of model parameters for the relationship between the moisture loss and the change in the resistivity

Mix Type	Total moisture loss (%)	C	n	R^2	RMSE ($\Omega.m$)
w/c=0.4	6.2±0.05	0.11	3.73	0.99	1.40
w/c=0.4 SMS=0.1%	5.8±0.03	0.31	3.12	0.99	2.17
w/c=0.4 SMS=0.2%	5.4±0.03	0.38	3.04	0.99	2.14
w/c=0.4 SMS=0.3%	5.3±0.02	0.43	2.98	0.99	1.79
w/c=0.4 SMS= 1%	4.9±0.02	0.54	2.89	0.99	1.50

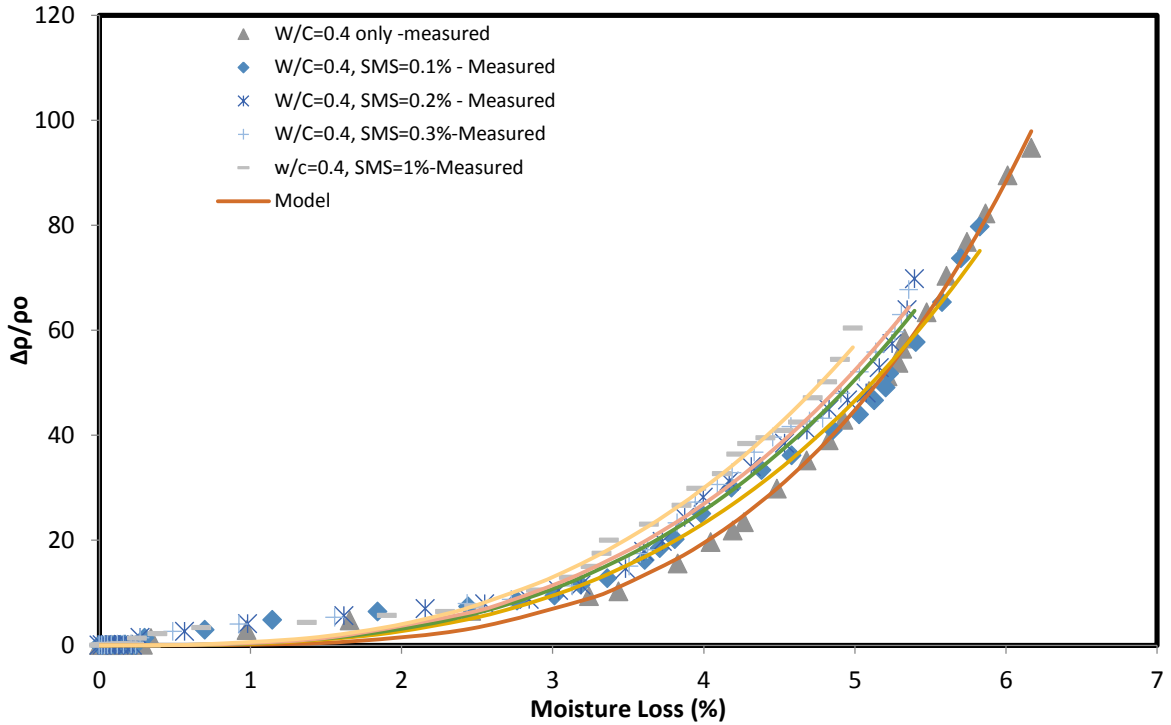


Figure 4-10: Change of resistivity with moisture loss of the cement specimens

4.2.3.3.1.3 Proposed relationship between resistivity and moisture loss

As we have seen that the rate of change of resistivity is related to the change of moisture loss, a relationship has been proposed for the resistivity of the cured specimen with the moisture loss (%) as

$$\rho = \rho_0 + D*(\Delta w/w_0)^m, \quad (4-5)$$

where,

ρ = Resistivity of the cement ($\Omega.m$)

ρ_0 = Initial resistivity of the cement without moisture loss ($\Omega.m$)

$\Delta w/w_0$ = Moisture loss of the specimen (%).

D and m are constants and are model parameters that can be determined from the experimental results. For the smart cement specimens with and without SMS, the experimental values fit very well with $R^2= 0.99$ and very good RMSE. The model

parameters are presented in Table 4-6. The constant D varies from 0.11 to 0.43 and the constant m varies from 2.89 to 3.72.

Table 4-6: Summary of model parameters for the relationship between the resistivity and the moisture loss

Mix Type	D	m	R ²	RMSE (Ω.m)
w/c=0.4	0.11	3.72	0.99	1.39
w/c=0.4, SMS=0.1%	0.28	3.12	0.99	1.97
w/c=0.4, SMS=0.2%	0.33	3.04	0.99	1.84
w/c=0.4, SMS=0.3%	0.36	2.98	0.99	1.51
w/c=0.4, SMS= 1%	0.43	2.89	0.99	1.20

4.2.3.3.2 Long time curing of the specimen without moisture loss at room temperature

The resistivity of the cement specimen with different percentage (0%, 0.1%, 0.2%, and 0.3%) of SMS was determined up to 12 months with airtight capping of the specimens and in an environment that provided no weight loss at room temperature.

Unit weight of the smart cement with w/c of 0.4 was 16.22±0.10 ppg (19.06 kN/m³) which was increased very little with SMS content. With 0.3% SMS, the unit weight increased to only 16.31±0.11 ppg (19.16 kN/m³). The initial electrical resistivity (ρ_o) of the smart cement with w/c ratio of 0.4 modified with 0.075% CF was 0.97±0.02 Ω-m and the electrical resistivity reduced to reach the ρ_{min} of 0.81±0.01 Ω-m after 180 minutes (t_{min}) as summarized in Table 4-6. Addition of SMS decreased the initial electrical resistivity and the minimum electrical resistivity but increased the time to reach the minimum (t_{min}). Addition of 0.3% SMS reduced the ρ_o by 10% and ρ_{min} by 24 %. The 24

hours electrical resistivity (ρ_{24hr}) of the smart cement was 2.34 $\Omega.m$. Hence the maximum change in electrical resistivity after 24 hours (RI_{24hr}) was 189% as summarized in Table 4-7. The 7 days and 28 days electrical resistivity (ρ_{7days} and ρ_{28days}) of the hardened smart cement were 7.24 $\Omega.m$ and 12.5 $\Omega.m$, hence the maximum change in electrical resistivity after 7 days and 28 days (RI_{7days} and $RI_{28 days}$) were 794% and 1443% respectively. The addition of SMS reduced the electrical resistivity compared to that of smart cement. Addition of 0.3% SMS reduced the 24 hours, 7 days and 28 days resistivity by about 13%, 14% and 5% respectively, hence, the maximum change in electrical resistivity i.e., RI_{24hr} , RI_{7days} and $RI_{28 days}$ were also reduced accordingly. For long term curing after 12 months, the resistivity of the smart cement was found about 26.3 $\Omega.m$, whereas the cement specimen with 0.3% SMS had a resistivity of 24.6 $\Omega.m$ which was 7% less than that of the smart cement.

The curing model parameter q_1 for smart cement only was 0.023 at 1 day of curing and increased to 0.660 with time up to 28 days and continued to increase 1.02 at 12 months. Addition of SMS increased the q_1 value and also followed the similar trend with curing time increased. The curing model parameter p_1 for smart cement only was 0.009 at 1 day of curing and increased continuously with curing time and reached to 3.823 with time up to 12 months (Table 4-8). Addition of SMS increased the parameter p_1 and reached to 0.050 with addition of 0.3% SMS and followed the similar trend with increased curing time. The curing model (Eqn. (3-11)) predicted the measured resistivity very well (Fig. 4-11). The coefficient of determination (R^2) varied from 0.95 to 0.99 and the root mean square of error (RMSE) varied from 0.041 $\Omega.m$ to 0.47 $\Omega.m$ for 1 day and 90 days of curing respectively.

4.2.3.3.3 Relationship between moisture loss and SMS content

When there is no moisture loss in the cement and the only factor that dominates is the electrical resistivity of the hardened cement with curing time is the SMS content, then the relationship between the resistivity of the cement and the SMS content are correlated with a polynomial relationship as

$$\rho = \rho_{\text{no SMS}}(t) + A \cdot (\text{SMS}\%)^n, \quad (4-6)$$

where, ρ = resistivity of the cement at any time of the moisture control specimen

$\rho_{\text{no SMS}}(t)$ = resistivity of the cement when there is no SMS and no moisture loss

A is a constant and n is model parameter that will be determined from experiment.

Table 4-7: Summary of bulk resistivity parameters for smart cement cured under no moisture loss condition at room temperature with and without SMS content

Mix Type	Density (ppg)	Initial resistivity, ρ_o ($\Omega.m$)	ρ_{min} ($\Omega.m$)	t_{min} (min)	$\rho_{24\text{hr}}$ ($\Omega.m$)	$\rho_{7 \text{ days}}$ ($\Omega.m$)	$\rho_{28 \text{ days}}$ ($\Omega.m$)	$RI_{24 \text{ hr}}$ (%)	$RI_{7 \text{ days}}$ (%)	$RI_{28 \text{ days}}$ (%)
w/c=0.4	16.22±0.10	0.97±0.02	0.81±0.01	180	2.34	7.24	12.5	189	794	1443
w/c=0.4 SMS=0.1%	16.24±0.12	0.93±0.02	0.80±0.02	240	2.28	6.70	12.0	185	738	1400
w/c=0.4 SMS=0.2%	16.26±0.12	0.89±0.01	0.75±0.02	240	2.17	6.45	11.2	189	760	1393
w/c=0.4 SMS=0.3%	16.31±0.11	0.87±0.01	0.61±0.01	300	2.02	6.20	10.8	231	916	1670

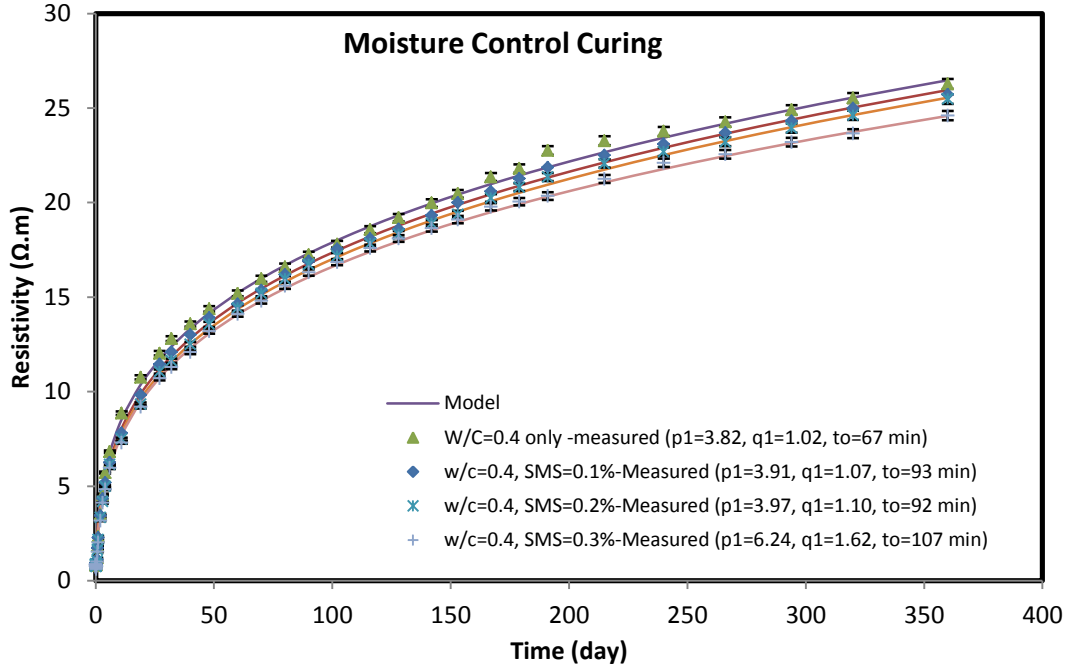


Figure 4-11: Variation of resistivity of curing cement specimen with time up to 12 months for specimens having no moisture loss modeled with curing model.

For the curing of the cement specimen cured under no moisture loss condition up to 12 months, constant A was calculated as -2.67 and parameter n was calculated as 0.7 with $R^2 = 0.98-0.99$.

After we have the model to calculate the resistivity under no moisture loss condition, we can develop relationship between the resistivity of the room condition specimen that has moisture loss. The relationship between the resistivity and the combined effect of moisture loss and SMS content are proposed as a polynomial relationship as

$$\rho = \rho_{no\ SMS}(t) + A*(SMS\%)^n + B*(\Delta w/w\%)^m + C*(SMS)^p*(\Delta w/w)^q, \quad (4-7)$$

where B and C are additional constant, and m, p, and q are model parameter that can be determined from experimental results. For the curing of the cement specimen cured under room curing condition up to 12 months, Constant B and C were calculated as 0.007 and -6.9E-05 respectively and m, p, and q were calculated as 4.95, 19.24, and 0.7 respectively

with $R^2 = 0.95-0.99$. Here the contribution of second term is 5% to 7%, third term is about 90% to 92% and the fourth term is 1% to 3%.

4.2.3.3.4 Long time curing of the specimen cured under water

4.2.3.3.4.1 Resistivity with curing time

The resistivity of the cement specimen with different percentage (0%, 0.1%, 0.2%, and 0.3%) of SMS was determined up to 360 days with specimens cured under water at room temperature. Unit weight of the smart cement with w/c of 0.4 was 16.23 ppg (19.07 kN/m³) which was increased very little with SMS content. With 0.3% SMS, the unit weight increased to only 16.32 ppg (19.17 kN/m³). The initial electrical resistivity (ρ_o) of the smart cement with w/c ratio of 0.4 modified with 0.075% CF was $0.98 \pm 0.01 \Omega\text{-m}$ and the electrical resistivity reduced to reach the ρ_{\min} of $0.80 \pm 0.01 \Omega\text{-m}$ after 180 minutes (t_{\min}) as summarized in Table 4-8.

Addition of SMS decreased the initial electrical resistivity and the minimum electrical resistivity but increased the time to reach the minimum (t_{\min}). Addition of 0.3% SMS reduced the ρ_o by 10% and ρ_{\min} by 21 %. The 24 hours electrical resistivity ($\rho_{24\text{hr}}$) of the smart cement was $2.27 \Omega\text{-m}$. Hence the maximum change in electrical resistivity after 24 hours ($RI_{24\text{hr}}$) was 184% as summarized in Table 4-9. The 7 days and 28 days electrical resistivity ($\rho_{7\text{days}}$ and $\rho_{28\text{days}}$) of the hardened smart cement were $5.23 \Omega\text{-m}$ and $8.2 \Omega\text{-m}$, hence the maximum change in electrical resistivity after 7 days and 28 days ($RI_{7\text{days}}$ and $RI_{28\text{days}}$) were 554% and 925% respectively. The addition of SMS reduced the electrical resistivity compared to that of smart cement. Addition of 0.3% SMS reduced the 24 hours, 7 days and 28 days resistivity by about 17%, 25% and 14% respectively, hence, the maximum change in electrical resistivity i.e. $RI_{24\text{hr}}$, $RI_{7\text{days}}$ and

RI_{28 days} were also reduced accordingly. For long term curing after 12 months, the resistivity of the smart cement was found about 19.93 $\Omega.m$, whereas the cement specimen with 0.3% SMS had a resistivity of 16.52 $\Omega.m$ which was 17% less than that of the smart cement.

Table 4-8: Model parameters for the curing model of the resistivity of smart cement modified with SMS cured under no moisture loss condition at room temperature up to 12 months

Mix Type	Curing Time (day)	P_{min} ($\Omega.m$)	t_{min} (min)	q_1	t_o (min)	P_1	RMSE ($\Omega.m$)	R^2
w/c=0.4	1 day	0.81	180	0.023	16	0.009	0.04	0.99
w/c=0.4 SMS=0.1%		0.80	240	0.026	28	0.010	0.04	0.98
w/c=0.4 SMS=0.2%		0.75	240	0.027	26	0.010	0.05	0.98
w/c=0.4 SMS=0.3%		0.61	300	0.110	48	0.050	0.08	0.95
w/c=0.4	7 days	0.81	180	0.305	55	0.428	0.24	0.98
w/c=0.4 SMS=0.1%		0.80	240	0.420	82	0.659	0.22	0.98
w/c=0.4 SMS=0.2%		0.75	240	0.411	80	0.628	0.19	0.98
w/c=0.4 SMS=0.3%		0.61	300	0.764	94	1.348	0.17	0.98
w/c=0.4	28 days	0.81	180	0.660	64	1.632	0.42	0.98
w/c=0.4 SMS=0.1%		0.80	240	0.721	88	1.832	0.29	0.99
w/c=0.4 SMS=0.2%		0.75	240	0.767	87	1.993	0.30	0.99
w/c=0.4 SMS=0.3%		0.61	300	1.252	103	3.764	0.25	0.99
w/c=0.4	90 days	0.81	180	0.899	66	2.996	0.47	0.99
w/c=0.4 SMS=0.1%		0.80	240	0.913	91	2.910	0.33	0.99
w/c=0.4 SMS=0.2%		0.75	240	0.885	89	2.679	0.29	0.99
w/c=0.4 SMS=0.3%		0.61	300	1.348	104	4.494	0.22	0.99
w/c=0.4	180 days	0.81	180	0.945	67	3.318	0.44	0.99
w/c=0.4 SMS=0.1%		0.80	240	0.976	92	3.321	0.33	0.99
w/c=0.4 SMS=0.2%		0.75	240	0.995	90	3.317	0.31	0.99
w/c=0.4 SMS=0.3%		0.61	300	1.444	105	5.147	0.22	0.99
w/c=0.4	360 days	0.81	180	1.021	67	3.823	0.45	0.99
w/c=0.4 SMS=0.1%		0.80	240	1.068	93	3.911	0.34	0.99
w/c=0.4 SMS=0.2%		0.75	240	1.100	92	3.976	0.32	0.99
w/c=0.4 SMS=0.3%		0.61	300	1.621	107	6.424	0.26	0.99

The curing model parameter q_1 for smart cement only was 0.022 at 1 day of curing and increased continuously to 0.668 with time up to 12 months of curing. Addition of SMS increased the q_1 value and also followed the similar trend with curing time increases. The curing model parameter p_1 for smart cement only was 0.009 at 1 day of curing and increased continuously with time up and reached to 2.279 after 12 months of curing (Table 4-10). Addition of SMS increases the parameter p_1 up to 0.055 with 0.3% SMS and followed the similar trend with increased curing time. The curing model (Eqn. (3-11)) predicted the measured resistivity very well (Fig. 4-12). The coefficient of determination (R^2) varied from 0.95 to 0.99 and the root mean square of error (RMSE) varied from 0.041 $\Omega.m$ to 0.44 $\Omega.m$ for 1 day and 360 days of curing respectively.

Table 4-9: Summary of bulk resistivity parameters for smart cement cured under water at room temperature with and without SMS content

Mix Type	Density (ppg)	Initial resistivity, ρ_o ($\Omega.m$)	ρ_{min} ($\Omega.m$)	t_{min} (min)	ρ_{24hr} ($\Omega.m$)	$\rho_{7\text{ days}}$ ($\Omega.m$)	$\rho_{28\text{ days}}$ ($\Omega.m$)	$RI_{24\text{ hr}}$ (%)	$RI_{7\text{ days}}$ (%)	$RI_{28\text{ days}}$ (%)
w/c=0.4	16.23±0.12	0.98±0.01	0.80±0.01	180	2.27	5.23	8.2	184	554	925
w/c=0.4 SMS=0.1%	16.25±0.12	0.94±0.01	0.88±0.01	240	2.13	4.18	7.6	142	375	764
w/c=0.4 SMS=0.2%	16.28±0.12	0.90±0.02	0.76±0.01	240	2.05	4.04	7.34	170	432	866
w/c=0.4 SMS=0.3%	16.32±0.12	0.88±0.02	0.63±0.02	300	1.89	3.90	7.04	200	519	1017

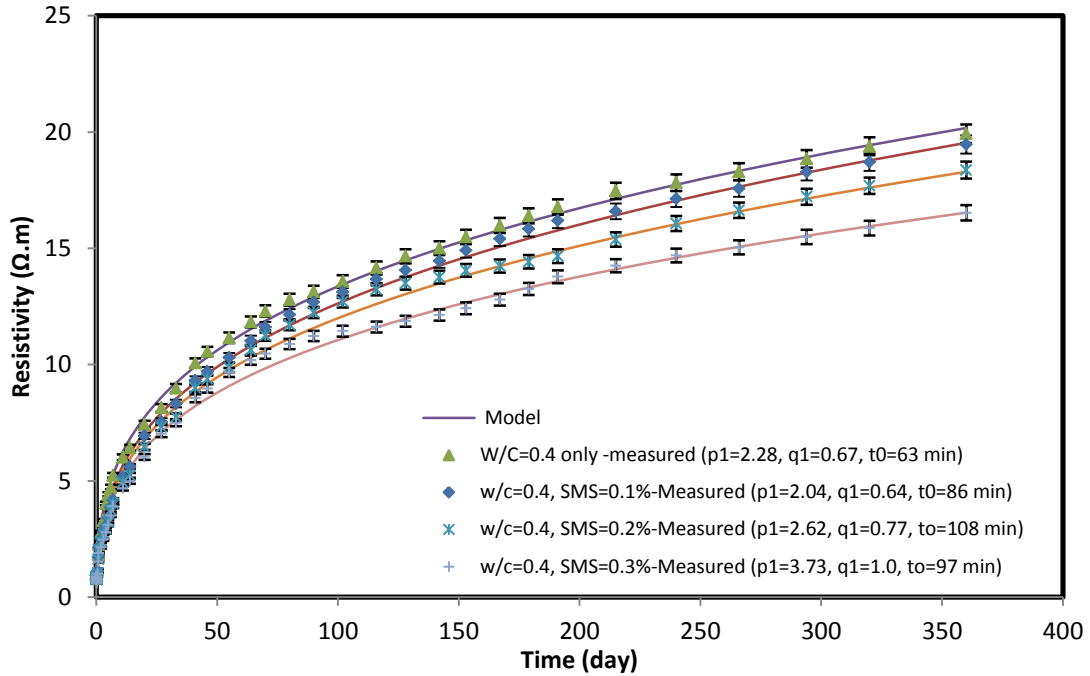


Figure 4-12: Variation of resistivity of curing cement specimen with time up to 12 months for specimens cured under water modeled with curing model

4.2.3.3.4.2 Moisture gain and its effect on the resistivity

During the curing period, the weight of the specimens was monitored to observe any change. This time, the specimens gained weight with time. The percent weight gain was calculated from the initial weight of the specimen. Here, the weight gain was almost equal for all of the specimens irrespective of the amount of SMS in the specimens. After 7 days, the weight gain was about 0.9% which increased to about 1.3 % after 28 days of curing. After 12 months of curing, the weight gain was about 1.89 ± 0.04 % (Fig. 4-13).

The relationship between the moisture gain ($\Delta w/w_0$) and the change in the resistivity ($\Delta \rho/\rho_0$) for the smart cement sample with and without SMS cured under water was observed and a polynomial relationship was found. The relation was

$$\Delta \rho/\rho_0 = E^*(\Delta w/w_0)^{n1}. \quad (4-6)$$

Table 4-10: Model parameters for the curing model of the resistivity of smart cement modified with SMS cured under water at room temperature up to 12 months

Mix Type	Curing Time (day)	ρ_{\min} ($\Omega.m$)	t_{\min} (min)	q_1	t_o (min)	p_1	RMSE ($\Omega.m$)	R^2
w/c=0.4	1 day	0.80	180	0.022	16	0.009	0.04	0.99
w/c=0.4 SMS=0.1%		0.88	240	0.029	30	0.011	0.03	0.99
w/c=0.4 SMS=0.2%		0.76	240	0.049	48	0.019	0.05	0.98
w/c=0.4 SMS=0.3%		0.63	300	0.117	48	0.055	0.08	0.99
w/c=0.4	7 days	0.80	180	0.176	18	0.217	0.32	0.95
w/c=0.4 SMS=0.1%		0.88	240	0.456	81	1.199	0.15	0.98
w/c=0.4 SMS=0.2%		0.76	240	0.599	104	1.812	0.15	0.98
w/c=0.4 SMS=0.3%		0.63	300	0.168	57	1.970	0.35	0.99
w/c=0.4	28 days	0.80	180	0.538	61	1.558	0.21	0.99
w/c=0.4 SMS=0.1%		0.88	240	0.387	79	0.885	0.15	0.99
w/c=0.4 SMS=0.2%		0.76	240	0.482	100	1.173	0.15	0.99
w/c=0.4 SMS=0.3%		0.63	300	0.643	88	1.565	0.24	0.99
w/c=0.4	90 days	0.80	180	0.507	60	1.411	0.19	0.99
w/c=0.4 SMS=0.1%		0.88	240	0.416	80	0.993	0.14	0.99
w/c=0.4 SMS=0.2%		0.76	240	0.482	100	1.160	0.14	0.99
w/c=0.4 SMS=0.3%		0.63	300	0.660	89	1.718	0.16	0.99
w/c=0.4	180 days	0.80	180	0.582	61	1.790	0.22	0.99
w/c=0.4 SMS=0.1%		0.88	240	0.505	83	1.365	0.23	0.99
w/c=0.4 SMS=0.2%		0.76	240	0.633	105	1.839	0.31	0.99
w/c=0.4 SMS=0.3%		0.63	300	0.920	96	3.145	0.35	0.99
w/c=0.4	360 days	0.80	180	0.668	63	2.280	0.33	0.99
w/c=0.4 SMS=0.1%		0.88	240	0.641	86	2.044	0.44	0.99
w/c=0.4 SMS=0.2%		0.76	240	0.771	108	2.624	0.41	0.99
w/c=0.4 SMS=0.3%		0.63	300	1.00	97	3.730	0.35	0.99

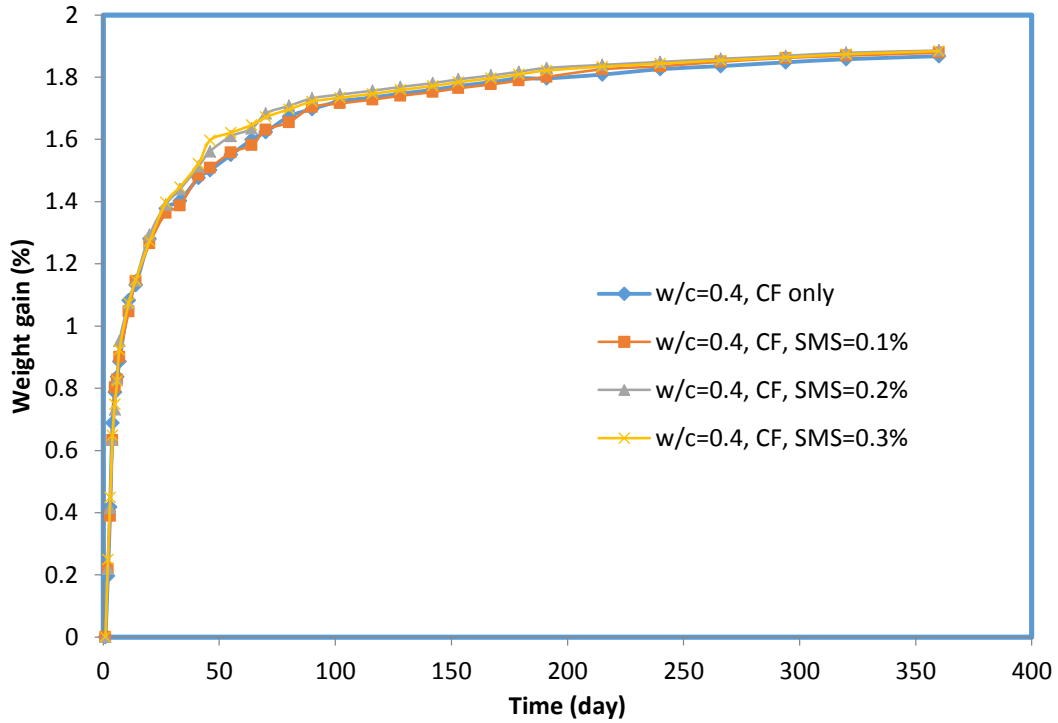


Figure 4-13: Weight gain of the cement specimens with time up to 12 months for specimens cured under water.

The experimental results was matched very well (Fig. 4-14) with the model equation (4-6) and the model parameters E and n1 are presented in Table 4-11. The constant E varies from 2.72 to 3.72 and the constant n1 varies from 2.48 to 2.97. We can see from Table that the R² values are 0.97-0.98 with very good RMSE.

Table 4-11: Summary of model parameters for the relationship between the moisture gain and the change in the resistivity

Mix Type	Total moisture gain (%)	E	n1	R ²	RMSE (Ω.m)
w/c=0.4	1.87±0.04	3.72	2.48	0.97	0.96
w/c=0.4 SMS=0.1%	1.87±0.03	3.12	2.79	0.98	0.78
w/c=0.4 SMS=0.2%	1.88±0.02	2.66	2.97	0.97	0.94
w/c=0.4 SMS=0.3%	1.89±0.04	2.72	2.81	0.98	0.86

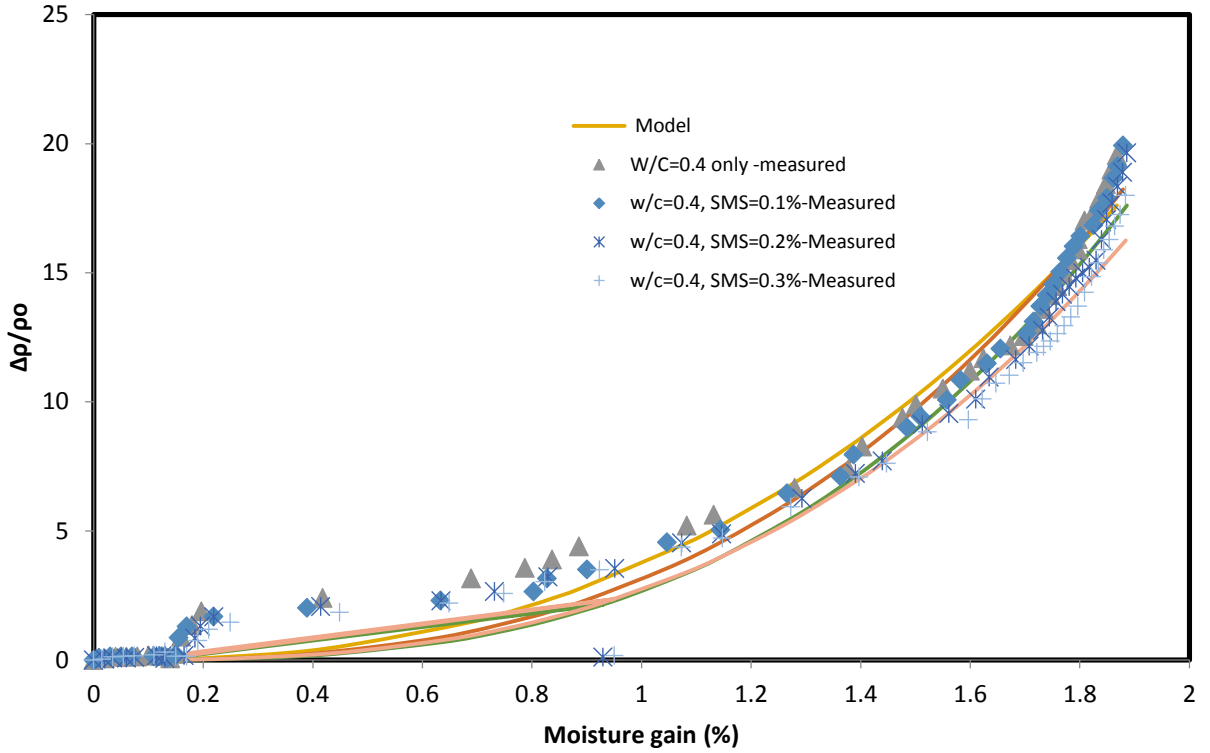


Figure 4-14: Change of resistivity with moisture gain of the cement specimens

4.2.3.3.4.3 Proposed relationship between resistivity and moisture gain

As we have seen that the rate of change of resistivity is related to the change of moisture gain, a relationship has been proposed for the resistivity of the cured specimen with the moisture gain (%) as

$$\rho = \rho_0 + F * (\Delta w / w_0)^{m1}, \quad (4-7)$$

where,

ρ = Resistivity of the cement ($\Omega.m$)

ρ_0 = Initial resistivity of the cement without moisture gain ($\Omega.m$)

$\Delta w / w_0$ = Moisture loss of the specimen (%).

F and m1 are constants and are model parameters that can be determined from the experimental results. For the smart cement specimens with and without SMS, the

experimental values fit very well with $R^2 = 0.99$ and very good RMSE. The model parameters are presented in Table 4-12. The constant F varies from 2.34 to 3.60 and the constant m1 varies from 2.49 to 2.98.

Table 4-12: Summary of model parameters for the relationship between the resistivity and the moisture loss

Mix Type	F	m1	R^2	RMSE ($\Omega.m$)
w/c=0.4	3.60	2.49	0.97	0.93
w/c=0.4, SMS=0.1%	2.90	2.79	0.98	0.73
w/c=0.4, SMS=0.2%	2.35	2.98	0.97	0.85
w/c=0.4, SMS=0.3%	2.34	2.84	0.97	0.77

4.2.3.3.5 Minimum resistivity with respect to SMS concentration

SMS decreased the minimum resistivity of the smart cement. The minimum resistivity (ρ_{\min}) of the smart cement decreased from 0.83 $\Omega.m$ to 0.54 $\Omega.m$ with 1% SMS, a 30% decrease. The relationship between minimum resistivity and SMS concentration has been modeled with hyperbolic model

$$\rho_{\min} = (\rho_{\min})_o - S/(G + HS), \quad (4-8)$$

where,

ρ_{\min} = minimum resistivity of the cement ($\Omega.m$)

$(\rho_{\min})_o$ = minimum resistivity of the cement without SMS ($\Omega.m$)

S = concentration of sodium meta-silicate (% by weight).

Parameters G and H are model parameters and parameter G represent the initial rate of change and parameter H determines the ultimate resistivity. Experimental results matched very well (Fig. 4-15) with the proposed model with coefficient of determination (R^2) of

0.95 and parameters G and H were found as $1.57 \text{ Ohm}^{-1}\text{-m}^{-1}$ and $2.28 \text{ Ohm}^{-1}\text{-m}^{-1}$.

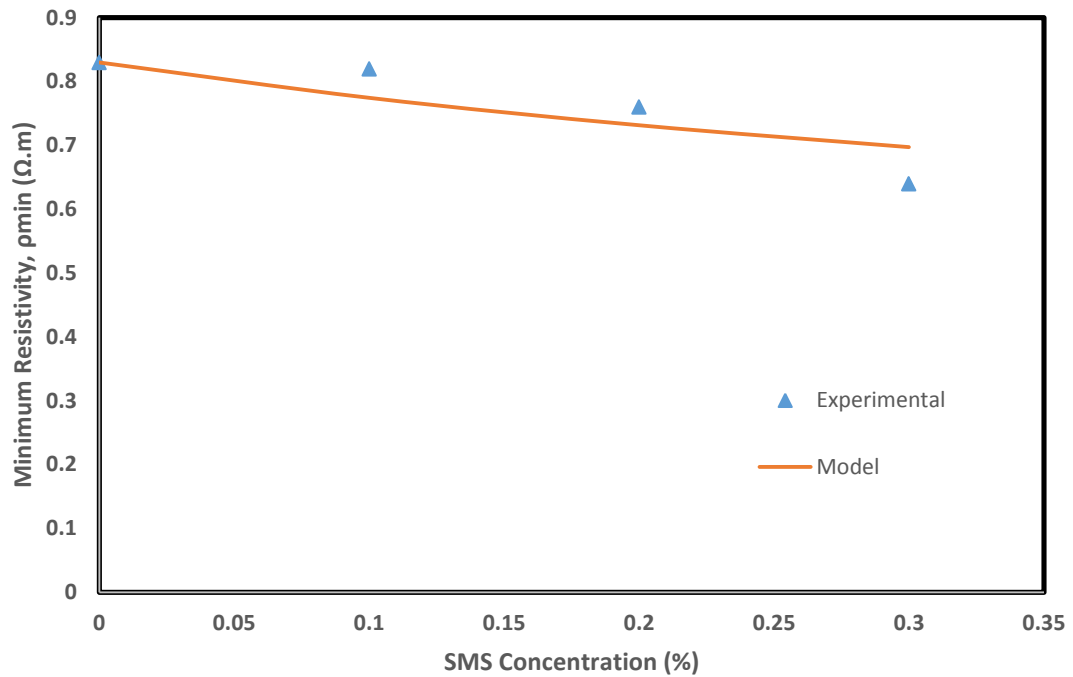


Figure 4-15: Relationship between the minimum resistivity and SMS concentration

4.2.4 Piezoresistivity and strength of smart cement

Addition of 0.1% conductive filler (CF) substantially improved piezoresistive behavior of the cement. Based on experimental results, p-q model developed by Vipulanandan and Paul (1990) was modified and used to predict the change in electrical resistivity of cement with applied stress for 1, 7 and 28 days of curing as described by Eqn 3-15.

4.2.4.1 1 day of curing

The compressive strength (σ_f) of the smart cement was 6.58 MPa which decreased to 6.55 MPa, 6.15 MPa and 5.71 MPa, by addition of 0.1%, 0.2% and 0.3% SMS respectively after 1 day of curing. So the strength of the smart cement decreased by

0.5%, 6% and 12% by addition of 0.1%, 0.2% and 0.3% SMS respectively as summarized in Table 4-13.

The change in electrical resistivity at failure $\left(\frac{\Delta\rho}{\rho_o}\right)_f$ for the unmodified smart cement was 545% which was reduced to 390%, 335% and 255% respectively as summarized in Table 4-13. With 0.3% SMS addition to the smart cement, the change in electrical resistivity at failure $\left(\frac{\Delta\rho}{\rho_o}\right)_f$ was reduced about 53% from that of the smart cement.

Using the p-q Piezoresistive model (Eqn. (3-15)), the relationships between compressive stress and the change in electrical resistivity $\left(\frac{\Delta\rho}{\rho_o}\right)$ of the smart cement with different SMS content of 0%, 0.1%, 0.2% and 0.3% for one day of curing were modeled. The piezoresistive model (Eqn. (3-15)) predicted the measured stress- change in resistivity relationship very well (Fig. 4-16). The model parameters q_2 and p_2 are summarized in Table 4-13. The coefficients of determination (R^2) were 0.97 to 0.99. The root mean square of error (RMSE) varied between 0.08 MPa and 0.14 MPa as summarized in Table 4-13.

Rate of change of resistivity with respect to stress change:

As we have considered the rate of resistivity change $\Delta\rho/\rho_o$ as X, and if we consider the stress as Y, then the slope dX/dY , which is rate of change of resistivity with respect to stress change could be another indicator of the piezoresistivity. For 1 day of curing, the rate of change of resistivity (dX/dY) without any sodium metasilicate is about 80 (%/MPa) which increases slowly and slightly changes the slope before the specimen cracks. With addition of 0.3% SMS, the rate of change of resistivity (dX/dY) decreased

upto 40 (%/MPa) which increases suddenly or changes the slope when the cement specimen experiences cracks (Figure 4-17).

Table 4-13: Peak stress, piezoresistivity, model parameters p₂, q₂ and R² & RMSE for the piezoresistivity model for the cement specimens under compressive stress after 1 day, 7 days and 28 days.

Mix Type	Curing Time (day)	Strength σ_f (MPa)	Piezoresistivity at peak stress, $(\Delta\rho/\rho_o)_f$ (%)	p ₂	q ₂	R ²	RMSE (MPa)
w/c=0.4	1 day	6.58	545	0.001	0.95	0.97	0.14
w/c=0.4 SMS=0.1%		6.55	390	0.001	1.34	0.99	0.09
w/c=0.4 SMS=0.2%		6.15	335	0.002	1.12	0.99	0.09
w/c=0.4 SMS=0.3%		5.71	255	0.319	1.05	0.99	0.08
w/c=0.4		28.54	523	0.05	1.23	0.97	1.45
w/c=0.4 SMS=0.1%	7 days	26.35	332	2.5	1.3	0.97	1.38
w/c=0.4 SMS=0.2%		25.23	300	3	1.4	0.95	1.54
w/c=0.4 SMS=0.3%		24.48	230	5.7	1.65	0.96	1.52
w/c=0.4		36.23	315	0.12	1.06	0.99	0.58
w/c=0.4 SMS=0.1%	28 days	36.10	250	0.75	1.25	0.97	1.81
w/c=0.4 SMS=0.2%		35.16	170	0.8	0.96	0.96	2.01
w/c=0.4 SMS=0.3%		34.68	145	0.68	0.8	0.95	1.74
w/c=0.4							

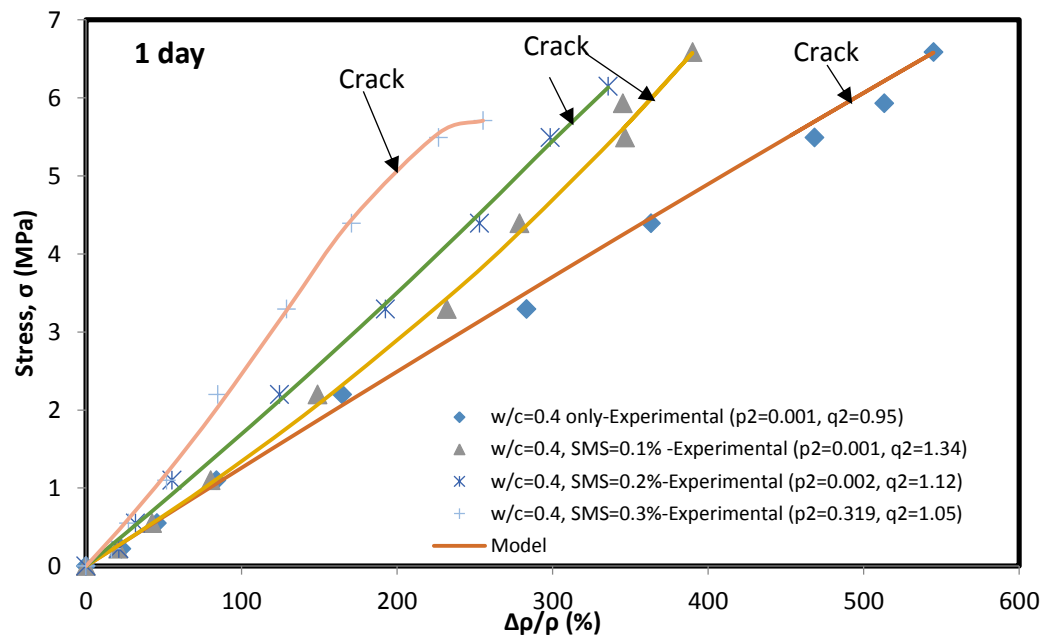


Figure 4-16: Piezoresistive response of the cement with and without SMS after 1 day of curing modeled with p-q model.

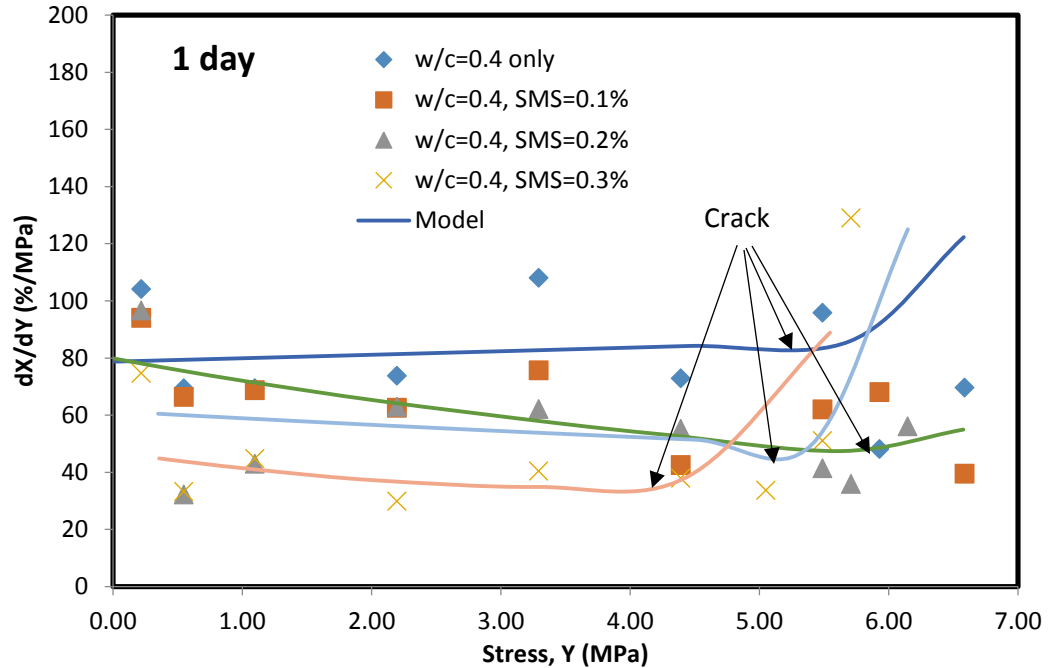


Figure 4-17: Rate of change of resistivity with respect to stress vs Stress for 1 day of curing

4.2.4.2 7 days of curing

The compressive strength (σ_f) of the smart cement was 28.54 MPa which decreased to 26.35 MPa, 25.23 MPa and 24.48 MPa, by addition of 0.1%, 0.2% and 0.3% SMS respectively after 7 days of curing. So the strength of the smart cement decreased by 7%, 11% and 14% by addition of 0.1%, 0.2% and 0.3% SMS respectively as summarized in Table 4-13.

The change in electrical resistivity at failure $\left(\frac{\Delta\rho}{\rho_0}\right)_f$ for the unmodified smart cement was 523% which was reduced to 332%, 300% and 230% respectively as summarized in Table 4-13. With 0.3% SMS addition to the smart cement, the change in electrical resistivity at failure $\left(\frac{\Delta\rho}{\rho_0}\right)_f$ was reduced about 56% from that of the smart cement.

Using the p-q Piezoresistive model (Eqn. (3-15)), the relationships between compressive stress and the change in electrical resistivity $\left(\frac{\Delta\rho}{\rho_0}\right)$ of the smart cement with different SMS content of 0%, 0.1%, 0.2% and 0.3% for one day of curing were modeled. The piezoresistive model (Eqn. (3-15)) predicted the measured stress- change in resistivity relationship very well (Fig. 4-18). The model parameters q_2 and p_2 are summarized in Table 4-13. The coefficients of determination (R^2) were 0.95 to 0.97. The root mean square of error (RMSE) varied between 1.38 MPa and 1.54 MPa as summarized in Table 4-13.

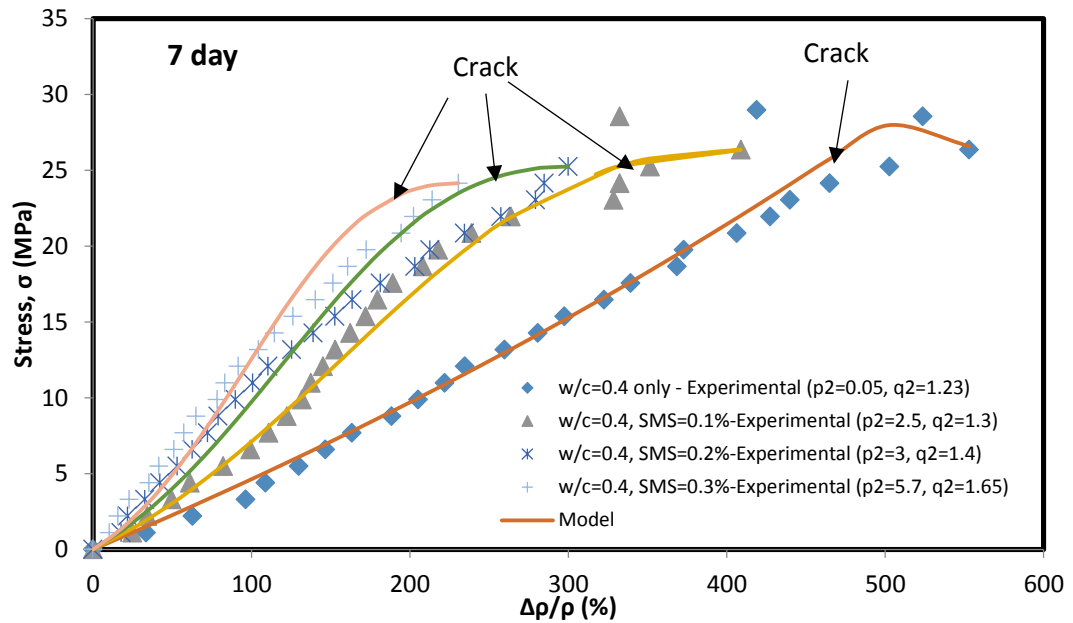


Figure 4-18: Piezoresistive response of the cement with and without SMS after 7 days of curing modeled with p-q model.

Rate of change of resistivity with respect to stress change:

For 7 days of curing, the rate of change of resistivity (dX/dY) without any sodium meta-silicate is about 22 (%/MPa) which decreases very slowly and then changes the

slope when the specimen cracks. With addition of 0.3% SMS, the rate of change of resistivity (dX/dY) decreased upto 8 (%/MPa) which increased sharply when the cement specimen experienced cracks (Fig. 4-19).

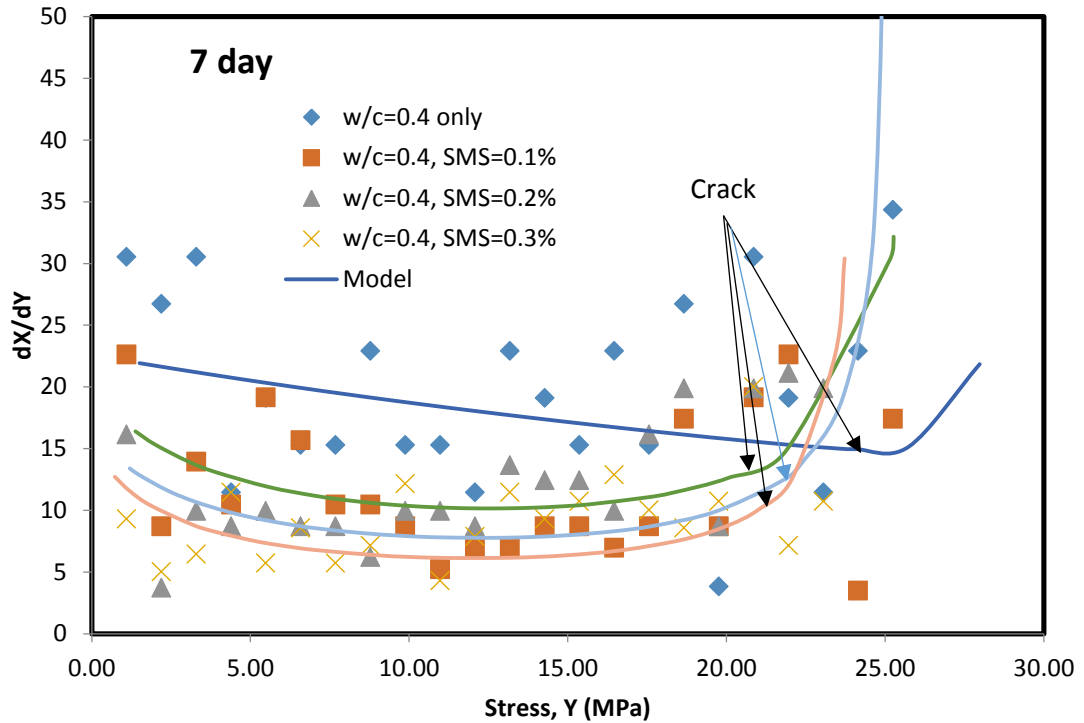


Figure 4-19: Rate of change of resistivity with respect to stress vs Stress for 7 days curing

4.2.4.3 28 days of curing

The compressive strength (σ_f) of the smart cement was 36.23 MPa which decreased to 36.10 MPa, 35.16 MPa and 34.68 MPa, by addition of 0.1%, 0.2% and 0.3% SMS respectively after 28 days of curing. So the strength of the smart cement decreased by 0.4%, 3% and 4% by addition of 0.1%, 0.2% and 0.3% SMS respectively as summarized in Table 4-13.

The change in electrical resistivity at failure $\left(\frac{\Delta\rho}{\rho_o}\right)_f$ for the unmodified smart cement was 315% which was reduced to 250%, 170% and 145% respectively as

summarized in Table 4-13. With 0.3% SMS addition to the smart cement, the change in electrical resistivity at failure $\left(\frac{\Delta\rho}{\rho_o}\right)_f$ was reduced about 54% from that of the smart cement.

Using the p-q Piezoresistive model (Eqn. (3-15)), the relationships between compressive stress and the change in electrical resistivity $\left(\frac{\Delta\rho}{\rho_o}\right)$ of the smart cement with different SMS content of 0%, 0.1%, 0.2% and 0.3% for one day of curing were modeled. The piezoresistive model (Eqn. (3-15)) predicted the measured stress- change in resistivity relationship very well (Fig. 4-20). The model parameters q_2 and p_2 are summarized in Table 4-13. The coefficients of determination (R^2) were 0.95 to 0.99. The root mean square of error (RMSE) varied between 0.58 MPa and 2.01 MPa as summarized in Table 4-13.

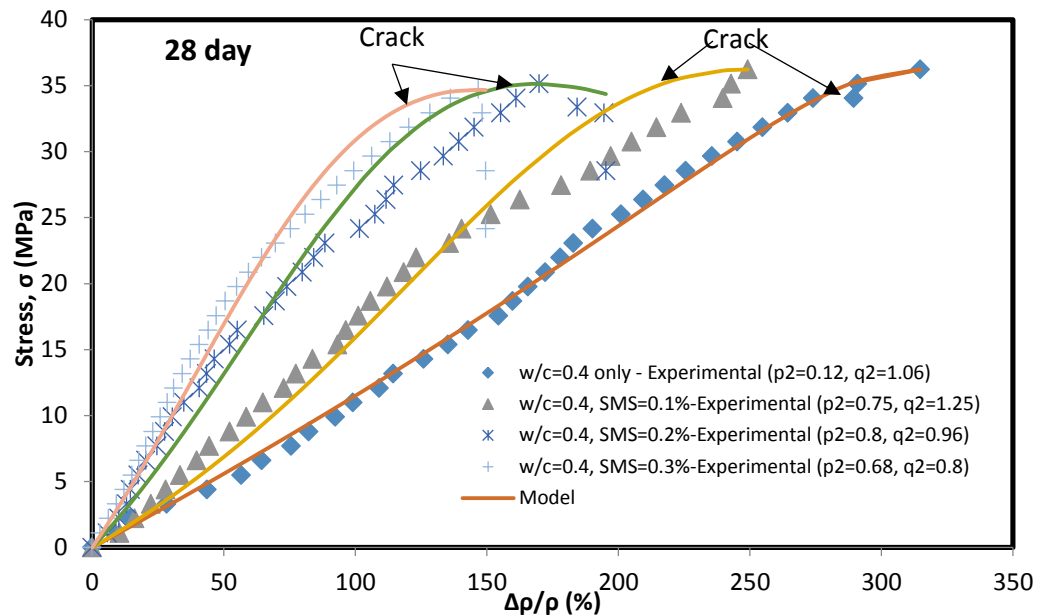


Figure 4-20: Piezoresistive response of the cement with and without SMS after 28 days of curing.

Rate of change of resistivity rate with respect to stress change:

For 28 days of curing, the rate of change of resistivity (dX/dY) without any sodium meta-silicate is about 10 (%/MPa) which almost remain constant and then increased sharply when the specimen cracks. With addition of 0.3% SMS, the rate of change of resistivity (dX/dY) decreased up to 4 (%/MPa) which increased sharply when the cement specimen experiences cracks (Fig. 4-21).

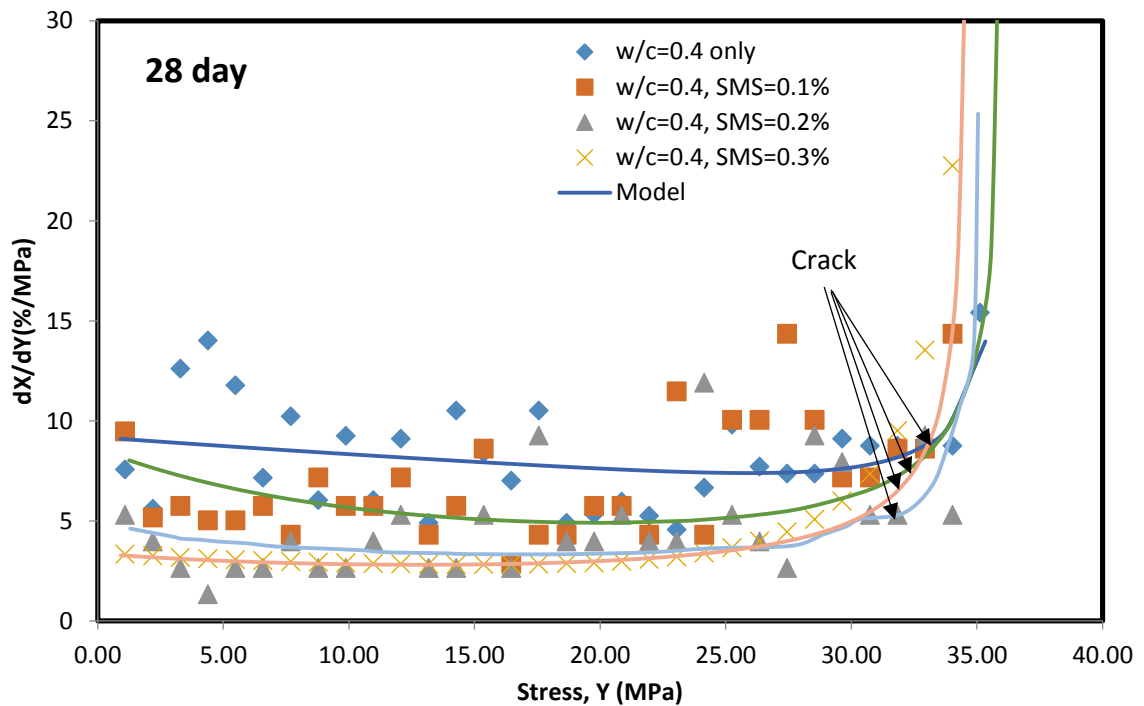


Figure 4-21: Rate of change of resistivity with respect to stress vs Stress for 28 days curing

4.2.4.4 Relationship between SMS concentration and strength/piezoresistivity

The strength of the cement specimen made with and without SMS was observed. The addition of SMS decreased the compressive strength of the smart cement. The relationship between the compressive strength of the cement and SMS concentration has been modeled with the hyperbolic model

$$\sigma_c = (\sigma_c)_o - S/(J + KS), \quad (4-9)$$

where,

σ_c = Compressive strength of the cement (MPa)

$(\sigma_c)_o$ = Compressive strength of the cement without SMS (MPa)

S = Concentration of sodium meta-silicate (% by weight)

Parameters J and K are model parameters and parameter J represent the initial rate of change and parameter K determines the ultimate strength. Experimental results matched very well (Fig. 4-22) with the proposed model with coefficient of determination (R^2) of 0.99. For 1 day strength test, parameters J and K were found as 0.93 MPa^{-1} and -1.95 MPa^{-1} . For 7 days strength test, parameters J and K were found as 0.03 MPa^{-1} and 0.14 MPa^{-1} . For 28 days strength test, parameters J and K were found as 0.35 MPa^{-1} and -0.54 MPa^{-1} .

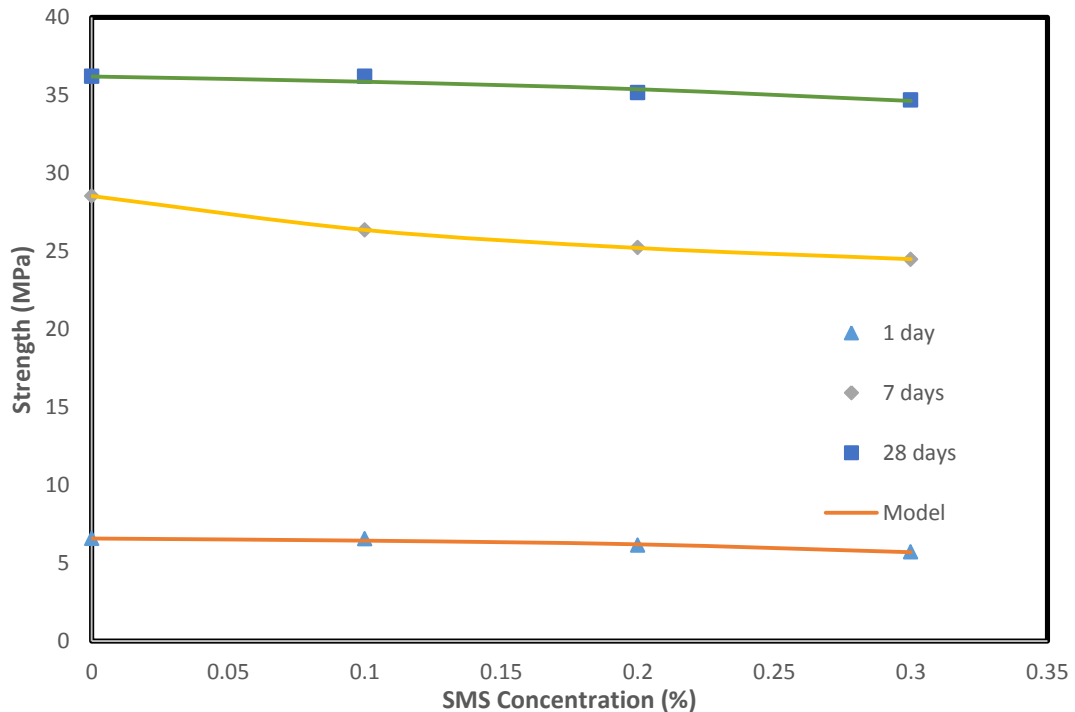


Figure 4-22: Relationship between compressive strength and SMS concentration

The piezoresistivity at failure of the cement specimen made with and without SMS was observed. The addition of SMS decreased the piezoresistivity at failure of the smart cement. The relationship between the piezoresistivity at failure of the cement and SMS concentration has been modeled with the hyperbolic model:

$$\Delta\rho/\rho_o = (\Delta\rho/\rho_o)_o - S/(L +MS), \quad (4-10)$$

where,

$\Delta\rho/\rho_o$ = Piezoresistivity at failure (%)

$(\Delta\rho/\rho_o)_o$ = Piezoresistivity at failure of the grout without SMS (%)

S = Concentration of sodium meta-silicate (% by weight)

Parameters L and M are model parameters and parameter L represent the initial rate of change and parameter M determines the ultimate piezoresistivity. Experimental results matched very well (Fig. 4-23) with the proposed model with coefficient of determination (R^2) of 0.99. For 1 day test, parameters L and M were found as 0.0005 and 0.0018. For 7 days, parameters L and M were found as 0.0003 and 0.0026. For 28 days strength test, parameters L and M were found as 0.0011 and 0.0019.

4.2.4.5 Relationship between RI_{24} and strength/piezoresistivity

The strength of the cement specimen and the resistivity index after 24 hours (RI_{24}) was observed to find whether any relationship can be obtained or not. The compressive strength has been found linearly related (Fig. 4-24) to the resistivity index after 24 hours (RI_{24}) of the cement grout. The relations are as follows:

- (i) For 1 day strength, $\sigma_c = -0.0176*(RI_{24}) + 9.52$, $R2 = 0.75$
- (ii) For 7 days strength, $\sigma_c = -0.0518*(RI_{24}) + 35.7$, and $R2 = 0.72$
- (iii) For 28 days strength, $\sigma_c = -0.0288*(RI_{24}) + 40.9$. $R2 = 0.65$

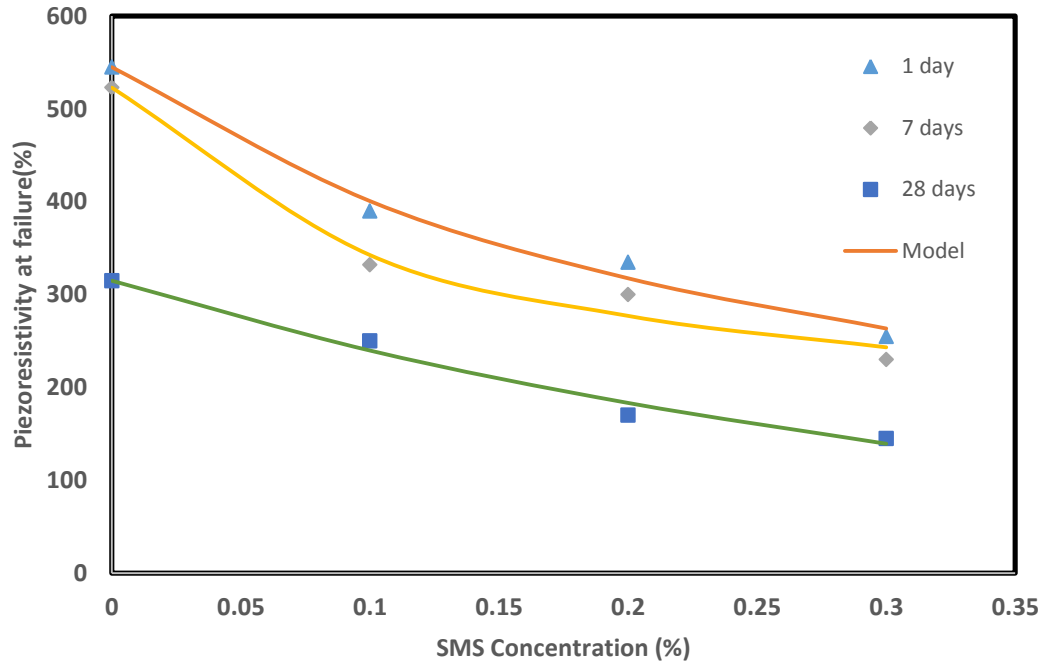


Figure 4-23: Relationship between piezoresistivity at failure and SMS concentration

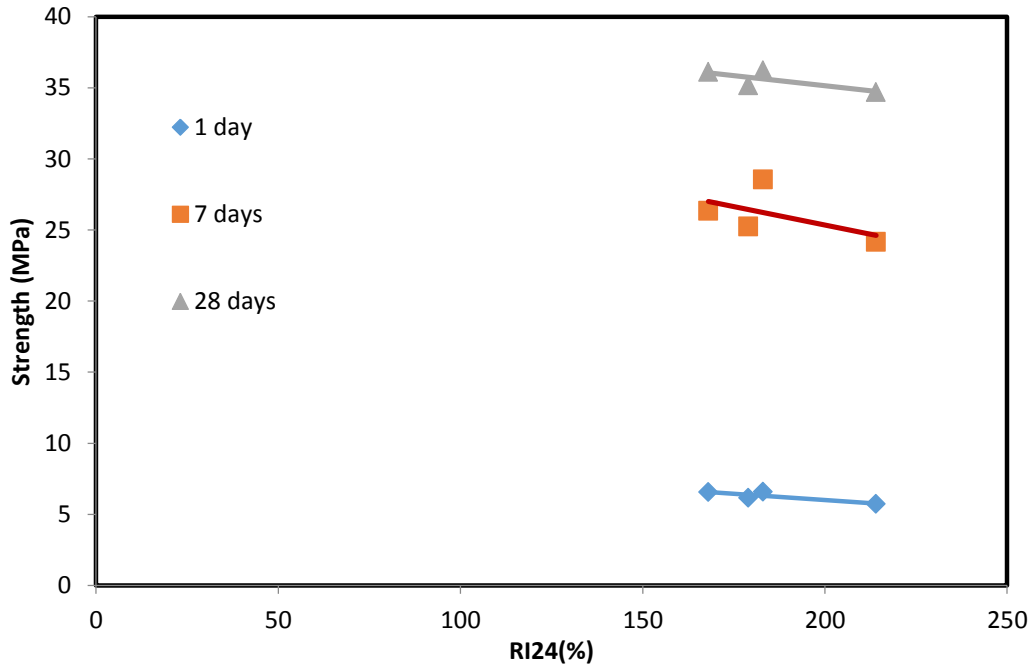


Figure 4-24: Relationship between RI24hr and compressive strength

4.2.4.6 Relationship between curing time and strength/piezoresistivity at failure

The strength of the cement specimen made with and without SMS was observed up to 28 days. With curing time increases, the compressive strength of the cement increased. The relationship between the compressive strength of the cement and curing time has been modeled with the hyperbolic model

$$\sigma_c = t/(N + Pt), \quad (4-11)$$

where,

σ_c = Compressive strength of the cement (MPa)

t = Curing time (day)

Parameters N and P are model parameters and parameter N represent the initial rate of change and parameter P determines the ultimate strength. For the smart cement, experimental results matched very well (Fig. 4-25, Table 4-14) with the proposed model with coefficient of determination (R^2) of 0.98-0.99.

Table 4-14: Model Parameters for the relationship between strength and curing time

Mix Type	N	P	R^2	RMSE (MPa)
w/c=0.4	0.094	0.023	0.98	1.50
w/c=0.4 SMS=0.1%	0.110	0.023	0.99	0.75
w/c=0.4 SMS=0.2%	0.117	0.024	0.99	0.69
w/c=0.4 SMS=0.3%	0.128	0.024	0.99	0.59

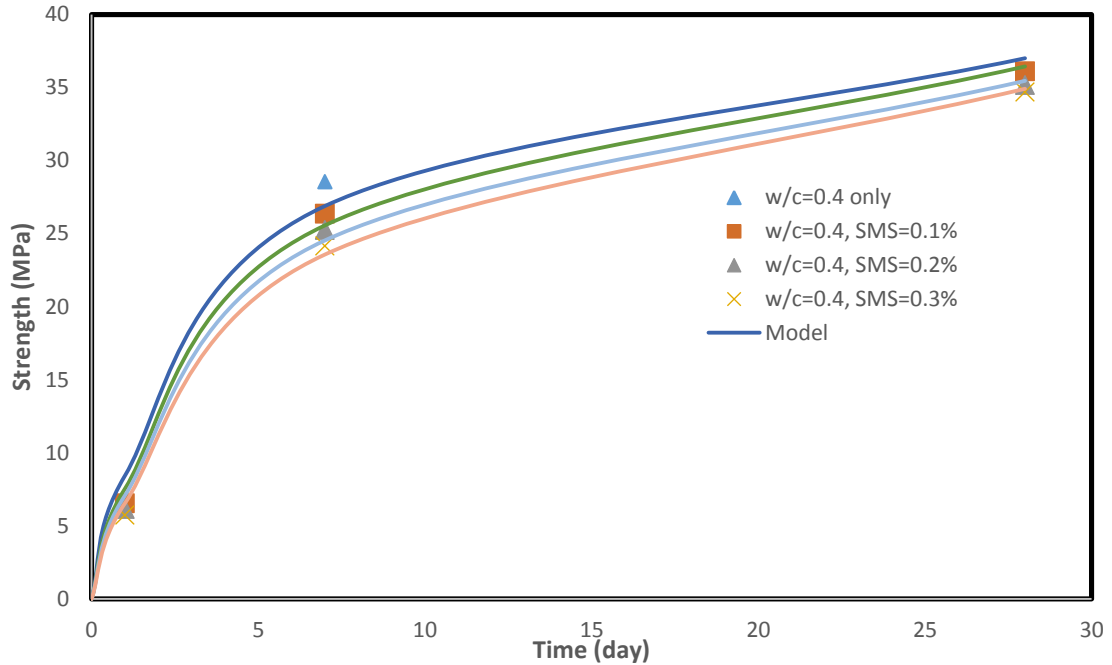


Figure 4-25: Relationship between compressive strength and curing time

The piezoresistivity at failure of the cement specimen made with and without SMS was observed up to 28 days. With curing time increases, the piezoresistivity at failure of the cement changes. The relationship between the piezoresistivity at failure of the cement grout and curing time has been modeled with the hyperbolic model

$$\Delta\rho/\rho_o = (\Delta\rho/\rho_o)_1 - t/(Q + Rt), \quad (4-12)$$

where,

$\Delta\rho/\rho_o$ = Piezoresistivity at failure (%)

$(\Delta\rho/\rho_o)_1$ = Piezoresistivity at failure of the cement after 1 day (%)

t = Curing time (day)

Parameters Q and R are model parameters and parameter Q represent the initial rate of change and parameter R determines the ultimate piezoresistivity. For the cement samples, experimental results matched very well (Fig. 4-26, Table 4-15) with the proposed model with coefficient of determination (R^2) of 0.95-0.99.

Table 4-15: Model Parameters for the relationship between strength and curing time

Mix Type	Q	R	R ²	RMSE (%)
w/c=0.4	0.390	-0.009	0.99	1.53
w/c=0.4 SMS=0.1%	0.102	0.003	0.99	5.68
w/c=0.4 SMS=0.2%	0.216	-0.001	0.99	2.73
w/c=0.4 SMS=0.3%	0.29	-0.001	0.99	1.98

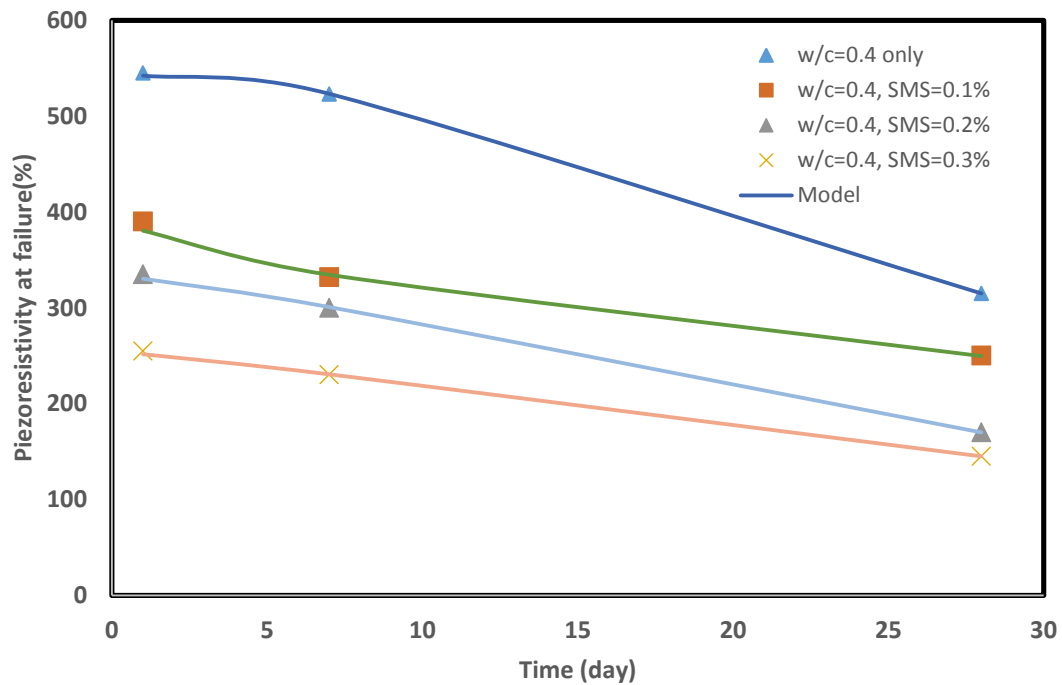


Figure 4-26: Relationship between piezoresistivity at failure and curing time

4.3 Effects of Temperature and Curing Environment on the Piezoresistive Behavior of the Smart Cement with and without Sodium Meta-silicate

4.3.1 Resistivity during curing at high temperature

The change of electrical resistivity with curing time for the cement specimens made with smart cement only and smart cement with 0.3% SMS cured in an oven at temperature 80° C under two different conditions was observed. The first condition is that

the sample is left in oven only and the second condition is that the sample is placed in saturated sand and then placed in the oven. The resistivity of the cement specimen for smart cement only and smart cement with 0.3% SMS both for oven cured and for oven cured in saturated sand was determined up to 28 days at 80° C temperature. The oven cured specimens were subjected to normal evaporation. Unit weight of the smart cement with w/c ratio of 0.4 was 16.2 ± 0.14 ppg (19.04 kN/m^3) which was increased to 16.3 ± 0.11 ppg (19.15 kN/m^3) with 0.3% SMS. The normal trend of the resistivity of the cured cement is that the resistivity is decreased up to a certain time (t_{\min}) and reached to a minimum resistivity (ρ_{\min}) and then starts increasing with time (Fig. 4-27).

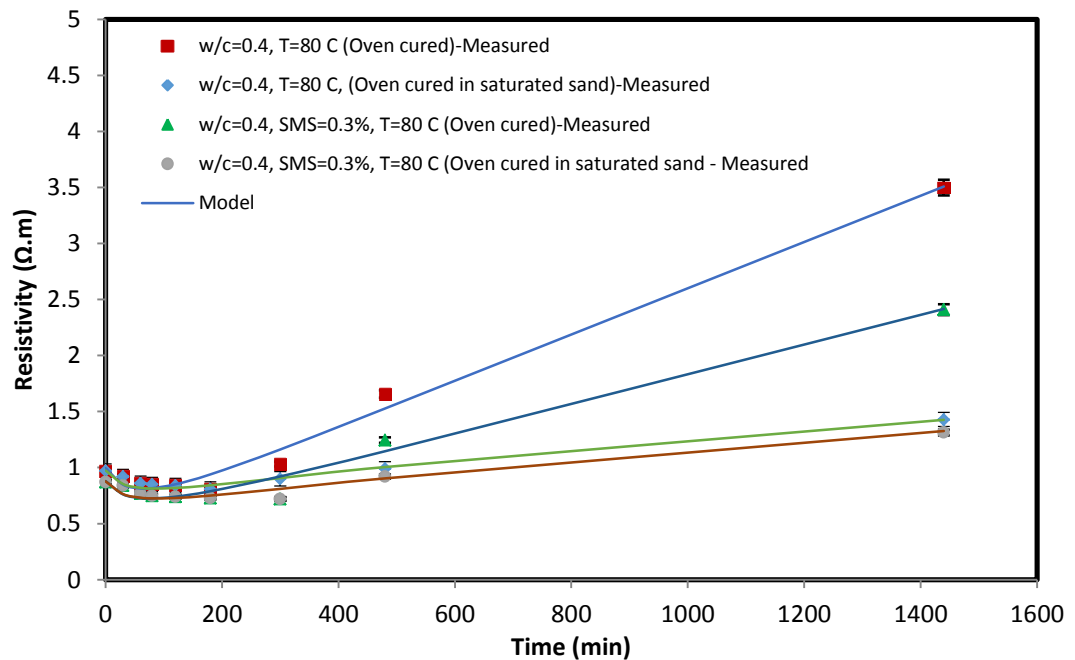


Figure 4-27: Variation of resistivity of smart cement during curing at high temperature with and without SMS up to 1 day

The initial electrical resistivity (ρ_o) of the smart cement with w/c ratio of 0.4 was $0.97 \pm 0.02 \text{ } \Omega\text{-m}$ and the electrical resistivity reduced to reach the ρ_{\min} of $0.81 \pm 0.01 \text{ } \Omega\text{-m}$

after 180 minutes (t_{\min}) as summarized in Table 4-16. With 0.3% SMS, the initial electrical resistivity and the minimum electrical resistivity was decreased and the time to reach the minimum (t_{\min}) was increased to 300 minutes. With 0.3% SMS, the ρ_o decreased by 10% and ρ_{\min} decreased by 12%. The 24 hours electrical resistivity (ρ_{24hr}) of the smart cement only that is oven cured was 3.49 $\Omega.m$. Hence the maximum change in electrical resistivity after 24 hours (RI_{24hr}) was 331% as summarized in Table 4-16. The 7 days and 28 days electrical resistivity (ρ_{7days} and ρ_{28days}) of the oven cured hardened cement were 12.73 $\Omega.m$ and 42.34 $\Omega.m$, hence the maximum change in electrical resistivity after 7 days and 28 days (RI_{7days} and $RI_{28 days}$) were 1472% and 5127% respectively. The addition of SMS decreased the electrical resistivity compared to that of smart cement only. Addition of 0.3% SMS decreased the 24 hours, 7 days and 28 days resistivity of the oven cured specimens by about 31%, 35% and 41% respectively and hence the maximum change in electrical resistivity i.e., RI_{24hr} , RI_{7days} and $RI_{28 days}$ were also decreased compared to that of smart cement only.

On the other hand, the 24 hours electrical resistivity (ρ_{24hr}) of the smart cement only that is oven cured in saturated sand was 1.42 $\Omega.m$. Hence the maximum change in electrical resistivity after 24 hours (RI_{24hr}) was 75% as summarized in Table 4-14. The 7 days and 28 days electrical resistivity (ρ_{7days} and $\rho_{28 days}$) of the hardened cement that was oven cured in saturated sand were 5.90 $\Omega.m$ and 10.24 $\Omega.m$, hence the maximum change in electrical resistivity after 7 days and 28 days ($RI_{7 days}$ and $RI_{28 days}$) were 628% and 1164% respectively. The addition of SMS decreased the electrical resistivity compared to that of smart cement only. Addition of 0.3% SMS decreased the 24 hours, 7 days and 28 days resistivity of the specimens that is oven cured in saturated sand by about 7%, 12%

and 18% respectively, and hence the maximum change in electrical resistivity i.e. RI_{24hr} , $RI_{7\text{ days}}$ and $RI_{28\text{ days}}$ were also decreased compared to that of smart cement only.

Table 4-16: Summary of bulk resistivity parameters for smart cement with and without SMS cured at high temperature up to 28 days

Mix Type	Density (ppg)	Initial resistivity, ρ_0 ($\Omega.m$)	ρ_{min} ($\Omega.m$)	t_{min} (min)	ρ_{24hr} ($\Omega.m$)	$\rho_{7\text{ days}}$ ($\Omega.m$)	$\rho_{28\text{ days}}$ ($\Omega.m$)	$RI_{2\text{ hr}}$ (%)	$RI_{7\text{ days}}$ (%)	$RI_{28\text{ days}}$ (%)
w/c=0.4, T=80°C (Oven cured)	16.2±0.14	0.97±0.02	0.81±0.01	180	3.49	12.73	42.34	331	1472	5127
w/c=0.4, T=80°C (Oven cured in saturated sand)	16.2±0.12	0.97±0.01	0.81±0.01	180	1.42	5.90	10.24	75	628	1164
w/c=0.4, SMS=0.3% T=80°C (Oven cured)	16.3±0.15	0.87±0.01	0.72±0.01	300	2.40	8.19	24.62	233	1038	3319
w/c=0.4, SMS=0.3% T=80°C (Oven cured in saturated sand)	16.3±0.11	0.87±0.01	0.72±0.01	300	1.31	5.16	8.34	82	617	1058

The curing model parameter q_1 for smart cement only that is oven cured was 0.366 at 1 day of curing and increased to 0.600 at time up to 7 days and then decreased to 0.296 at 28 days. Addition of 0.3% SMS decreased the q_1 value up to about 0.247 and then followed the similar trend with increase in curing time. For smart cement specimen that is oven cured in saturated sand, the model parameter q_1 was 0.178 at 1 day of curing and decreased to 0.117 at time up to 7 days and then increased to 0.384 at 28 days. Addition of 0.3% SMS decreased the q_1 value up to about 0.173 and then followed the similar trend with increase in curing time (Table 4-17).

The curing model parameter p_1 for smart cement only that is oven cured was 0.393 at 1 day of curing and increased to 0.928 at time up to 7 days and then decreased to

0.341 at time 28 days (Table 4-17). Addition of 0.3% SMS decreased the parameter p_1 to about 0.252 after 1 day of curing and then followed the similar trend curing time and reached to 0.263 after 28 days of curing. For the smart cement specimen that is oven cured in saturated sand, the curing model parameter p_1 was 0.315 after 1 day of curing which was decreased to 0.128 after 7 days of curing and then increased to 0.809 after 28 days of curing. The specimen having 0.3% SMS and oven cured in saturated sand, the model parameter p_1 was 0.270 after 1 day and then followed the similar trend like smart cement and reached to 1.061 after 28 days of curing. The curing model (Eqn. (3-11)) predicted the measured resistivity very well (Fig. 4-28). The coefficient of determination (R^2) varied from 0.96 to 0.99 and the root mean square of error (RMSE) varied from 0.03 $\Omega.m$ to 0.72 $\Omega.m$ for 1 day and 28 days of curing respectively.

4.3.2 Moisture loss/gain and its effect on the resistivity of the cement specimen

During the curing period, the weight of the specimens was monitored to observe any change. The oven cured samples lost the weight and the oven cured samples in saturated sand gained the weight. The percent weight loss/gain was calculated from the initial weight of the specimen. The oven cured smart cement sample lost about 18% weight after 28 days whereas the smart cement with 0.3% SMS lost about 16% weight (Fig. 4-29). The smart cement sample and the smart cement with 0.3% SMS both of which was oven cured in saturated sand gained about 2.75% weight (Fig. 4-30).

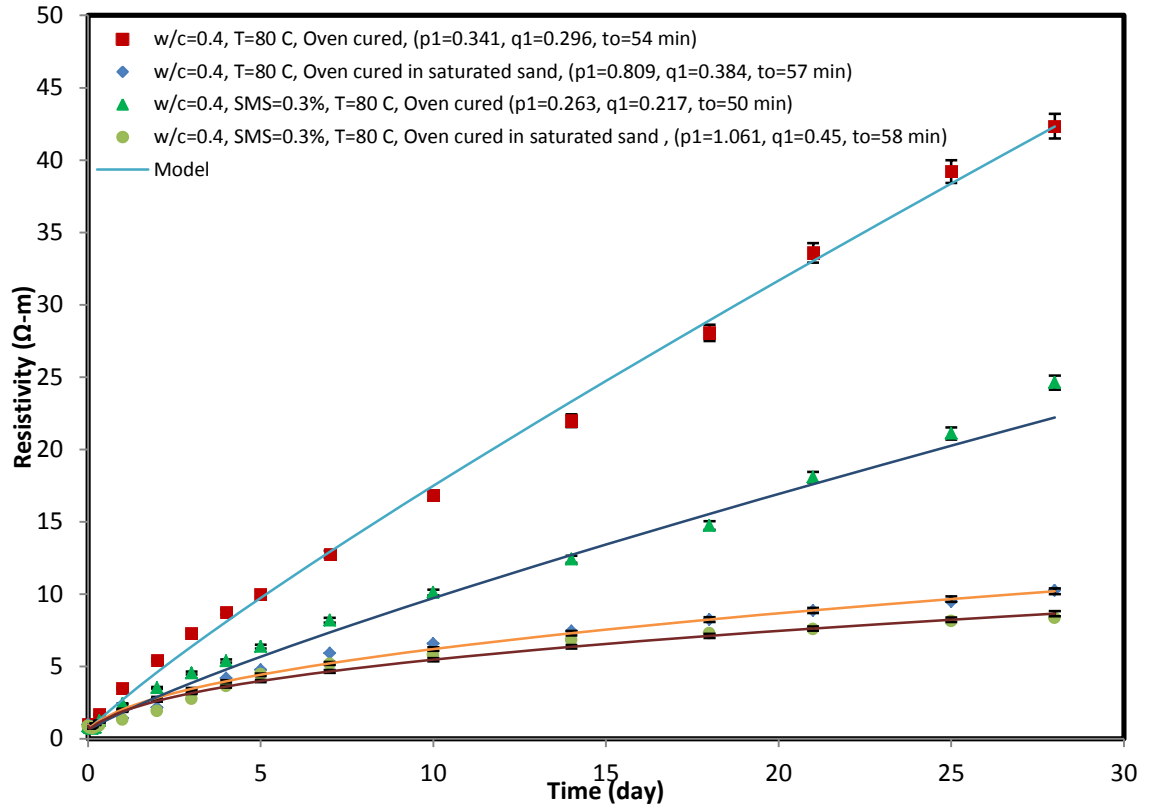


Figure 4-28: Variation of resistivity of smart cement during curing at high temperature with and without SMS up to 28 days

A relationship has been proposed for the resistivity of the cured specimen with the moisture loss/gain (%) as

$$\rho = \rho_o + A*(\Delta w/w_o)^n, \quad (4-12)$$

where,

ρ = Resistivity of the cement ($\Omega.m$)

ρ_o = Initial resistivity of the cement without moisture loss/gain ($\Omega.m$)

$\Delta w/w_o$ = Moisture loss/gain of the specimen (%)

A and n are constants and are model parameters that can be determined from the experimental results.

Table 4-17: Model parameters for the curing model of the resistivity of modified smart cement with and without SMS cured at high temperature up to 28 days

Mix Type	Curing Time (day)	ρ_{\min} ($\Omega.m$)	t_{\min} (min)	q_1	t_0 (min)	p_1	RMSE ($\Omega.m$)	R^2
w/c=0.4, T=80°C (Oven cured)	1 day	0.81	180	0.366	57	0.393	0.08	0.99
w/c=0.4, T=80°C (Oven cured in saturated sand)		0.81	180	0.178	46	0.315	0.03	0.96
w/c=0.4, SMS=0.3% T=80°C (Oven cured)		0.72	300	0.247	52	0.252	0.07	0.98
w/c=0.4, SMS=0.3% T=80°C (Oven cured in saturated sand)		0.72	300	0.173	45	0.270	0.03	0.96
w/c=0.4, T=80°C (Oven cured)	7 days	0.81	180	0.600	64	0.928	0.25	0.99
w/c=0.4, T=80°C (Oven cured in saturated sand)		0.81	180	0.117	41	0.128	0.14	0.99
w/c=0.4, SMS=0.3% T=80°C (Oven cured)		0.72	300	0.369	57	0.532	0.13	0.99
w/c=0.4, SMS=0.3% T=80°C (Oven cured in saturated sand)		0.72	300	0.127	41	0.143	0.14	0.99
w/c=0.4, T=80°C (Oven cured)	28 days	0.81	180	0.296	54	0.341	0.58	0.98
w/c=0.4, T=80°C (Oven cured in saturated sand)		0.81	180	0.384	57	0.809	0.30	0.99
w/c=0.4, SMS=0.3% T=80°C (Oven cured)		0.72	300	0.217	50	0.263	0.72	0.99
w/c=0.4, SMS=0.3% T=80°C (Oven cured in saturated sand)		0.72	300	0.450	58	1.061	0.31	0.98

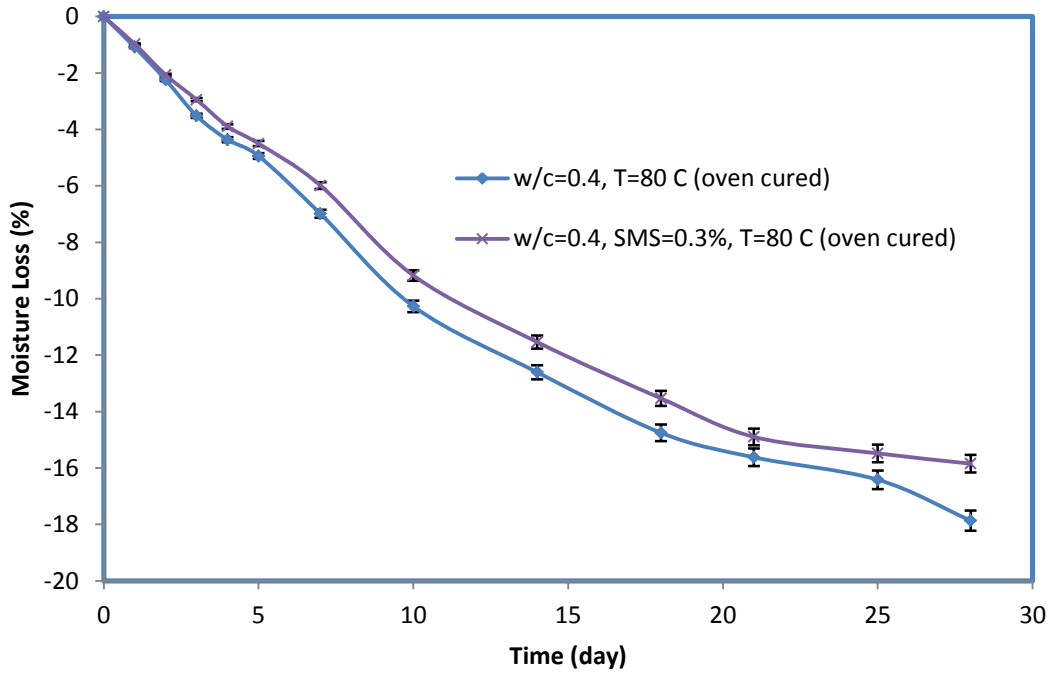


Figure 4-29: Moisture loss of cement specimens cured at high temperature in oven with and without SMS up to 28 days

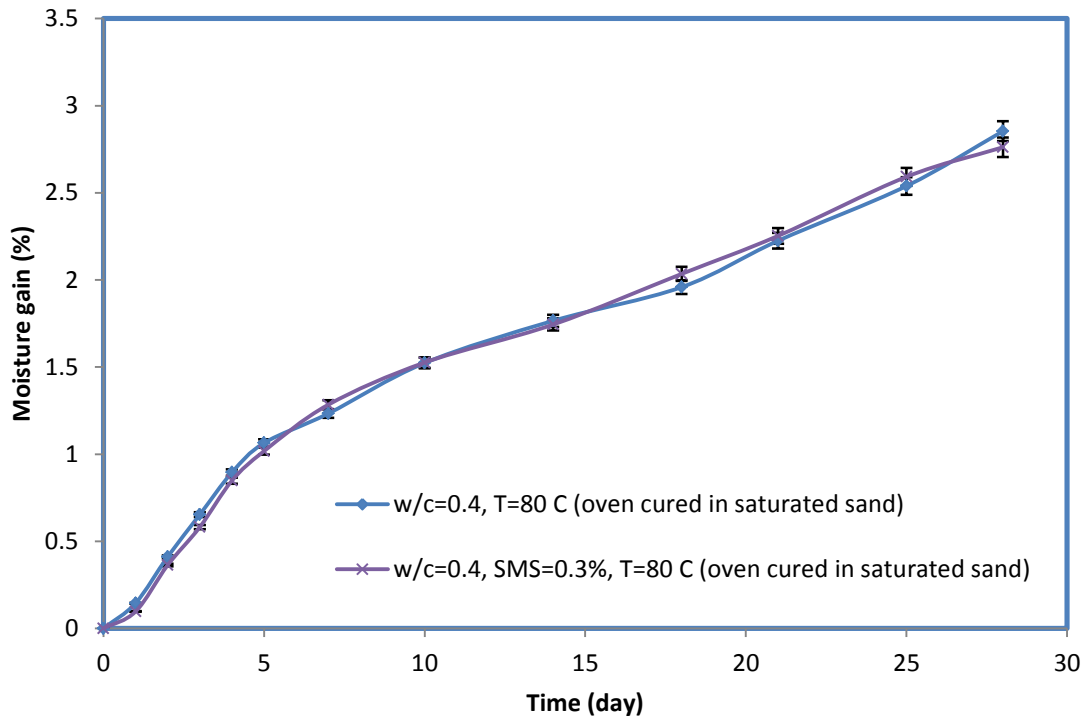


Figure 4-30: Moisture gain of cement specimens cured at high temperature in saturated sand with and without SMS up to 28 days

For the cement specimen that is oven cured and for the cement specimens that is oven cured in saturated sand, the experimental values fit very well with the proposed model (Fig. 4-31, 32). For the cement specimens that oven cured (here $\Delta w/w_o$ represents moisture loss), the determined model parameters are as

- (i) For the specimen without SMS, $A = 0.813$, $n = 1.34$ and $R^2 = 0.98$
- (ii) For the specimen with 0.3% SMS, $A = 0.735$, $n = 1.20$. $R^2 = 0.97$

For the cement specimens that is oven cured in saturated sand (here $\Delta w/w_o$ represents moisture gain), the determined model parameters are as

- (i) For the specimen without SMS, $A = 3.59$, $n = 0.96$ and $R^2 = 0.99$
- (ii) For the specimen with 0.3% SMS, $A = 3.31$, $n = 0.86$. $R^2 = 0.99$

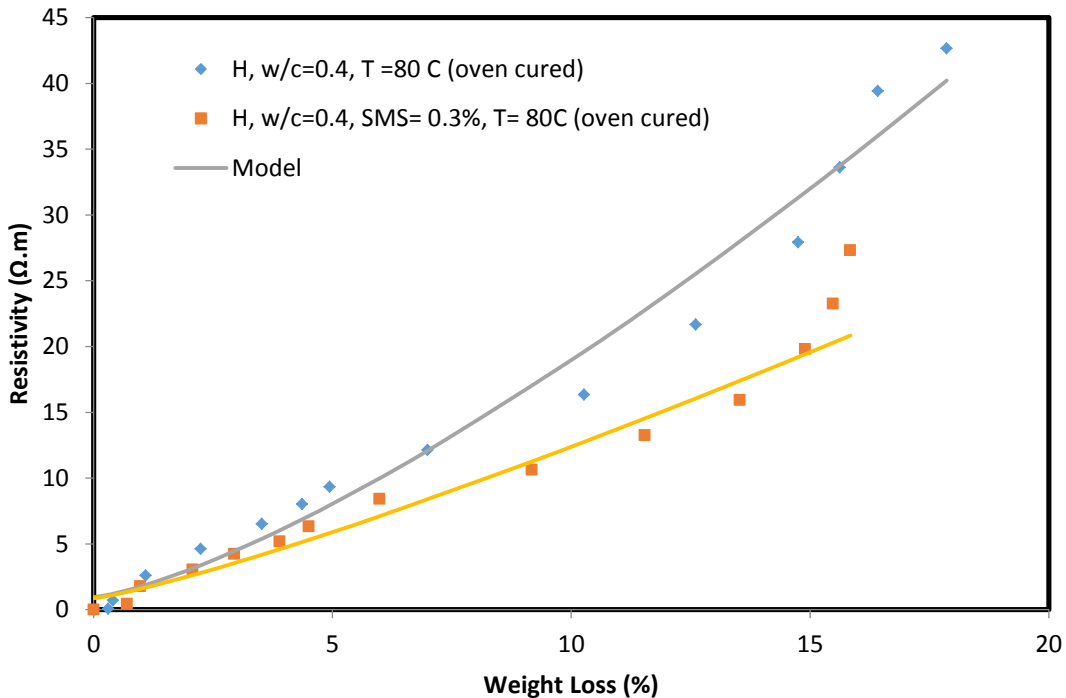


Figure 4-31: Relationship between resistivity and moisture loss of the smart cement cured in oven at 80°C

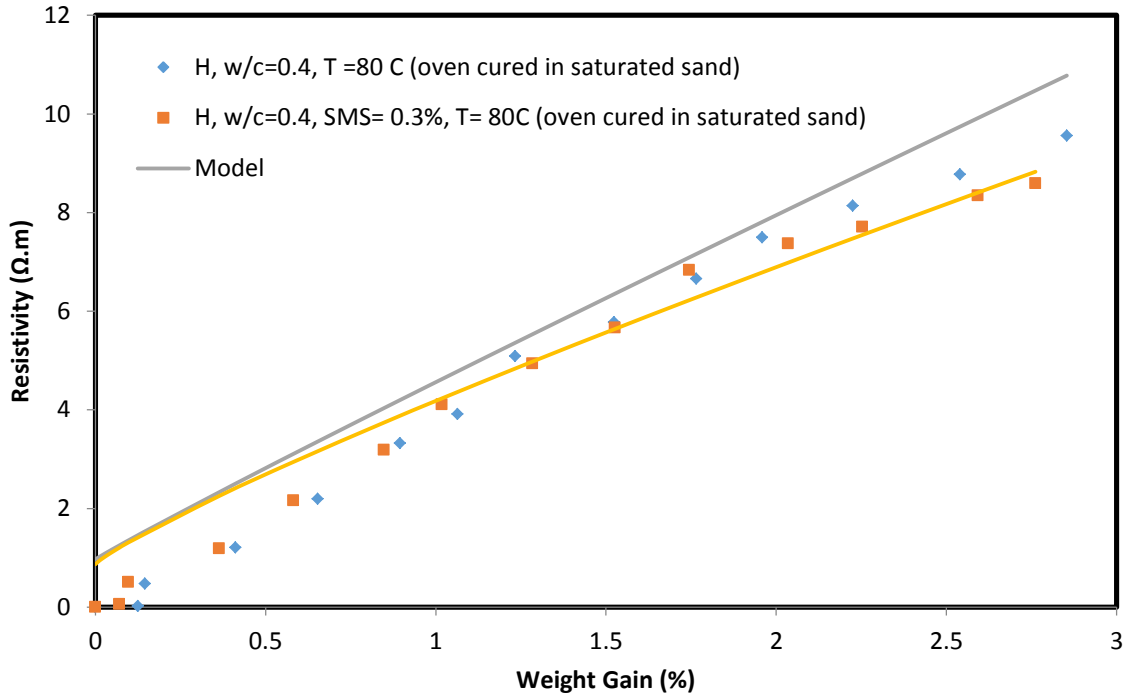


Figure 4-32: Relationship between resistivity and moisture gain of the smart cement cured in saturated sand at 80°C

4.3.3 Piezoresistivity and strength of smart cement cured at high temperature

Addition of 0.075% CF substantially improved piezoresistive behavior of the cement. Based on experimental results, p-q model developed by Vipulanandan and Paul (1990) was modified and used to predict the change in electrical resistivity of cement with applied stress for 1, 7 and 28 days of curing.

4.3.3.1 1 day of curing

The compressive strength (σ_f) of the smart cement cured in oven after one day of curing was 15.81 MPa which was increased to 18.00 MPa for smart cement oven cured in saturated sand, a 14% increase. The smart cement with 0.3% SMS cured in oven had a compressive strength of 14.93 MPa which was increased to 16.91 MPa for specimen oven cured in saturated sand, a 13% increase (Table 4-18).

The change in electrical resistivity at failure $\left(\frac{\Delta\rho}{\rho_o}\right)_f$ for the smart cement cured in oven was 433% which was increased to 475% for smart cement oven cured in saturated sand. The smart cement with 0.3% SMS cured in oven showed the change in electrical resistivity at failure $\left(\frac{\Delta\rho}{\rho_o}\right)_f$ as 331% which was increased to 345% for specimen oven cured in saturated sand (Table 4-18).

Using the p-q Piezoresistive model (Eqn. (3-15)), the relationships between compressive stress and the change in electrical resistivity $\left(\frac{\Delta\rho}{\rho_o}\right)$ of the smart cement with and without 0.3% SMS for one day of oven curing and oven cure in saturated sand were modeled. The piezoresistive model (Eqn. (3-15)) predicted the measured stress- change in resistivity relationship very well (Fig. 4-33). The model parameters q_2 and p_2 are summarized in Table 3. The coefficients of determination (R^2) were 0.98 to 0.99. The root mean square of error (RMSE) varied between 0.11 MPa and 0.38 MPa as summarized in Table 4-18.

Rate of change of resistivity with respect to stress change:

As we have considered the rate of resistivity change $\Delta\rho/\rho_o$ as X, and if we consider the stress as Y, then the slope dX/dY , which is rate of change of resistivity with respect to stress change could be another indicator of the piezoresistivity. For 1 day of curing, the rate of change of resistivity (dX/dY) without any SMS was about 22-30 (%/MPa) which increased to 48 (%/MPa) and changed the slope before the specimen cracks. With 0.3% SMS, the rate of change of resistivity (dX/dY) decreases upto 16-25 (%/MPa) which

increased suddenly to 50 (%/MPa) and changes the slope when the cement specimen experiences cracks (Fig. 4-34).

4.3.3.2 7 days of Curing

The compressive strength (σ_f) of the smart cement cured in oven after 7 days of curing was 29.65 MPa which was increased to 30.08 MPa for smart cement oven cured in saturated sand, a 2% increase. The smart cement with 0.3% SMS cured in oven had a compressive strength of 27.88 MPa which was increased to 28.54 MPa for specimen oven cured in saturated sand, a 2.3% increase (Table 4-18).

The change in electrical resistivity at failure $\left(\frac{\Delta\rho}{\rho_o}\right)_f$ for the smart cement cured in oven was 360% which was increased to 420% for smart cement oven cured in saturated sand. The smart cement with 0.3% SMS cured in oven showed the change in electrical resistivity at failure $\left(\frac{\Delta\rho}{\rho_o}\right)_f$ as 250% which was increased to 290% for specimen oven cured in saturated sand (Table 4-18).

Using the p-q Piezoresistive model (Eqn. (3-15)), the relationships between compressive stress and the change in electrical resistivity $\left(\frac{\Delta\rho}{\rho_o}\right)$ of the smart cement with and without 0.3% SMS for 7 days of oven curing and oven cured in saturated sand were modeled. The piezoresistive model (Eqn. (3-15)) predicted the measured stress-change in resistivity relationship very well (Fig. 4-35). The model parameters q_2 and p_2 are summarized in Table 4-16. The coefficients of determination (R^2) were 0.98 to 0.99. The root mean square of error (RMSE) varied between 0.18 MPa and 0.47 MPa as summarized in Table 4-18.

Table 4-18: Peak stress, piezoresistivity, model parameters p₂, q₂ and R² & RMSE for the piezoresistivity model for the smart cement specimens under compressive stress after 1 day, 7 days and 28 days.

Mix Type	Curing Time (day)	Peak Stress σ_f (Mpa)	Piezoresistivity at peak stress, $(\Delta\rho/\rho_o)_f$ (%)	p ₂	q ₂	R ²	RMS E (MPa)
w/c=0.4, T=80°C (Oven cured)	1 day	15.81	433	0.010	0.673	0.99	0.12
w/c=0.4, T=80°C (Oven cured in saturated sand)		18.00	475	0.030	0.802	0.98	0.38
w/c=0.4, SMS=0.3% T=80°C (Oven cured)		14.93	331	0.048	0.730	0.99	0.16
w/c=0.4, SMS=0.3% T=80°C (Oven cured in saturated sand)		16.91	345	0.081	0.897	0.99	0.11
w/c=0.4, T=80°C (Oven cured)	7 days	29.65	360	0.070	0.768	0.99	0.37
w/c=0.4, T=80°C (Oven cured in saturated sand)		30.08	420	0.040	0.612	0.98	0.47
w/c=0.4, SMS=0.3% T=80°C (Oven cured)		27.88	250	0.010	0.813	0.99	0.23
w/c=0.4, SMS=0.3% T=80°C (Oven cured in saturated sand)		28.54	290	0.038	0.668	0.99	0.18
w/c=0.4, T=80°C (Oven cured)	28 days	33.59	245	0.010	0.626	0.98	0.39
w/c=0.4, T=80°C (Oven cured in saturated sand)		37.98	302	0.019	0.744	0.99	0.26
w/c=0.4, SMS=0.3% T=80°C (Oven cured)		33.15	160	0.050	0.825	0.99	0.30
w/c=0.4, SMS=0.3% T=80°C (Oven cured in saturated sand)		38.42	220	0.010	0.487	0.97	0.46

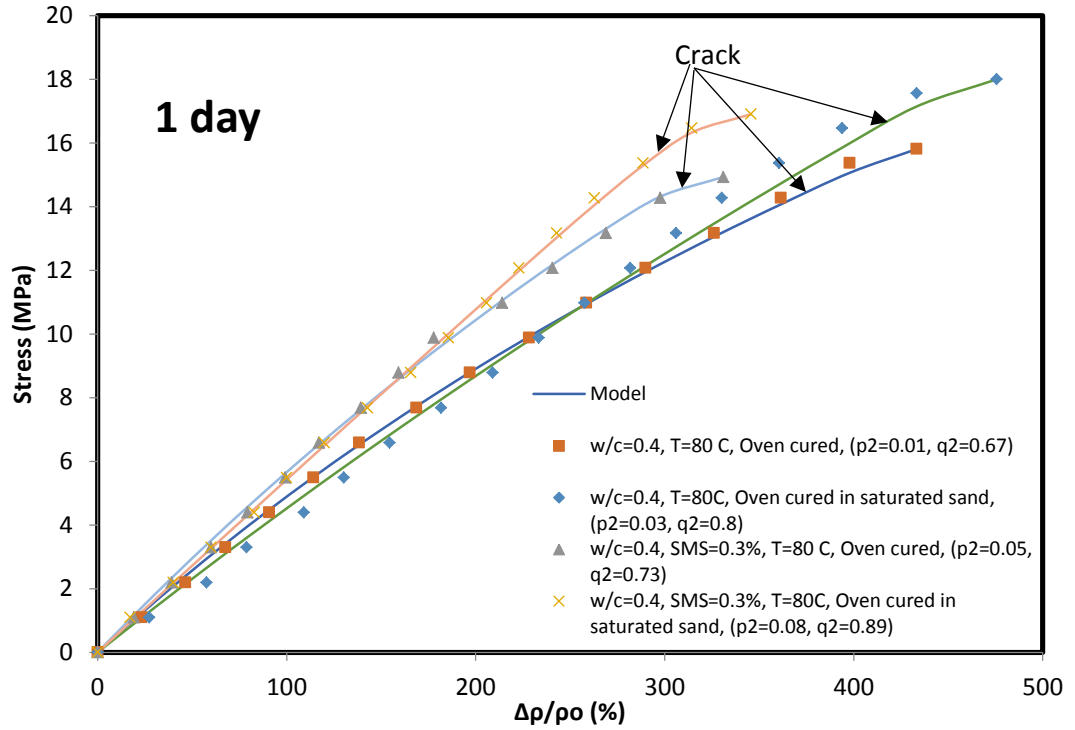


Figure 4-33: Piezoresistive response of the smart cement with and without SMS after 1 day of high temperature curing.

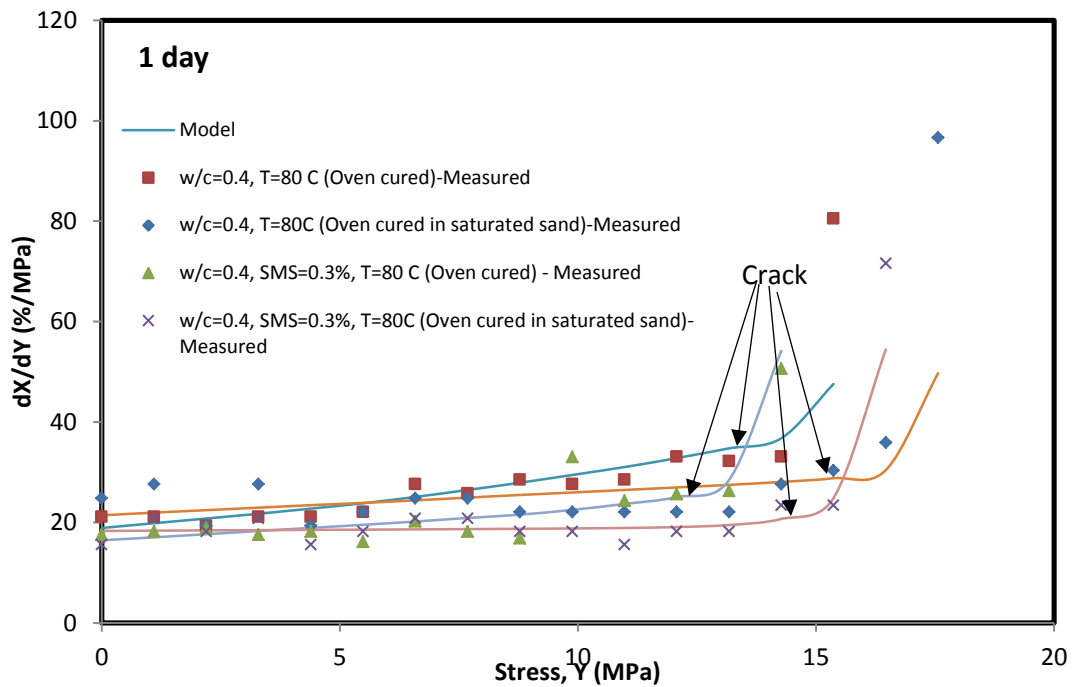


Figure 4-34: Rate of change of resistivity with respect to stress vs Stress for 1 day of curing

Rate of change of resistivity with respect to stress change:

For 7 days of curing, the rate of change of resistivity (dX/dY) without any SMS was about 9-15 (%/MPa) which increased to 44 (%/MPa) and changed the slope before the specimen cracks. With 0.3% SMS, the rate of change of resistivity (dX/dY) decreases upto 6-10 (%/MPa) which increased suddenly to 15-25 (%/MPa) and changes the slope when the cement specimen experiences cracks (Fig. 4-36).

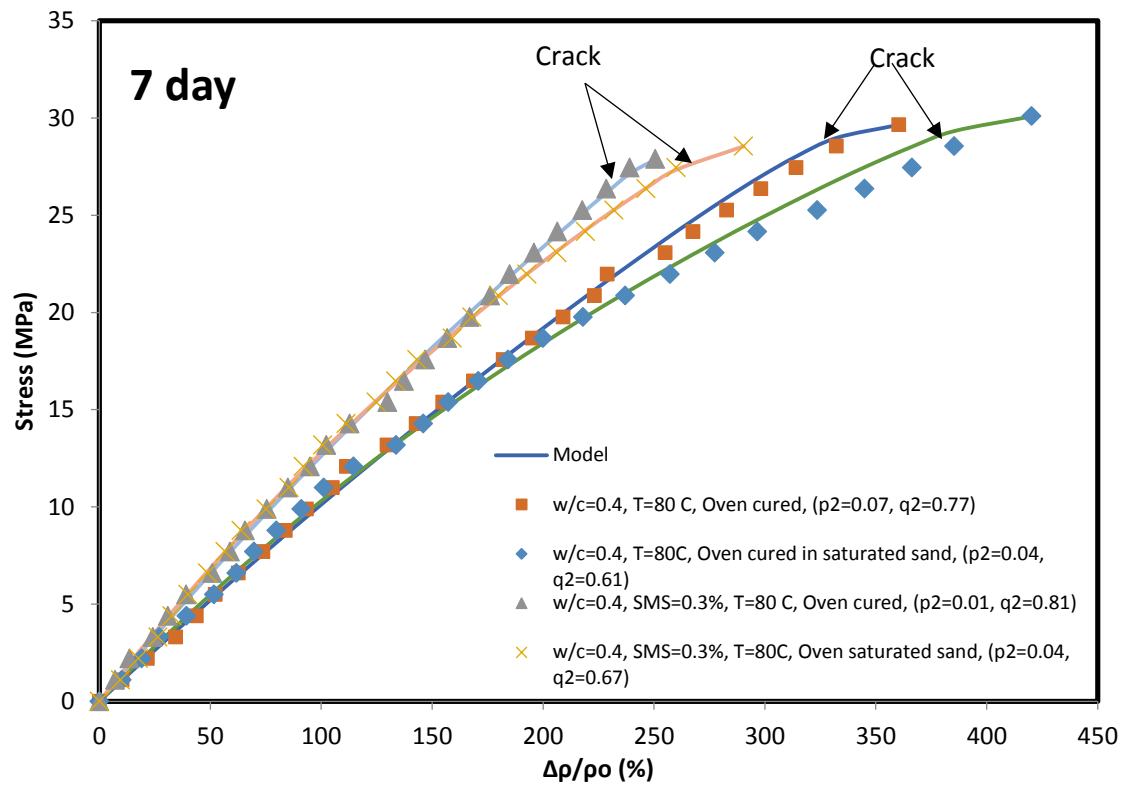


Figure 4-35: Piezoresistive response of the smart cement with and without SMS after 7 days of high temperature curing modeled with p-q model.

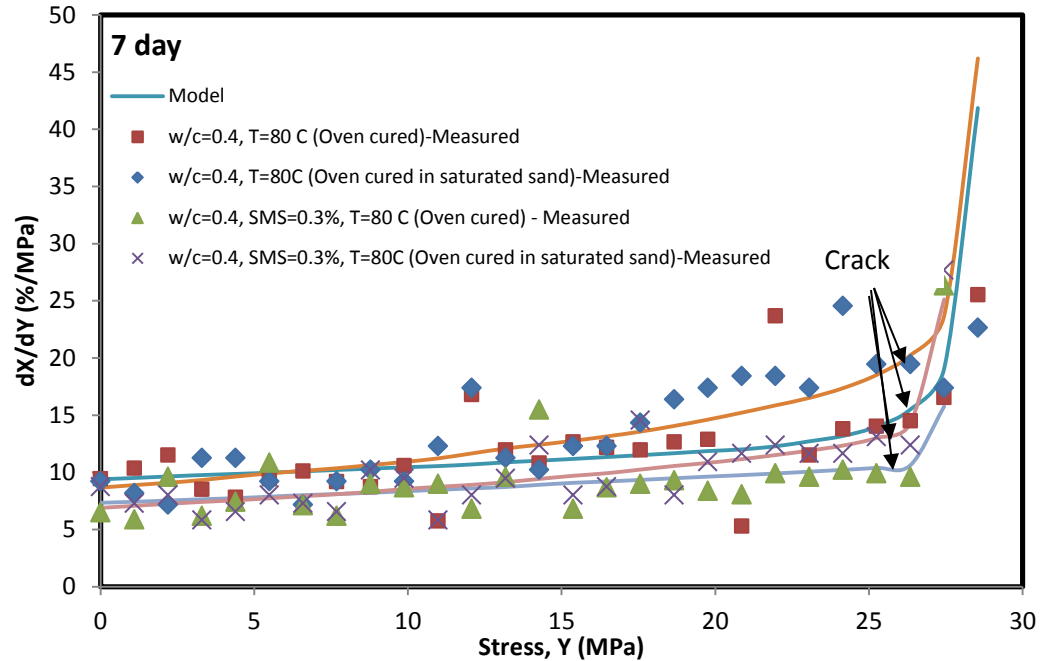


Figure 4-36: Rate of change of resistivity with respect to stress vs Stress for 7 days curing

4.3.3.3 28 days of Curing

The compressive strength (σ_f) of the smart cement cured in oven after 28 days of curing was 33.56 MPa which was increased to 37.98 MPa for smart cement oven cured in saturated sand, a 13% increase. The smart cement with 0.3% SMS cured in oven had a compressive strength of 33.15 MPa which was increased to 38.42 MPa for specimen oven cured in saturated sand, a 16% increase (Table 4-18).

The change in electrical resistivity at failure $\left(\frac{\Delta\rho}{\rho_o}\right)_f$ for the smart cement cured in oven was 245% which was increased to 302% for smart cement oven cured in saturated sand. The smart cement with 0.3% SMS cured in oven showed the change in electrical resistivity at failure $\left(\frac{\Delta\rho}{\rho_o}\right)_f$ as 160% which was increased to 220% for specimen oven cured in saturated sand (Table 4-18).

Using the p-q Piezoresistive model (Eqn. (3-15)), the relationships between compressive stress and the change in electrical resistivity ($\frac{\Delta\rho}{\rho_0}$) of the smart cement with and without 0.3% SMS for 28 days of oven curing and oven cured in saturated sand were modeled. The piezoresistive model (Eqn. (3-15)) predicted the measured stress-change in resistivity relationship very well (Fig. 4-37). The model parameters q_2 and p_2 are summarized in Table 4-18. The coefficients of determination (R^2) were 0.97 to 0.99. The root mean square of error (RMSE) varied between 0.26 MPa and 0.46 MPa as summarized in Table 4-18.

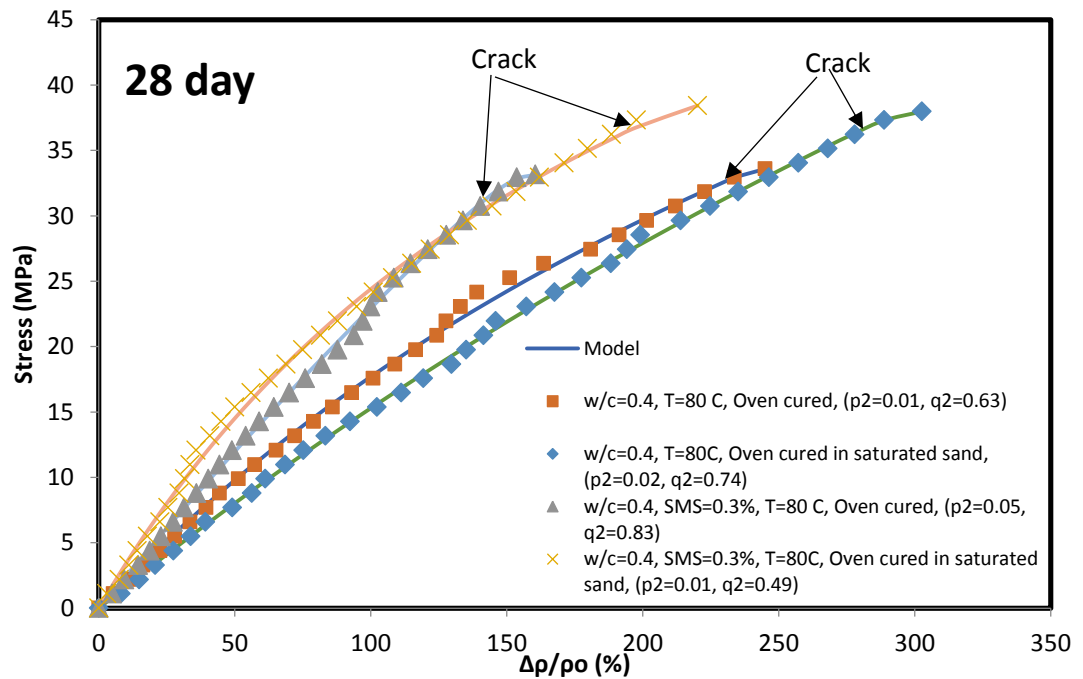


Figure 4-37: Piezoresistive response of the smart cement with and without SMS after 28 days of high temperature curing

Rate of change of resistivity rate with respect to stress change:

For 28 days of curing, the rate of change of resistivity (dX/dY) without any SMS was about 4-9 (%/MPa) which increased to 16-20 (%/MPa) and changed the slope before the specimen cracks. With 0.3% SMS, the rate of change of resistivity (dX/dY) decreased upto 3-7 (%/MPa) which increased suddenly to 16-22 (%/MPa) and changes the slope when the cement specimen experienced cracks (Fig. 4-38).

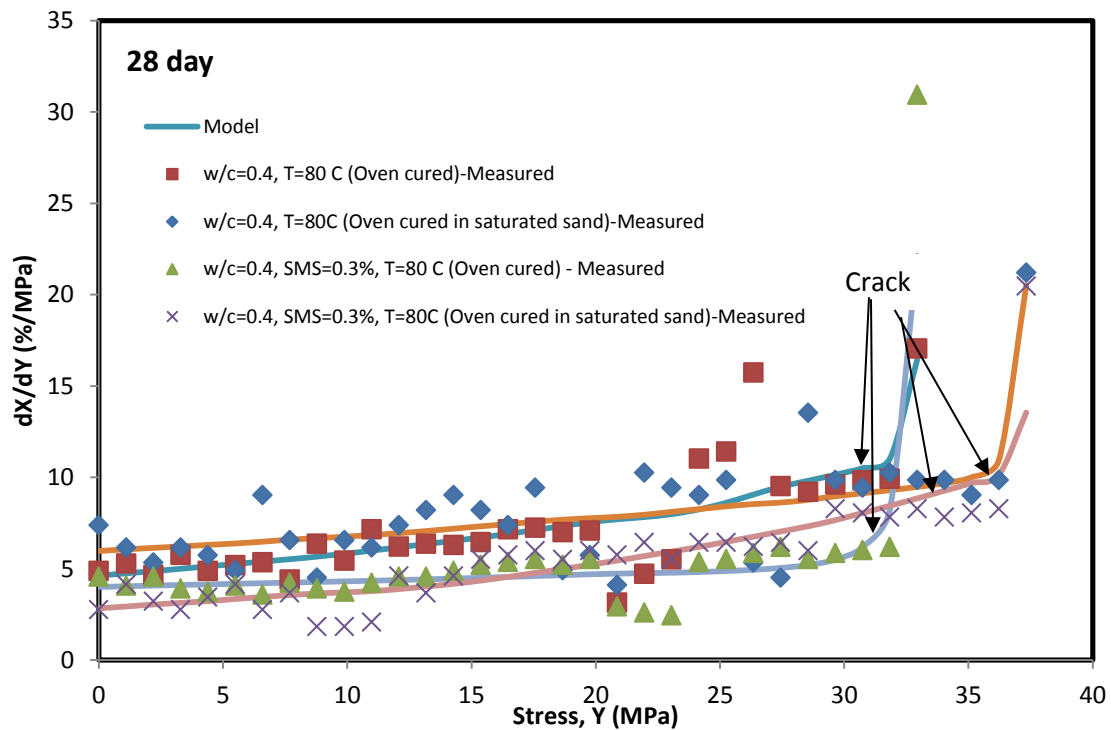


Figure 4-38: Rate of change of resistivity with respect to stress vs Stress for 28 days curing

4.3.4 Relationship between curing time and strength/piezoresistivity at failure

The strength of the cement specimen made with and without SMS oven cured and oven cured in saturated sand was observed up to 28 days. With curing time increases, the compressive strength of the cement specimen increased. The relationship between the

compressive strength of the cement and curing time has been modeled with the hyperbolic model

$$\sigma_c = t/(C + Dt), \quad (4-13)$$

where,

σ_c = Compressive strength of the grout (MPa)

t = Curing time (day)

Parameters C and D are model parameters and parameter C represent the initial rate of change and parameter D determines the ultimate strength. For the cement specimens cured in oven, experimental results matched very well (Fig. 4-39) with the proposed model with coefficient of determination (R^2) of 0.99. For smart cement only, parameters C and D were found as 0.035 MPa^{-1} and 0.028 MPa^{-1} . For smart cement with 0.3% SMS, parameters C and D were found as 0.039 MPa^{-1} and 0.029 MPa^{-1} . For the cement specimens oven cured in saturated sand, experimental results also matched very well (Fig. 4-39) with the proposed model with coefficient of determination (R^2) of 0.94-0.95. For smart cement only, parameters C and D were found as 0.032 MPa^{-1} and 0.026 MPa^{-1} . For smart cement with 0.3% SMS, parameters C and D were found as 0.038 MPa^{-1} and 0.026 MPa^{-1} .

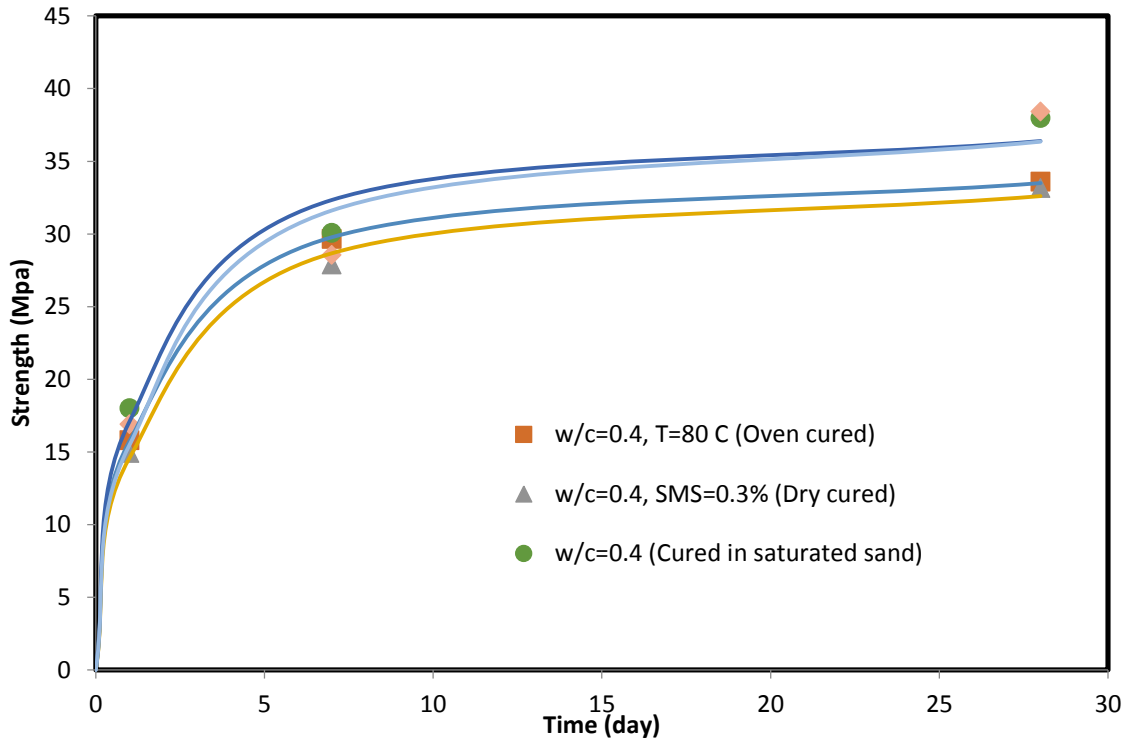


Figure 4-39: Relationship between compressive strength and the curing time for the smart cement modeled with hyperbolic model

The piezoresistivity at failure of the cement specimen made with and without SMS oven cured and oven cured in saturated sand was observed up to 28 days. With curing time increases, the piezoresistivity at failure of the cement specimen changes. The relationship between the piezoresistivity at failure of the cement grout and curing time has been modeled with the hyperbolic model

$$\Delta\rho/\rho_o = (\Delta\rho/\rho_o)_1 - t/(E + Ft), \quad (4-14)$$

where,

$\Delta\rho/\rho_o$ = Piezoresistivity at failure (%)

$(\Delta\rho/\rho_o)_1$ = Piezoresistivity at failure after 1 day (%)

t = Curing time (day)

Parameters E and F are model parameters and parameter E represent the initial rate of change and parameter F determines the ultimate piezoresistivity. For the cement specimens cured in oven, experimental results matched very well (Fig. 4-40) with the proposed model with coefficient of determination (R^2) of 0.98-0.99. For smart cement only, parameters E and F were found as 0.083 MPa^{-1} and 0.002 MPa^{-1} . For smart cement with 0.3% SMS, parameters E and F were found as 0.067 MPa^{-1} and 0.003 MPa^{-1} . For the cement specimens oven cured in saturated sand, experimental results also matched very well (Fig. 4-40) with the proposed model with coefficient of determination (R^2) of 0.98-0.99. For smart cement only, parameters E and F were found as 0.121 MPa^{-1} and 0.001 MPa^{-1} . For smart cement with 0.3% SMS, parameters E and F were found as 0.104 MPa^{-1} and 0.004 MPa^{-1} .

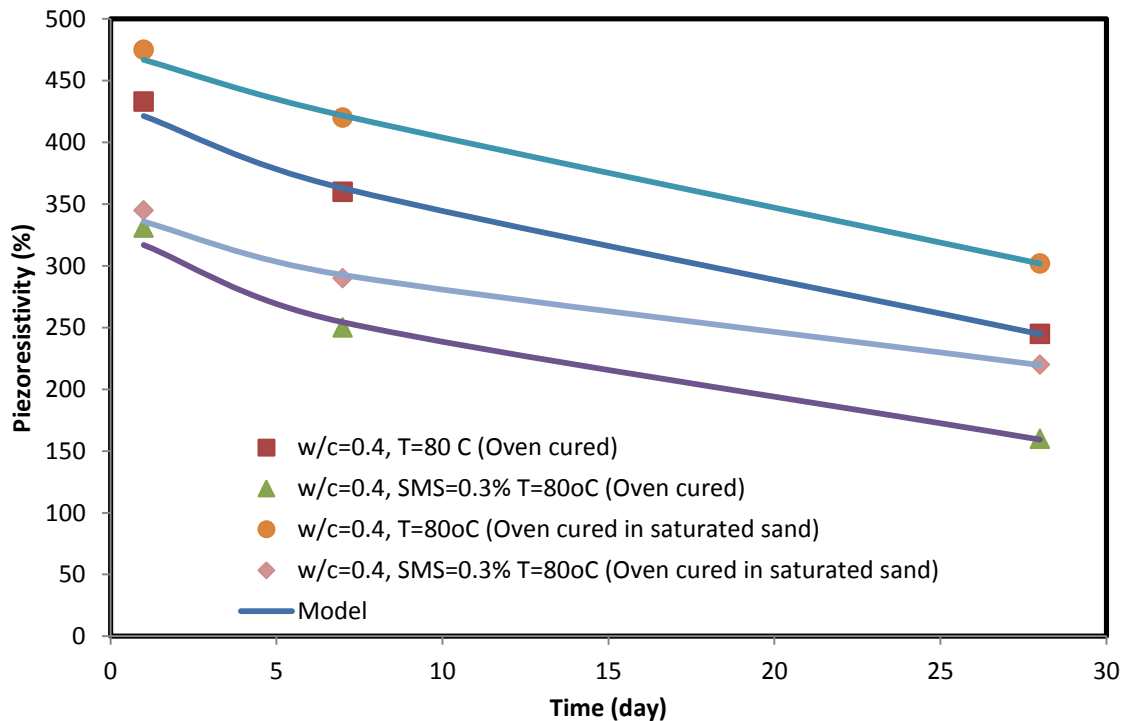


Figure 4-40: Relationship between Piezoresistivity at failure and the curing time for the smart cement specimen modeled with hyperbolic model

4.4 Curing and Piezoresistive Behavior of Modified Portland Cement Contaminated with Clay

4.4.1 Initial Resistivity.

The electrical resistivity of the modified Portland cement slurry with and without clay contamination was determined. The initial resistivity of the modified Portland cement slurry was $0.92 \pm 0.02 \text{ } \Omega \cdot \text{m}$ and it was increased with clay contamination as shown in Fig. 4-41. With 1% clay contamination, the initial resistivity was increased to $0.94 \pm 0.01 \text{ } \Omega \cdot \text{m}$ and with 5% clay contamination, the initial resistivity was $1.15 \pm 0.03 \text{ } \Omega \cdot \text{m}$, a 25% increase. Hence the initial resistivity was sensitive to the clay contamination with the cement.

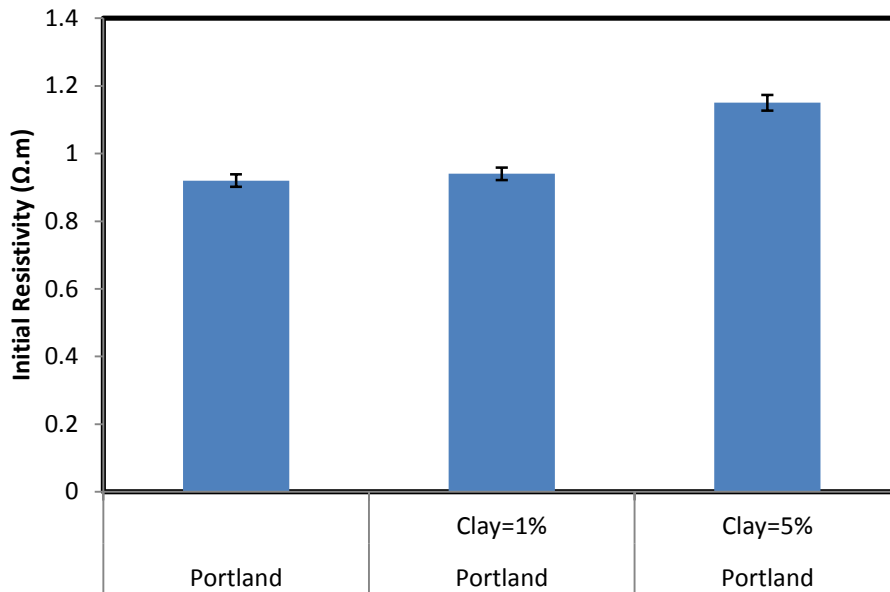


Figure 4-41: Initial resistivity of the Portland cement slurry with different amount of clay contamination

4.4.2 Resistivity with curing of cement

The change of electrical resistivity with curing time for the modified Portland cement with different clay contamination such as 0%, 1% 5% was observed for different

curing condition. The normal trend of the resistivity of the cured cement is that the resistivity is decreased up to a certain time (t_{\min}) and reached to a minimum resistivity (ρ_{\min}) and then starts increasing with time.

4.4.2.1 Long time curing of the specimen at room temperature

The resistivity of the cement specimen with different percentage (0%, 1% and 5%) of clay contamination was determined up to 28 days at room temperature. The specimens were subject to normal evaporation. Unit weight of modified Portland cement with w/c ratio of 0.38 was 16.8 ± 0.12 ppg (19.74 kN/m^3) which was decreased with clay contamination. With 5% clay contamination, the unit weight decreased to 15.1 ± 0.15 ppg (17.74 kN/m^3). The initial electrical resistivity (ρ_o) of class modified Portland cement with w/c ratio of 0.38 was $0.92 \pm 0.02 \text{ } \Omega\text{-m}$ and the electrical resistivity reduced to reach the ρ_{\min} of $0.84 \pm 0.01 \text{ } \Omega\text{-m}$ after 180 minutes (t_{\min}) as summarized in Table 4-19. With clay contamination, the initial electrical resistivity and the minimum electrical resistivity was increased but the time to reach the minimum (t_{\min}) was same. With 5% clay contamination, the ρ_o increased by 25% and ρ_{\min} increased by 27%. The 24 hours electrical resistivity ($\rho_{24\text{hr}}$) of the cement without contamination was $2.48 \text{ } \Omega\text{-m}$. Hence the maximum change in electrical resistivity after 24 hours ($RI_{24\text{hr}}$) was 195% as summarized in Table 4-19. The 7 days and 28 days electrical resistivity ($\rho_{7\text{days}}$ and $\rho_{28\text{days}}$) of the hardened cement were $6.79 \text{ } \Omega\text{-m}$ and $11.37 \text{ } \Omega\text{-m}$, hence the maximum change in electrical resistivity after 7 days and 28 days ($RI_{7\text{days}}$ and $RI_{28 \text{ days}}$) were 708% and 1253% respectively. The clay contamination increased the electrical resistivity compared to that of cement only. Addition of 5% clay contamination increased the 24 hours, 7 days and 28 days resistivity by about 13%, 20% and 24% respectively, but, the maximum change in

electrical resistivity i.e., RI_{24hr} , RI_{7days} and $RI_{28 days}$ were not showing that increase accordingly due to the difference in ρ_{min} .

Table 4-19: Summary of bulk resistivity parameters for modified Portland cement with and without clay contamination cured under room temperature up to 28 days

Mix Type	Density (ppg)	Initial resistivity, ρ_o ($\Omega.m$)	ρ_{min} ($\Omega.m$)	t_{min} (min)	ρ_{24hr} ($\Omega.m$)	$\rho_{7 days}$ ($\Omega.m$)	$\rho_{28 days}$ ($\Omega.m$)	$RI_{24 hr}$ (%)	$RI_{7 days}$ (%)	$RI_{28 days}$ (%)
w/c=0.38	16.8±0.12	0.92±0.02	0.84±0.01	180	2.48	6.79	11.37	195	708	1253
w/c=0.38 Clay = 1%	16.6±0.10	0.94±0.01	0.85±0.01	180	2.62	6.57	12.30	208	673	1347
w/c=0.38 Clay = 5%	15.1±0.15	1.15±0.03	1.07±0.02	180	2.82	8.17	15.10	164	664	1311

The curing model parameter q_1 for modified Portland cement only was 0.010 at 1 day of curing and increased to 0.366 at time up to 7 days and to 0.542 at 28 days. Clay contamination increased the q_1 value up to about 0.04 and then followed the similar trend with increase in curing time. The curing model parameter p_1 for modified Portland cement only was 0.004 at 1 day of curing and increased to 0.638 at time up to 7 days and then increased to 1.263 after curing time of 28 days. (Table 4-20). Clay contamination increased the parameter p_1 to about 0.019 for 5% clay contamination and then followed the similar trend with increase in curing time and reached to 0.896 after 28 days of curing. The curing model (Eqn. (3-11)) predicted the measured resistivity very well (Fig. 4-42). The coefficient of determination (R^2) varied from 0.98 to 0.99 and the root mean square of error (RMSE) varied from 0.02 $\Omega.m$ to 0.51 $\Omega.m$ for 1 day and 28 days of curing respectively.

4.4.2.2 Moisture loss and its effect on the resistivity of the cement specimen

During the curing period, the weight loss of the specimens was monitored to observe any change. The percent weight loss was calculated from the initial weight of the specimen. We can see from Fig. 4-43 that the rapid weight loss was happened within

initial 7 days of curing. After 7 days, the weight loss were 0.71%, 0.7%, and 0.45% for specimens having 0%, 1% and 5% clay contamination respectively. After 28 days of curing, the weight loss were 0.97%, 0.95% and 0.74% for specimens having 0% 1% and 5% clay contamination respectively. Here we found that the specimens having more amount of clay contamination losing less amount of moisture from the specimens. The specimen having 5% clay contamination losing 22% less weight compared to the specimen which had no clay contamination (i.e., modified Portland cement only).

Table 4-20: Model parameters for the curing model of the resistivity of modified Portland cement with and without clay contamination cured under room temperature up to 28 days

Mix Type	Curing Time (day)	ρ_{\min} ($\Omega.m$)	t_{\min} (min)	q_1	t_o (min)	p_1	RMSE ($\Omega.m$)	R^2
w/c=0.38	1 day	0.84	180	0.010	16	0.004	0.02	0.99
w/c=0.38 Clay = 1%		0.85	180	0.043	37	0.022	0.02	0.99
w/c=0.38 Clay = 5%		1.07	180	0.037	40	0.019	0.04	0.99
w/c=0.38	7 days	0.84	180	0.366	65	0.638	0.21	0.99
w/c=0.38 Clay = 1%		0.85	180	0.393	66	0.741	0.13	0.99
w/c=0.38 Clay = 5%		1.07	180	0.205	63	0.287	0.14	0.99
w/c=0.38	28 days	0.84	180	0.542	69	1.263	0.38	0.99
w/c=0.38 Clay = 1%		0.85	180	0.485	68	1.075	0.16	0.99
w/c=0.38 Clay = 5%		1.07	180	0.432	70	0.896	0.51	0.98

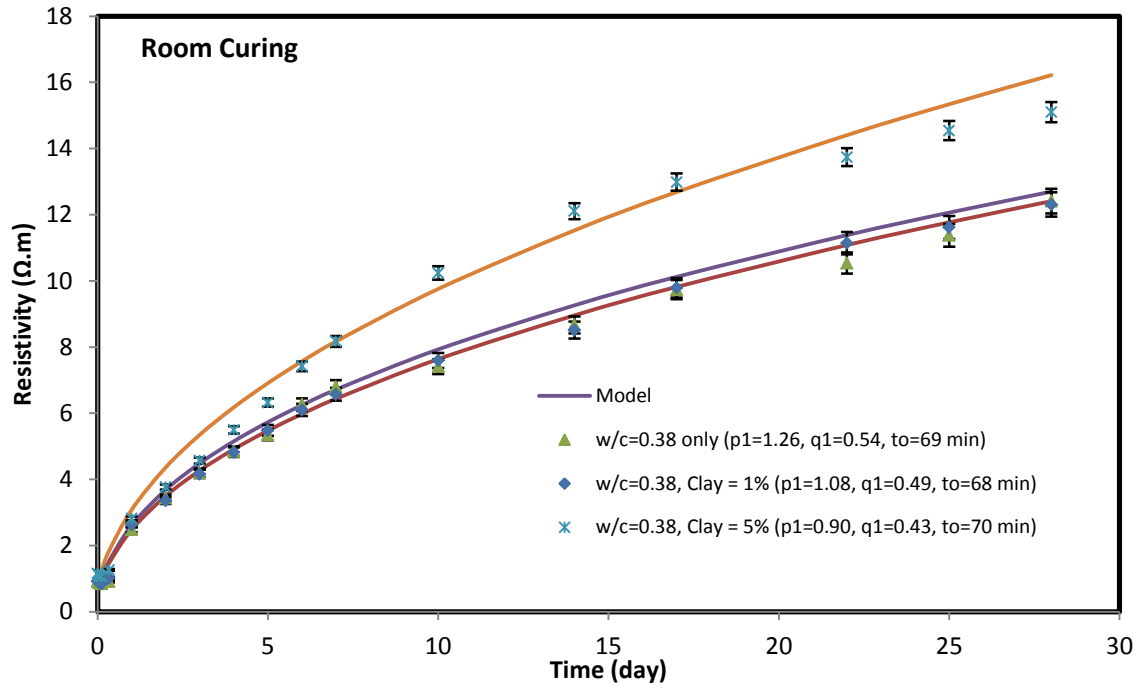


Figure 4-42: Variation of resistivity for cement specimens cured at room temperature with and without clay contamination up to 28 days modeled with curing model.

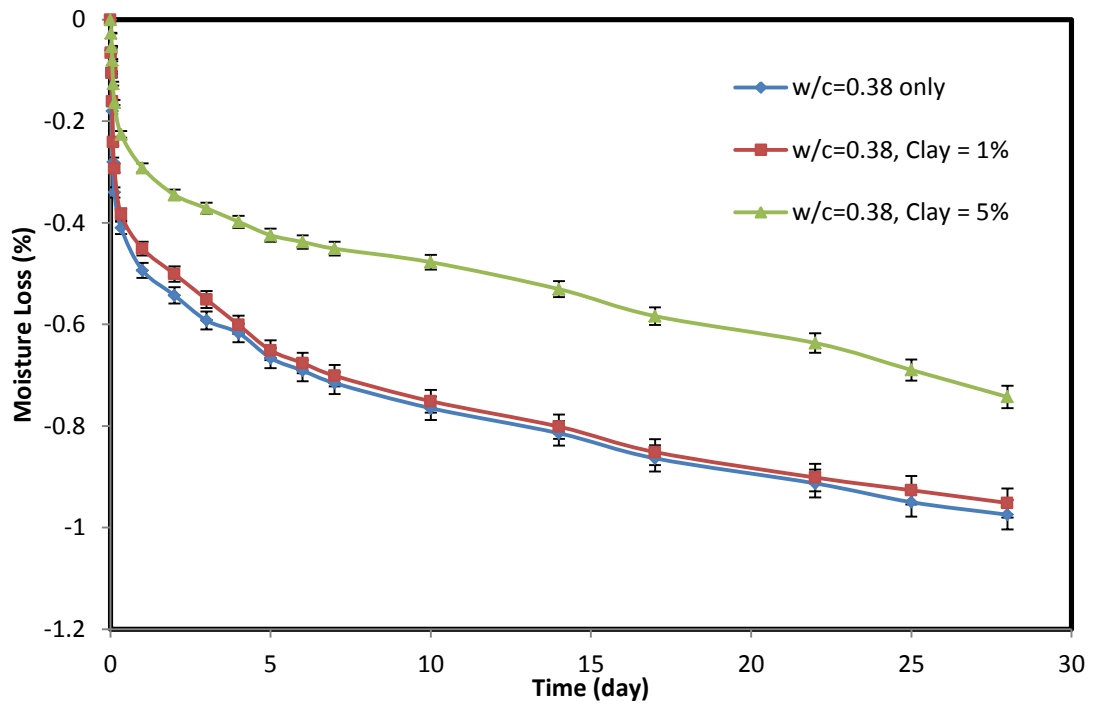


Figure 4-43: Moisture loss of cement specimens cured at room temperature with and without clay contamination up to 28 days

A relationship has been proposed for the resistivity of the cured specimen with the moisture loss (%) as

$$\rho = \rho_0 + D * (\Delta w / w_0)^m, \quad (4-15)$$

where, ρ = Resistivity of the cement ($\Omega.m$)

ρ_0 = Initial resistivity of the cement without moisture loss ($\Omega.m$)

$\Delta w / w_0$ = Moisture loss of the specimen (%)

D and m are constants and are model parameters that can be determined from the experimental results. For the Portland cement specimens with and without clay contamination, the experimental values fit very well (Fig. 4-44) with the proposed model.

The determined model parameters are as follows:

- (i) For Portland cement only, $D = 12.47$, $m = 2.57$, $R^2 = 0.98$
- (ii) For Portland cement with 1% clay, $D = 12.66$, $m = 2.60$, and $R^2 = 0.99$
- (iii) For Portland cement with 5% clay, $D = 16.17$, $m = 2.68$. $R^2 = 0.97$

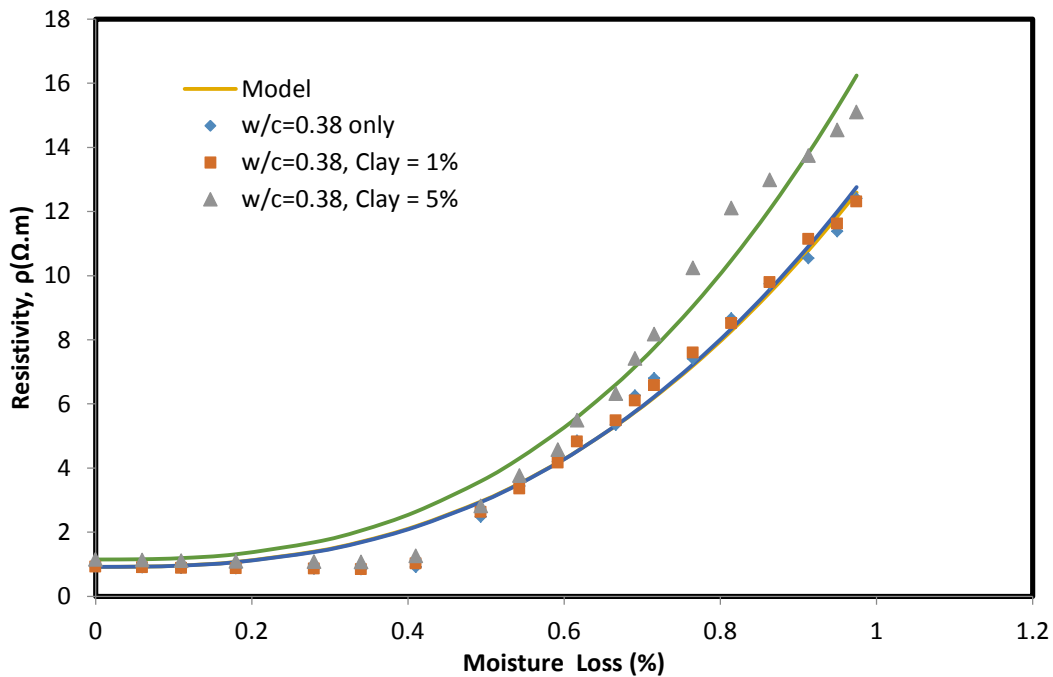


Figure 4-44: Change of resistivity with moisture loss of the cement specimens

4.4.2.3 Long time curing of the specimen without moisture loss at room temperature

The resistivity of the cement specimen with different percentage (0%, 1% and 5%) of clay contamination was determined up to 28 days at room temperature. The specimens were cured in an environment that ensures no moisture loss from the specimens. Unit weight of modified Portland cement with w/c ratio of 0.38 was 16.8 ± 0.10 ppg (19.74 kN/m^3) which was decreased with clay contamination. With 5% clay contamination, the unit weight decreased to 15.1 ± 0.08 ppg (17.74 kN/m^3). The initial electrical resistivity (ρ_o) of Portland cement with w/c ratio of 0.38 modified with 0.075% CF was 0.92 ± 0.01 $\Omega\text{-m}$ and the electrical resistivity reduced to reach the ρ_{\min} of 0.84 ± 0.01 $\Omega\text{-m}$ after 180 minutes (t_{\min}) as summarized in Table 4-21. With clay contamination, the initial electrical resistivity and the minimum electrical resistivity was increased but the time to reach the minimum (t_{\min}) was same. With 5% clay contamination, the ρ_o increased by 25% and ρ_{\min} increased by 27%. The 24 hours electrical resistivity ($\rho_{24\text{hr}}$) of the cement without contamination was 2.29 $\Omega\text{-m}$. Hence the maximum change in electrical resistivity after 24 hours ($RI_{24\text{hr}}$) was 172% as summarized in Table 4-21. The 7 days and 28 days electrical resistivity ($\rho_{7\text{days}}$ and $\rho_{28\text{days}}$) of the hardened cement were 5.62 $\Omega\text{-m}$ and 9.07 $\Omega\text{-m}$, hence the maximum change in electrical resistivity after 7 days and 28 days ($RI_{7\text{days}}$ and $RI_{28\text{days}}$) were 569% and 979% respectively. The addition of clay contamination increased the electrical resistivity compared to that of cement only. Addition of 5% clay contamination increased the 24 hours, 7 days and 28 days resistivity by about 18%, 36% and 52% respectively, and, the maximum change in electrical resistivity i.e. $RI_{24\text{hr}}$, $RI_{7\text{days}}$ and $RI_{28\text{days}}$ were also increased accordingly.

Table 4-21: Summary of bulk resistivity parameters for modified Portland cement with and without clay contamination cured under no moisture loss condition at room temperature up to 28 days

Mix Type	Density (ppg)	Initial resistivity ρ_o ($\Omega.m$)	ρ_{min} ($\Omega.m$)	t_{min} (min)	ρ_{24hr} ($\Omega.m$)	$\rho_{7\text{ days}}$ ($\Omega.m$)	$\rho_{28\text{ days}}$ ($\Omega.m$)	RI ₂₄ hr (%)	RI ₇ d _{ays} (%)	RI ₂₈ d _{ays} (%)
w/c=0.38	16.8±0.10	0.92±0.01	0.84±0.01	180	2.29	5.62	9.07	172	569	979
w/c=0.38 Clay = 1%	16.6±0.08	0.92±0.01	0.85±0.01	180	2.33	5.69	10.00	174	569	1076
w/c=0.38 Clay = 5%	15.1±0.08	1.15±0.03	1.07±0.02	180	2.70	7.65	13.85	152	615	1194

The curing model parameter q_1 for modified Portland cement only was 0.027 at 1 day of curing and increased to 0.485 at time up to 7 days and to 0.60 at 28 days. Clay contamination increased the q_1 value up to about 0.047 and then followed the similar trend with increase in curing time. The curing model parameter p_1 for modified Portland cement only was 0.0012 at 1 day of curing and increased to 1.151 at time up to 7 days and to 1.741 after curing time 28 days. (Table 4-22). Clay contamination decreased the parameter p_1 to 0.009 with 5% clay and followed the similar trend with increase in curing time and reached to 0.895 after curing time of 28 days. The curing model (Eqn. (3-11)) predicted the measured resistivity very well (Fig. 4-45). The coefficient of determination (R^2) varied from 0.98 to 0.99 and the root mean square of error (RMSE) varied from 0.02 $\Omega.m$ to 0.37 $\Omega.m$ for 1 day and 28 days of curing respectively.

Table 4-22: Model parameters for the curing model of the resistivity of modified Portland cement with and without clay contamination cured under no moisture loss condition at room temperature up to 28 days

Mix Type	Curing Time (day)	P_{\min} ($\Omega.m$)	t_{\min} (min)	q_1	t_0 (min)	p_1	RMSE ($1/\Omega.m$)	R^2
w/c=0.38	1 day	0.92	180	0.027	30	0.012	0.03	0.99
w/c=0.38 Clay = 1%		0.92	180	0.047	38	0.026	0.02	0.99
w/c=0.38 Clay = 5%		1.15	180	0.020	31	0.009	0.02	0.99
w/c=0.38	7 days	0.92	180	0.485	68	1.151	0.19	0.98
w/c=0.38 Clay = 1%		0.92	180	0.260	62	0.421	0.14	0.99
w/c=0.38 Clay = 5%		1.15	180	0.184	62	0.253	0.15	0.99
w/c=0.38	28 days	0.92	180	0.600	69	1.741	0.27	0.99
w/c=0.38 Clay = 1%		0.92	180	0.491	68	1.217	0.17	0.99
w/c=0.38 Clay = 5%		1.15	180	0.408	69	0.895	0.37	0.99

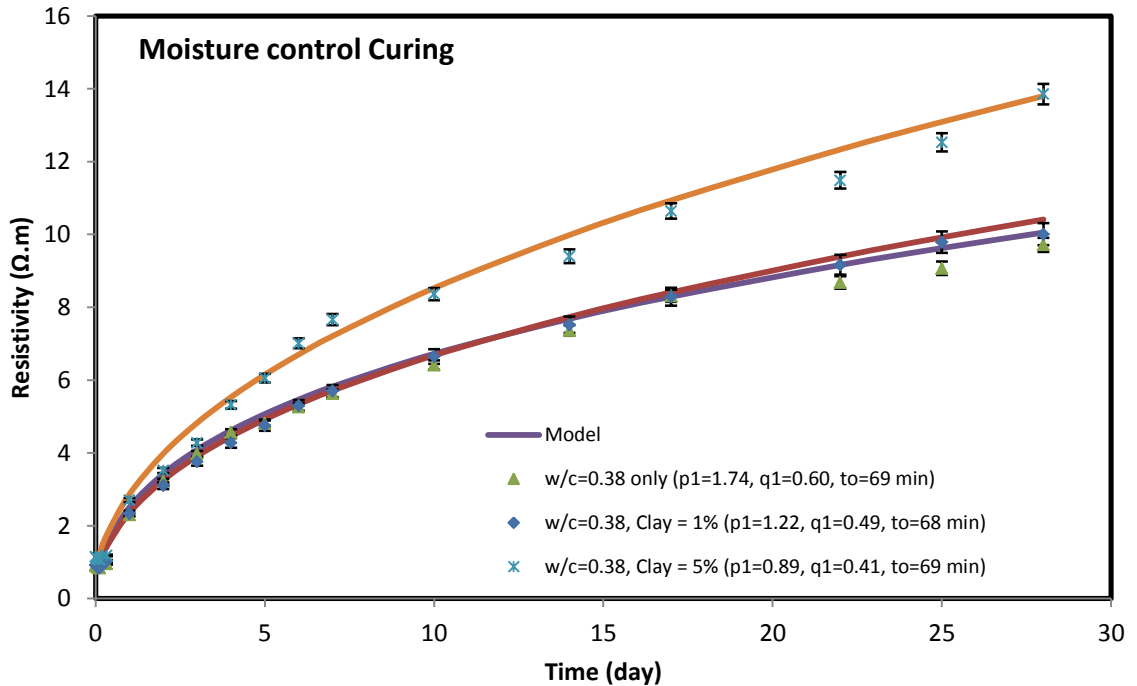


Figure 4-45: Variation of resistivity of curing cement specimen with time up to 28 days for Portland cement with and without clay contamination having no moisture loss modeled with curing model.

4.4.3 Piezoresistivity and strength of modified Portland cement

Addition of 0.075% conductive filler (CF) substantially improved piezoresistive behavior of the cement. Based on experimental results, p-q model developed by Vipulanandan and Paul (1990) was modified and used to predict the change in electrical resistivity of cement with applied stress for 1, 7 and 28 days of curing.

4.4.3.1 1 day of curing

The compressive strength (σ_f) of the modified Portland cement with 0%, 1%, and 5% clay contamination for one day of curing were 9.88 MPa, 9.44 MPa and 8.12 MPa; a 4%, and 18% reduction when the clay content increased about 1% and 5% respectively as summarized in Table 4-23.

The change in electrical resistivity at failure $\left(\frac{\Delta\rho}{\rho_o}\right)_f$ for the modified Portland cement was 432% which was reduced to 411% and 230% respectively as summarized in Table 4-23. With 5% clay contamination to the modified Portland cement, the change in electrical resistivity at failure $\left(\frac{\Delta\rho}{\rho_o}\right)_f$ was reduced about 45% from that of the modified Portland cement.

Using the p-q Piezoresistive model (Eqn. (3-15)), the relationships between compressive stress and the change in electrical resistivity $\left(\frac{\Delta\rho}{\rho_o}\right)$ of the modified Portland cement with different clay content of 0%, 1% and 5% for one day of curing were modeled. The piezoresistive model (Eqn. (3-15)) predicted the measured stress- change in resistivity relationship very well (Fig. 4-46). The model parameters q_2 and p_2 are summarized in Table 4-23. The coefficients of determination (R^2) were 0.97 to 0.99. The

root mean square of error (RMSE) varied between 0.21 MPa and 0.43 MPa as summarized in Table 4-23.

Table 4-23: Peak stress, piezoresistivity, model parameters p_2 , q_2 and R^2 & RMSE for the piezoresistivity model for the cement specimens under compressive stress after 1 day, 7 days and 28 days.

Mix Type	Curing Time (day)	Strength σ_f (MPa)	Piezoresistivity at peak stress, $(\Delta\rho/\rho_0)_f$ (%)	p_2	q_2	R^2	RMSE (MPa)
w/c=0.38	1 day	9.88	432	0.047	2.77	0.99	0.21
w/c=0.38 Clay = 1%		9.44	411	0.025	1.48	0.98	0.43
w/c=0.38 Clay = 5%		8.12	230	0.031	1.64	0.97	0.43
w/c=0.38	7 days	20.86	338	0.0002	0.95	0.98	0.69
w/c=0.38 Clay = 1%		18.66	280	0.002	0.80	0.98	0.70
w/c=0.38 Clay = 5%		16.47	216	0.002	0.59	0.97	0.84
w/c=0.38	28 days	31.40	270	0.062	0.75	0.98	0.44
w/c=0.38 Clay = 1%		30.08	209	0.052	0.75	0.99	0.34
w/c=0.38 Clay = 5%		27.44	158	0.125	0.78	0.99	0.34

Rate of change of resistivity with respect to stress change:

As we have considered the rate of resistivity change $\Delta\rho/\rho_0$ as X, and if we consider the stress as Y, then the slope dX/dY , which is rate of change of resistivity with respect to stress change could be another indicator of the piezoresistivity. For 1 day of curing, the rate of change of resistivity (dX/dY) without any clay contamination was decreased from 120 to 20 (%/MPa) which increased to 30 (%/MPa) and changes the slope before the specimen cracks. With 5% clay contamination, the rate of change of resistivity (dX/dY) decreased from 40 to 17 (%/MPa) which increased suddenly or changes the slope when the cement specimen experiences cracks (Figure 4-47).

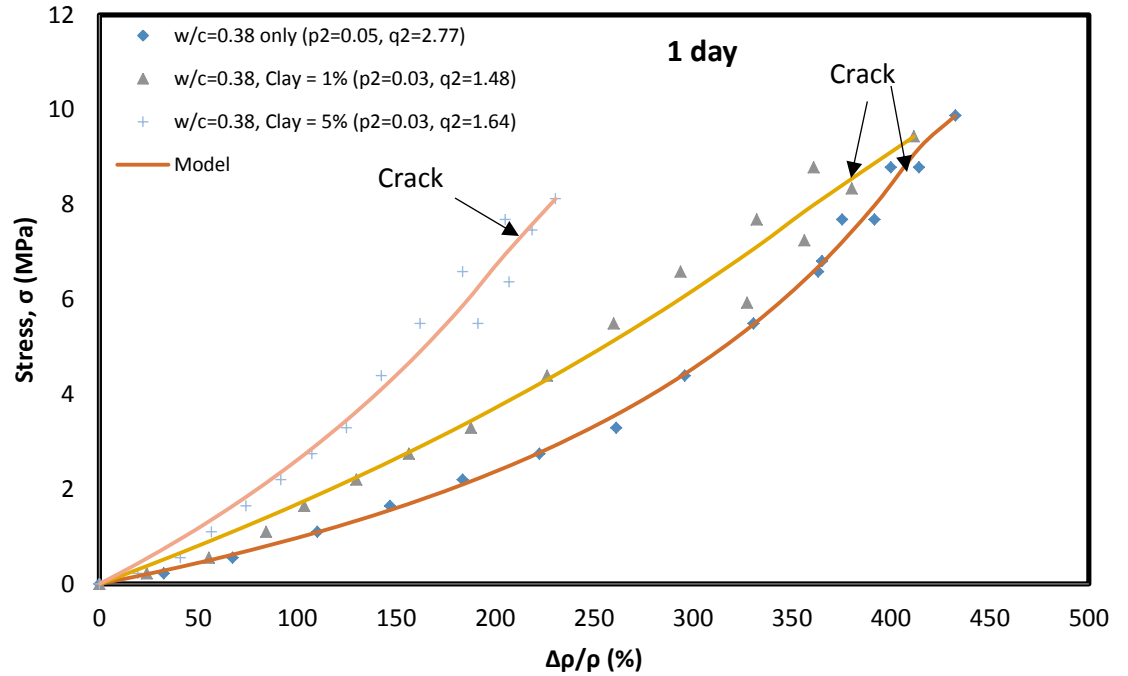


Figure 4-46: Piezoresistive response of the cement with and without clay contamination after 1 day of curing.

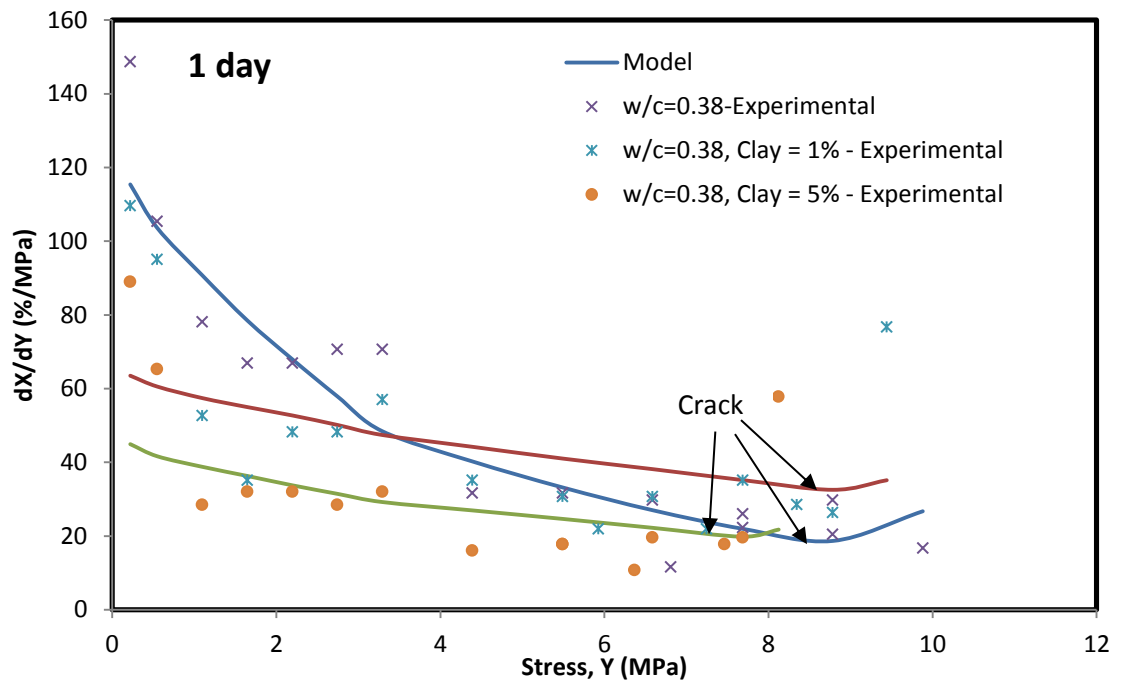


Figure 4-47: Rate of change of resistivity with respect to stress vs Stress for 1 day of curing

4.4.3.2 7 days of Curing

The compressive strength (σ_f) of the modified Portland cement with 0%, 1%, and 5% clay contamination for one day of curing were 20.86 MPa, 18.66 MPa and 16.47 MPa; a 10%, and 21% reduction when the clay content increased about 1% and 5% respectively as summarized in Table 4-23.

The change in electrical resistivity at failure $\left(\frac{\Delta\rho}{\rho_o}\right)_f$ for the modified Portland cement was 338% which was reduced to 280% and 216% respectively as summarized in Table 4-23. With 5% clay contamination to the modified Portland cement, the change in electrical resistivity at failure $\left(\frac{\Delta\rho}{\rho_o}\right)_f$ was reduced about 36% from that of the modified Portland cement.

Using the p-q Piezoresistive model (Eqn. (3-15)), the relationships between compressive stress and the change in electrical resistivity $\left(\frac{\Delta\rho}{\rho_o}\right)$ of the modified Portland cement with different clay content of 0%, 1% and 5% for one day of curing were modeled. The piezoresistive model (Eqn. (3-15)) predicted the measured stress- change in resistivity relationship very well (Fig. 4-48). The model parameters q_2 and p_2 are summarized in Table 4-23. The coefficients of determination (R^2) were 0.97 to 0.98. The root mean square of error (RMSE) varied between 0.69 MPa and 0.84 MPa as summarized in Table 4-23.

Rate of change of resistivity with respect to stress change:

For 7 day of curing, the rate of change of resistivity (dX/dY) without any clay contamination was about 15 (%/MPa) which was almost unchanged and suddenly changed the slope before the specimen cracks. With 5% clay contamination, the rate of

change of resistivity (dX/dY) decreases upto 8 (%/MPa) which increased slowly but increased suddenly and changed the slope when the cement specimen experienced cracks (Figure 4-49).

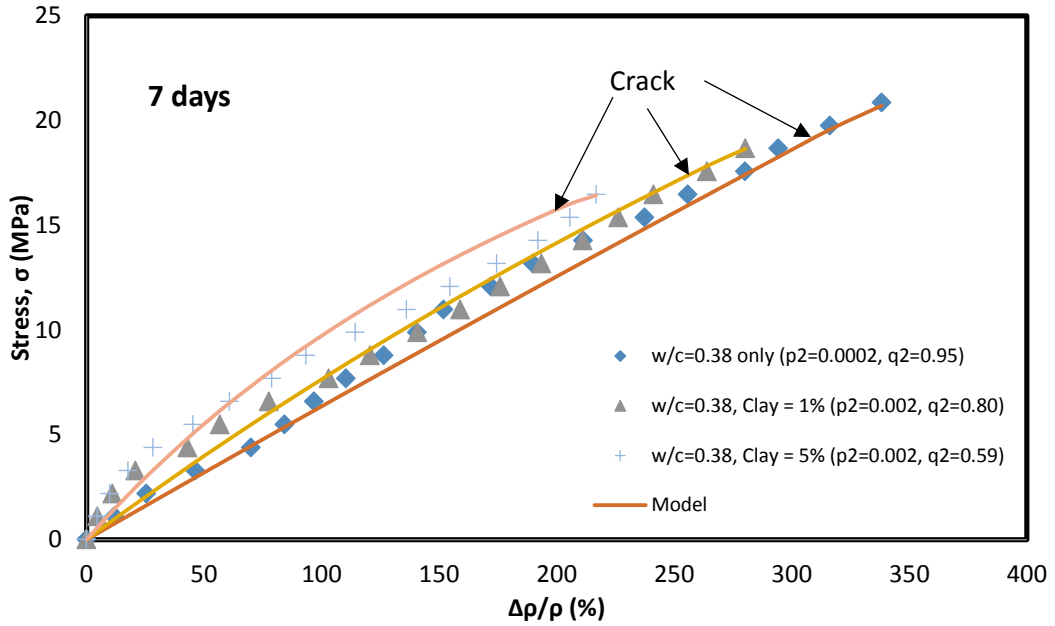


Figure 4-48: Piezoresistive response of the cement with and without clay contamination after 7 days of curing

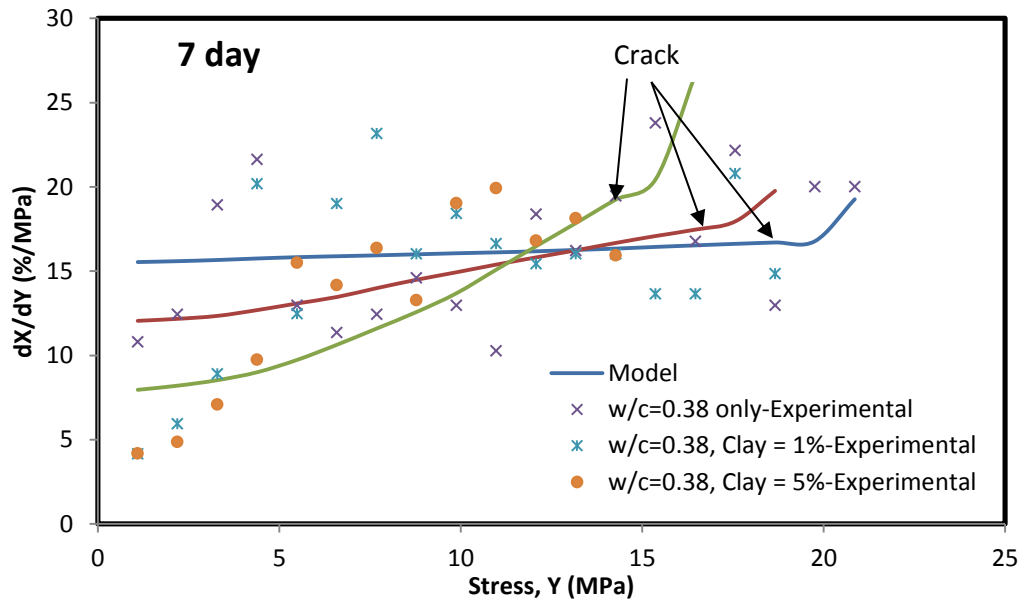


Figure 4-49: Rate of change of resistivity with respect to stress vs Stress for 7 days curing

4.4.3.3 28 days of Curing

The compressive strength (σ_f) of the modified Portland cement with 0%, 1%, and 5% clay contamination for one day of curing were 31.40 MPa, 30.08 MPa and 27.44 MPa; a 4%, and 13% reduction when the clay content increased about 1% and 5% respectively as summarized in Table 4-23.

The change in electrical resistivity at failure $\left(\frac{\Delta\rho}{\rho_o}\right)_f$ for the modified Portland cement was 270% which was reduced to 209% and 158% respectively as summarized in Table 4-23. With 5% clay contamination to the modified Portland cement, the change in electrical resistivity at failure $\left(\frac{\Delta\rho}{\rho_o}\right)_f$ was reduced about 40% from that of the modified Portland cement.

Using the p-q Piezoresistive model (Eqn. (3-15)), the relationships between compressive stress and the change in electrical resistivity $\left(\frac{\Delta\rho}{\rho_o}\right)$ of the modified Portland cement with different clay content of 0%, 1% and 5% for one day of curing were modeled. The piezoresistive model (Eqn. (3-15)) predicted the measured stress- change in resistivity relationship very well (Fig. 4-50). The model parameters q_2 and p_2 are summarized in Table 4-23. The coefficients of determination (R^2) were 0.98 to 0.99. The root mean square of error (RMSE) varied between 0.34 MPa and 0.44 MPa as summarized in Table 4-23.

Rate of change of resistivity rate with respect to stress change

For 28 days of curing, the rate of change of resistivity (dX/dY) without any clay contamination was about 6-12 (%/MPa) which was suddenly increased to 37 (%/MPa) and changed the slope before the specimen cracks. With 5% clay contamination, the rate

of change of resistivity (dX/dY) decreased upto 4-7 (%/MPa) which was suddenly increased to 20 (%/MPa) and changed the slope before the specimen cracks (Figure 4-51).

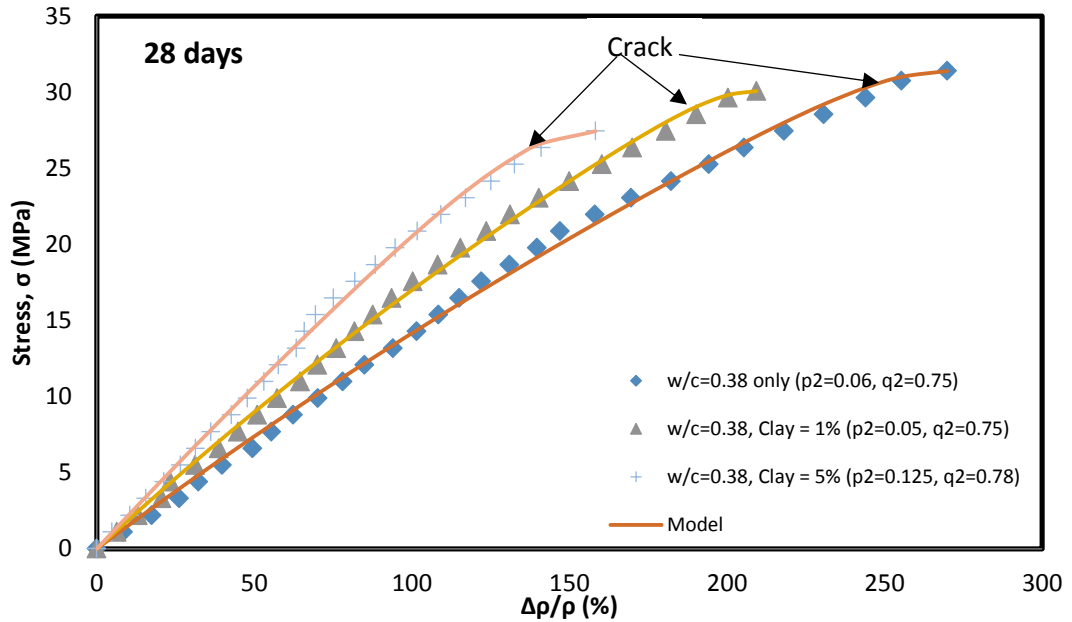


Figure 4-50: Piezoresistive response of the cement with and without clay contamination after 28 days of curing.

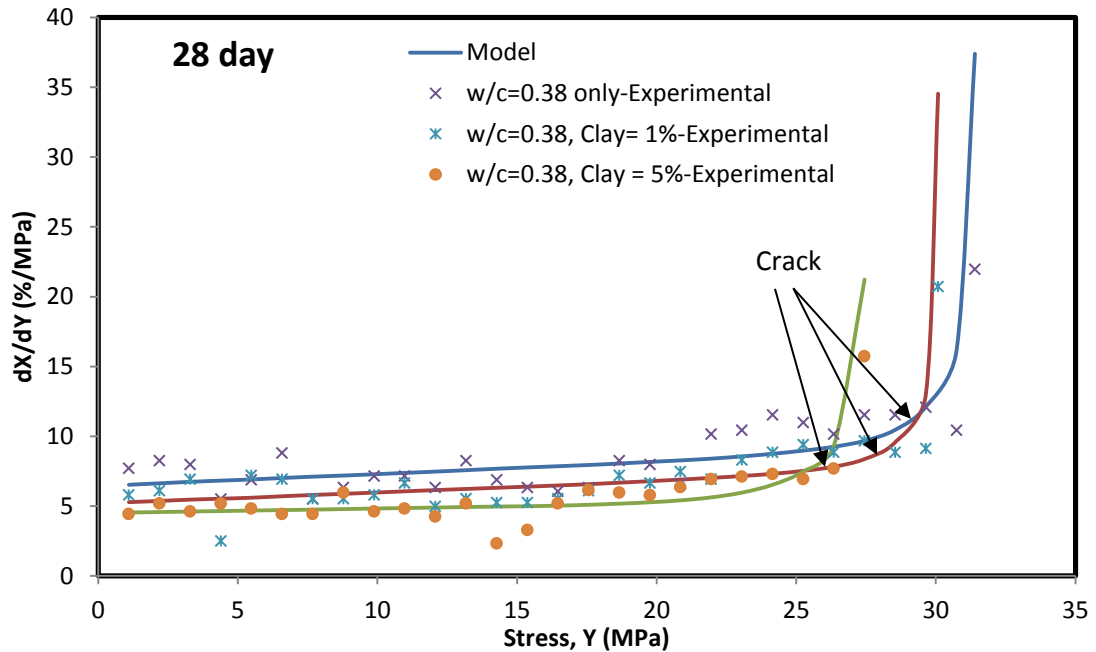


Figure 4-51: Rate of change of resistivity with respect to stress vs Stress for 28 days curing

4.4.3.4 Relationship between curing time and strength/piezoresistivity at failure

The strength of the cement specimen made with and without clay contamination was observed up to 28 days. With curing time increases, the compressive strength of the cement specimen increased. The relationship between the compressive strength of the cement and curing time has been modeled with the hyperbolic model

$$\sigma_c = t/(E + Ft), \quad (4-16)$$

where,

σ_c = Compressive strength of the grout (MPa)

t = Curing time (day)

Parameters E and F are model parameters and parameter E represent the initial rate of change and parameter F determines the ultimate strength. The experimental results matched very well (Fig. 4-52) with the proposed model with coefficient of determination (R^2) of 0.95-0.96. For modified Portland cement only, parameters E and F were found as 0.098 MPa^{-1} and 0.029 MPa^{-1} . For modified Portland cement with 1% clay, parameters E and F were found as 0.119 MPa^{-1} and 0.030 MPa^{-1} . For modified Portland cement with 5% clay, parameters E and F were found as 0.151 MPa^{-1} and 0.032 MPa^{-1} .

The piezoresistivity at failure of the cement specimen made with and without clay contamination was observed up to 28 days. With curing time increases, the piezoresistivity at failure of the cement specimen changes. The relationship between the piezoresistivity at failure of the cement grout and curing time has been modeled with the hyperbolic model

$$\Delta\rho/\rho_o = (\Delta\rho/\rho_o)_1 - t/(G + Ht), \quad (4-17)$$

where,

$\Delta\rho/\rho_o$ = Piezoresistivity at failure (%)

$(\Delta\rho/\rho_0)_1$ = Piezoresistivity at failure after 1 day (%)

t = Curing time (day)

Parameters G and H are model parameters and parameter G represent the initial rate of change and parameter H determines the ultimate piezoresistivity. The experimental results matched very well (Fig. 4-53) with the proposed model with coefficient of determination (R^2) of 0.95-0.99. For modified Portland cement only, parameters G and H were found as 0.051 MPa^{-1} and 0.004 MPa^{-1} . For modified Portland cement with 1% clay, parameters G and H were found as 0.033 MPa^{-1} and 0.003 MPa^{-1} . For modified Portland cement with 5% clay, parameters G and H were found as 0.551 MPa^{-1} and 0.006 MPa^{-1} .

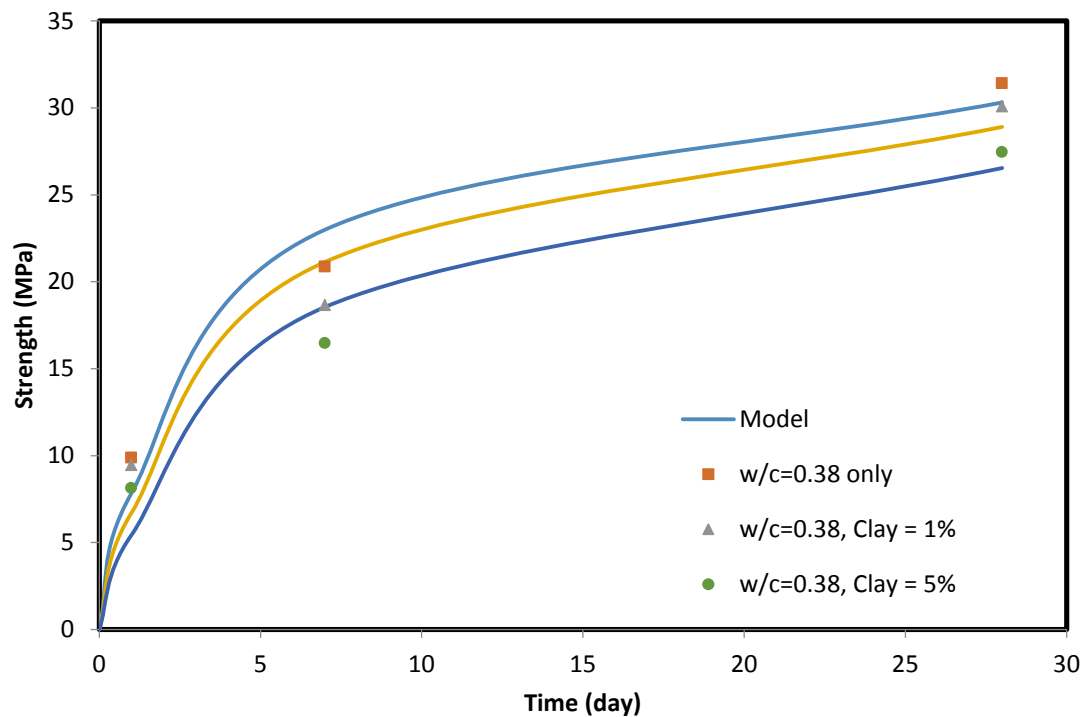


Figure 4-52: Relationship between compressive strength and the curing time for the cement specimen modeled with hyperbolic model

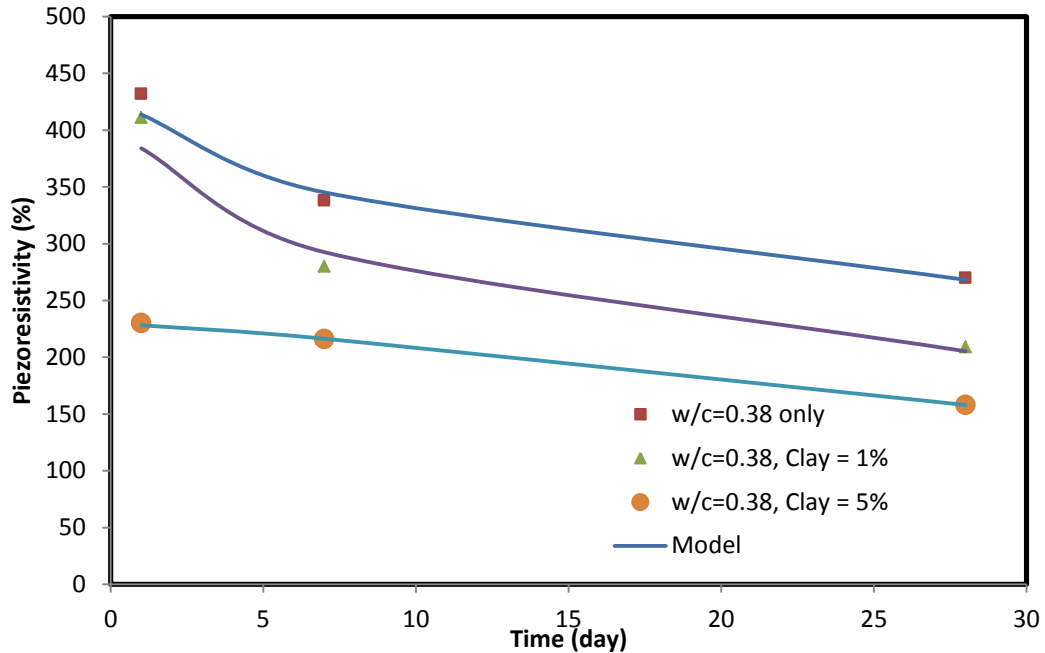


Figure 4-53: Relationship between Piezoresistivity at failure and the curing time for the cement specimen modeled with hyperbolic model

4.5 Summary

Based on experimental and analytical study on smart cement with the addition of sodium meta-silicate (SMS), at different curing temperature and condition, and on the modified Portland cement with and without clay contamination, the following observations are advanced:

- 1) Addition of 0.1% SMS increased the pH and reduced the resistivity of water by 50% and 80% respectively. The change in resistivity of water with the addition of SMS has been modeled.
- 2) Addition of 0.3% SMS increased the 10 second and 10 minute gel strength of smart cement slurry by over 30%, and also increased the yield stress by about 280%. The apparent viscosity of smart cement slurry at 100 sec^{-1} was increased

by 85% with addition of 0.3% SMS. Shear stress and shear strain rate relationships have been modeled.

- 3) Addition of 0.2% SMS increased the fluid loss of the smart cement slurry by 6%.
- 4) The initial resistivity (ρ_o) of the smart cement decreased from 0.97 Ω -m to 0.87 Ω -m with 0.3% SMS, a 10% decrease. The minimum resistivity (ρ_{min}) of the smart cement decreased from 0.81 Ω -m to 0.61 Ω -m with 0.3% SMS, a 24% decrease. The changes in the electrical resistivity were higher than the changes in the unit weight of the cement. Hence the electrical resistivity can also be used for quality control
- 5) Electrical resistivity developments with hydration time of the cement with different amount of SMS follow a similar pattern: they first drop to a minimum point and then gradually increase with time. The resistivity index ($RI_{24 \text{ hour}}$, $RI_{7 \text{ days}}$, $RI_{28 \text{ days}}$) of the smart cement were 183%, 1239% and 2810% which decreased from 5-14% with 0.3% SMS content.
- 6) A hyperbolic relationship has been observed between the minimum resistivity and the SMS concentration.
- 7) For long term curing under room temperature after 1 year, the resistivity of the smart cement was found about 95 Ω .m, whereas the cement specimen with 0.3% SMS had a resistivity of 58 Ω .m which was 38% less than that of the smart cement. The moisture loss of the smart cement specimen 6.2% which was also reduced with addition of SMS. The specimen with 0.3% SMS lost 5.4% moisture, an 11% less weight than the specimen with no SMS.

- 8) For long term curing under no moisture loss condition after 12 months, the resistivity of the smart cement was found about 26.27 Ω .m which is 72% less than that of room curing condition (94.8 Ω .m). On the other hand, the cement specimen with 0.3% SMS had a resistivity of 24.6 Ω .m which was 6% less than that of the smart cement under no moisture loss condition.
- 9) For long term curing under water after 12 months, the resistivity of the smart cement was found about 19.93 Ω .m which is 78% less than that of room curing condition (94.8 Ω .m). On the other hand, the cement specimen with 0.3% SMS had a resistivity of 16.52 Ω .m which was 17% less than that of the smart cement cured under water.
- 10) The resistivity with curing time under different curing condition was modeled with curing model developed from p-q model and the model parameters were determined with very good coefficient of correlation and RMSE.
- 11) A polynomial relationship has been proposed for the resistivity of the cured specimen (ρ) with the moisture loss/gain (%) and found matched very well with the experimental results with very good coefficient of determination.
- 12) The smart cement showed piezoresistive behavior under compressive stress. Without any SMS piezoresistivity at peak stress was varying from 315% to 545% which is reduced up to 145% to 230% with addition of 0.3% SMS. The nonlinear piezoresistive model predicated the compressive stress – change in resistivity relationship of the smart cement very well
- 13) The rate of change of resistivity with respect to stress change was found to be another indicator of the piezoresistivity. During the application of the stress, this

indicator changes very slowly but after the initial crack happens, the rate of change of resistivity with respect to stress changes sharply or changes the slope which indicates prior to failure of the specimen.

- 14) A linear relationship has been found between the RI_{24} and the compressive strength of the cement.
- 15) A hyperbolic relationship has been observed between the compressive strength and SMS concentration. The piezoresistivity also showed same kind of relationship with the SMS concentration.
- 16) The relationship between the compressive strength of the cement and curing time has been modeled with the hyperbolic model and the experimental values matched very well with the model having very good coefficient of determination. The relationship between the piezoresistivity at failure and curing time was also modeled with the hyperbolic model and fits very well with the experimental results
- 17) The resistivity index ($RI_{24 \text{ hour}}$, $RI_{7 \text{ days}}$, $RI_{28 \text{ days}}$) of the smart cement oven cured at 80°C temperature were 331%, 1472% and 5127% but for the smart cement oven cured in saturated sand at 80°C temperature those index were 75%, 628% and 1164% respectively. Thus the smart cement oven cured in saturated condition had 77%, 57% and 77% less resistivity for 1 day, 7 days, and 28 days curing compared to that of dry oven curing.
- 18) The resistivity index ($RI_{24 \text{ hour}}$, $RI_{7 \text{ days}}$, $RI_{28 \text{ days}}$) of the smart cement with 0.3% SMS oven cured at 80°C temperature were 233%, 1038% and 3319% but for the same sample oven cured in saturated sand at 80°C temperature those index were

82%, 617% and 1058% respectively. Thus the smart cement with 0.3% SMS oven cured in saturated condition had 65%, 41% and 68% less resistivity for 1 day, 7 days, and 28 days curing compared to that of dry oven curing.

19) The resistivity with curing time under different curing condition was modeled with curing model developed from p-q model and the model parameters were determined with very good coefficient of correlation and RMSE.

20) A linear relationship between the moisture loss/gain ($\Delta w/w_0$) and the change in the resistivity ($\Delta \rho/\rho_0$) for smart cement sample with and without SMS for both types of high temperature curing was observed. A polynomial relationship has been proposed for the resistivity of the cured specimen (ρ) with the moisture loss/gain (%) and found matched very well with the experimental results with very good coefficient of determination.

21) The smart cement cured at high temperature (80°C) showed piezoresistive behavior under compressive stress. Without any SMS, piezoresistivity at peak stress was varying from 245% to 475% which is reduced up to 160% to 345% with 0.3% SMS. The high temperature (80°C) curing in saturated sand showed comparatively higher (about 15% to 25% more) piezoresistivity compared to that of the dry high temperature curing. The nonlinear piezoresistive model predicated the compressive stress – change in resistivity relationship of the smart cement with and without SMS very well.

22) The rate of change of resistivity with respect to stress change was found to be another indicator of the piezoresistivity. During the application of the stress, this indicator changes very slowly but after the initial crack happens, the rate of

change of resistivity with respect to stress changes sharply or changes the slope which indicates prior to failure of the specimen.

- 23) The relationship between the compressive strength of the cement and curing time has been modeled with the hyperbolic model and the experimental values matched very well with the model having very good coefficient of determination. The relationship between the piezoresistivity at failure and curing time was also modeled with the hyperbolic model and fits very well with the experimental results.
- 24) The initial resistivity (ρ_o) of the modified Portland cement increased from 0.92 $\Omega\cdot\text{m}$ to 1.15 $\Omega\cdot\text{m}$ with 5% clay contamination, a 25% increase. The minimum resistivity (ρ_{min}) of the modified Portland cement increased from 0.84 $\Omega\cdot\text{m}$ to 1.07 $\Omega\cdot\text{m}$ with 5% clay contamination, a 27% increase. The changes in the electrical resistivity were higher than the changes in the unit weight of the cement. Hence the electrical resistivity can also be used for quality control of Portland cement.
- 25) The resistivity index ($\text{RI}_{24 \text{ hour}}$, $\text{RI}_{7 \text{ days}}$, $\text{RI}_{28 \text{ days}}$) of the modified Portland cement were 195%, 708% and 1253%. With 5% clay contamination, $\text{RI}_{24 \text{ hr}}$ and $\text{RI}_{7 \text{ days}}$ were decreased by about 15% and 6% respectively but $\text{RI}_{28 \text{ days}}$ was increased by 5%.
- 26) For long term curing under room temperature after 28 days, the resistivity of the modified Portland cement was found about 11.37 $\Omega\cdot\text{m}$, whereas the cement specimen with 5% clay contamination had a resistivity of 15.10 $\Omega\cdot\text{m}$ which was 32% higher than that of the modified Portland cement. The moisture loss of the modified Portland cement specimen was about 1% which was also reduced with

clay contamination. The specimen with 5% clay contamination lost 0.75% moisture, a 25% less weight loss than the specimen with no clay contamination.

- 27) For long term curing under no moisture loss condition after 28 days, the resistivity of the modified Portland cement was found about 9.07 $\Omega\cdot\text{m}$ which is 20% less than that of room curing condition (11.37 $\Omega\cdot\text{m}$). On the other hand, the cement specimen with 5% clay contamination had a resistivity of 13.85 $\Omega\cdot\text{m}$ which was 52% higher than that of the cement specimen having no clay contamination under no moisture loss condition.
- 28) The resistivity with curing time under different curing condition was modeled with curing model developed from p-q model and the model parameters were determined with very good coefficient of correlation and RMSE.
- 29) A polynomial relationship between the moisture loss ($\Delta w/w_0$) and the change in the resistivity ($\Delta\rho/\rho_0$) for modified Portland cement sample with and without clay contamination was observed. Another polynomial relationship has been proposed for the resistivity of the cured specimen (ρ) with the moisture loss (%) and found matched very well with the experimental results with very good coefficient of determination.
- 30) The modified Portland cement showed piezoresistive behavior under compressive stress. Without any clay contamination, piezoresistivity at peak stress was varying from 270-430% which is reduced up to 160-230% with 5% clay contamination. The nonlinear piezoresistive model predicated the compressive stress – change in resistivity relationship of the modified Portland cement very well.

- 31) The rate of change of resistivity with respect to stress change was found to be another indicator of the piezoresistivity. During the application of the stress, this indicator changes very slowly but after the initial crack happens, the rate of change of resistivity with respect to stress changes sharply or changes the slope which indicates prior to failure of the specimen.
- 32) The relationship between the compressive strength of the cement and curing time has been modeled with the hyperbolic model and the experimental values matched very well with the model having very good coefficient of determination. The relationship between the piezoresistivity at failure and curing time was also modeled with the hyperbolic model and fits very well with the experimental results.

CHAPTER 5 CHARACTERIZING THE SMART CEMENT GROUTS

5.1 Curing

The change of electrical resistivity with curing time for the smart cement grout with and without SMS and for repaired cement with those grouts was observed up to 28 days of curing. The normal trend of the resistivity of the cured cement is that the resistivity decreased up to a certain time (t_{min}) and reached to a minimum resistivity (ρ_{min}) and then increased with time. Hence the model proposed by Vipulanandan and Paul (1990) was modified (Eqn. (3-11)) was used to predict the electrical resistivity of cement during hydration for different curing condition and curing time.

Several resistivity parameters can be used in monitoring the curing (hardening process) of the smart cement grout. The parameters are initial resistivity (ρ_o), minimum electrical resistivity (ρ_{min}), time to reach the minimum resistivity (t_{min}) and percentage of maximum change in resistivities at the end of 24 hours (RI_{24hr}), 7 days (RI_{7days}), and 28 days ($RI_{28 days}$) as defined in (Eqn. (3-12)), (Eqn. (3-13)) and (Eqn. (3-14)).

5.1.1 Room Temperature

The resistivity of the smart cement grout with and without 3% SMS cured under room temperature was observed for 28 days. Unit weight of the smart cement grout with w/c ratio of 0.8 was 13.44 ppg (15.79 kN/m³) which increased to 13.52 ppg (15.88 kN/m³) with 1% SMS and further increased to 13.56 ppg (15.93 kN/m³) with 3% SMS. The initial electrical resistivity (ρ_o) of the smart cement grout with w/c ratio of 0.8 was 1.08±0.01 Ω-m and the electrical resistivity reduced to reach the ρ_{min} of 1.04±0.01 Ω-m

after 180 minutes (t_{\min}) as summarized in Table 5-1. With 1% and 3% SMS, the initial electrical resistivity and the minimum electrical resistivity was decreased and the time to reach the minimum (t_{\min}) increased to 300 minutes. With 1% SMS, the ρ_o was 0.69 ± 0.02 $\Omega.m$, decreased by 36% and ρ_{\min} was 0.54 $\Omega.m$, decreased by 44%. And with 3% SMS, the ρ_o was 0.52 ± 0.02 $\Omega.m$, decreased by 51% and ρ_{\min} was 0.41 $\Omega.m$, decreased by 60%. The 24 hours electrical resistivity (ρ_{24hr}) of the smart cement grout was 2.16 $\Omega.m$. Hence the maximum change in electrical resistivity after 24 hours (RI_{24hr}) was 108% as summarized in Table 5-1. The 7 days and 28 days electrical resistivity (ρ_{7days} and ρ_{28days}) for the smart cement grout were 6.16 $\Omega.m$ and 9.37 $\Omega.m$, hence the maximum change in electrical resistivity after 7 days and 28 days (RI_{7days} and $RI_{28 days}$) were 492% and 801% respectively. The addition of SMS decreased the electrical resistivity of the smart cement grout. Addition of 1% SMS decreased the 24 hours, 7 days and 28 days resistivity of the smart cement grout by about 52%, 60% and 48% respectively and hence the maximum change in electrical resistivity i.e. RI_{24hr} , RI_{7days} and $RI_{28 days}$ were also decreased compared to that of smart cement grout only. Addition of 3% SMS decreased the 24 hours, 7 days and 28 days resistivity of the smart cement grout by about 74%, 79% and 65% respectively and hence the maximum change in electrical resistivity indices RI_{24hr} , RI_{7days} and $RI_{28 days}$ were also decreased accordingly.

Table 5-1: Bulk resistivity parameters for smart cement grout with and without SMS cured at room temperature up to 28 days

Mix Type	Density (ppg)	Initial resistivity, ρ_o ($\Omega.m$)	ρ_{min} ($\Omega.m$)	t_{min} (min)	ρ_{24hr} ($\Omega.m$)	$\rho_{7\text{ days}}$ ($\Omega.m$)	$\rho_{28\text{ days}}$ ($\Omega.m$)	$RI_{24\text{ hr}}$ (%)	$RI_{7\text{ days}}$ (%)	$RI_{28\text{ days}}$ (%)
Grout (H, w/c=0.8 only)	13.44±0.02	1.08±0.01	1.04	180	2.16	6.16	9.37	108	492	801
Grout (H, w/c=0.8, SMS = 1%)	13.52±0.01	0.69±0.02	0.54	300	1.01	2.20	4.85	87	307	798
Grout (H, w/c=0.8, SMS = 3%)	13.56±0.02	0.52±0.02	0.41	300	0.56	1.28	3.29	37	212	702

Table 5-2: Curing model parameters for smart grout repaired cement

Mix Type	Density (ppg)	Initial resistivity, ρ_o ($\Omega.m$)	ρ_{min} ($\Omega.m$)	t_{min} (min)	ρ_{24hr} ($\Omega.m$)	$\rho_{7\text{ days}}$ ($\Omega.m$)	$\rho_{28\text{ days}}$ ($\Omega.m$)	$RI_{24\text{ hr}}$ (%)	$RI_{7\text{ days}}$ (%)	$RI_{28\text{ days}}$ (%)
Repaired cement with grout (H, w/c=0.8 only)	16.20±0.05	12.5	12.42	180	18.45	27.88	35.2	49	124	183
Repaired cement with grout (H, w/c=0.8, SMS = 1%)	16.40±0.04	3.30	3.21	300	8.74	19.34	25.17	172	502	684
Repaired cement with grout (H, w/c=0.8, SMS = 3%)	16.44±0.04	1.64	1.54	300	3.09	9.46	17.76	101	514	1053

The resistivity of the repaired cement specimen with smart cement grout only and with smart cement grout with 1% and 3% SMS cured under room temperature was observed for 28 days. Unit weight of the cement repaired with smart cement grout with w/c ratio of 0.8 was 16.20±0.05 ppg (19.04 kN/m³) which was increased to 16.40±0.04 ppg (19.27 kN/m³) for the specimen repaired with smart cement grout with the 1% SMS and to 16.44±0.04 ppg (19.31 kN/m³) for the specimen repaired with smart cement grout with the 3% SMS. The initial electrical resistivity (ρ_o) of the specimen repaired with smart

cement grout with w/c ratio of 0.8 was 12.5 Ω -m and the electrical resistivity reduced to reach the ρ_{\min} of 12.42 Ω -m after 180 minutes (t_{\min}) as summarized in Table 5-2. For the specimen repaired with smart cement grout with the 1% SMS, the initial electrical resistivity was 3.30 Ω -m and the minimum electrical resistivity was 3.21 Ω -m; and the time to reach the minimum (t_{\min}) was 300 minutes and for the specimen repaired with smart cement grout with the 3% SMS, the initial electrical resistivity was 1.64 Ω -m and the minimum electrical resistivity was 1.54 Ω -m; and the time to reach the minimum (t_{\min}) was 300 minutes. Here, the curing of the repaired specimen followed similar trend of curing like the grout specimens. The 24 hours electrical resistivity ($\rho_{24\text{hr}}$) of the specimen repaired with smart cement grout only was 18.45 Ω .m. Hence the maximum change in electrical resistivity after 24 hours ($RI_{24\text{hr}}$) was 49% as summarized in Table 5-2. The 7 days and 28 days electrical resistivity ($\rho_{7\text{days}}$ and $\rho_{28\text{days}}$) of the specimen repaired with smart cement grout only were 27.88 Ω .m and 35.2 Ω .m, hence the maximum change in electrical resistivity after 7 days and 28 days ($RI_{7\text{days}}$ and $RI_{28\text{days}}$) were 124% and 183% respectively. For the specimen repaired with smart cement grout with the 1% SMS, the 24 hours, 7 days and 28 days resistivity were 8.74 Ω -m, 19.34 Ω -m and 25.17 Ω -m, hence the maximum change in electrical resistivity i.e. $RI_{24\text{hr}}$, $RI_{7\text{days}}$ and $RI_{28\text{days}}$ were 172%, 502% and 684% respectively. For the specimen repaired with smart cement grout with the 3% SMS, the 24 hours, 7 days and 28 days resistivity were 3.09 Ω -m, 9.46 Ω -m and 17.11 Ω -m, hence the maximum change in electrical resistivity i.e. $RI_{24\text{hr}}$, $RI_{7\text{days}}$ and $RI_{28\text{days}}$ were 101%, 514% and 1053% respectively.

Modeling:

The curing model parameter p_1 for smart cement grout was 0.286 at 1 day of

curing and decreased to 0.085 at time up to 7 days and increased to 0.709 at time 28 days (Table 5-3). Addition of 1% SMS decreased the parameter p_1 to about 0.244 after 1 day of curing and then increased to 0.328 at 7 days and the decreased to 0.236 after 28 days of curing. Addition of 3% SMS further decreased the parameter p_1 to about 0.174 after 1 day of curing and then decreased to 0.148 at 7 days of curing and again increased to 0.113 after 28 days of curing. The curing model parameter q_1 for smart cement grout only was 0.188 after 1 day of curing and decreased to 0.072 after 7 days of curing and then increased to 0.295 at 28 days as summarized in Table 5-3. Addition of 1% SMS increased the q_1 value up to about 0.217 and it was decreased to 0.199 at 7 days and then decreased to 0.161 at 28 days. But addition of 3% SMS decreased the q_1 value up to about 0.131 and it decreased to 0.111 at 7 days and then decreased to 0.092 at 28 days.

Table 5-3: Curing Model parameters

Mix Type	Curing Time (day)	ρ_{min} ($\Omega.m$)	t_{min} (min)	p_1	q_1	t_o (min)	RMSE ($\Omega.m$)	R^2
Grout (H, w/c=0.8 only)	1 day	1.04	180	0.286	0.188	63	0.04	0.98
Grout (H, w/c=0.8, SMS = 1%)		0.54	300	0.244	0.217	70	0.03	0.95
Grout (H, w/c=0.8, SMS = 3%)		0.41	300	0.174	0.131	61	0.03	0.97
Grout (H, w/c=0.8 only)	7 days	1.04	180	0.085	0.072	100	0.09	0.99
Grout (H, w/c=0.8, SMS = 1%)		0.54	300	0.328	0.199	70	0.09	0.97
Grout (H, w/c=0.8, SMS = 3%)		0.41	300	0.148	0.111	56	0.03	0.98
Grout (H, w/c=0.8 only)	28 days	1.04	180	0.709	0.295	110	0.45	0.97
Grout (H, w/c=0.8, SMS = 1%)		0.54	300	0.236	0.161	70	0.09	0.99
Grout (H, w/c=0.8, SMS = 3%)		0.41	300	0.113	0.092	51	0.03	0.99

For specimen repaired with smart cement grout, the curing model parameter p_1 was 0.003 after 1 day of curing which was increased to 0.343 after 7 days of curing and

then increased to 4.538 at 28 days (Table 5-4). For the specimen repaired with smart cement grout with 1% SMS, the model parameter p_1 was 0.011 after 1 day and then followed the similar trend like the specimen repaired with smart cement grout only and reached to 1.027 after 28 days. For the specimen repaired with smart cement grout with 3% SMS, the model parameter p_1 was 0.011 after 1 day and then followed the similar trend like the specimen repaired with smart cement grout only and reached to 1.173 after 28 days. For specimen repaired with smart cement grout only, the model parameter q_1 was 0.007 at 1 day of curing and increased to 0.122 at time up to 7 days and then increased to 0.282 at 28 days. For the specimen repaired with smart cement grout with 1% SMS, the q_1 value was 0.016 for 1 day which increased to 0.024 and then again increased to 0.345 at 28 days (Table 5-4). For the specimen repaired with smart cement grout with 3% SMS, the q_1 value was 0.028 for 1 day which increased to 0.315 after 7 days and then again increased to 0.499 after 28 days.

The curing model (Eqn. (3-11)) predicted the measured resistivity very well (Fig. 5-1, Fig. 5-2). The coefficient of determination (R^2) varied from 0.95 to 0.99 and the root mean square of error (RMSE) varied from 0.033 $\Omega.m$ to 1.52 $\Omega.m$ for 1 day and 28 days of curing respectively.

Table 5-4: Model parameters for the curing model of the resistivity of damaged cement repaired with smart cement grout with and without SMS cured at room temperature up to 28 days

Mix Type	Curing Time (day)	ρ_{\min} ($\Omega.m$)	t_{\min} (min)	p_1	q_1	t_0 (min)	RMSE ($\Omega.m$)	R^2
Repaired cement with grout (H, w/c=0.8 only)	1 day	12.42	180	0.003	0.007	51	0.12	0.99
Repaired cement with grout (H, w/c=0.8, SMS = 1%)		3.21	180	0.008	0.016	40	0.03	0.99
Repaired cement with grout (H, w/c=0.8, SMS = 3%)		1.54	300	0.011	0.028	63	0.03	0.99
Repaired cement with grout (H, w/c=0.8 only)	7 days	12.42	180	0.343	0.122	70	0.67	0.98
Repaired cement with grout (H, w/c=0.8, SMS = 1%)		3.21	180	0.024	0.024	140	0.40	0.99
Repaired cement with grout (H, w/c=0.8, SMS = 3%)		1.54	300	0.505	0.315	114	0.20	0.99
Repaired cement with grout (H, w/c=0.8 only)	28 days	12.42	180	4.538	0.282	80	1.09	0.98
Repaired cement with grout (H, w/c=0.8, SMS = 1%)		3.21	180	1.027	0.345	110	1.52	0.96
Repaired cement with grout (H, w/c=0.8, SMS = 3%)		1.54	300	1.173	0.499	120	0.40	0.99

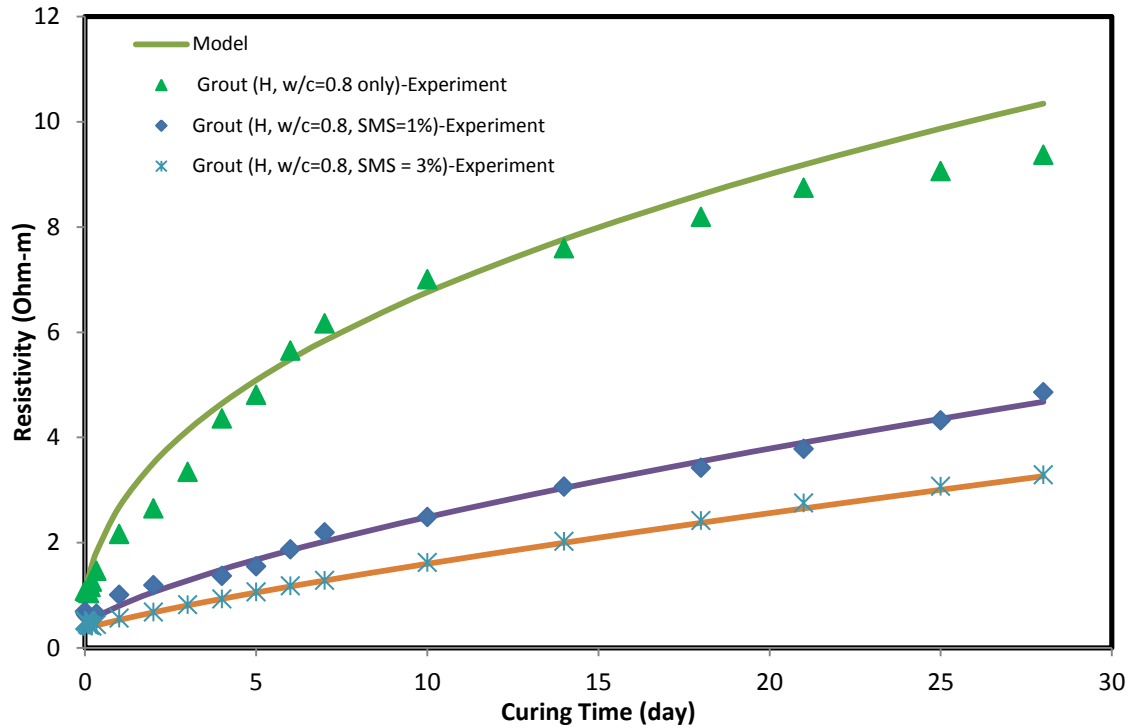


Figure 5-1: Variation of resistivity of smart cement grout with and without SMS up to 28 days of curing modeled with curing model

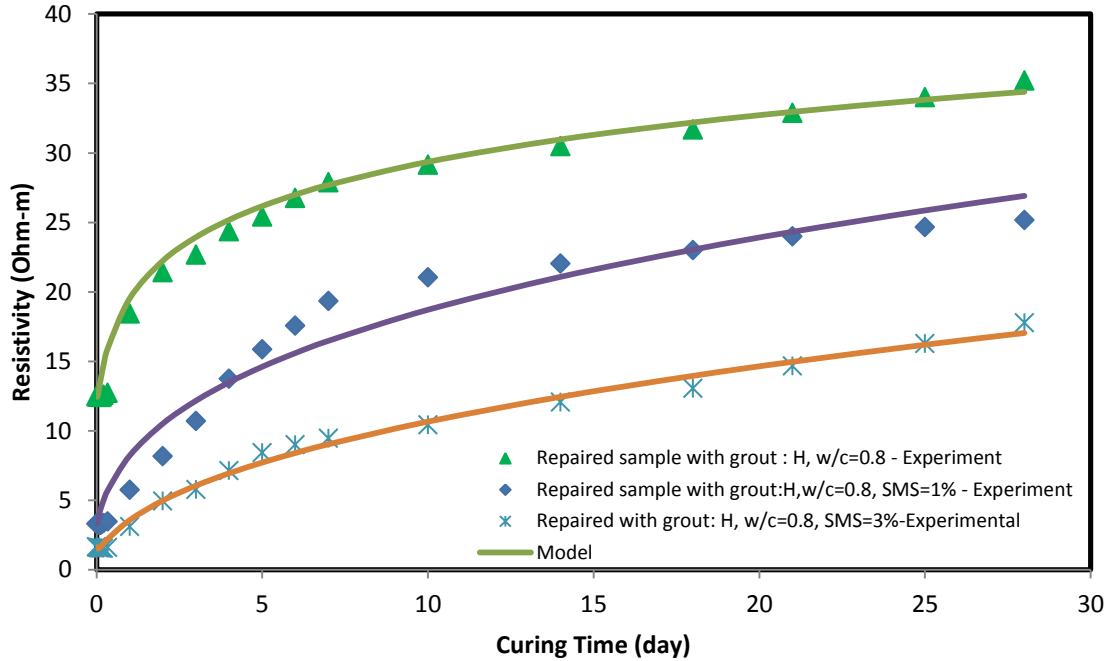


Figure 5-2: Variation of resistivity for repaired cement specimens repaired with smart cement grout with and without SMS cured up to 28 days modeled with curing model

5.1.2 Moisture loss and resistivity

During the curing period, the weight of the specimens was monitored to observe any change in the moisture loss. The smart cement grout only samples lost about 6% moisture during 28 days of curing whereas, the grout sample made with smart cement and 1% SMS lost about 4.2% moisture during 28 days, a 30% less moisture loss with the addition of 1% SMS (Fig. 5-3); and the grout sample made with 3% SMS lost about 3.7% moisture during 28 days, about 38% less moisture loss. The cement specimen repaired with smart cement grout only lost about 1% moisture after 28 days of curing whereas the specimen repaired with smart cement grout with 1% SMS lost about 0.8% moisture after 28 days of curing, a 20 less moisture loss (Fig. 5-4); and the specimen repaired with smart cement grout with 3% SMS lost about 0.67% moisture after 28 days of curing, about 33% less moisture loss.

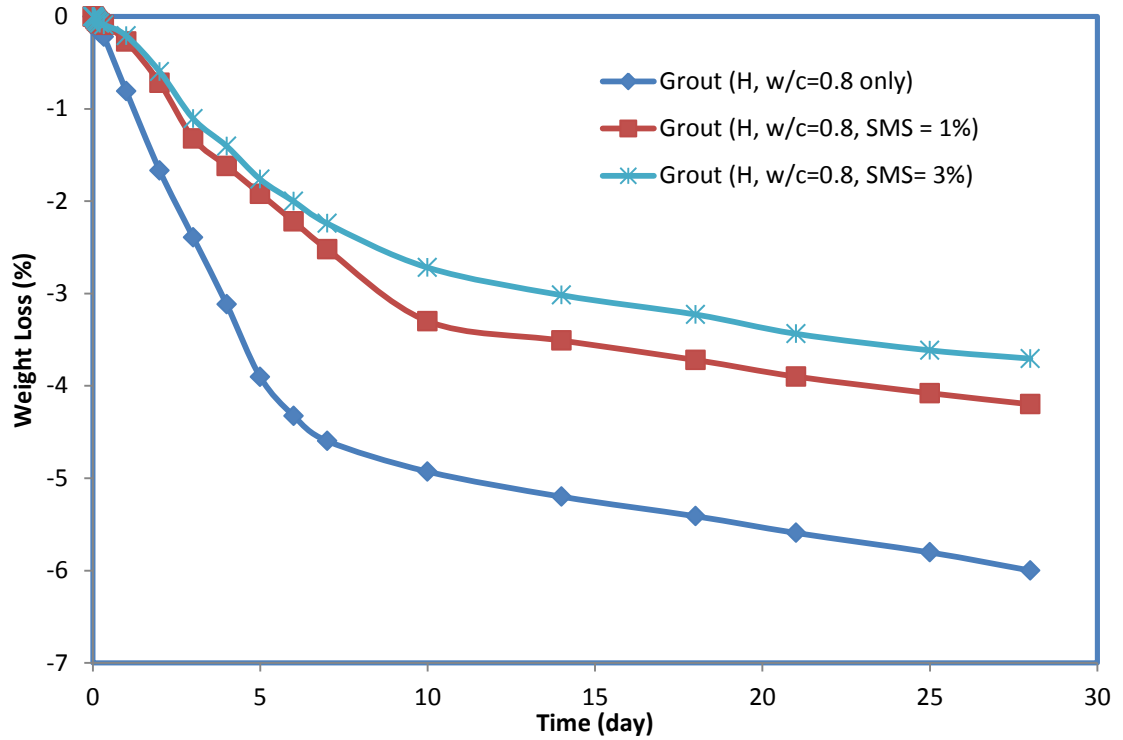


Figure 5-3: Weight loss of smart cement grout specimens cured at room temperature with and without SMS up to 28 days

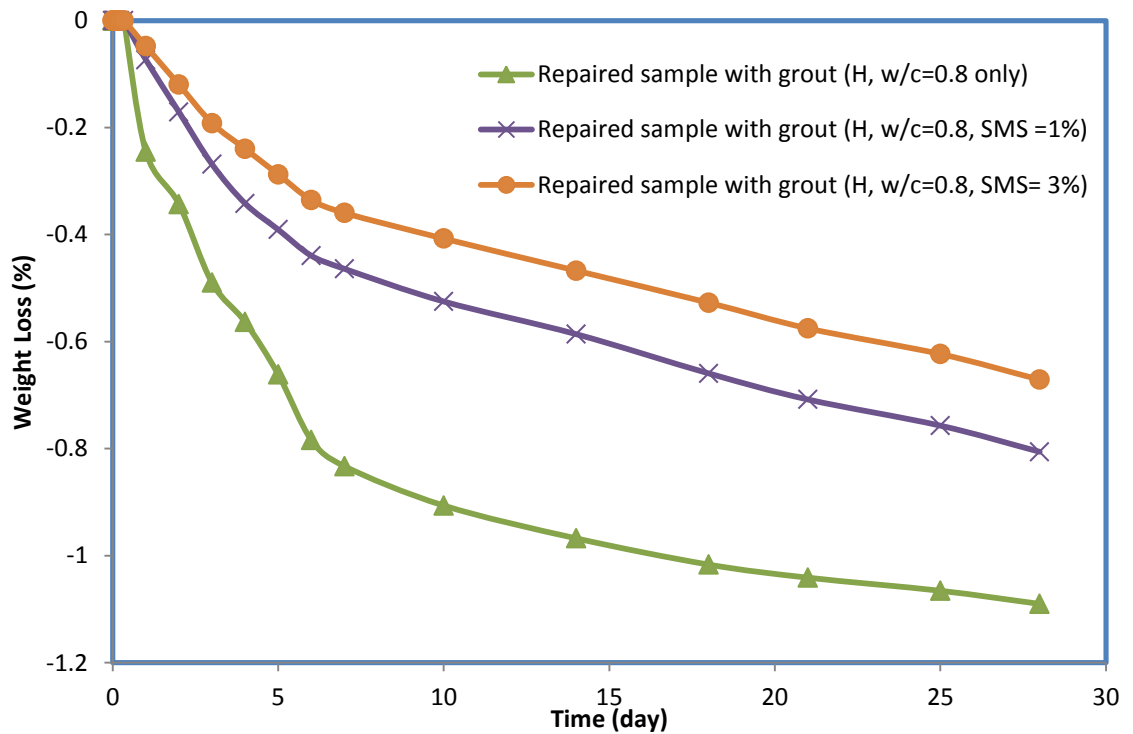


Figure 5-4: Weight loss of the specimens repaired with grouts cured at room temperature up to 28 days

Modeling:

A relationship has been proposed for the resistivity of the cured specimen with the moisture loss (%) as

$$\rho = \rho_o + A*(\Delta w/w_o)^n, \quad (5-1)$$

where,

ρ = Resistivity of the grout ($\Omega.m$)

ρ_o = Initial resistivity of the grout without moisture loss ($\Omega.m$)

$\Delta w/w_o$ = moisture loss of the specimen (%)

A and n are constants and are model parameters that can be determined from the experimental results. For the grouts and for the repaired specimens with the grouts, the experimental values fit very well with the proposed model (Fig. 5-5, Fig. 5-6). For the grouts, the determined model parameters are as follows:

(iii) For grout without SMS, $A = 0.587$, $n = 1.47$, $R^2 = 0.99$ (5-2.a)

(iv) For grout with 1% SMS, $A = 0.198$, $n = 2.05$, $R^2 = 0.97$ (5-2.b)

(v) For grout with 3% SMS, $A = 0.11$, $n = 2.4$, $R^2 = 0.98$ (5-2.c)

For the repaired specimens with grouts, the determined model parameters are as follows:

(iii) Repaired by grout without SMS, $A = 19.33$, $n = 0.89$, $R^2 = 0.99$ (5-3.a)

(iv) Repaired by grout with 1% SMS, $A = 28.11$, $n = 0.87$, $R^2 = 0.99$ (5-3.b)

(v) Repaired by grout with 3% SMS, $A = 23.4$, $n = 1.03$, $R^2 = 0.99$ (5-3.c)

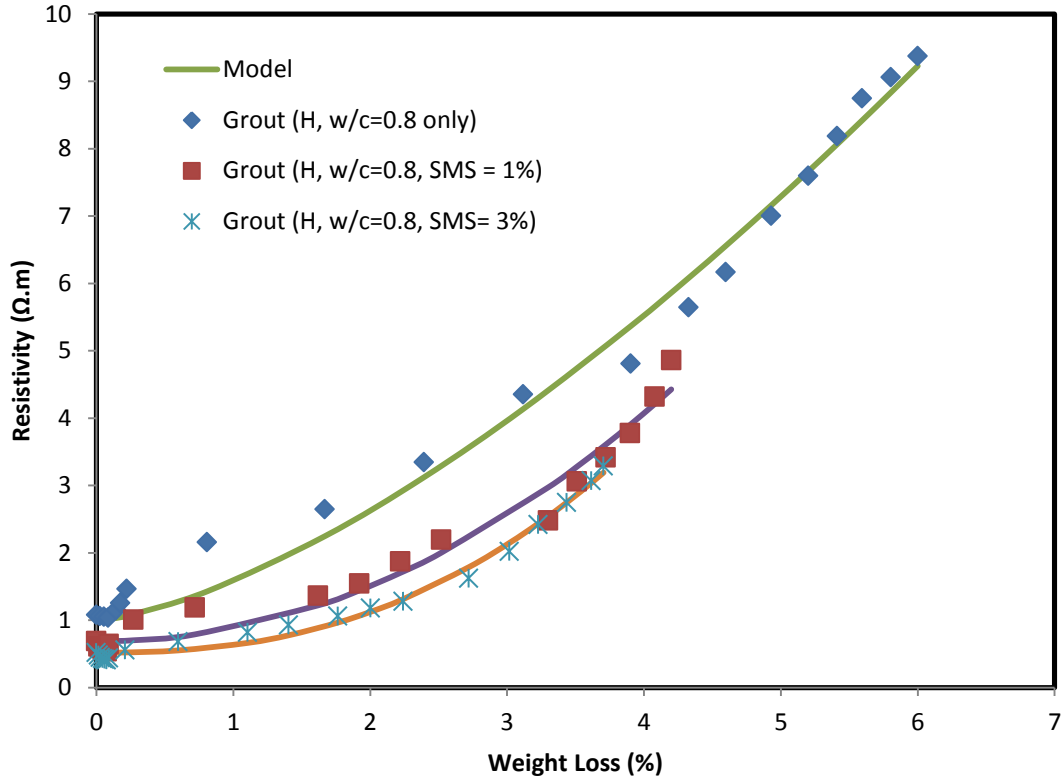


Figure 5-5: Relationship between resistivity and the moisture loss of the grout sample 1

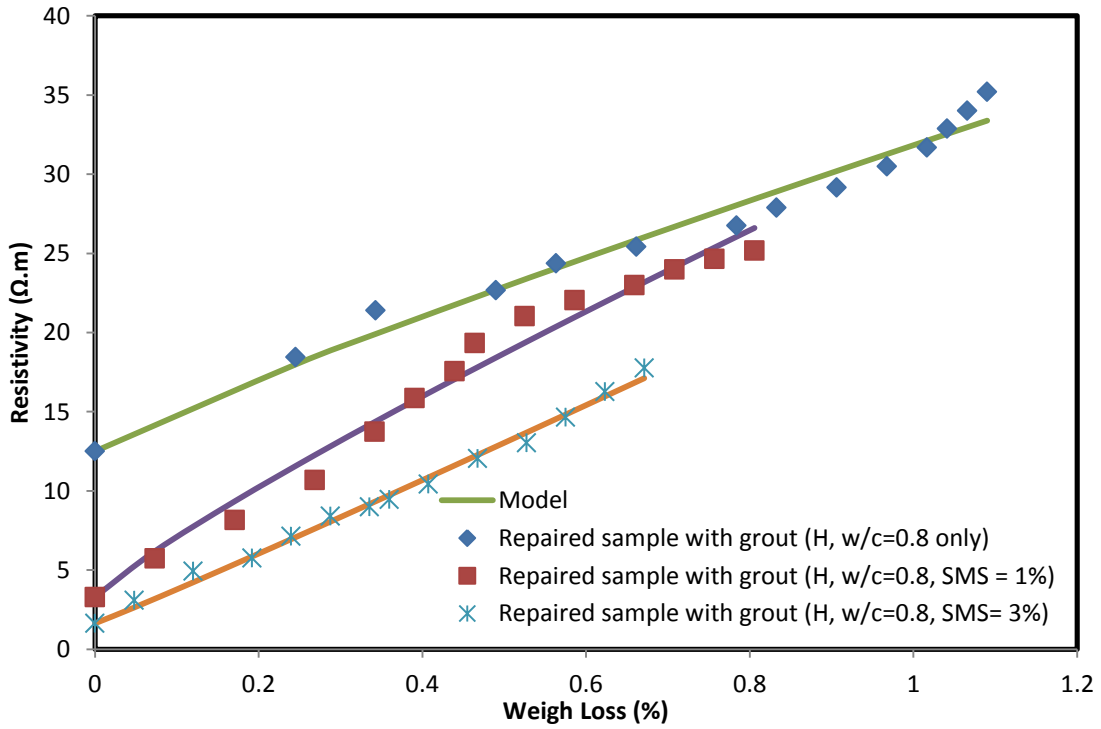


Figure 5-6: Relationship between resistivity and the moisture loss of the specimens repaired with grouts

5.1.3 Minimum resistivity

SMS decreased the minimum resistivity of the cement grout. The minimum resistivity (ρ_{\min}) of the smart cement grout decreased from 1.04 $\Omega\text{-m}$ to 0.54 $\Omega\text{-m}$ with 1% SMS, a 44% decrease. By addition of 3% SMS, the minimum resistivity of the grout was further decreased to 0.41, a 60% decrease. The relationship between minimum resistivity and SMS concentration has been modeled with hyperbolic model

$$\rho_{\min} = (\rho_{\min})_o - S/(C + DS), \quad (5-2)$$

where,

ρ_{\min} = minimum resistivity of the grout ($\Omega\text{.m}$)

$(\rho_{\min})_o$ = minimum resistivity of the grout without SMS ($\Omega\text{.m}$)

S = concentration of sodium meta-silicate (% by weight)

Parameters C and D are model parameters and parameter C represent the initial rate of change and parameter D determines the ultimate resistivity. Experimental results matched very well (Fig. 5-7) with the proposed model with coefficient of determination (R^2) of 0.99 and parameters C and D were found as 0.62 $\text{Ohm}^{-1}\text{-m}^{-1}$ and 1.38 $\text{Ohm}^{-1}\text{-m}^{-1}$.

5.2 Piezoresistivity and strength of smart cement grout and repaired specimens

Addition of 0.075% CF substantially improved piezoresistive behavior of the cement. Based on experimental results, p-q model developed by Vipulanandan and Paul (1990) was modified and used (Eqn. (3-15)) to predict the change in electrical resistivity of cement with applied stress for 1, 7 and 28 days of curing.

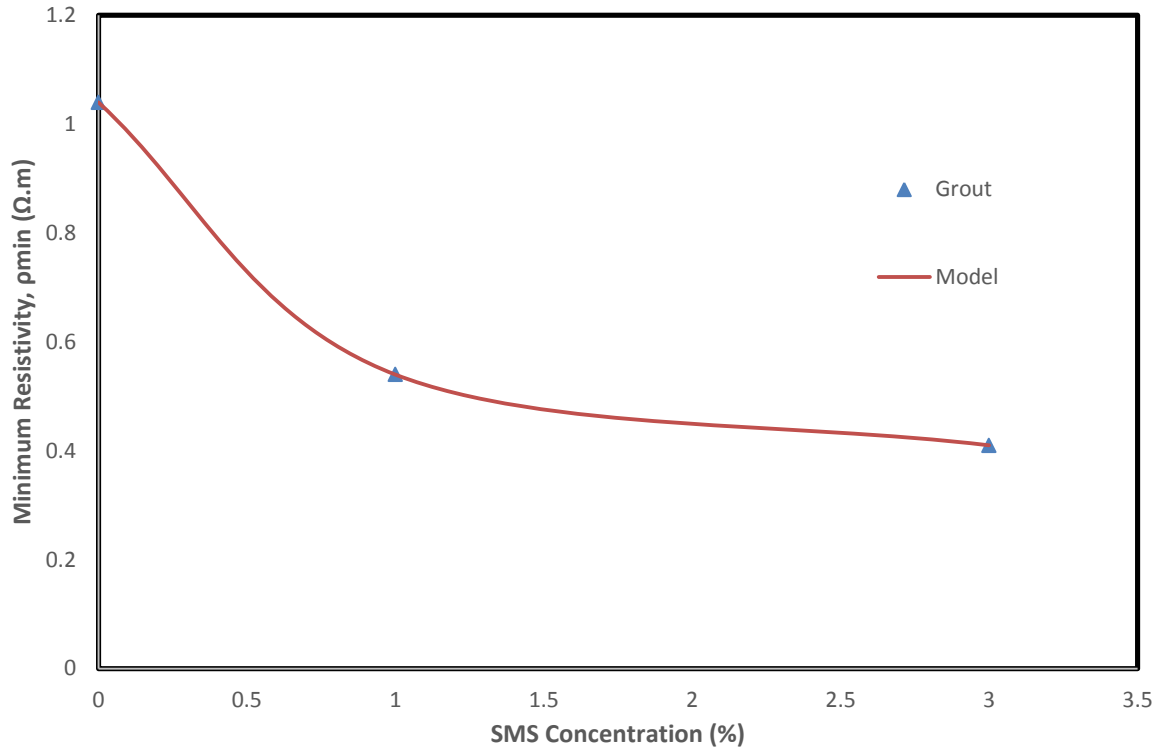


Figure 5-7: Variation of minimum resistivity with SMS concentration

5.2.1 Compressive behavior

(a) Smart cement grout: The compressive strength (σ_f) of the smart cement grout after 1day, 7 days and 28 days of curing were 2.96 MPa, 9.94 MPa and 16.47 MPa.

(b) Smart cement grout with 1% SMS: The compressive strength (σ_f) of the smart cement grout with 1% SMS decreased to 2.23 MPa, 6.98 MPa and 13.42 MPa respectively after 1day, 7 days and 28 days of curing (Table 5-5).

(c) Smart cement grout with 3% SMS: The compressive strength (σ_f) of the smart cement grout with 3% SMS decreased to 1.82 MPa, 5.45 MPa and 11.75 MPa, which are 38%, 45% and 28% reduction respectively after 1day, 7 days and 28 days of curing (Table 5-5).

Table 5-5: Compressive strength, piezoresistivity and model parameters p₂, q₂ for smart cement grout

Mix Type	Curing Time (day)	Strength σ_f (MPa)	Piezoresistivity at peak stress, $(\Delta\rho/\rho_o)_f$ (%)	p ₂	q ₂	R ²	RMSE (MPa)
Grout (H, w/c=0.8 only)	1 day	2.96	155	0.031	0.607	0.99	0.08
Grout (H, w/c=0.8, SMS = 1%)		2.23	117	0.037	0.706	0.95	0.17
Grout (H, w/c=0.8, SMS = 3%)		1.82	106	0.183	1.193	0.99	0.04
Grout (H, w/c=0.8 only)	7 days	9.94	156	0.035	0.642	0.99	0.18
Grout (H, w/c=0.8, SMS = 1%)		6.98	116	0.052	0.596	0.99	0.15
Grout (H, w/c=0.8, SMS = 3%)		5.45	94	0.07	1.582	0.99	0.16
Grout (H, w/c=0.8 only)	28 days	16.47	179	0.012	0.613	0.99	0.10
Grout (H, w/c=0.8, SMS = 1%)		13.42	125	0.01	0.561	0.97	0.64
Grout (H, w/c=0.8, SMS = 3%)		11.75	103	0.03	0.492	0.99	0.20

Piezoresistivity:

(a) Smart cement grout: The change in electrical resistivity at failure $\left(\frac{\Delta\rho}{\rho_o}\right)_f$ of the smart cement grout after 1day, 7 days and 28 days of curing were 155%, 156% and 179%.

(b) Smart cement grout with 1% SMS: The change in electrical resistivity at failure $\left(\frac{\Delta\rho}{\rho_o}\right)_f$ of the smart cement grout with 1% SMS decreased to 117%, 116% and 125% respectively after 1day, 7 days and 28 days of curing (Table 5-5). Thus the piezoresistivity of the grouts were reduced by 24%, 25% and 30% after 1day, 7 days and 28 days of curing with addition of 1% SMS.

(c) Smart cement grout with 3% SMS: By addition of 3% SMS, the piezoresistivity after 1 day, 7 days and 28 days of curing were 106%, 94% and 103%, which are 31%, 40% and 42% reduction respectively (Table 5-5).

Using the p-q piezoresistive model (Eqn. (3-15)), the relationships between compressive stress and the change in electrical resistivity $\left(\frac{\Delta\rho}{\rho_0}\right)$ of the smart cement grout with and without SMS for 1 day, 7 days and 28 days of curing were modeled. The piezoresistive model (Eqn. (3-15)) predicted the measured stress-change in resistivity relationship very well (Fig. 5-8, Fig. 5-10, Fig. 5-12). The model parameters q_2 and p_2 are summarized in Table 5-5. The coefficients of determination (R^2) were 0.95 to 0.99. The root mean square of error (RMSE) varied between 0.04 MPa and 0.64 MPa as summarized in Table 5-5.

Change in resistivity per stress change

As we have considered the rate of resistivity change $\Delta\rho/\rho_0$ as X, and if we consider the stress as Y, then the slope dX/dY , which is rate of change of resistivity with respect to stress change could be another indicator of the piezoresistivity. For smart cement grout only, after 1 day of curing, the rate of change of resistivity (dX/dY) was about 40-70 (%/MPa) which increased to 100 and changed the slope before the specimen cracks; after 7 days of curing, the rate of change of resistivity (dX/dY) was about 11-20 (%/MPa) which increased to 27 (%/MPa) and changed the slope before the specimen cracks; and after 28 days of curing, the rate of change of resistivity (dX/dY) was about 7-13 (%/MPa) which increased to 18 and changed the slope before the specimen cracks (Fig. 5-9) . For the smart grout with 1% SMS, after 1 day of curing, the rate of change of resistivity

(dX/dY) was about 40-50 (%/MPa) which increased to 80 and changed the slope before the specimen cracks; after 7 days of curing, the rate of change of resistivity (dX/dY) was about 10-20 (%/MPa) which increased to 40 (%/MPa) and changed the slope before the specimen cracks; and after 28 days of curing, the rate of change of resistivity (dX/dY) was about 6-12 (%/MPa) which increased to 40 (%/MPa) and changed the slope before the specimen cracks (Fig. 5-11). For the smart grout with 3% SMS, after 1 day of curing, the rate of change of resistivity (dX/dY) was about 55-65 (%/MPa) which increased to 130 and changed the slope before the specimen cracks; after 7 days of curing, the rate of change of resistivity (dX/dY) was decreasing from 22 to 12 (%/MPa) and then suddenly increased to 20 (%/MPa) and changed the slope before the specimen cracks; and after 28 days of curing, the rate of change of resistivity (dX/dY) was about 5-13 (%/MPa) which increased to 25 v and changed the slope before the specimen cracks (Fig. 5-13)

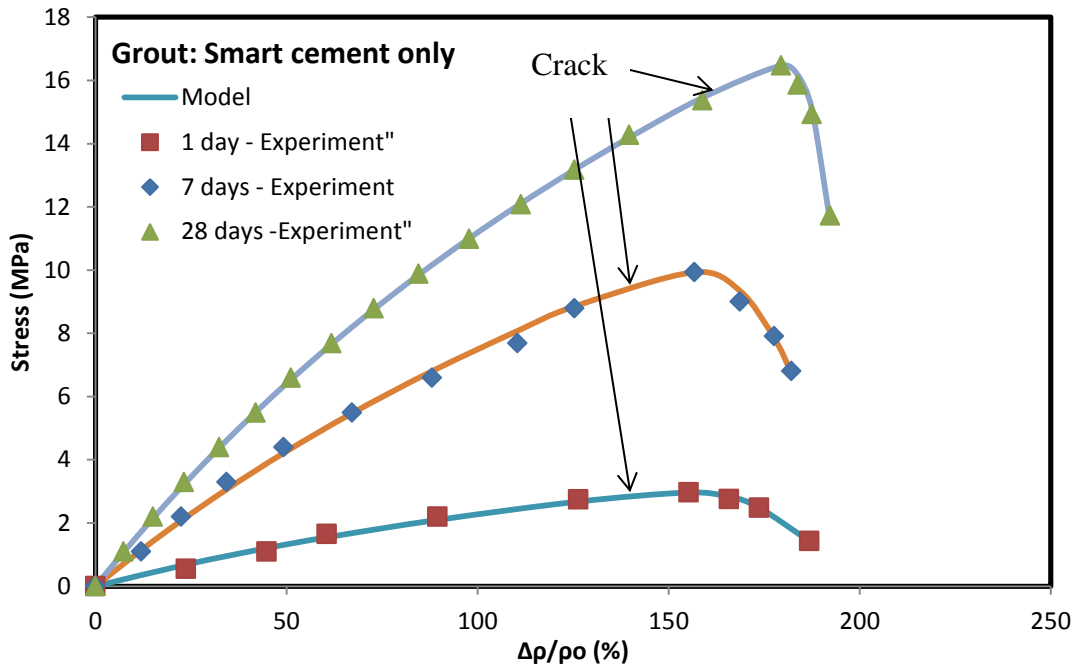


Figure 5-8: Piezoresistive response of the smart cement grout after 1 day, 7 days and 28 days of curing modeled with p-q model

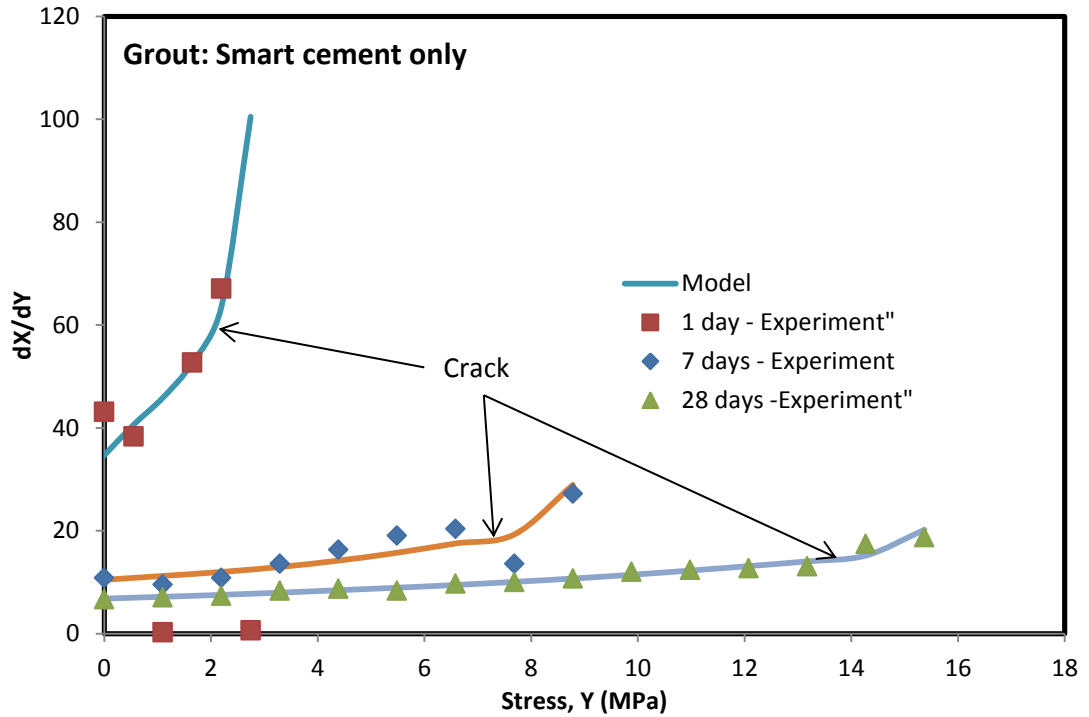


Figure 5-9: Rate of change of resistivity with respect to stress vs Stress for smart cement grout only after 1 day, 7 days and 28 days of curing

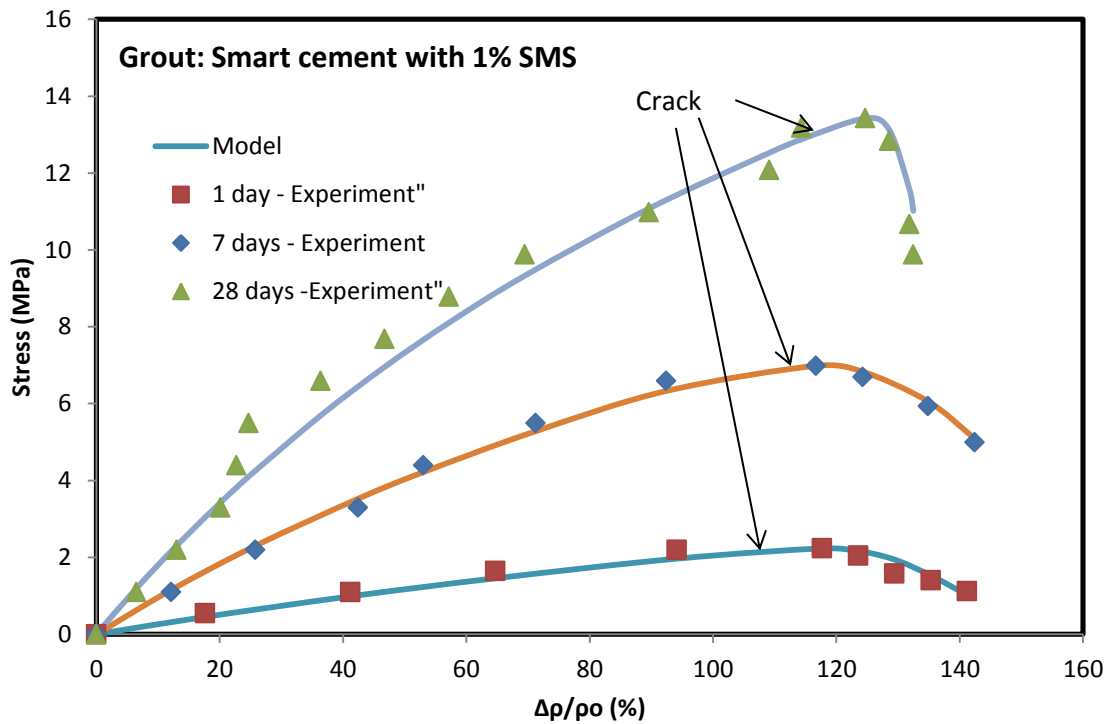


Figure 5-10: Piezoresistive response of the smart cement with 1% SMS after 1 day, 7 days and 28 days of curing modeled with p-q model

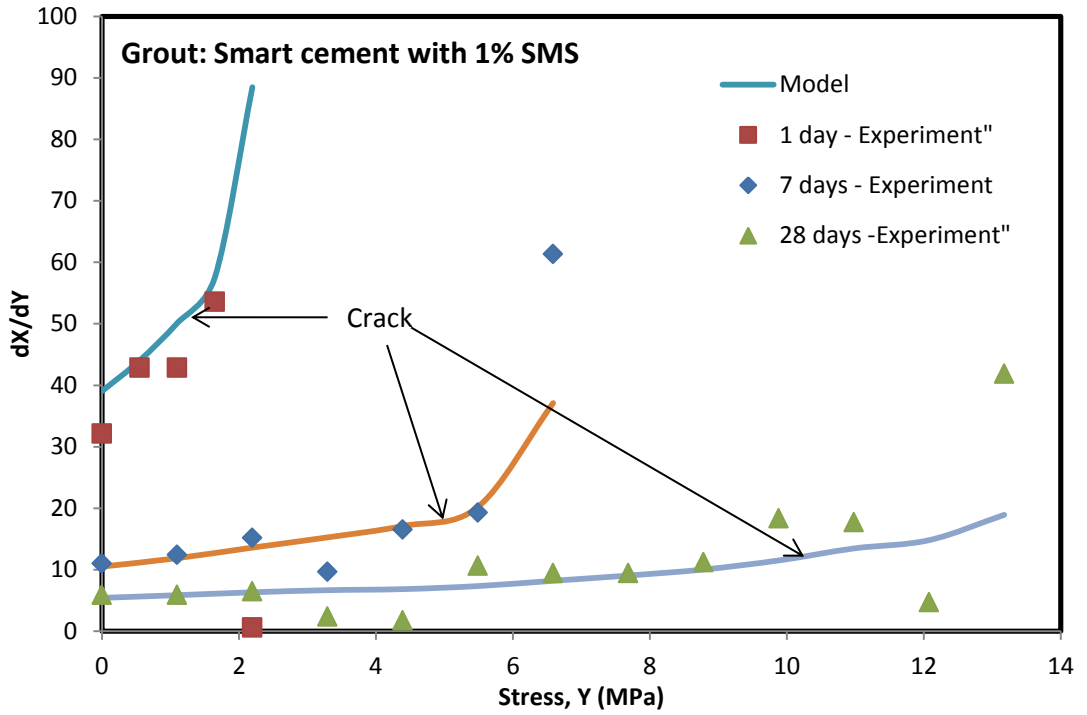


Figure 5-11: Rate of change of resistivity with respect to stress vs Stress for smart cement grout with 1% SMS after 1 day, 7 days and 28 days of curing

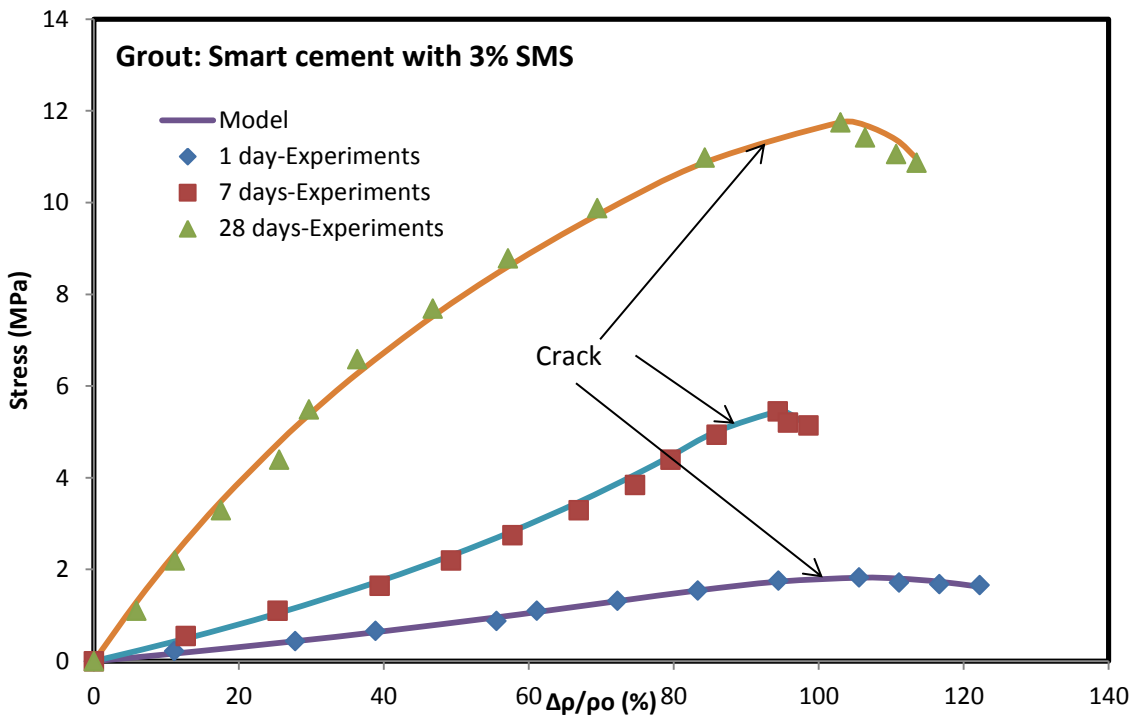


Figure 5-12: Piezoresistive response of the smart cement with 3% SMS after 1 day, 7 days and 28 days of curing modeled with p-q model

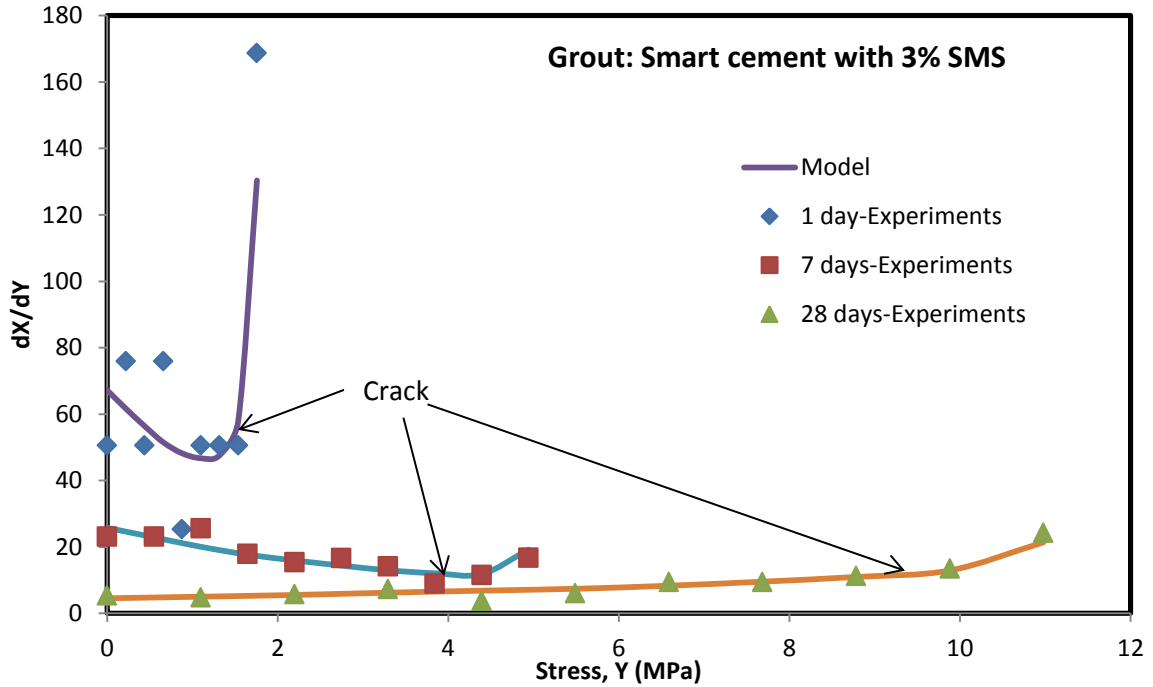


Figure 5-13: Rate of change of resistivity with respect to stress vs Stress for smart cement grout with 3% SMS after 1 day, 7 days and 28 days of curing

5.2.2 Repairing of Smart Cement

5.2.2.1 1 day of Curing

The specimen repaired with smart cement grout had a compressive strength of 10.09 MPa (which had a previous strength of 12.00 MPa), an 84% strength regain (Table 5-6, Fig. 5-14). The specimen repaired with smart cement grout with 1% SMS had a compressive strength of 5.80 MPa (which had a previous strength of 11.37 MPa), a 51% strength regain (Table 5-6, Fig. 5-16). The specimen repaired with smart cement grout with 3% SMS had a compressive strength of 4.63 MPa (which had a previous strength of 10.82 MPa), a 43% strength regain (Table 5-6, Fig. 5-18).

The specimen repaired with smart cement grout only showed the change in electrical resistivity at failure $\left(\frac{\Delta\rho}{\rho_o}\right)_f$ as 48% (which failed previously at piezoresistivity of 300%), a 16% regain of piezoresistivity (Table 6, Fig. 14). The specimen repaired with

smart cement grout with 1% SMS showed the change in electrical resistivity at failure $\left(\frac{\Delta\rho}{\rho_o}\right)_f$ as 56% (which failed previously at piezoresistivity of 294%), a 19% regain of piezoresistivity (Table 6, Fig. 16). The specimen repaired with smart cement grout with 3% SMS showed the change in electrical resistivity at failure $\left(\frac{\Delta\rho}{\rho_o}\right)_f$ as 44% (which failed previously at piezoresistivity of 268%), a 16% regain of piezoresistivity (Table 6, Fig. 18).

Using the p-q Piezoresistive model (Eqn. (3-15)), the relationships between compressive stress and the change in electrical resistivity $\left(\frac{\Delta\rho}{\rho_o}\right)$ of the smart cement and the specimen repaired with smart cement grout with and without SMS for 1 day of curing were modeled. The piezoresistive model (Eqn. (3-15)) predicted the measured stress-change in resistivity relationship very well (Fig. 5-14, Fig. 5-16, Fig. 5-18). The model parameters q_2 and p_2 are summarized in Table 5-6. The coefficients of determination (R^2) were 0.98 to 0.99. The root mean square of error (RMSE) varied between 0.08 MPa and 0.21 MPa as summarized in Table 5-6.

Table 5-6: Model parameters p_2 , q_2 , R^2 & RMSE for the piezoresistivity model for the smart cement specimens repaired with grout after 1 day, 7 days and 28 days

Mix Type	Curing Time (day)	Strength σ_f (MPa)	Piezoresistivity at peak stress, $(\Delta\rho/\rho_0)_f$ (%)	p_2	q_2	R^2	RMSE (MPa)	Strength Regain (%)	Piezoresistivity Regain (%)
Initial smart cement	1 day	12.00	300	0.01	0.693	0.99	0.14	N/A	N/A
Repaired cement (Grout: w/c=0.8 only)		10.09	48	0.039	0.601	0.99	0.19	84	16
Initial smart cement	1 day	11.37	294	0.01	0.639	0.99	0.21	N/A	N/A
Repaired cement (Grout: w/c=0.8, SMS = 1%)		5.80	56	0.046	0.793	0.99	0.17	51	19
Initial smart cement	1 day	10.82	268	0.016	0.684	0.99	0.19	N/A	N/A
Repaired cement (Grout: w/c=0.8, SMS = 3%)		4.63	44	0.072	0.628	0.99	0.078	43	16
Initial smart cement	7 days	19.75	276	0.017	0.825	0.99	0.30	N/A	N/A
Repaired cement (Grout: w/c=0.8 only)		13.82	58	0.028	0.629	0.99	0.07	70	21
Initial smart cement	7 days	18.92	238	0.09	0.777	0.99	0.31	N/A	N/A
Repaired cement (Grout: w/c=0.8, SMS = 1%)		14.57	62	0.03	0.73	0.98	0.31	77	26
Initial smart cement	7 days	18.48	218	0.048	0.838	0.99	0.21	N/A	N/A
Repaired cement (Grout: w/c=0.8, SMS = 3%)		12.74	56	0.05	0.704	0.99	0.19	69	26
Initial smart cement	28 days	26.54	241	0.02	0.672	0.99	0.42	N/A	N/A
Repaired cement (Grout: w/c=0.8 only)		18.05	53	0.009	0.747	0.99	0.17	68	22
Initial smart cement	28 days	26.11	262	0.02	0.735	0.99	0.35	N/A	N/A
Repaired cement (Grout: w/c=0.8, SMS = 1%)		16.71	42	0.02	0.487	0.99	0.49	64	16
Initial smart cement	28 days	26.74	278	0.03	0.707	0.99	0.31	N/A	N/A
Repaired cement (Grout: w/c=0.8, SMS = 3%)		15.50	39	0.17	0.59	0.99	0.14	58	14

Rate of change of resistivity with respect to stress change:

For 1 day of curing, the rate of change of resistivity (dX/dY) for initial smart cement specimen only was about 17-30 which increased to 40 and changed the slope before the specimen cracks. For the repaired sample with smart cement grout only, the rate of change of resistivity (dX/dY) varied from 3-7 and increased to 20 and changes the slope when the cement specimen experiences cracks (Figure 5-15). For the repaired sample with smart cement grout with 1% SMS, the rate of change of resistivity (dX/dY) varied from 6-11 and increased to 23 and changes the slope when the cement specimen experiences cracks (Figure 5-17). For the repaired sample with smart cement grout with 3% SMS, the rate of change of resistivity (dX/dY) varied from 6-12 and increased to 30 and changes the slope when the cement specimen experiences cracks (Figure 5-19).

5.2.2.2 7 days of Curing

The specimen repaired with smart cement grout had a compressive strength of 13.82 MPa (which had a previous strength of 19.75 MPa), a 70% strength regain (Table 5-6, Fig. 5-20). The specimen repaired with smart cement grout with 1% SMS had a compressive strength of 14.57 MPa (which had a previous strength of 18.92 MPa), a 77% strength regain (Table 5-6, Fig. 5-22). The specimen repaired with smart cement grout with 3% SMS had a compressive strength of 12.74 MPa (which had a previous strength of 18.48 MPa), a 69% strength regain (Table 5-6, Fig. 5-24).

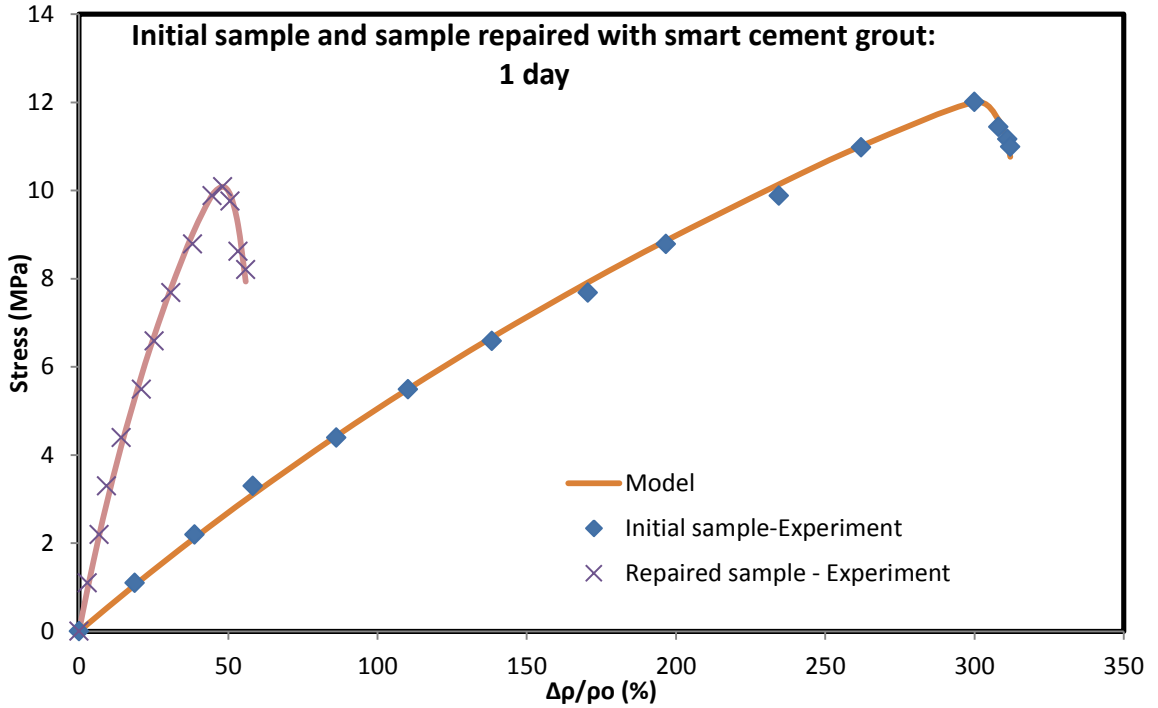


Figure 5-14: Piezoresistive response of the initial smart cement sample and the specimen repaired with grout after 1 day of curing modeled with p-q model

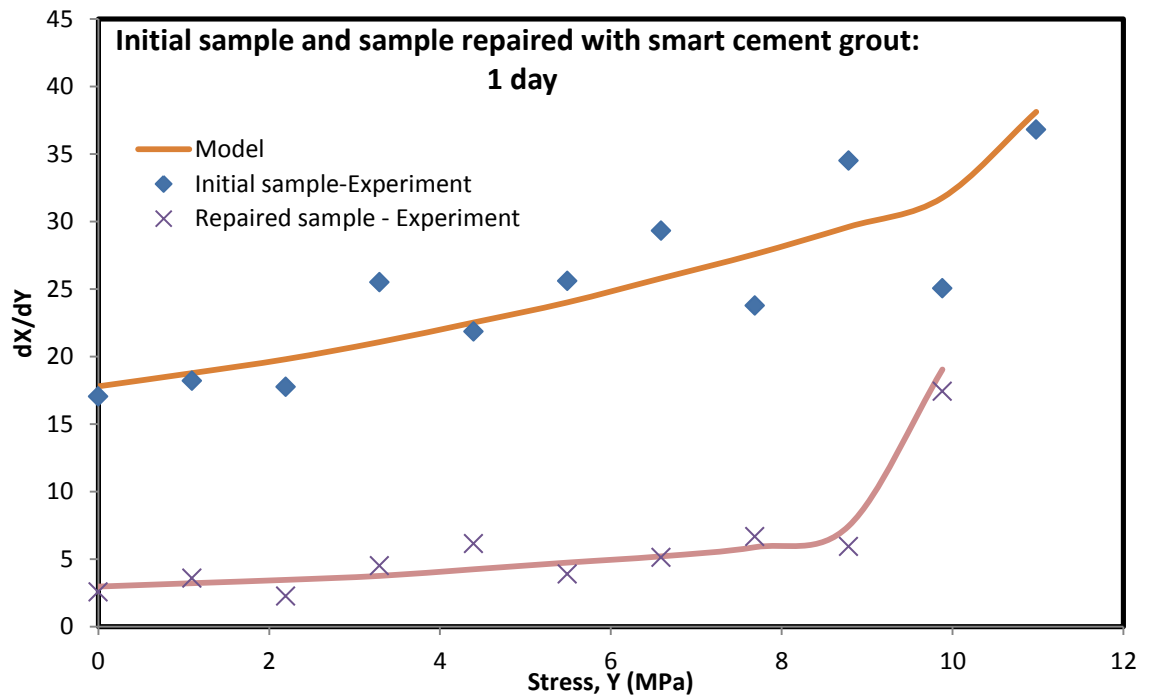


Figure 5-15: Rate of change of resistivity with respect to stress vs Stress for 1 day curing of the initial smart cement sample and the specimen repaired with grout

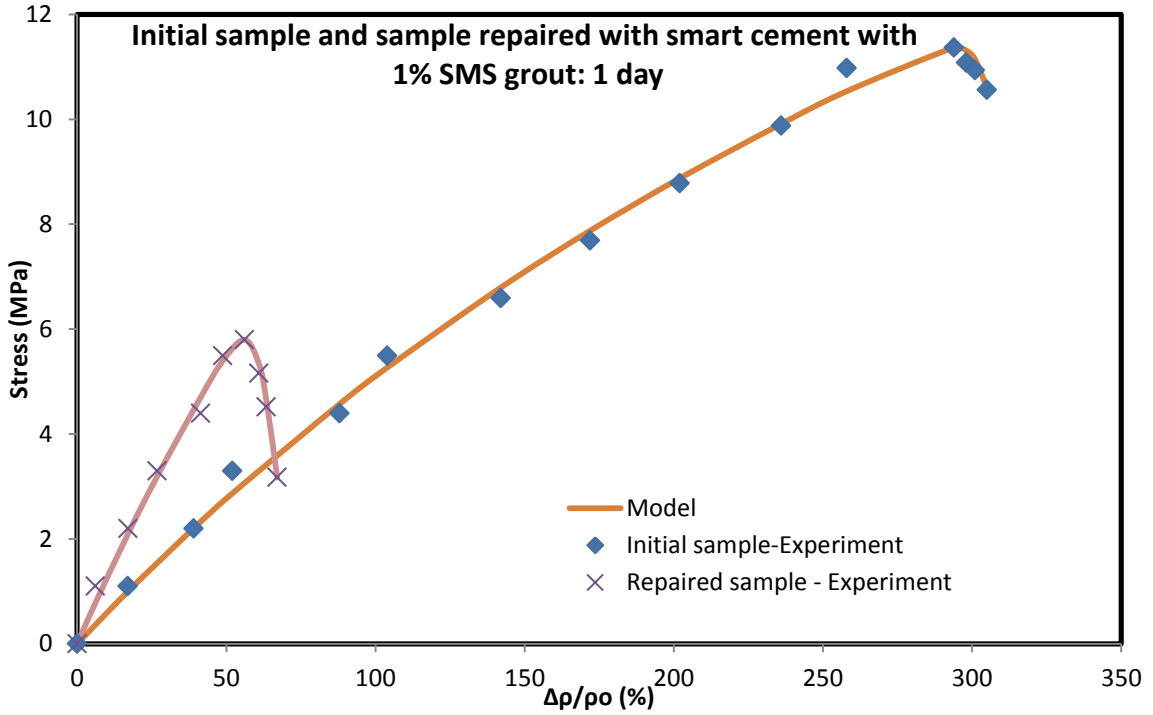


Figure 5-16: Piezoresistive response of the initial smart cement sample and the specimen repaired with grout with 1% SMS after 1 day of curing modeled with p-q model

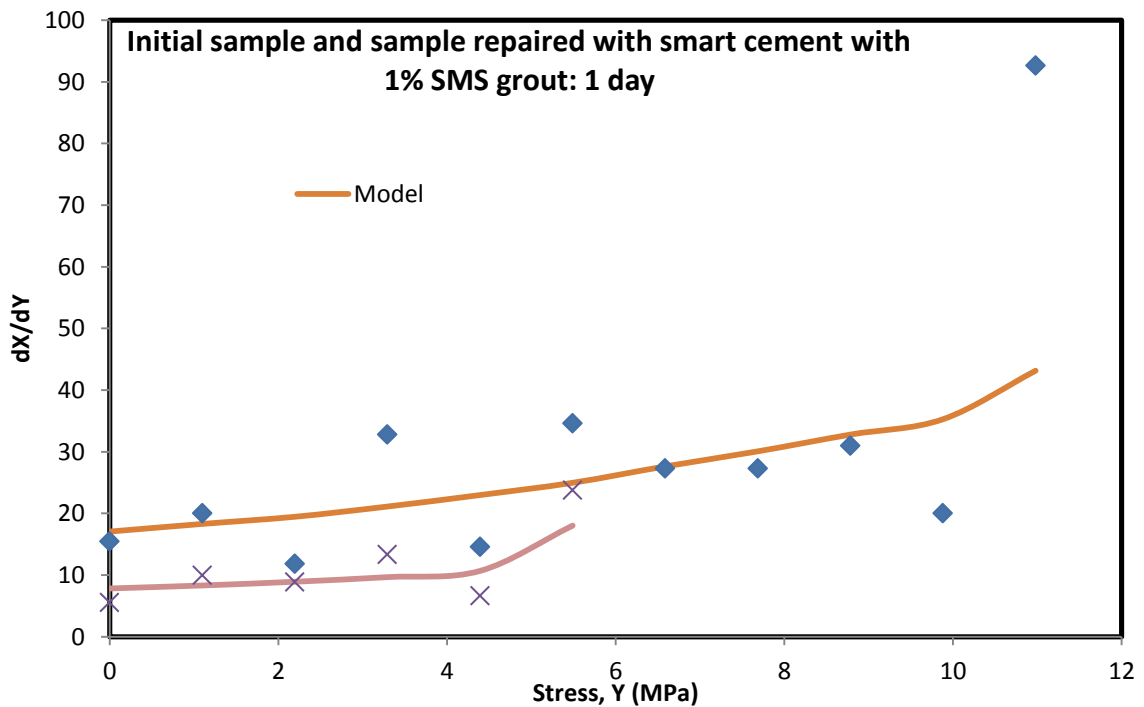


Figure 5-17: Rate of change of resistivity with respect to stress vs Stress for 1 day curing of the initial smart cement sample and the specimen repaired with grout with 1% SMS

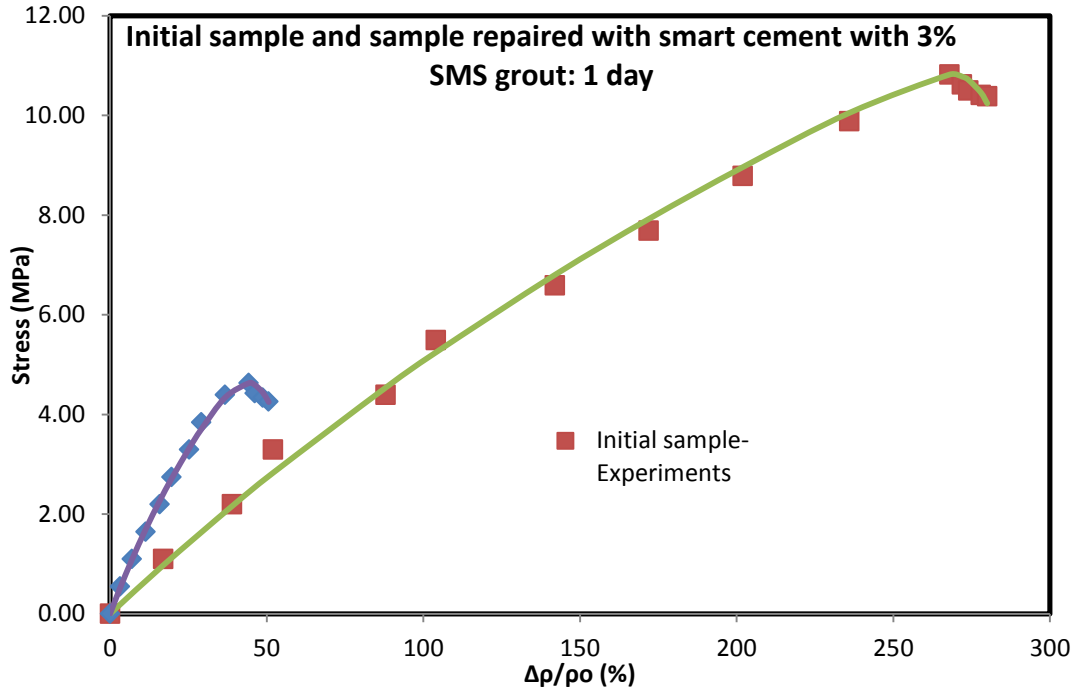


Figure 5-18: Piezoresistive response of the initial smart cement sample and the specimen repaired with grout with 3% SMS after 1 day of curing modeled with p-q model

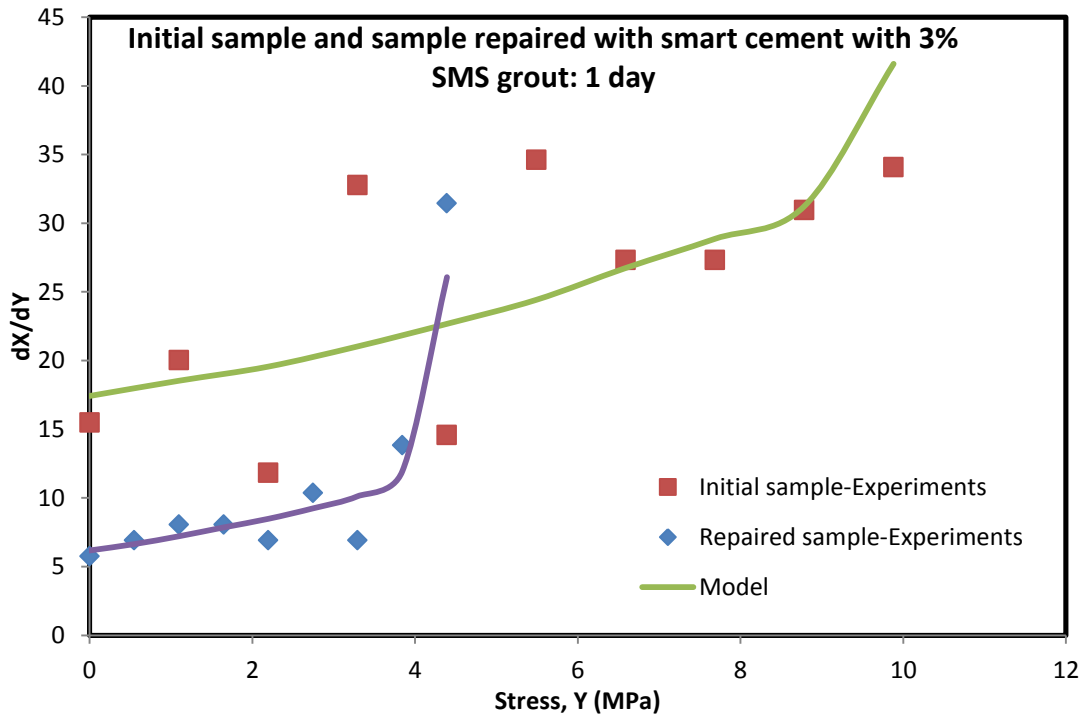


Figure 5-19: Rate of change of resistivity with respect to stress vs Stress for 1 day curing of the initial smart cement sample and the specimen repaired with grout with 3% SMS

The specimen repaired with smart cement grout only showed the change in electrical resistivity at failure $\left(\frac{\Delta\rho}{\rho_o}\right)_f$ as 58% (which failed previously at piezoresistivity of 276%), a 21% regain of piezoresistivity (Table 5-6, Fig. 5-20). The specimen repaired with smart cement grout with 1% SMS showed the change in electrical resistivity at failure $\left(\frac{\Delta\rho}{\rho_o}\right)_f$ as 62% (which failed previously at piezoresistivity of 238%), a 26% regain of piezoresistivity (Table 5-6, Fig. 5-22). The specimen repaired with smart cement grout with 3% SMS showed the change in electrical resistivity at failure $\left(\frac{\Delta\rho}{\rho_o}\right)_f$ as 56% (which failed previously at piezoresistivity of 218%), a 26% regain of piezoresistivity (Table 5-6, Fig. 5-24).

Using the p-q Piezoresistive model (Eqn. (3-15)), the relationships between compressive stress and the change in electrical resistivity $\left(\frac{\Delta\rho}{\rho_o}\right)$ of the smart cement and the specimen repaired with smart cement grout with and without SMS for 7 days of curing were modeled. The piezoresistive model (Eqn. (3-15)) predicted the measured stress- change in resistivity relationship very well (Fig. 5-20, Fig 5-22, Fig. 5-24). The model parameters q_2 and p_2 are summarized in Table 5-4. The coefficients of determination (R^2) were 0.98 to 0.99. The root mean square of error (RMSE) varied between 0.07 MPa and 0.31 MPa as summarized in Table 5-6.

Rate of change of resistivity with respect to stress change:

For 7 days of curing, the rate of change of resistivity (dX/dY) for initial smart cement specimen only was about 12 to 16 (%/MPa) which increased to 22 (%/MPa) and changed the slope before the specimen cracks. For the repaired sample with smart cement grout only, the rate of change of resistivity (dX/dY) varied from 2.5 to 5.5 (%/MPa) and

increased to 10 (%/MPa) and changes the slope when the cement specimen experiences cracks (Fig. 5-21). For the repaired sample with smart cement grout with 1% SMS, the rate of change of resistivity (dX/dY) varied from 2.6 to 5.6 (%/MPa) and increased to 17 (%/MPa) and changes the slope when the cement specimen experiences cracks (Figure 5-23). For the repaired sample with smart cement grout with 3% SMS, the rate of change of resistivity (dX/dY) varied from 3.3 to 5.4 (%/MPa) and increased to 12 (%/MPa) and changes the slope when the cement specimen experiences cracks (Figure 5-25).

5.2.2.3 28 days of Curing

The specimen repaired with smart cement grout had a compressive strength of 18.05 MPa (which had a previous strength of 26.54 MPa), a 68% strength regain (Table 5-6, Fig. 5-26). The specimen repaired with smart cement grout with 1% SMS had a compressive strength of 16.71 MPa (which had a previous strength of 26.11 MPa), a 64% strength regain (Table 5-6, Fig. 5-28). The specimen repaired with smart cement grout with 3% SMS had a compressive strength of 15.50 MPa (which had a previous strength of 26.74 MPa), a 58% strength regain (Table 5-6, Fig. 5-30).

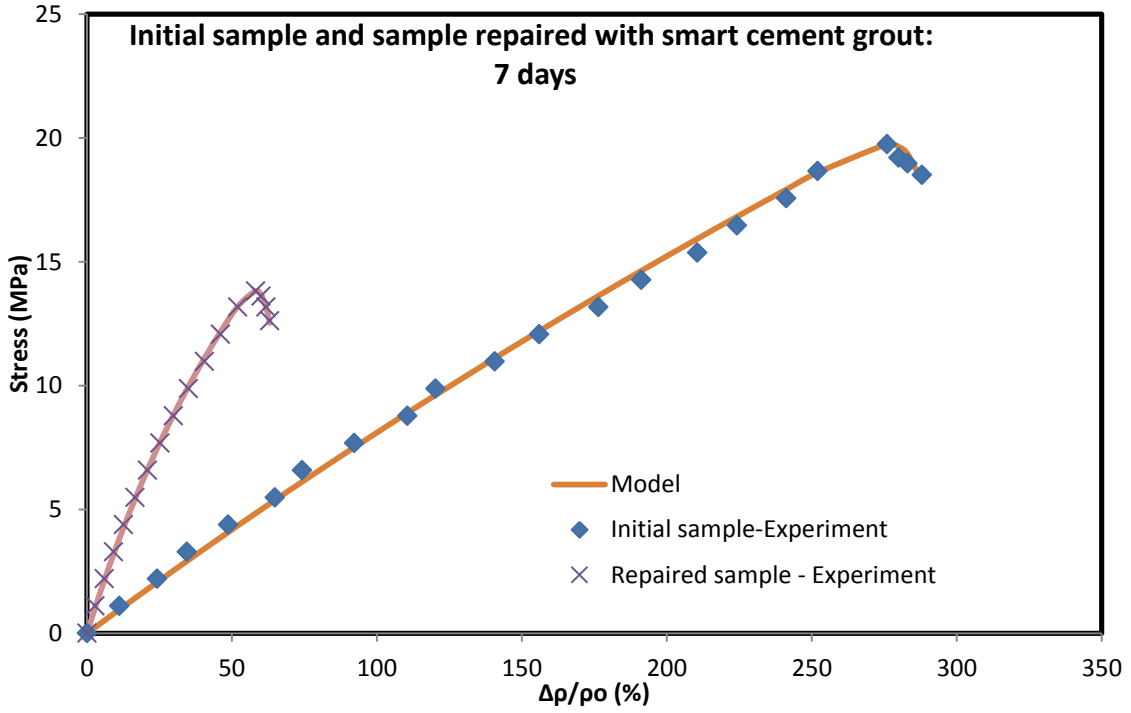


Figure 5-20: Piezoresistive response of the initial smart cement sample and the specimen repaired with grout after 7 days of curing modeled with p-q model

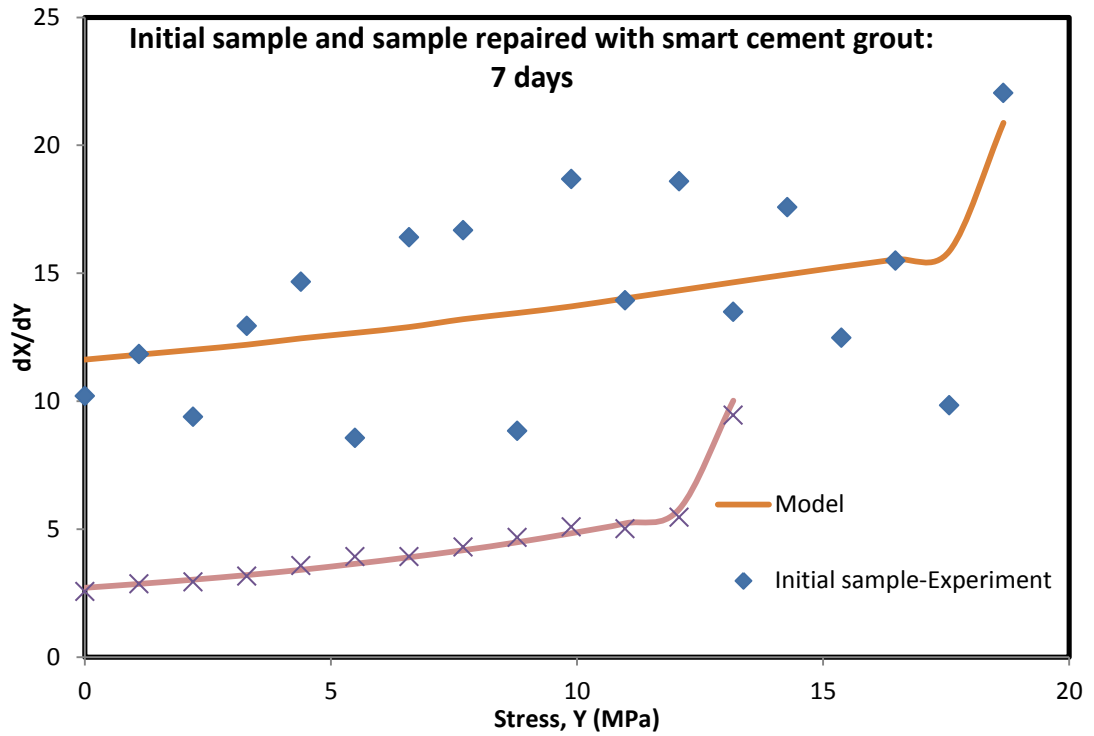


Figure 5-21: Rate of change of resistivity with respect to stress vs Stress for 7 days curing of the initial smart cement sample and the specimen repaired with grout

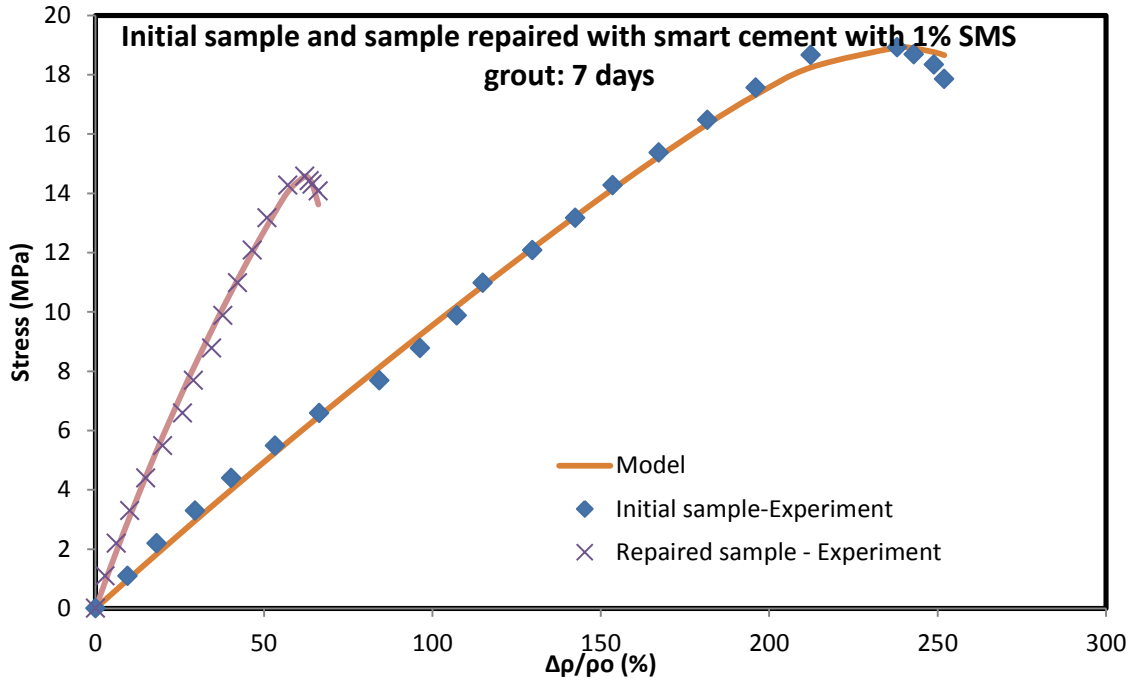


Figure 5-22: Piezoresistive response of the initial smart cement sample and the specimen repaired with grout with 1% SMS after 7 days of curing modeled with p-q model

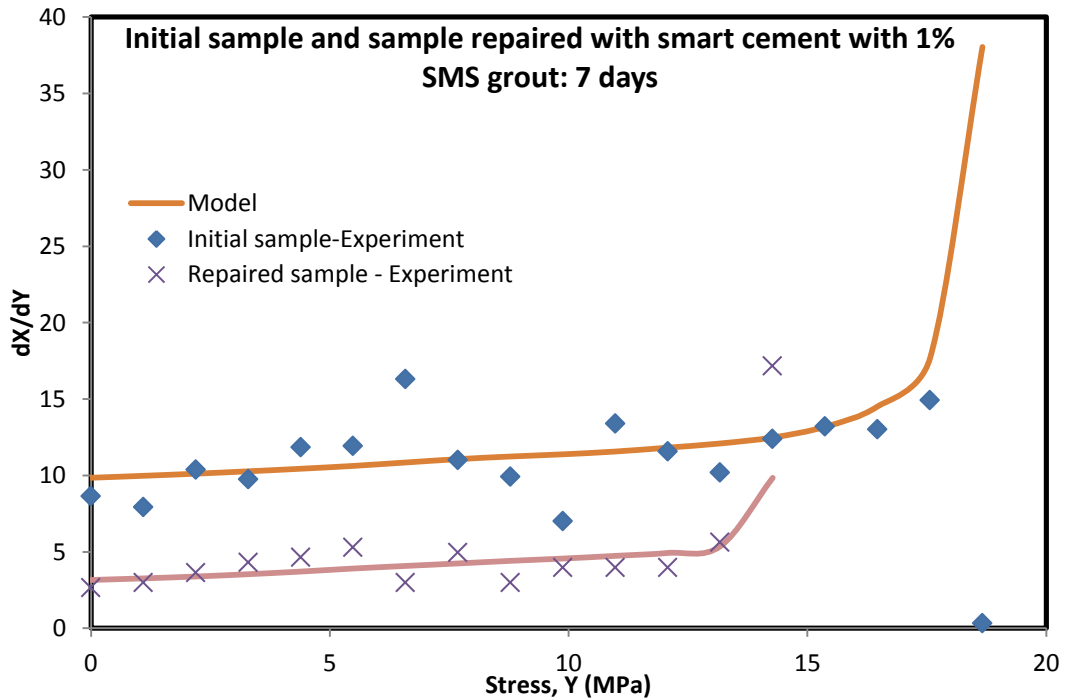


Figure 5-23: Rate of change of resistivity with respect to stress vs Stress for 7 days curing of the initial smart cement sample and the specimen repaired with grout with 1% SMS

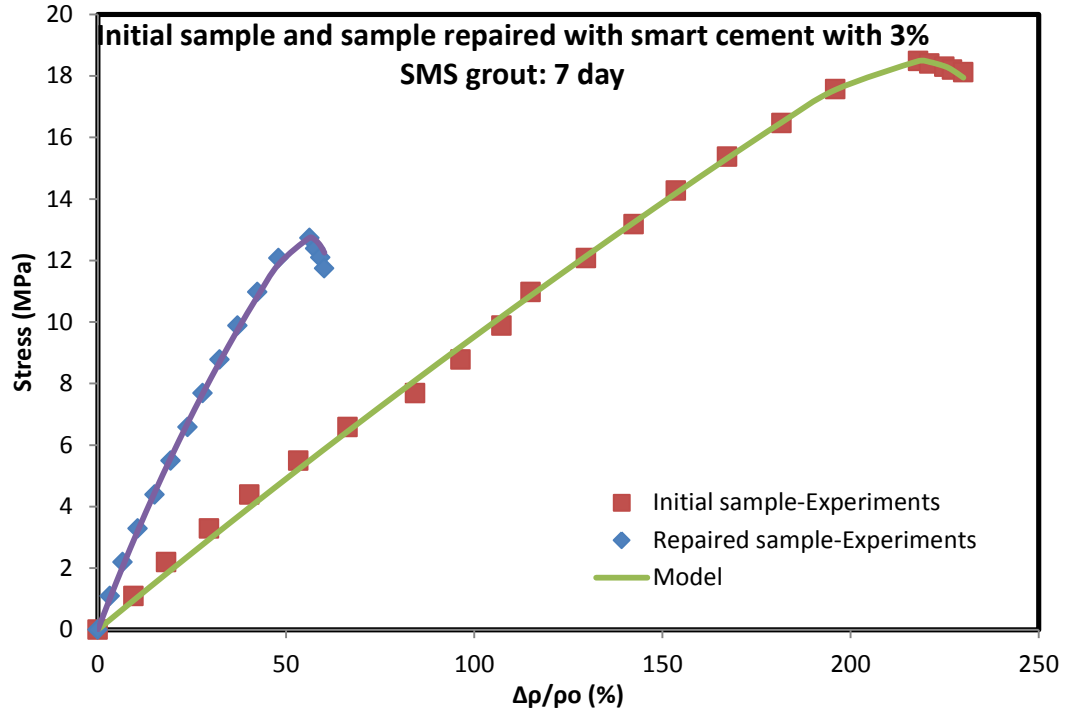


Figure 5-24: Piezoresistive response of the initial smart cement sample and the specimen repaired with grout with 3% SMS after 7 days of curing modeled with p-q model

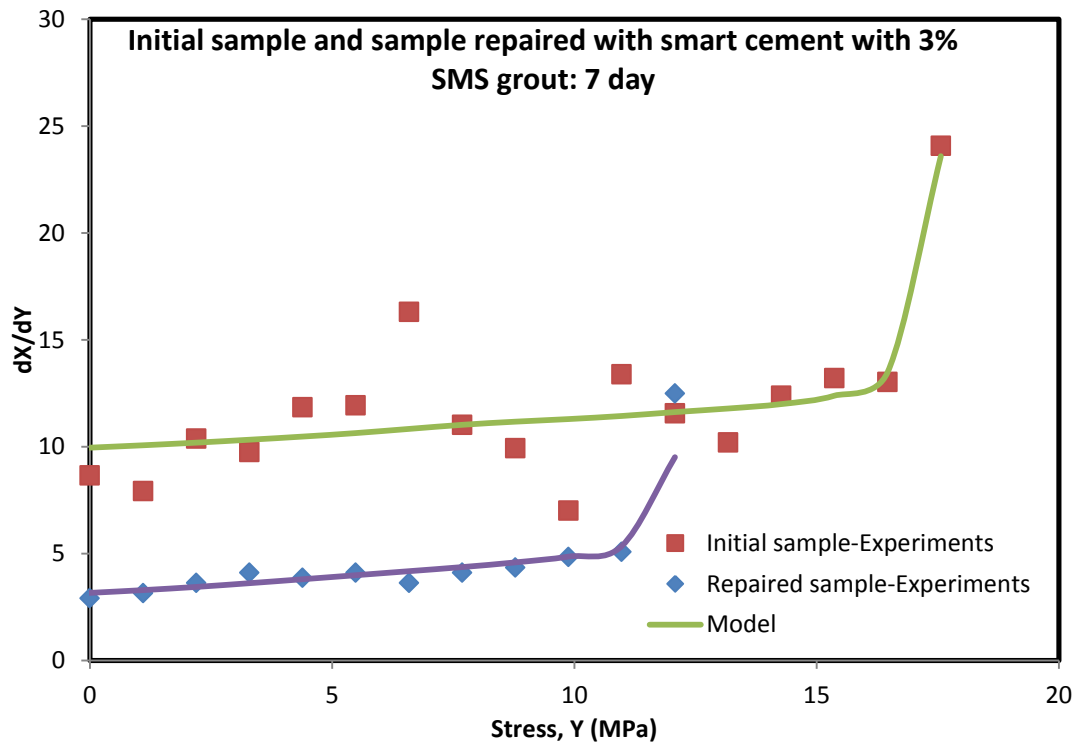


Figure 5-25: Rate of change of resistivity with respect to stress vs Stress for 7 days curing of the initial smart cement sample and the specimen repaired with grout with 3% SMS

The specimen repaired with smart cement grout only showed the change in electrical resistivity at failure $\left(\frac{\Delta\rho}{\rho_o}\right)_f$ as 53% (which failed previously at piezoresistivity of 241%), a 22% regain of piezoresistivity (Table 5-6, 5-26). The specimen repaired with smart cement grout with 1% SMS showed the change in electrical resistivity at failure $\left(\frac{\Delta\rho}{\rho_o}\right)_f$ as 42% (which failed previously at piezoresistivity of 262%), a 16% regain of piezoresistivity (Table 5-6, 5-28). The specimen repaired with smart cement grout with 3% SMS showed the change in electrical resistivity at failure $\left(\frac{\Delta\rho}{\rho_o}\right)_f$ as 39% (which failed previously at piezoresistivity of 278%), a 14% regain of piezoresistivity (Table 5-6, 5-30).

Using the p-q Piezoresistive model (Eqn. (3-15)), the relationships between compressive stress and the change in electrical resistivity $\left(\frac{\Delta\rho}{\rho_o}\right)$ of the smart cement and the specimen repaired with smart cement grout with and without SMS for 28 days of curing were modeled. The piezoresistive model (Eqn. (3-15)) predicted the measured stress- change in resistivity relationship very well (Fig. 5-26, Fig 5-28, Fig. 5-30). The model parameters q_2 and p_2 are summarized in Table 5-6. The coefficients of determination (R^2) were 0.97 to 0.99. The root mean square of error (RMSE) varied between 0.17 MPa and 0.49 MPa as summarized in Table 5-6.

Rate of change of resistivity with respect to stress change:

For 28 days of curing, the rate of change of resistivity (dX/dY) for initial smart cement specimen only was about 6 to 12 (%/MPa) which increased to 31 (%/MPa) and changed the slope before the specimen cracks. For the repaired sample with smart cement grout only, the rate of change of resistivity (dX/dY) varied from 2.25 to 4 (%/MPa) and

increased to 7 (%/MPa) and changes the slope when the cement specimen experiences cracks (Fig. 5-27). For the repaired sample with smart cement grout with 1% SMS, the rate of change of resistivity (dX/dY) varied from 2 to 4 (%/MPa) and increased to 18 (%/MPa) and changes the slope when the cement specimen experiences cracks (Fig. 5-29). For the repaired sample with smart cement grout with 3% SMS, the rate of change of resistivity (dX/dY) varied from 1.5 to 3 (%/MPa) and increased to 13 (%/MPa) and changes the slope when the cement specimen experiences cracks (Fig. 5-31).

5.2.3 Relationship between SMS concentration and strength/piezoresistivity

The strength of the grout specimen made with and without SMS was observed. The addition of SMS decreased the compressive strength of the cement grout. The relationship between the compressive strength of the cement grout and SMS concentration has been modeled with the hyperbolic model

$$\sigma_c = (\sigma_c)_o - S/(E + FS), \quad (5-3)$$

where,

σ_c = Compressive strength of the grout (MPa)

$(\sigma_c)_o$ = Compressive strength of the grout without SMS (MPa)

S = Concentration of sodium meta-silicate (% by weight)

Parameters E and F are model parameters and parameter E represent the initial rate of change and parameter F determines the ultimate strength. Experimental results matched very well (Fig. 5-32) with the proposed model with coefficient of determination (R^2) of 0.99. For 1 day strength test, parameters E and F were found as 0.74 MPa^{-1} and 0.63 MPa^{-1} . For 7 days strength test, parameters E and F were found as 0.17 MPa^{-1} and 0.16 MPa^{-1} . For 28 days strength test, parameters E and F were found as 0.17 MPa^{-1} and 0.15 MPa^{-1} .

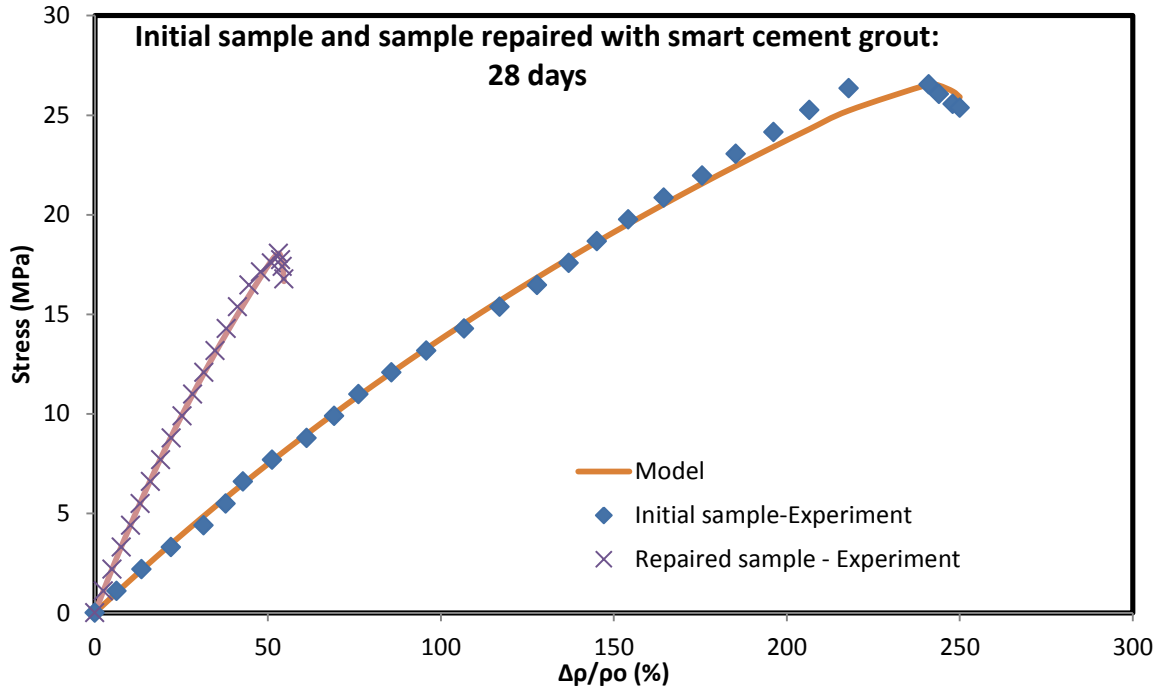


Figure 5-26: Piezoresistive response of the initial smart cement sample and the specimen repaired with grout after 28 days of curing modeled with p-q model

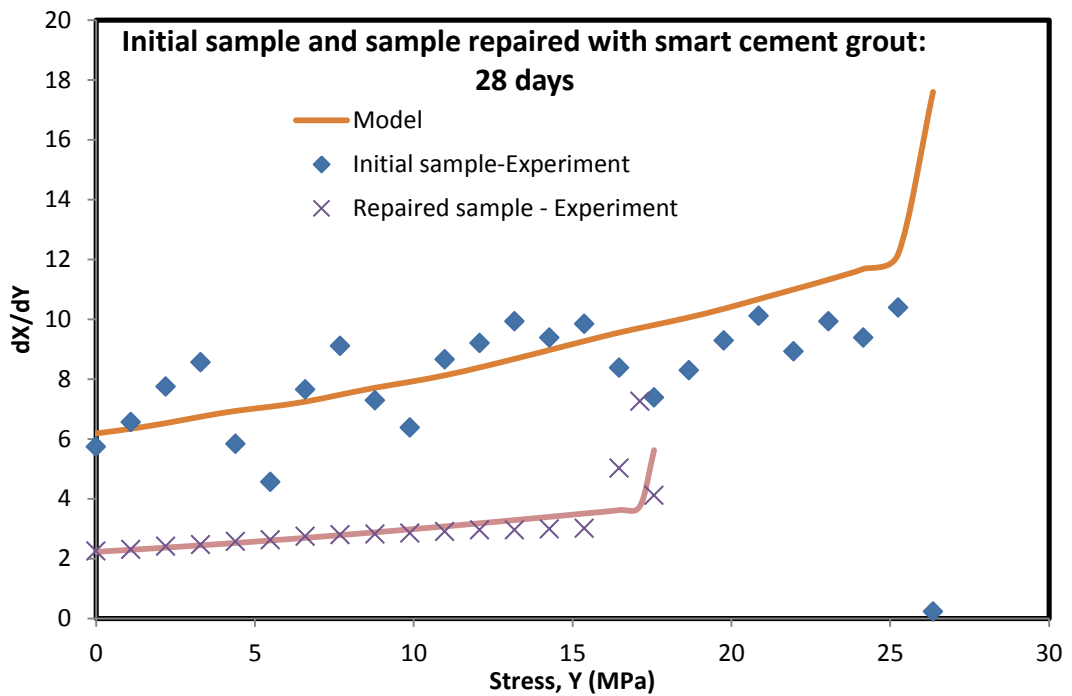


Figure 5-27: Rate of change of resistivity with respect to stress vs Stress for 28 days curing of the initial smart cement sample and the specimen repaired with grout

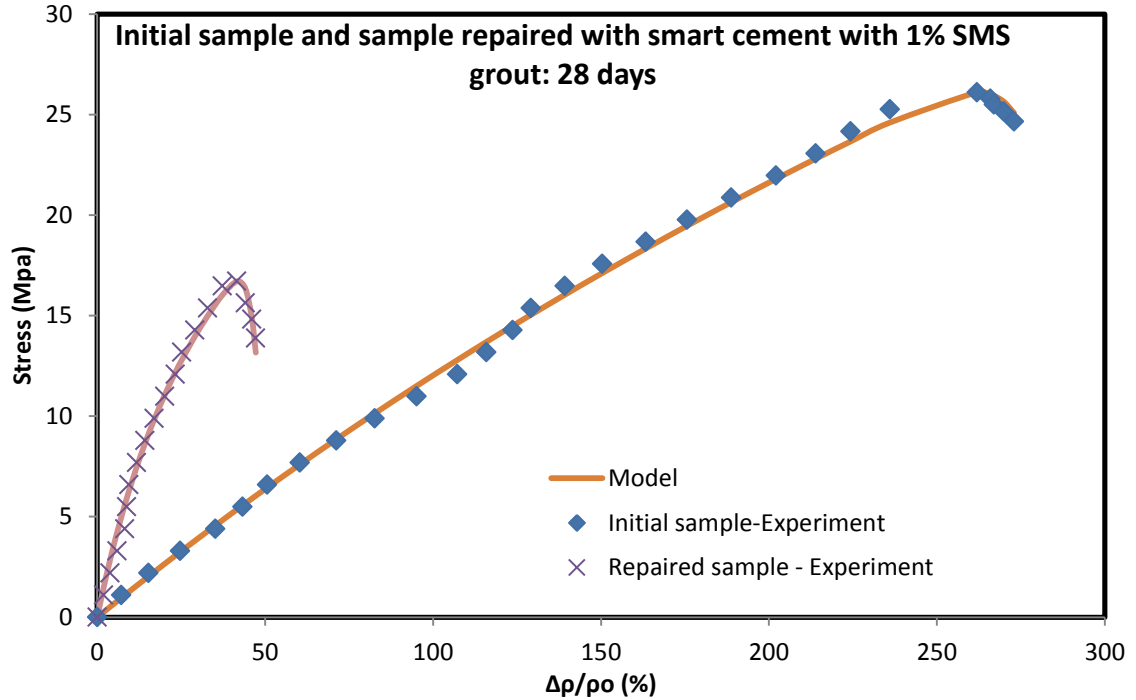


Figure 5-28: Piezoresistive response of the initial smart cement sample and the specimen repaired with grout with 1% SMS after 28 days of curing modeled with p-q model

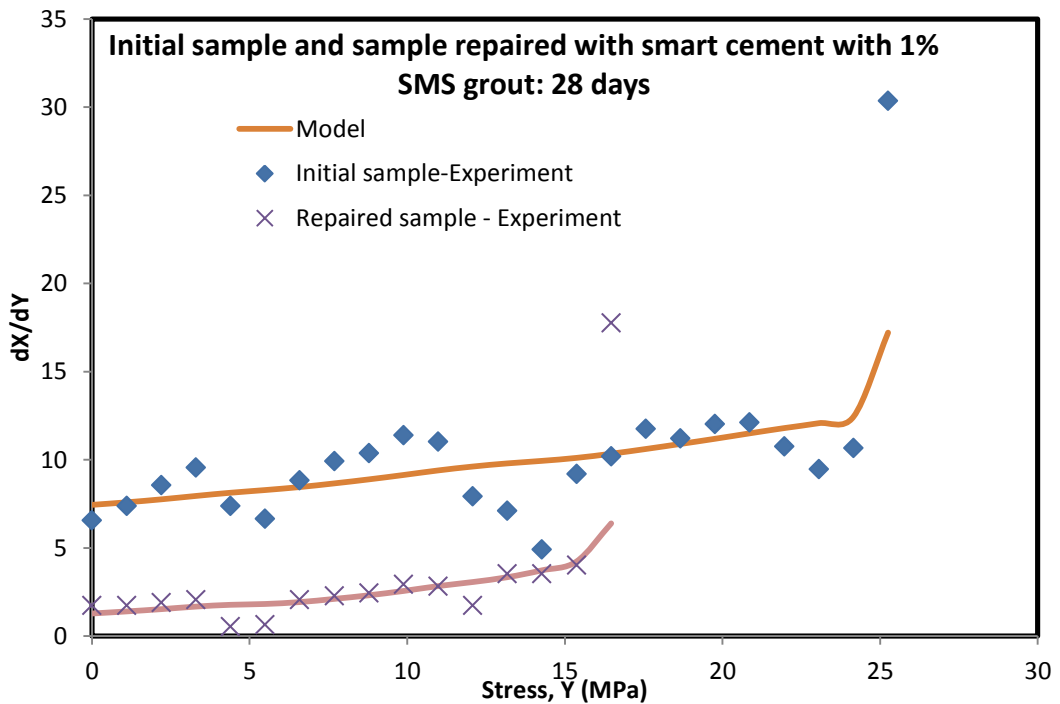


Figure 5-29: Rate of change of resistivity with respect to stress vs Stress for 28 days curing of the initial smart cement sample and the specimen repaired with grout with 1% SMS

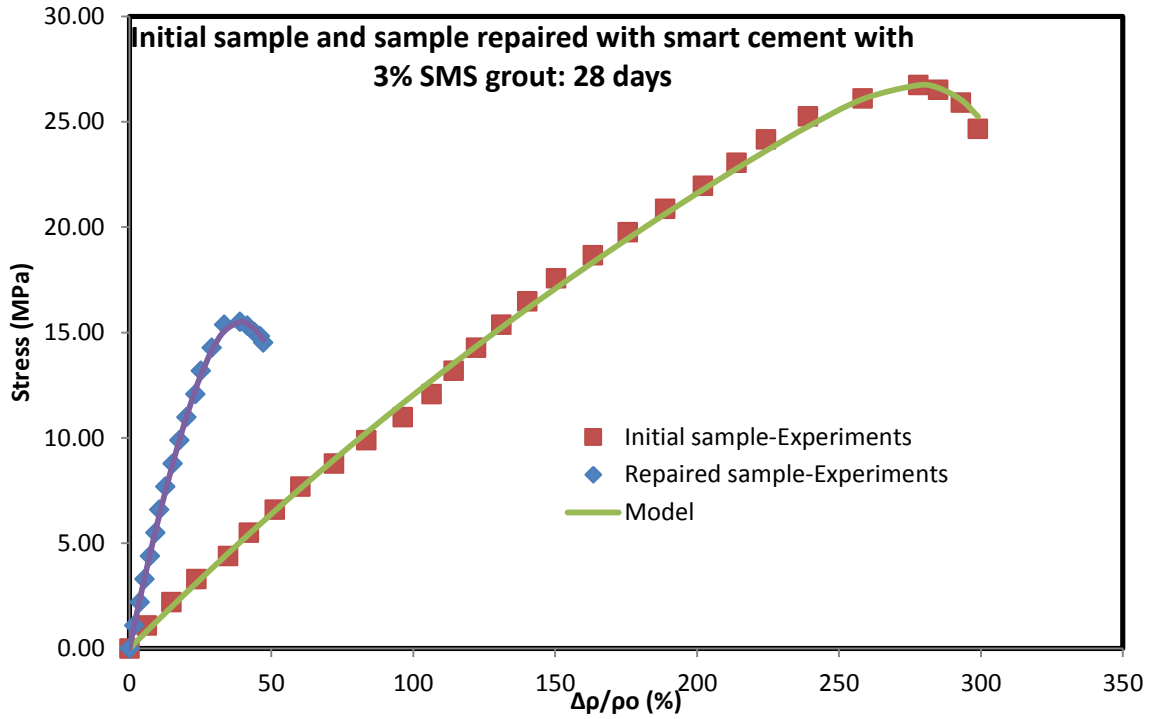


Figure 5-30: Piezoresistive response of the initial smart cement sample and the specimen repaired with grout with 3% SMS after 28 days of curing modeled with p-q model

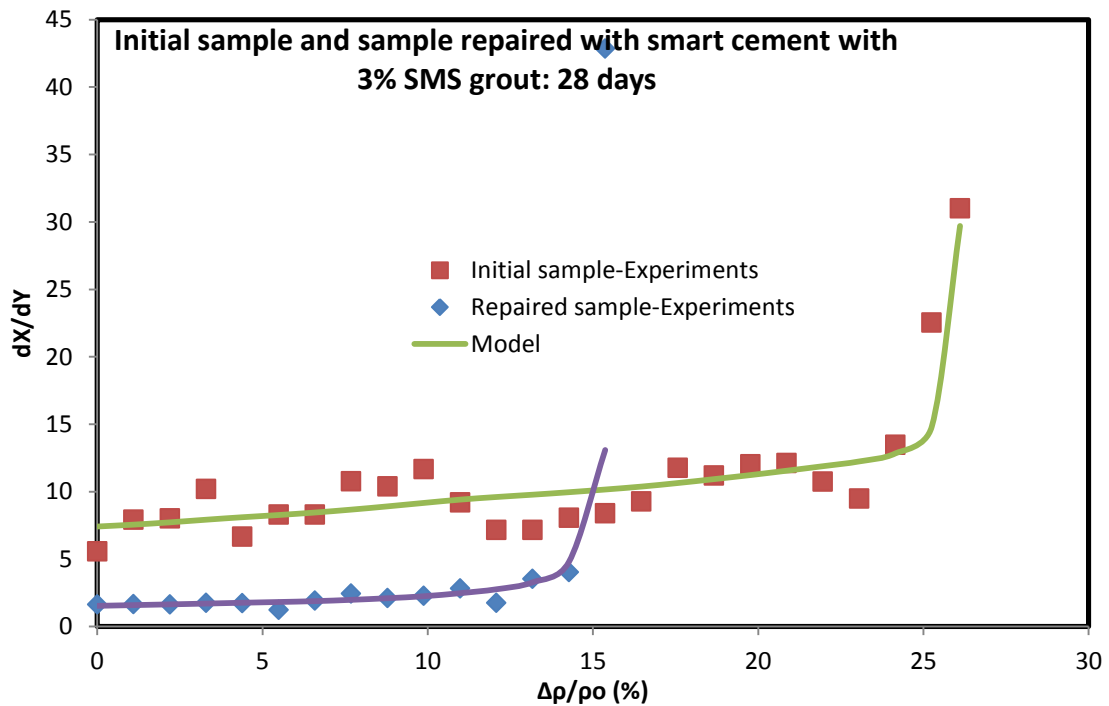


Figure 5-31: Rate of change of resistivity with respect to stress vs Stress for 28 days curing of the initial smart cement sample and the specimen repaired with grout with 3% SMS

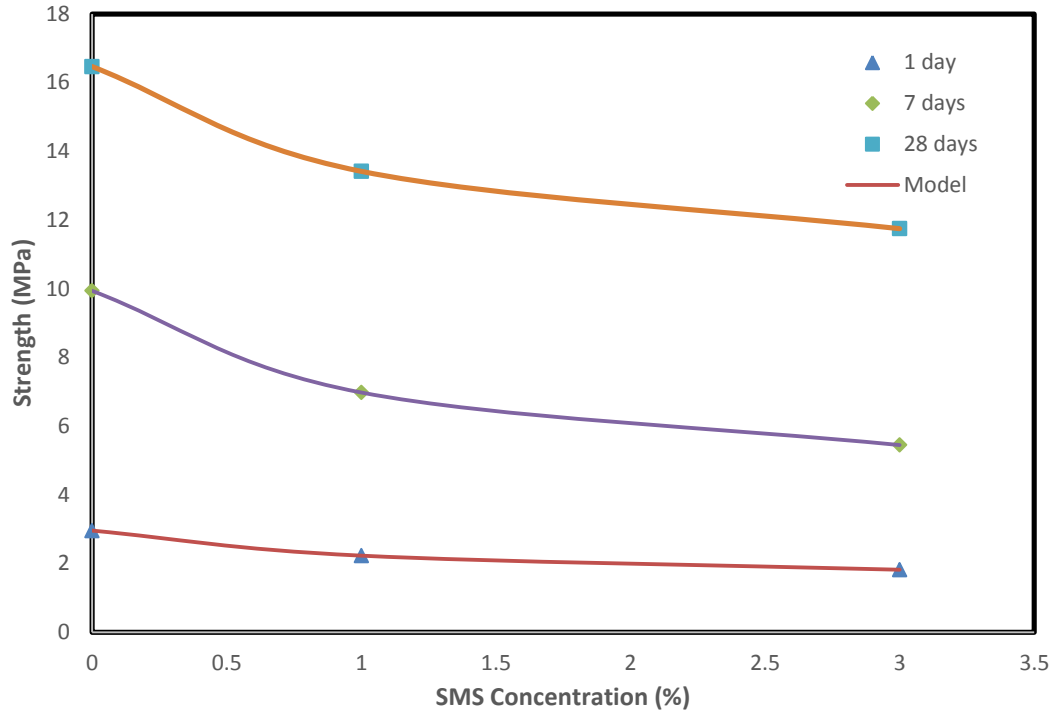


Figure 5-32: Relationship between compressive strength and SMS concentration

The piezoresistivity at failure of the grout specimen made with and without SMS was observed. The addition of SMS decreased the piezoresistivity at failure of the cement grout. The relationship between the piezoresistivity at failure of the cement grout and SMS concentration has been modeled with the hyperbolic model

$$\Delta\rho/\rho_o = (\Delta\rho/\rho_o)_o - S/(G + HS), \quad (5-4)$$

where,

$\Delta\rho/\rho_o$ = Piezoresistivity at failure (%)

$(\Delta\rho/\rho_o)_o$ = Piezoresistivity at failure of the grout without SMS (%)

S = Concentration of sodium meta-silicate (% by weight)

Parameters E and F are model parameters and parameter E represent the initial rate of change and parameter F determines the ultimate piezoresistivity. Experimental results matched very well (Fig. 5-33) with the proposed model with coefficient of determination

(R^2) of 0.99. For 1 day test, parameters E and F were found as 0.009 and 0.017. For 7 days, parameters E and F were found as 0.013 and 0.011. For 28 days strength test, parameters E and F were found as 0.008 and 0.010.

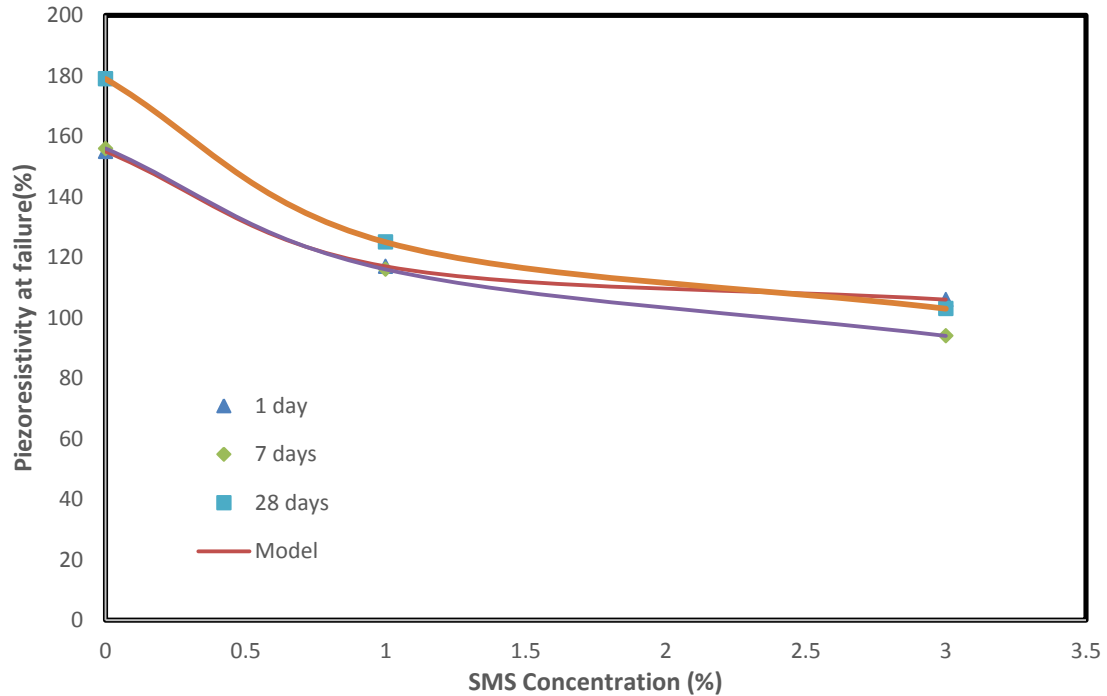


Figure 5-33: Relationship between piezoresistivity at failure strength and SMS concentration

5.2.4 Relationship between RI_{24} and strength/piezoresistivity

The strength of the grout specimen and the resistivity index after 24 hours (RI_{24}) was observed to find whether any relationship can be obtained or not. The compressive strength has been found linearly related (Fig. 5-34) to the resistivity index after 24 hours (RI_{24}) of the cement grout. The relations are as follows:

- (i) For 1 day strength, $\sigma_c = 0.015*(RI_{24}) + 1.2$, $R^2 = 0.95$
- (ii) For 7 days strength, $\sigma_c = 0.057*(RI_{24}) + 3.02$, and $R^2 = 0.95$
- (iii) For 28 days strength, $\sigma_c = 0.06*(RI_{24}) + 9.2$. $R^2 = 0.85$

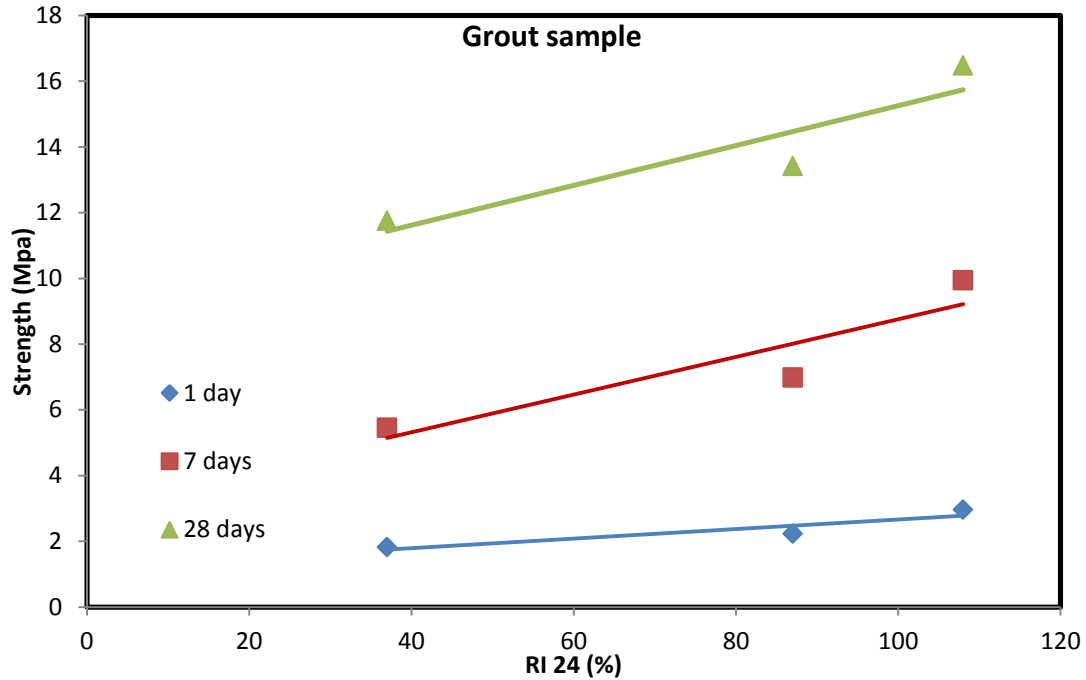


Figure 5-34: Relationship between compressive strength and resistivity index after 24 hours (RI₂₄) for the cement grout

The same relationship between the piezoresistivity ($\Delta\rho/\rho_o$) at failure and resistivity index after 24 hours (RI₂₄) was observed to find whether any relationship can be obtained or not for the grout specimens. The relationship was found linear for the grouts (Fig. 5-35). The relations are as follows:

- (i) For 1 day, $\Delta\rho/\rho_o = 0.8*(RI_{24}) + 60.5$, $R^2 = 0.95$
- (ii) For 7 days, $\Delta\rho/\rho_o = 0.6*(RI_{24}) + 79.2$, and $R^2 = 0.95$
- (iii) For 28 days, $\Delta\rho/\rho_o = 0.95*(RI_{24}) + 61.7$. $R^2 = 0.85$

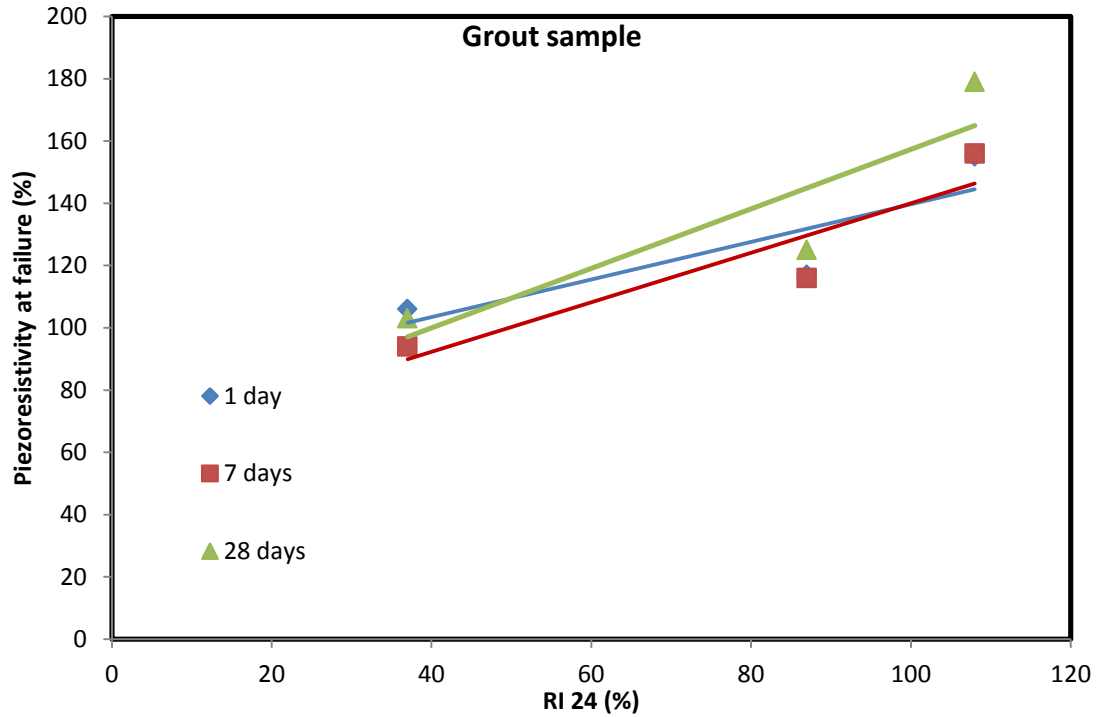


Figure 5-35: Relationship between piezoresistivity at failure and resistivity index after 24

5.2.5 Relationship between curing time and strength/piezoresistivity at failure

The strength of the grout specimen made with and without SMS was observed up to 28 days. With curing time increases, the compressive strength of the cement grout increased. The relationship between the compressive strength of the cement grout and curing time has been modeled with the hyperbolic model

$$\sigma_c = t/(J + Kt), \quad (5-5)$$

where,

σ_c = Compressive strength of the grout (MPa)

t = Curing time (day)

Parameters J and K are model parameters and parameter J represent the initial rate of change and parameter K determines the ultimate strength. For the cement grouts, experimental results matched very well (Fig. 5-36) with the proposed model with

coefficient of determination (R^2) of 0.95-0.99. For smart cement grout only, parameters J and K were found as 0.347 MPa^{-1} and 0.048 MPa^{-1} . For smart cement grout with 1% SMS, parameters J and K were found as 0.586 MPa^{-1} and 0.054 MPa^{-1} . For smart cement grout with 3% SMS, parameters J and K were found as 0.841 MPa^{-1} and 0.055 MPa^{-1} .

For the cement specimens repaired with grout, experimental results also matched very well (Fig. 5-37) with the proposed model with coefficient of determination (R^2) of 0.95-0.99. For the specimen repaired with smart cement grout only, parameters J and K were found as 0.046 MPa^{-1} and 0.058 MPa^{-1} . For the specimen repaired with smart cement grout with 1% SMS, parameters J and K were found as 0.110 MPa^{-1} and 0.055 MPa^{-1} . For the specimen repaired with smart cement grout with 3% SMS, parameters J and K were found as 0.149 MPa^{-1} and 0.058 MPa^{-1} .

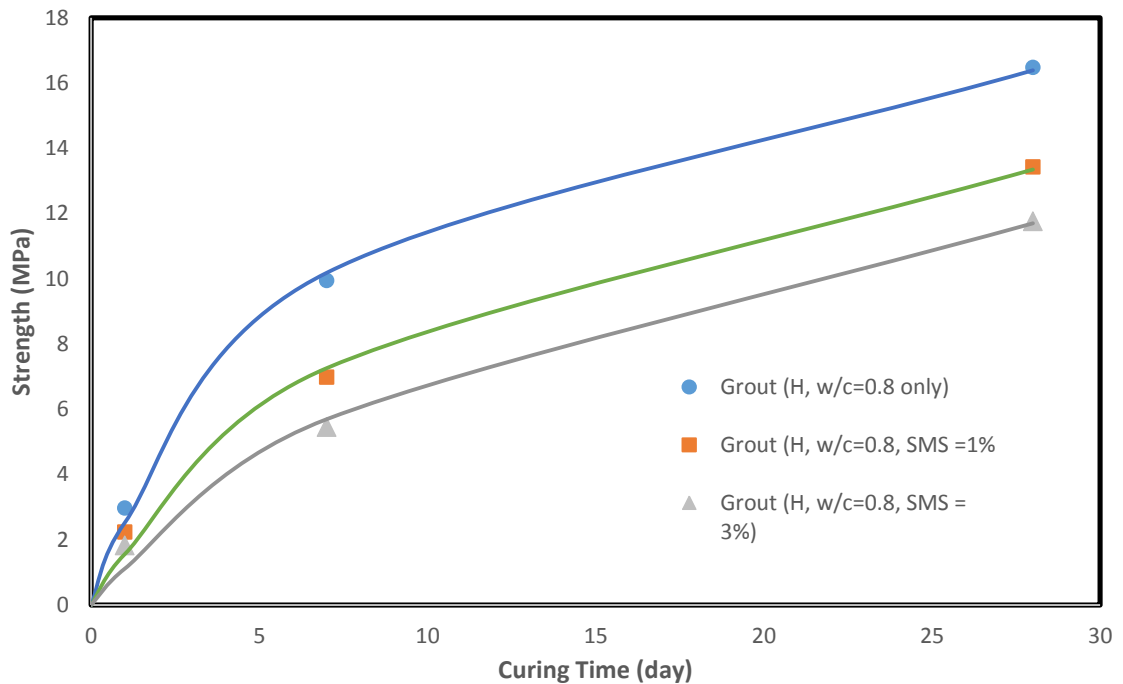


Figure 5-36: Relationship between compressive strength and the curing time for the grout modeled with hyperbolic model

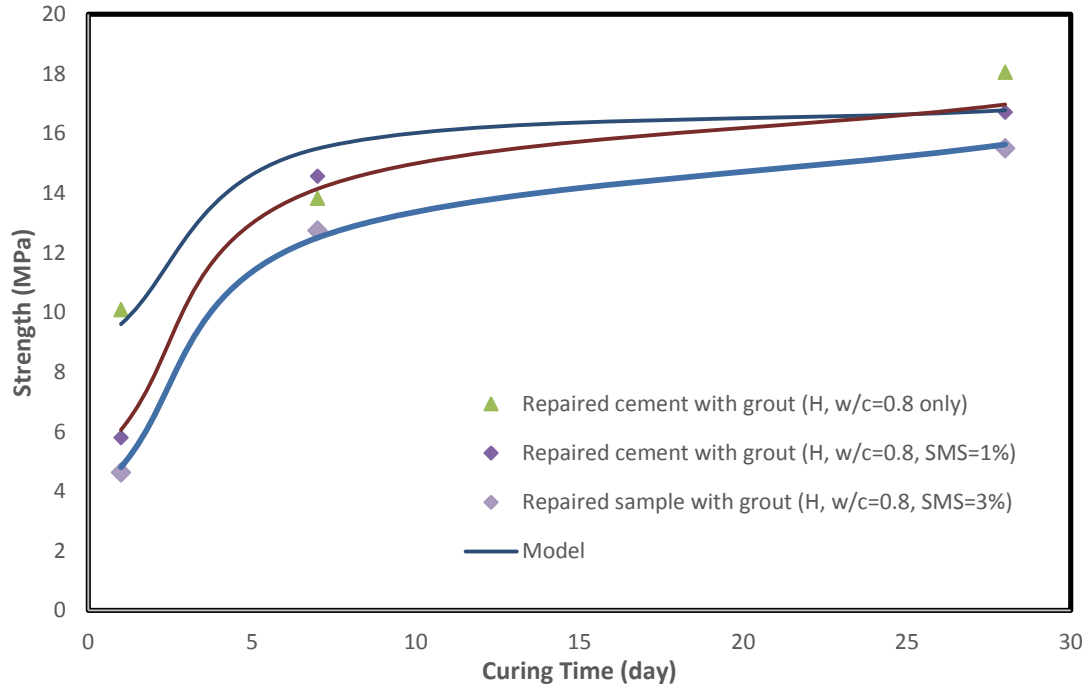


Figure 5-37: Relationship between compressive strength and the curing time for the repaired cement with grout modeled with hyperbolic model

The piezoresistivity at failure of the grout specimen made with and without SMS was observed up to 28 days. With curing time increases, the piezoresistivity at failure of the cement grout changes. The relationship between the piezoresistivity at failure of the cement grout and curing time has been modeled with the hyperbolic model

$$\Delta\rho/\rho_o = (\Delta\rho/\rho_o)_1 - t/(L + Mt) \quad (5-6)$$

where,

$\Delta\rho/\rho_o$ = Piezoresistivity at failure (%)

$(\Delta\rho/\rho_o)_1$ = Piezoresistivity at failure of the grout after 1 day (%)

t = Curing time (day)

Parameters L and M are model parameters and parameter L represent the initial rate of change and parameter M determines the ultimate piezoresistivity. For the cement grouts,

experimental results matched very well (Fig. 5-38) with the proposed model with coefficient of determination (R^2) of 0.95-0.99. For smart cement grout only, parameters L and M were found as 1.64 and -0.019. For smart cement grout with 1% SMS, parameters L and M were found as 2.5 and 0.036. For smart cement grout with 3% SMS, parameters L and M were found as 3.5 and 0.1.

For the cement specimens repaired with grout, experimental results also matched very well (Fig. 5-39) with the proposed model with coefficient of determination (R^2) of 0.95-0.99. For the specimen repaired with smart cement grout only, parameters L and M were found as 0.270 MPa^{-1} and 0.126 MPa^{-1} . For the specimen repaired with smart cement grout with 1% SMS, parameters L and M were found as 2.97 MPa^{-1} and -0.035 MPa^{-1} . For the specimen repaired with smart cement grout with 3% SMS, parameters L and M were found as 0.158 MPa^{-1} and 0.367 MPa^{-1} .

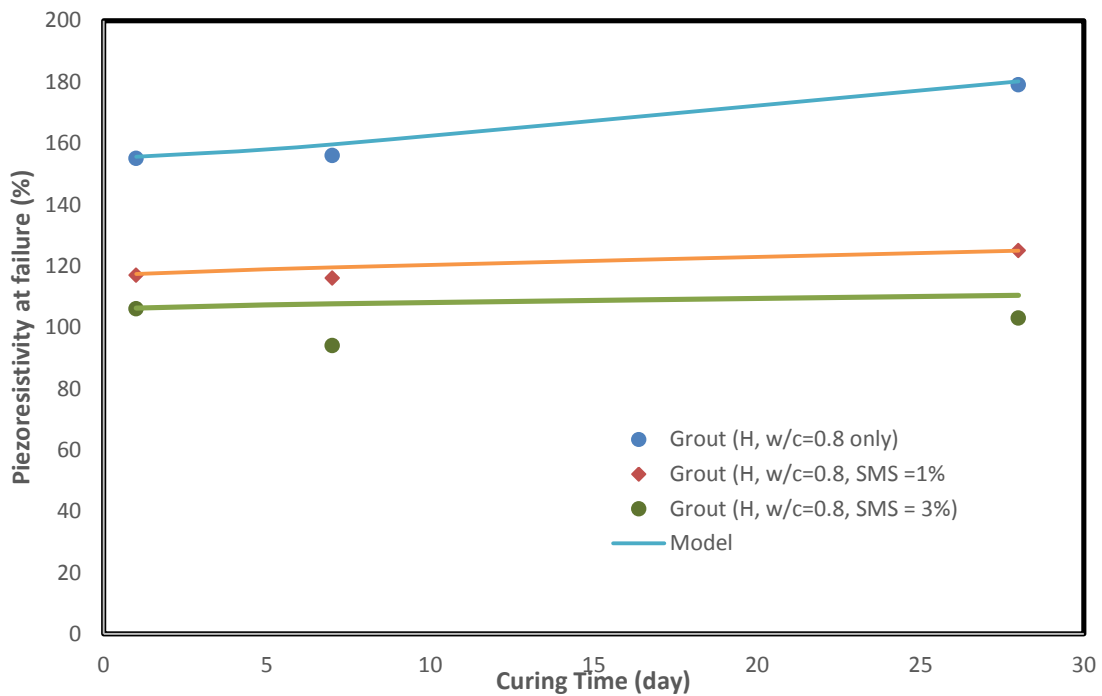


Figure 5-38: Relationship between Piezoresistivity at failure and the curing time for the grout modeled with hyperbolic model

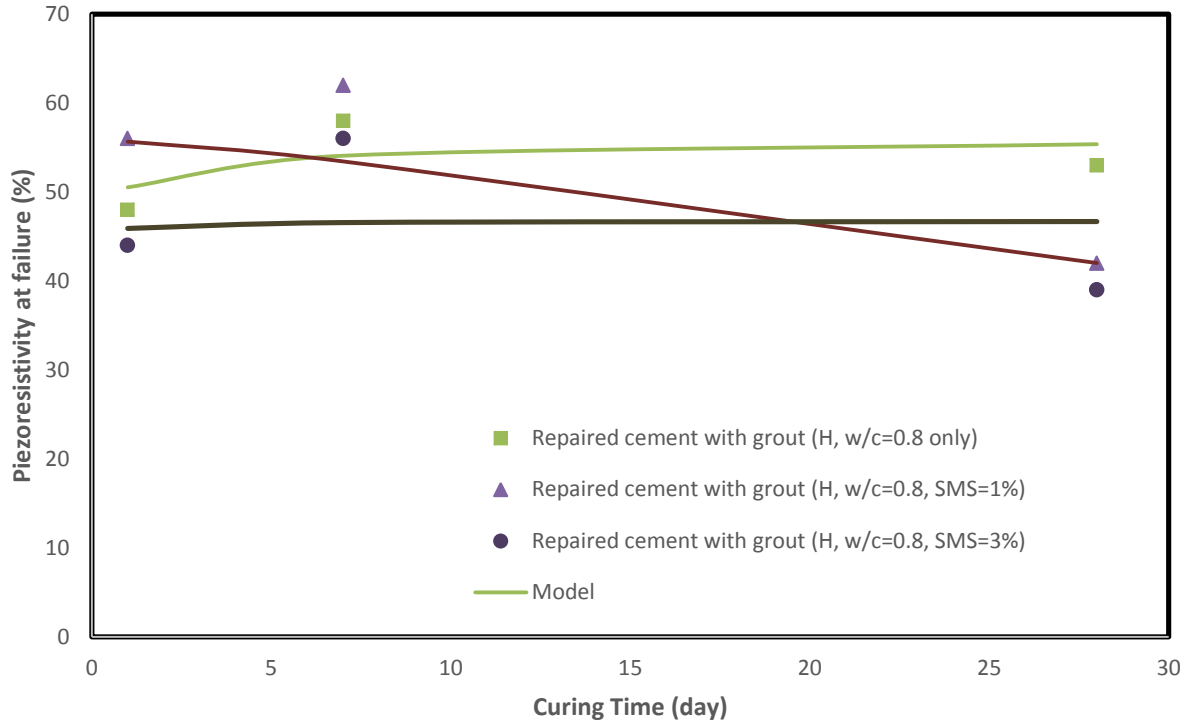


Figure 5-39: Relationship between Piezoresistivity at failure and the curing time for the cement specimens repaired with grout modeled with hyperbolic model

5.3 Summary

Based on experimental and analytical study on smart cement grout with and without SMS cured room temperature, the following observations are advanced:

1. The initial resistivity (ρ_o) of the smart cement grout decreased from $1.08 \Omega\text{-m}$ to $0.69 \Omega\text{-m}$ with 1% SMS, a 36% decrease. The minimum resistivity (ρ_{\min}) of the smart cement grout decreased from $1.04 \Omega\text{-m}$ to $0.54 \Omega\text{-m}$ with 1% SMS, a 44% decrease. The changes in the electrical resistivity were higher than the changes in the unit weight of the cement. Hence the electrical resistivity can also be used for quality control of smart cement grout curing.
2. Electrical resistivity developments with hydration time of the cement with addition of SMS followed a similar pattern: they first drop to a minimum point

and then gradually increase with time. The resistivity index ($RI_{24 \text{ hour}}$, $RI_{7 \text{ days}}$, $RI_{28 \text{ days}}$) of the smart cement grout 108%, 492% and 801% but for the smart cement grout with 1% SMS, those indices were reduced to 87%, 307% and 798% respectively. And the smart cement grout with 1% SMS had 52%, 60% and 48% less resistivity for 1 day, 7 days, and 28 days curing compared to that of smart cement grout.

3. The resistivity index ($RI_{24 \text{ hour}}$, $RI_{7 \text{ days}}$, $RI_{28 \text{ days}}$) of the repaired cement specimen with smart cement grout only were 49%, 124% and 183% but for the specimen repaired with smart cement grout with 1% SMS, those indices were 172%, 502% and 684% respectively. The RI_{24} was found linearly related to the strength and piezoresistivity of the grout.
4. The resistivity with curing time for both types of grout and for the repaired sample was modeled with curing model developed from p-q model and the model parameters were determined with very good coefficient of correlation and RMSE. The rate of change of resistivity was linearly related to the rate of moisture loss. The resistivity was modeled with the moisture loss by a polynomial relationship and found matched with a very good coefficient of determination.
5. The smart cement grout showed piezoresistive behavior under compressive stress. Without any SMS, piezoresistivity at peak stress was varying from 155-179% which is reduced up to 116-125% with 1% SMS. The repaired samples showed piezoresistivity varying from 48-62%. The strength regain was varying from 51-84% and the piezoresistivity regain were 16-26%. The nonlinear piezoresistive model predicated the compressive stress–change in resistivity relationship of the

smart cement grout with and without SMS very well.

6. The rate of change of resistivity with respect to stress change was found to be another indicator of the piezoresistivity. During the application of the stress, this indicator changes very slowly but after the initial crack happens, the rate of change of resistivity with respect to stress changes sharply or changes the slope which indicates prior to failure of the specimen.
7. The compressive strength and piezoresistivity was modeled by hyperbolic relationship with the SMS content and the curing time.

CHAPTER 6 CHARACTERIZATION OF DRILLING MUD

6.1 Rheological Properties

The rheological test was done with a rotational viscometer with rotational speed 0.3 RPM to 600 RPM. From the test gel strength at 10 seconds and 10 minutes and the shear stress at different shear strain rate were measured. After modeling the experimental data with Herschel-Bulkley model (Eqn. (3-4)) and hyperbolic model (Eqn. (3-5)) the yield points were determined from the model. The yield points, gel strength, model parameters A and B, and R^2 and RMSE determined from hyperbolic model are presented in Table 6-1. Also the apparent viscosity at shear strain rate 510 (1/sec) is calculated from the data and presented in Table 6-1. The hyperbolic model fitted the experimental data with a very good coefficient of determination ($R^2=0.98$ to 0.99) and RMSE (1.26 to 2.93 Pa) both for the 6% bentonite mud with and without sodium alumino-silicate (SAS) (Fig. 6-1) and 6% bentonite mud with and without sodium meta-silicate (SMS) (Fig. 6-2). Parameter A was 2.32 Pa^{-1} for 6% bentonite mud only which increased with the addition of SAS and was 3.25 Pa^{-1} with 0.3% SAS. With the addition of SMS parameter A increased to 2.91 Pa^{-1} with 0.3% SMS. Parameter B was $0.012 \text{ Pa}\cdot\text{sec}^{-1}$ for 6% bentonite mud only and reduced to 0.009 with the addition of 0.1% SAS and increased to $0.014 \text{ Pa}\cdot\text{sec}^{-1}$ with 0.3% SAS. The addition of SMS followed the similar trend and the parameter B reached to 0.015 by addition of 0.3% SMS (Table 6-1). The experimental results were also modeled with Herschel–Bulkley model (Eqn. (3-4)) and the model parameters k and n are presented in Table 3-2. The Herschel–Bulkley model fitted the experimental data with a coefficient of determination ($R^2=0.97$ to 0.99) and RMSE (1.4 to 2.34 Pa) both for the 6% bentonite mud with and without SAS (Fig. 6-3) and 6%

bentonite mud with and without SMS (Fig. 6-4). Parameter k was found as 8.35 for 6% bentonite mud only which was decreased by addition of SAS and reached to about 5.05 by addition of 0.3% SAS. By addition of SMS parameter k was also decreased and reached to 4.98 by addition of 0.3% SMS. Parameter n was found as 0.32 for 6% bentonite mud only which was increases to 0.41 by addition of 0.1% SAS and then decreased to 0.37 by addition of 0.3% SAS. The addition of SMS followed the similar trend and the parameter n reached to 0.36 by addition of 0.3% SMS (Table 6-2).

Table 6-1: Hyperbolic model parameters for drilling muds

Mud Type	Apparent viscosity at 510 (1/sec)	Gel Strength (Pa)		Hyperbolic Model				
		10 sec	10 min	Yield Stress (Pa)	A (Pa ⁻¹)	B (Pa.sec ⁻¹)	R ²	RMSE (Pa)
Bentonite (B)	14.7	26	32	19	2.32	0.012	0.99	1.26
B+0.1%SAS	17.4	26	31	22.2	2.57	0.009	0.99	2.93
B+0.2%SAS	13.9	11	14	16.6	2.59	0.012	0.99	2.10
B+0.3%SAS	9.9	4.2	5.8	5.6	3.25	0.014	0.98	2.22
B+0.1%SMS	16.8	25.5	31.4	23.5	2.54	0.009	0.98	2.93
B+0.2%SMS	14.1	12	15	17	2.58	0.012	0.99	1.58
B+0.3%SMS	10.0	4	6	4.2	2.91	0.015	0.99	2.05

Table 6-2: Herschel–Bulkley model parameters for drilling muds

Mud Type	Hyperbolic Model				
	Yield Stress (Pa)	k	n	R ²	RMSE (Pa)
Bentonite (B)	10.5	8.35	0.32	0.97	2.34
B+0.1%SAS	18.3	5.13	0.41	0.99	1.75
B+0.2%SAS	10.8	6.16	0.36	0.98	2.04
B+0.3%SAS	0	5.05	0.37	0.99	1.40
B+0.1%SMS	19.2	5.29	0.40	0.99	1.77
B+0.2%SMS	10.6	6.58	0.35	0.98	2.11
B+0.3%SMS	0	4.98	0.36	0.99	1.5

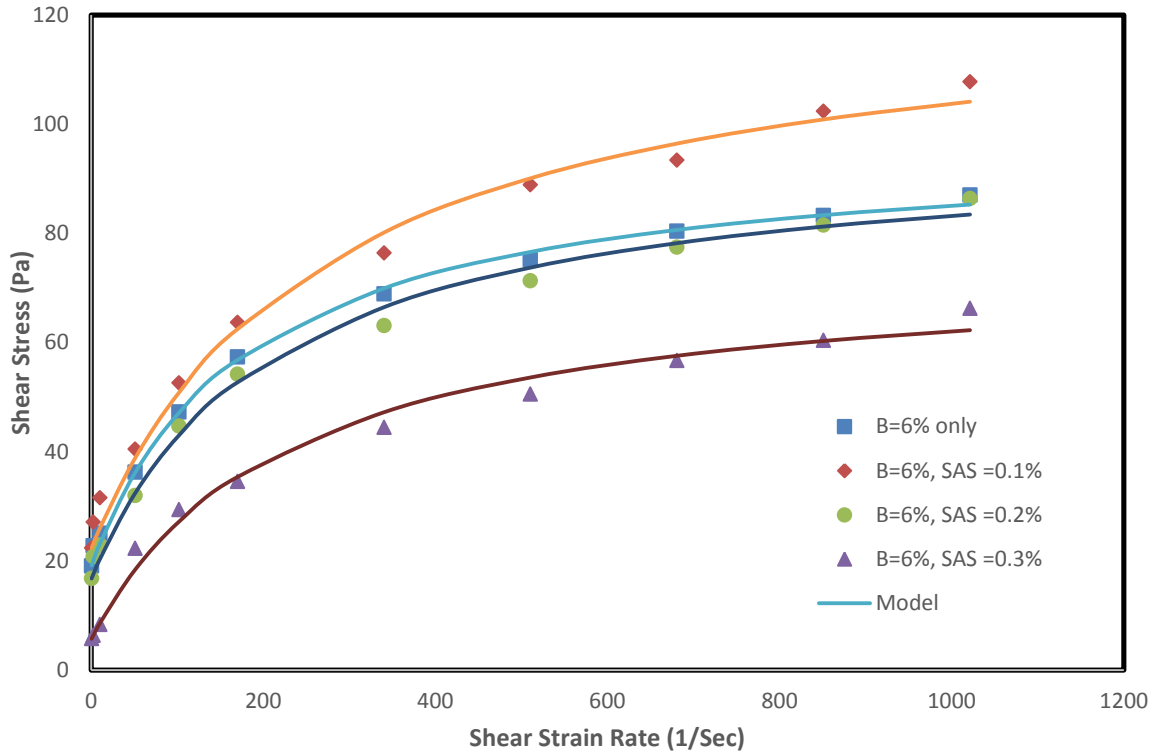


Figure 6-1: Measured and predicted shear stress vs shear strain rate (hyperbolic model) for bentonite mud with and without SAS

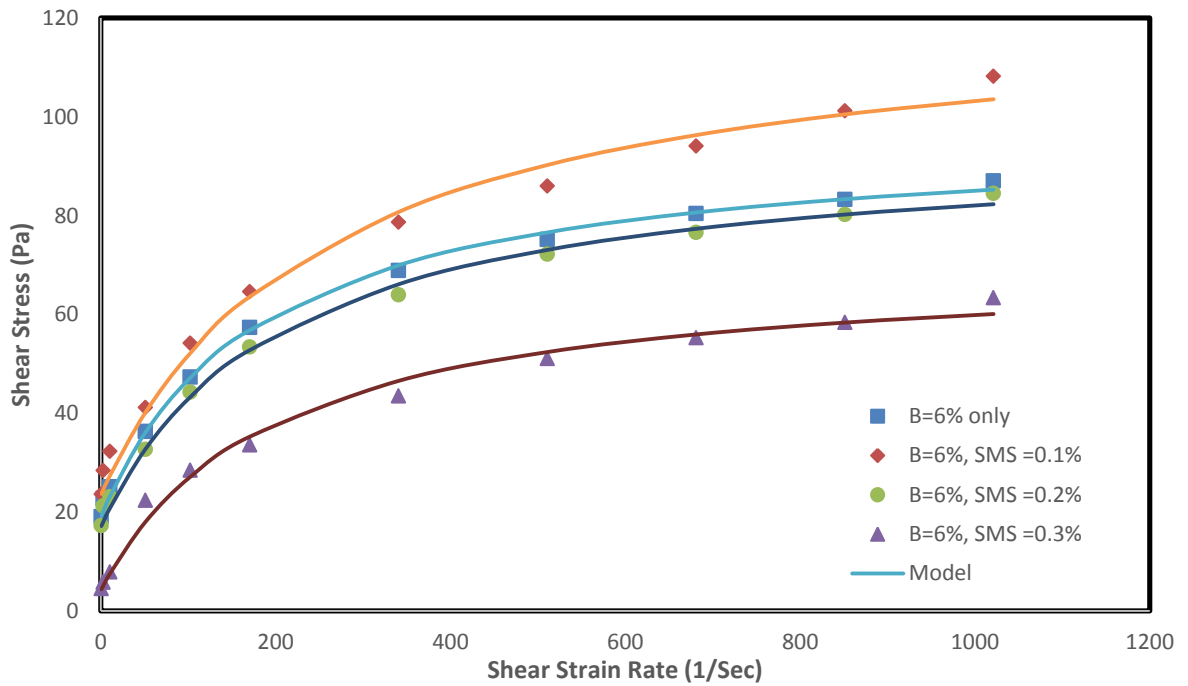


Figure 6-2: Measured and predicted shear stress vs shear strain rate (hyperbolic model) for bentonite mud with and without SMS

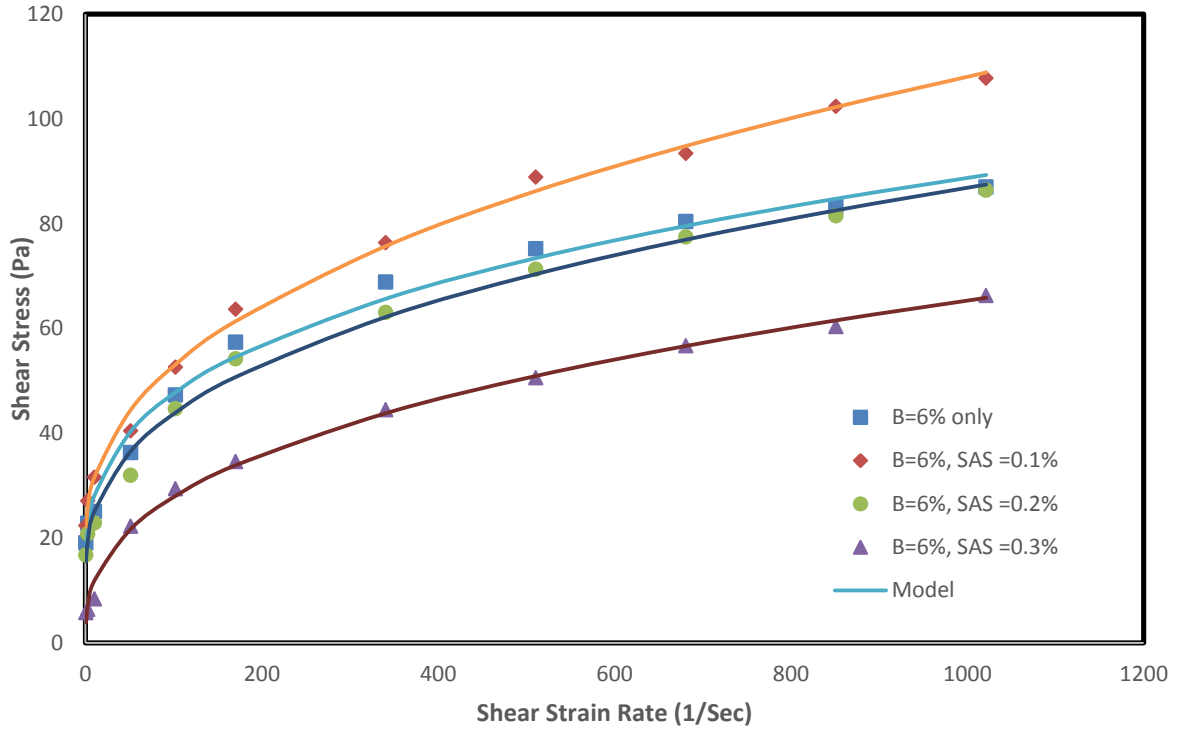


Figure 6-3: Measured and predicted shear stress vs shear strain rate (Herschel–Bulkley model) for bentonite mud with and without SAS

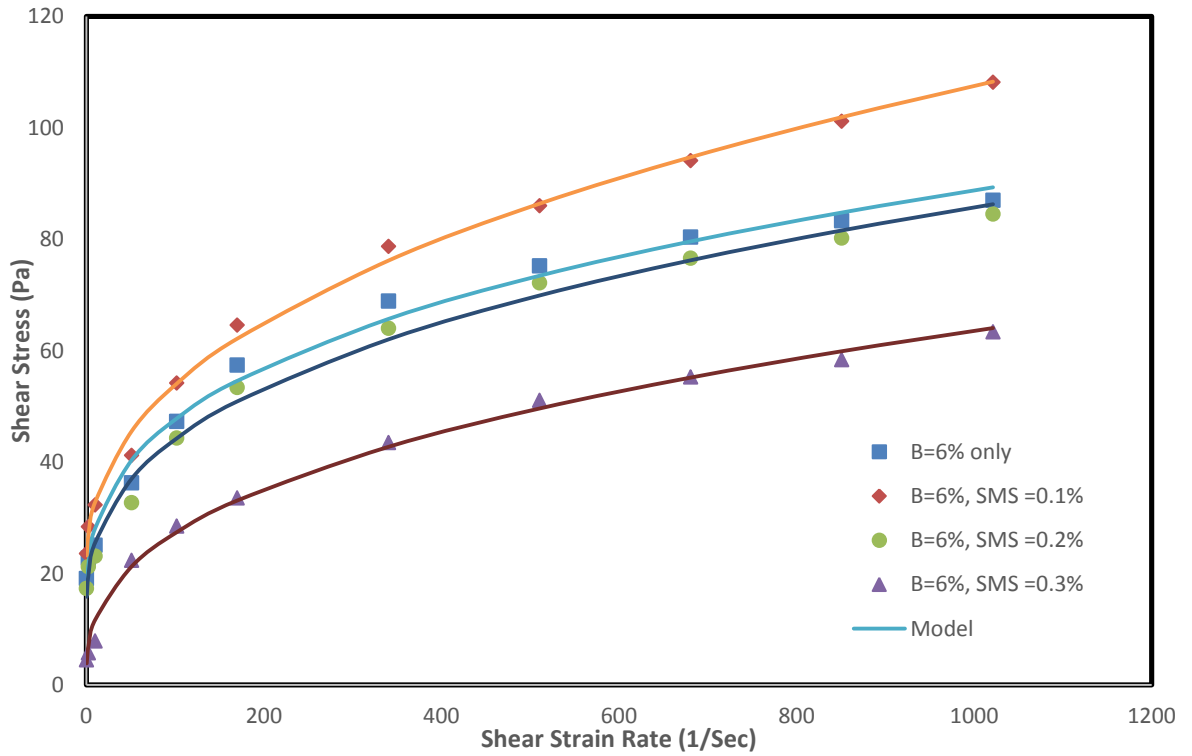


Figure 6-4: Measured and predicted shear stress vs shear strain rate (Herschel–Bulkley model) for bentonite mud with and without SMS

6.1.1 Apparent viscosity

Apparent viscosity of a 6% (w/w) bentonite mud with different percentage (0 to 0.3% w/w) of sodium alumino-silicate (SAS) and sodium meta-silicate (SMS) content was calculated at 510 sec^{-1} shear strain rate and the results are summarized in Table 6-1. The results were as follows:

(a) For 6% bentonite mud: The apparent viscosity of a 6% bentonite mud at 510 sec^{-1} was 14.7 cP.

(b) 6% bentonite mud with 0.1% silicate: The apparent viscosity of a 6% bentonite mud with 0.1% silicate solution at 510 sec^{-1} was increased to about 17 to 17.4 cP, a 18% increase.

(c) 6% bentonite mud with 0.3% silicate: The apparent viscosity of a 6% bentonite mud with 0.3% silicate solution at 510 sec^{-1} was decreased to about 10 cP, a 30% decrease.

Bentonites are highly colloidal and swell in water providing viscosity to the mix (Fink, 2012). Thus a lesser silicate content (0.1%) increased the colloidal properties and that's why decreased the pump ability of the bentonite mud, but a higher content (0.3%) decreased the colloidal properties and hence increased the pump ability of the drilling mud.

6.1.2 Yield Point

The yield point (YP) or yield stress is described as the stress that must be applied to a material to initiate flow or it is the shear stress corresponding to a shear strain rate of zero (Power and Zamora, 2003). If the applied stress is below the yield stress, then the fluid will display strain recovery when the stress is removed. Once the yield stress has

been exceeded, the fluid displays viscous flow characteristics. In this study, the yield point determined from hyperbolic model also behaves in the same way that plastic viscosity behaves with both silicates as summarized in Table 6-1 and Table 6-2 and described as follows:

(a) For 6% bentonite mud: The yield point of a 6% bentonite mud was 19 Pa.

(b) 6% bentonite mud with 0.1% silicate: The yield point of a 6% bentonite mud with 0.1% silicate solution was increased to 22.2 Pa by addition of 0.1% SAS and to 23.5 Pa by addition of 0.1% SMS, a 20% increase.

(c) 6% bentonite mud with 0.3% silicate: The yield of a 6% bentonite mud with 0.3% SAS and SMS was decreased to 5.6 Pa and 4.4 Pa respectively, a 73% reduction (Table 6-1, 6-2).

YP is used to evaluate the ability of a mud to lift cuttings out of the annulus (Nazari et al., 2010) and YP is lowered by adding deflocculant to a clay-based mud and increased by adding freshly dispersed clay or a flocculant, such as lime (Smithson, 2015). Thus, in this study, 0.1% silicate was acting as a flocculant which increased the YP and hence increased the ability to lift cuttings; and the higher amount (0.3%) was acting as a deflocculant which decreased the YP and hence decreased the ability to lift cuttings.

6.1.3 Gel strength

The gel strength is defined as the shear stress of drilling mud which is measured at low shear strain rate after the drilling mud is left static/quiescent for a certain period of time i.e. 10 second or 10 minutes and actually it is a measure of the attractive forces between the particles in fluid under static condition (Nelson, 2006). The gel strength demonstrates the ability of the drilling mud to suspend drill solid and weighting material when circulation is ceased. In this study, gel strength showed a slightly different trend

than the apparent viscosity and yield point with addition of silicate solution as summarized in Table 6-1 and described as follows:

(a) For 6% bentonite mud: The 10 second and 10 minutes gel strength were 26 Pa and 32 Pa for 6% bentonite mud.

(b) 6% bentonite mud with 0.1% silicate: The 10 second and 10 minutes gel strength of a 6% bentonite mud with 0.1% silicate solution was decreased to 25.5 Pa and 31 Pa by addition of 0.1% silicate solution, a 3% decrease.

(c) 6% bentonite mud with 0.3% silicate: The 10 second and 10 minutes gel strength of a 6% bentonite mud with 0.3% SAS and SMS was decreased to 4 Pa and 6 Pa, a 81 to 84% reduction (Table 6-1, 6-2)

Thus, the addition of silicate solution was decreasing the attractive forces between the particles in drilling mud and hence reducing the ability to suspend drill solid and weighing material when circulation is ceased.

6.2 Electrical Resistivity of Bentonite Drilling Mud

Electrical resistivity of 6% bentonite drilling mud was determined with conductivity meter and converting it to resistivity. Fig. 6-5 shows the effect of SMS and SAS on the resistivity of 6% bentonite drilling mud. Here the resistivity is very sensitive to the silicate content. The resistivity of 6% bentonite was found 5.3 Ω .m which reduced to 4.70 and 4.95 Ω .m for only 0.1% (w/w) SMS and SAS respectively. With 0.3% SMS the resistivity was found 4.42 Ω .m (a 17% reduction) and for 0.3% SAS, the resistivity was 4.54 Ω .m, a 14% reduction.

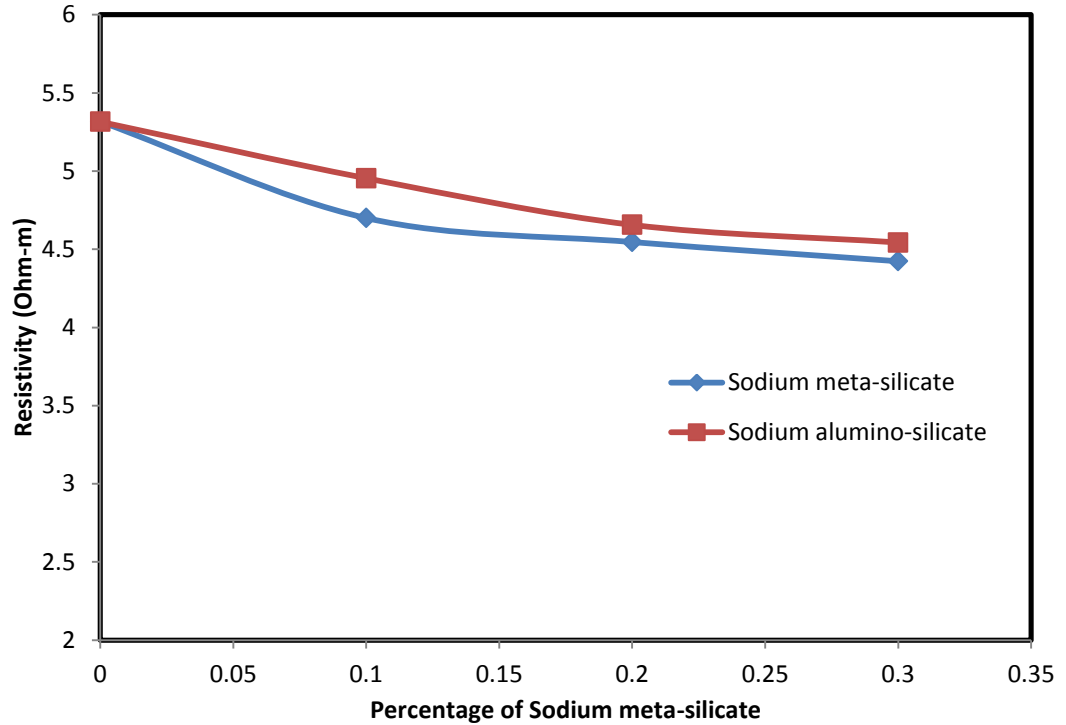


Figure 6-5: Effect of SMS and SAS on the resistivity of a 6% bentonite mud.

6.3 Fluid loss analysis

Different amount of SAS and SMS (0.1% and 0.3%) is added to 6% bentonite mud to determine the filtration loss until the last drop of filtrate comes out. The applied pressure was about 80-100 psi. For 6% bentonite drilling mud, the API (30 minutes) fluid loss was found as 22.5 mL. With addition of 0.1% SMS and SAS, the fluid loss was reduced to 18.2 ml, but with 0.3% of both of the silicates, the fluid loss again increased a little bit which is about 20.5 mL. As the sample was allowed to loss fluid for long time until the end of the fluid loss, the 6% bentonite losses fluid until 2 days and the total loss happened was about 200 mL (Table 6-3). With 0.1% SAS, the sample stayed until 4.1 days with a fluid loss of 202 mL (Fig. 6-6) whereas with 0.1% SMS, the sample stayed until 4.9 days with a fluid loss of about 220 mL (Fig. 6-7). But with the addition of 0.3% SAS and SMS, the time of fluid loss is reduced to about 3.2 days and the total fluid loss

is increased to about 230 ml. Thus, the addition of 0.1% SAS and SMS increased the time of fluid loss by about 140%; and for SAS the total fluid loss was almost same but for SMS the total fluid loss increased by about 9-10%. The addition of 0.3% of both silicates increased the time about 60% and the total fluid loss about 15%. The results are summarized in Table 6-3.

Table 6-3: Summary of fluid loss with SAS and SMS for a bentonite mud.

Combination	API (30 Minutes) Fluid Loss (mL)		Total Fluid Loss (mL)		Total Time (Days)	
	Test 1	Test 2	Test 1	Test 2	Test 1	Test 2
6% B (Bentonite)	22.5	22	201	198	1.94	2.23
6%B + 0.1%SAS	18.2	20	200	204	4.10	3.88
6%B + 0.3%SAS	20	19.7	226	228	3.14	3.22
6%B + 0.1%SMS	18.2	20	218	220	4.88	4.93
6%B + 0.3%SMS	20.5	22.2	230	228	3.25	2.84

6.3.1 Modeling of the filtration process

The filtration process were modeled and predicted using API model (Eqn. (3-6)) and the model parameter M , R^2 and RMSE values are presented in Table 6-4. Here, the parameter M is calculated using initial 30 min fluid loss and then the predictions are made for the long time fluid loss. The value of M was about 4.25 for 6% bentonite mud which is decreased to about 3.5 by 0.1% SAS and then increased to about 3.65 by addition of 0.3% SAS. Addition of SMS had the same kind of effect on the parameter M . The value of M decreased to about 3.5 by addition of 0.1% SMS and then increased to about 3.9 by addition of 0.3% SMS. The coefficient of determination varied from 0.79 to 0.98 and the RMSE varied from 8 mL to 35.5 mL. The predictions are presented in Fig. 6-6 and Fig. 6-7.

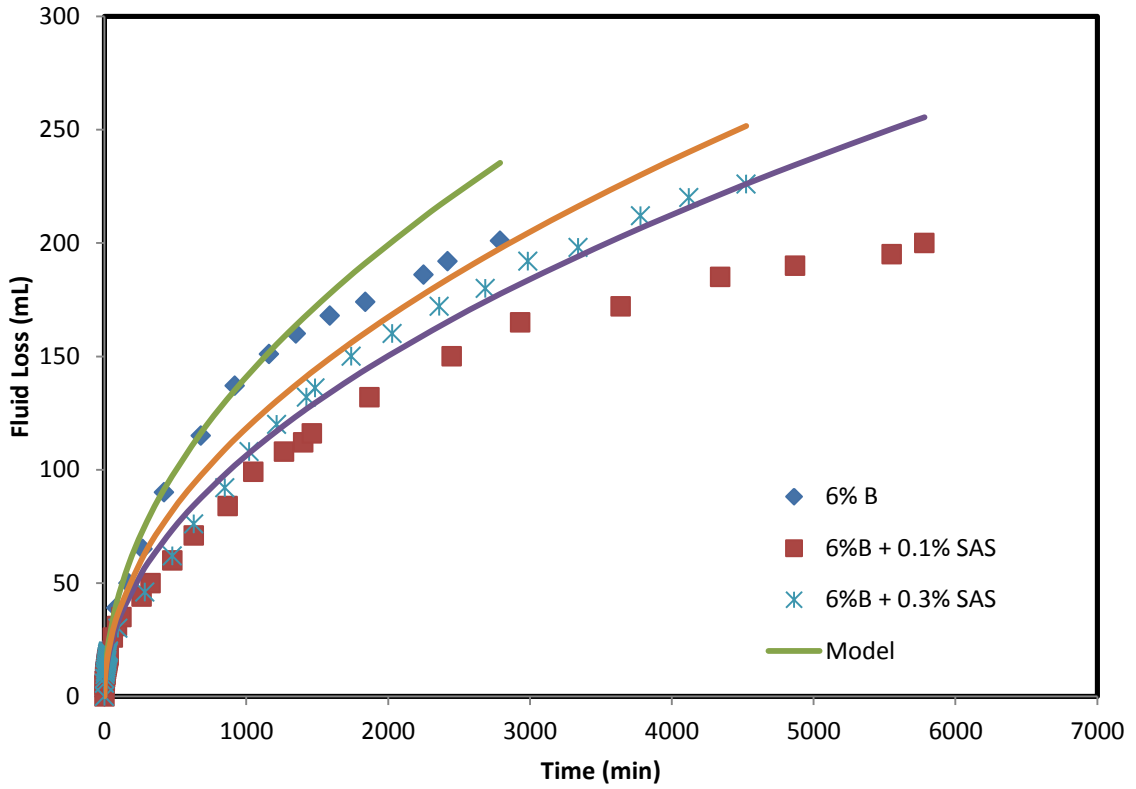


Figure 6-6: Effect of SAS on the fluid loss of a bentonite mud modeled with API Model

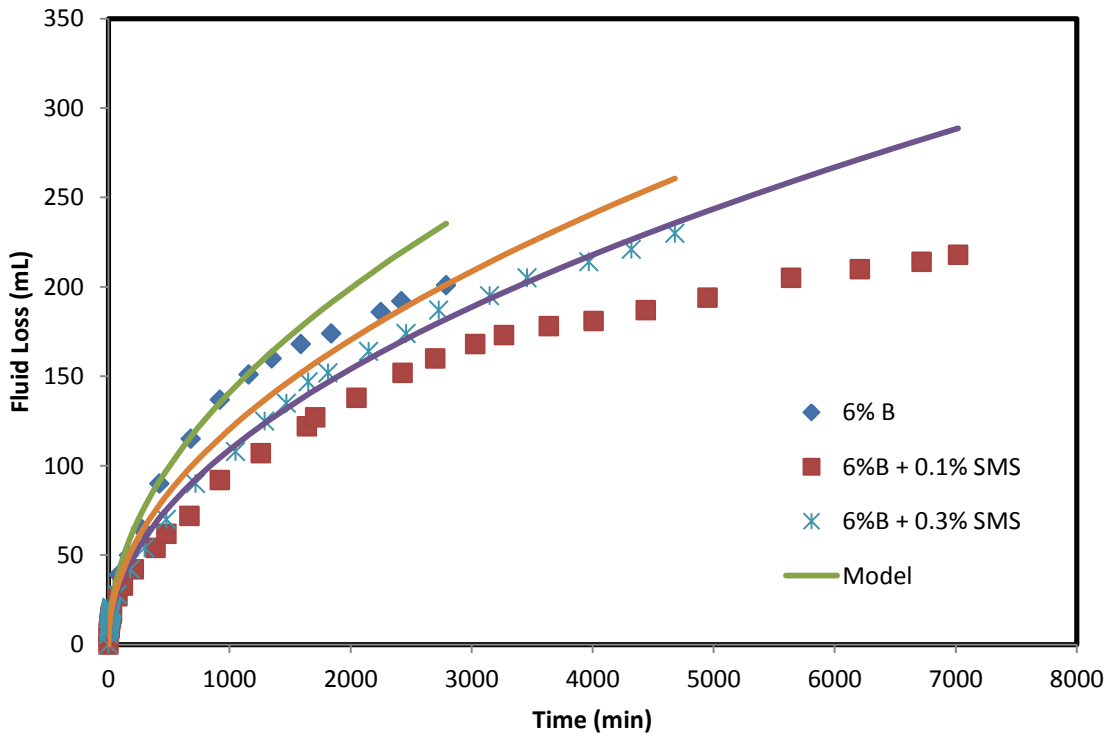


Figure 6-7: Effect of SMS on the fluid loss of a bentonite mud modeled with API Model

The prediction done using API model did not show very good coefficient of correlation (0.79-0.98) and RMSE (Table 6-4). So the prediction is also done using the Kinetic model (Eqn. (3-8)) for 6% bentonite mud with and without SAS and the constant N and model parameters C and D are summarized in Table 6-4. The test results fitted very well with the model (Fig. 6-8, 6-9) for all of the experiments having coefficients of determination (R^2) values varying from 0.97 to 0.98. The root mean square of error (RMSE) varied between 8.4 ml. and 62 9.7 as summarized in Table 6-4. We can see from the results that for 6% bentonite mud, the constant N was between 3.78 to 4.10 which decreased to 2.83 to 3.00 with addition of 0.1% SAS but then increased to 3.38 to 3.43 with addition of 0.3% SAS. For addition of SMS, the constant N decreased to 2.81 to 2.82 by 0.1% SMS which then increased to 3.45 to 3.88 by 0.3% SMS. For 6% bentonite mud, the parameter C was 10.7 which increased to 17.1 to 17.4 with addition of 0.1% SAS and again increased to 21.1 with addition of 0.3% SAS. For addition of SMS, the parameter C increased to about 18.5 by 0.1% SMS which again increased to about 17 by 0.3% SMS. The parameter D was 0.016 for 6% bentonite mud which decreased to 0.011 with addition of 0.1% SAS and again decreased to 0.010 with addition of 0.3% SAS. For addition of SMS, the parameter D decreased to 0.010 by 0.1% SMS which then increased to 0.013 by 0.3% SMS.

Table 6-4: Model parameters for the fluid loss tests modeled with new Kinetic Model

Materials	Test Nos.	Kinetic Model					API Model		
		N	C	D	RMSE (mL)	R ²	M	RMSE (mL)	R ²
6% B (Bentonite)	Test 1	4.1	10.7	0.017	9.1	0.98	4.45	10.2	0.97
	Test 2	3.78	10.7	0.016	8.4	0.98	4.03	8.7	0.98
6% B + 0.1% SAS	Test 1	2.83	17.1	0.011	8.8	0.98	3.36	18.4	0.92
	Test 2	3.00	17.4	0.011	9.7	0.97	3.81	29.7	0.83
6% B + 0.3% SAS	Test 1	3.43	21.1	0.010	8.7	0.98	3.74	10.7	0.98
	Test 2	3.38	21.1	0.010	9.8	0.97	3.66	9.6	0.98
6% B + 0.1% SMS	Test 1	2.82	18.2	0.010	8.4	0.98	3.44	25.7	0.88
	Test 2	2.81	18.6	0.010	9.0	0.97	3.67	35.5	0.79
6% B + 0.3% SMS	Test 1	3.45	19.5	0.011	9.3	0.98	3.81	11.9	0.97
	Test 2	3.88	15.7	0.013	9.7	0.97	4.10	8.0	0.98

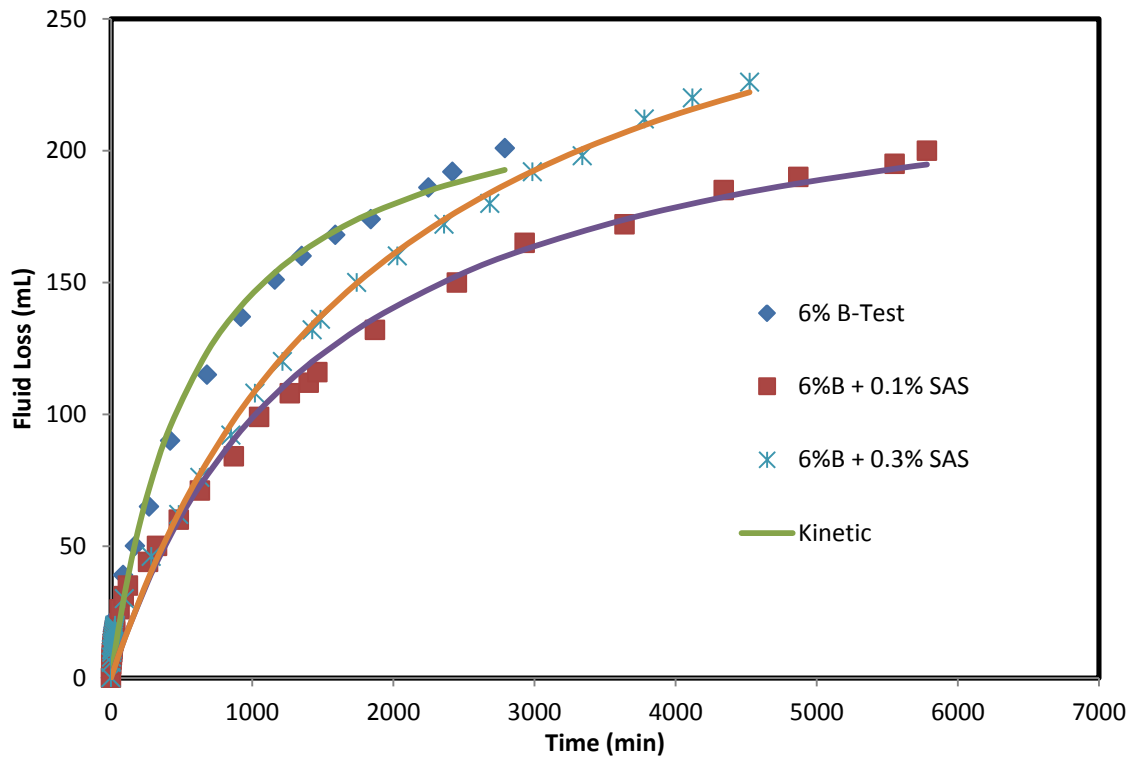


Figure 6-8: Effect of SAS on the fluid loss of a bentonite mud modeled with new Kinetic Model

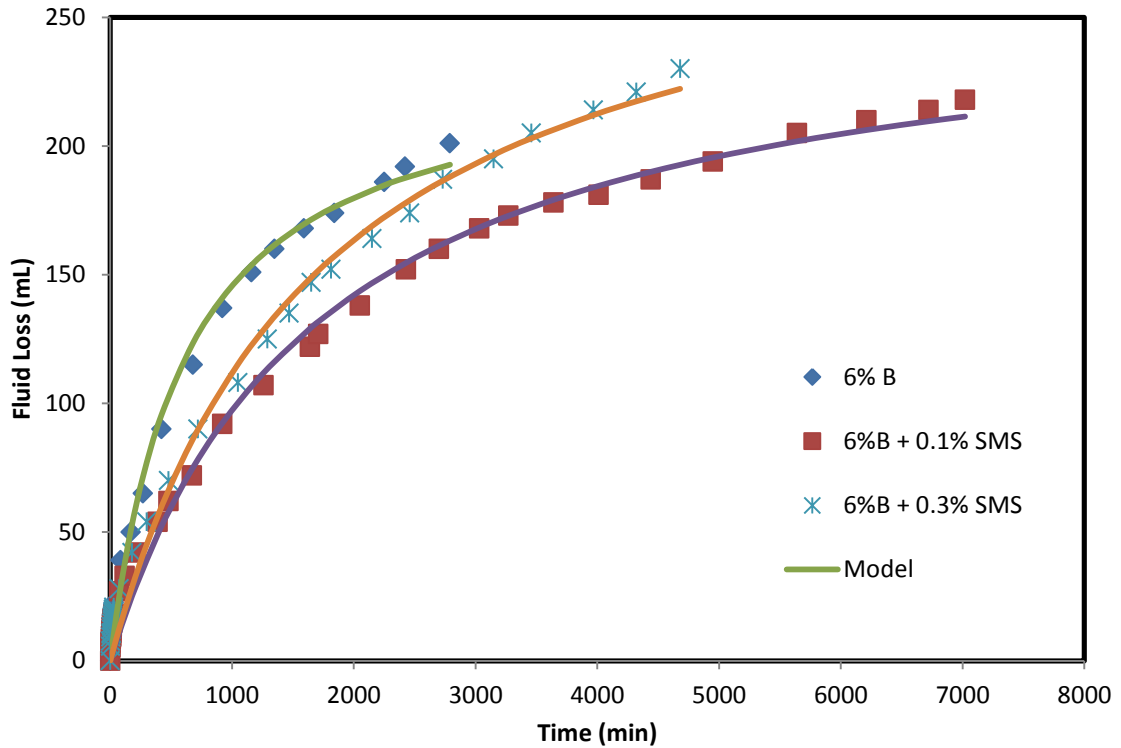


Figure 6-9: Effect of SMS on the fluid loss of a bentonite mud modeled with new Kinetic Model

6.3.2 Filter cake characterization

After the end of fluid loss test (i.e. when no more fluid is coming out from the test cell) the filter cake is taken out of the mold and characterized. For different types of mud, the filter cake was different in size and the water content was also different (Fig. 6-10). The measurement of the filter cake thickness, initial weight and the oven dry weight after putting the cake in an oven for 24 hours was recorded. From the measurements the void ratio, porosity and density of the filter cake was calculated.

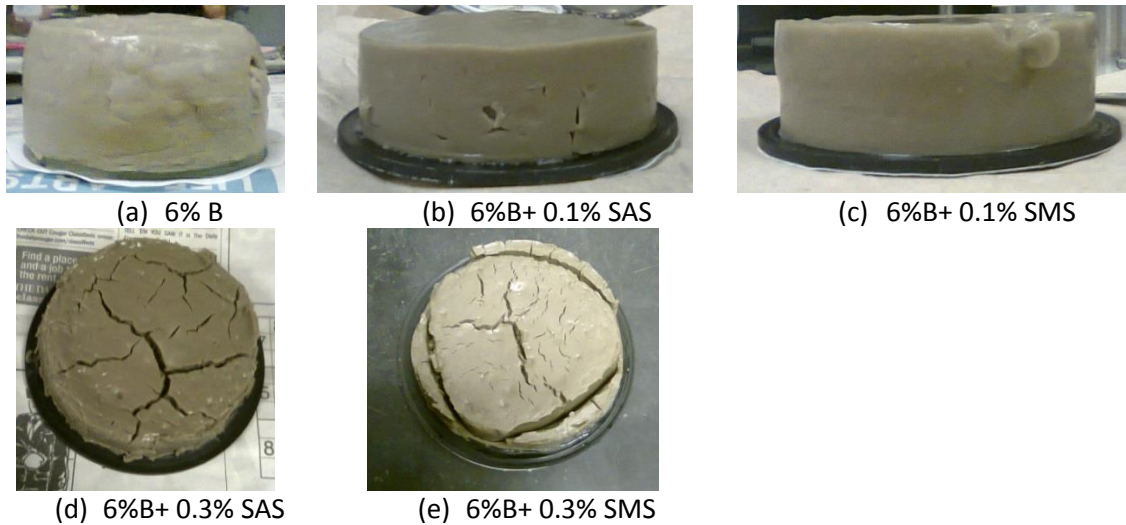


Figure 6-10: Filter cake collected after fluid loss test with: (a) 6% bentonite (B) only, (b) 6%B+ 0.1% SAS, (c) 6%B+ 0.1% SMS, (d) 6%B+ 0.3% SAS and (e) 6%B+ 0.3% SMS

Filter cake thickness was reduced with addition of both types of silicates. The filter cake thickness was found about 37 mm for a drilling mud of 6% bentonite only which was reduced to 28.5 mm with 0.1% SAS/SMS. It is further reduced to about 19 mm with addition of 0.3% SAS/SMS (Table 6-5, Fig. 6-11). Thus 0.3% silicate reduced the cake thickness by about 48%.

Table 6-5: Filter cake properties of 6% bentonite mud with and without silicates (SAS/SMS)

Materials	Test No.	Filter cake properties			
		Thickness (mm)	Void ratio	Porosity	Density
6% B (Bentonite)	Test 1	38	21.3	0.95	1.02
	Test 2	36.3	21.1	0.95	1.02
6%B + 0.1%SAS	Test 1	28.7	16.9	0.94	1.04
	Test 2	29.8	16.1	0.94	1.05
6%B + 0.3%SAS	Test 1	19.4	11.4	0.92	1.05
	Test 2	19.3	11.5	0.92	1.06
6%B + 0.1%SMS	Test 1	27	14.7	0.94	1.05
	Test 2	28.3	15.8	0.94	1.04
6%B + 0.3%SMS	Test 1	18.3	10.3	0.91	1.05
	Test 2	19.3	10.7	0.91	1.06

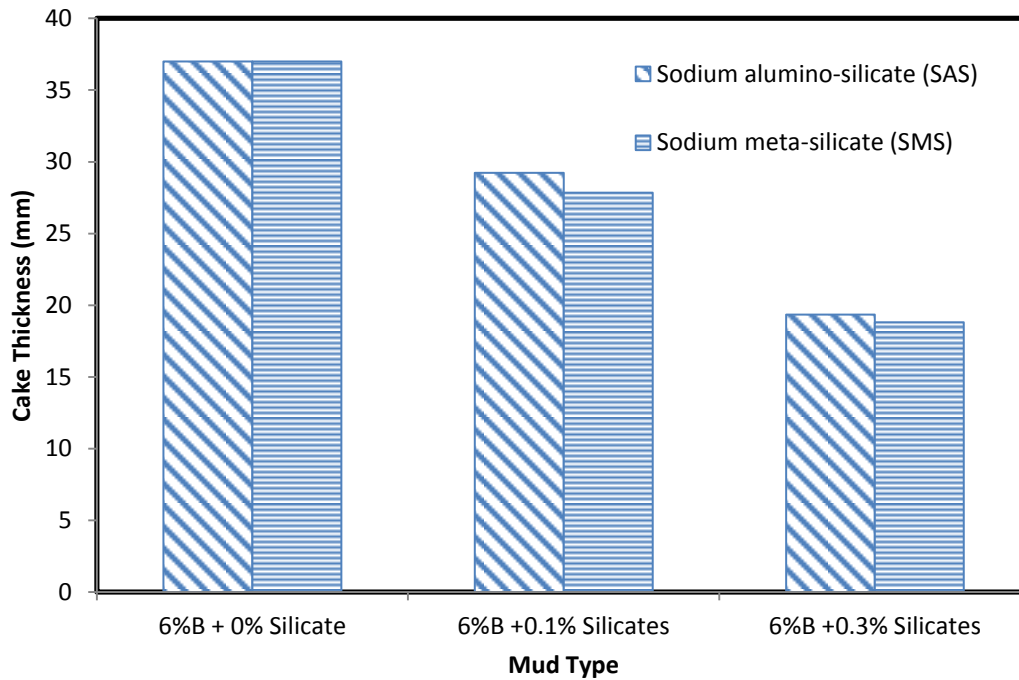


Figure 6-11: Effect of SAS and SMS on the measured filter cake thickness of 6% bentonite mud

The void ratio of the filter cake also showed a similar trend with filter cake thickness. Filter cake void ratio was about 21 for a drilling mud of 6% bentonite only which was reduced to 15-16.5 with 0.1% SAS/SMS and further reduced to about 10.5-11.5 with addition of 0.3% SAS/SMS (Table 6-5, Fig. 6-12). Thus 0.3% silicate reduced the void ratio of filter cake by about 46%.

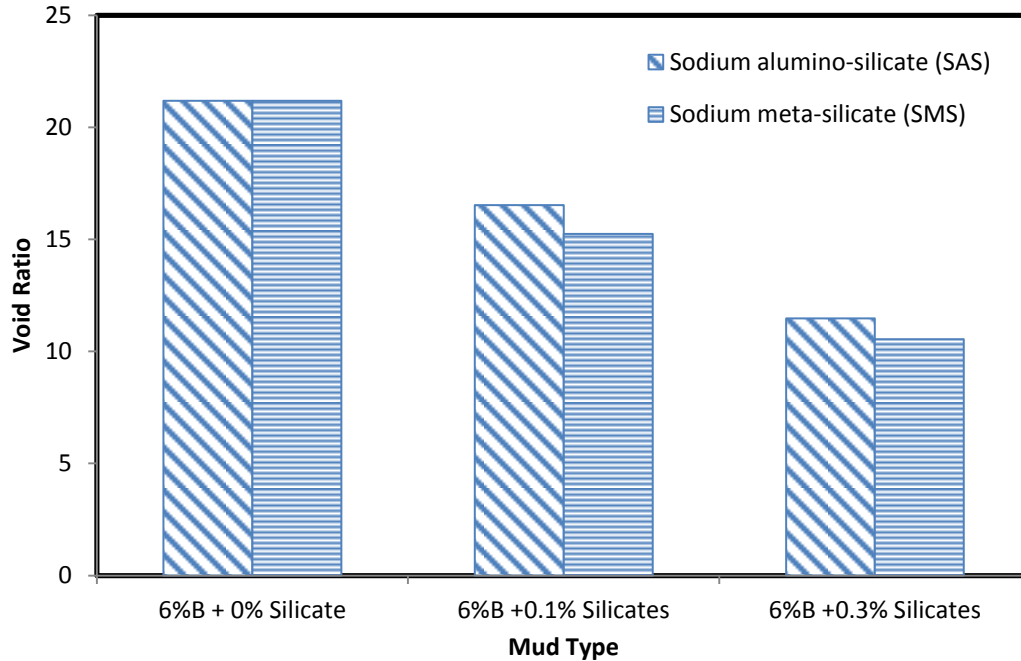


Figure 6-12: Effect of SAS and SMS on the measured filter cake void ratio of 6% bentonite mud

As the filter cake contains more amount of water than solids content, it is highly porous. The calculation showed that the solids content was from 11 to 22 % and the water content was from 78 to 89%. The porosity was calculated and found that for 6% bentonite, it was about 0.95 which was reduced to 0.93 with 0.1% silicate (Table 6-5, Figure 6-13) and further reduced to 0.91 with 0.3% SAS/SMS (a 4% reduction in porosity).

The density of the filter cake was calculated and found that addition of silicate increases the density of the filter cake. The density of the cake was about 1.02 gm/cc for filter cake with 6% bentonite which was increased to 1.04-1.05 with addition of 0.1% silicates and also with 0.3% SAS/SMA, the cake density was found about 1.06 (Table 6-5, Figure 6-14).

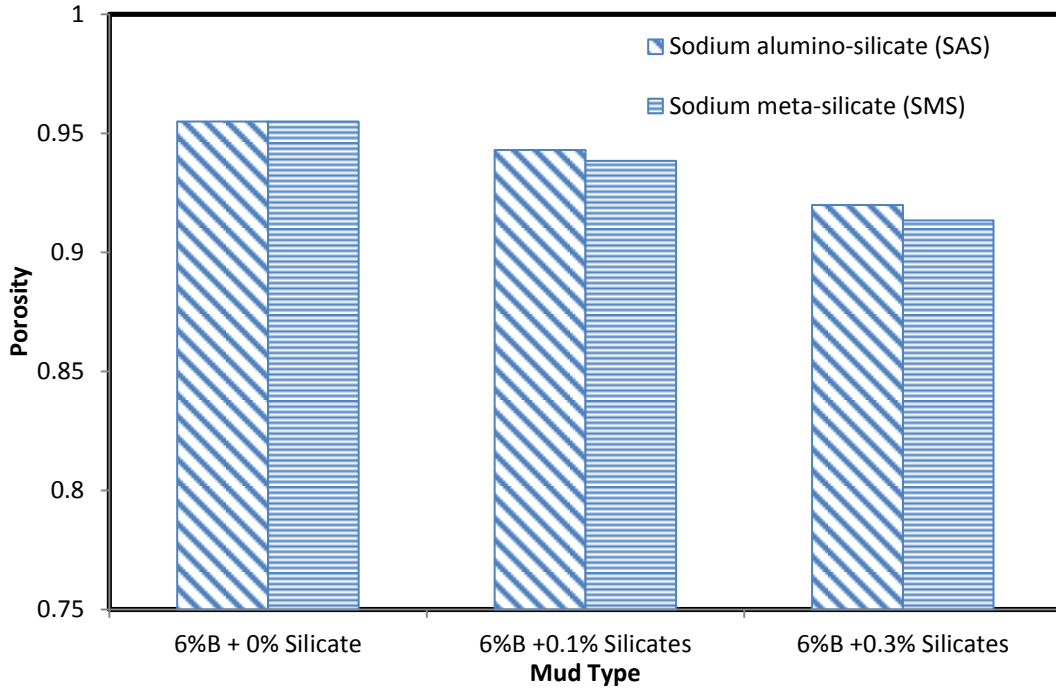


Figure 6-13: Effect of SAS and SMS on the filter cake porosity of 6% bentonite mud

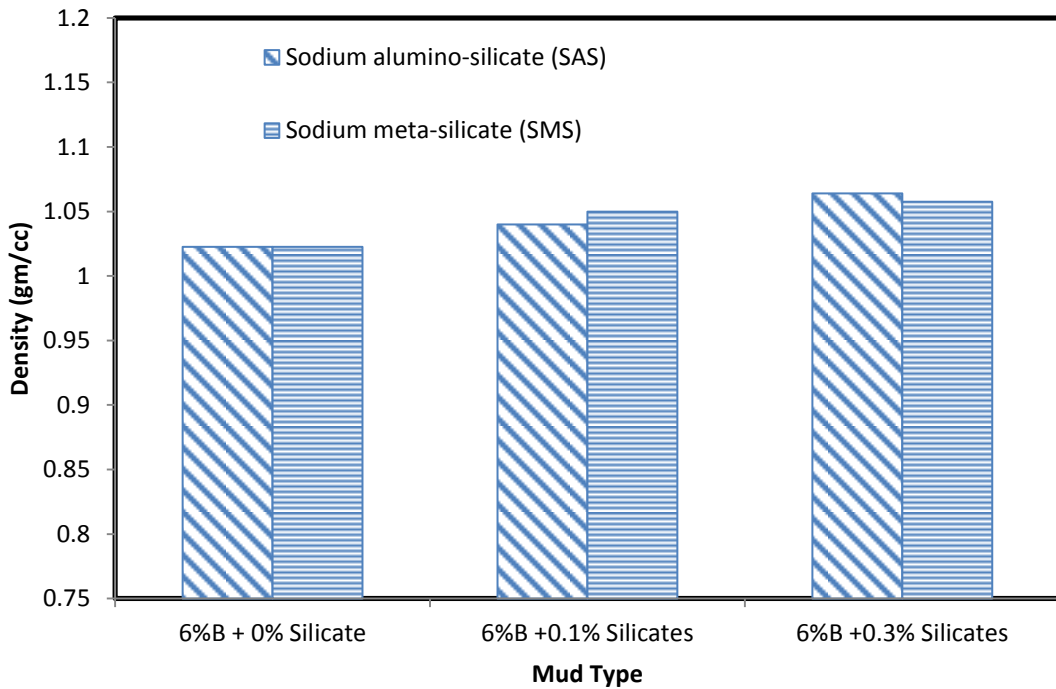


Figure 6-14: Effect of SAS and SMS on the measured filter cake density of 6% bentonite mud

6.4 Summary

Based on experimental and analytical study on bentonite mud with and without SAS and SMS, the following observations are advanced:

1. The apparent viscosity at 500 Sec^{-1} shear strain rate of a 6% bentonite mud was 14.7 cP which was increased to about 17 cP with addition of 0.1% SAS and SMS, a 18% increase. But with 0.3% SMS and SAS, the apparent viscosity decreased to about 10 cP, a 30% decrease. Thus a lesser silicate content (0.1%) increased the colloidal properties and that's why decreased the pump ability of the bentonite mud but a higher content (0.3%) decreased the colloidal properties and hence increased the pump ability of the drilling mud.
2. For 6% bentonite mud, the yield point was 19 Pa which was increased to about 23 Pa with addition of 0.1% SAS and SMS, a 20% increase. But with addition of 0.3% SAS and SMS, it reduced to about 5 Pa, a 73% reduction. YP is used to evaluate the ability of a mud to lift cuttings out of the annulus and thus, in this study, 0.1% silicate was acting as a flocculant which increased the YP and hence increased the ability to lift cuttings; and the higher amount (0.3%) was acting as a deflocculant which decreased the YP and hence decreased the ability to lift cuttings.
3. The 10 second and 10 minutes gel strengths were 26 Pa and 32 Pa for 6% bentonite mud which reduced to about 4 Pa and 6 Pa respectively with addition of 0.3% SAS and SMS solution, a 81% to 84% reduction. Thus, the addition of silicate solution was decreasing the attractive forces between the particles in drilling mud and hence reducing the ability to suspend drill solid and weighing material when circulation is ceased.

4. The electrical resistivity was very sensitive to the silicate content. The resistivity of 6% bentonite mud was found 5.3 Ω .m which reduced to 4.70 and 4.95 Ω .m for only 0.1% (w/w) SMS and SAS respectively. With 0.3% SMS the resistivity was found 4.42 Ω .m, a 17% reduction, and for 0.3% SAS, the resistivity was 4.54 Ω .m, a 14% reduction.
5. For 6% bentonite drilling mud, the API (30 minutes) fluid loss was found as 22.5 mL. With addition of 0.1% SMS and SAS, the fluid loss was reduced to 18.2 ml, but with 0.3% of both of the silicates, the fluid loss again increased a little bit which is about 20.5 mL. As the sample was allowed to loss fluid for long time until the end of the fluid loss, the 6% bentonite losses fluid until 2 days and the total loss happened was about 200 mL. With 0.1% SAS and SMS, the sample stayed until 4.1-4.9 days with a fluid loss of 202-220 mL. But with the addition of 0.3% SAS and SMS, the time of fluid loss was reduced to about 3.2 days and the total fluid loss was increased to about 226-230 ml. Thus, the addition of 0.1% SAS and SMS increased the time of fluid loss by about 105-145%, but the total fluid loss increased by about 9-10%. The addition of 0.3% both silicate increased the time about 60% and the total fluid loss about 15%.
6. The filter loss vs time for 6% bentonite mud with and without SAS and SMS was modeled by using Kinetic (Hyperbolic) model and it was found that the test results fitted very well with the model for all of the experiments having very good coefficients of determination (R^2) values and acceptable root mean square of error (RMSE) values. The experimental values also modeled with API model but the

model predicted very well up to 30 min fluid loss but for long term test it did not show good matching with the experimental results.

7. The filter cake thickness was found about 36-38 mm for a drilling mud of 6% bentonite only which was reduced to about 19 mm with addition of 0.3% SAS/SMS, a reduction of 48%. Filter cake void ratio was about 21 for a drilling mud of 6% bentonite only which was reduced to about 10.5-11.5 with addition of 0.3% SAS/SMS, a reduction of 46%. The porosity of the filter cake was calculated and found that for 6% bentonite, it was about 0.95 which was reduced to 0.91 with 0.3% SAS/SMS, a 4% reduction in porosity. The density of the filter cake was about 1.02 gm/cc for filter cake with 6% bentonite which was increased to about 1.06 with addition of 0.3% SAS and SMS, a 4 % increase in density.

CHAPTER 7 REAL TIME MONITORING OF MODEL WELLBORE

7.1 Small lab model

7.1.1 Installation

7.1.1.1 Stage 1: Drilling Mud

Bentonite drilling mud (6% w/w) was taken to fill the casing step by step and the resistance was measured to check whether the presence of drilling can be known from the change of resistance. Fig. 7-1 shows the vertical wire setup A resistance change with partial change of drilling mud height. Hence as shown in Fig. 7-1, 7-2, and 7-3 the vertical resistance before the drilling mud was filled to any level was around 15-30 k-Ohm which reduced to around 500-700 Ohm. Whenever two levels of wires were in the cement slurry, the resistance dropped down sharply. For example, the vertical resistance between wires 1 and 2 along wire setup A was 28 k-Ohm which dropped to 570 Ohm when both of the wires were under drilling mud. This indicated that the drilling mud has reached up to the wire level 2.

For wire setup B (Fig 7-2), the vertical resistance before the cement slurry was varying from 18-70 k-Ohm which dropped to about 550-750 Ohm (Fig. 7-2). For example, the resistance between wire 1 and 2 along wire setup B was 18 K-Ohm which dropped to 575 Ohm when both of the wires are under drilling mud. This tells us that the drilling mud reached up to the wire level 2.

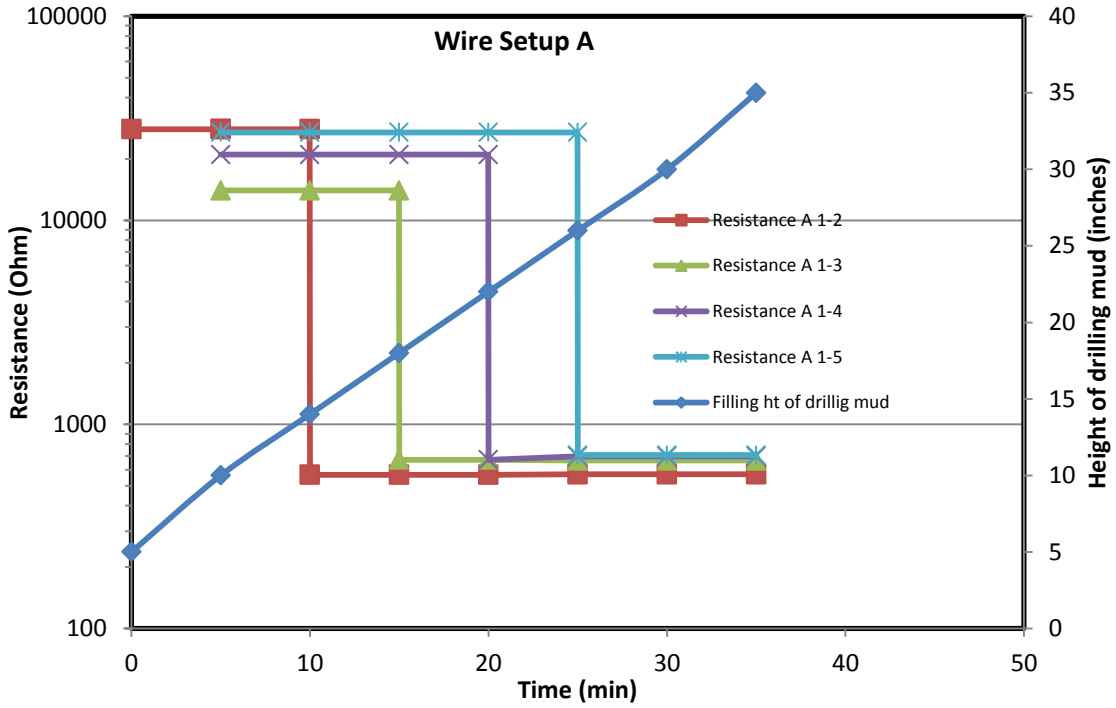


Figure 7-1: The change of vertical resistance along wire setup A with drilling mud filling.

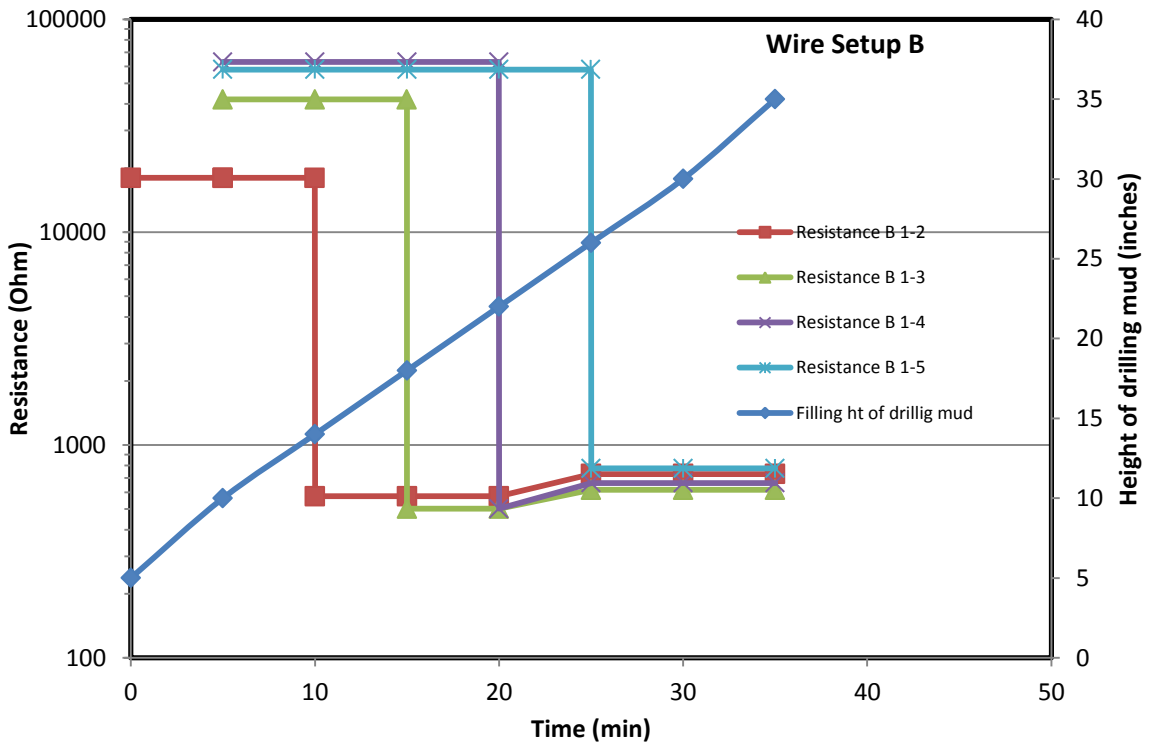


Figure 7-2: The change of vertical resistance along wire setup B with drilling mud filling.

For wire setup C, the resistance before the cement slurry was varying from 12-39 k-Ohm which dropped to about 550-670 Ohm (Figure 7-3). For example, the resistance between wire 1 and 2 along wire setup B was 29 K-Ohm which dropped to 630 Ohm when both of the wires are under drilling mud. This tells us that the drilling mud reached up to the wire level 2.

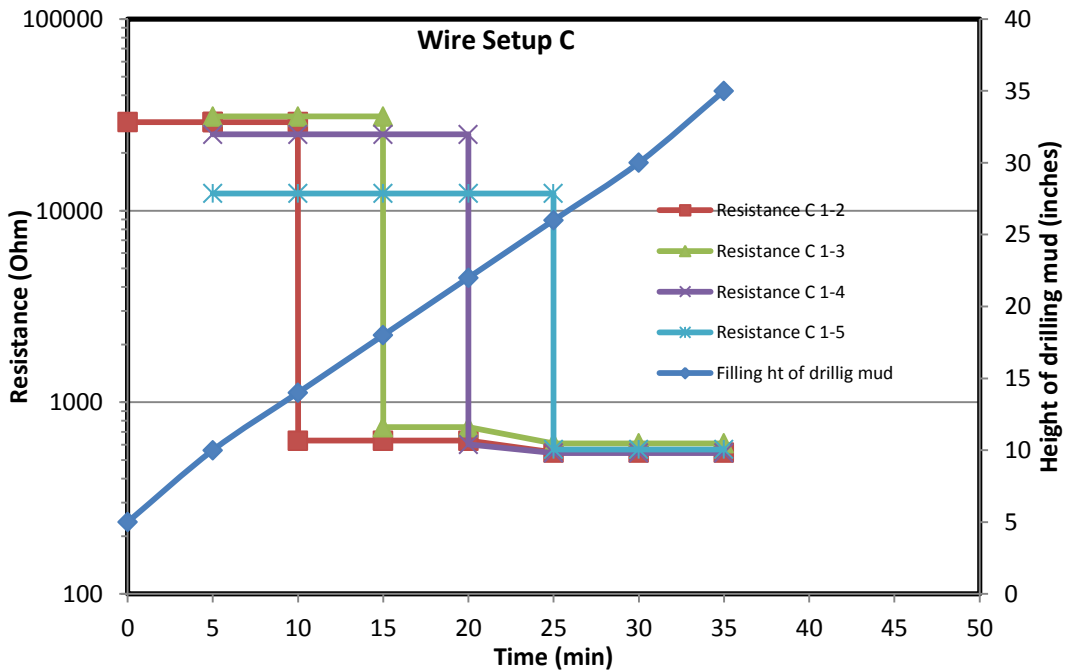


Figure 7-3: The change of vertical resistance along wire setup C with drilling mud filling

7.1.1.2 Stage 2: Cement Slurry

Cement slurry was injected taken to fill the casing step by step and the resistance was measured to check whether the presence of cement slurry can be known from the change of resistance. Fig. 7-4 showed the vertical wire setup A resistance change with partial change of cement slurry height. As shown in Fig. 7-4, 7-5, and 7-6 the resistance before the cement slurry was filled to any level was around 400-250 Ohm (representing the

drilling mud) which reduced to 60-45 Ohm. Whenever two levels of wires both are in the cement slurry, the resistance was dropped down sharply. For example, the resistance between wire 1 and 2 along wire setup A was 380 Ohm which dropped to 68 Ohm when both of the wires are under cement slurry. This tells us that the cement slurry reached up to the wire level 2.

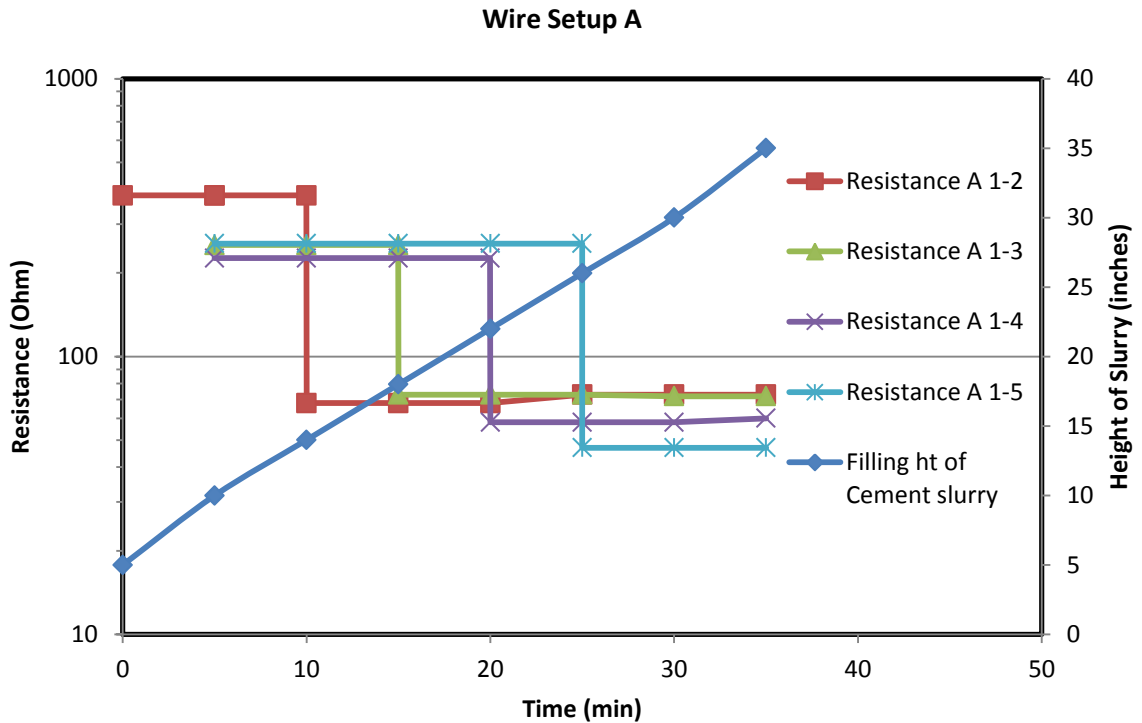


Figure 7-4: The change of vertical resistance along wire setup A with cement slurry filling

For wire setup B, the resistance before the cement slurry was varying from 990-250 Ohm which dropped to about 60-40 Ohm (Fig. 7-5). For example, the resistance between wire 1 and 2 along wire setup B was 704 Ohm which dropped to 55 Ohm when both of the wires are under cement slurry. This tells us that the cement slurry reached up to the wire level 2.

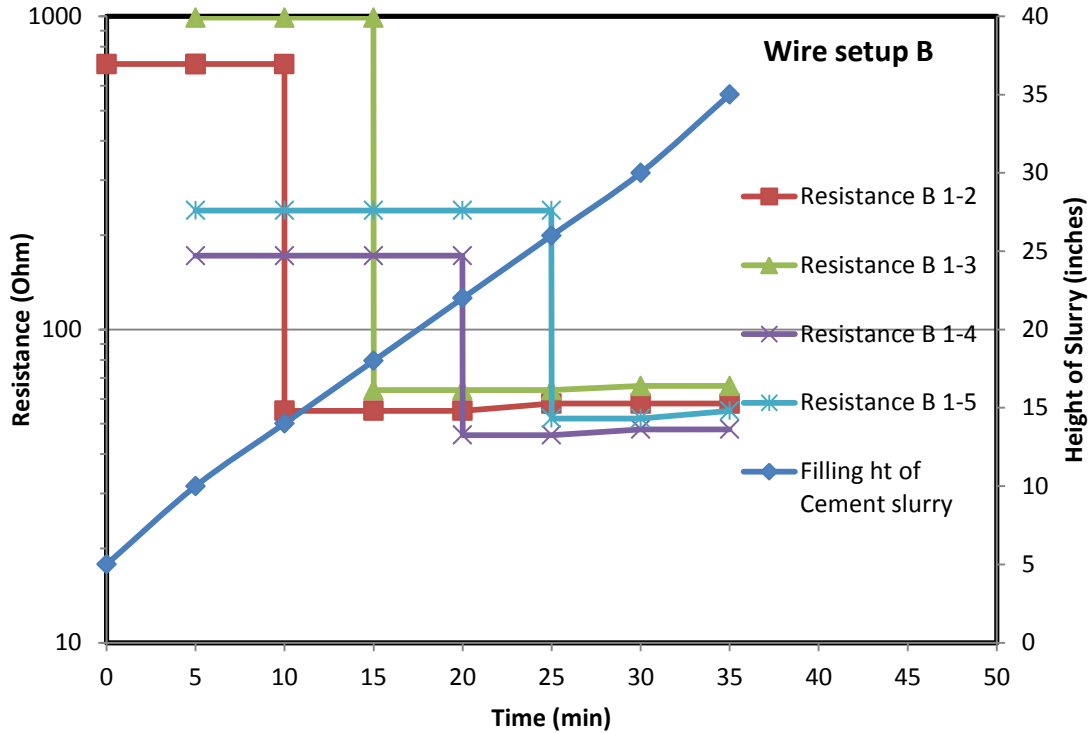


Figure 7-5: The change of vertical resistance along wire setup B with cement slurry filling

For wire setup C, the resistance before the cement slurry was varying from 850-250 Ohm which dropped to about 60-25 Ohm (Figure 7-6). For example, the resistance between wire 1 and 2 along wire setup B was 827 Ohm which dropped to 68 Ohm when both of the wires are under cement slurry. This tells us that the cement slurry reached up to the wire level 2.

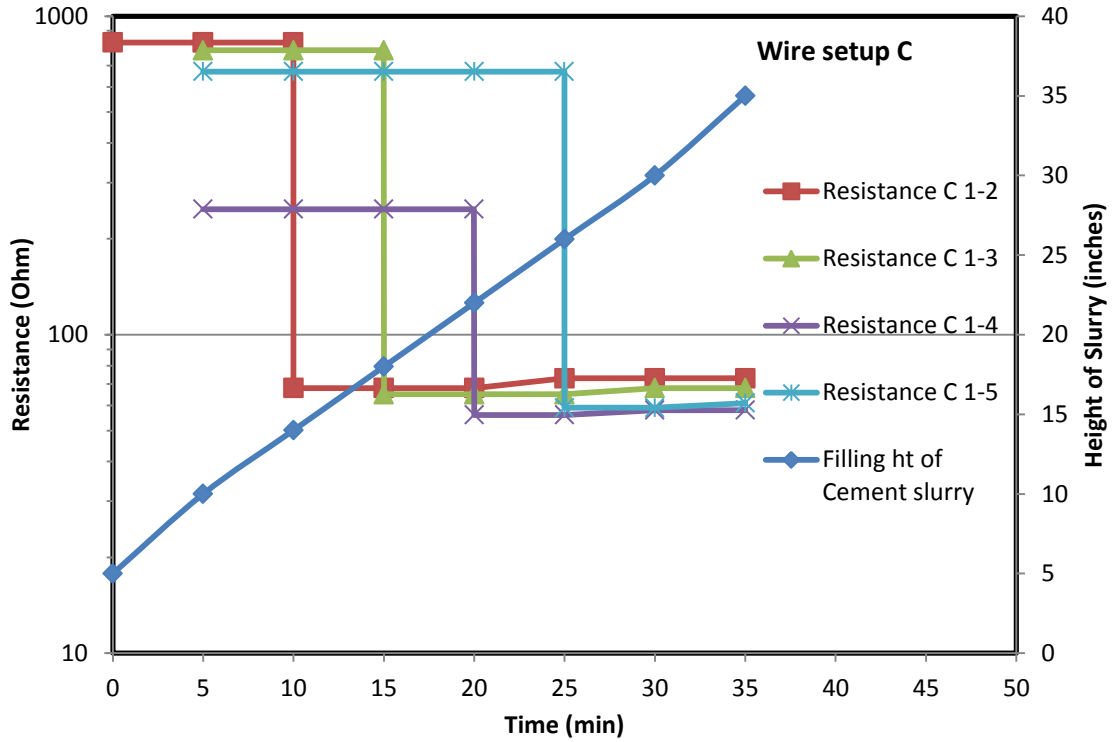


Figure 7-6: The change of vertical resistance along wire setup C with cement slurry filling

7.1.2 Prediction of resistance in curing cement

7.1.2.1 Parameter K

The parameter K (i.e., L/A) for the wire setup A, B, and C with different wire spacing were first determined filling the cement slurry. To do this, the resistivity of the cement slurry was determined by direct resistivity measurement device and the resistance between the wire combinations was determined with resistance measurement device (LCR meter). The results of the K values are shown below (Fig. 7-7 to 7-10) and the average value, maximum value, and minimum values are shown in the tables below (Table 7-1 to 7-4).

For wire setup A, the average K parameter are found to be varied from 57.9 to 58.6 m⁻¹ with standard deviations varying from 4.5 to 9.1 for different wire spacing (Fig. 7-7, Table 7-1).

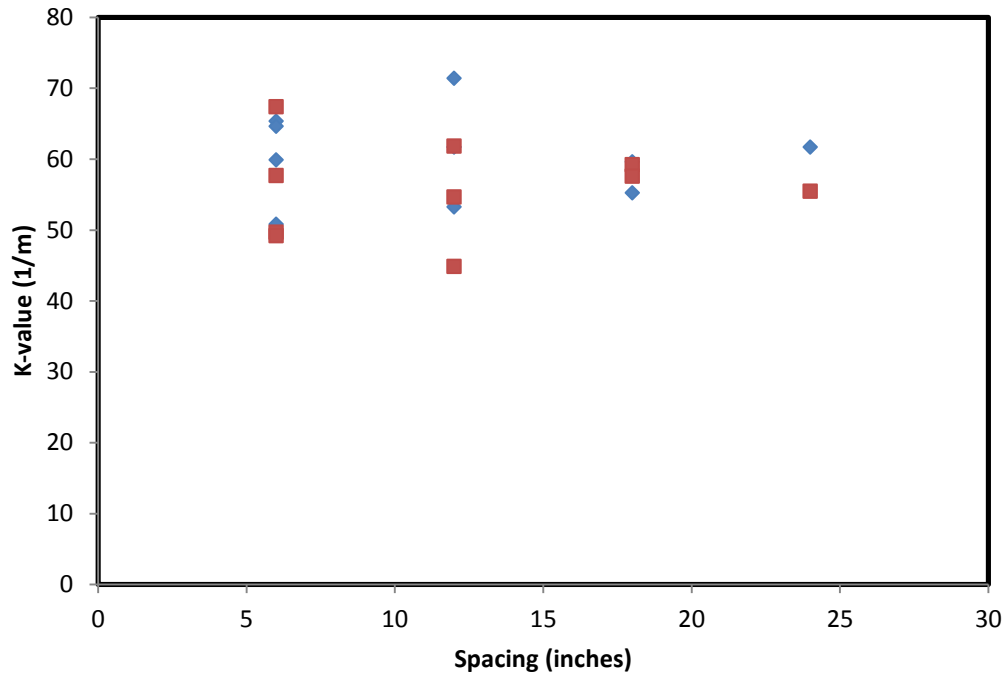


Figure 7-7: K parameter for wire setup A

Table 7-1: Variations of K parameter for wire setup A for model 2

	6 inch	12 inch	18 inch	24 inch
Avg	58.0	57.9	57.9	58.6
Min	49.1	44.8	55.2	55.4
Max	67.4	71.4	59.6	61.7
Std. dev	3.4	3.1	2.0	2.5
Number of data	12	12	12	12

For wire setup B, the average K parameter are found to be varied from 49.8 to 56.2 m⁻¹ with standard deviations varying from 3.9 to 5.4 for different wire spacing (Fig. 7-8, Table 7-2).

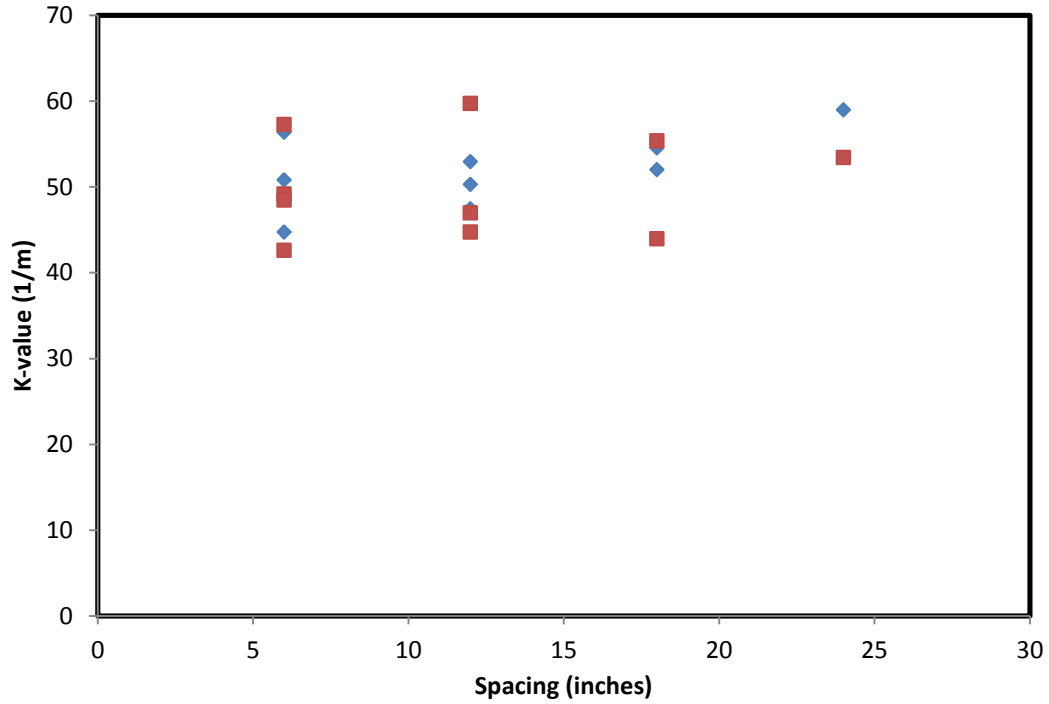


Figure 7-8: K parameter for wire setup B

Table 7-2: Variations of K parameter for wire setup B for model 2

	6 inch	12 inch	18 inch	24 inch
Avg	49.8	50.3	51.5	56.2
Min	42.6	44.7	43.9	53.4
Max	57.2	59.7	55.4	58.9
Std. dev	2.1	2.4	2.2	2.9
Number of data	12	12	12	12

And For wire setup C, the average K parameter are found to be varied from 58.7 to 68.1 m^{-1} with standard deviations varying from 10.6 to 13.7 for different wire spacing (Fig. 7-9, Table 7-3).

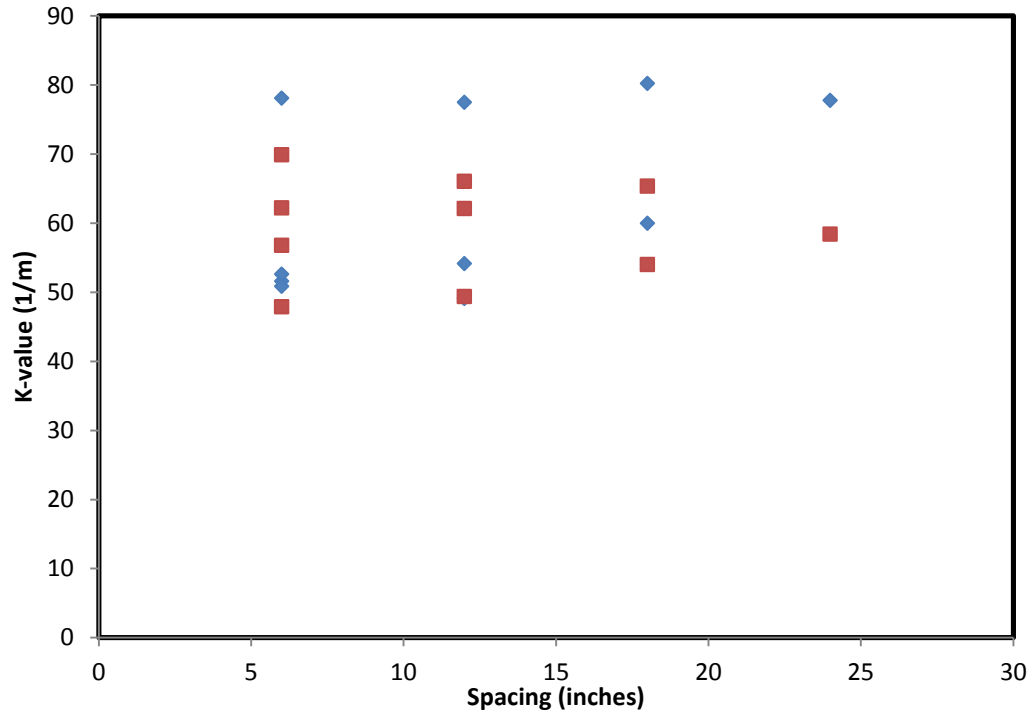


Figure 7-9: K parameter for wire setup C

Table 7-3: Variations of K parameter for wire setup C for model 2

	6 inch	12 inch	18 inch	24 inch
Avg	58.7	59.7	64.9	68.1
Min	47.9	49.0	54.0	58.4
Max	78.0	77.4	80.0	77.8
Std. dev	2.6	3.1	3.4	3.7
Number of data	12	12	12	12

And for horizontal wire combination, the average K parameter are found to be varied from 38 to 69 m⁻¹ with standard deviations varying from 6 to 11 for different wire level (Fig. 7-10, Table 7-4).

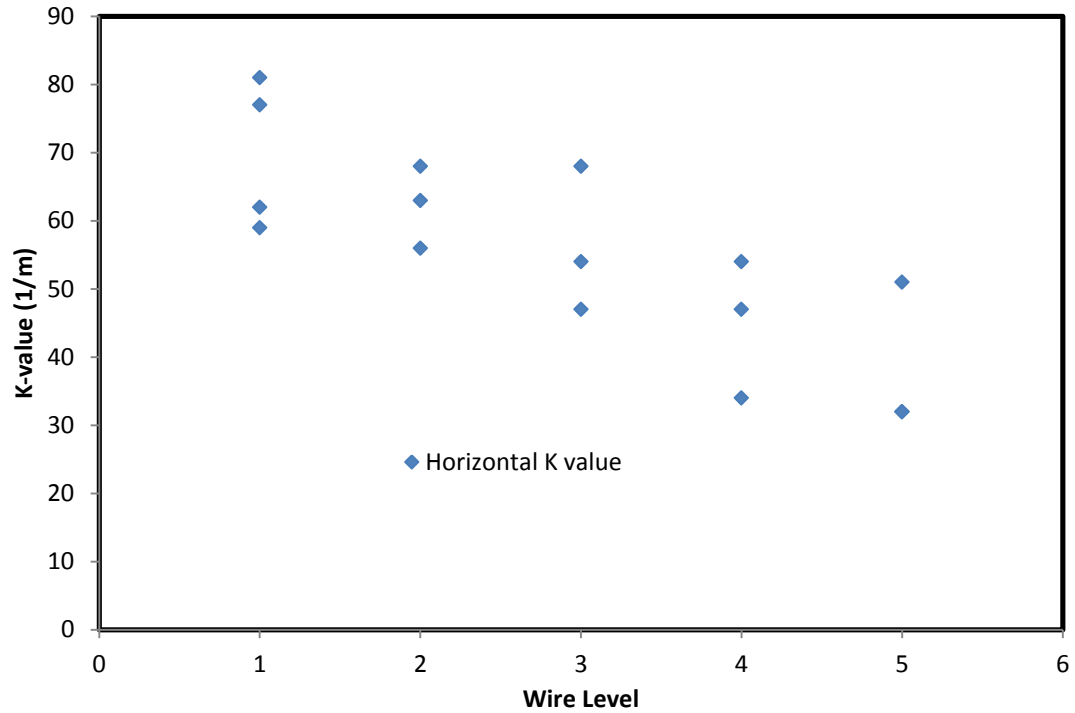


Figure 7-10: K parameter for horizontal wire combinations at different levels

Table 7-4: Variations of K parameter for horizontal wire combination at different level for model 2

Level	1	2	3	4	5
Avg	69.8	62.3	56.3	45.0	38.3
Min	59.0	56.0	47.0	34.0	32.0
Max	81.0	68.0	68.0	54.0	51.0
Std. dev	2.9	2.0	2.7	2.1	2.2
No of data	12	12	12	12	12

7.1.2.2 Resistivity of the cement slurry with time

The Resistivity of the cement slurry with curing time of up to 360 days is determined using a small mold (2 inches diameter and 4 inches height cylindrical mold) with the same cement slurry that was used for the model and cured under room temperature curing conditions. The resistivity showed an increasing trend with curing time (Fig. 7-11). The total weight loss calculated for the sample under room temperature curing was about

5.4% up to 366 days. The resistivity trend was modeled with the curing model which is developed by modified the p-q model proposed by Vipulanandan and Paul (1990) (Eqn. 3-11) and the model parameters were found as $p_1= 2.02$, $q_1= 0.68$, $t_0= 63$ min.

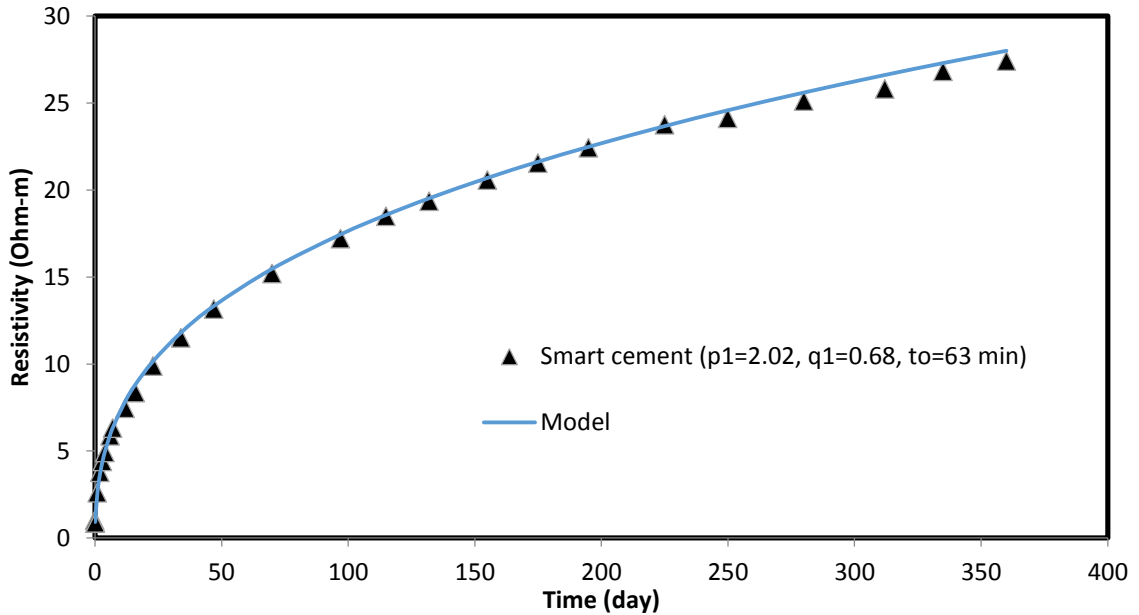


Figure 7-11: Resistivity of cement slurry with curing time

7.1.2.3 Predicted Resistance Vs Measured Resistance:

From Fig. 7-11, we know the resistivity of cement slurry with curing time. From Figure 7-7 to 7-10 and Table 7-1 to 7-4 we know the K parameter that can be used to calculate the resistivity of the cement slurry at different time having the resistance measured. If we back calculate the possible values of resistance from the same equation using the average, minimum, and maximum K parameter, we can find the predicted resistance values. Fig. 7-12 to Fig. 7-23 shows the variations of the predicted resistance value and also the actual measured values for different wire setup/combinations. Fig. 7-24 to Fig. 7-26 shows the

variations of the predicted resistance value and also the actual measured values for horizontal wire combination at different levels.

For wire setup A, the wire combination A 1-2 shows that the measured values are within the range of predicted range with a little exception that up to initial 14 days the values are little bit higher than the predictions (Fig. 7-12). And for wire combination A 1-3, the measured values are very close to the predicted values (Figure 7-13).

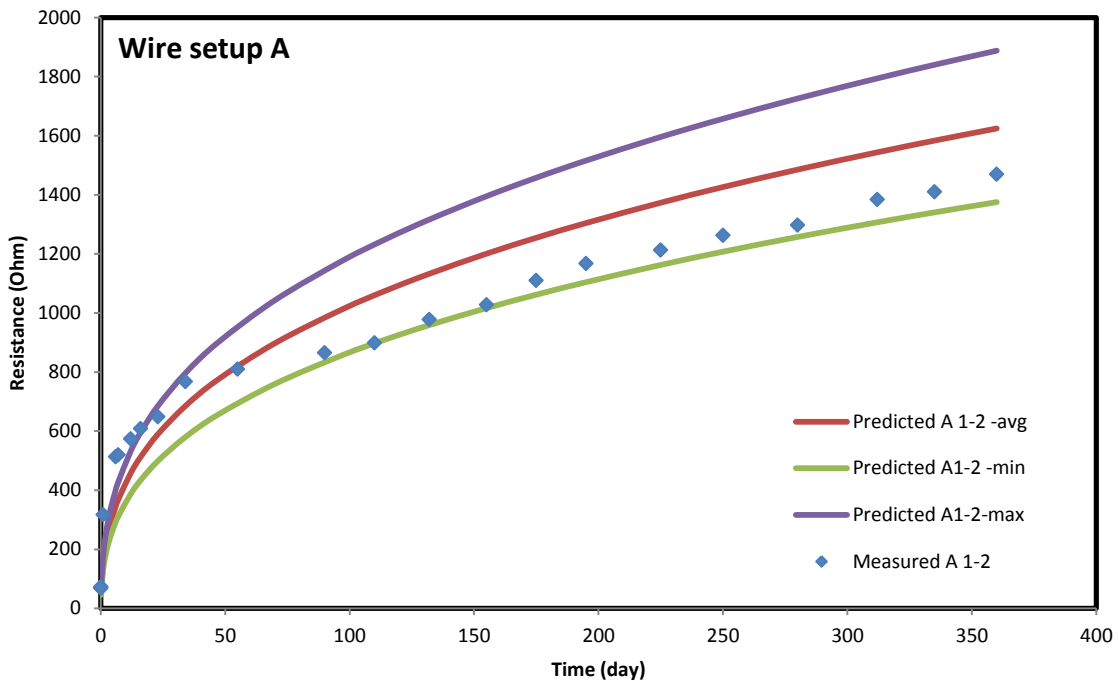


Figure 7-12: Predicted and measured resistance for wire setup A for wire combination 1-2

The wire combination A 1-4 shows that the measured values are within the range of predicted range with a little exception that up to initial 14 days the values are little bit lower than the predictions (Fig. 7-14). And for wire combination A 1-5, the measured values are very close to the predicted values (Figure 7-15) with only exceptions is that some of the values are below the prediction which can be explained as outliers.

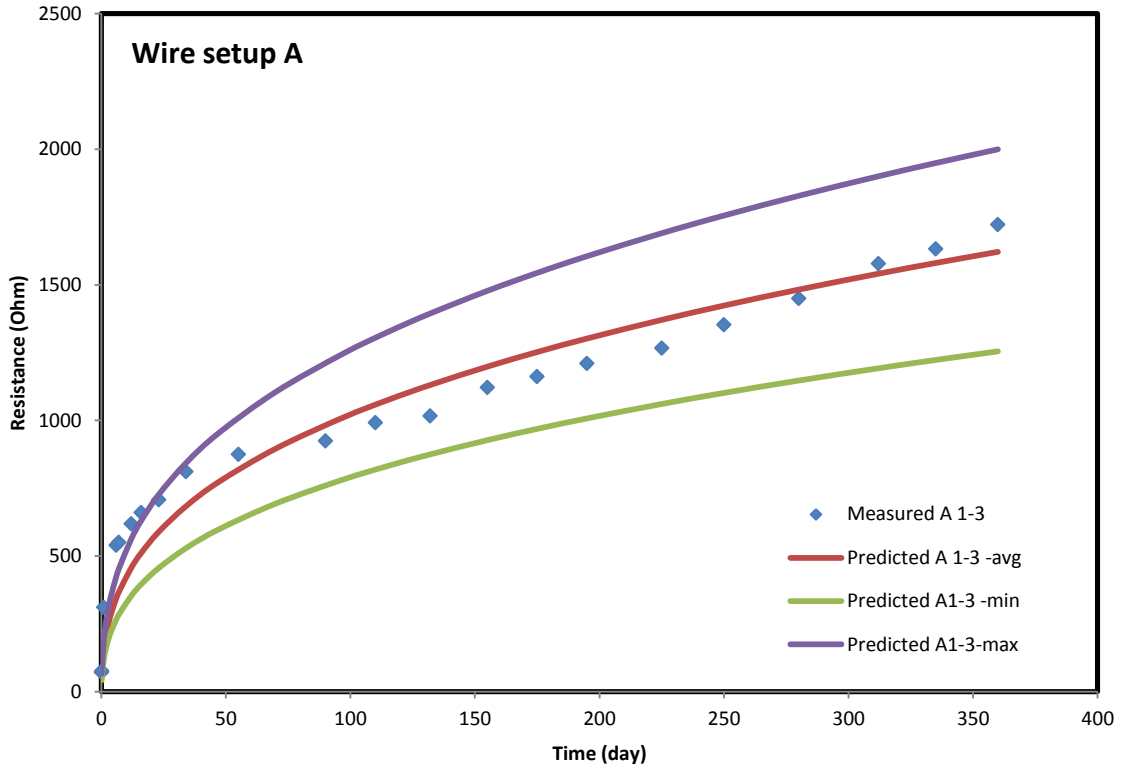


Figure 7-13: Predicted and measured resistance for wire setup A for wire combination 1-3

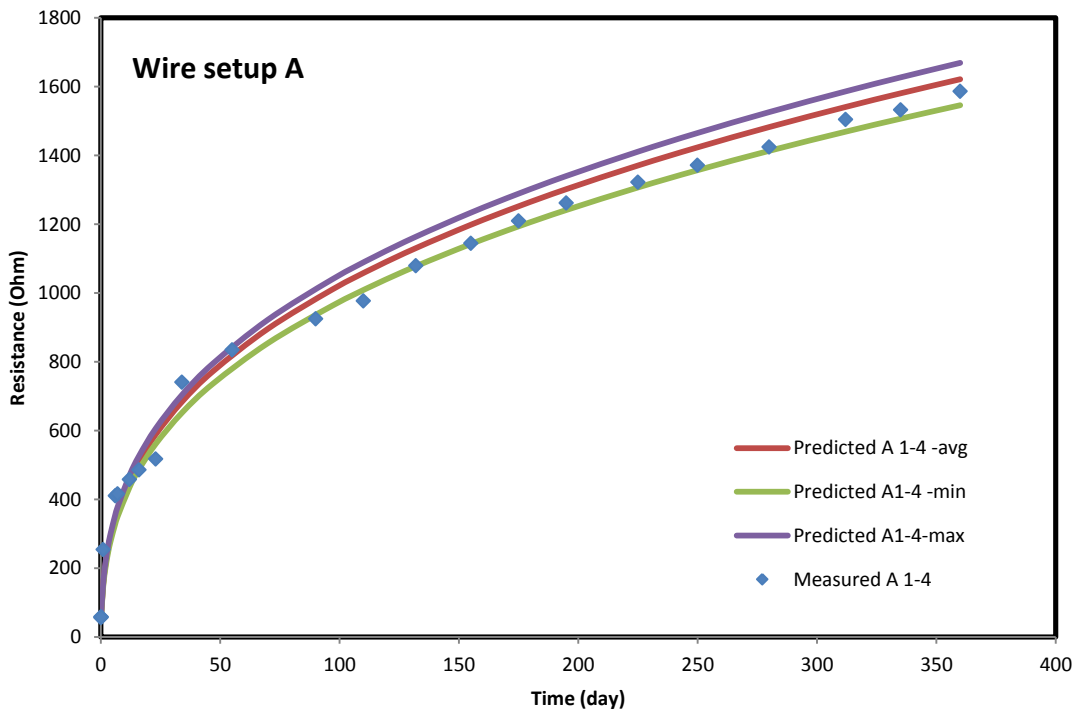


Figure 7-14: Predicted and measured resistance for wire setup A for wire combination 1-4

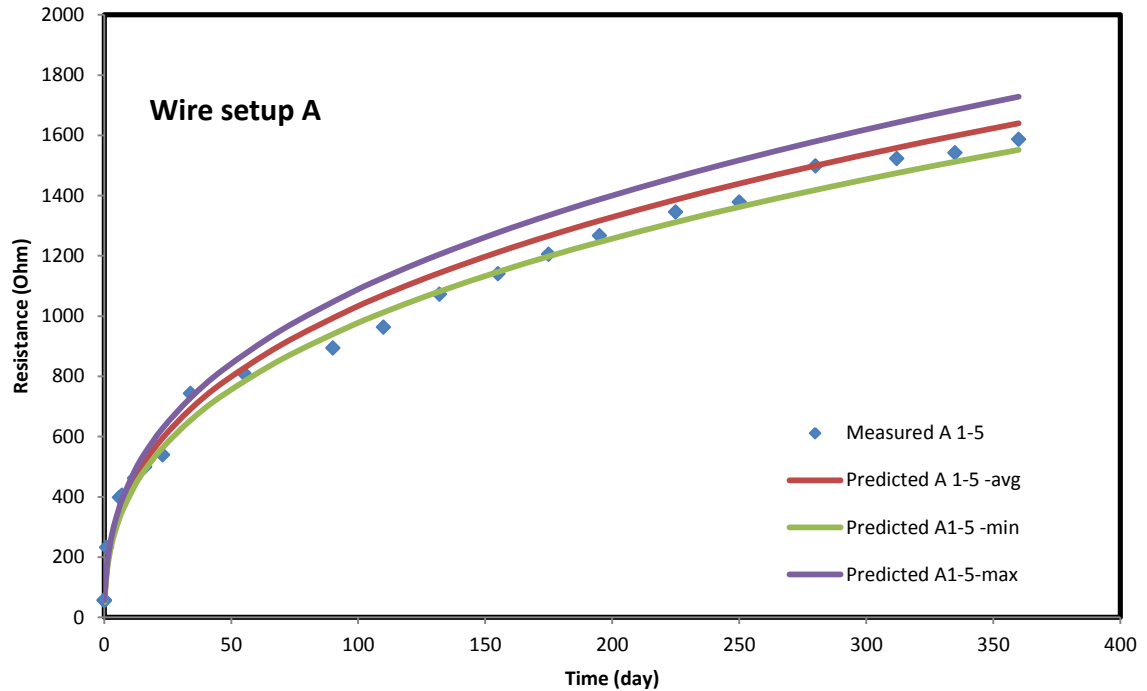


Figure 7-15: Predicted and measured resistance for wire setup A for wire combination 1-5

For wire setup B, the wire combination B 1-2 shows that the predicted values are a little bit lower but fits within the range of the measured values (Fig. 7-16). And for wire combination B 1-3, the measured values up to 150 days of curing are within the predicted range but after 150 days of curing the measured values are less than the predicted range (Fig. 7-17) which could be due to different curing condition of the small sample and the model.

For the wire combination B 1-4, the measured values are mostly within the range of the predicted values (Fig. 7-18) with a little exception of lower values which can be considered as outliers. And for wire combination B 1-5, the measured values from curing time 50 days to 195 days of curing are lower than the predicted range but other values are

within the predicted range (Fig. 7-19). This different could be due to different curing condition of the small sample and the model.

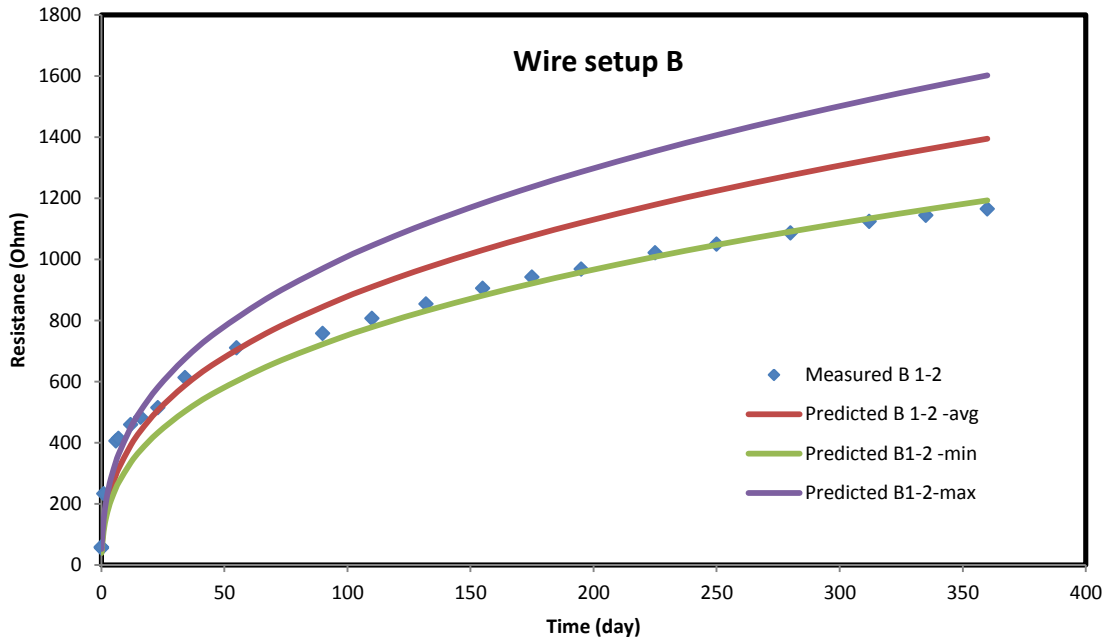


Figure 7-16: Predicted and measured resistance for wire setup B for wire combination 1-2

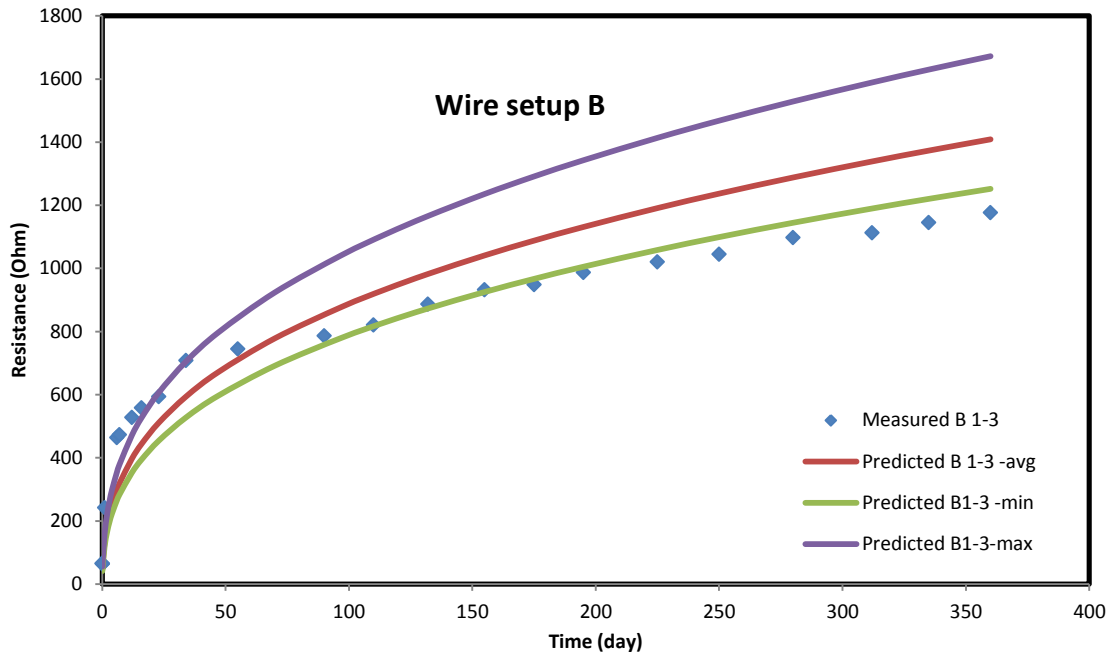


Figure 7-17: Predicted and measured resistance for wire setup B for wire combination 1-3

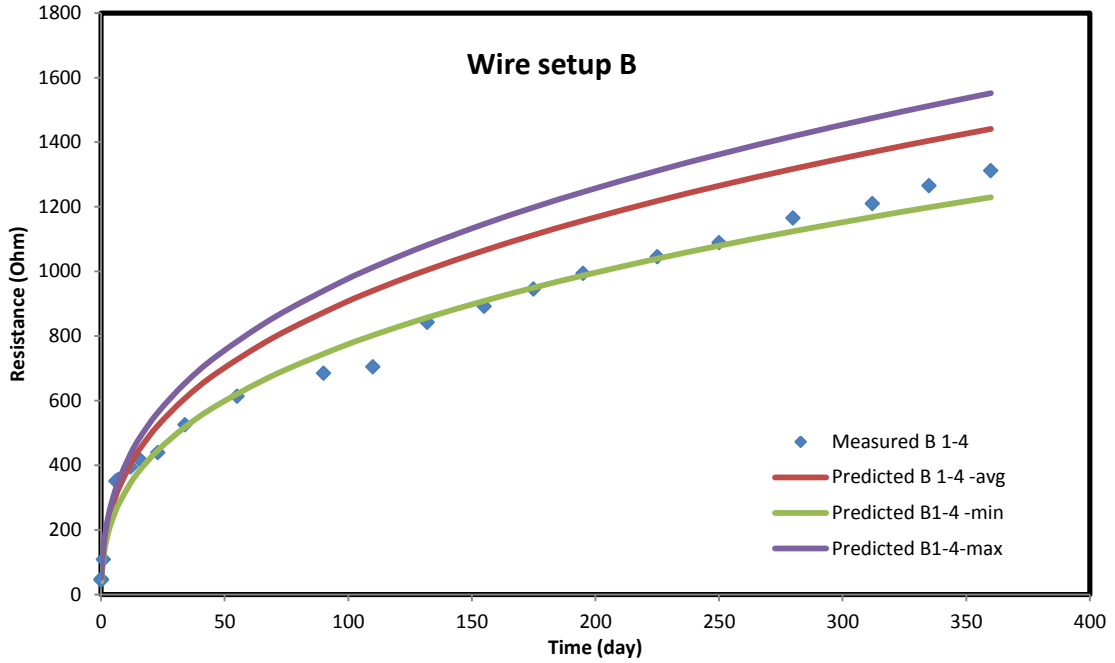


Figure 7-18: Predicted and measured resistance for wire setup B for wire combination 1-4

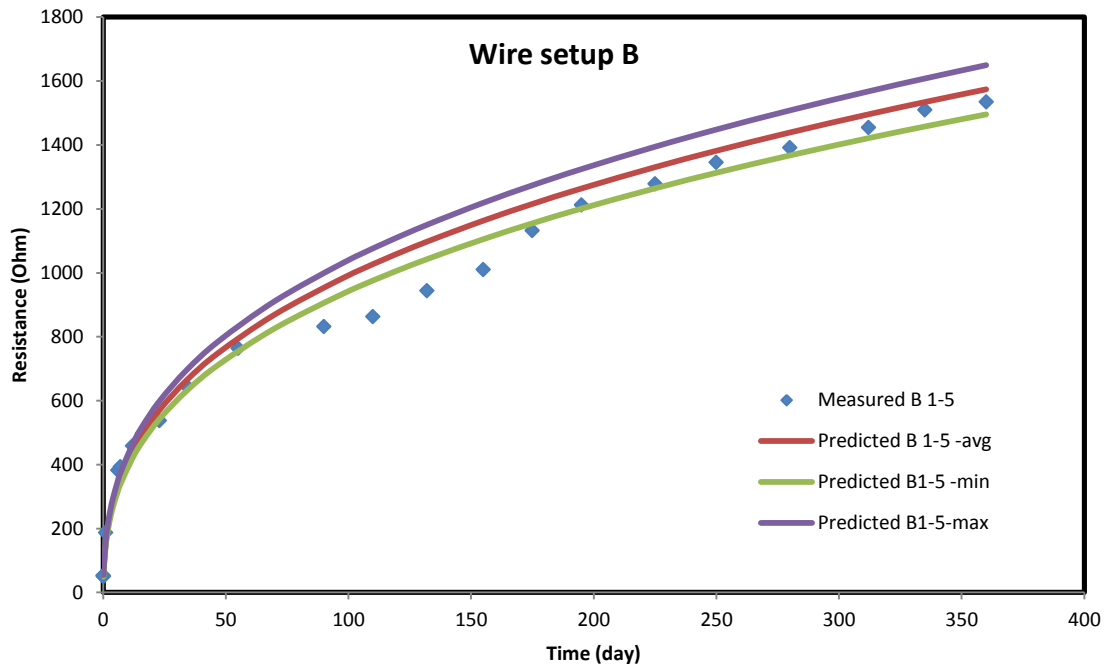


Figure 7-19: Predicted and measured resistance for wire setup B for wire combination 1-5

For wire setup C, the wire combination C 1-2 shows that the measured values are within the predicted range of values (Fig. 7-20). And for wire combination C 1-3, the measured values are also fitted nicely within the range of the predicted values (Fig. 7-21).

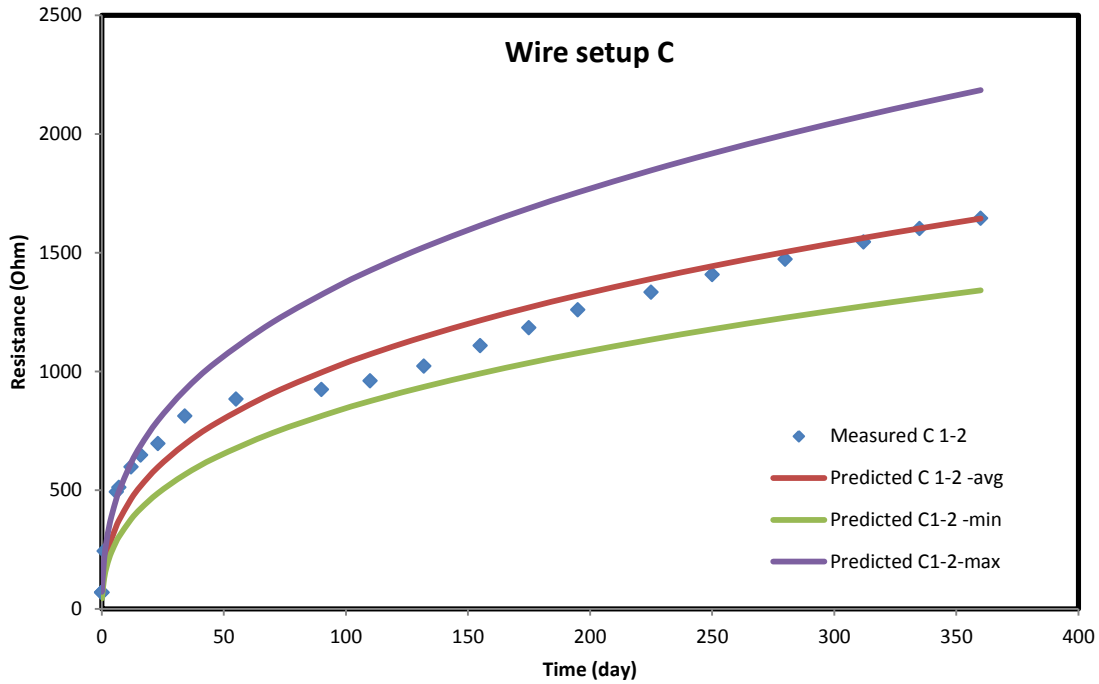


Figure 7-20: Predicted and measured resistance for wire setup C for wire combination 1-2

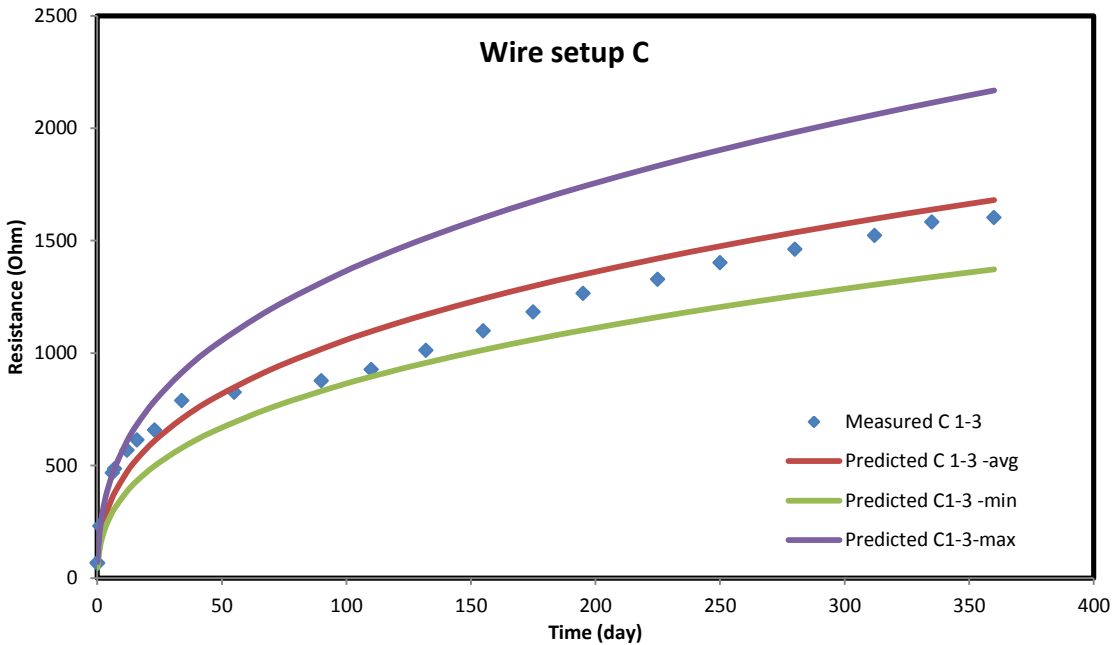


Figure 7-21: Predicted and measured resistance for wire setup C for wire combination 1-3

For the wire combination C 1-4, the measured values are mostly within the predicted range of values (Fig. 7-22) with a little exception. And for wire combination C 1-5, the measured values up to curing time 70 days are higher than the predicted range but after that the measured values are within the range of the predicted values (Fig. 7-23). The reason could be because the wire level at C 5 is at the top of the cementing layer and the initial moisture loss could be higher than the small sample moisture loss. For horizontal wire setup A-B at level 1, the measured values are lower than the predicted values (Fig. 7-24). This could be because of the reason that the level 1 is at the bottom of the cementing and the moisture loss is very less compared to that of the other part of the cementing. At level 3, the measured values are very close to the predicted values (Fig. 7-25). But at level 5, the measured values are above the predicted range of values. The reason could be that the level 5 is at the top of the cementing and the moisture loss could be higher than the small sample. And for higher moisture loss, the measured resistance could be higher.

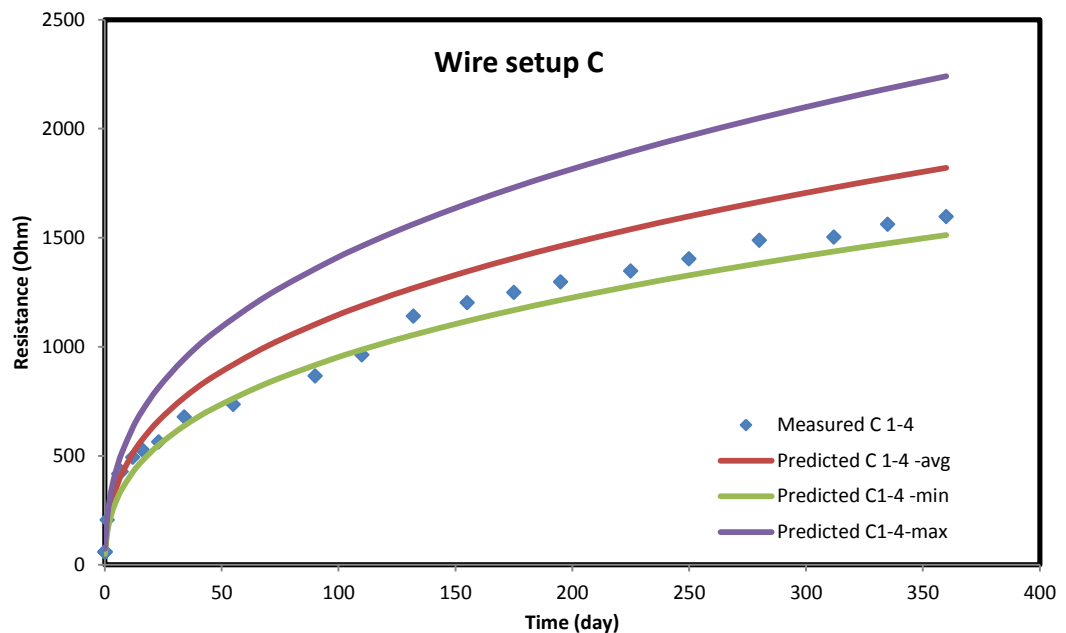


Figure 7-22: Predicted and measured resistance for wire setup C for wire combination 1-4

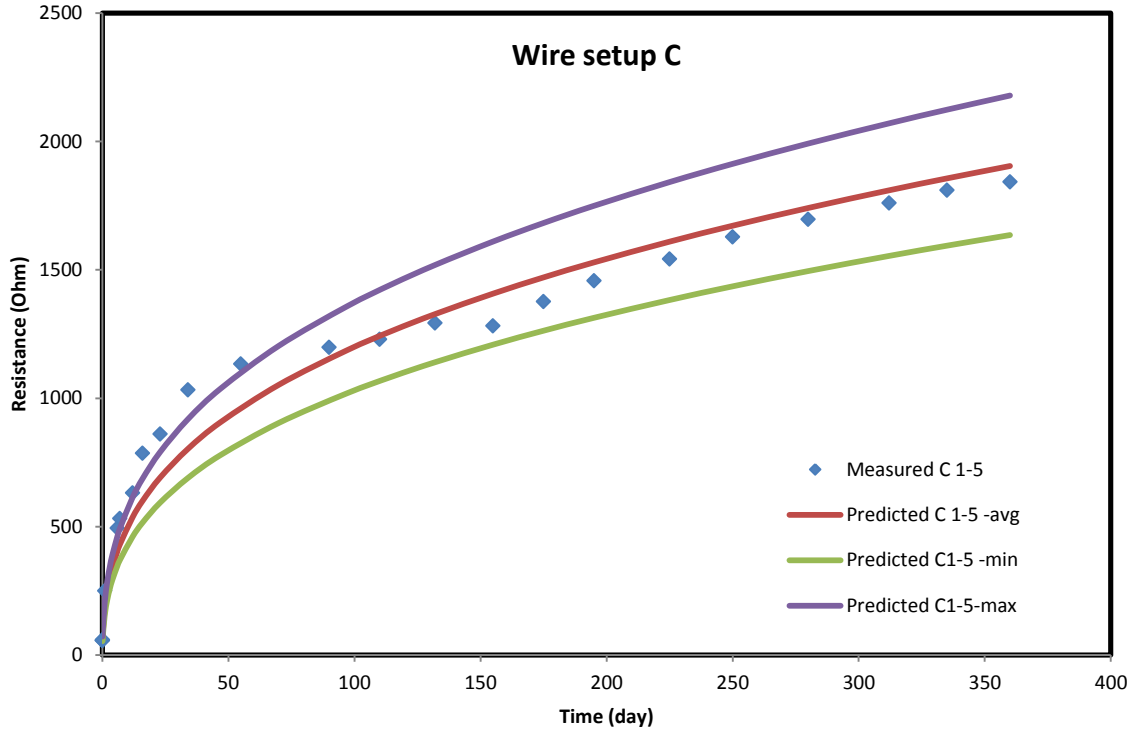


Figure 7-23: Predicted and measured resistance for wire setup C for wire combination 1-5

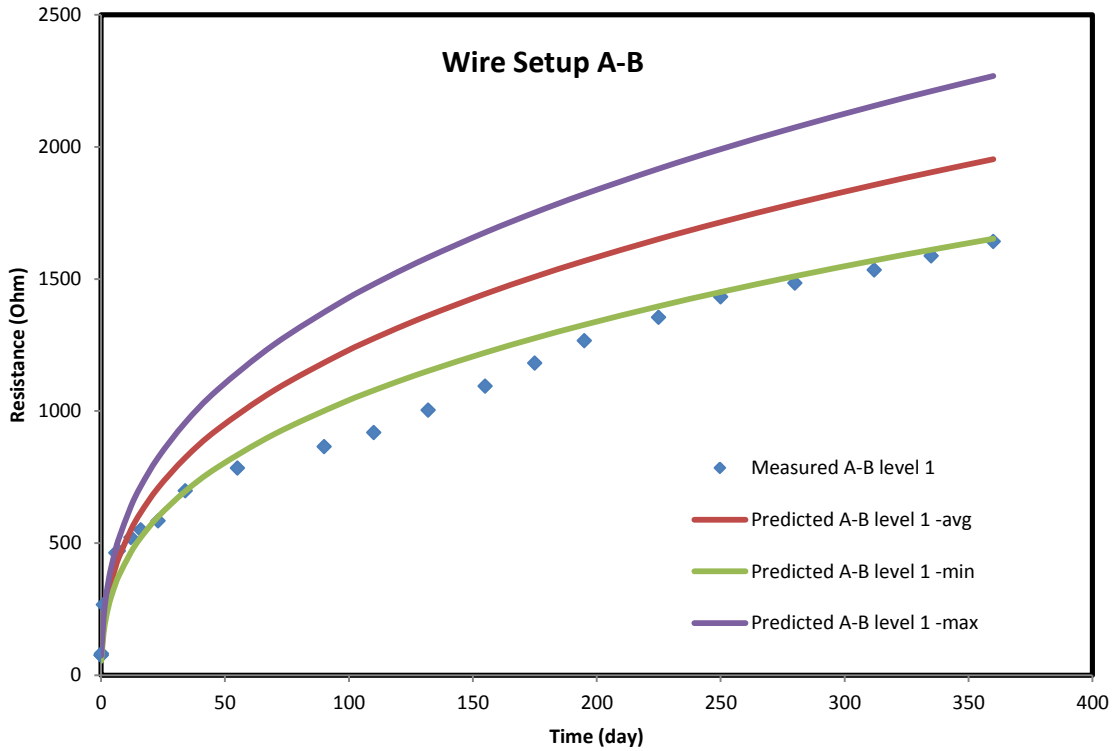


Figure 7-24: Predicted and measured resistance for horizontal wire setup A-B at level 1

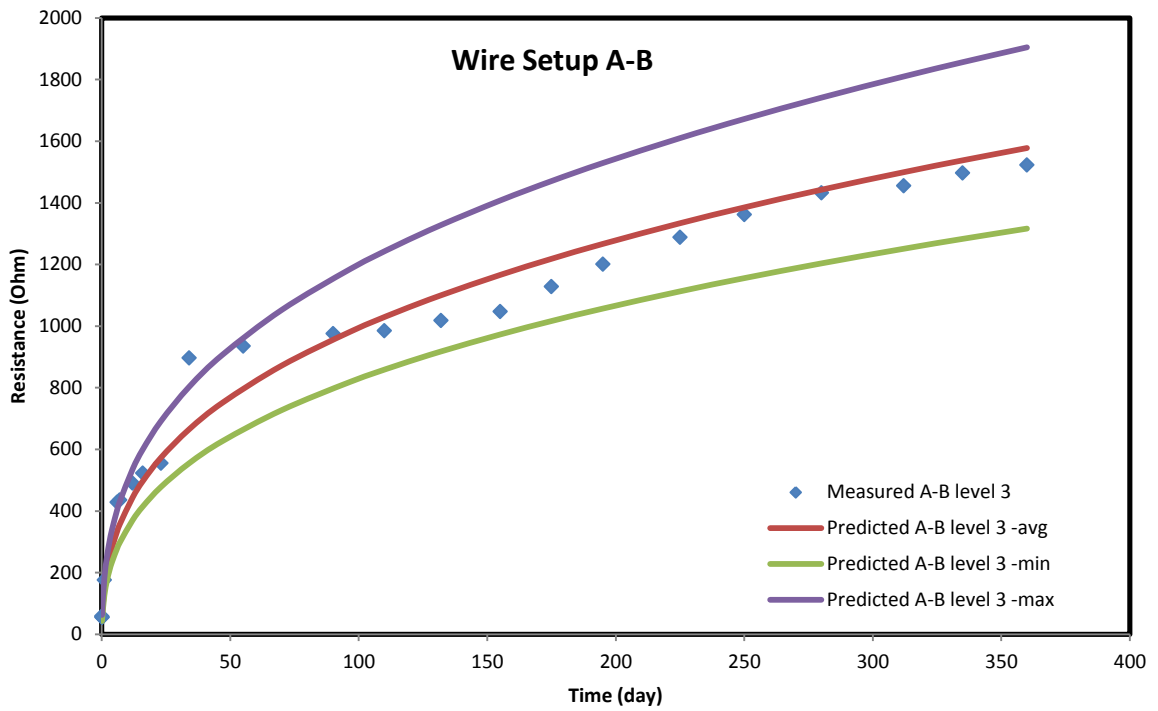


Figure 7-25: Predicted and measured resistance for horizontal wire setup A-B at level 3

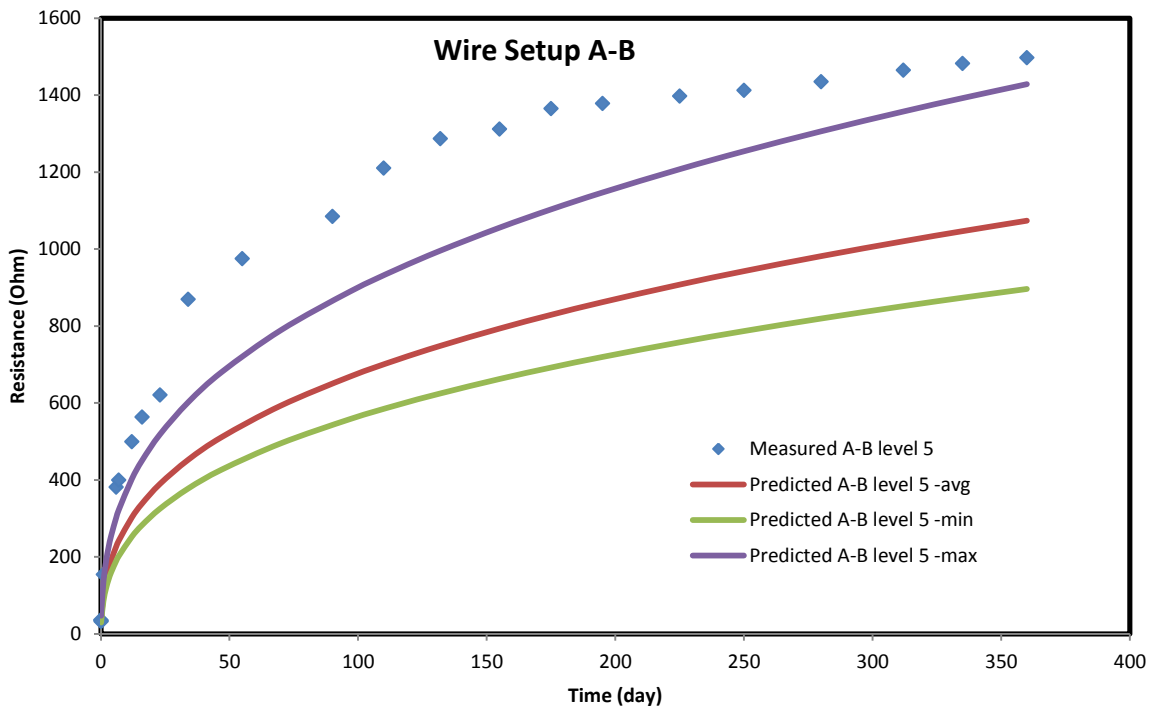


Figure 7-26: Predicted and measured resistance for horizontal wire setup A-B at level 5

7.2 Big lab model 1

7.2.1 Detecting the presence of cement slurry by resistance measurements in big lab model 1 during installation

Cement slurry is taken to fill the casing step by step and the resistance was measured to check whether the presence of cement slurry can be known from the change of resistance. Figure 7-27 showed the resistance change through the vertical wire setup A while cement slurry is being filled up to a certain wire level. We can see from the plot that the resistance between wire combination A1-A3 before the cement slurry is filled to level 3 was about 12.5 k Ω which becomes around 16-17 Ω only when the cement slurry reached level 3. Similarly, for wire combinations A1-A5 , A1-A7, A1-A9, A1-A11, A1-A13 the resistance varied from 10.8 k Ω to 13.1 k Ω before both the two levels of wires became in the cement slurry, but as long as both wires were inside the cement slurry, the resistance was dropping down sharply to about 16-19 Ω only. This sharp dropping down of the resistance value tells us that the cement slurry reached up to that certain wire level.

For wire level C, we can see from the plot (Fig. 7-28) that the vertical resistance between wire combination C1-C3 before the cement slurry is filled to level 3 was about 17.5 k Ω which becomes around 18-19 Ω only when the cement slurry reached level 3. Similarly, for wire combinations C1-C5 , C1-C7, C1-C9, C1-C11, C1-C13 the resistance varied from 13.9 k Ω to 16.4 k Ω before both the two levels of wires became in the cement slurry, but as long as both wires were inside the cement slurry, the resistance was dropping down sharply to about 17-20 Ω only. This sharp dropping down of the resistance value tells us that the cement slurry reached up to that certain wire level.

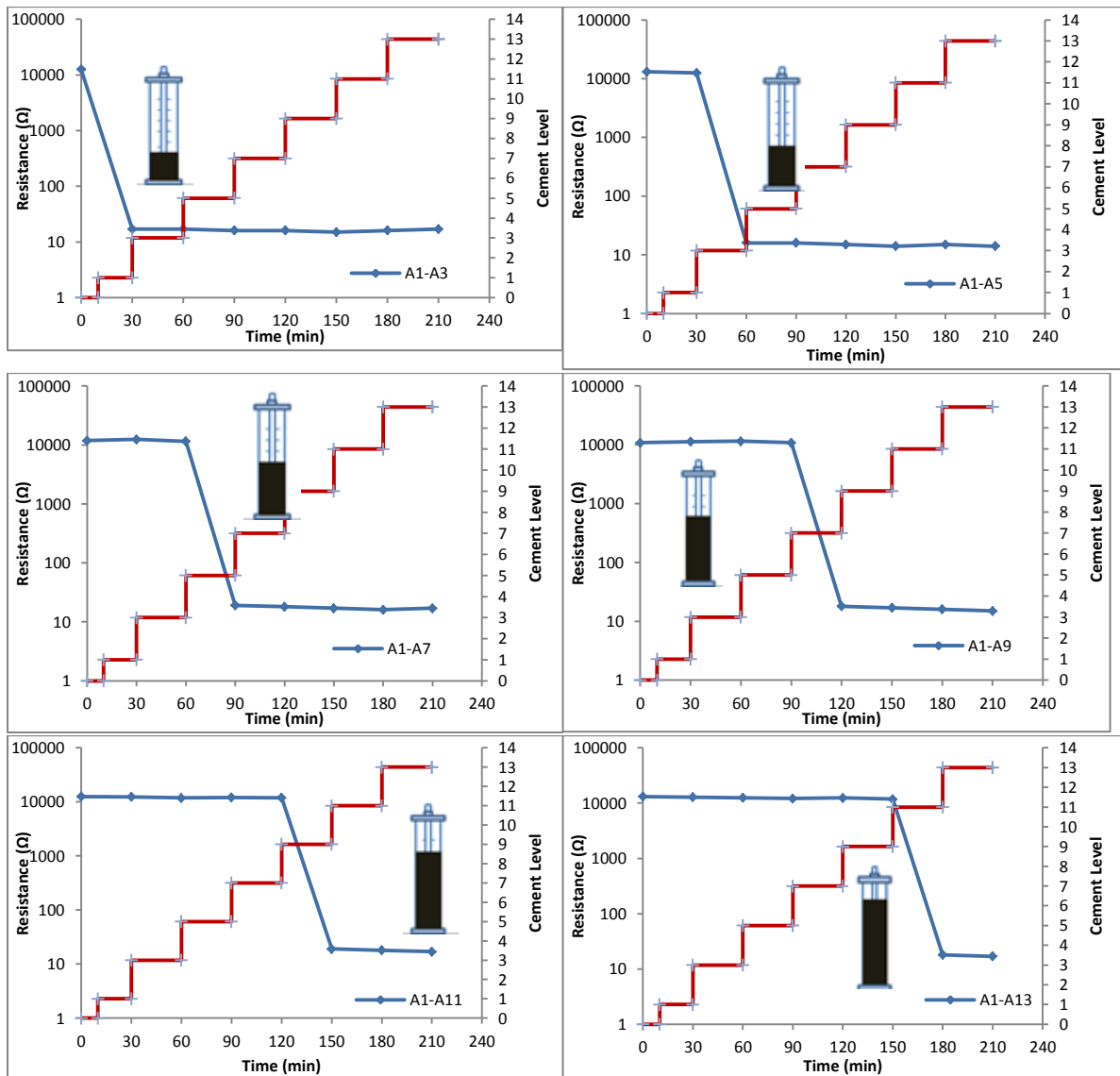


Figure 7-27: The change of vertical resistance along wire setup A with cement slurry filling for big lab model 1

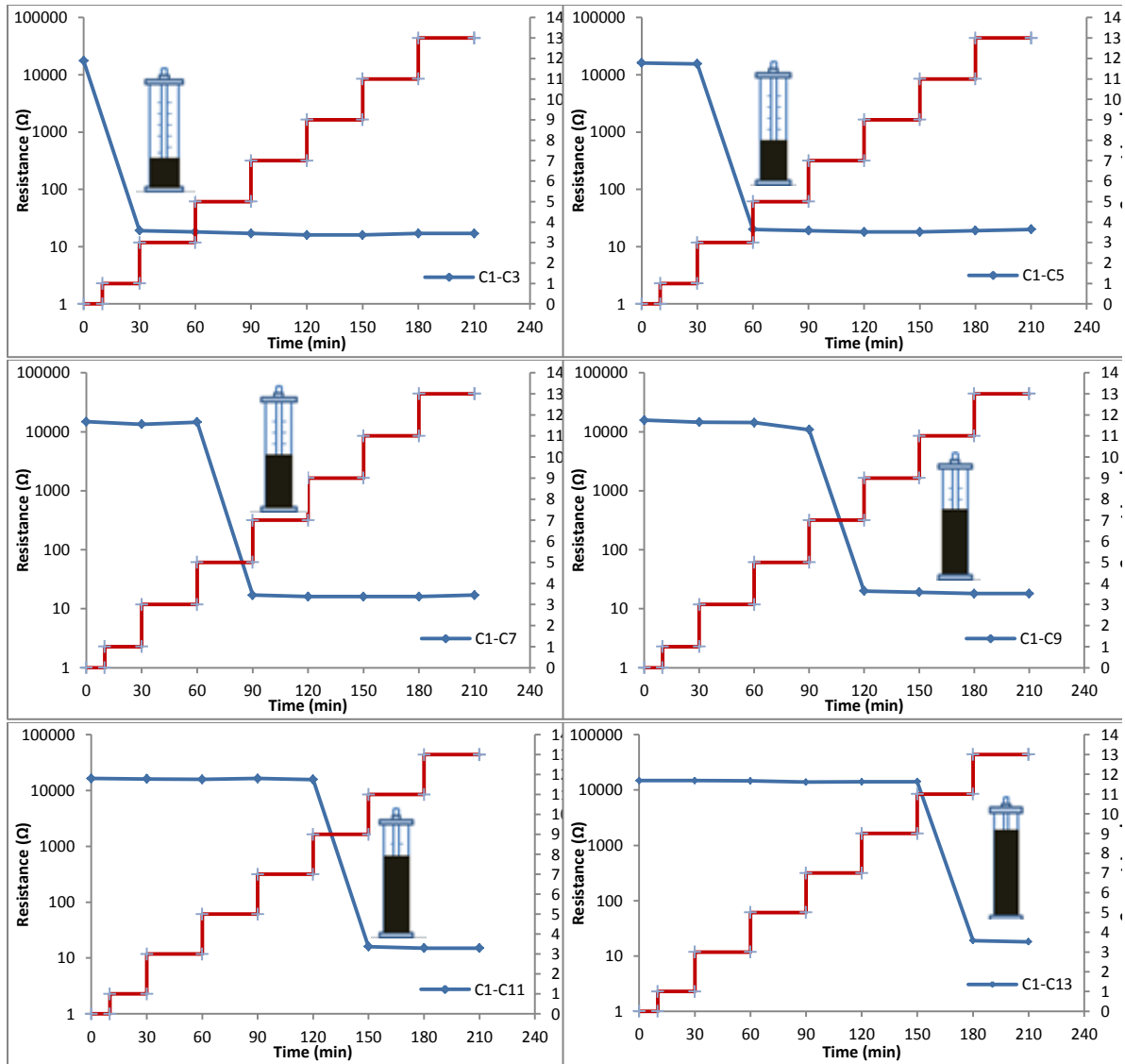


Figure 7-28: The change of vertical resistance along wire setup C with cement slurry filling for big lab model 1

For variation of resistance for the horizontal wire combination A-C at level different level are showed in Figure 7-29. We can see from the plot that the horizontal resistance between wire combination A3-C3 before the cement slurry is filled to level 3 was about 15.7 kΩ which becomes around 16-17Ω only when the cement slurry reached level 3. Similarly, for wire combinations A5-C5 , A7-C7, A9-C9, A11-C11, A13-C13

the resistance varied from 14.8 k Ω to 17.5 k Ω before levels of wires became in the cement slurry, but as long as wire level became inside the cement slurry, the resistance was dropping down sharply to about 17-20 Ω only. This sharp dropping down of the resistance value tells us that the cement slurry reached up to that certain wire level.

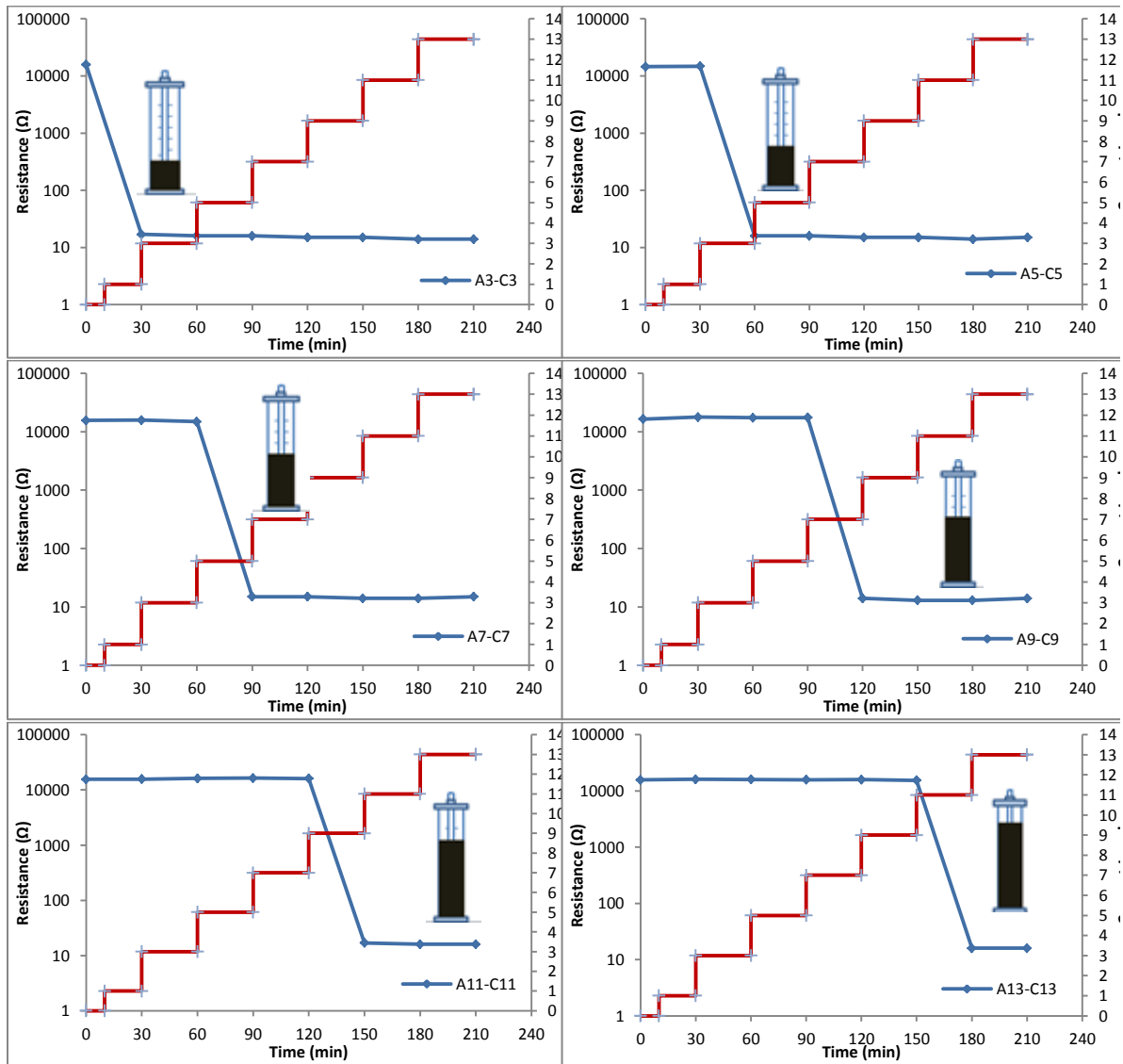


Figure 7-29: The change of horizontal resistance for wire set up A-C at different level with cement slurry filling for big lab model 1

7.2.2 Prediction and compare the measured resistance value during different curing time after cement slurry is placed in the wellbore around casing

7.2.2.1 Determination of Geometric parameter K for the different wire combination

The K parameter (i.e. L/A) for the wire setup A, B, C and D with different wire spacing were first determined filling the cement slurry. To do this, the resistivity of the cement slurry was determined by direct resistivity measurement device and the resistance between the wire combinations was determined with resistance measurement device (LCR meter). The results of the K values are shown below (Fig. 7-30 to 7-32) and the average value, maximum value, and minimum values are shown in the table below (Table 7-5 to 7-7) for wire setup A, C and horizontal combination A-C respectively.

For wire setup A, the average K parameter are found to be varied from 18.5 to 25 m^{-1} with standard deviations varying from 1.3 to 8.6 m^{-1} for different wire spacing (Fig. 7-30 and Table 7-5).

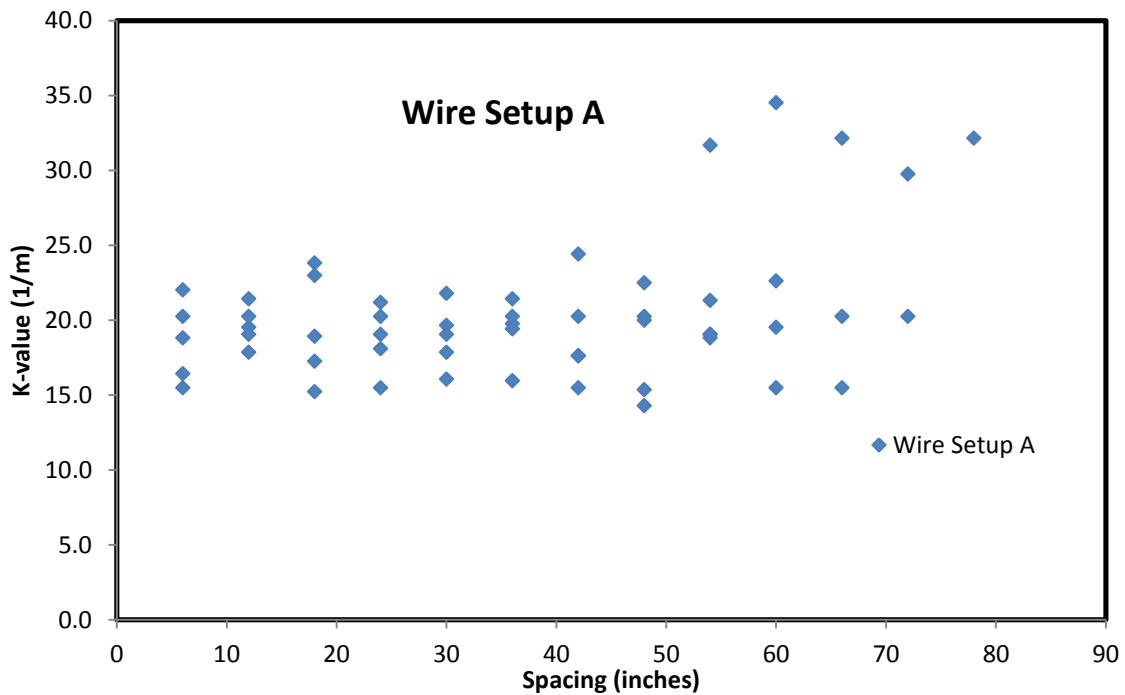


Figure 7-30: K parameter for wire setup A for big lab model 1

Table 7-5: Variations of K parameter for wire setup A for big lab model 1

	6 inches	12 inches	18 inches	24 inches	30 inches	36 inches	42 inches	48 inches	54 inches	60 inches	66 inches	72 inches
Avg	18.6	19.6	19.6	18.8	18.9	19.4	19.1	18.5	22.0	23.0	22.6	25.0
Min	15.5	17.9	15.2	15.5	16.1	16.0	15.5	14.3	18.8	15.5	15.5	20.2
Max	22.0	21.4	23.8	21.2	21.8	21.4	24.4	22.5	31.7	34.5	32.1	29.8
Std. dev	1.7	0.7	1.2	1.3	1.1	1.1	1.4	1.5	1.2	1.9	1.6	1.7
No of data	24	24	24	24	18	18	18	18	12	12	12	12

And for wire setup C, the average K parameter were found to be varied from 21.2 to 35.6 m⁻¹ with standard deviations varying from 2 to 6.2 for different wire spacing (Fig. 7-31 and Table 7-6).

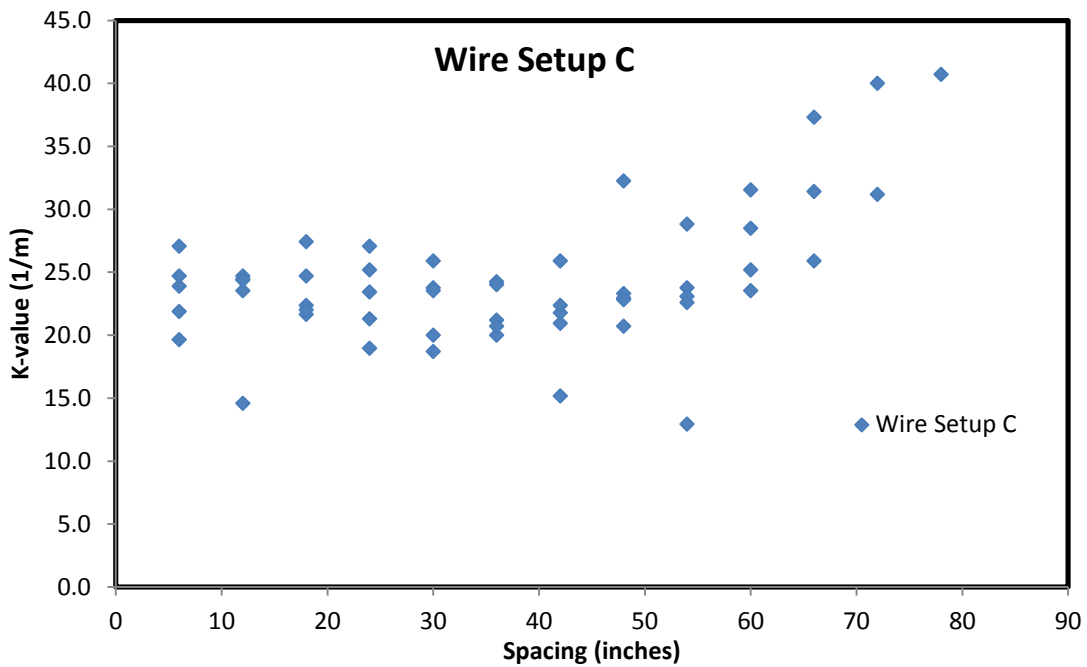


Figure 7-31: K parameter for wire setup C for big lab model 1

Table 7-6: Variations of K parameter for wire setup C for big lab model 1

	6 inches	12 inches	18 inches	24 inches	30 inches	36 inches	42 inches	48 inches	54 inches	60 inches	66 inches	72 inches
Avg	23.4	22.3	23.6	23.2	22.4	22.0	21.2	24.4	22.2	27.2	31.5	35.6
Min	19.6	14.6	21.6	18.9	18.7	20.0	15.2	20.7	12.9	23.5	25.9	31.2
Max	27.1	24.7	27.4	27.1	25.9	24.2	25.9	32.2	28.8	31.5	37.3	40.0
Std. dev	1.8	1.4	1.4	1.2	1.9	1.0	1.9	1.5	1.8	1.6	1.7	2.2
No of data	24	24	24	24	18	18	18	18	12	12	12	12

And for horizontal wire combination A-C, the average K parameter are found to be varied from 16.2 to 18.1 m^{-1} with standard deviations varying from 1 to 1.9 for different wire level (Figure 7-32 and Table 7-7).

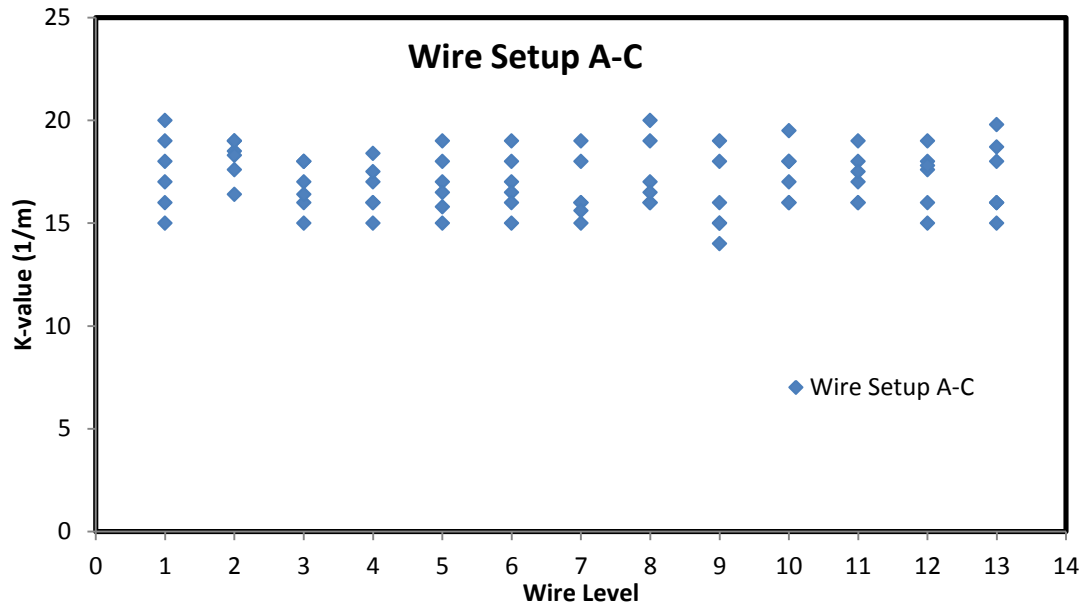


Figure 7-32: K parameter for wire setup A-C for big lab model 1

Table 7-7: Variations of K parameter for wire setup A-C for big lab model 1

Level	1	2	3	4	5	6	7	8	9	10	11	12	13
Avg	17.5	18.1	16.7	16.7	16.9	16.9	16.6	17.4	16.2	17.4	17.3	17.2	17.3
Min	15.0	16.4	15.0	15.0	15.0	15.0	15.0	16.0	14.0	16.0	16.0	15.0	15.0
Max	20.0	19.0	18.0	18.4	19.0	19.0	19.0	20.0	19.0	19.5	19.0	19.0	19.8
Std. dev	1.9	1.0	1.2	1.2	1.5	1.4	1.5	1.7	1.9	1.4	1.2	1.5	1.9
No of data	12	12	12	12	12	12	12	12	12	12	12	12	12

7.2.2.2 Resistivity of the cement slurry with time

The Resistivity of the cement slurry with curing time of up to 255 days is determined using a small mold (2 inches diameter and 4 inches height cylindrical mold) with the same cement slurry that was used for the model and cured under different curing conditions. The resistivity shows an increasing trend with curing time (Fig. 7-33). The total weight loss calculated for the sample under room temperature curing was about

3.4% up to 255 days. The no moisture loss curing sample was cured in an environment where there was no moisture loss of the specimen. The sample which was cured under water gained about 1.7 % weight after 255 days. The resistivity trend was modeled with the curing model which is developed by modified the p-q model proposed by Vipulanandan and Paul (1990) (Eqn. (3-11)). The model parameters for room cured sample were $p_1= 1.82$, $q_1=0.61$, and $t_0=140$ min; for moisture control sample were $p_1= 1.77$, $q_1=0.55$, and $t_0=140$ min; and for sample cured under water were $p_1= 1.24$, $q_1=0.40$, and $t_0=140$ min.

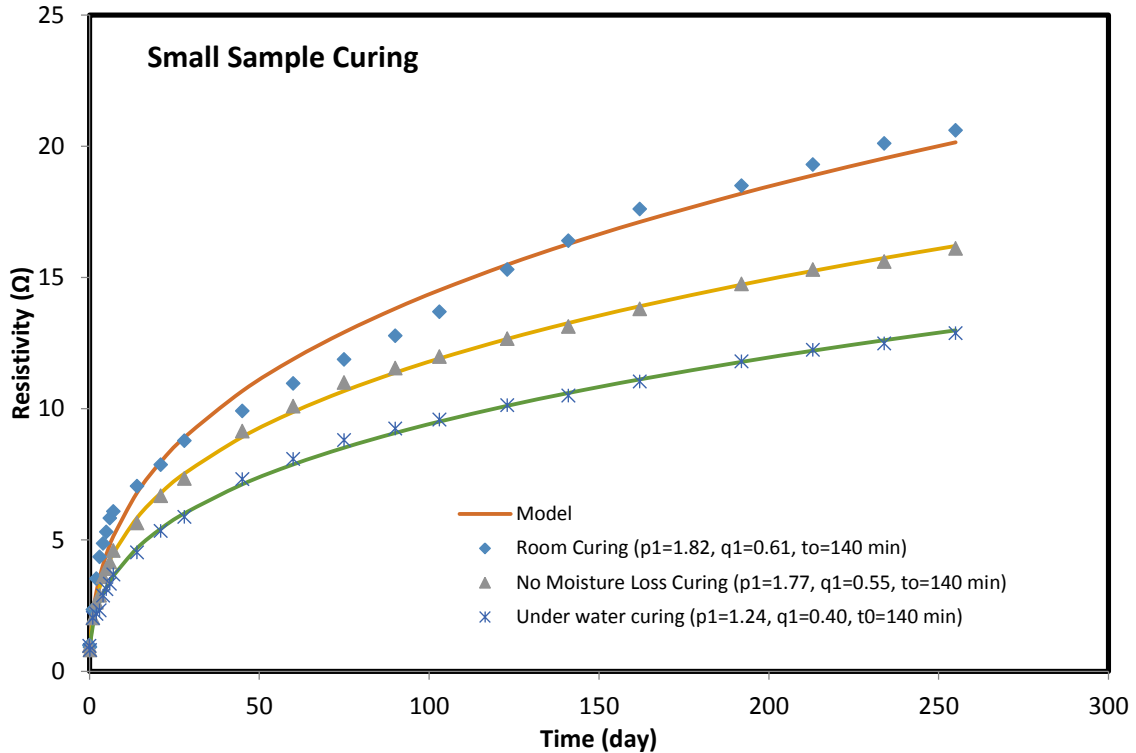


Figure 7-33: Resistivity of cement slurry with curing time

7.2.2.3 Predicted Resistance Vs Measured Resistance

From Fig. 7-33, we know the resistivity of cement slurry with curing time. From Fig. 7-30 to 7-32 and Table 7-5 to 7-7 we know the K parameter that can be used to calculate the resistivity of the cement slurry at different time having the resistance

measured. If we back calculate the possible values of resistance from the same equation using the average, minimum, and maximum K parameter, we can find the predicted Resistance values. Fig. 7-34 to Fig. 7-39 shows the variations of the predicted resistance value and also the actual measured values for wire setup A. Fig. 7-40 to Fig. 7-45 shows the variations of the predicted resistance value and also the actual measured values for wire setup C. Also, Fig. 7-46 to Fig. 7-52 shows the variations of the predicted resistance value and also the actual measured values for horizontal wire setup A-C at different level.

The measured resistance for wire combination 1-3 in wire setup A were little bit less than the predicted values for that combination. It may be due to the less moisture loss of that bottom part of the cement level (Fig. 7-34). The measured resistances for wire combination 1-5 in wire setup A were very much within the range except for the initial 10 days of curing (Fig. 7-35). This may be because of the different curing condition of the small sample and the big physical model.

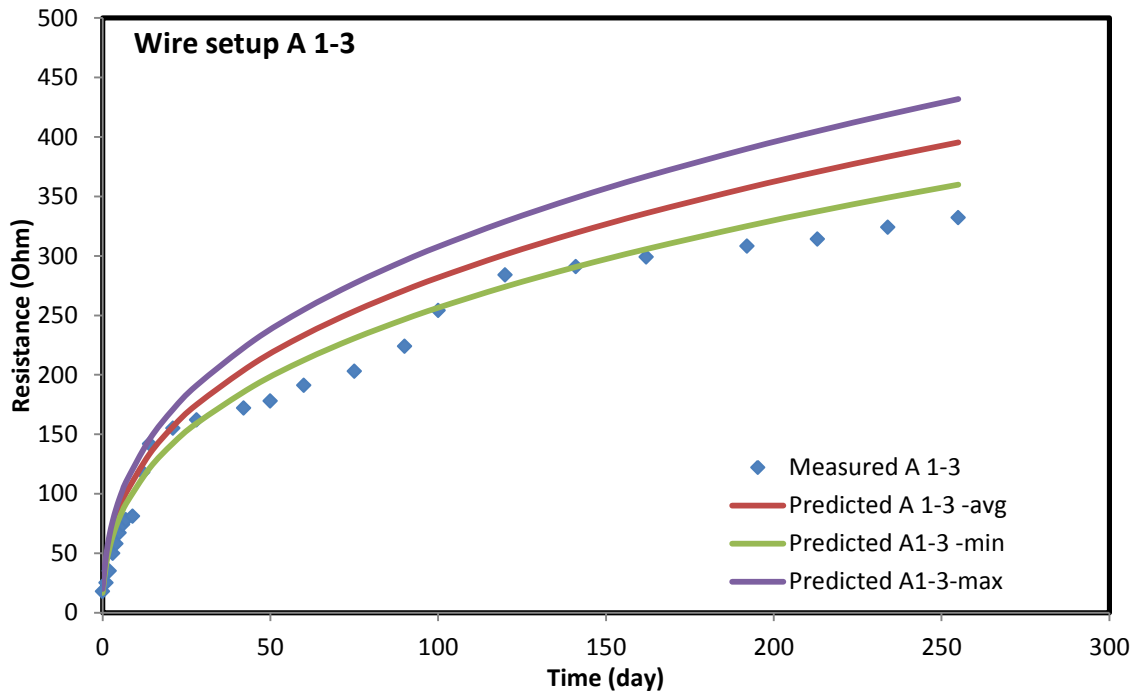


Figure 7-34: Predicted and measured resistance for wire setup A for wire combination 1-3

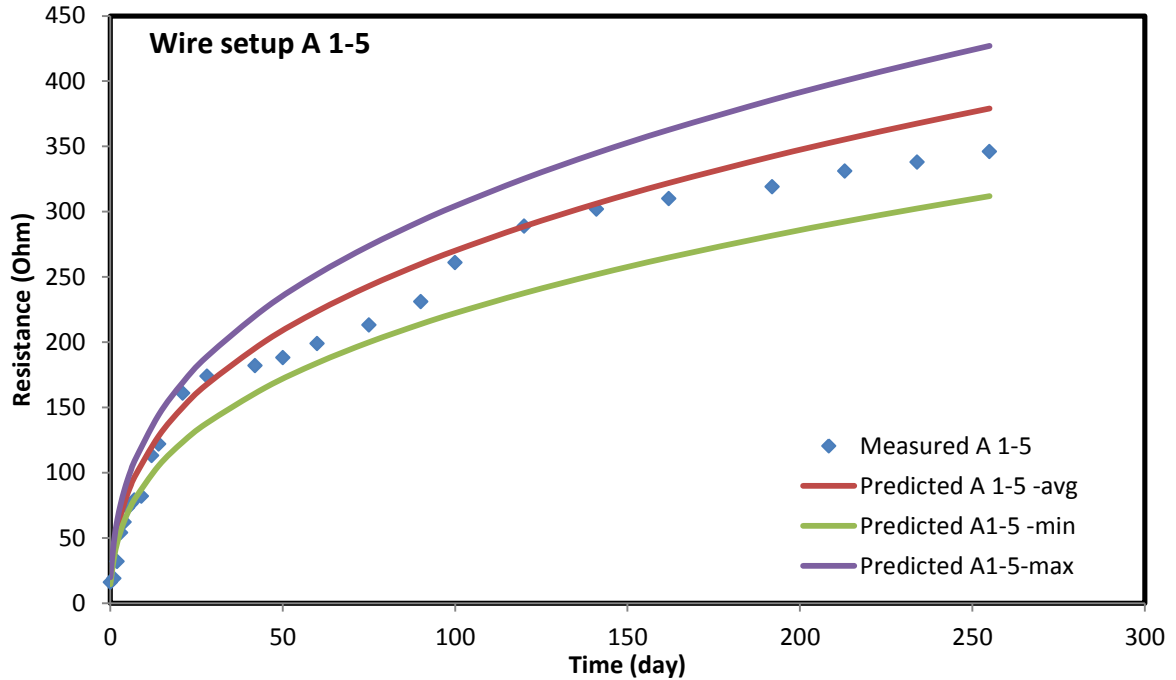


Figure 7-35: Predicted and measured resistance for wire setup A for wire combination 1-5

The wire combination 1-7 and 1-9 show similar trend like wire setup 1-5, i.e., the measured values matches very close to the predicted values but a little bit lower than the predicted values for initial curing days up to 10 days (Fig. 7-36, Fig. 7-37). The measured resistances for wire combination 1-11 and 1-13 are also in between the range of predicted values of the resistance (Fig. 7-38, Fig. 7-39). Only little exception is that there is some values go slightly away of the range for initial curing days which can be considered as outliers.

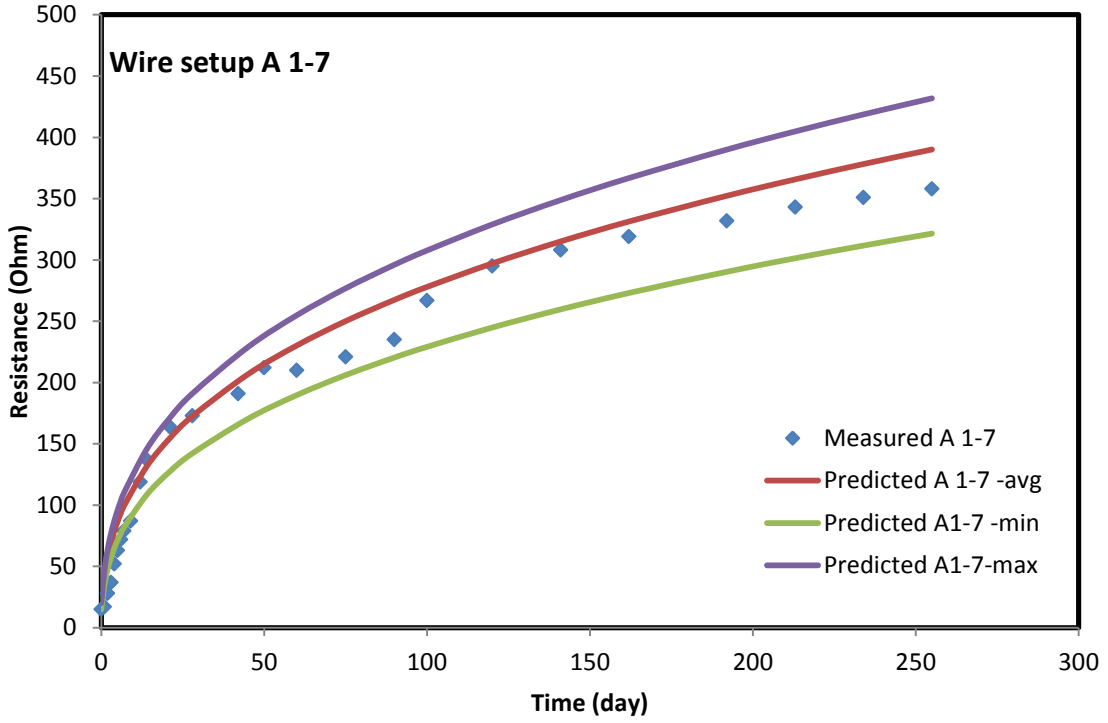


Figure 7-36: Predicted and measured resistance for wire setup A for wire combination 1-7

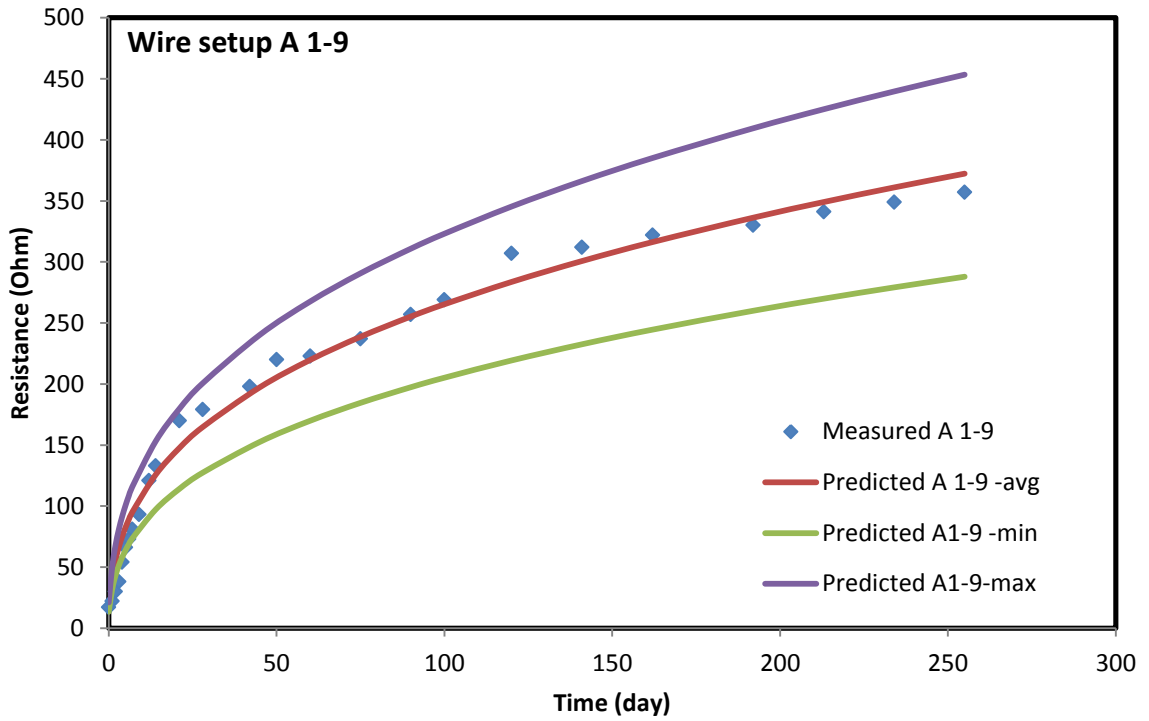


Figure 7-37: Predicted and measured resistance for wire setup A for wire combination 1-9

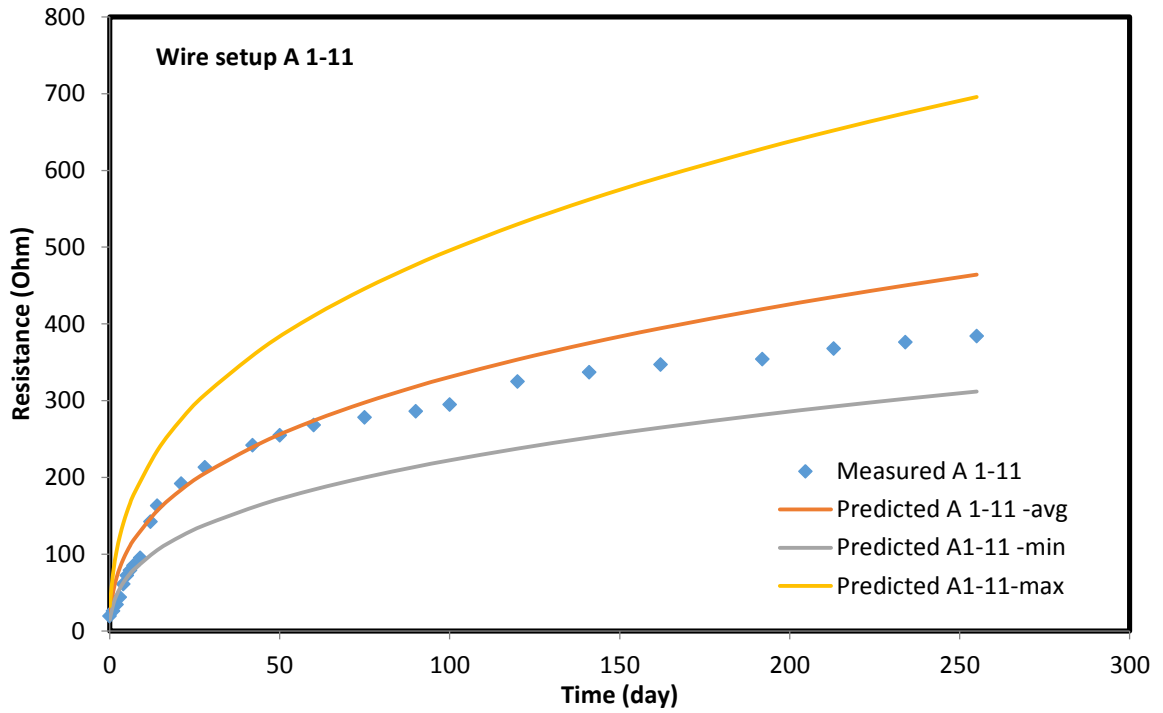


Figure 7-38: Predicted and measured resistance for wire setup A for wire combination 1-11

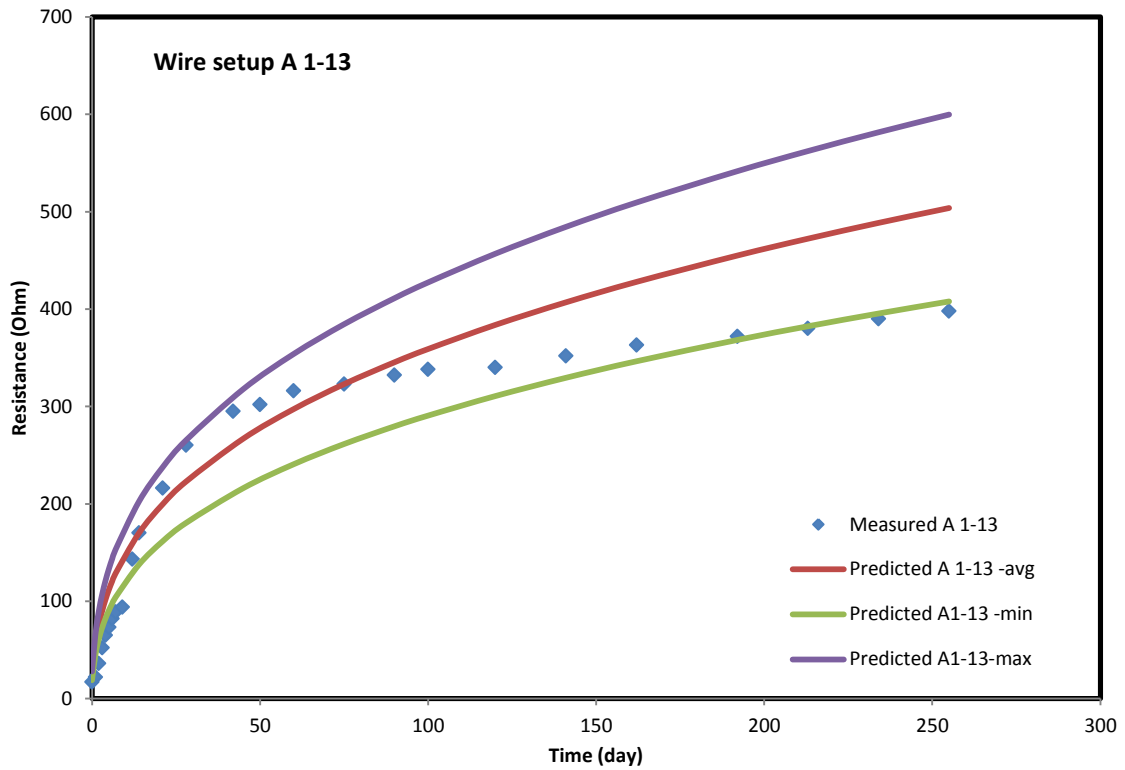


Figure 7-39: Predicted and measured resistance for wire setup A for wire combination 1-13

The measured resistances for wire combination 1-3 and 1-5 in wire setup C were less than the predicted values for those combinations (Fig. 7-40, Fig. 7-41). We can see that these levels are at lower part of the model where the moisture loss may be very less compare to that of small samples. That's why the measured resistances are less than the predicted range. For wire setup 1-7 and 1-9, the measured resistances are also lower than the range of predicted resistances (Fig. 7-42, 7-43). These may be caused due to low moisture loss of the cement compared to that of small samples. The similar trend was found for wire combination 1-11 and 1-13 where the measured resistances were less than the predicted resistances (Fig. 7-44, Fig. 7-45). That can be explained as different curing condition of the model and small sample.

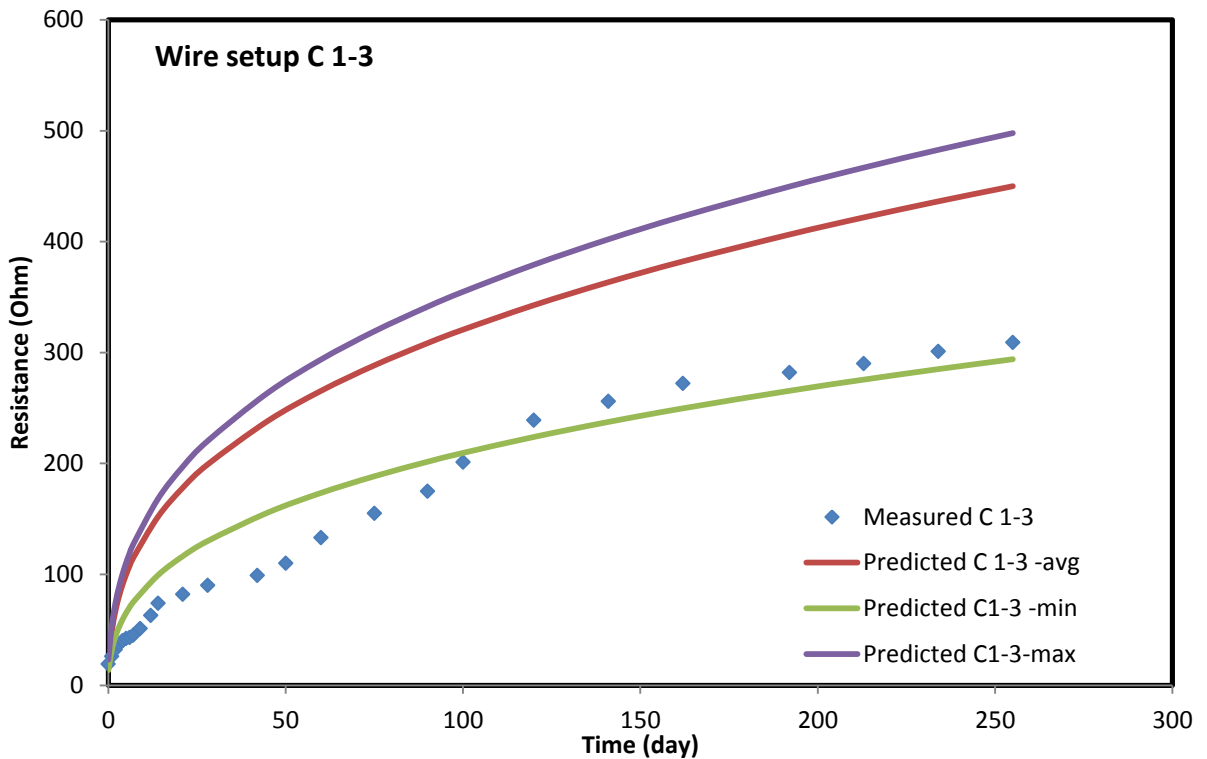


Figure 7-40: Predicted and measured resistance for wire setup C for wire combination 1-3

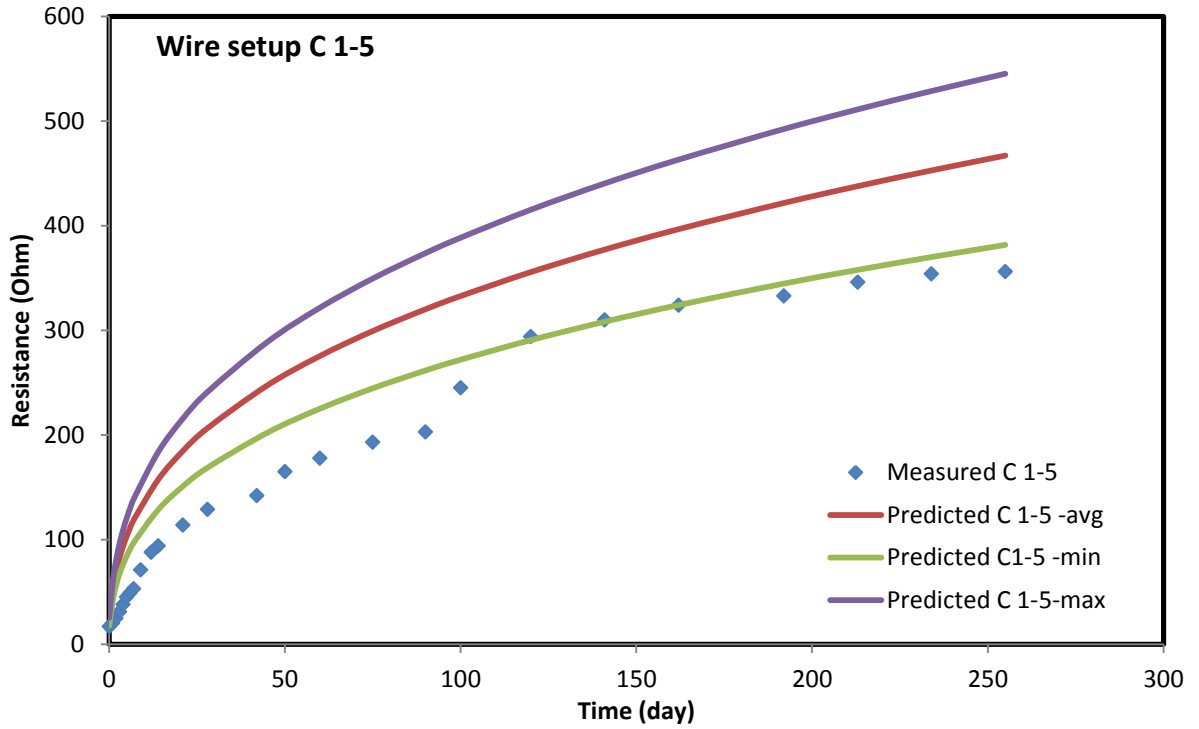


Figure 7-41: Predicted and measured resistance for wire setup C for wire combination 1-5

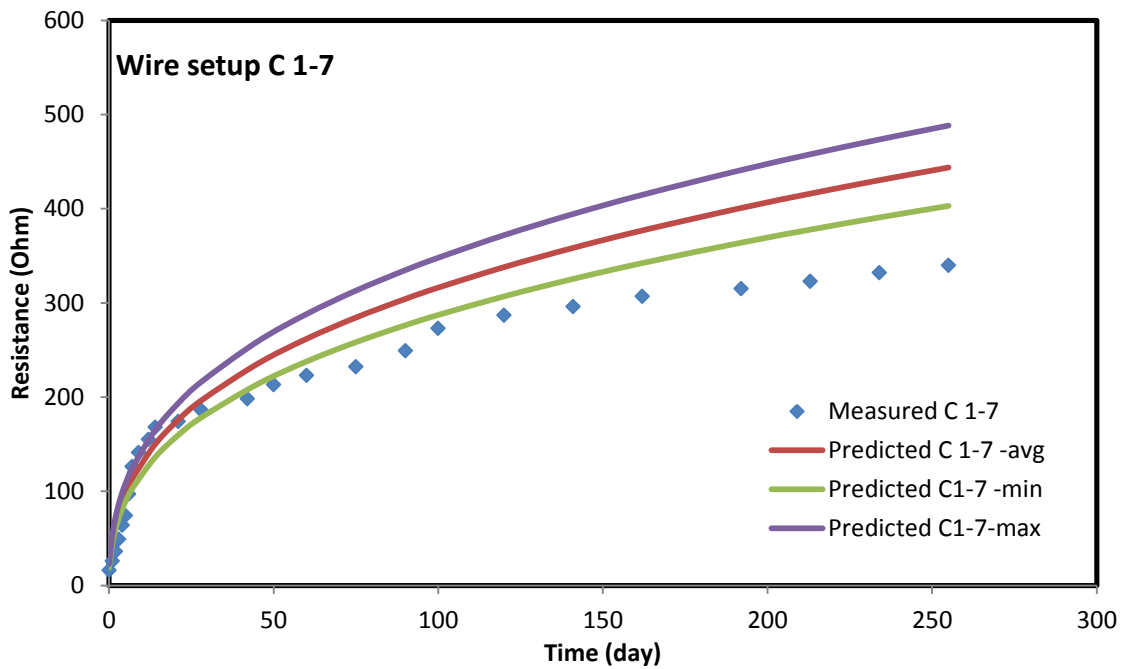


Figure 7-42: Predicted and measured resistance for wire setup C for wire combination 1-7

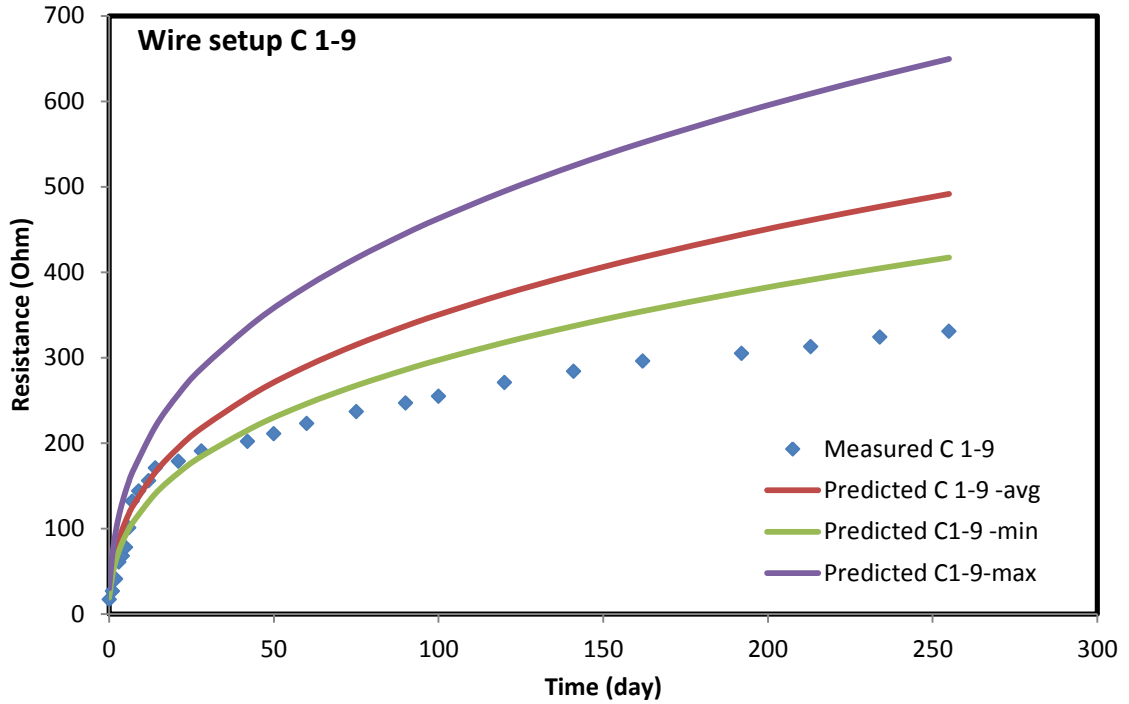


Figure 7-43: Predicted and measured resistance for wire setup C for wire combination 1-9

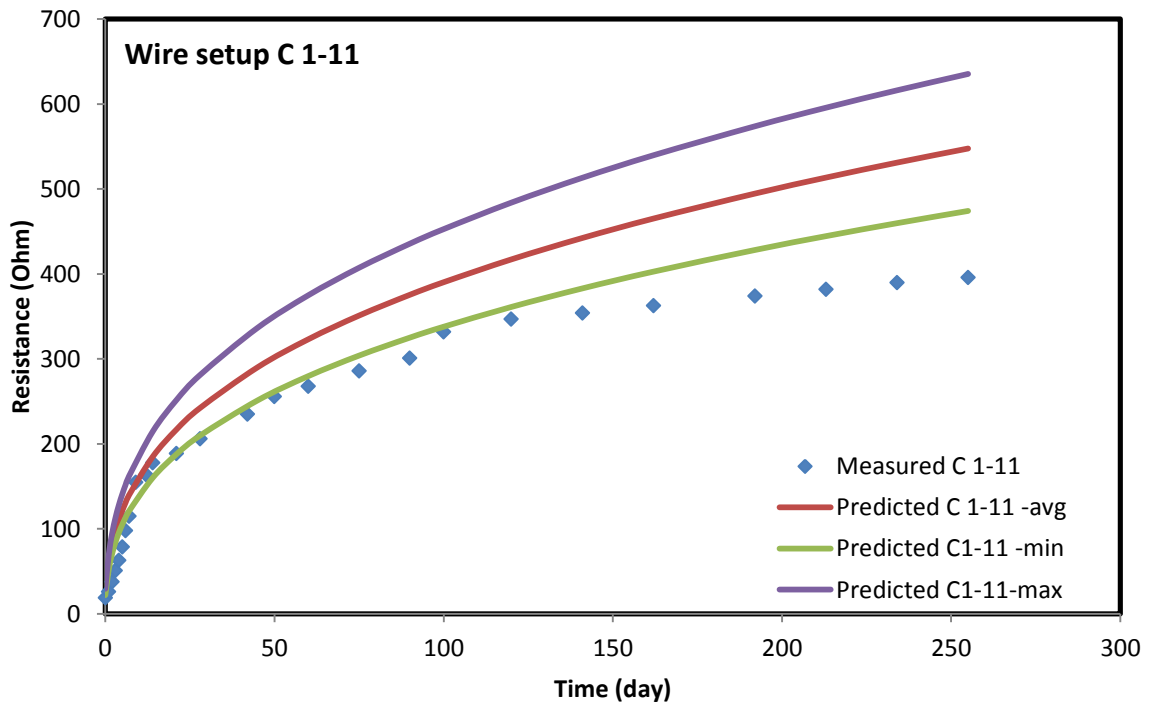


Figure 7-44: Predicted and measured resistance for wire setup C 1-11

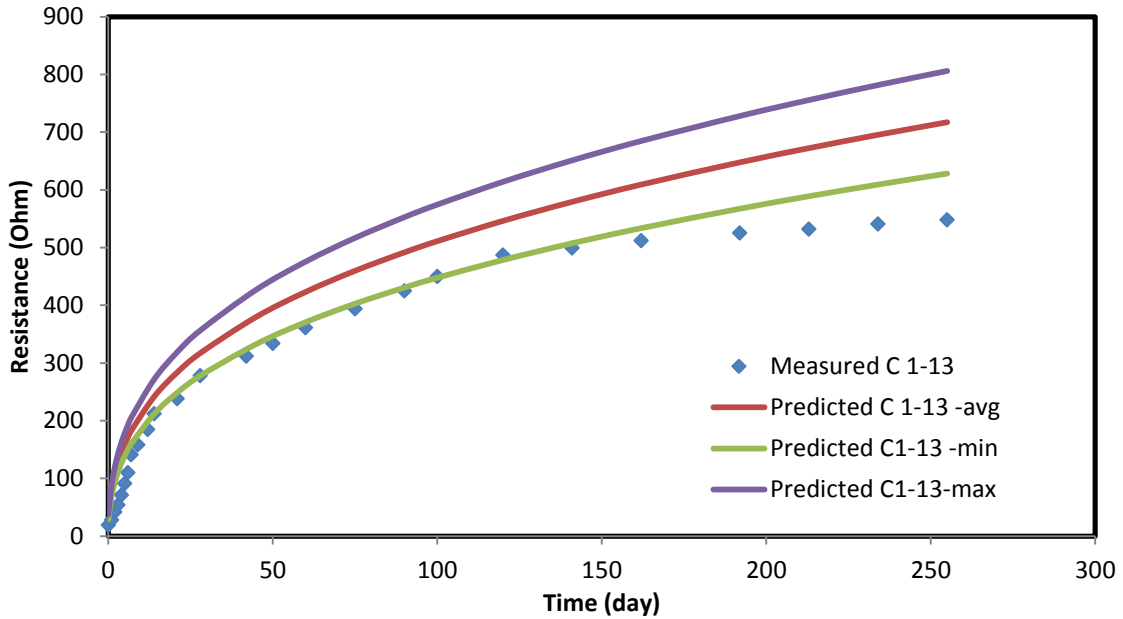


Figure 7-45: Predicted and measured resistance for wire setup C 1-13

For the horizontal wire combination A-C at level 1 and 3, the measured values are less than those of the range of the predicted values (Fig. 7-46, Fig. 7-47). We can see that these levels are at lower part of the model where the moisture loss may be very less compare to that of small samples. That's why the measured resistances are less than the predicted range. At level 5, 7, and 9 the measured values are matching very well within the range of the predicted values (Fig. 7-48, 7-49, 7-50). This supports that the curing condition are similar to those of the small sample. At level 11 and 13, the measured values are matching well with the predicted values up to 45 days of curing (Fig. 7-51, 7-52) but after that the values are higher than the predicted range. We can say that the moisture loss may be higher than for those levels as it is near the top of the model.

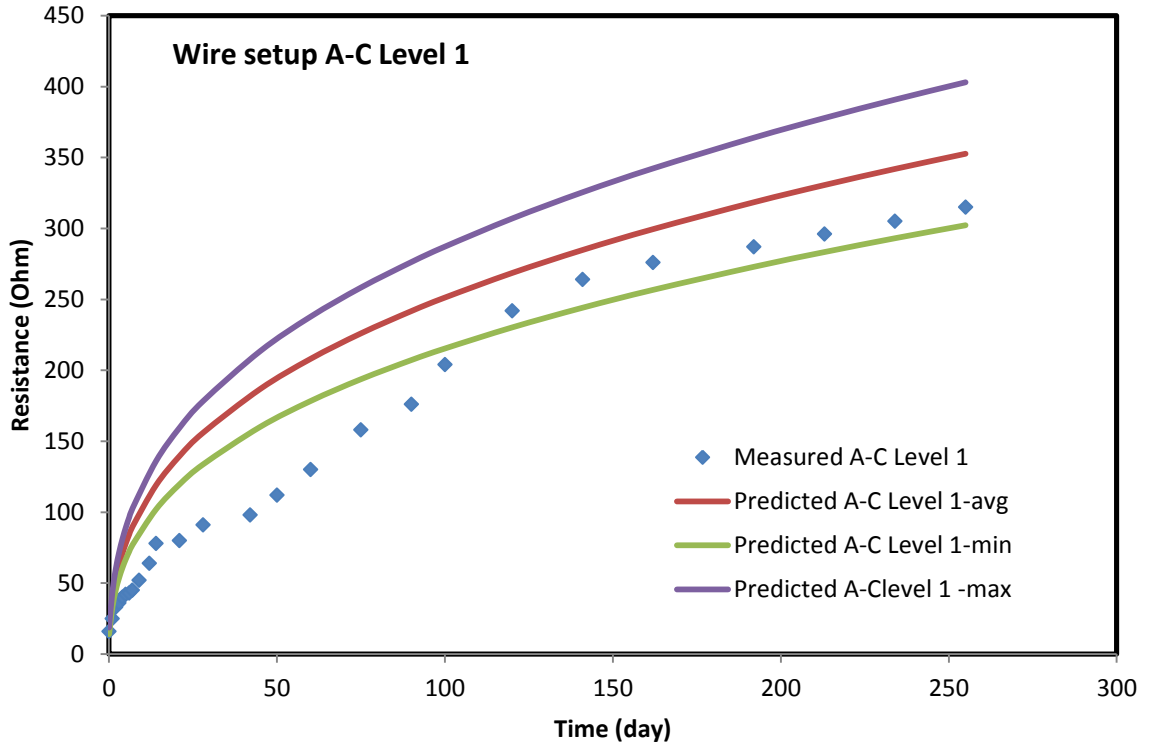


Figure 7-46: Predicted and measured resistance for wire setup A-C at level 1

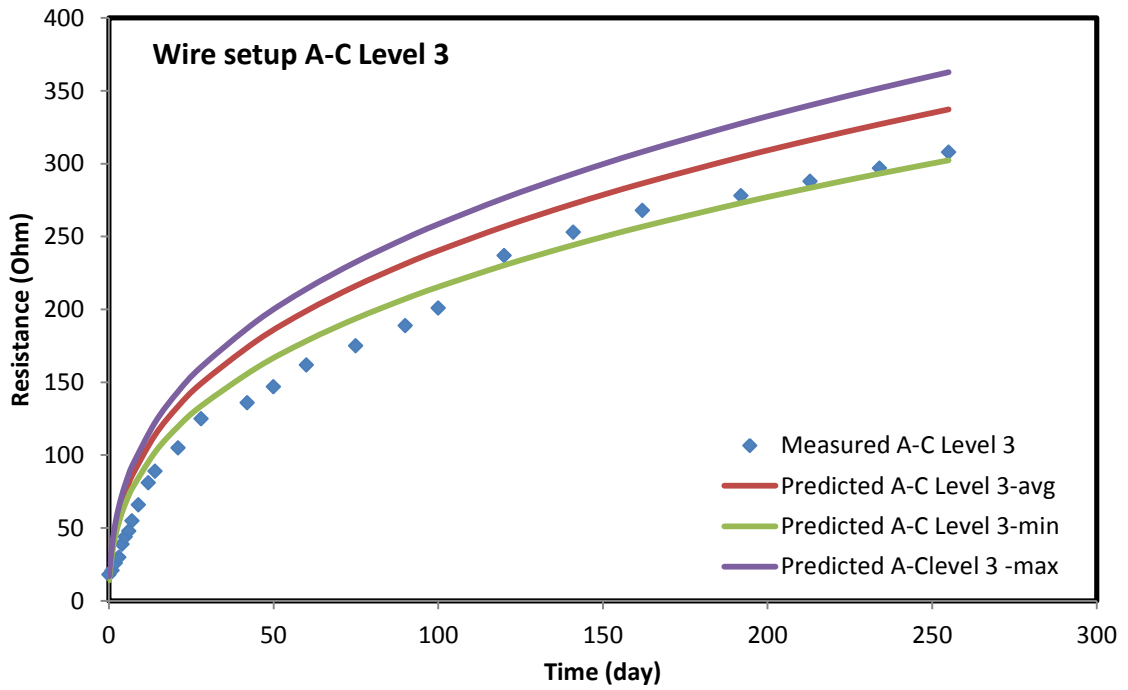


Figure 7-47: Predicted and measured resistance for wire setup A-C at level 3

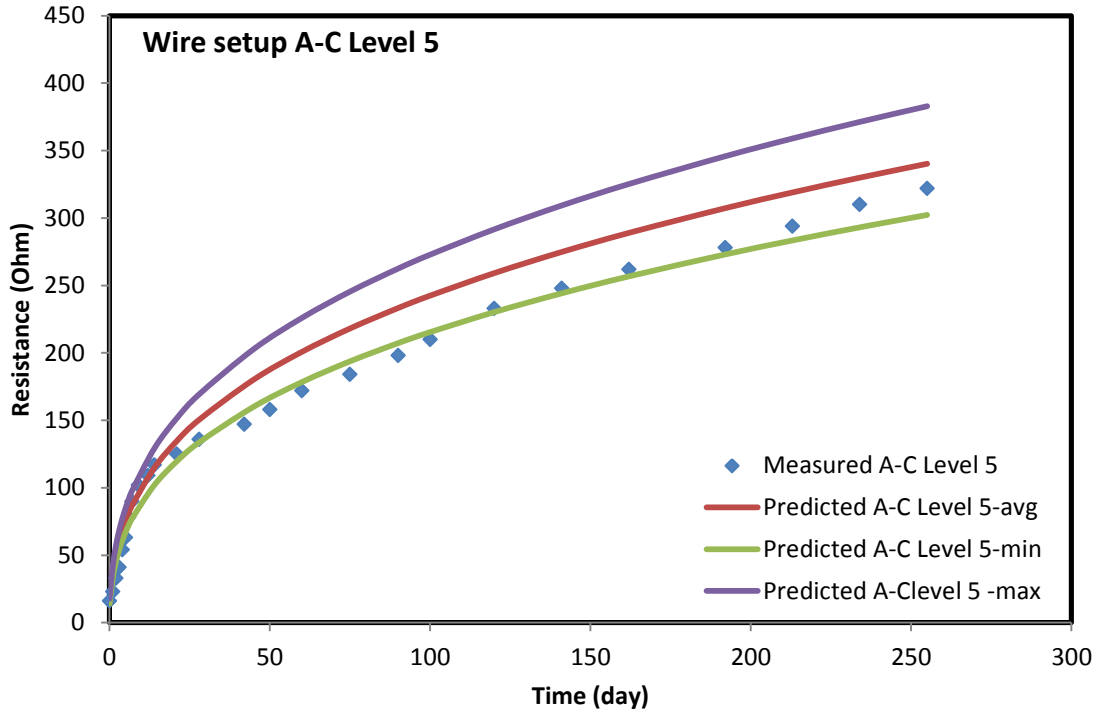


Figure 7-48: Predicted and measured resistance for wire setup A-C at level 5

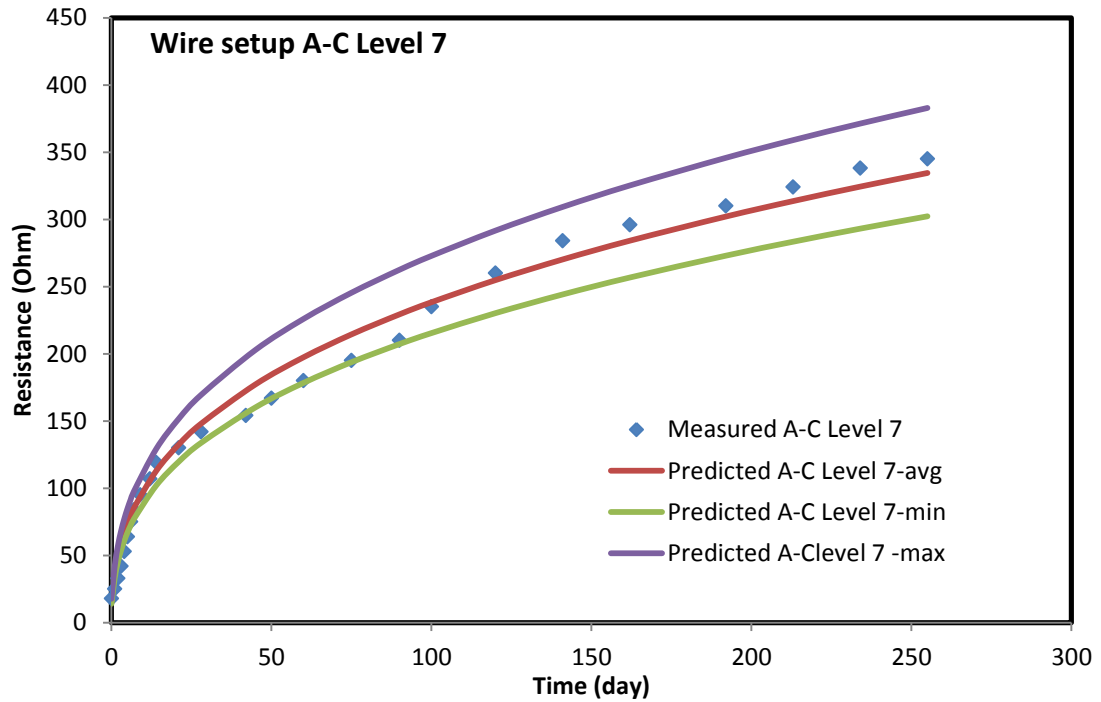


Figure 7-49: Predicted and measured resistance for wire setup A-C at level 7

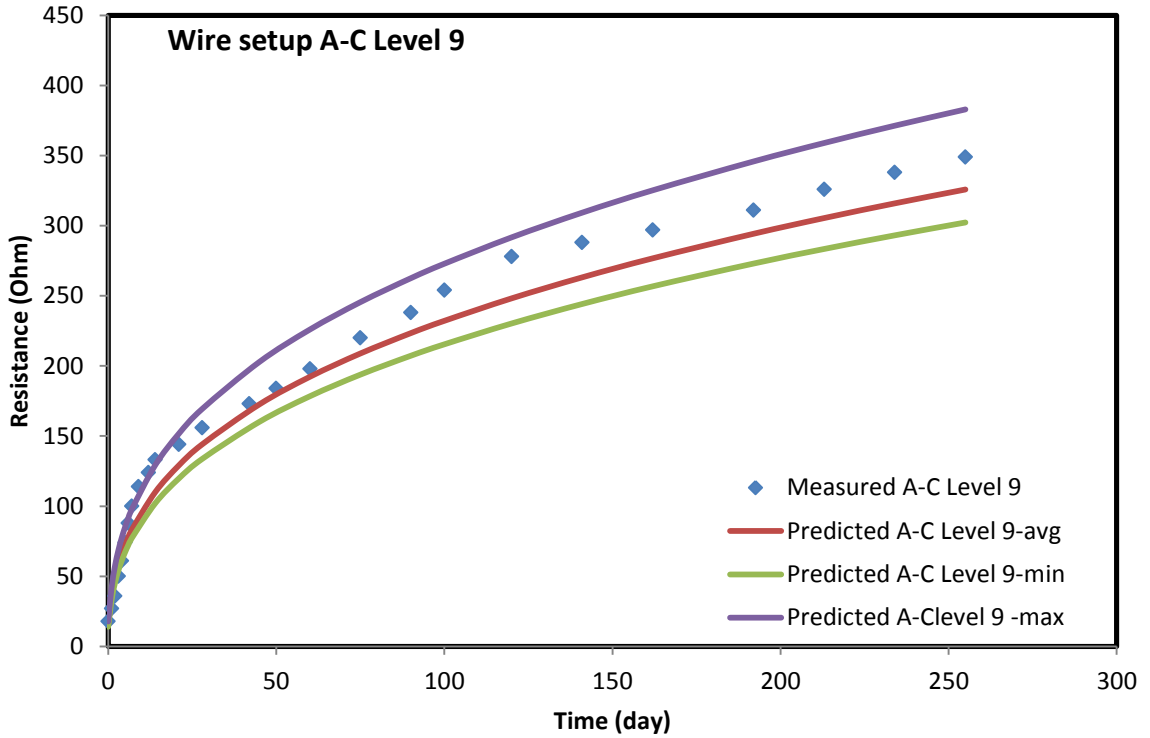


Figure 7-50: Predicted and measured resistance for wire setup A-C at level 9

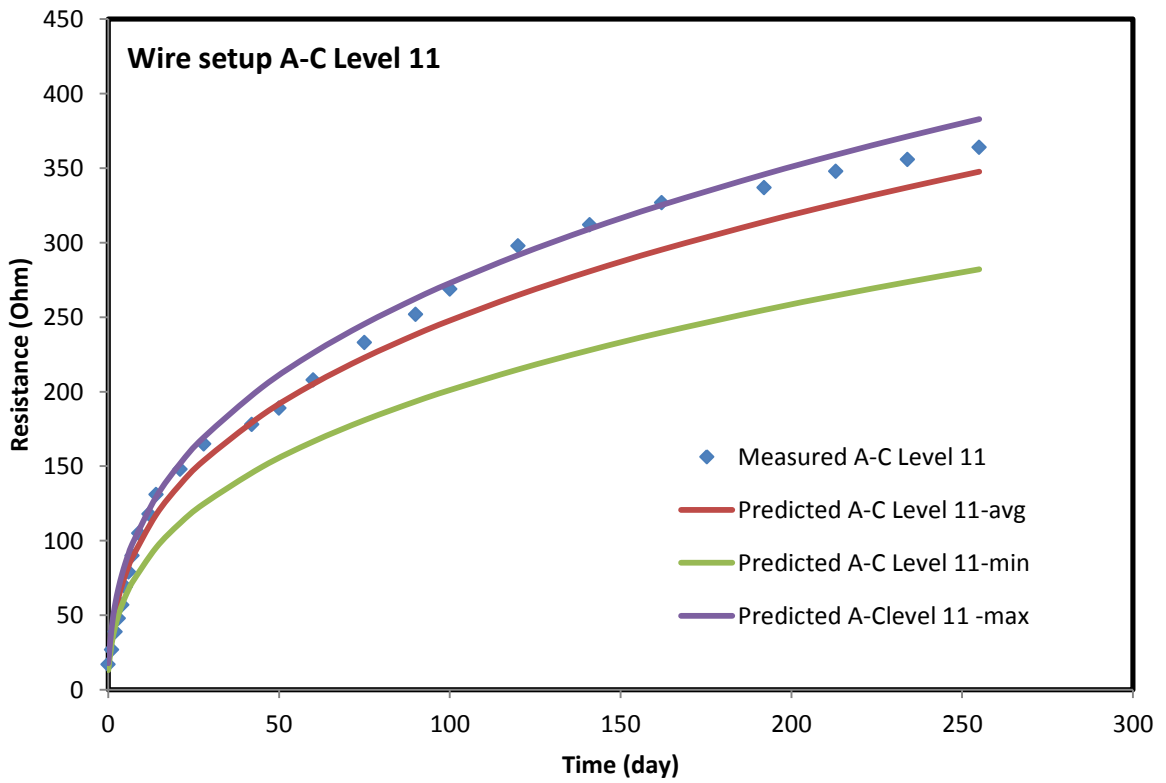


Figure 7-51: Predicted and measured resistance for wire setup A-C at level 11

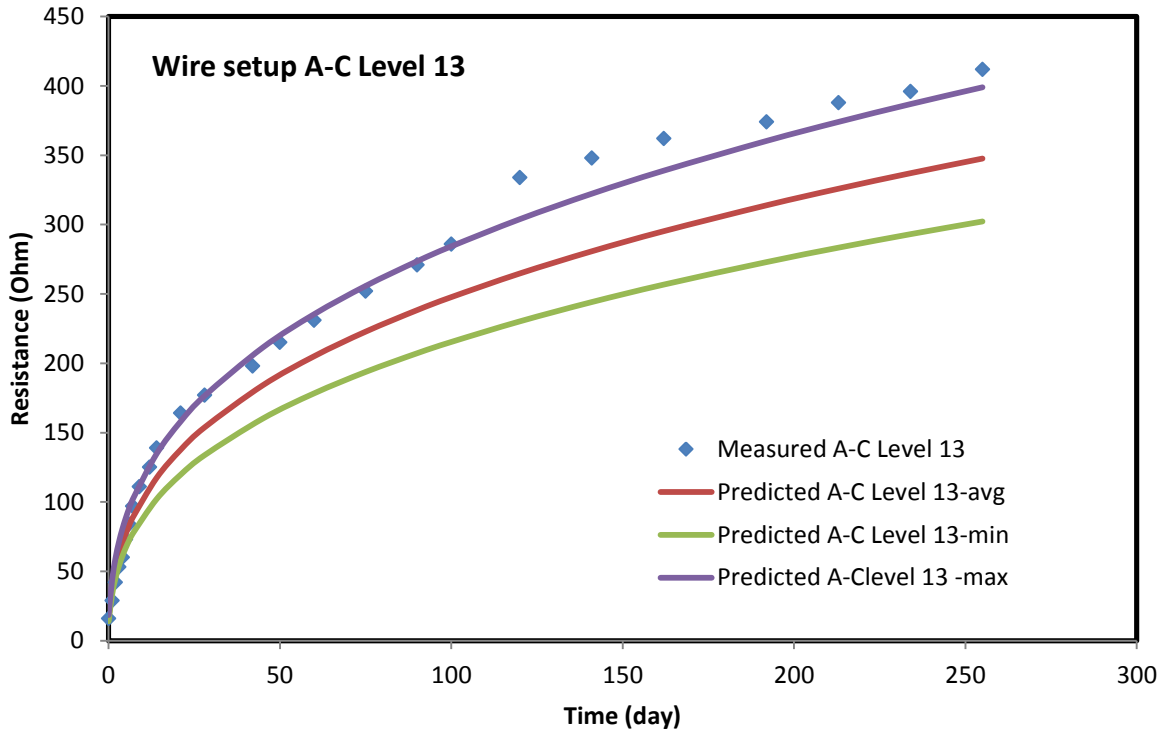


Figure 7-52: Predicted and measured resistance for wire setup A-C at level 13

7.2.3 Temperature variation at different levels

Thermocouples were placed to determine the variation of temperature during the curing time. With wire setup A, two thermocouples were placed at level 1 and 8; and for wire setup C, two thermocouples were placed at level 4 and 12. For wire setup A at level 1, the temperature started from 31° C and increased up to 32.8 °C after several hours and then decreased steadily up to 60 days to reach the room temperature (Fig. 7-53). The temperature at level 8 showed the similar trend throughout the curing period with a very little difference in the temperature. For wire setup C at level 4, the temperature started from 30.5 °C and increased up to 31 °C after several hours and then decreased steadily up to 50 days to reach the room temperature (Fig. 7-54). The temperature at level 12 showed the similar trend throughout the curing period with a very little difference in the temperature.

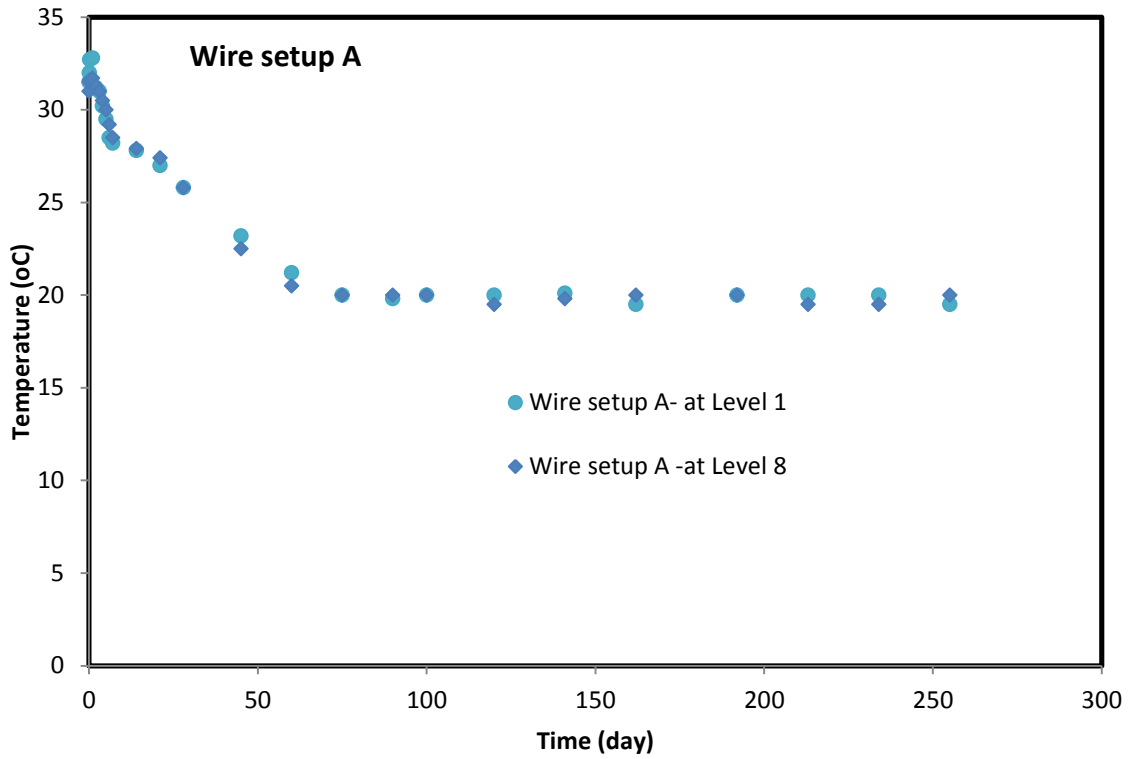


Figure 7-53: The variation of temperature throughout the curing period for thermocouples placed along wire setup A

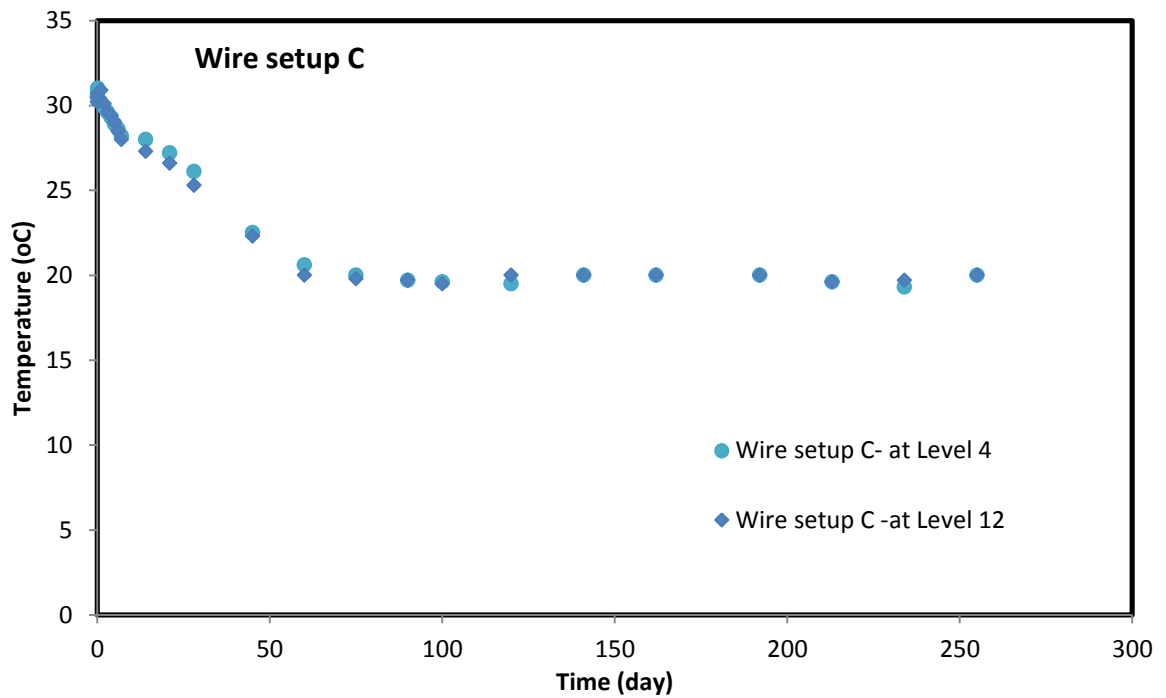


Figure 7-54: The variation of temperature throughout the curing period for thermocouples placed along wire setup C

7.3 Big lab model 2

7.3.1 Detecting the presence of cement slurry by resistance measurements in big lab model 2 during installation

Cement slurry is taken to fill the casing step by step and the resistance was measured to check whether the presence of cement slurry can be known from the change of resistance. Fig. 7-55 showed the resistance change through the vertical wire setup B while cement slurry is being filled up to a certain wire level. We can see from the plot that the resistance between wire combination B1-B3 before the cement slurry is filled to level 3 was about 22.7 k Ω which becomes around 22-24 Ω only when the cement slurry reached level 3. Similarly, for wire combinations B1-B5 , B1-B7, B1-B9, B1-B11, B1-B13 the resistance varied from 16.5 k Ω to 20.7 k Ω before both the two levels of wires became in the cement slurry, but as long as both wires were inside the cement slurry, the resistance was dropping down sharply to about 18-21 Ω only. This sharp dropping down of the resistance value tells us that the cement slurry reached up to that certain wire level. For wire level D, we can see from the plot (Fig. 7-56) that the vertical resistance between wire combination D1-D3 before the cement slurry is filled to level 3 was about 17.5 k Ω which becomes around 12-13 Ω only when the cement slurry reached level 3. Similarly, for wire combinations D1-D5 , D1-D7, D1-D9, D1-D11, D1-D13 the resistance varied from 15.9 k Ω to 17.8 k Ω before both the two levels of wires became in the cement slurry, but as long as both wires were inside the cement slurry, the resistance was dropping down sharply to about 12-14 Ω only. This sharp dropping down of the resistance value tells us that the cement slurry reached up to that certain wire level.

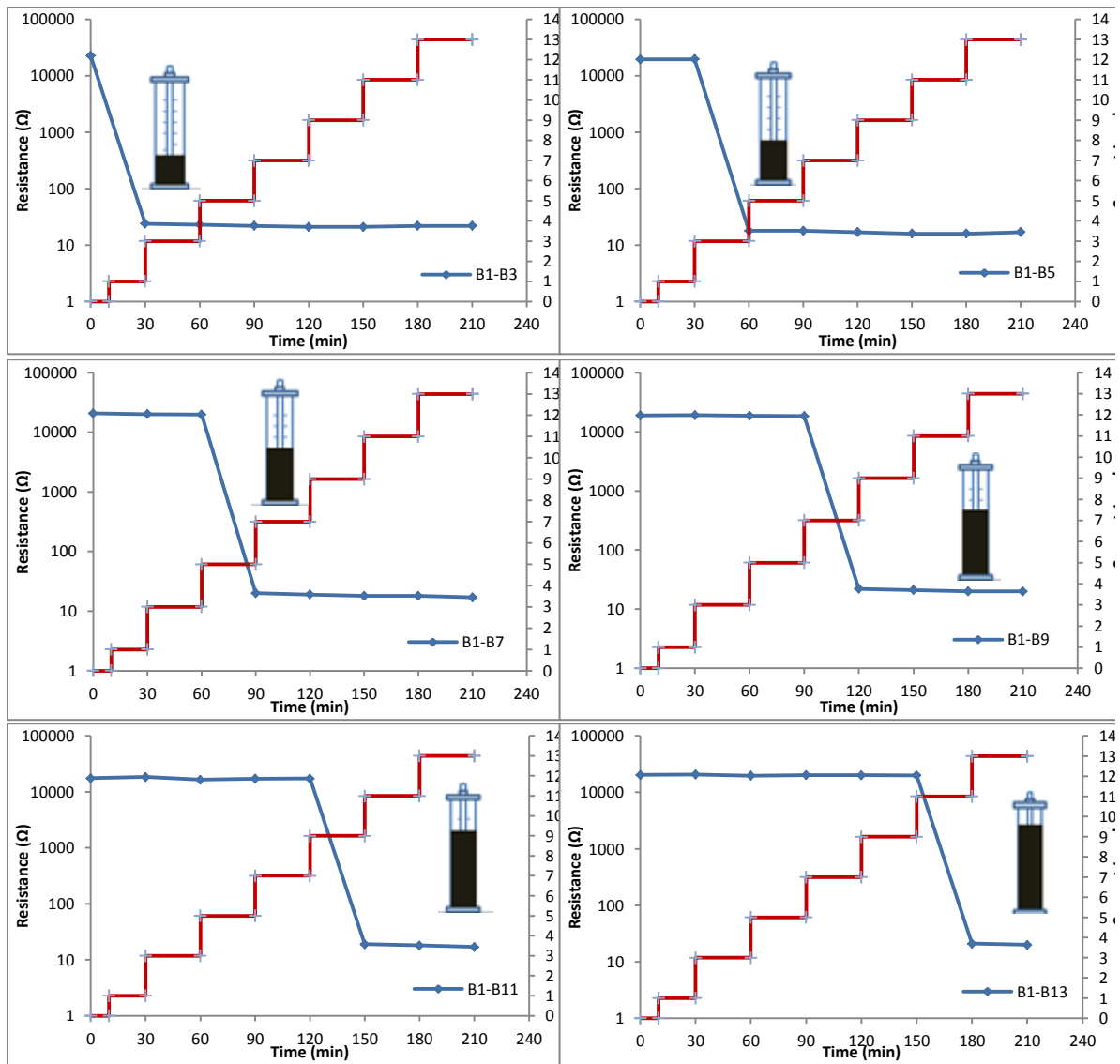


Figure 7-55: The change of vertical resistance along wire setup B with cement slurry filling for big lab model 2

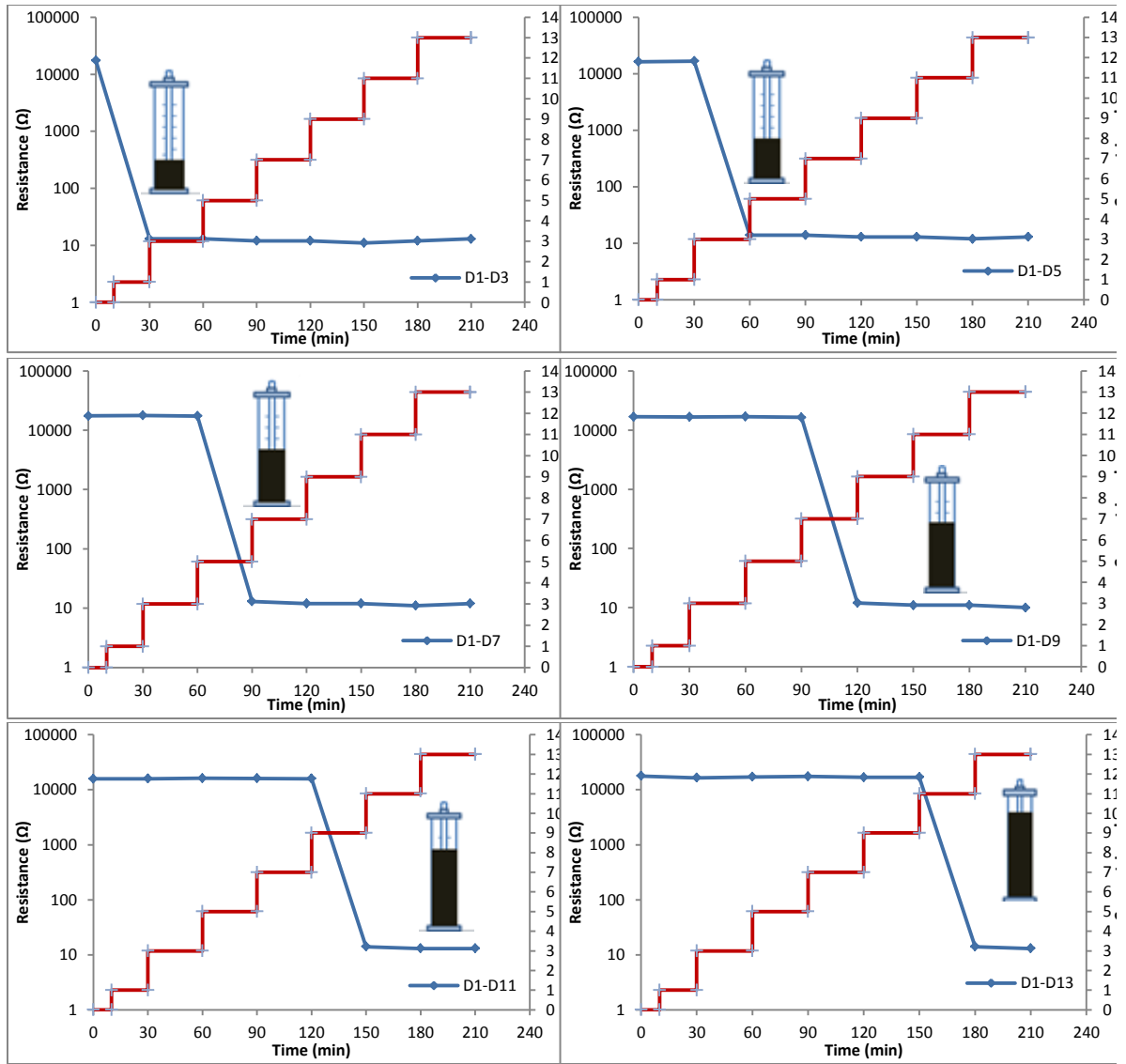


Figure 7-56: The change of vertical resistance along wire setup D with cement slurry filling for big lab model 2

For variation of resistance for the horizontal wire combination B-D at level different level are showed in Fig. 7-57. We can see from the plot that the horizontal resistance between wire combination B3-D3 before the cement slurry is filled to level 3 was about 16.5 kΩ which becomes around 17-18Ω only when the cement slurry reached level 3. Similarly, for wire combinations B5-D5 , B7-D7, B9-D9, B11-D11, B13-D13 the resistance varied from 16.4 kΩ to 17.5 kΩ before levels of wires became in the

cement slurry, but as long as wire level became inside the cement slurry, the resistance was dropping down sharply to about 17-19Ω only. This sharp dropping down of the resistance value tells us that the cement slurry reached up to that certain wire level.

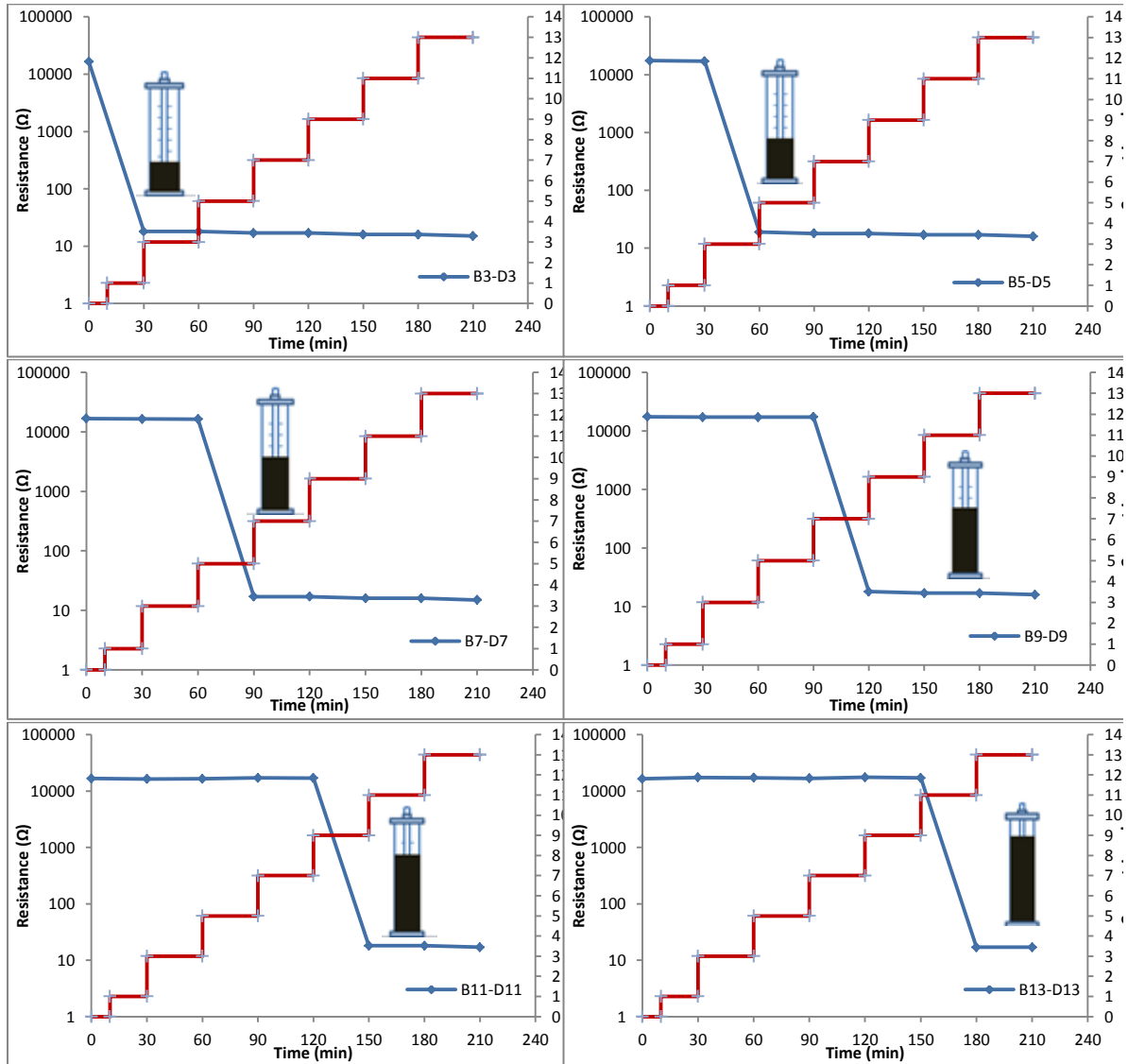


Figure 7-57: The change of horizontal resistance for wire set up B-D at different level with cement slurry filling for big lab model 2

7.3.2 Prediction and compare the measured resistance value during different curing time after cement slurry is placed in the wellbore around casing

7.3.2.1 Determination of Geometric parameter K for the different wire combination

The K parameter (i.e. L/A) for the wire setup A, B, C and D with different wire spacing were first determined filling the cement slurry. To do this, the resistivity of the cement slurry was determined by direct resistivity measurement device and the resistance between the wire combinations was determined with resistance measurement device (LCR meter). The results of the K values are shown below (Fig. 7-58 to 7-60) and the average value, maximum value, and minimum values are shown in the table below (Table 7-8 to 7-10) for wire setup B, B and horizontal combination B-D respectively.

For wire setup B, the average K parameter are found to be varied from 18.5 to 25 m^{-1} with standard deviations varying from 1.3 to 8.6 m^{-1} for different wire spacing (Fig. 7-58 and Table 7-8).

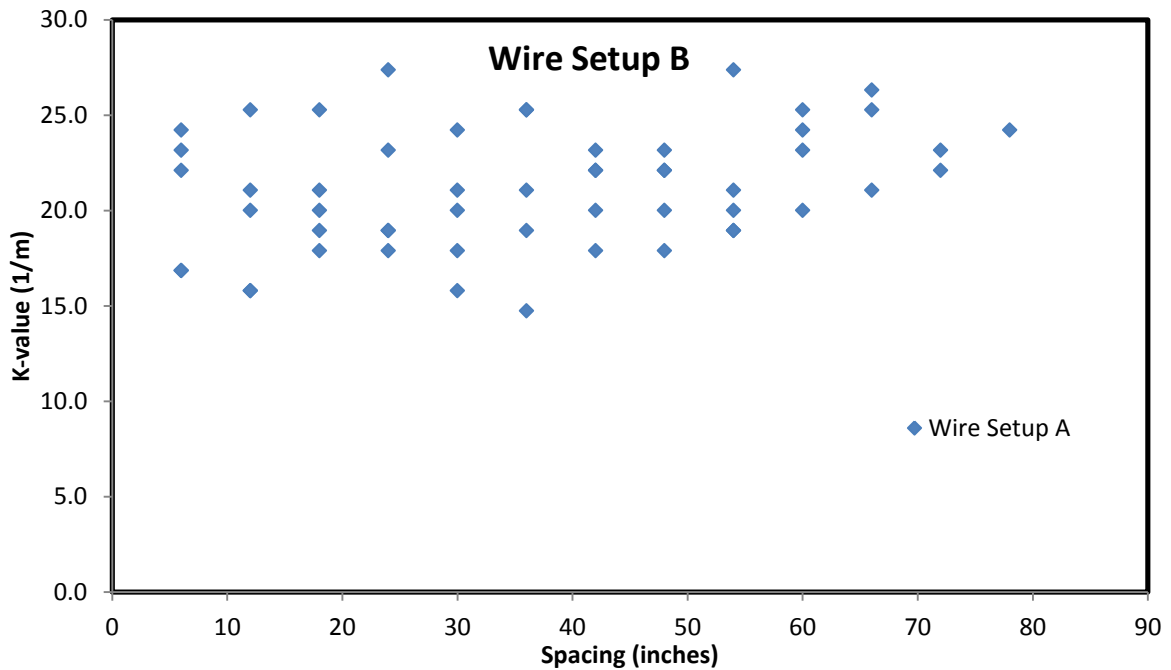


Figure 7-58: K parameter for wire setup B for big lab model 2

Table 7-8: Variations of K parameter for wire setup B for big lab model 2

	6 inches	12 inches	18 inches	24 inches	30 inches	36 inches	42 inches	48 inches	54 inches	60 inches	66 inches	72 inches
Avg	20.6	19.6	20.6	21.3	19.8	21.1	21.1	21.1	21.3	23.2	24.2	20.6
Min	16.8	15.8	17.9	17.9	15.8	14.7	17.9	17.9	18.9	20.0	21.1	18.1
Max	24.2	25.3	25.3	27.4	24.2	25.3	23.2	23.2	27.4	25.3	26.3	23.2
Std. dev	1.5	1.0	1.8	1.0	1.2	1.5	1.1	1.1	1.5	1.3	1.8	1.6
No of Data	24	24	24	24	18	18	18	18	12	12	12	12

And for wire setup D, the average K parameter were found to be varied from 15.3 to 19.2 m⁻¹ with standard deviations varying from 0.8 to 6.8 for different wire spacing (Fig. 7-59 and Table 7-9).

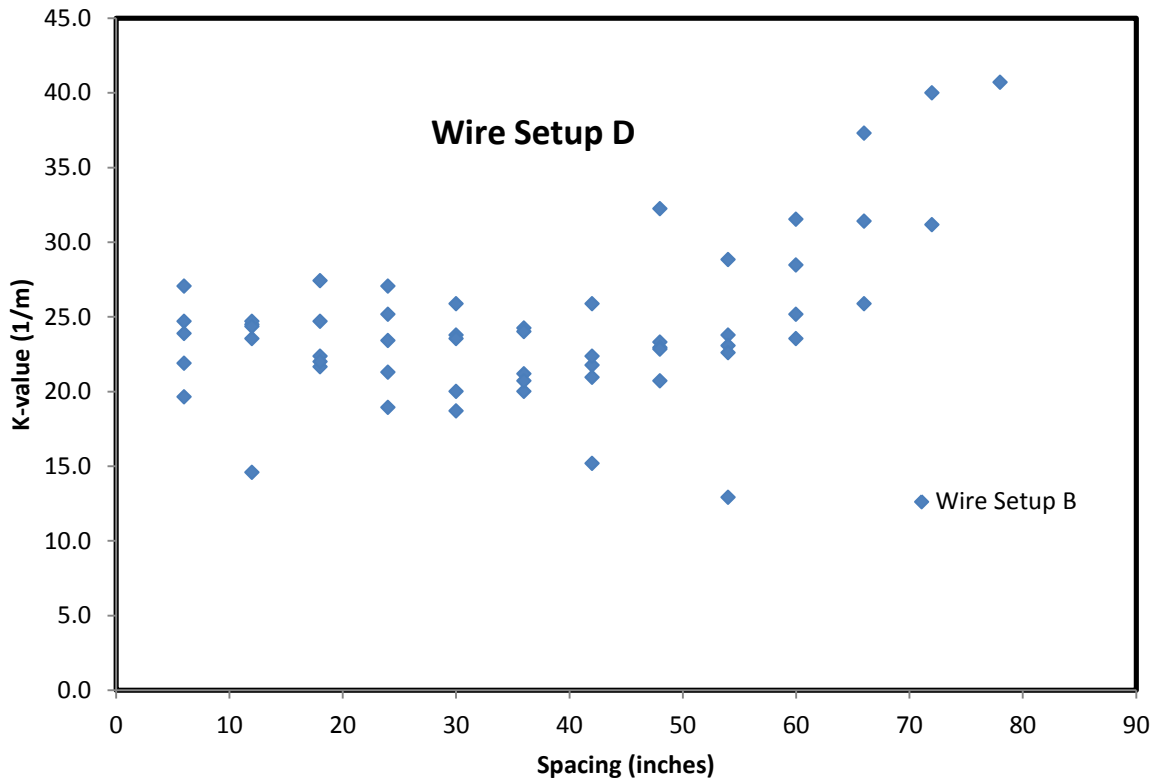


Figure 7-59: K parameter for wire setup D for big lab model 2

Table 7-9: Variations of K parameter for wire setup D for big lab model 2

	6 inches	12 inches	18 inches	24 inches	30 inches	36 inches	42 inches	48 inches	54 inches	60 inches	66 inches	72 inches
Avg	15.3	16.5	16.2	16.0	17.6	17.4	16.5	16.0	15.8	16.1	19.2	15.3
Min	14.1	15.3	12.9	14.1	16.5	15.3	14.1	14.1	14.1	14.0	15.3	13.0
Max	18.8	17.6	20.0	17.6	18.8	18.8	18.8	17.6	21.2	17.6	27.1	17.6
Std. dev	1.0	0.8	1.7	1.3	1.2	1.5	0.9	1.6	1.1	1.5	1.8	0.8
No of Data	24	24	24	24	18	18	18	18	12	12	12	12

And for horizontal wire combination B-D, the average K parameter are found to be varied from 16.7 to 19.2 m⁻¹ with standard deviations varying from 2 to 3.6 for different wire level (Fig. 7-60 and Table 7-10).

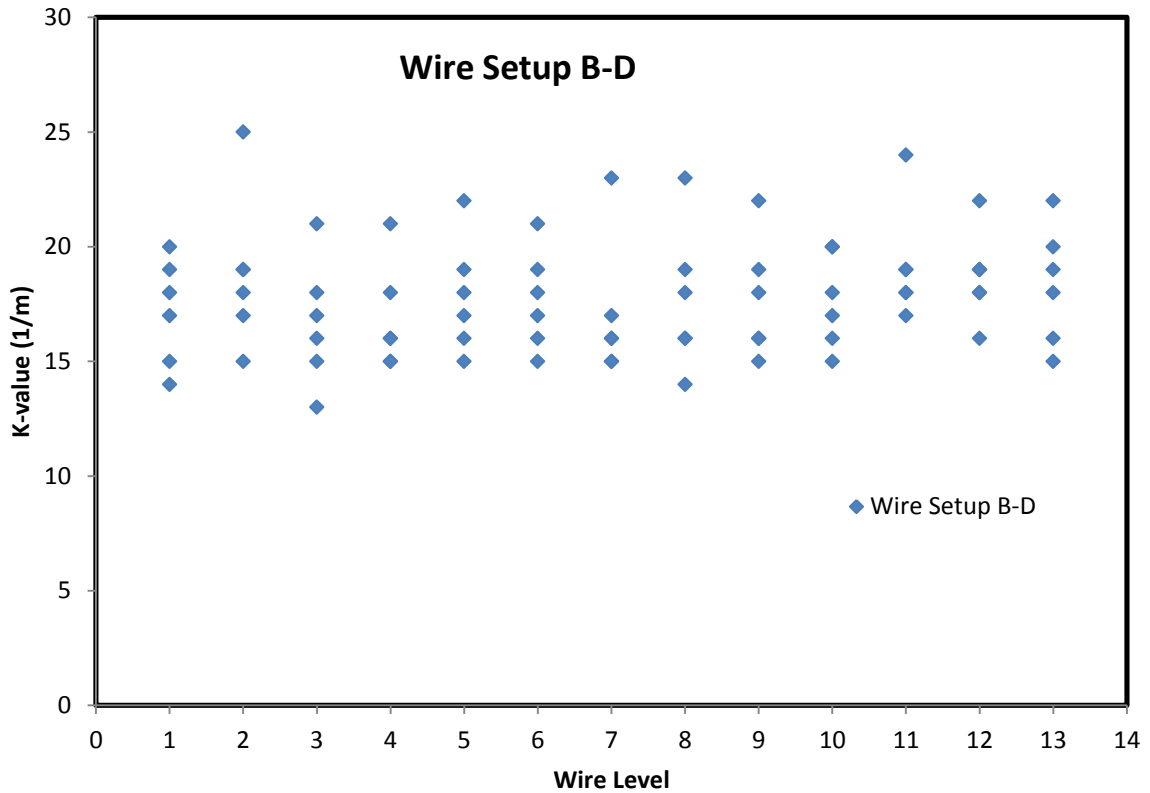


Figure 7-60: K parameter for wire setup B-D for big lab model 2

Table 7-10: Variations of K parameter for wire setup B-D for big lab model 1

Level	1	2	3	4	5	6	7	8	9	10	11	12	13
Avg	17.2	18.8	16.7	16.8	17.8	17.7	17.0	17.7	17.7	17.7	19.2	18.7	18.3
Min	14.0	15.0	13.0	15.0	15.0	15.0	15.0	14.0	15.0	15.0	17.0	16.0	15.0
Max	20.0	25.0	21.0	21.0	22.0	21.0	23.0	23.0	22.0	20.0	24.0	22.0	22.0
Std. dev	1.3	1.4	1.7	1.3	1.5	1.2	1.0	1.1	1.6	1.1	1.5	1.0	1.6
No of data	12	12	12	12	12	12	12	12	12	12	12	12	12

7.3.2.2 Predicted resistance Vs measured resistance

From Fig. 7-33, we know the resistivity of cement slurry with curing time. From Fig. 7-58 to 7-60 and Table 7-8 to 7-10 we know the K parameter that can be used to

calculate the resistivity of the cement slurry at different time having the resistance measured. If we back calculate the possible values of resistance from the same equation using the average, minimum, and maximum K parameter, we can find the predicted resistance values. Fig. 7-61 to Fig. 7-66 shows the variations of the predicted resistance value and also the actual measured values for wire setup B. Fig. 7-67 to Fig. 7-72 shows the variations of the predicted resistance value and also the actual measured values for wire setup D. Also, Fig. 7-73 to Fig. 7-79 shows the variations of the predicted resistance value and also the actual measured values for horizontal wire setup B-D at different level.

The measured resistances for wire combination 1-3 and 1-5 are lower than the range of minimum values of the predicted range of resistances (Fig. 7-61, 7-62). It may be due to the less moisture loss of that bottom part of the cement level.

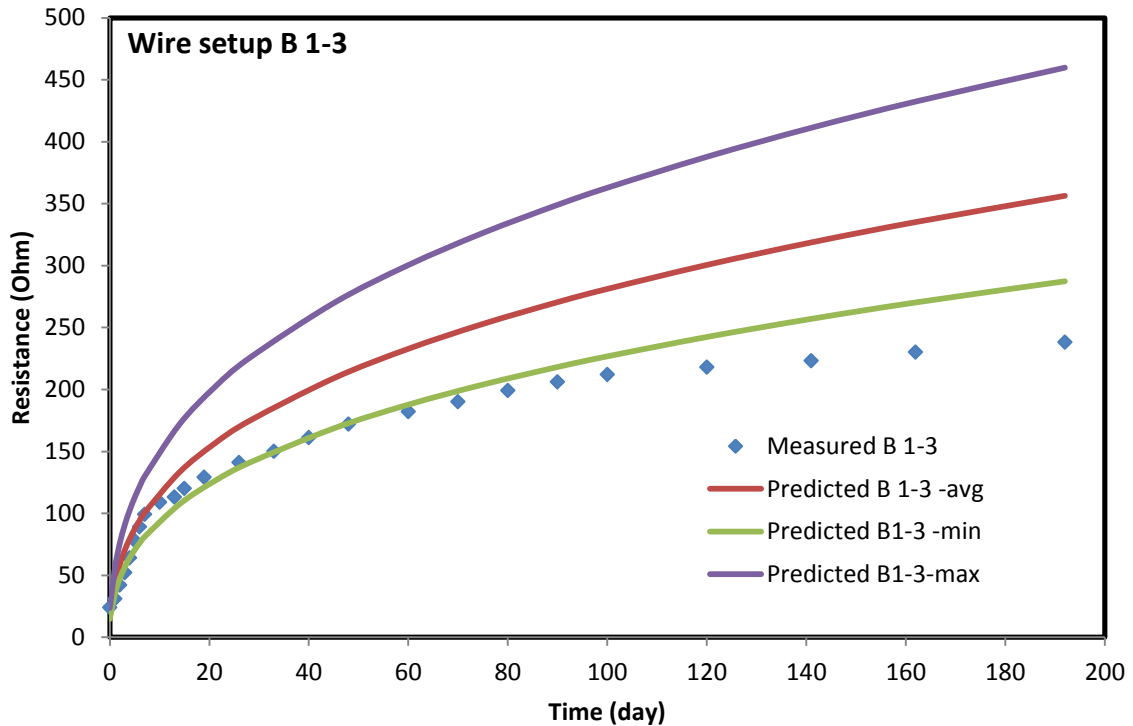


Figure 7-61: Predicted and measured resistance for wire setup B for wire combination 1-3

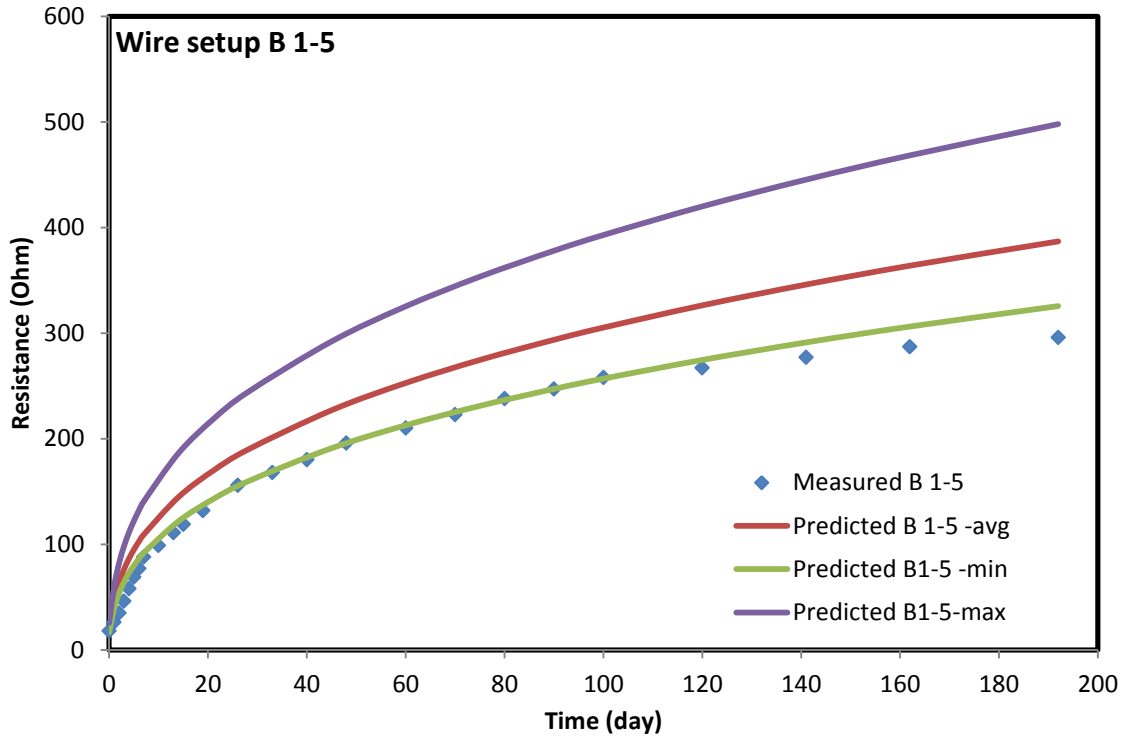


Figure 7-62: Predicted and measured resistance for wire setup B for wire combination 1-5

For the wire combination 1-7 and 1-9, the predicted values are matching very well with those of the predicted values (Fig. 7-63, Fig. 7-64). This supports the curing condition of the small samples are similar with that of big physical model. The measured resistances for wire combination 1-11 and 1-13 are also in between the range of predicted values of the resistance (Fig. 7-65, Fig. 7-66). Only little exception is that there is some values go slightly away of the range which can be explained as having little more moisture loss than that of small sample.

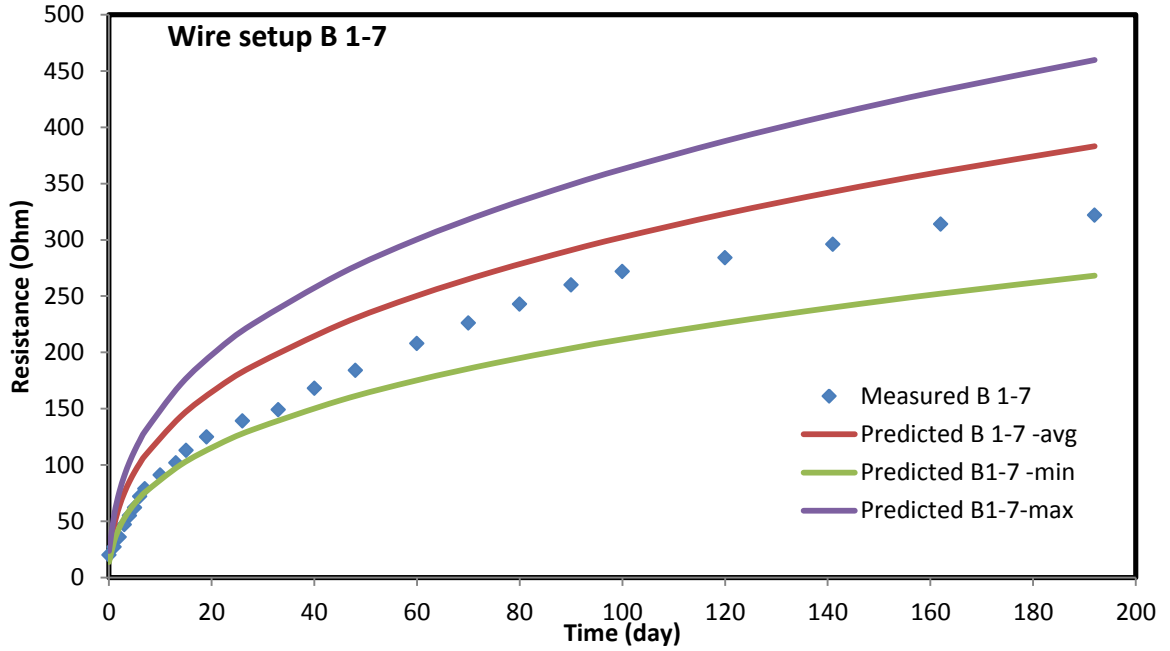


Figure 7-63: Predicted and measured resistance for wire setup B for wire combination 1-7

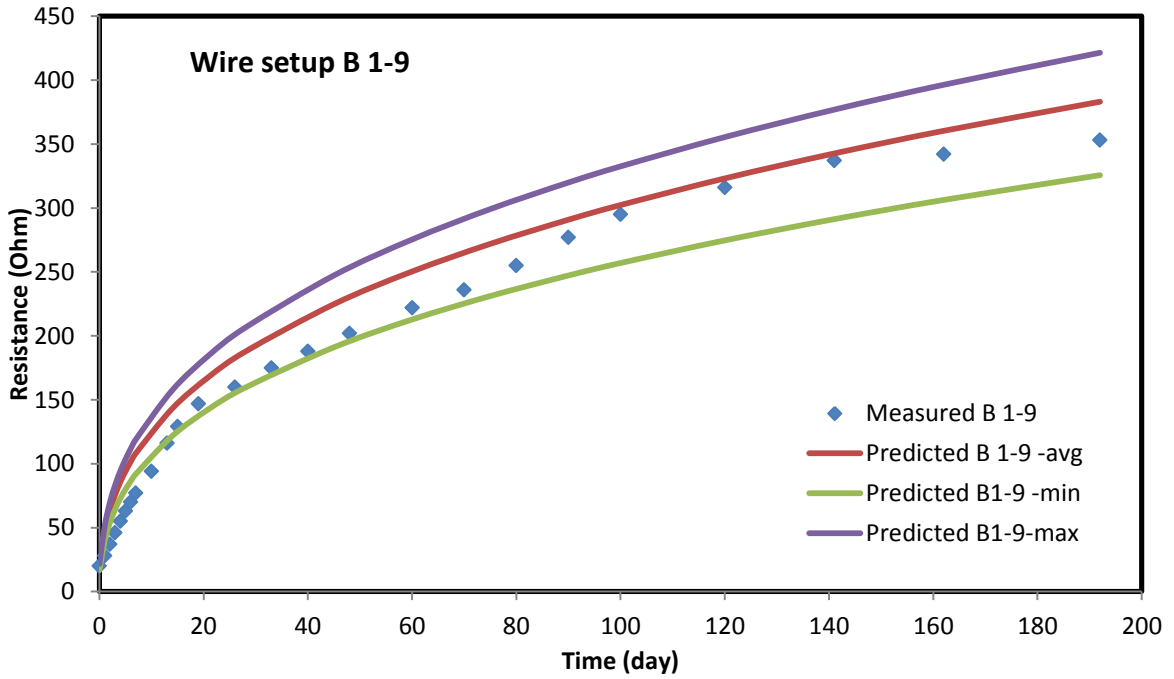


Figure 7-64: Predicted and measured resistance for wire setup B for wire combination 1-9

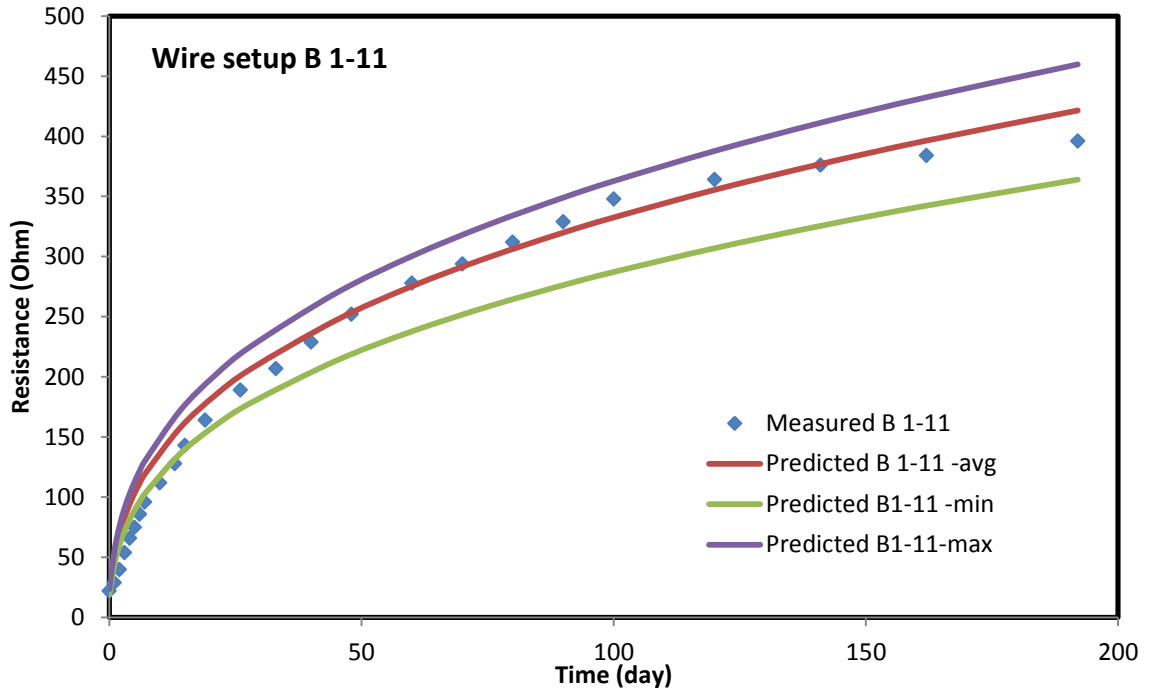


Figure 7-65: Predicted and measured resistance for wire setup B 1-11

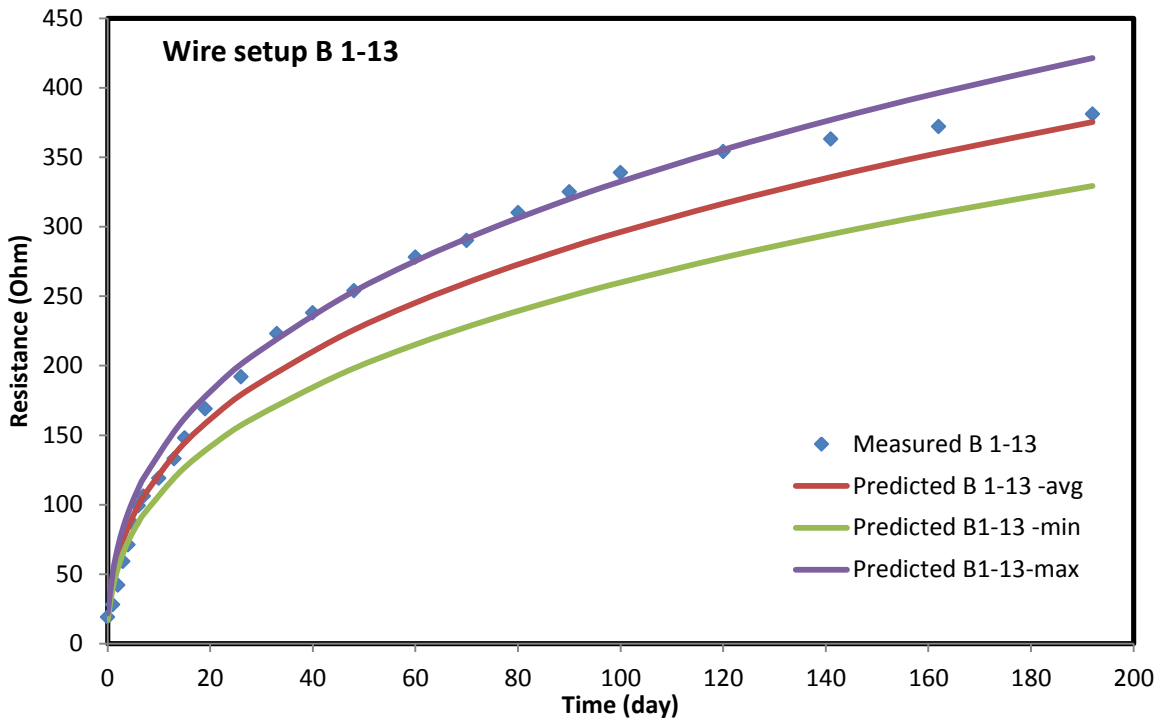


Figure 7-66: Predicted and measured resistance for wire setup B 1-13

The measured resistance for wire combination 1-3 and 1-5 in wire setup D were less than the predicted values for those combinations (Fig. 7-67, Fig. 7-68). We can see that these levels are at lower part of the model where the moisture loss may be very less compare to that of small samples. That's why the measured resistances are less than the predicted range. For wire setup 1-7 and 1-9, the measured resistances are little lower than the predicted resistances (Fig. 7-69, 7-70). These may be due to the different curing condition of the model and the small samples.

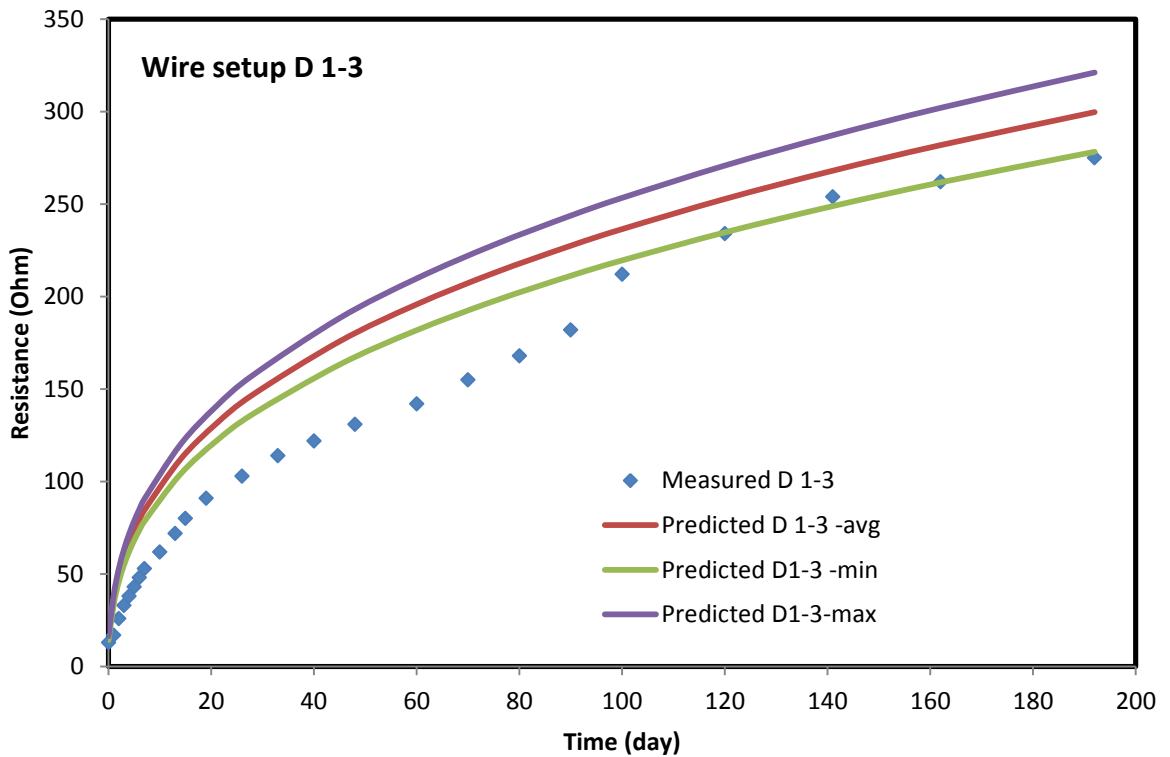


Figure 7-67: Predicted and measured resistance for wire setup D for wire combination 1-3

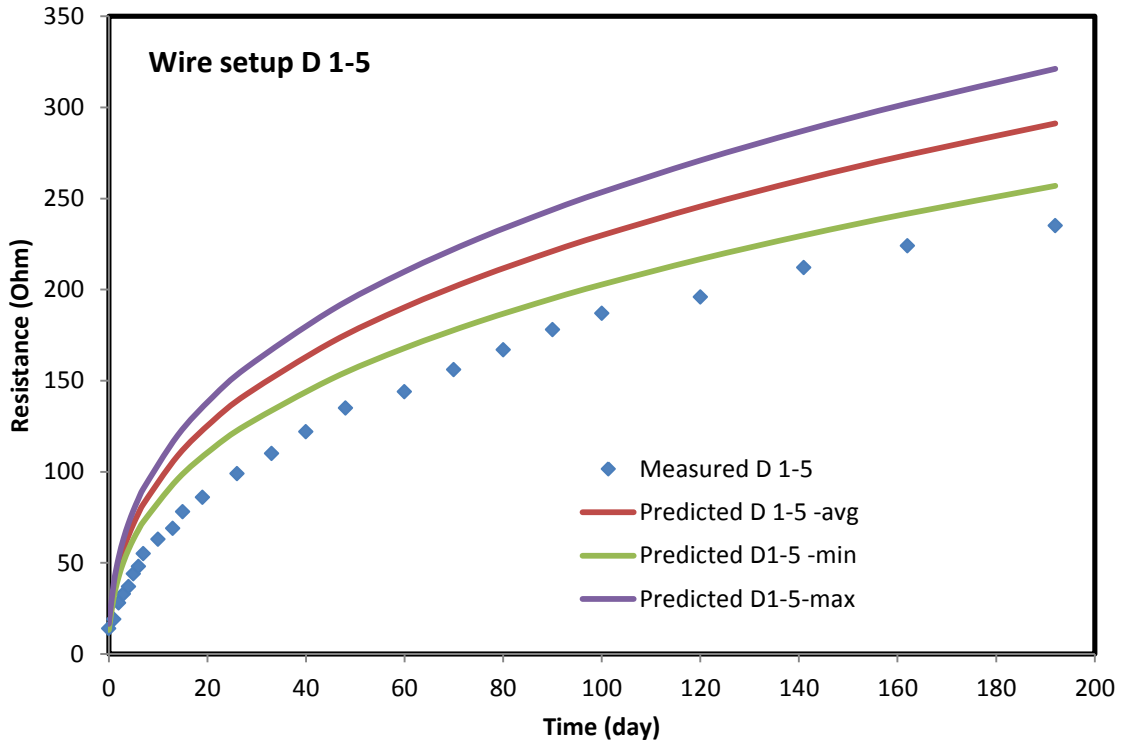


Figure 7-68: Predicted and measured resistance for wire setup D for wire combination 1-5

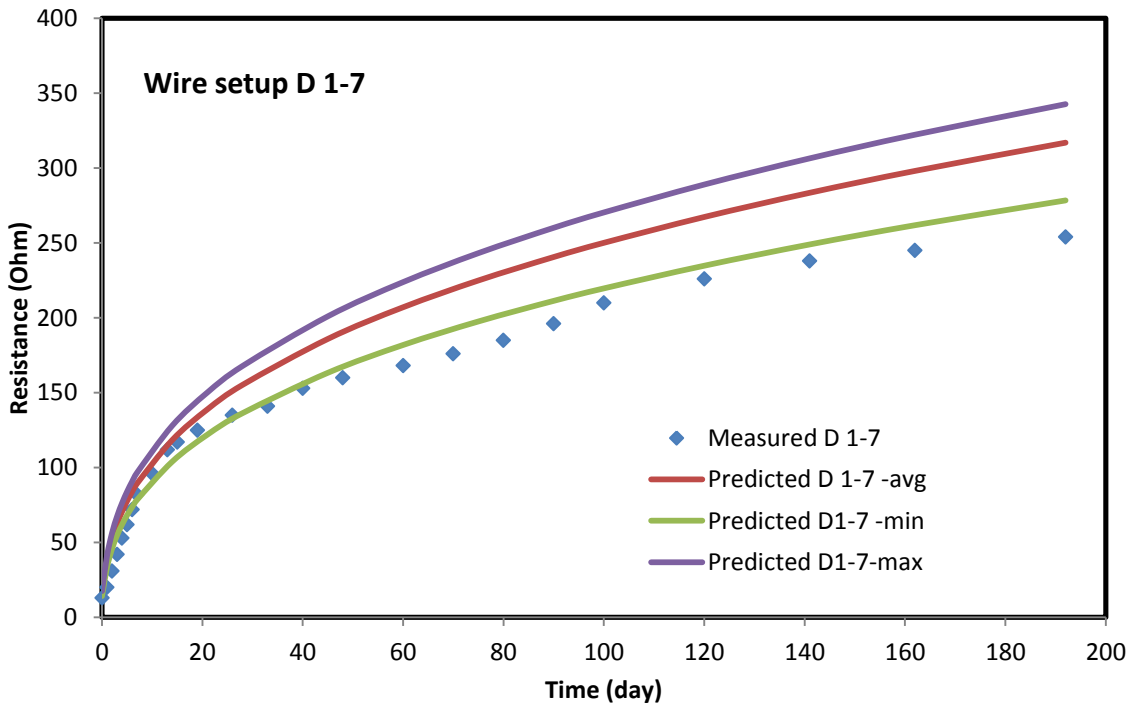


Figure 7-69: Predicted and measured resistance for wire setup D for wire combination 1-7

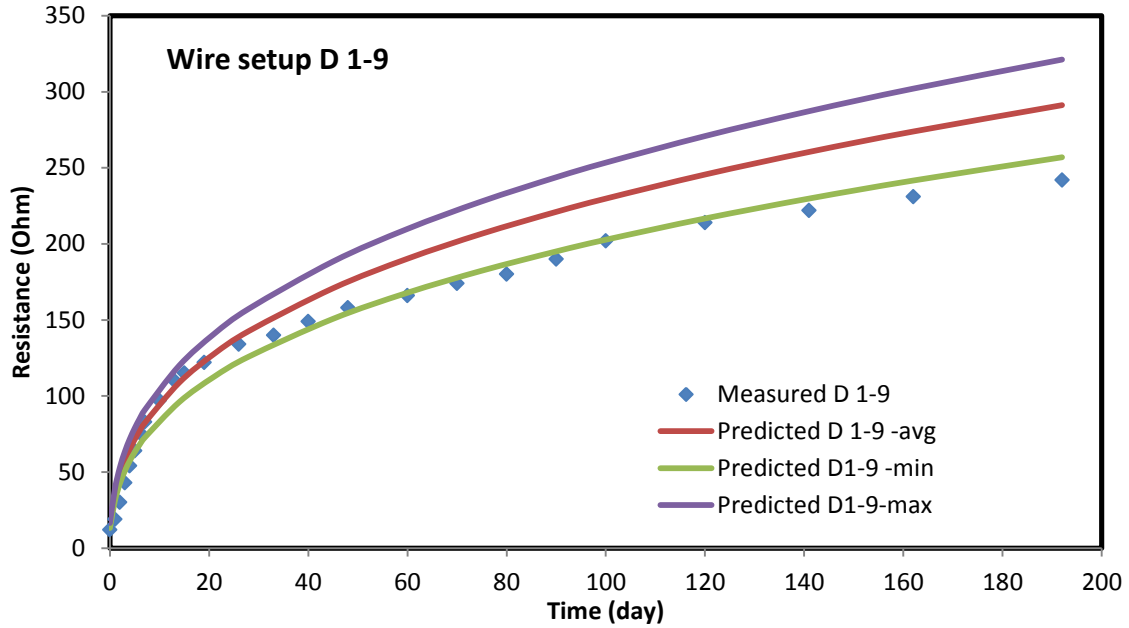


Figure 7-70: Predicted and measured resistance for wire setup D for wire combination 1-9

The measured resistance for wire combination 1-11 and 1-13 were very much within the range of predicted values (Fig. 7-71, 7-72). This supports the curing condition of the small samples are similar with that of big physical model. For the horizontal wire combination B-D at level 1 and 3, the measured values are less than those of the range of the predicted values (Fig. 7-73, 7-74) for initial curing time up to 30 days. As these levels are at lower part of the model where the moisture loss may be very less compare to that of small samples. That's why the measured resistances are less than the predicted range.

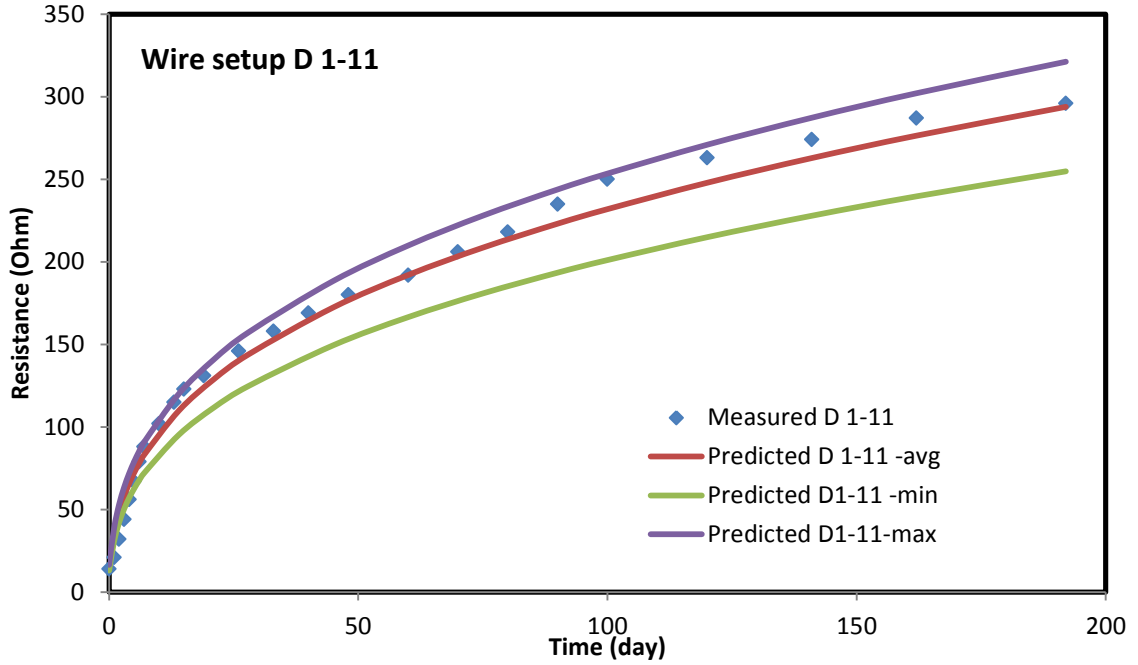


Figure 7-71: Predicted and measured resistance for wire setup D 1-11

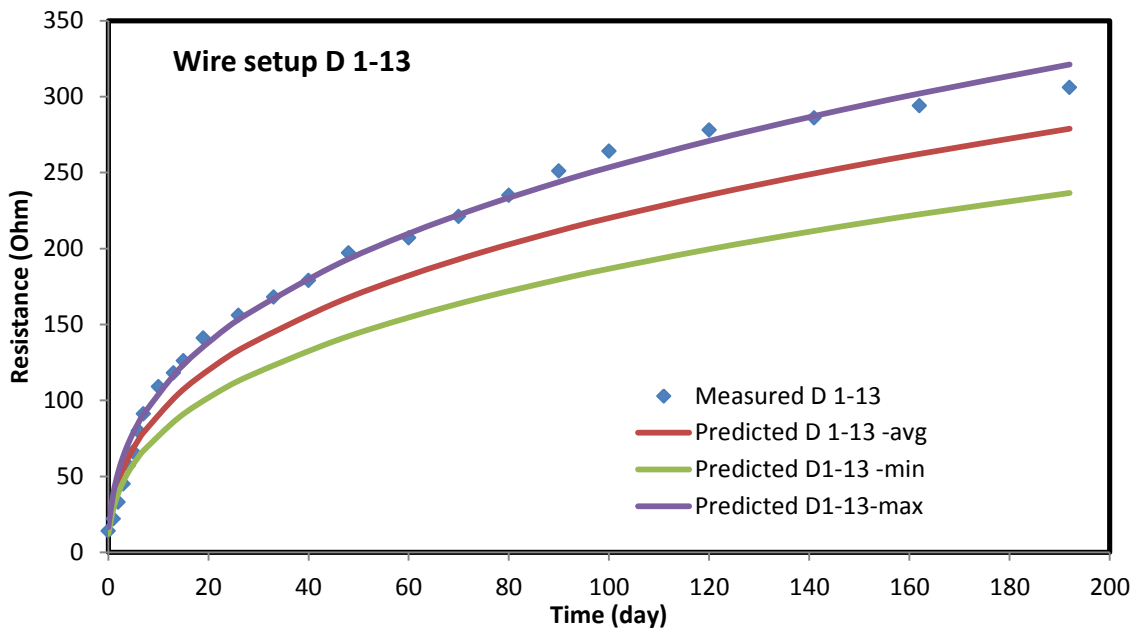


Figure 7-72: Predicted and measured resistance for wire setup D 1-13

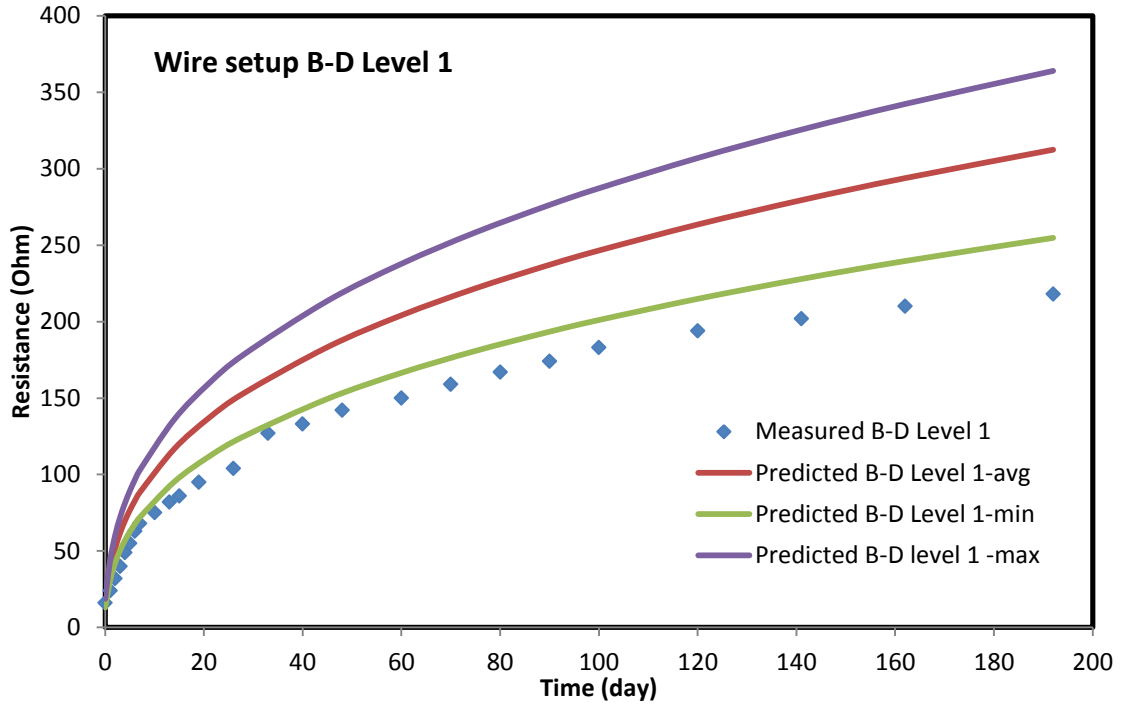


Figure 7-73: Predicted and measured horizontal resistance for wire setup B-D at level 1

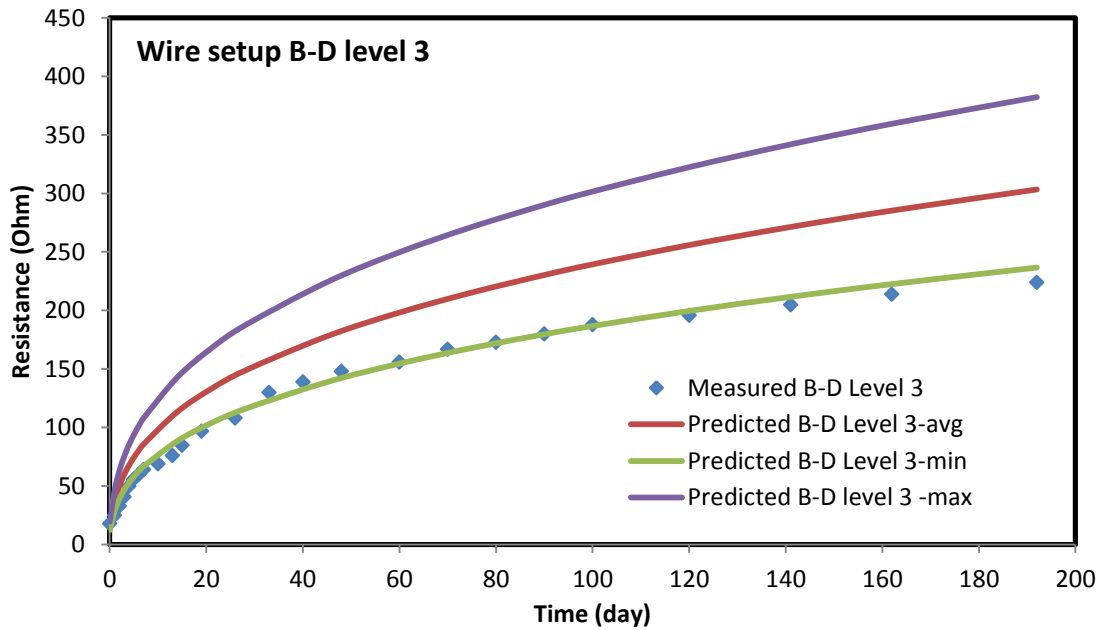


Figure 7-74: Predicted and measured horizontal resistance for wire setup B-D at level 3

At level 5, 7, and 9 the measured values are matching very well within the range of the predicted values (Fig. 7-75, 7-76, 7-77). This supports that the curing condition are similar to those of the small sample. At level 11, the measured values are matching well with the predicted values (Fig. 7-78) but at level 13, the measured values are higher than the predicted range (Fig. 7-79). We can say that the moisture loss may be higher than for that level as it is near the top of the model.

7.3.3 Temperature variation at different levels

Thermocouples were placed to determine the variation of temperature during the curing time. With wire setup B, two thermocouples were placed at level 2 and 9; and for wire setup D, two thermocouples were placed at level 5 and 13. For wire setup B at level 2, the temperature started from 29.5 °C and increased up to 31.8 °C after several hours and the decreased steadily up to 60 days to reach the room temperature (Fig. 7-80). The temperature at level 9 showed the similar trend throughout the curing period with a very little difference in the temperature. For wire setup D at level 4, the temperature started from 30.2 °C and increased up to 30.9 °C after several hours and the decreased steadily up to 50 days to reach the room temperature (Fig. 7-81). The temperature at level 13 showed the similar trend throughout the curing period with a very little difference in the temperature.

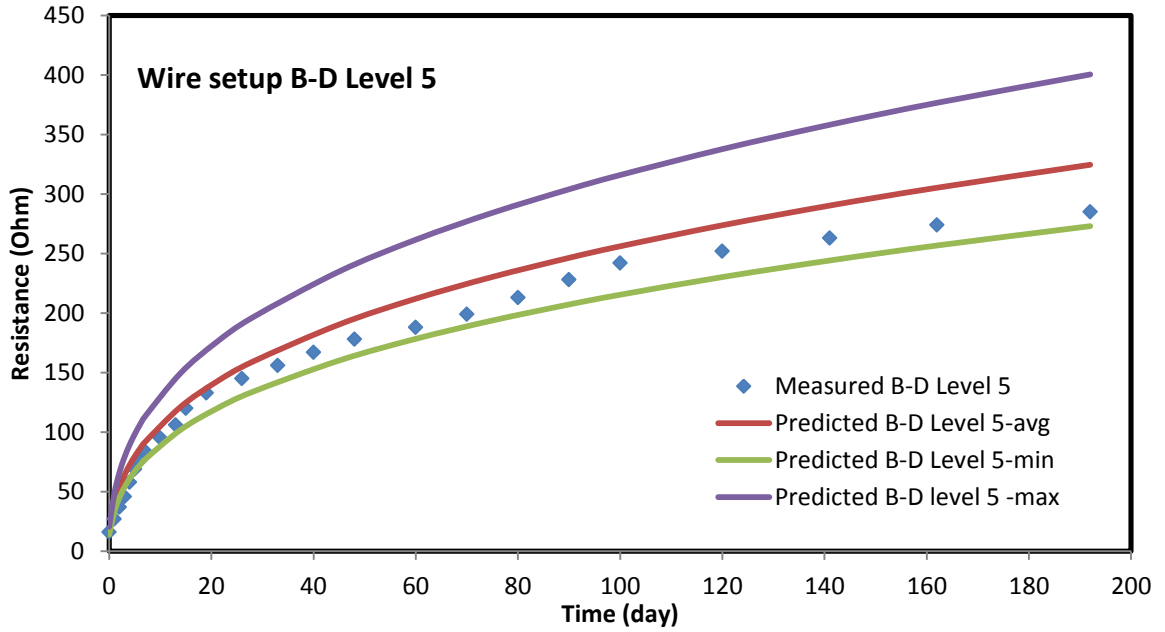


Figure 7-75: Predicted and measured horizontal resistance for wire setup B-D at level 5

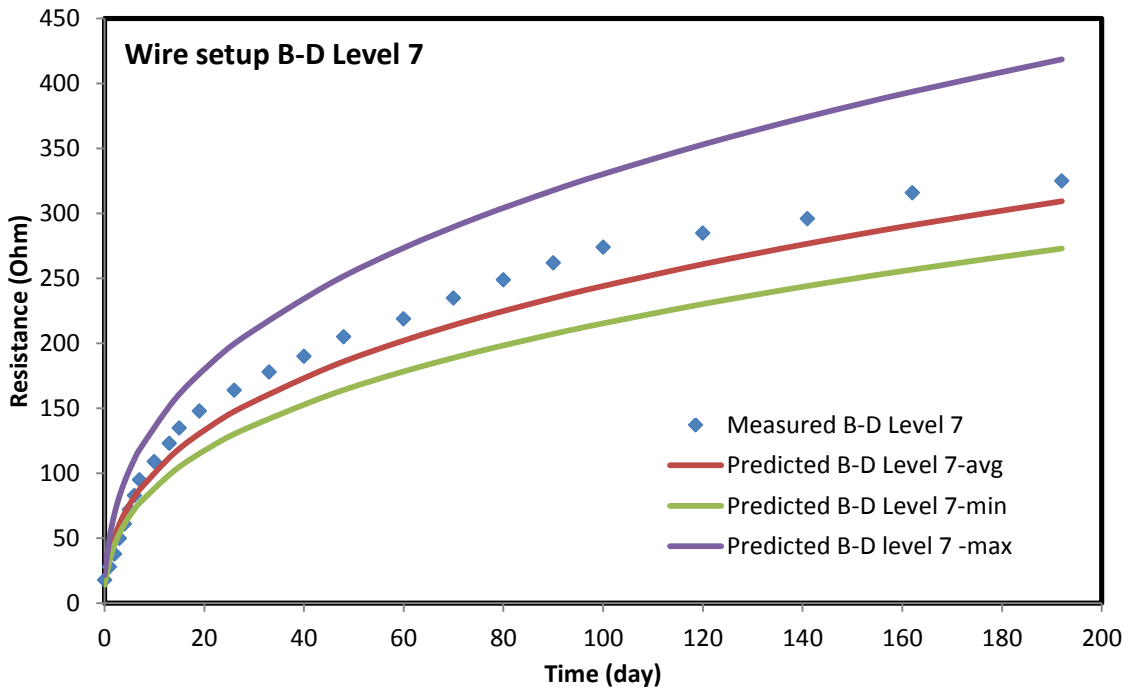


Figure 7-76: Predicted and measured horizontal resistance for wire setup B-D at level 7

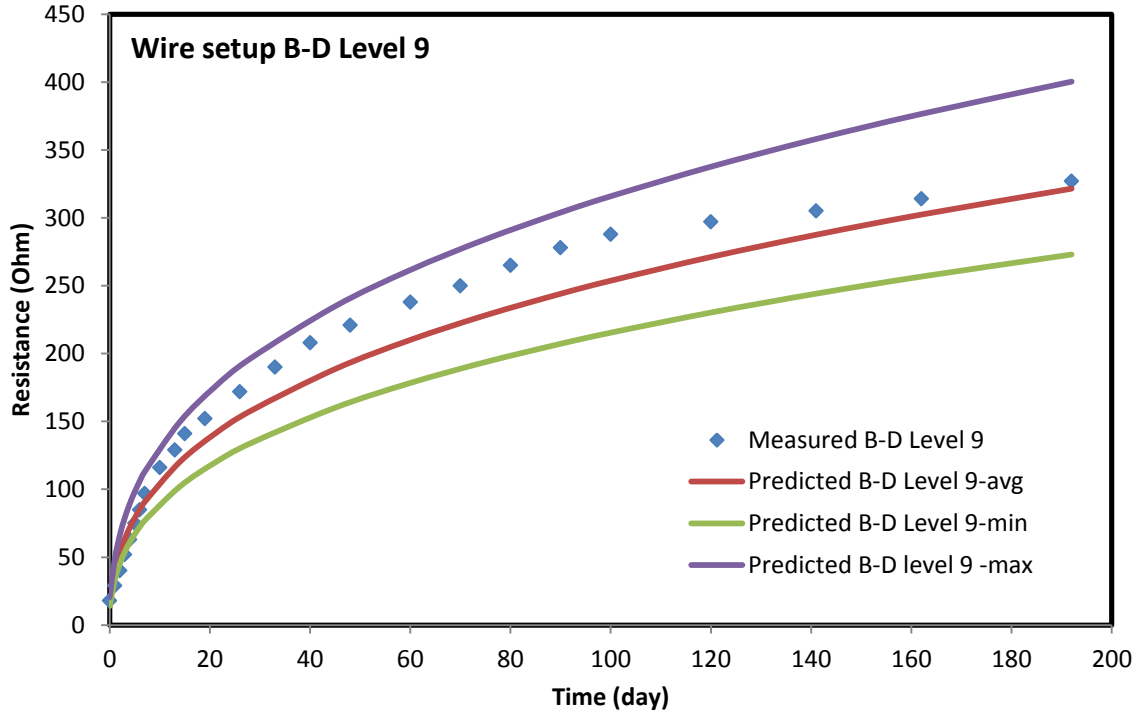


Figure 7-77: Predicted and measured horizontal resistance for wire setup B-D at level 9

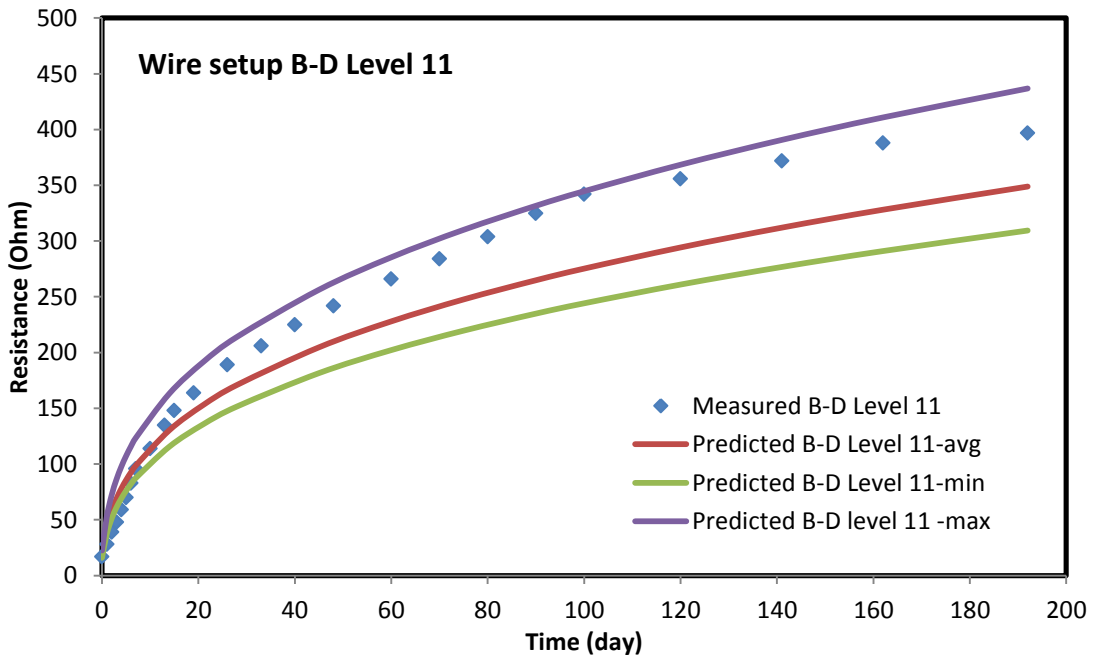


Figure 7-78: Predicted and measured horizontal resistance for wire setup B-D at level 11

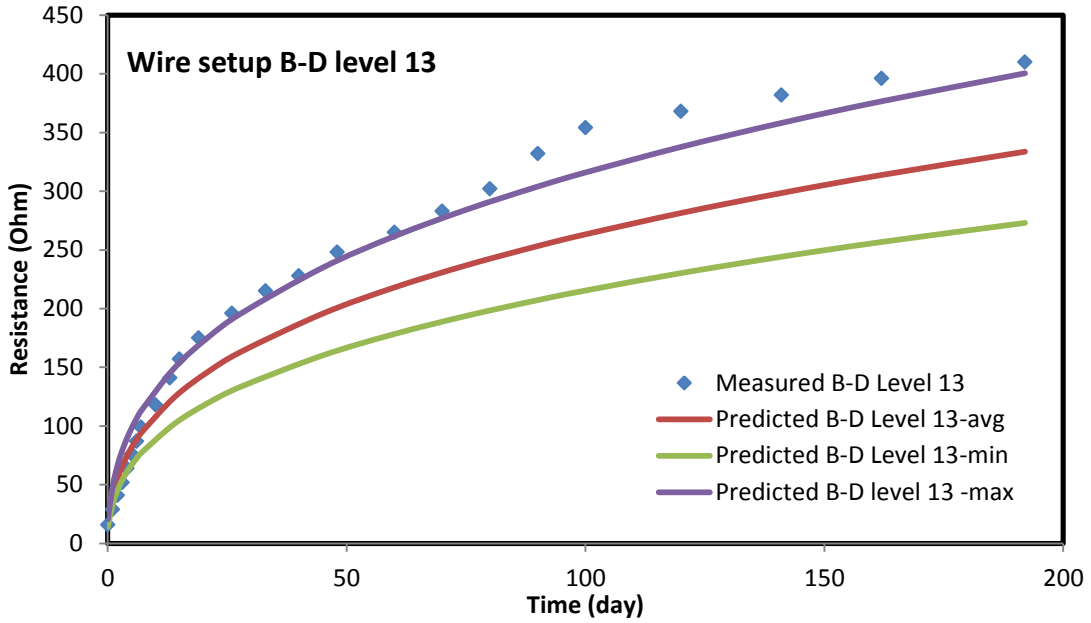


Figure 7-79: Predicted and measured horizontal resistance for wire setup B-D at level 13

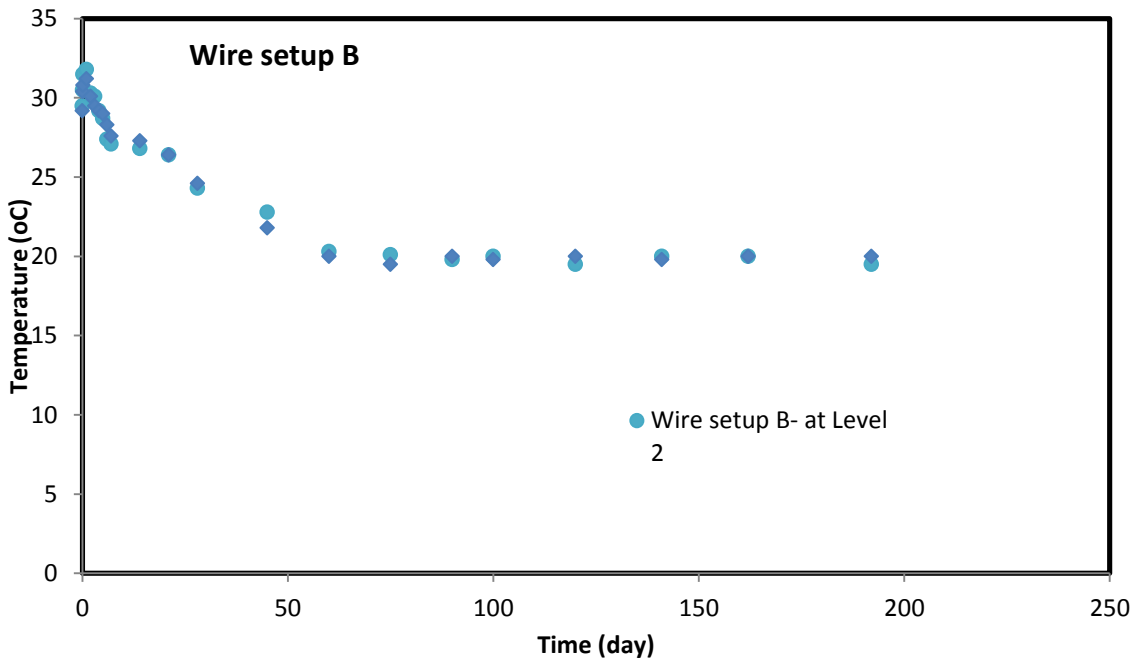


Figure 7-80: The variation of temperature throughout the curing period for thermocouples placed along wire setup B

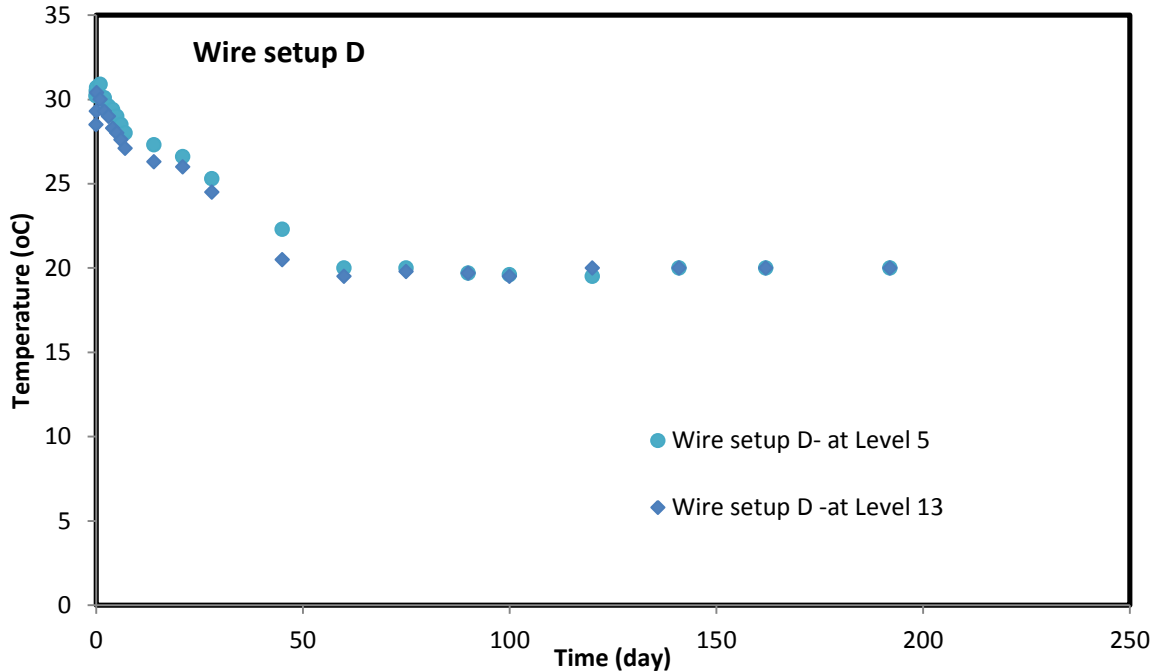


Figure 7-81: The variation of temperature throughout the curing period for thermocouples placed along wire setup D

7.4 Field model study

7.4.1 Prediction and measured resistance .

7.4.1.1 Determination of Geometric parameter K for the different wire combination

The K parameter (i.e. L/A) for the wire setup A, B, C, D, E, F, G and H with different wire spacing were first determined filling the cement slurry. To do this, the resistivity of the cement slurry was determined by direct resistivity measurement device and the resistance between the wire combinations was determined with resistance measurement device (LCR meter). The results of the K values are shown below (Fig. 7-82) and the average value, maximum value, and minimum values are shown in the table below (Table 7-11) for different wire combination.

For different wire combination, the average K parameter are found to be varied from 14.6 to 29.8 m^{-1} with standard deviations varying from 1.6 to 8.3 m^{-1} (Fig. 7-82 and Table 7-11).

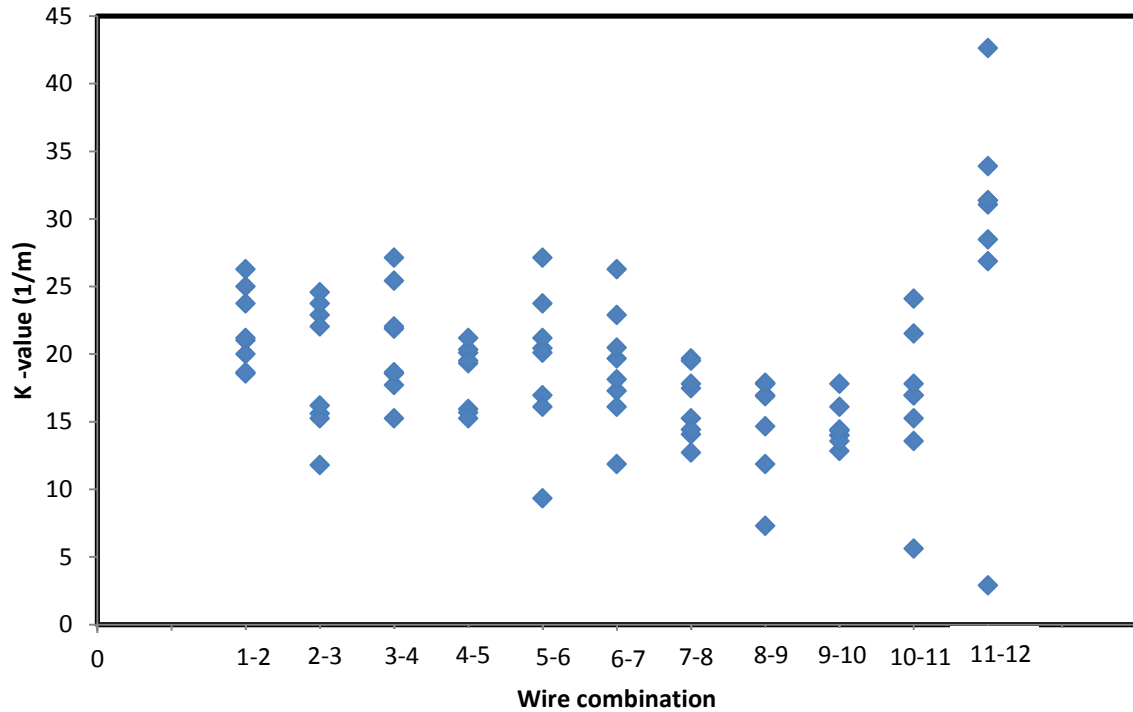


Figure 7-82: K parameter for different wire combination of the field model study

Table 7-11: Variations of K parameter for different wire combination of the field model

	1-2	2-3	3-4	4-5	5-6	6-7	7-8	8-9	9-10	10-11	11-12
	48 inches	48 inches	48 inches	24 inches	30 inches	36 inches	42 inches	48 inches	54 inches	60 inches	66 inches
Avg	21.8	19.0	20.8	18.4	19.4	19.1	16.4	15.1	14.6	16.5	29.8
Min	18.6	11.8	15.3	15.3	9.3	11.9	12.7	7.3	12.8	5.6	12.9
Max	26.3	24.6	27.1	21.2	27.1	26.3	19.7	17.9	17.8	24.1	42.6
Std. dev	1.9	1.8	2.0	1.4	2.4	2.4	2.6	2.8	1.6	2.5	3.3
No of data	16	16	16	16	16	16	16	16	16	16	16

7.4.1.2 Resistivity of the cement slurry with time

The Resistivity of the cement slurry with curing time of up to 110 days is determined using a small mold (2 inches diameter and 4 inches height cylindrical mold) with the same cement slurry that was used for the field model and cured under different curing conditions. The electrical resistivity was determined for a sample cured under moisture control (no moisture loss) condition, for a sample cured under room condition (a moisture loss of 2.8 % was calculated up to 110 days), and for a sample cured under water condition (a moisture gain of 1.2 % was calculated up to 110 days) . The resistivity shows an increasing trend with curing time (Fig. 7-83) which has been modeled with the curing model which is developed by modifying the p-q model proposed by Vipulanandan and Paul (1990) (Eqn. 3-11). The model parameters were for moisture control curing: $p_1=7.6$, $q_1=0.6$, and $t_0=70$ min; for room curing: $p_1=6.5$, $q_1=0.82$, and $t_0=72$ min; and for under water curing: $p_1=0.83$, $q_1=0.21$, and $t_0=58$ min

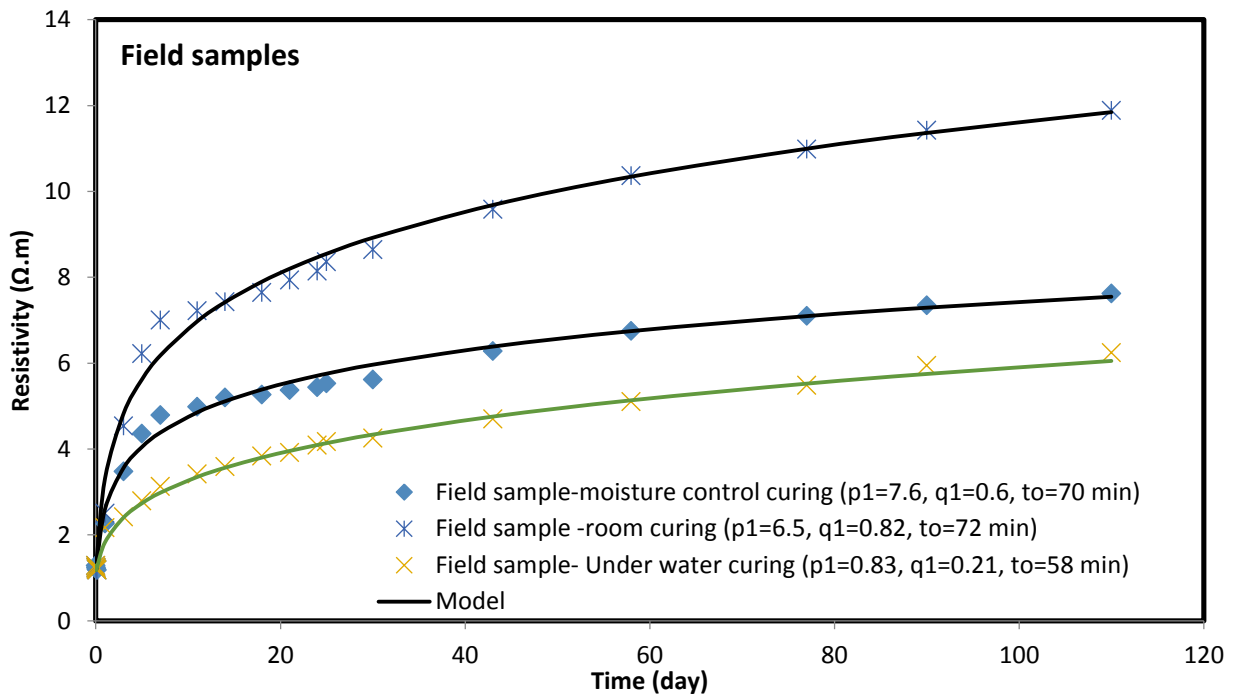


Figure 7-83: Resistivity of cement slurry with curing time

7.4.1.3 Predicted Resistance Vs Measured Resistance

From Fig. 7-83, we know the resistivity of cement slurry with curing time. From Fig. 7-82 and Table 7-11, we know the K parameter that can be used to calculate the resistivity of the cement slurry at different time having the resistance measured. If we back calculate the possible values of resistance from the same equation using the average, minimum, and maximum K parameter, we can find the predicted Resistance values. Fig. 7-84 to Fig. 7-94 show the variations of the predicted resistance value and also the actual measured values for wire setup E. Fig. 7-95 to Fig. 7-105 show the variations of the predicted resistance value and also the actual measured values for wire setup F. Also, Fig. 7-106 to Fig. 7-117 show the variations of the predicted resistance value and also the actual measured values for horizontal wire setup E-F at different level.

The measured resistance for wire combination 1-2 in wire setup E were in between the predicted range up to 11 days of curing but a little bit less than the predicted values after 11 days of curing. It may be due to the excess moisture inside the formation as wire combination 1-2 is inside the ground water level (Fig. 7-84). The measured resistance for wire combination 2-3 in wire setup E were very much within the range except for the initial 3-5 days of curing shows a little higher values than that of predicted values (Fig. 7-85). This may be because of the different curing condition of the small sample and the big physical model.

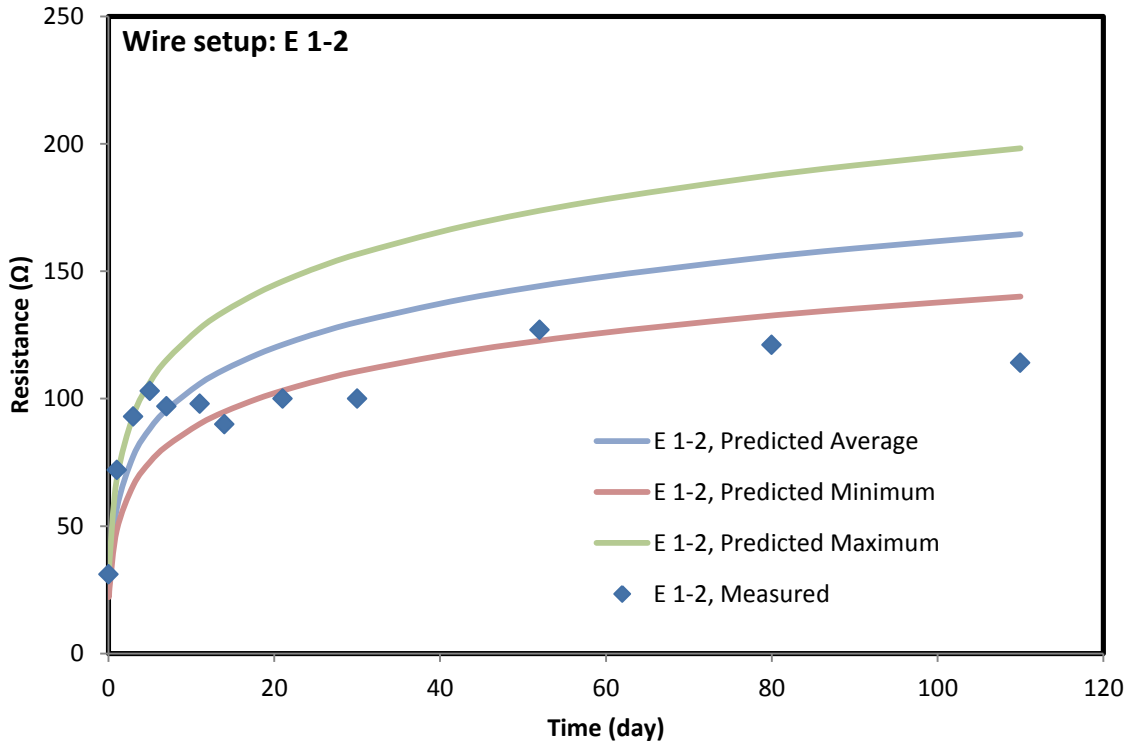


Figure 7-84: Predicted and measured vertical resistance for wire setup E 1-2

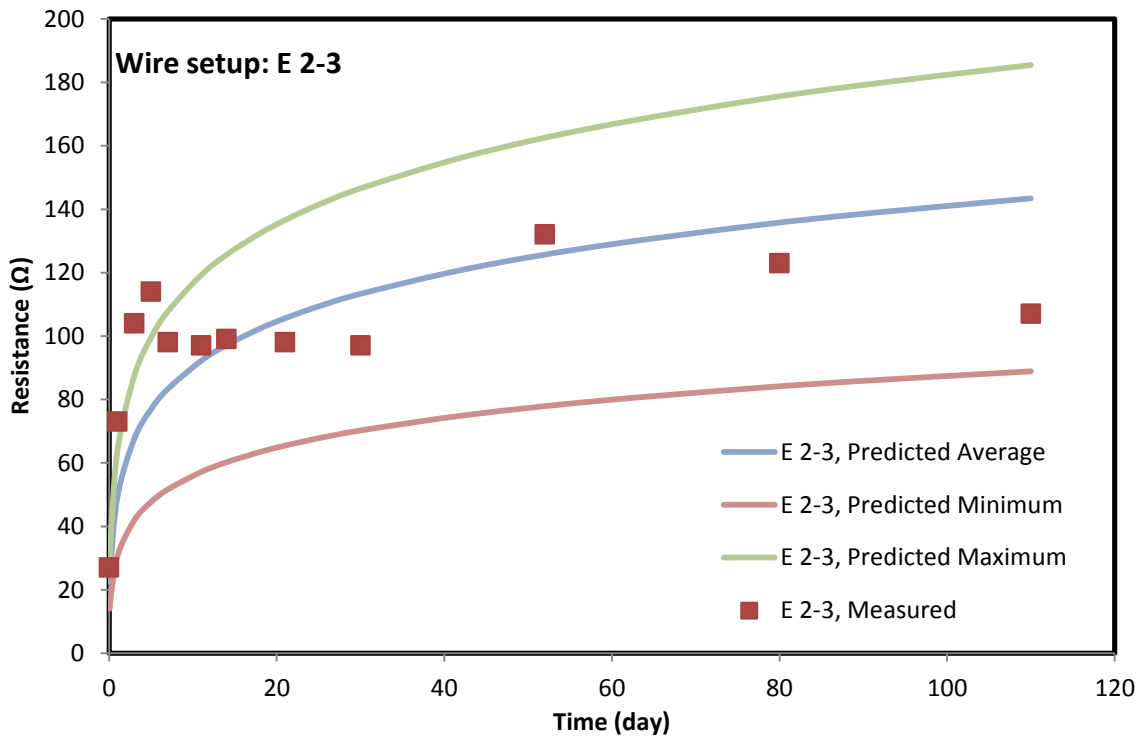


Figure 7-85: Predicted and measured vertical resistance for wire setup E 2-3

The wire combination 3-4 shows well matching of the measured resistance values with the predicted range (Fig. 7-86). But the measured resistance values for wire combination 4-5 does not matches with the predicted values (Fig. 7-87). That can be caused due to the difference between the lab curing condition and the curing inside the formation is not totally identical. The measured resistances for wire combination 5-6 and 6-7 are also in between the range of predicted values of the resistance (Fig. 7-88, Fig. 7-89). Only little exception is that there are some values for wire combination 5-6 go slightly away of the range which can be considered as outliers.

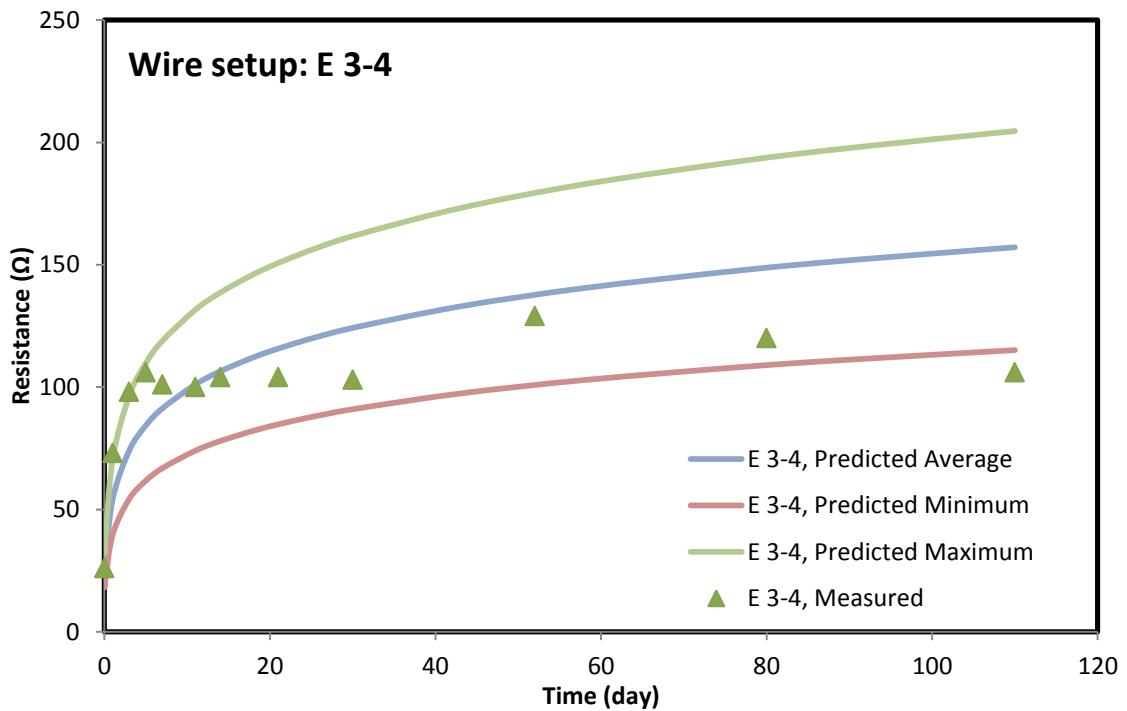


Figure 7-86: Predicted and measured vertical resistance for wire setup E 3-4

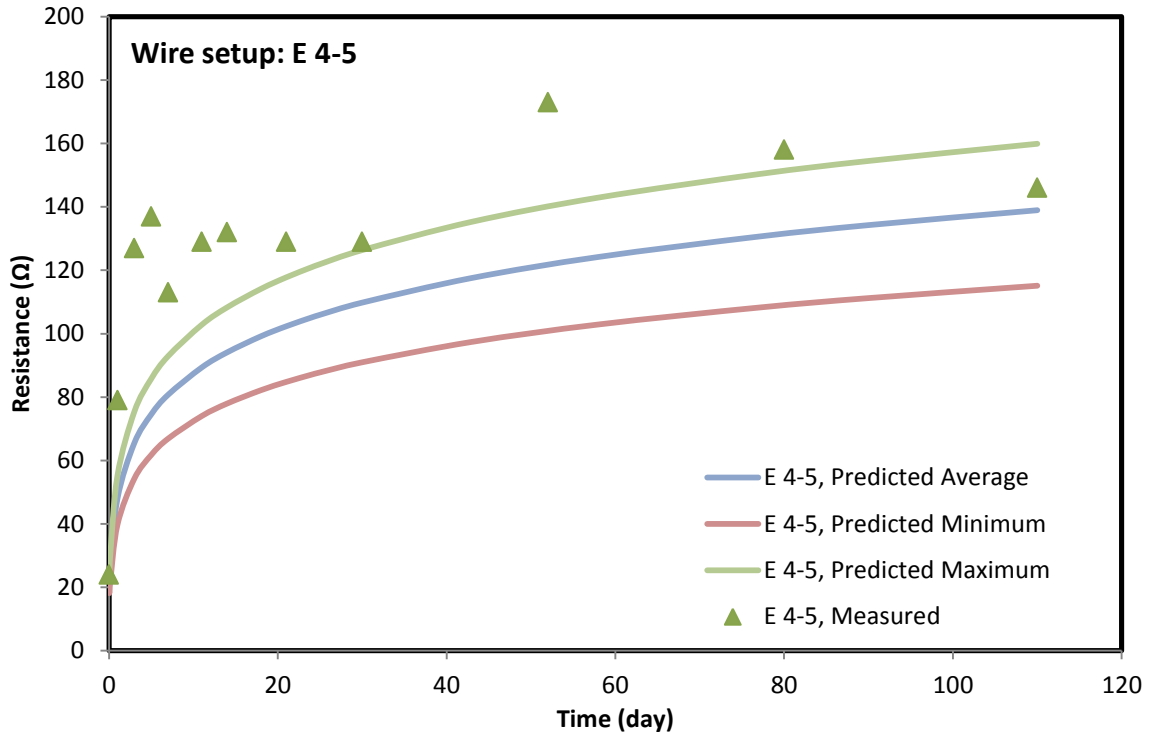


Figure 7-87: Predicted and measured vertical resistance for wire setup E 4-5

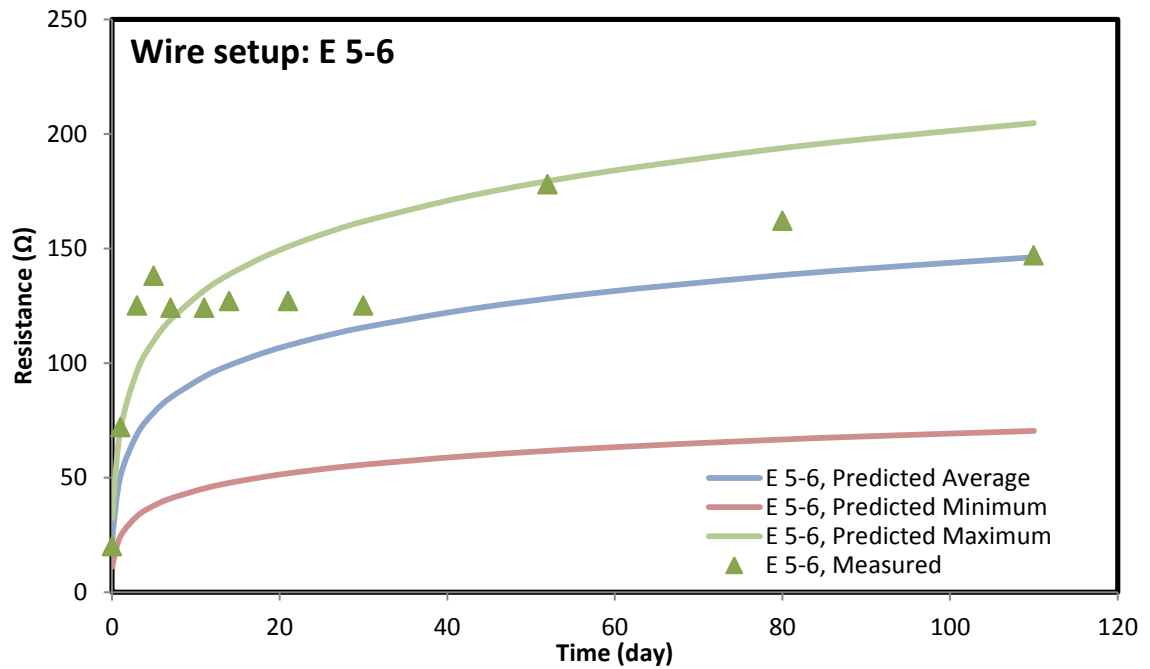


Figure 7-88: Predicted and measured vertical resistance for wire setup E 5-6

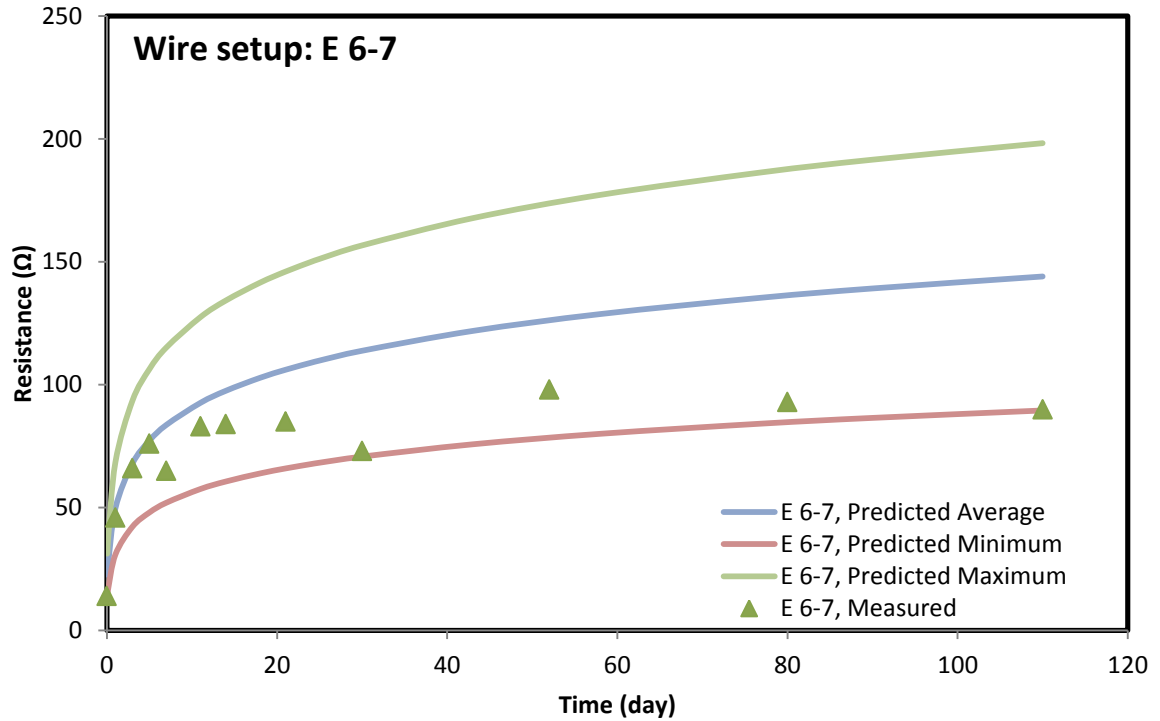


Figure 7-89: Predicted and measured vertical resistance for wire setup E 6-7

The measured resistance for wire combination 7-8 was in between the predicted range up to 21 days but after that the measured values are less than the predicted range. This may be because of the moisture in the ground at that level (Fig. 7-90). For the wire combination 8-9 in wire setup E was found closely matching with those of the predicted values for those combinations (Fig. 7-91). This shows the curing condition of the lab matching with those of the field condition.

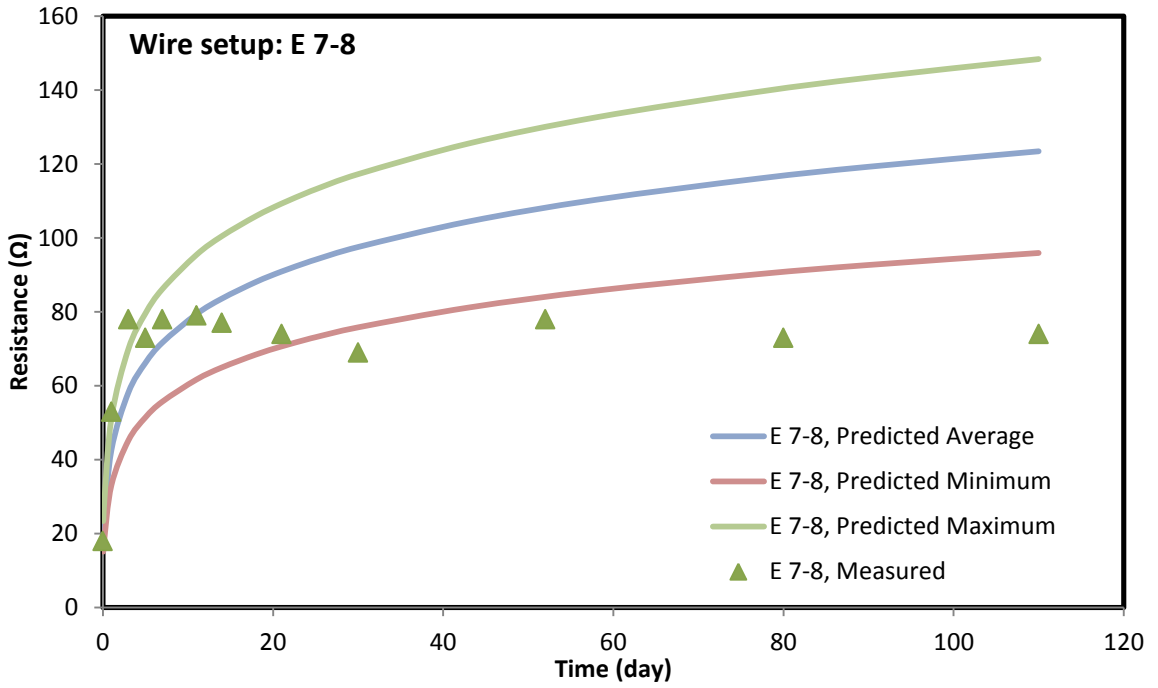


Figure 7-90: Predicted and measured vertical resistance for wire setup E 7-8

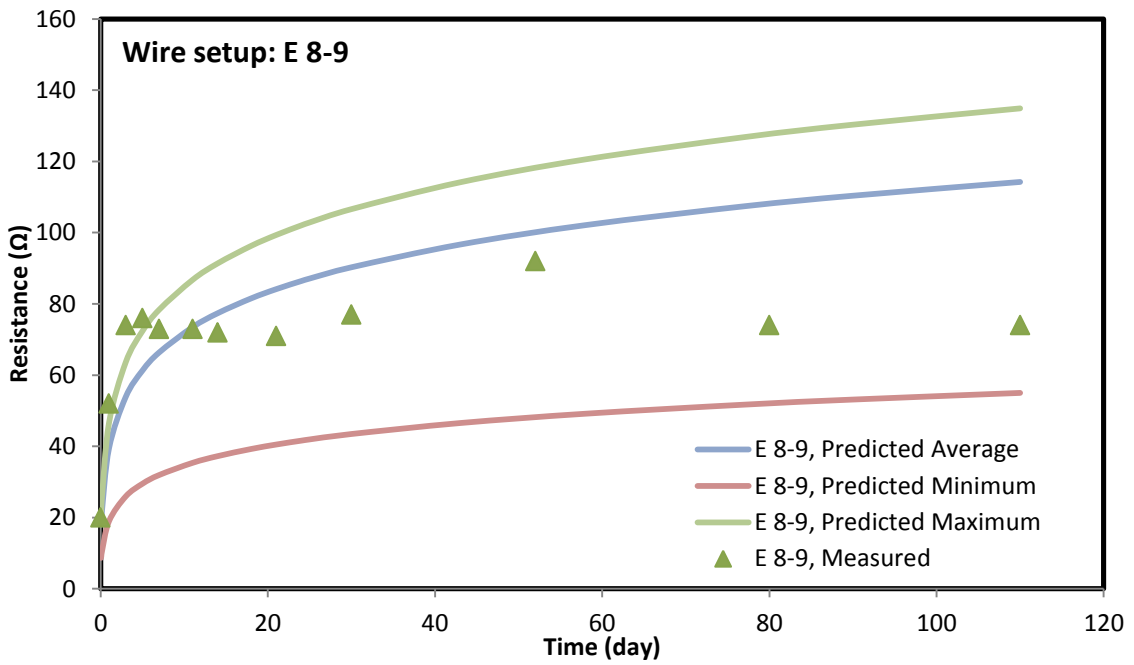


Figure 7-91: Predicted and measured vertical resistance for wire setup E 8-9

For wire setup 9-10 and 10-11, the measured resistances are very much within the range of predicted resistances (Fig. 7-92, 7-93). There are some values outside the range which we can consider as outliers.

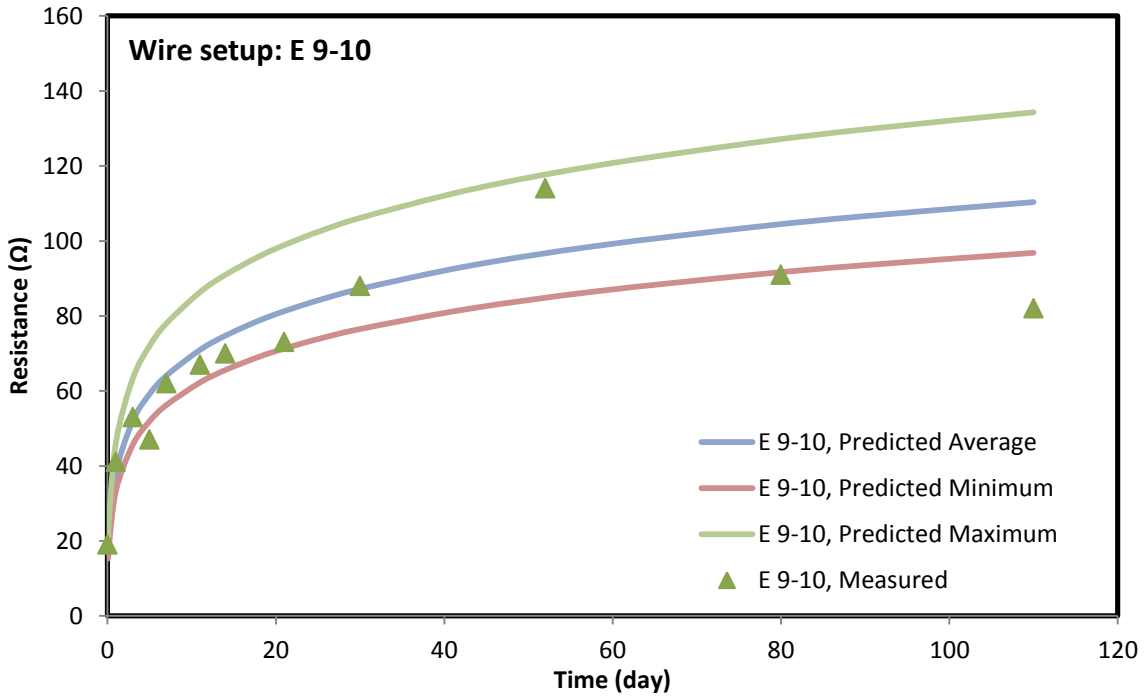


Figure 7-92: Predicted and measured vertical resistance for wire setup E 9-10

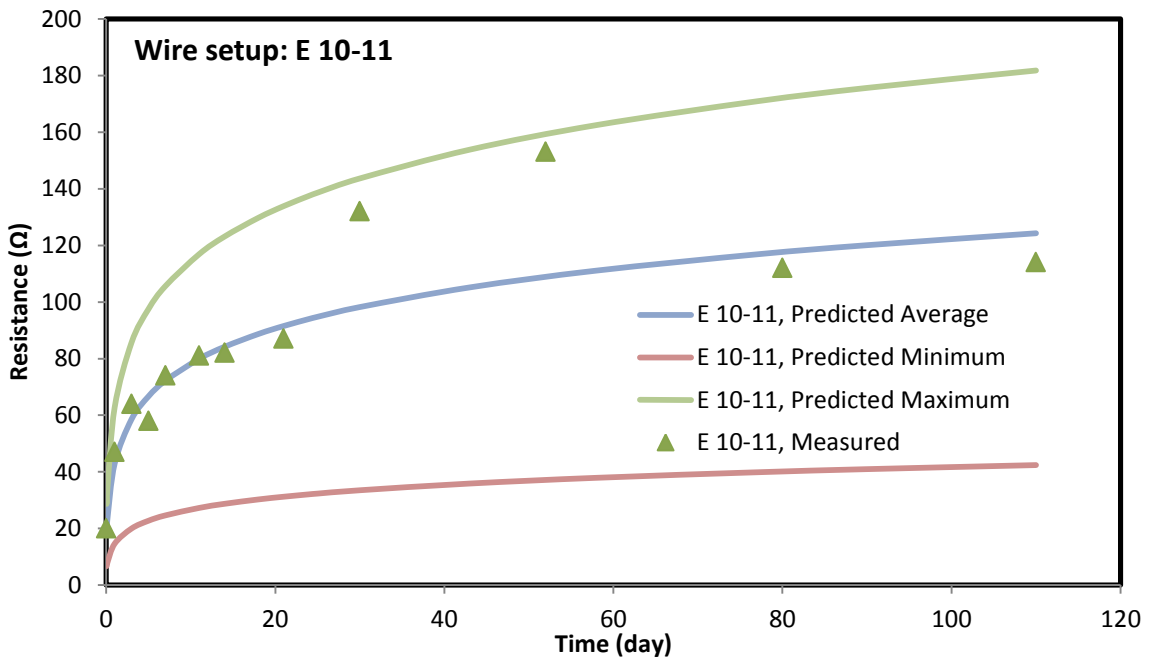


Figure 7-93: Predicted and measured vertical resistance for wire setup E 10-11

The measured values for wire combination 11-12 are higher than that of the predicted range (Fig. 7-94). From field observation, we found that the wire E -12 is above the ground level which is exposed to atmosphere. That's why moisture from the cement may be lost due to drying of the cured cement which is causing the higher resistance values.

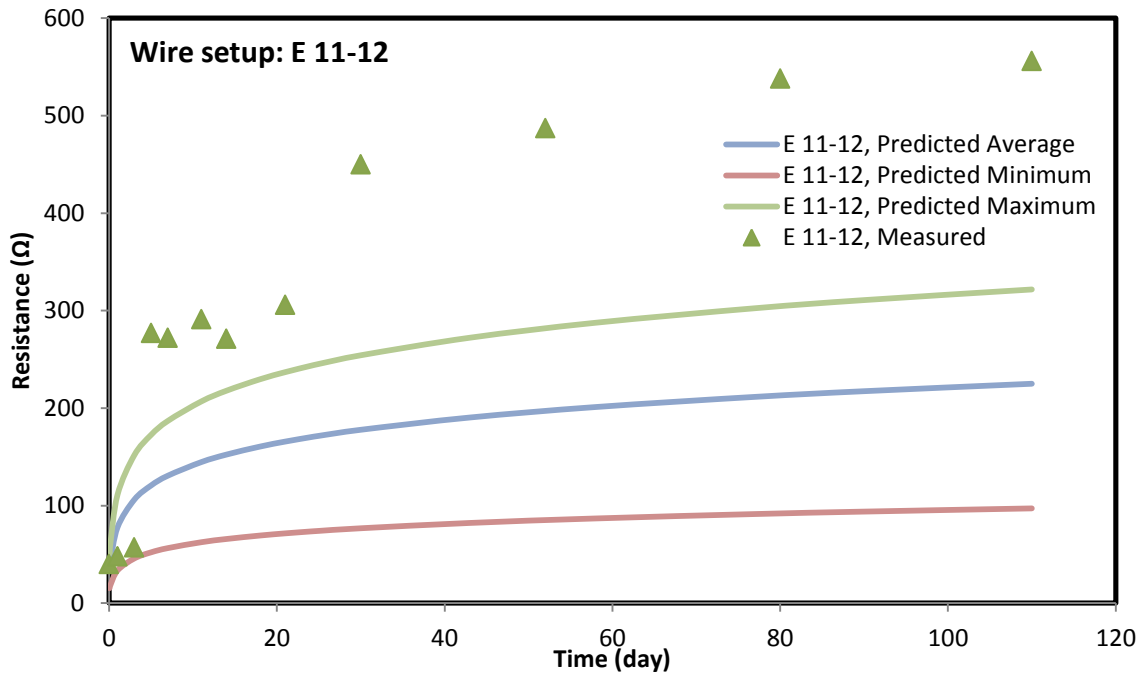


Figure 7-94: Predicted and measured vertical resistance for wire setup E 11-12

The measured resistance for wire combination 1-2 in wire setup F were below the predicted range. It may be due to the excess moisture inside the formation as wire combination 1-2 is inside the ground water level (Fig. 7-95). The measured resistance for wire combination 2-3 in wire setup E were very much within the range (Fig. 7-96).

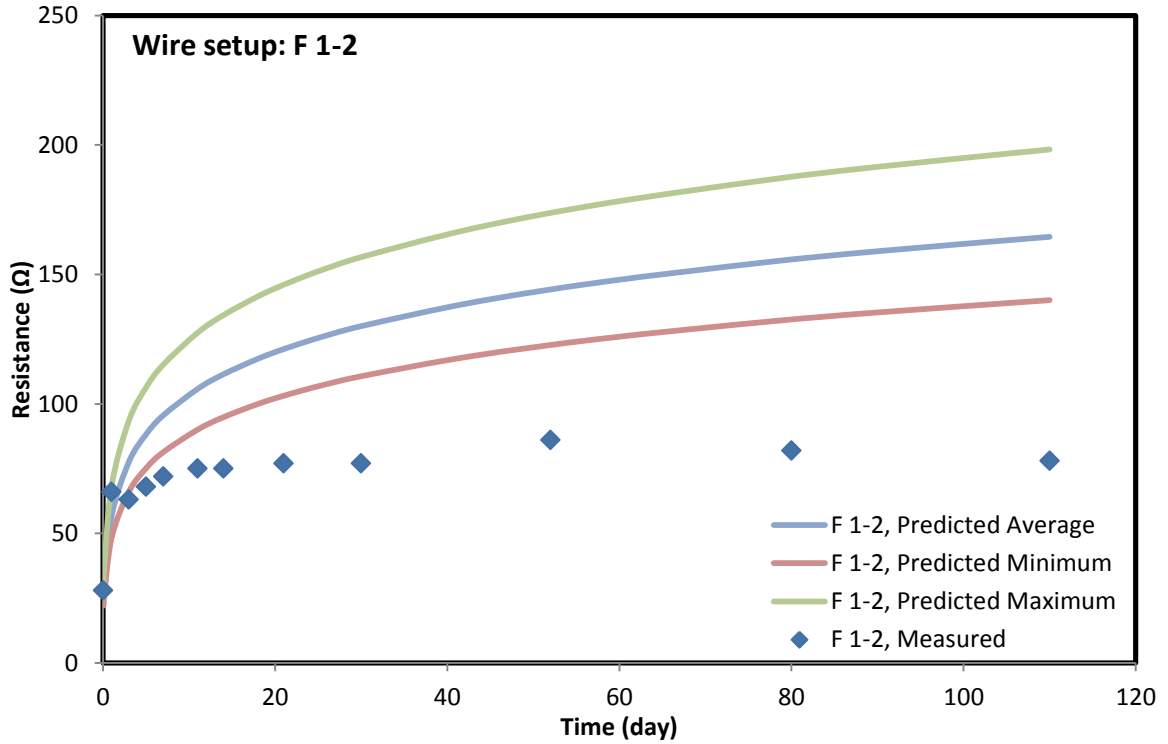


Figure 7-95: Predicted and measured vertical resistance for wire setup F 1-2

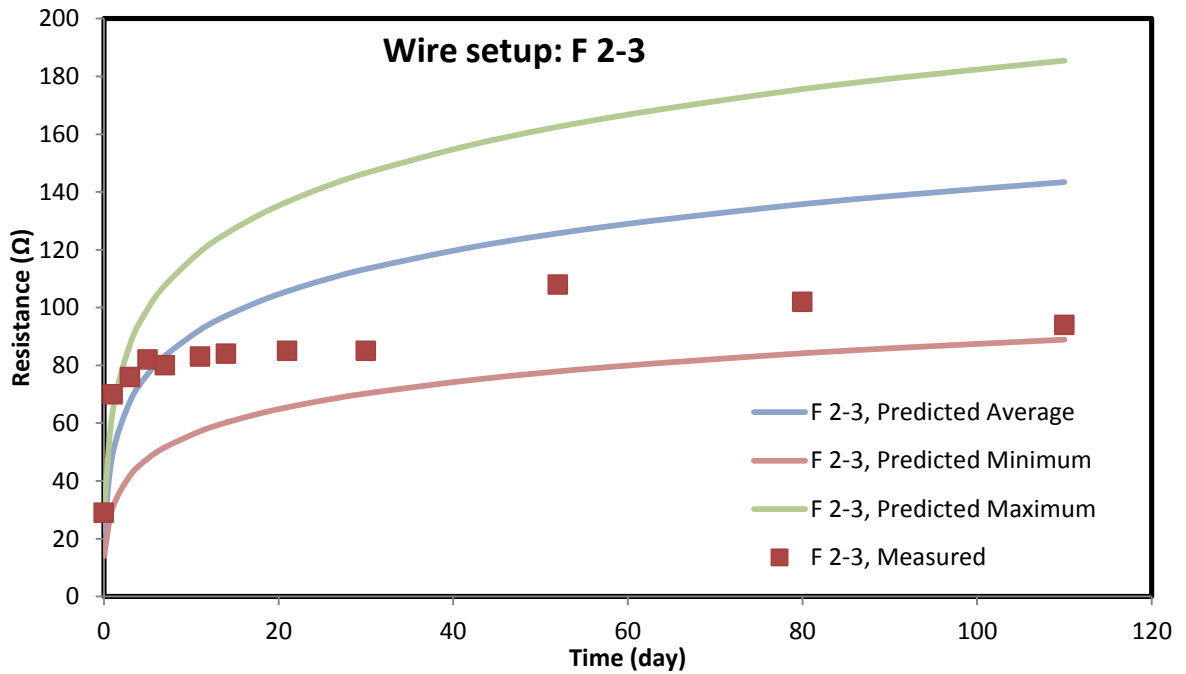


Figure 7-96: Predicted and measured vertical resistance for wire setup F 2-3

The wire combination 3-4 and 4-5 both shows well matching of the measured resistance values with the predicted range up to 15 days of curing (Fig. 7-97 and 7-98). But the measured resistance values after 15 days of curing are a little bit lower than the predicted range of values. That can be caused due to the difference between the lab curing condition and the curing inside the formation does not totally identical. The measured resistances for wire combination 5-6 and 6-7 are also in between the range of predicted values of the resistance (Fig. 7-99, Fig. 7-100). This shows the curing condition of the lab matching with those of the field condition.

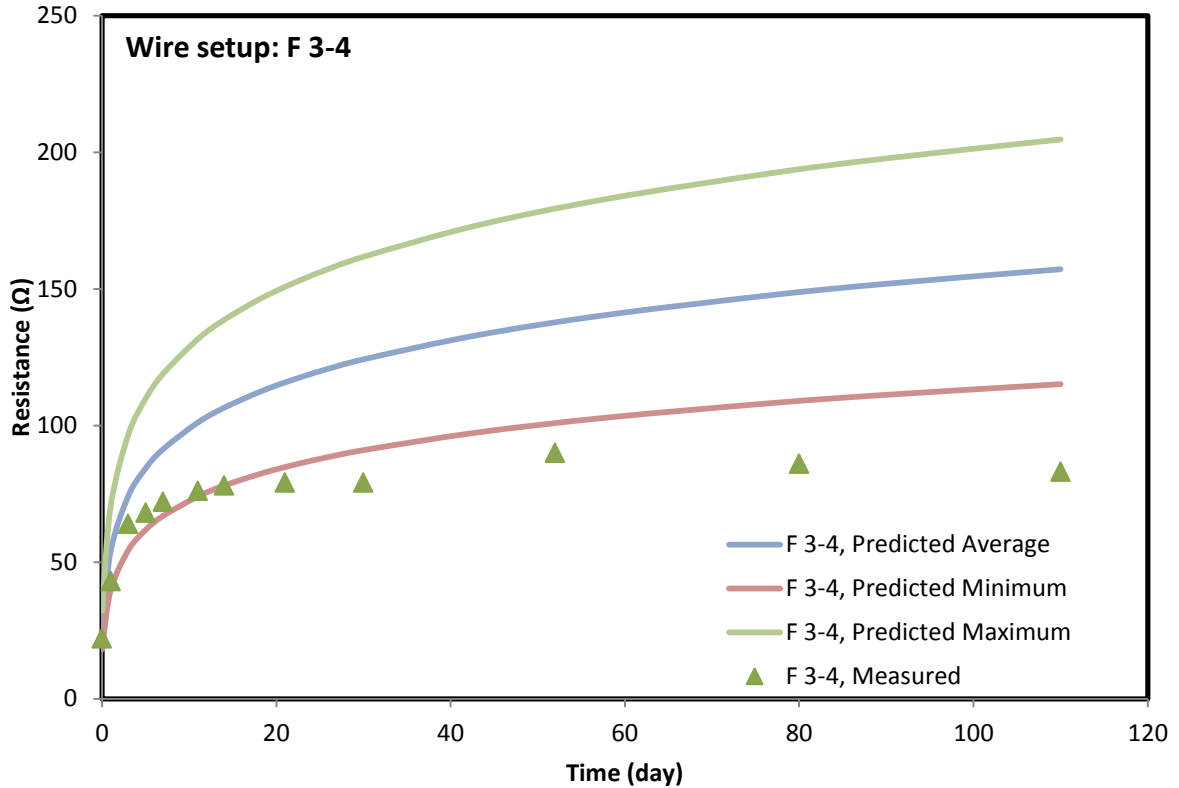


Figure 7-97: Predicted and measured vertical resistance for wire setup F 3-4

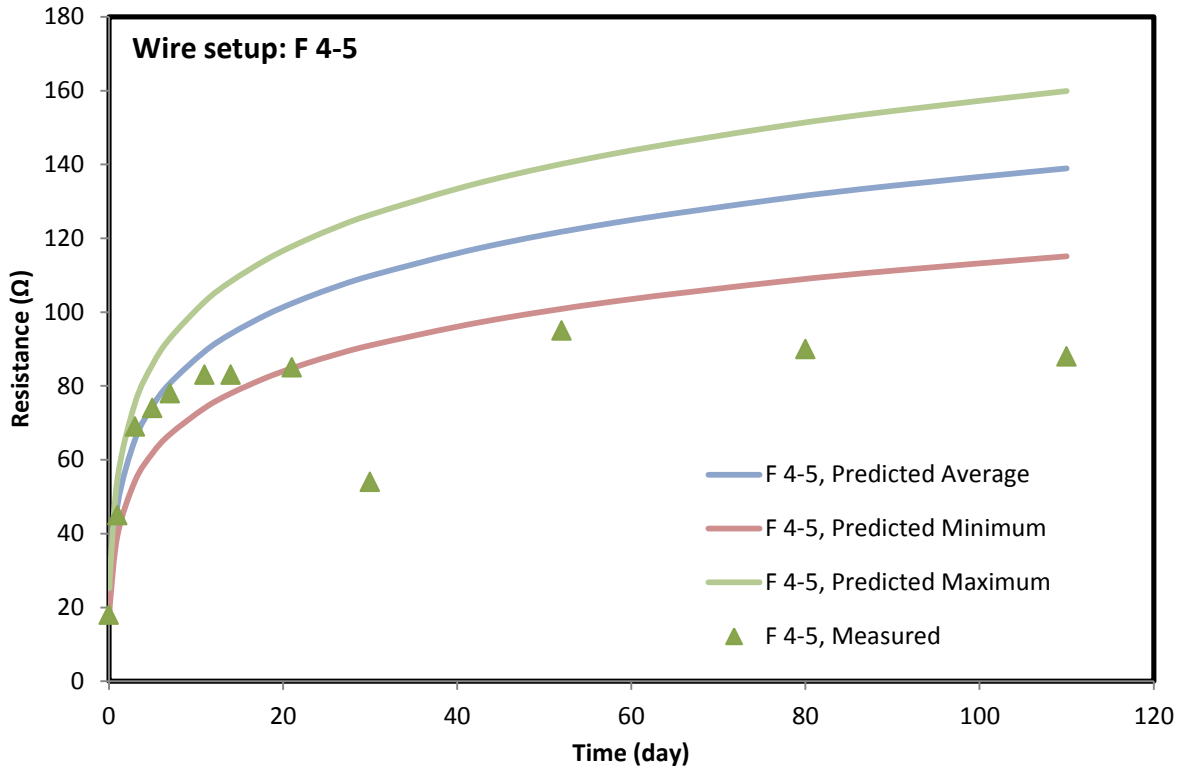


Figure 7-98: Predicted and measured vertical resistance for wire setup F 4-5

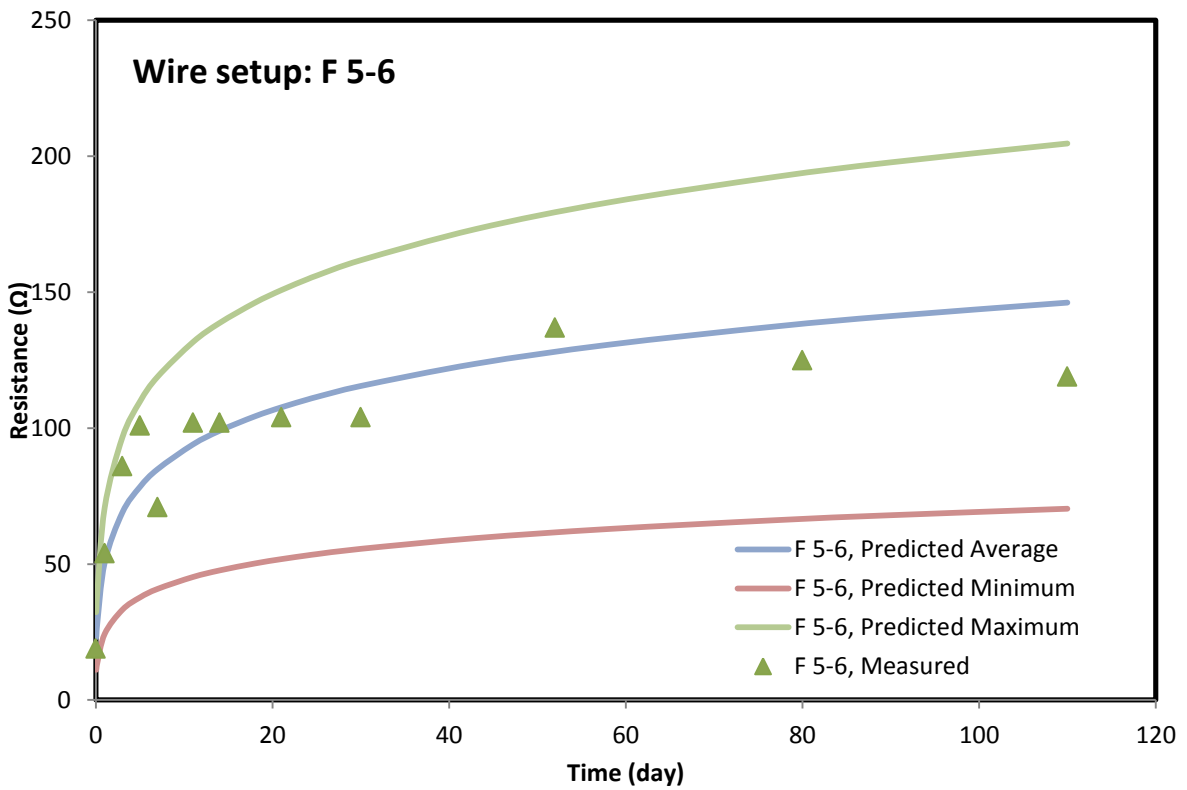


Figure 7-99: Predicted and measured vertical resistance for wire setup F 5-6

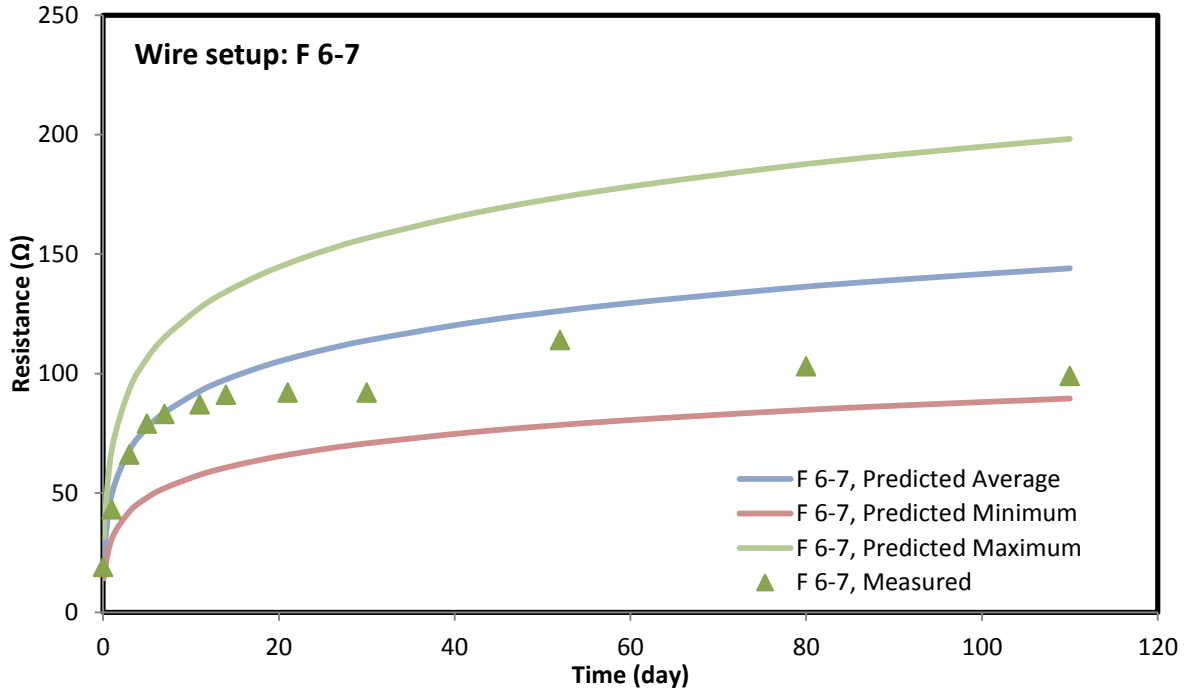


Figure 7-100: Predicted and measured vertical resistance for wire setup F 6-7

The measured resistance for wire combination 7-8 matches well up to 21 days but lower than the predicted values after that. This may be because of the different curing condition of lab and field (Fig. 7-101). But for wire combination 8-9 in wire setup F was found closely matching with those of the predicted values for those combinations (Fig. 7-102). This shows the curing condition of the lab matching with those of the field condition. The measured resistances for wire setup 9-10 are a little below the predicted range and for 10-11, the measured resistances are a little higher than the predicted range (Fig. 7-103, 7-104). In both cases the difference is very less. We can consider them as within the close vicinity of the predicted range.

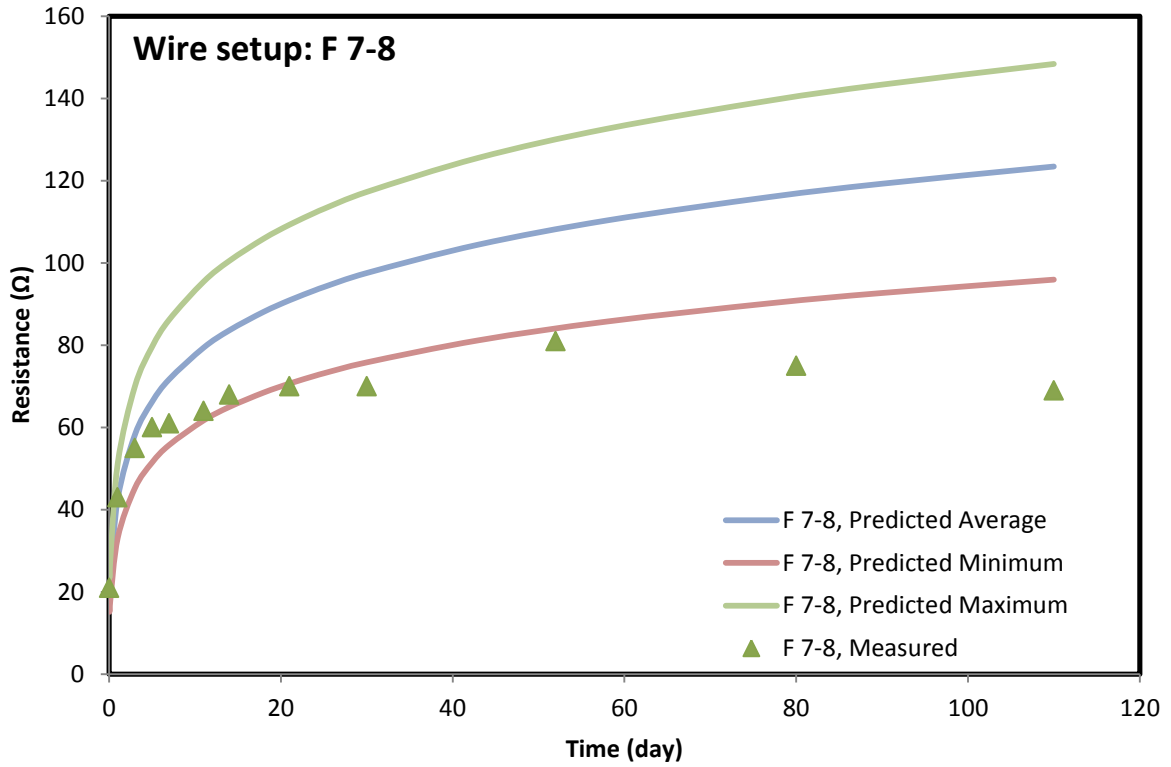


Figure 7-101: Predicted and measured vertical resistance for wire setup F 7-8

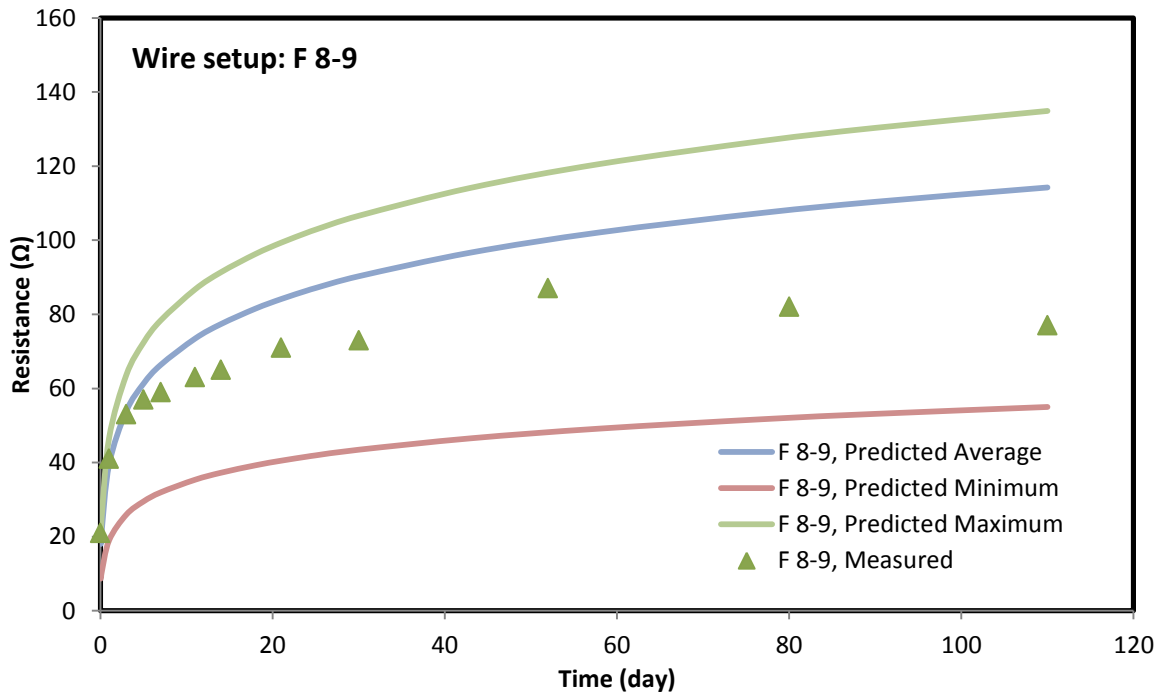


Figure 7-102: Predicted and measured vertical resistance for wire setup F 8-9

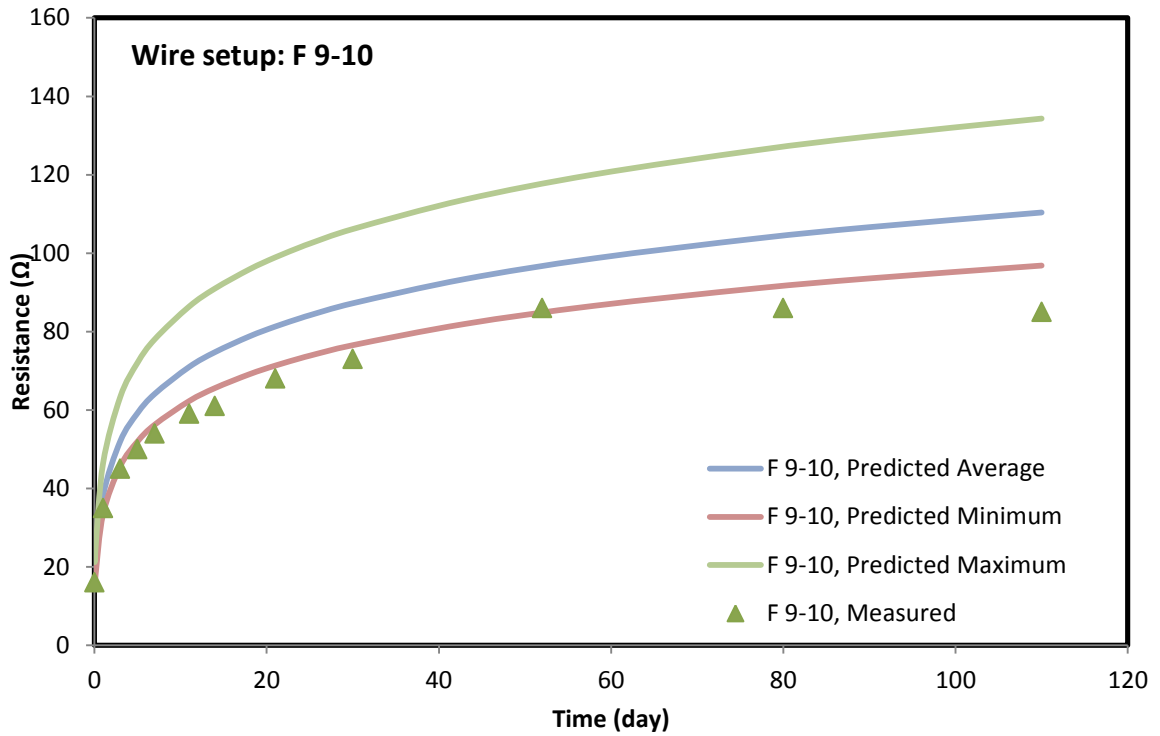


Figure 7-103: Predicted and measured vertical resistance for wire setup F 9-10

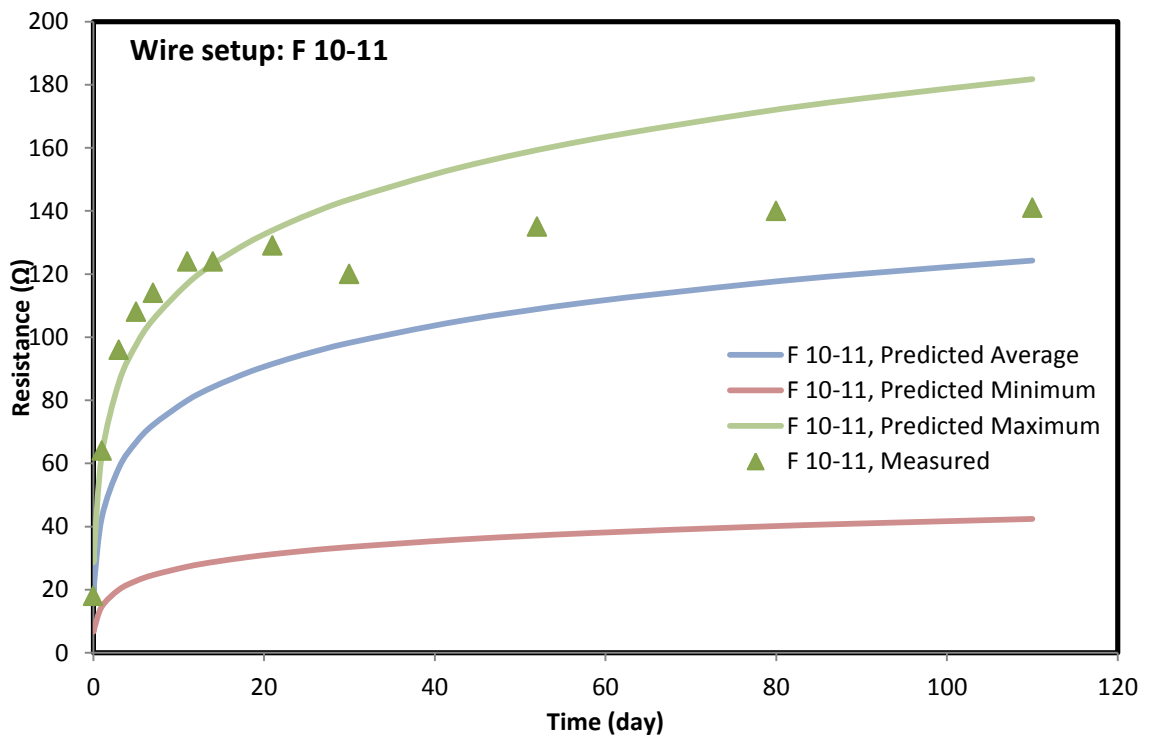


Figure 7-104: Predicted and measured vertical resistance for wire setup F 10-11

Some of the measured values for wire combination 11-12 are higher than that of the predicted range (Fig. 7-105). From field observation, we found that the wire E 11-12 is above the ground level which is exposed to atmosphere. That's why moisture from the cement may be lost due to drying of the cured cement which is causing the higher resistance values. The measured resistances for horizontal wire combination E-F at level 1 were below the predicted range. It may be due to the excess moisture inside the formation as wire level 1 is inside the ground water level (Fig. 7-106). The measured resistances for wire combination E-F at level 2 were very much within the range (Fig. 7-107).

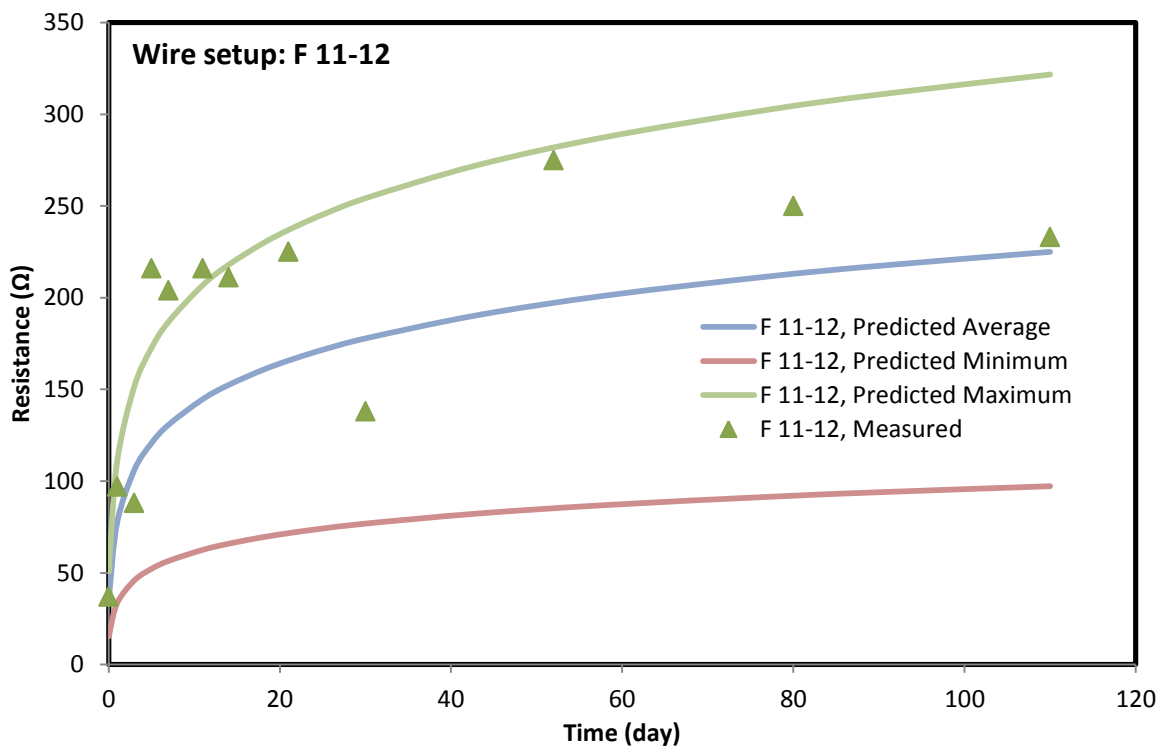


Figure 7-105: Predicted and measured vertical resistance for wire setup F 11-12

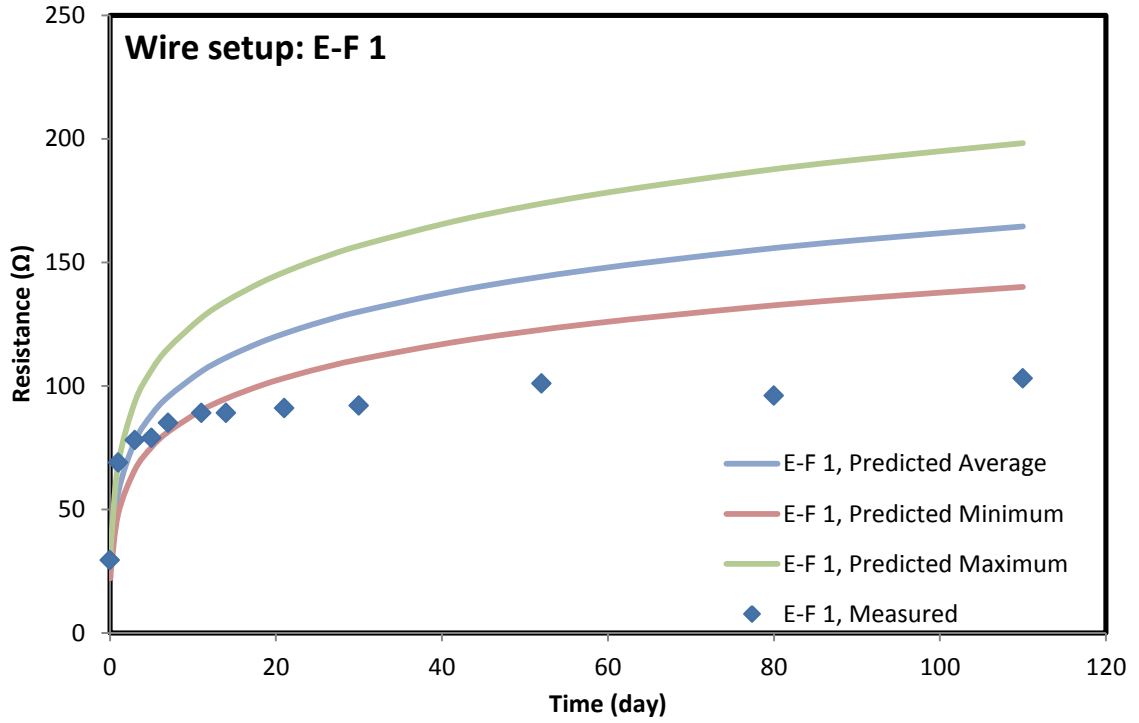


Figure 7-106: Predicted and measured resistance for horizontal wire setup E-F at level 1

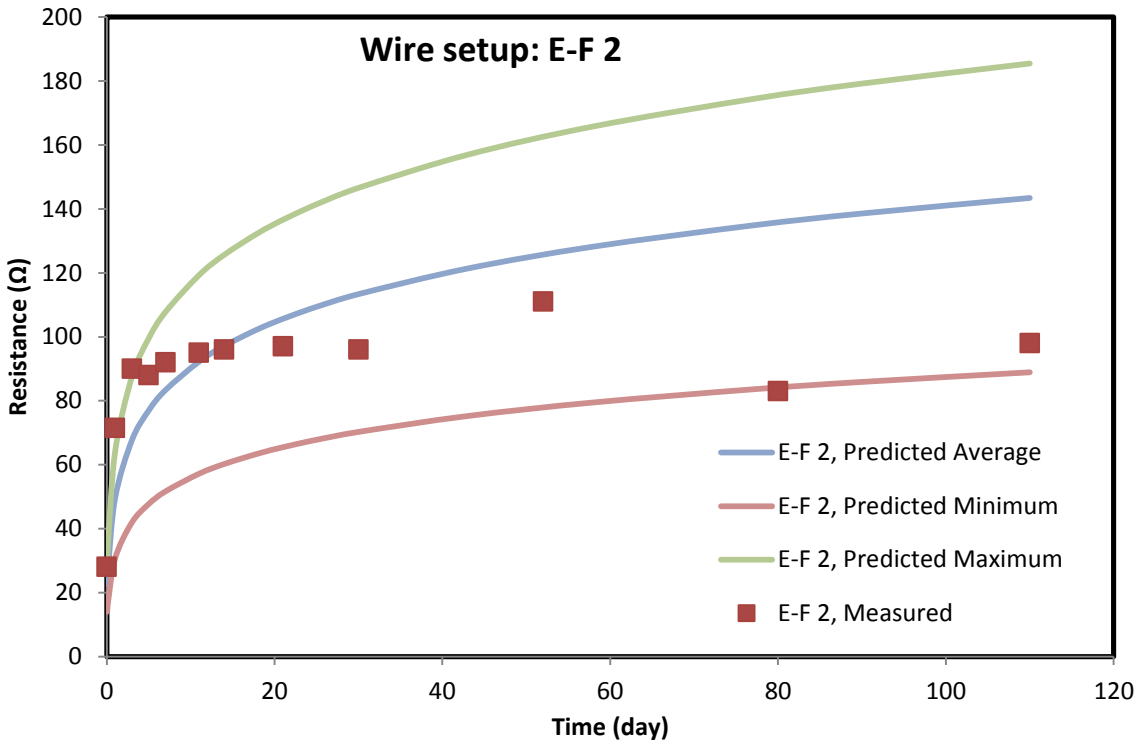


Figure 7-107: Predicted and measured resistance for horizontal wire setup E-F at level 2

The wire combination E-F at level 3 shows well matching of the measured resistance values with the predicted range (Fig. 7-108). But the measured resistance values for wire combination E-F at level 4 after 15 days of curing are a little bit lower than the predicted range of values. That can be caused due to the difference between the lab curing condition and the curing inside the formation does not totally identical (Fig. 7-109). The measured resistances for wire combination and E-F at level 5 and at level 6 both are also in between the range of predicted values of the resistance (Fig. 7-110, Fig. 7-111) with a little exception for level 5 which shows some higher values. This shows the curing condition of the lab closely matching with those of the field condition.

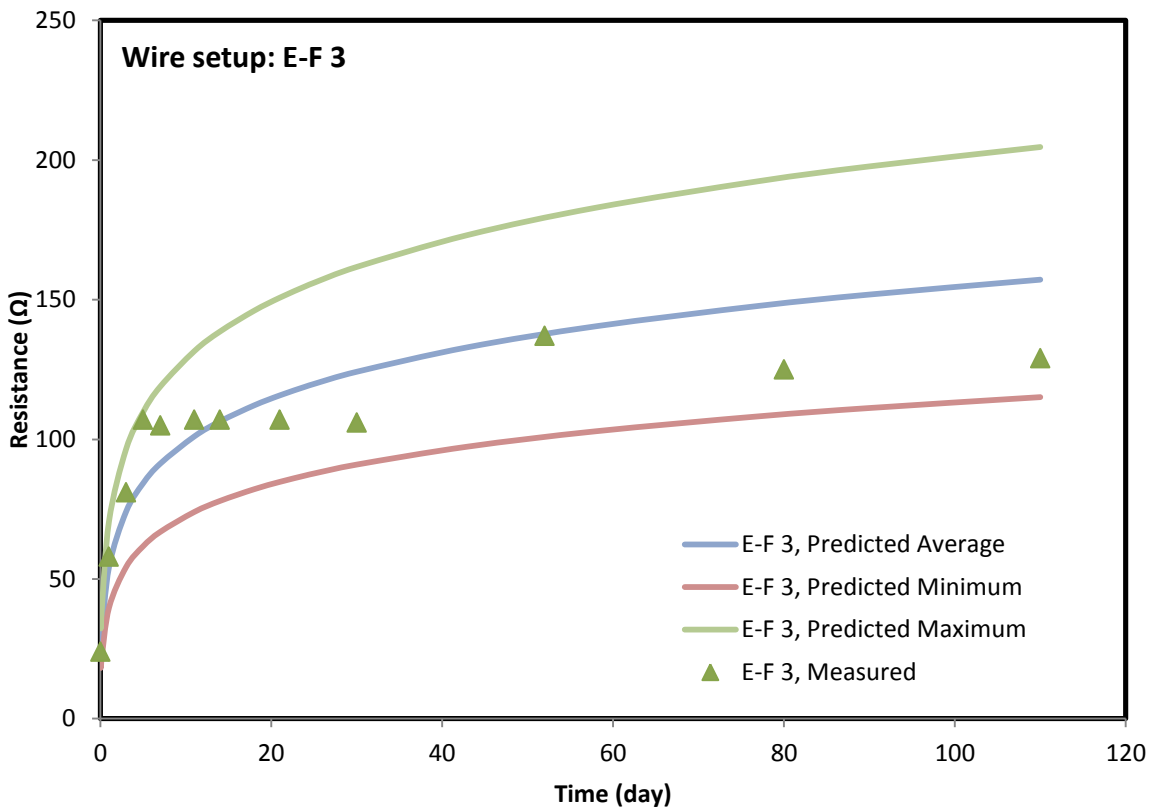


Figure 7-108: Predicted and measured resistance for horizontal wire setup E-F at level 3

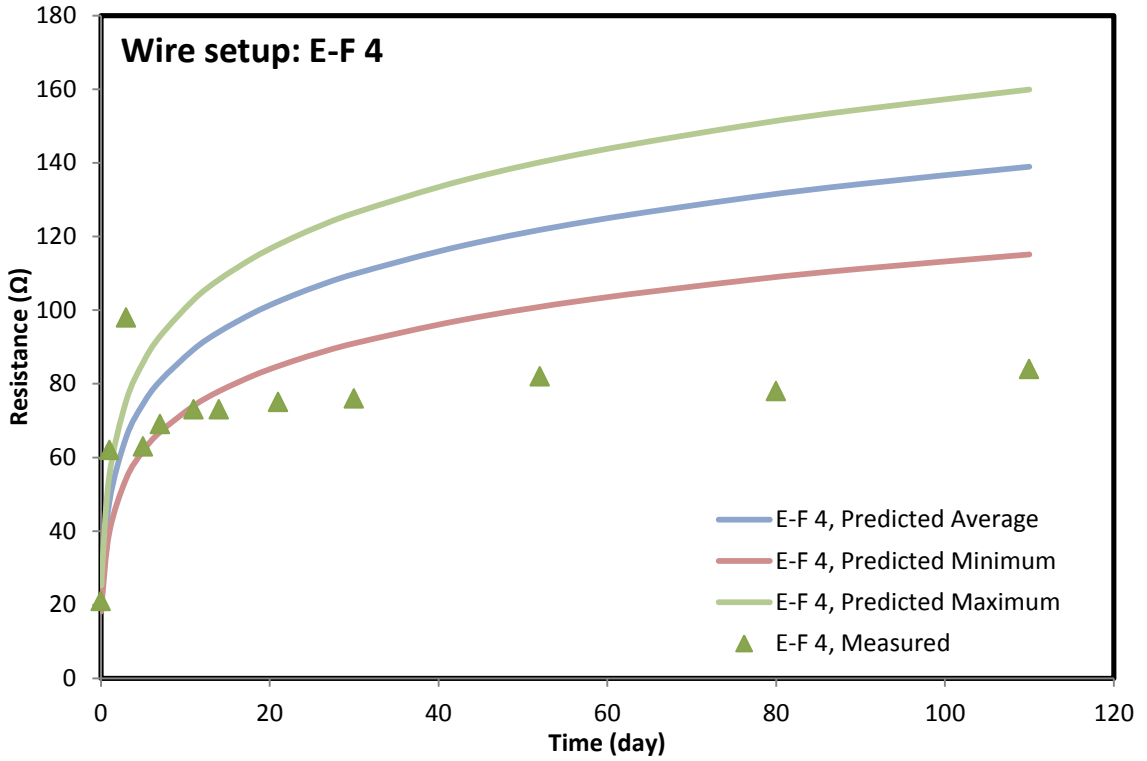


Figure 7-109: Predicted and measured resistance for horizontal wire setup E-F at level 4

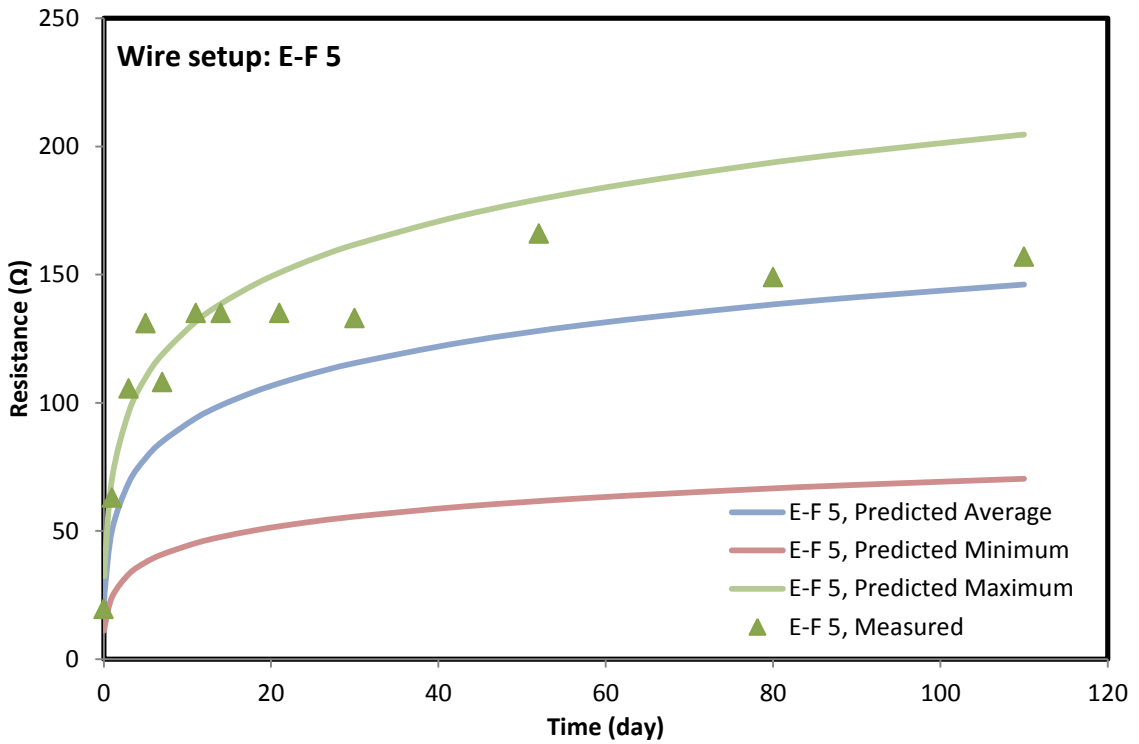


Figure 7-110: Predicted and measured resistance for horizontal wire setup E-F at level 5

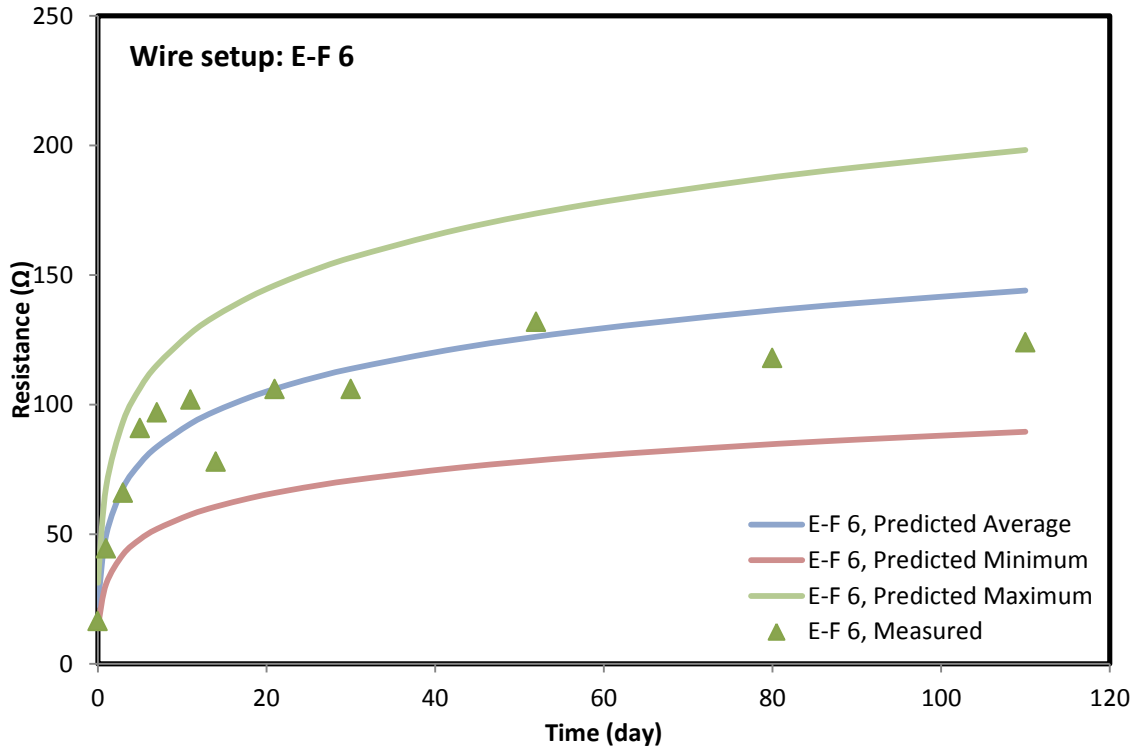


Figure 7-111: Predicted and measured resistance for horizontal wire setup E-F at level 6

The measured resistance for wire combination and E-F at level 7 and at level 8 was also found closely matching with those of the predicted values for those combinations (Fig. 7-112, Fig. 7-113) with a little exception for level 7. This shows the curing condition of the lab matching with those of the field condition. The measured resistances for wire setup and E-F at level 9 closely matches with the minimum range of the predicted values whereas at level 10, the measured values are within the range of predicted values (Fig. 7-114, 7-115). In both cases the results showing very good match with lab curing condition with a little exception.

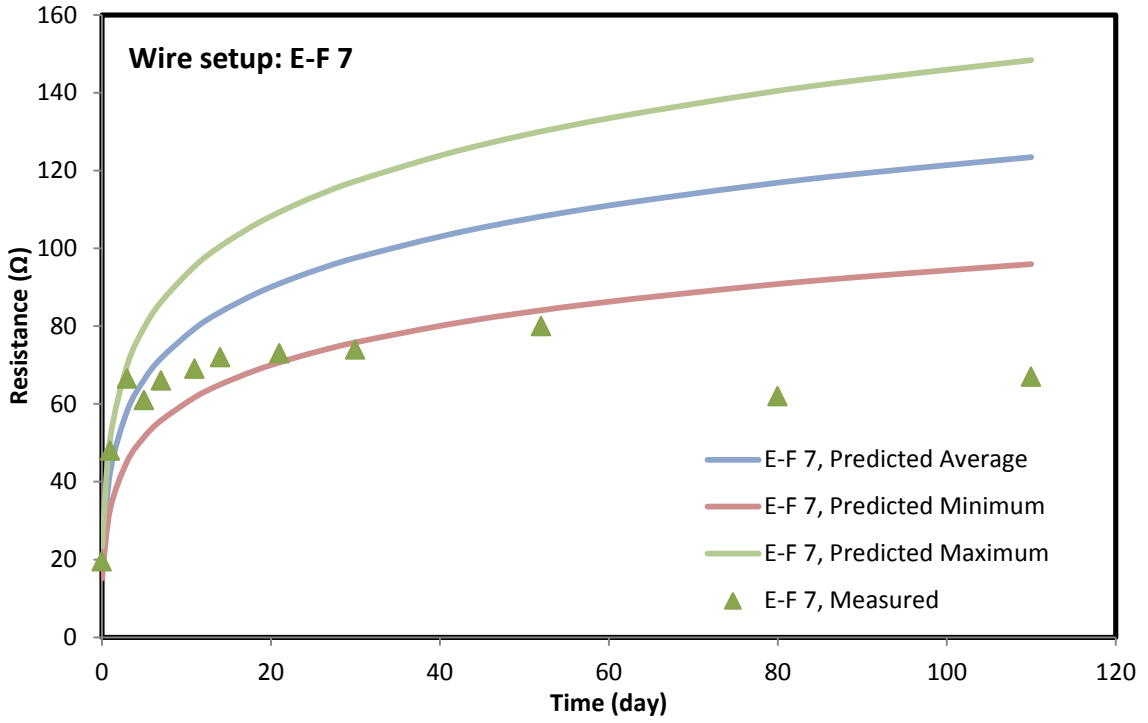


Figure 7-112: Predicted and measured resistance for horizontal wire setup E-F at level 7

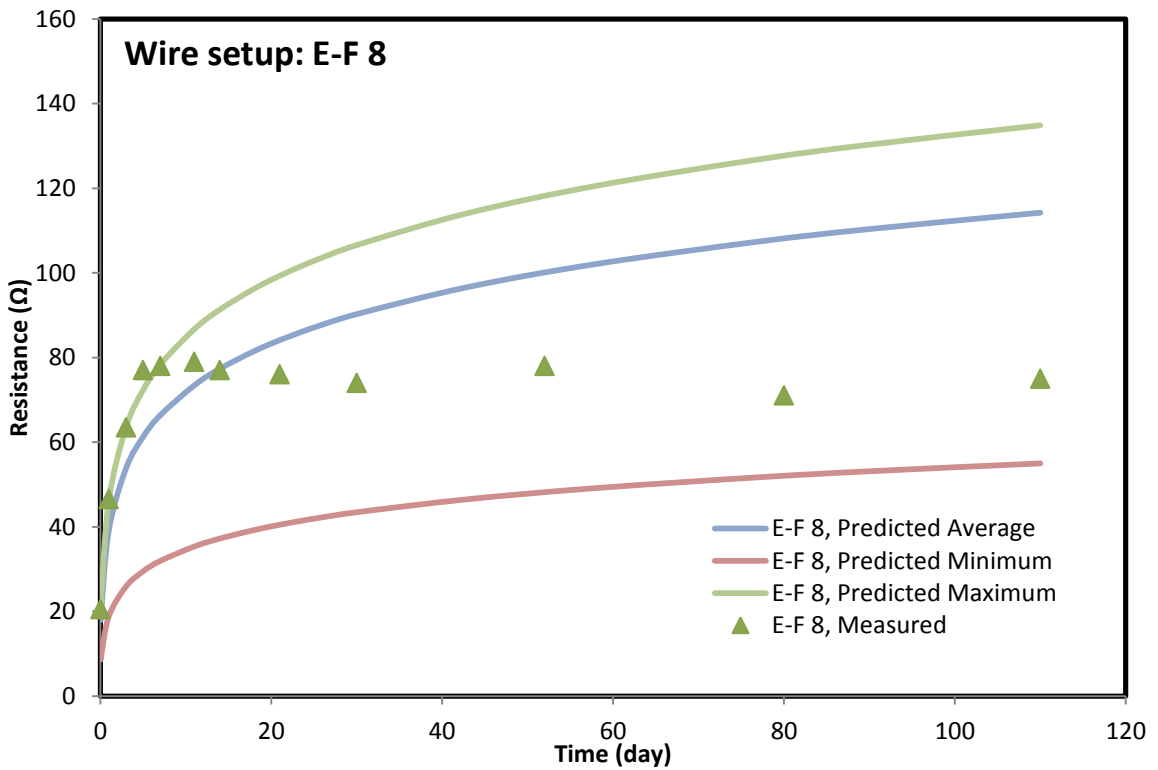


Figure 7-113: Predicted and measured resistance for horizontal wire setup E-F at level 8

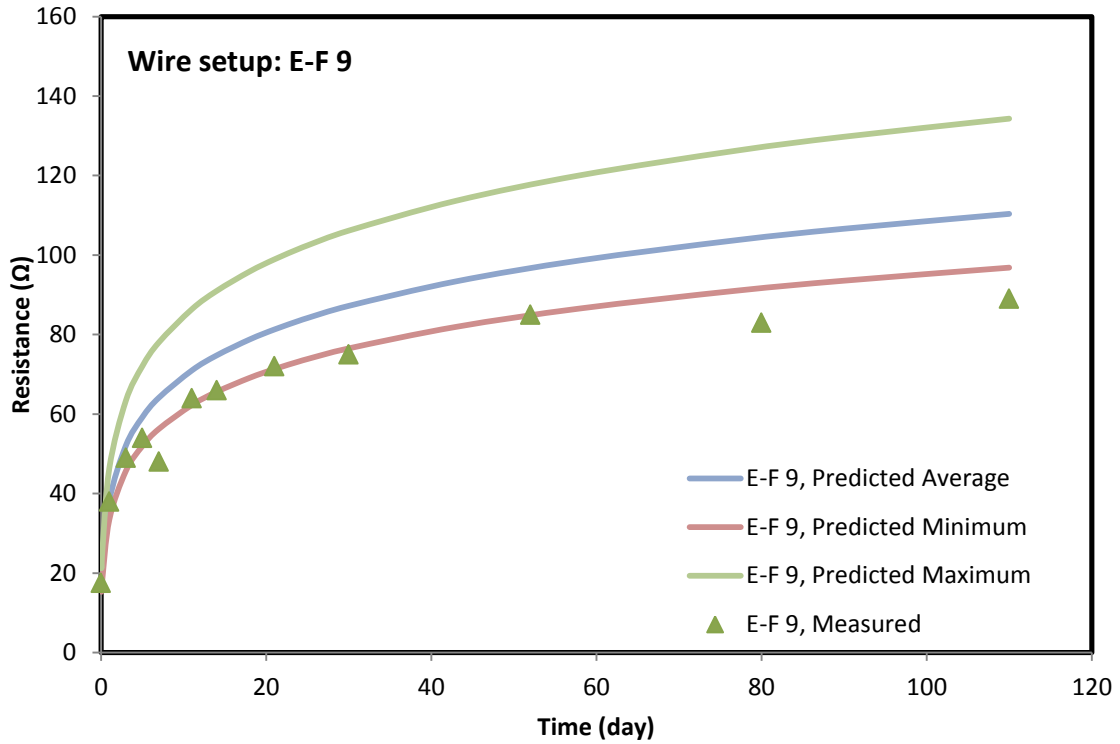


Figure 7-114: Predicted and measured resistance for horizontal wire setup E-F at level 9

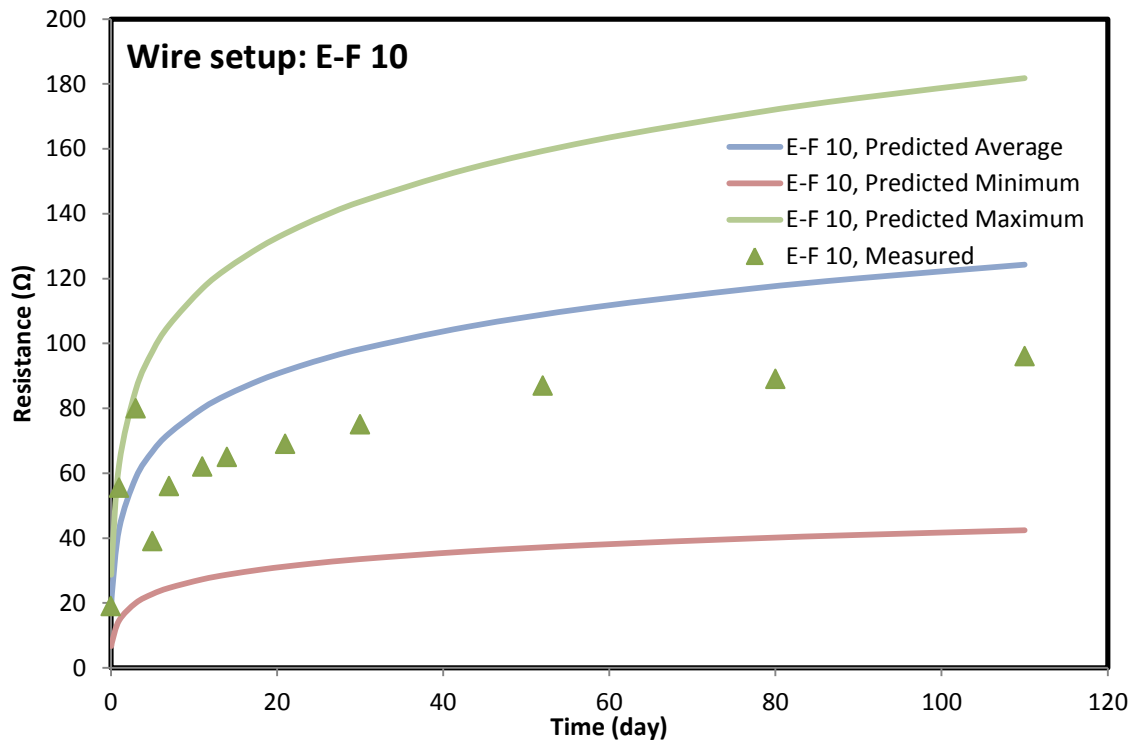


Figure 7-115: Predicted and measured resistance for horizontal wire setup E-F at level 10.

Due to the high deviations of the K parameter at level 11 and level 12, the predicted range for those levels are also very high. The measured values are also falling within the range of predicted values (Fig. 7-116, 7-117).

7.5 Summary

Based on the lab model study and field model study, the following observations are advanced:

1. The detection of drilling mud and slurry filling by way of resistance measurements was found effective. From the change of resistance value we were able to decide that the drilling mud or cement slurry have reached to a certain level.
2. The determination of resistance of the hardened cement and comparing with the predicted values were also found effective. The predictions of the resistance which was based on the calibrated geometric factor and the resistivity of the small samples cured in lab under different curing condition matched in most of the cases and agreed well with the measured resistance values for both the lab models and field model.

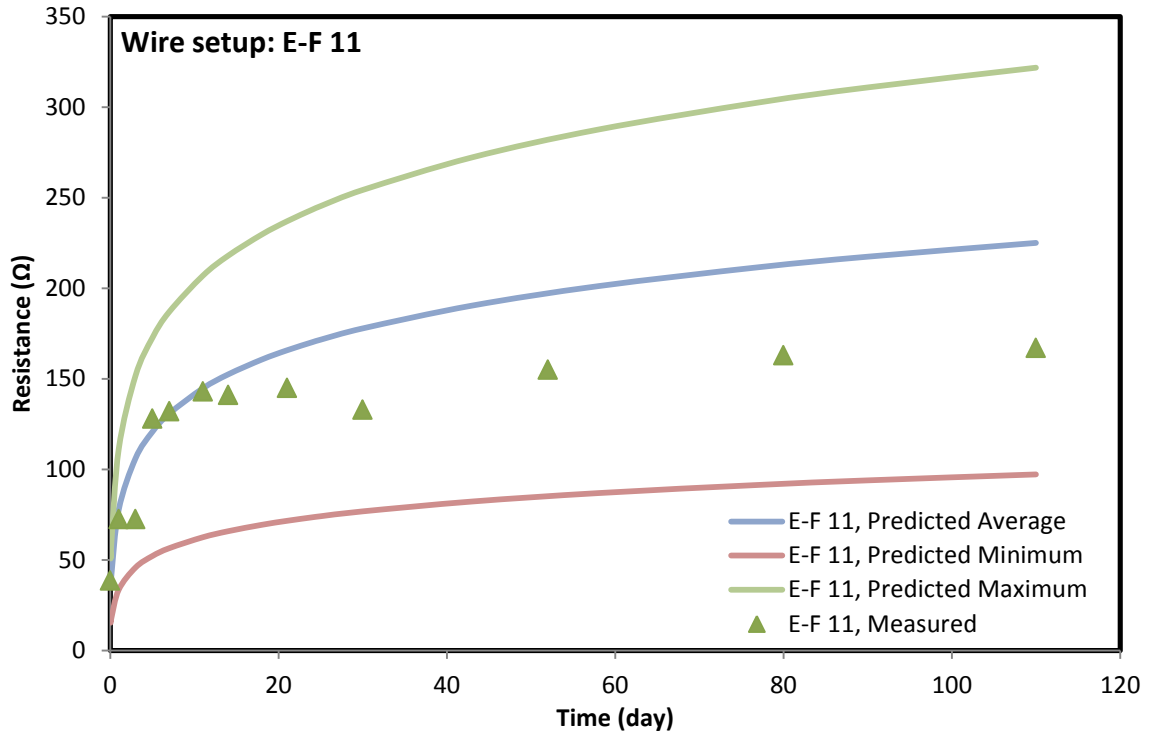


Figure 7-116: Predicted and measured resistance for horizontal wire setup E-F at level 11

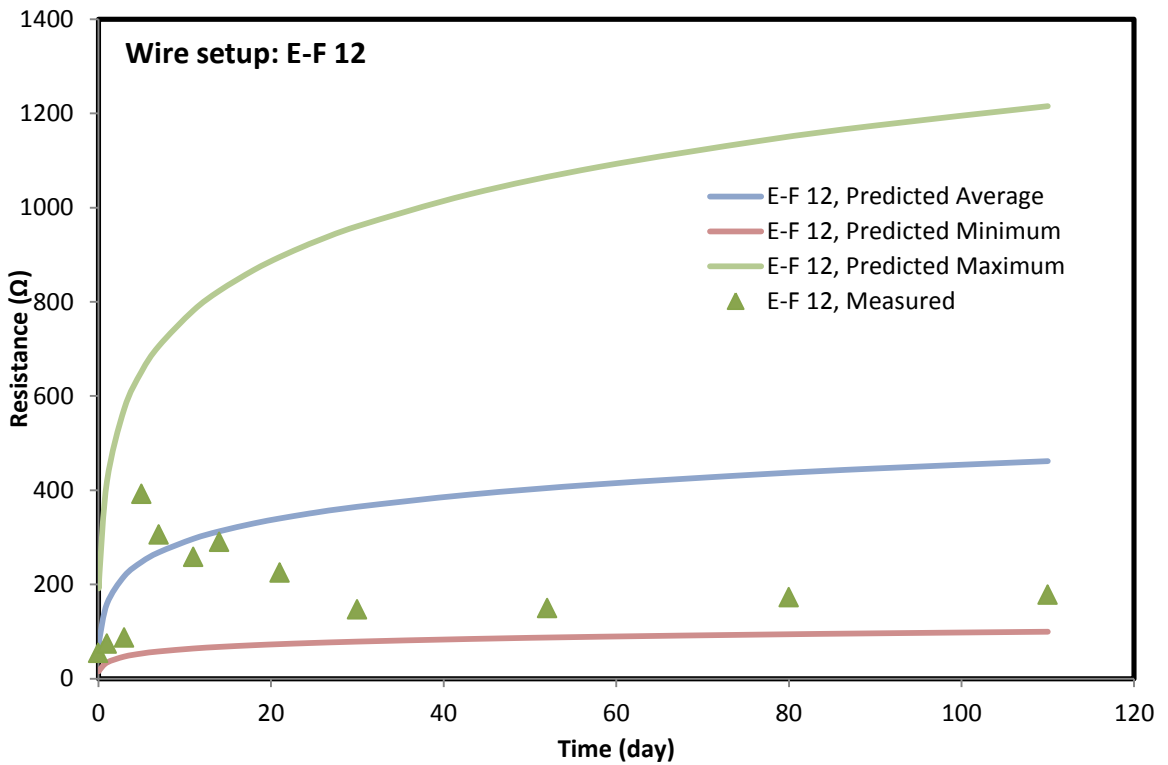


Figure 7-117: Predicted and measured resistance for horizontal wire setup E-F at level 12

CHAPTER 8 CONCLUSIONS AND RECOMMENDATIONS

8.1 Conclusions

The objective of this study was to investigate the effects of sodium meta-silicate on the rheological, curing and piezoresistive properties of smart oil well cement under various curing condition, of grouts made of smart cement and the effectiveness of the grout to repair damaged cement, of the water based drilling mud, and the verification of the real time monitoring of the smart oil well cement by electrical resistivity measurement with physical model study. Based on the experimental results, the following conclusions were advanced:

- 1) The initial resistivity (ρ_o) and minimum resistivity (ρ_{min}) of the smart cement decreased with addition of SMS. A hyperbolic relationship was developed to relate the minimum resistivity and the SMS concentration.
- 2) For long term curing under room temperature after 1 year, the resistivity of the smart cement was found about 95 $\Omega.m$, whereas the cement specimen with 0.3% SMS had a resistivity of 58 $\Omega.m$ which was 38% less than that of the smart cement. The moisture loss of the smart cement specimen 6.2% which was also reduced with addition of SMS. The specimen with 0.3% SMS lost 5.4% moisture, an 11% less weight than the specimen with no SMS.
- 3) For long term curing under no moisture loss condition after 12 months, the resistivity of the smart cement was found about 26.27 $\Omega.m$ which is 72% less than that of room curing condition (94.8 $\Omega.m$). On the other hand, the cement specimen with 0.3% SMS had a resistivity of 24.6 $\Omega.m$ which was 6% less than that of the smart cement under no moisture loss condition.

- 4) For long term curing under water after 12 months, the resistivity of the smart cement was found about 19.93 $\Omega.m$ which is 78% less than that of room curing condition (94.8 $\Omega.m$). On the other hand, the cement specimen with 0.3% SMS had a resistivity of 16.52 $\Omega.m$ which was 17% less than that of the smart cement cured under water.
- 5) The resistivity with curing time under different curing condition was modeled with curing model developed from p-q model and the model parameters were determined with very good coefficient of correlation and RMSE.
- 6) The smart cement showed piezoresistive behavior under compressive stress. Without any SMS piezoresistivity at peak stress was varying from 315% to 545% which is reduced up to 145% to 230% with addition of 0.3% SMS. The nonlinear piezoresistive model predicated the compressive stress – change in resistivity relationship of the smart cement very well
- 7) A linear relationship has been found between the RI_{24} and the compressive strength of the cement.
- 8) The relationship between the compressive strength of the cement and curing time has been modeled with the hyperbolic model and the experimental values matched very well with the model having very good coefficient of determination. The relationship between the piezoresistivity at failure and curing time was also modeled with the hyperbolic model and fits very well with the experimental results
- 9) The smart cement cured at high temperature (80°C) showed piezoresistive behavior under compressive stress. Without any SMS, piezoresistivity at peak

stress was varying from 245% to 475% which is reduced up to 160% to 345% with 0.3% SMS. The high temperature (80°C) curing in saturated sand showed comparatively higher (about 15% to 25% more) piezoresistivity compared to that of the dry high temperature curing. The nonlinear piezoresistive model predicated the compressive stress – change in resistivity relationship of the smart cement with and without SMS very well.

- 10) The rate of change of resistivity with respect to stress change was found to be another indicator of the piezoresistivity. During the application of the stress, this indicator changes very slowly but after the initial crack happens, the rate of change of resistivity with respect to stress changes sharply or changes the slope which indicates prior to failure of the specimen.
- 11) For long term curing under room temperature after 28 days, the resistivity of the modified Portland cement was found about 11.37 Ω .m, whereas the cement specimen with 5% clay contamination had a resistivity of 15.10 Ω .m which was 32% higher than that of the modified Portland cement. The moisture loss of the modified Portland cement specimen was about 1% which was also reduced with clay contamination. The specimen with 5% clay contamination lost 0.75% moisture, a 25% less weight loss than the specimen with no clay contamination.
- 12) For long term curing under no moisture loss condition after 28 days, the resistivity of the modified Portland cement was found about 9.07 Ω .m which is 20% less than that of room curing condition (11.37 Ω .m). On the other hand, the cement specimen with 5% clay contamination had a resistivity of 13.85 Ω .m which was 52% higher than that of the cement specimen having no clay contamination under

no moisture loss condition.

- 13) The resistivity with curing time under different curing condition was modeled with curing model developed from p-q model and the model parameters were determined with very good coefficient of correlation and RMSE.
- 14) The modified Portland cement showed piezoresistive behavior under compressive stress. Without any clay contamination, piezoresistivity at peak stress was varying from 270-430% which is reduced up to 160-230% with 5% clay contamination. The nonlinear piezoresistive model predicated the compressive stress – change in resistivity relationship of the modified Portland cement very well.
- 15) The rate of change of resistivity with respect to stress change was found to be another indicator of the piezoresistivity. During the application of the stress, this indicator changes very slowly but after the initial crack happens, the rate of change of resistivity with respect to stress changes sharply or changes the slope which indicates prior to failure of the specimen.
- 16) The initial resistivity (ρ_0) of the smart cement grout decreased from 1.08 Ω -m to 0.69 Ω -m with 1% SMS, a 36% decrease. The minimum resistivity (ρ_{min}) of the smart cement grout decreased from 1.04 Ω -m to 0.54 Ω -m with 1% SMS, a 44% decrease.
- 17) The smart cement grout showed piezoresistive behavior under compressive stress. Without any SMS, piezoresistivity at peak stress was varying from 155-179% which is reduced up to 116-125% with 1% SMS. The repaired samples showed piezoresistivity varying from 48-62%. The strength regain was varying from 51-84% and the piezoresistivity regain were 16-26%. The nonlinear piezoresistive

model predicated the compressive stress–change in resistivity relationship of the smart cement grout with and without SMS very well.

18) The apparent viscosity and yield stress of a water based 6% bentonite mud was increased with 0.1% silicate but decreased with higher content. The 10 second and 10 minutes gel strengths were reduced by addition of silicate content.

19) The API (30 minutes) fluid loss and the total fluid loss of a water based 6% bentonite mud was decreased with addition of 0.1% silicate but increased with higher content. The total fluid loss was modeled with API fluid loss model and new Kinetic (Hyperbolic) model. The filter cake thickness was reduced with addition of silicate.

8.2 Recommendation

The recommendation for future research in continuation of my current research is that the relationship between the moisture loss of cement cured under different conditions and temperature can be continued to make correlation for different additives and contamination.

REFERENCES

1. API Recommended Practice 10B, 1997. “Recommended Practice for Testing Well Cements Exploration and Production Department.” 22nd Edition.
2. API Recommended Practice 65, 2002. “Cementing Shallow Water Flow Zones in Deepwater Wells.”
3. API Spec 10, 1988. “Specification for Materials and Testing for Well Cements.” Fourth Edition, API, Dallas, August, 1988.
4. Anagnostopoulos, C.A., 2014. “Effect of different superplasticisers on the physical and mechanical properties of cement grouts.” Construction and Building Materials, Volume 50, January 2014, Pages 162–168
5. Baltazar, L.G., Henriques, F.M.A., and Jorne, F., 2012. “Optimisation of flow behaviour and stability of superplasticized fresh hydraulic lime grouts through design of experiments.” Constr Build Mater, 2012;35:838–45
6. Baker, C.L. and Garrison, A.D., 1939. “The chemical control of heaving shale.” Petroleum Eng. part 1, 50, January 1939; part 2, 102, February, 1939.
7. Bowen, R., 1981. Grouting in engineering practice. (2nd ed.) Apply Science Pub, London (1981)

8. Brazzel, R.L., 2009. "Multi-component drilling fluid additive, and drilling fluid system incorporating the additive." US Patent 7 635 667, assigned to Ambar Lonestar Fluid Services, LLC (Layfayette, LA), December 22, 2009.
9. Cai, J., Chenevert, M.E., Sharma, M.M., and Friedheim, J.E., 2012. "Decreasing Water Invasion Into Atoka Shale Using Nonmodified Silica Nanoparticles." SPE Drilling & Completion, Volume-27, Issue-01, March, 2012
10. Calvert, D.G., 2006. Preface, In: Nelson, E.B. and Guillot, D. (Ed.), Well Cementing, Schlumberger, Texas, 1-11.
11. Calvert, D. G., Smith, D. K., 1990. "API Oil Well Cementing Practices." Journal of Petroleum Technology, Volume 42, Issue 11, November, 1990.
12. Chun, B.S., Yang, H.C., Park, D.H., and Jung, H.S., 2008. "Chemical And Physical Factors Influencing Behavior of Sodium Silicate-Cement Grout." The Eighteenth International Offshore and Polar Engineering Conference, Vancouver, Canada, 6-11 July, 2008.
13. Cristou, M., and Konstantinidou, M., 2012. "Safety of Offshore Oil and Gas Operations: Lessons from Past Accident Analysis." Joint Research Centre of the European Commission, Luxembourg. (<http://publications.jrc.ec.europa.eu/repository/bitstream/111111111/27463/1/offshore-accident-analysis-draft-final-report-dec-2012-rev6-online.pdf>).

14. Darley, H.C.H., 1970. "Stabilization of Hard Shaly Formations with Alkali Metal Silicate." U.S. patent 3,640,343.
15. Detroit, W.J., Sanford, M.E., Chatterji, J., George, C.R., Childs, J.D., and Love, R. 1983. "Oil well Cementing Process." United States Patent RE31190, 1983.
16. Deville, J., Fritz, B., and Jarrett, M., 2011. "Development of water based drilling fluids customized for shale reservoirs." Proceeding-International Oilfield symposium on Oilfield Chemistry, Woodlands, Texas, 11-13 April, 2011
17. Dom, P.B., and S. Rabke 2007. "Development, verification, and improvement of a sediment-toxicity test for regulatory compliance." SPE Drilling & Completion, Vol. 22(2), 90-97.
18. Draganovic, A., Stille, H., 2014. "Filtration of cement-based grouts measured using a long slot." Tunnelling and Underground Space Technology. Volume 43, July 2014, Pages 101–112
19. Duncan, J., and McDonald, M., 2004. "Exceeding Drilling Performance and Environmental Requirements with Potassium Silicate Based Drilling Fluid." Proceeding-SPE International Conference on Health, Safety, and Environment in Oil and Gas Exploration and Production, Calgary, Alberta, Canada, 29-31 March, 2004
20. Durand, C., and T. Forsans, 1995. "Influence of Clays on Borehole Stability - A Literature Survey." Revue De L Institut Francais Du Petrole, Vol. 50(2),

187-218.

21. Eilers, L.H., Nelson, E.B., and Moran, L.K., 1983. "High-Temperature Cement Compositions-Pectolite, Scawtite, Truscottite, or Xonotlite: Which Do You Want?" *Journal of Petroleum Technology*, Volume-35, Issue-07, July, 1983, pp 1373-1377.
22. Eoff, L. and Waltman, B. 2009. "Polymer Treatment Controls Fluid Loss While Maintaining Hydrocarbon Flow." *Journal of Petroleum Technology*, pp. 28-30.
23. Eoff, L.S., and Buster, D., 1995. "High Temperature Synthetic Cement Retarder." *Proceeding- SPE International Symposium on Oilfield Chemistry, San Antonio, TX, February, 1995.*
24. Famous Gushers of the world. <http://www.sjgs.com/gushers.html#> Famous Gusher of the world
25. Fasesan, O.A., Heinze, L.R., and Wasler, D.W., 2005. "Incremental Improvements in 50:50 Poz Cementing Yields Enhanced Properties & Cost-effective Application." *Proceeding-SPE Production Operations Symposium, Oklahoma City, Oklahoma, 16-19 April, 2005.*
26. Fink, J.K., 2012. "Petroleum Engineer's Guide to Oil Field Chemicals and Fluids." Gulf Professional Publishing- an imprint of Elsevier. Waltham, MA 02451, USA, 2012

27. Franzoni, E., Pigino, B., Pistolesi, C., 2013. "Ethyl silicate for surface protection of concrete: performance in comparison with other inorganic surface treatments." *Cement Concrete Comp*, 44 (2013), pp. 69–76
28. Fuller, G., Souza, P., Ferreira, L., and Rouat, D. 2002. "High-Strength Lightweight Blend Improves Deepwater Cementing." *Oil & Gas Journal*, Vol. 100, No.8, pp. 86-95.
29. Garba, M.D., Petitt, I., and MacPhee, D.E., 2014. "Sodium Silicate Cement Squeeze Best Practice." *Proceeding- SPE Nigeria Annual International Conference and Exhibition, Lagos, Nigeria, 5-7 August, 2014.*
30. Gill, C., Fuller, G. A., and Faul, R. 2005. "Deepwater Cementing Best Practices for the Riserless Section." *AADE-05-NTCE-70*, pp. 1-14.
31. Griffith, J. and Faul, R. 1997. "Mud Management Special Slurries Improve Deepwater Cementing Operations." *Oil and Gas Journal*, Vol. 95, No. 42, pp. 49-51.
32. Guichard, B., Wood, B., and Vongphouthone, P., 2008. "Fluid loss reducer for high temperature high pressure water based-mud application." *US Patent 7 449 430*, assigned to Eliokem S.A.S. (Villejust, FR), November 11, 2008.
33. Guo, J., Yan, J., Fan, W., and Zhang, 2006. "Applications of strongly inhibitive silicate-based drilling fluids in troublesome shale formations in Sudan." *Journal of Petroleum Science and Engineering*. Volume 50, Issues 3–4, 16 March 2006,

Pages 195–203.

34. Heinold, T., Dillenbeck, R. L., Rogers, M. J., 2002. “The Effect of Key Cement Additives on the Mechanical Properties of Normal Density Oil and Gas Well Cement Systems.” Proceeding-SPE Asia Pacific Oil and Gas Conference and Exhibition, Melbourne, Australia, 8-10 October, 2002.
35. Izon, D., Danenberger, E.P., and Mayes, M., 2007. “Absence of fatalities in blowouts encouraging in MMS study of OCS incidents 1992-2006.” Well Control Magazine, July/August 2007, pp. 86-90
36. Jianga, L., Xuea, X., Zhanga, W., Yangc, J., Zhanga, H., Lia, Y., Zhanga, R., Zhanga, Z., Xub, L., Qua, J., Songa, J., and Qina, J., 2015. “The investigation of factors affecting the water impermeability of inorganic sodium silicate-based concrete sealers.” Construction and Building Materials. Volume 93, 15 September 2015, Pages 729–736
37. John B. (1992). “Class G and H Basic Oil Well Cements,” World Cement.
38. Joshi, R.C., and Lohtia, R.P. 1997. “Advances in Concrete Technology, V 2, Fly Ash in Concrete: Production, Properties and Uses.” Amsterdam, Netherlands: Gordon and Breach Science Publishers, 1997, pp:1-271.
39. Kennerley, R.A., 1961. “Products of Hydrothermal Hydration of Cements from Geothermal Bores.” New Zealand J. Science, Volume- 4, 1961, pp453-68.
40. Kim, J. and Vipulanandan, C. 2006. “Removal of Lead from Contaminated

Water and Clay Soil Using a Biosurfactant.” *Journal of Environmental Engineering*, Vol. 132, No. 7, pp.857-865.

41. Kim, J. and Vipulanandan, C. 2003. “Effect of pH, Sulfate and Sodium on the EDTA titration of Calcium.” *Cement and Concrete Research*, Vol. 33(5), pp. 621-627.
42. Labibzadeh, M., Zhhabizadeh, B., and Khajehdezfuly, A. 2010. “Early Age Compressive Strength Assessment of Oil Well Class G Cement Due to Borehole Pressure and Temperature Changes.” *Journal of American Science*, Vol. 6, No.7, pp.38-47.
43. Larrondo, L.E., Urness, C.M., and Milosz, G.M., 1985. “Laboratory Evaluation of Sodium Hydroxide, Sodium Orthosilicate, and Sodium Metasilicate as Alkaline Flooding Agents for a Western Canada Reservoir.” *Proceeding- SPE Oilfield and Geothermal Chemistry Symposium*, Phoenix, Arizona, 9-11 March, 1985.
44. Lea, F.M., 1971. “The Chemistry of Cement and Concrete.” Third edition, Chemical Publishing Co., New York City, 1971, pp 177-202.
45. Lim, S.K., Tan, C.S., Chen, K.P., Lee, M.L., Lee, W.P., 2013. “Effect of different sand grading on strength properties of cement grout.” *Construction and Building Materials*. Volume 38, January 2013, Pages 348–355
46. Liu, J., Vipulanandan, C., and Richardson, D. 2013. “Piezoresistive Behavior of Modified oil Well Cement with Nickel.” *Proceedings, CIGMAT -2013*

http://cigmat.cive.uh.edu/sites/cigmat/files/conference/poster/2013/7_2.pdf

47. Malyshev, A., Doronina, T., Popov, M., Ryabchikov, A., and Shulga, V., 2013. “Optimized Particles Size Distribution Lightweight Cement at Low Temperatures: Case Study from Eastern Siberia, Russia.” Proceeding- SPE Arctic and Extreme Environments Technical Conference and Exhibition, Moscow, Russia, 15-17 October, 2013.
48. Mangadlao, J.D., Cao, P., and Advincula, R.C., 2015. “Smart cements and cement additives for oil and gas operations.” *Journal of Petroleum Science and Engineering* 129 (2015) 63–76
49. Mbaba, P.E. and Caballero, E.P. 1983. “Field Application of an Additive Containing Sodium Metasilicate During Steam Stimulation.” Proceeding-SPE Annual Technical Conference and Exhibition, San Francisco, California, 5-8 October, 1983.
50. McDonald, M., 2012. “A Novel Potassium Silicate for Use in Drilling Fluids Targeting Unconventional Hydrocarbons.” Proceeding- SPE Canadian Unconventional Resources Conference, Calgary, Alberta, Canada, 30 October-1 November, 2012.
51. Mebarkia, S. and Vipulanandan, C. (1992). “Compressive behavior of glass-fiber-reinforced polymer concrete.” *Journal of Materials in Civil Engineering*, Vol. 4, No. 1, pp. 91-105, 1992.

52. Melbouci, M., and Sau, A.C., 2008. "Water-based drilling fluids." US Patent 7 384 892, assigned to Hercules Incorporated (Wilmington, DE), June 10, 2008
53. Moradi, S.S.T., and Nikolaeb, N.I., 2014. "Optimization of Cement Spacer System for Zonal Isolation in High-Pressure High-Temperature Wells." SPE Russian Oil and Gas Exploration & Production Technical Conference and Exhibition, Moscow, Russia, 14-16 October, 2014.
54. Morales, M., Morris, W., Criado, M.A., Robles, J., and Bianchi, G., 2003. "Improving the Sulfate Resistance Performance of API cement Portland upon Appropriate Slurry Design." Proceeding-SPE Latin American and Caribbean Petroleum Engineering Conference, Port-of-Spain, Trinidad and Tobago, 27-30 April, 2003
55. Morgan, B.E., 1958. Drilling and Production Practice, 1 January, New York, New York, 1958
56. Nazari, T., Hareland, G., and Azar, J.J., 2010. "Review of Cuttings Transport in Directional Well Drilling: Systematic Approach." Proceeding-SPE 132372, Presentation at the SPE Western Regional Meeting held in Anaheim, California, USA, 27-29 May 2010
57. Nelson, E.B., Guillot, D., 2006. Well cementing (2nd edition), Schlumberger Dowell, Sugar Land, TX (2006)
58. Nelson, E.B., 1990. Well Cementing. Elsevier Science BV, Amsterdam, The

Netherlands, 1990, 3-10.

59. Nelson, E.B. and Casabonne, J.M., 1992. "New Method for Better Control of Cement Performance in High-Temperature Wells." Proceeding- 67th Annual Technical Conference and Exhibition of the Society of Petroleum Engineers held in Washington, DC, October 4-7, 1992.
60. Nonveiller, E., 1989. "Grouting theory and practice." Elsevier, Amsterdam (1989)
61. Park, J., Vipulanandan, C., Kim, J., and Oh, M. H. 2006. "Effect of Surfactants and Electrolyte Solutions on the Properties of Soils." Journal of Environmental Geology, Vol. 49, pp.977-989.
62. Power, D., and Zamora, M., 2003. "Drilling Fluid Yield Stress: Measurement Techniques for Improved Understanding of Critical Drilling Fluid Parameters." Proceeding-AADE 2003 National Technology Conference "Practical Solutions for Drilling Challenges," held at the Radisson Astrodome Houston, Texas, April 1 - 3, 2003 in Houston, Texas.
63. Powers, C.A., Holman, G.B., and Smith, R.C. 1977. "Process and Composition For Cementing Casing In A Well." United States Patent 4036301, 1977
64. Ravi, K., McMechan, D.E., Reddy, B.R., Crook, R.J., 2007. "A Comparative Study of Mechanical Properties of Density-Reduced Cement Compositions." SPE Drilling & Completion, Vol. 22, No. 2, June, 2007, pp. 119-126.

65. Radenti, G., and Ghiringhelli, L., 1972. "Cementing Materials for Geothermal Wells." *Geothermics*, Volume-3, 1972, pp119-23.
66. Saasen, A., Marken, C., Dawson, J., and Rogers, M., 1991. "Oscillating rheometer measurements on oilfield cement slurries." Volume 21, Issue 1, January 1991, pp 109–119.
67. Sabins, F.L., Sutton, D.L., and Cook, C. Jr., 1984. "Effect of Excessive Retardation on the Physical Properties of Cement Slurries." *Journal of Petroleum Technology*, Volume-36, Issue-08, August 1984.
68. Satoh, H., Sasaki, T., and Yamaguchi, Y., 2012. "Laboratory Grouting Tests using Ultrafine Cement Based Grouts of Smooth Surface Particles by Dry Impact Blending Method." *Proceeding-7th Asian Rock Mechanics Symposium*, Seoul, Korea, 15-19 October, 2012
69. Shaw Gusher. "The Village of Oil Springs". <http://www.oilsprings.ca/activities.htm>
70. Smith, D.K., 1987. Cementing. Monograph Series, SPE, Richardson, TX (1987) 4.
71. Smithson, T., 2015. "Schlumberger Oilfield Glossary." Schlumberger Limited, 2015
72. Stewart, M.R., Kosich, B., Warren, B.K., Urquhart, J.C., and McDonald, M.J., 2000. "Use of Silicate Mud to Control Borehole Stability and over pressured Gas

Formations in Northeastern British Columbia.” Proceeding -SPE/CERI Gas Technology Symposium, Calgary, Alberta, Canada, 3-5 April, 2000.

73. Stille, B. and Gustafson G. 2010. “A review of the Namntall tunnel project with regard to grouting performance.” *Tunn Undergr Sp Tech* 2010;25(4):346–56.
74. Sugama, T., and Carciello, N., 1996. “Sodium metasilicate-modified lightweight high alumina cements for use as geothermal well-cementing materials.” *Advanced Cement Based Materials*, Volume 3, Issue 2, March 1996, Pages 45-53.
75. Sutton, I.S., 2013. “Summarizing the Deepwater Horizon/Macondo Reports.” *Proceedings- Offshore Technology Conference*, Houston, Texas, USA, 6-9 May, 2013.
76. Taylor, H.F.W., 1964. The Chemistry of Cements, Academic Press Inc., London, 1964, 1, 212.
77. Taehee, K., Kwon, L.H., Deok, K.G., Woo, L.S., Tak, C.G., and Woo, Y.B., 2013. “Analysis on the Chemical and Mechanical Stability of the Grouting Cement for CO2 Injection Well.” *Energy Procedia*, Volume 37, 2013, Pages 5702–5709
78. Thaemlitz, J., and Patel, A.D., 1999. “New environmentally safe high-temperature water-based drilling-fluid system.” *SPE Drilling & Completion* Vol. 14(3), 185-189.

79. Urquhart, J.C., 1998. "Back to the Future in Silicate Drilling Fluids." *World Oil*, October, 1998
80. Venditto, J.J., and George, C.R., 1984: "Better Wellbore Temperature Data Equal Better Cement Job." *World Oil*, February, 1984.
81. Vietti, W.V., Garrison, A.D., 1939. "Method of Drilling Wells." U.S. patent 2,165,824.
82. Vipulanandan, C. and Paul, E., 1990. "Performance of Epoxy and Polyester Polymer Concrete." *ACI Materials Journal*, Vol. 87, No. 3, May-June, 1990, p. 241-251
83. Vipulanandan, C. and Prashanth, P. 2013. "Impedance Spectroscopy Characterization of a Piezoresistive Structural Polymer Composite Bulk Sensor." *Journal of Testing and Evaluation*, ASTM, Vol. 41, No. 6, pp. 898-904.
84. Vipulanandan, C. and Garas, V. 2008. "Electrical Resistivity, Pulse Velocity and Compressive Properties of Carbon Fiber Reinforced Cement Mortar." *Journal of Materials in Civil Engineering*, Vol. 20, No. 2 , pp. 93-101.
85. Vipulanandan, C. and Liu, J. 2005. "Polyurethane Based Grouts for Deep Off-Shore Pipe-in-Pipe Application." *Proceedings, Pipelines 2005, ASCE*, Houston, TX, pp. 216-227.

86. Vipulanandan, C., and Garas, V. 2006. "Piezoresistivity of Carbon Fiber Reinforced Cement Mortar", Proceedings, Engineering, Construction and Operations in Challenging Environments." Earth & Space 2006, Proceedings ASCE Aerospace Division, League City, TX, CD-ROM.
87. Vipulanandan, C. and Sett, K. 2004. "Development and Characterization of Piezoresistive Smart Structural Materials," Proceedings, Engineering, Construction and Operations in Challenging Environments, Earth & Space 2004, ASCE Aerospace Division, League City, TX, pp. 656-663.
88. Vipulanandan, C., Krishnamoorti, R., Saravanan, R., Liu, J., Qu, Q., Narvaez, G.G., Richardson, D.A., and Pappas, J.M., 2014. "Development and Characterization of Smart Cement for Real Time Monitoring of Ultra Deepwater Oil Well Cementing Applications." Proceeding- Offshore Technology Conference, 05-08 May, 2014, Houston, Texas.
89. Vipulanandan, C., Ali, K., Narvaez, G., Richardson, D.A., and Pappas, J.M., 2014. "Characterizing Smart Cement with Sodium Metasilicate for Real Time Monitoring of Ultra-Deepwater Oil Well Cementing Applications." Proceeding- AADE Fluids Technical Conference and Exhibition held at the Hilton Houston North Hotel, Houston, Texas, April 15-16, 2014.
90. Vipulanandan, C., Mohammed, A.S., 2014. "Hyperbolic rheological model with shear stress limit for acrylamide polymer modified bentonite drilling muds."

Journal of Petroleum Science and Engineering, Volume 122, October 2014, Pages 38–47

91. Vipulanandan, C., Raheem, A., Basirat, B., Mohammed, A.S., and Richardson, D. A., 2014. “New Kinetic Model to Characterize the Filter Cake Formation and Fluid Loss in HPHT Process.” Proceeding-Offshore Technology Conference, Houston, Texas, 05-08 May, 2014
92. Vipulanandan, C., and Mohammed, A., 2015a. “Smart cement rheological and piezoresistive behavior for oil well applications.” Journal of petroleum Science and Engineering, V-135, 2015, pp. 50-58.
93. Vipulanandan, C., and Mohammed, A., 2015b. “Smart cement modified with iron oxide nanoparticles to enhance the piezoresistive behavior and compressive strength for oil well applications.” Journal of Smart Materials and Structures (In Press, 2015).
94. Wang, S. Y., and Vipulanandan, C. 1996. “Leachability of Lead From Solidified Cement-Fly Ash Binders.” Cement and Concrete Research, Vol. 26, No. 6, pp. 895-905.
95. Ward, I., Chapman, J.W., and Williamson, R., 1999. “Silicate Based Muds: Chemical Optimization Based on Field Experience.” SPE Drilling & Completion, V-14, No-1, March, 1999, pp 57-63

96. Wingrave, J.A., Kubena, E., Jr., Douty, C.F., Whitfill, D.L., Cords, D.P., 1987.
“New chemical package produces an improved shale inhibitive water-based
drilling fluid system.” SPE Annual Technical Conference and Exhibition, Dallas,
Texas, 27-30 September, 1987
97. Yeon, K.S., and Han, M.Y., 1997. “Fundamental properties of polymer–cement
mortars for concrete repair.” Proceeding- 7th International Conference on
Structural Faults and Repair, vol. 2. Edinburgh. 1997. p. 469–76.